

Tomy J. Gutiérrez *Editor*

Reactive and Functional Polymers Volume Two

Modification Reactions, Compatibility
and Blends



Springer

Reactive and Functional Polymers Volume Two

Tomy J. Gutiérrez

Editor

Reactive and Functional Polymers Volume Two

Modification Reactions, Compatibility
and Blends

 Springer

Editor

Tomy J. Gutiérrez

Thermoplastic Composite Materials (CoMP) Group, Faculty of Engineering

Institute of Research in Materials Science and Technology (INTEMA)

National University of Mar del Plata (UNMdP) and National Scientific

and Technical Research Council (CONICET)

Mar del Plata, Buenos Aires, Argentina

ISBN 978-3-030-45134-9

ISBN 978-3-030-45135-6 (eBook)

<https://doi.org/10.1007/978-3-030-45135-6>

© The Editor(s) (if applicable) and The Author(s), under exclusive license to Springer Nature Switzerland AG 2020

This work is subject to copyright. All rights are reserved by the Publisher, whether the whole or part of the material is concerned, specifically the rights of translation, reprinting, reuse of illustrations, recitation, broadcasting, reproduction on microfilms or in any other physical way, and transmission or information storage and retrieval, electronic adaptation, computer software, or by similar or dissimilar methodology now known or hereafter developed.

The use of general descriptive names, registered names, trademarks, service marks, etc. in this publication does not imply, even in the absence of a specific statement, that such names are exempt from the relevant protective laws and regulations and therefore free for general use.

The publisher, the authors, and the editors are safe to assume that the advice and information in this book are believed to be true and accurate at the date of publication. Neither the publisher nor the authors or the editors give a warranty, expressed or implied, with respect to the material contained herein or for any errors or omissions that may have been made. The publisher remains neutral with regard to jurisdictional claims in published maps and institutional affiliations.

This Springer imprint is published by the registered company Springer Nature Switzerland AG

The registered company address is: Gewerbestrasse 11, 6330 Cham, Switzerland

I would like to dedicate this book:

To my God (Father, Son and Holy Spirit), to the Virgin Mary and to my Guardian Angel, Its energy stimulates me to enjoy the landscape we call life, and its peace encourages me to always continue towards the future, a place where we will all go and each one will be under the law of the creative father.

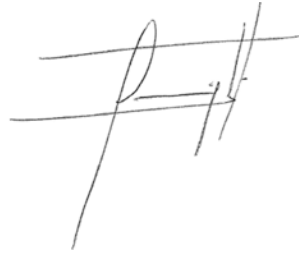
*To my Mother (Dr. Mirian Arminda Carmona Rodríguez),
For forming my character and attitude towards life.*

*To my Grandmother (Mrs. Arminda Teresa Rodríguez Romero),
A person who unfortunately left before this world's time, but I am sure that she is up watching me and supporting me in all facets of my life. You are in my most beautiful memories.*

*To my firstborn daughter (Miranda
V. Gutiérrez),
I will give you a lot of love!!!🌍❤️*

*To all anonymous people,
Those who give me their love, friendship,
patience and support in various situations.*

*To Venezuela and Argentina,
The first for giving me my academic and
professional training, and the second for
welcoming me with love and friendship
before the dictatorship that my country
(Venezuela) is experiencing today.*

A handwritten signature in black ink, appearing to be 'Tomy J. Gutiérrez', written over two horizontal lines.

*Tomy J. Gutiérrez, Ph.D.
Editor*

Preface

Reactive and functional polymers are essentially linked to the chemistry of the polymers and their applications. The multiple tasks that they have accomplished in our recent history, and how they will help new advances in different crucial fields such as agriculture, environmental remediation, food, medicine, among others are indisputable. Volume 2 of this book has been focused on coupling, crosslinking and grafting reactions to improve the compatibility of reactive and functional polymer blends. I thank Dr. Sabu Thomas (Editor-in-chief for the journal ‘Nano-Structures & Nano-Objects’) and his research group for their valuable contribution to this volume.

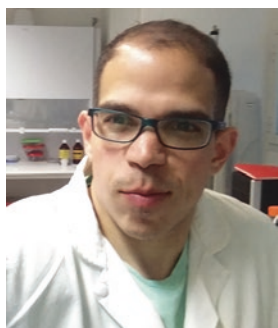
Tomy J. Gutiérrez, Ph.D
National Scientific and Technical Research Council (CONICET)
Institute of Research in Materials Science and Technology (INTEMA)
Thermoplastic Composite Materials (CoMP) Group
Mar del Plata, Argentina

Contents

1	Advances in Reactive and Functional Polymers: Editor's Perspective	1
	Tomy J. Gutiérrez	
2	Role of Functional Polymers in the Compatibilization of Polymer Blends	5
	Ajitha Anthickamalil Ramachandran, Arunima Reghunadhan, Hanna J. Maria, and Sabu Thomas	
3	Compatibilization and Crosslinking in Biodegradable Thermoplastic Polyester Blends	23
	M. Z. Ahmad Thirmizir, Z. A. Mohd Ishak, and M. S. Salim	
4	Crosslinked Polymer Hydrogels	91
	Reem K. Farag and Salma Hani	
5	Crosslinking of Polymers: Rubber Vulcanization	117
	Gordana Marković, Milena Marinović-Cincović, Suzana Samaržija-Jovanović, Vojislav Jovanović, and Jaroslava Budinski-Simendić	
6	Cross-Linkable Bio and Mineral Fillers for Reactive Polymer Composites: Processing and Characterization	135
	Jelena D. Rusmirović, Tihomir M. Kovačević, Saša J. Brzić, and Aleksandar D. Marinković	
7	Functional Crosslinked Hydrogels	165
	Saminu M. Magami	
8	Grafting Polymers	199
	Sonal Choudhary, Kashma Sharma, Vishal Sharma, and Vijay Kumar	

9	Grafting Functional Groups onto Biodegradable Thermoplastic Polyesters	245
	Casparus J. R. Verbeek and Chanelle Gavin	
10	Grafting of Electroactive Polymers	283
	Arun K. Nandi, Radhakanta Ghosh, and Dhruva P. Chatterjee	
11	Reinforced Polymers for Electroactive Devices	325
	Anupama Gaur and Pralay Maiti	
	Index	349

About the Editor



Tomy J. Gutiérrez received his degrees chemistry and in Education (Chemical Mention) from the Central University of Venezuela (UCV) in December 2007 and July 2008, respectively. He completed his specialization in International Negotiation of Hydrocarbons from the National Polytechnic Experimental University of the National Armed Force (UNEFA), Venezuela, in July 2011, and his Master's and PhD degrees in Food Science and Technology in October 2013 and April 2015, respectively, both from the UCV. He has also PhD studies in Metallurgy and Materials Science from

the UCV and postdoctoral studies in the Research Institute in Materials Science and Technology (INTEMA). He has been a Professor/Researcher both at the Institute of Food Science and Technology (ICTA) and the School of Pharmacy at the UCV. Currently, he is an Adjunct Researcher in the INTEMA, National Scientific and Technical Research Council (CONICET), Argentina. Dr. Gutiérrez has at least 20 book chapters, 40 publications in international journals of high-impact factor, and 5 published books. He has been a Lead Guest Editor of several international journals such as *Journal of Food Quality*, *Polymers for Advanced Technologies*, and *Current Pharmaceutical Design*. He is also an Editorial Board Member of different international journals such as *Food and Bioprocess Technology* (from April 2019 to the present, 2019 impact factor 3.356), *Current Nutraceuticals* (from May 2019 to the present) and *Journal of Renewable Materials* (from June 2019 to the present, 2019 impact factor 1.341). Currently, he is developing a line of research in nano-structured materials based on polymers (composite materials), which are obtained on a pilot scale to be transferred to the agricultural, food, pharmaceutical and polymer industries. He is also a collaborator of international projects between Argentina and Brazil, Colombia, France, Poland, Spain, Italy, Sweden and Venezuela.

Chapter 1

Advances in Reactive and Functional Polymers: Editor's Perspective



Tomy J. Gutiérrez

Abstract Reactive and functional polymers are generally obtained *via* coupling, crosslinking and grafting reactions using different processing methodologies such as extrusion reactive in order to improve the compatibility of polymer blends, as well as to obtain active and functional polymer surfaces. These polymers have proven important for the development of advanced materials for different applications. With this chapter, we open the main topics that will be analyzed in this volume.

Keywords Block copolymers · Coupling · Crosslinking · Grafting · Natural and synthetic polymers · Surface

1.1 Fundamentals for Reactive and Functional Polymers

Reactive and functional polymers are mainly obtained *via* chemical or physical modifications of the polymer structures using different coupling, crosslinking and grafting reactions in order to improve the compatibility of polymer blends based on natural and synthetic polymers, as well as to obtain active and functional polymer surfaces (Gutiérrez 2017a, b, 2018a, b; Gutiérrez, Herniou-Julien et al. 2018a; Gutiérrez and Álvarez 2016; Gutiérrez and Alvarez 2017a,b,c,d; Gutiérrez and Alvarez 2018; Gutiérrez and González 2016, 2017; Gutiérrez, Guarás et al. 2017; Gutiérrez, Guzmán et al. 2016a; Gutiérrez, Morales et al. 2015a; Gutiérrez, Ollier et al. 2018b; Gutiérrez, Suniaga, et al. 2016b; Gutiérrez, Tapia et al. 2015b; Gutiérrez et al. 2019; Herniou--Julien et al. 2019; Merino

T. J. Gutiérrez (✉)

Thermoplastic Composite Materials (CoMP) Group, Faculty of Engineering, Institute of Research in Materials Science and Technology (INTEMA), National University of Mar del Plata (UNMDP) and National Scientific and Technical Research Council (CONICET), Colón 10850, Mar del Plata, Argentina
e-mail: tomy.gutierrez@fi.mdp.edu.ar

et al. 2019a,b; Merino, Gutiérrez et al. 2018a; Merino, Mansilla et al. 2018b; Toro-Márquez et al. 2018; Zarrintaj et al. 2019). These aspects are the focus of this volume.

Acknowledgements The author would like to thank the Consejo Nacional de Investigaciones Científicas y Técnicas (CONICET) (Postdoctoral internal fellowship PDTs-Resolution 2417), Agencia Nacional de Promoción Científica y Tecnológica (ANPCyT) (grant PICT-2017-1362), Universidad Nacional de Mar del Plata (UNMdP) for financial support, and Dr. Mirian Carmona-Rodríguez.

Conflicts of Interest The author declares no conflict of interest.

References

- Gutiérrez, T. J. (2017a). Effects of exposure to pulsed light on molecular aspects of edible films made from cassava and taro starch. *Innovative Food Science and Emerging Technologies*, 41, 387–396. <https://doi.org/10.1016/j.ifset.2017.04.014>.
- Gutiérrez, T. J. (2017b). Surface and nutraceutical properties of edible films made from starchy sources with and without added blackberry pulp. *Carbohydrate Polymers*, 165, 169–179. <https://doi.org/10.1016/j.carbpol.2017.02.016>.
- Gutiérrez, T. J. (2018a). Active and intelligent films made from starchy sources/blackberry pulp. *Journal Polymers and the Environment*, 26(6), 2374–2391. <https://doi.org/10.1007/s10924-017-1134-y>.
- Gutiérrez, T. J. (2018b). Are modified pumpkin flour/plum flour nanocomposite films biodegradable and compostable? *Food Hydrocolloids*, 83, 397–410. <https://doi.org/10.1016/j.foodhyd.2018.05.035>.
- Gutiérrez, T. J., Herniou-Julien, C., Álvarez, K., & Alvarez, V. A. (2018a). Structural properties and *in vitro* digestibility of edible and pH-sensitive films made from Guinea arrowroot starch and wastes from wine manufacture. *Carbohydrate Polymers*, 184, 135–143. <https://doi.org/10.1016/j.carbpol.2017.12.039>.
- Gutiérrez, T. J., & Álvarez, K. (2016). Physico-chemical properties and *in vitro* digestibility of edible films made from plantain flour with added *Aloe vera* gel. *Journal of Functional Foods*, 26, 750–762. <https://doi.org/10.1016/j.jff.2016.08.054>.
- Gutiérrez, T. J., & Alvarez, V. A. (2017a). Cellulosic materials as natural fillers in starch-containing matrix-based films: A review. *Polymer Bulletin*, 74(6), 2401–2430. <https://doi.org/10.1007/s00289-016-1814-0>.
- Gutiérrez, T. J., & Alvarez, V. A. (2017b). Data on physicochemical properties of active films derived from plantain flour/PCL blends developed under reactive extrusion conditions. *Data in Brief*, 15, 445–448. <https://doi.org/10.1016/j.dib.2017.09.071>.
- Gutiérrez, T. J., & Alvarez, V. A. (2017c). Eco-friendly films prepared from plantain flour/PCL blends under reactive extrusion conditions using zirconium octanoate as a catalyst. *Carbohydrate Polymers*, 178, 260–269. <https://doi.org/10.1016/j.carbpol.2017.09.026>.
- Gutiérrez, T. J., & Alvarez, V. A. (2017d). Properties of native and oxidized corn starch/polystyrene blends under conditions of reactive extrusion using zinc octanoate as a catalyst. *Reactive and Functional Polymers*, 112, 33–44. <https://doi.org/10.1016/j.reactfunctpolym.2017.01.002>.
- Gutiérrez, T. J., & Alvarez, V. A. (2018). Bionanocomposite films developed from corn starch and natural and modified nano-clays with or without added blueberry extract. *Food Hydrocolloids*, 77, 407–420. <https://doi.org/10.1016/j.foodhyd.2017.10.017>.
- Gutiérrez, T. J., & González, G. (2016). Effects of exposure to pulsed light on surface and structural properties of edible films made from cassava and taro starch. *Food and Bioprocess Technology*, 9(11), 1812–1824. <https://doi.org/10.1007/s11947-016-1765-3>.

- Gutiérrez, T. J., & González, G. (2017). Effect of cross-linking with *Aloe vera* gel on surface and physicochemical properties of edible films made from plantain flour. *Food Biophysics*, 12(1), 11–22. <https://doi.org/10.1007/s11483-016-9458-z>.
- Gutiérrez, T. J., Guarás, M. P., & Alvarez, V. A. (2017). Chapter 9. Reactive extrusion for the production of starch-based biopackaging. In M. A. Masuelli (Ed.), *Biopackaging* (pp. 287–315). Miami, EE.UU. ISBN: 978-1-4987-4968-8: CRC Press Taylor & Francis Group. <https://doi.org/10.1201/9781315152349-9>.
- Gutiérrez, T. J., Guzmán, R., Medina Jaramillo, C., & Famá, L. (2016a). Effect of beet flour on films made from biological macromolecules: Native and modified plantain flour. *International Journal of Biological Macromolecules*, 82, 395–403. <https://doi.org/10.1016/j.ijbiomac.2015.10.020>.
- Gutiérrez, T. J., Morales, N. J., Pérez, E., Tapia, M. S., & Famá, L. (2015a). Physico-chemical properties of edible films derived from native and phosphated cush-cush yam and cassava starches. *Food Packaging and Shelf Life*, 3, 1–8. <https://doi.org/10.1016/j.foodpack.2014.09.002>.
- Gutiérrez, T. J., Ollier, R., & Alvarez, V. A. (2018b). Chapter 5. Surface properties of thermo-plastic starch materials reinforced with natural fillers. In V. K. Thakur & M. K. Thakur (Eds.), *Functional biopolymers* (pp. 131–158). EE.UU: Springer International Publishing. https://doi.org/10.1007/978-3-319-66417-0_5. isbn:978-3-319-66416-3. eISBN: 978-3-319-66417-0.
- Gutiérrez, T. J., Suniaga, J., Monsalve, A., & García, N. L. (2016b). Influence of beet flour on the relationship surface-properties of edible and intelligent films made from native and modified plantain flour. *Food Hydrocolloids*, 54, 234–244. <https://doi.org/10.1016/j.foodhyd.2015.10.012>.
- Gutiérrez, T. J., Tapia, M. S., Pérez, E., & Famá, L. (2015b). Structural and mechanical properties of native and modified cush-cush yam and cassava starch edible films. *Food Hydrocolloids*, 45, 211–217. <https://doi.org/10.1016/j.foodhyd.2014.11.017>.
- Gutiérrez, T. J., Toro-Márquez, L. A., Merino, D., & Mendieta, J. R. (2019). Hydrogen-bonding interactions and compostability of bionanocomposite films prepared from corn starch and nano-fillers with and without added Jamaica flower extract. *Food Hydrocolloids*, 89, 283–293. <https://doi.org/10.1016/j.foodhyd.2018.10.058>.
- Herniou--Julien, C., Mendieta, J. R., & Gutiérrez, T. J. (2019). Characterization of biodegradable/non-compostable films made from cellulose acetate/corn starch blends processed under reactive extrusion conditions. *Food Hydrocolloids*, 89, 67–79. <https://doi.org/10.1016/j.foodhyd.2018.10.024>.
- Merino, D., Gutiérrez, T. J., & Alvarez, V. A. (2019a). Potential agricultural mulch films based on native and phosphorylated corn starch with and without surface functionalization with chitosan. *Journal Polymers and the Environment*, 27(1), 97–105. <https://doi.org/10.1007/s10924-018-1325-1>.
- Merino, D., Gutiérrez, T. J., & Alvarez, V. A. (2019b). Structural and thermal properties of agricultural mulch films based on native and oxidized corn starch nanocomposites. *Starch-Stärke*, 71(7–8), 1800341. <https://doi.org/10.1002/star.201800341>.
- Merino, D., Gutiérrez, T. J., Mansilla, A. Y., Casalengué, C. A., & Alvarez, V. A. (2018a). Critical evaluation of starch-based antibacterial nanocomposites as agricultural mulch films: Study on their interactions with water and light. *ACS Sustainable Chemistry & Engineering*, 6(11), 15662–15672. <https://doi.org/10.1021/acssuschemeng.8b04162>.
- Merino, D., Mansilla, A. Y., Gutiérrez, T. J., Casalengué, C. A., & Alvarez, V. A. (2018b). Chitosan coated-phosphorylated starch films: Water interaction, transparency and antibacterial properties. *Reactive and Functional Polymers*, 131, 445–453. <https://doi.org/10.1016/j.reactfunctpolym.2018.08.012>.
- Toro-Márquez, L. A., Merino, D., & Gutiérrez, T. J. (2018). Bionanocomposite films prepared from corn starch with and without nanopackaged Jamaica (*Hibiscus sabdariffa*) flower extract. *Food and Bioprocess Technology*, 11(11), 1955–1973. <https://doi.org/10.1007/s11947-018-2160-z>.
- Zarrintaj, P., Jouyandeh, M., Ganjali, M. R., Hadavand, B. S., Mozafari, M., Sheiko, S. S., Vatankeh-Varnoosfaderani, M., Gutiérrez, T. J., & Saeb, M. R. (2019). Thermo-sensitive polymers in medicine: A review. *European Polymer Journal*, 117, 402–423. <https://doi.org/10.1016/j.eurpolymj.2019.05.024>.

Chapter 2

Role of Functional Polymers in the Compatibilization of Polymer Blends



Ajitha Anthickamalil Ramachandran, Arunima Reghunadhan,
Hanna J. Maria, and Sabu Thomas

Abstract Polymer mixing is one of the direct and practical strategies for creating new superior materials for commercial and industrial applications. The polymer blend can reinforce the setting of the properties according to the focused need. The compatibility of the immiscible polymer mixing system by incorporating a new material, helps in the development of high-performance materials. In general, graft, block or random copolymers have widespread applications as compatibilizers. Compatibilization is based on a specific chemical reaction between two functional polymer components during mixing, and is known as a reactive mixing. The introduction of reactive and functional polymers into an immiscible polymer blend with a strong interaction between the two polymer components of the mixtures can improve the adhesion between the components. Functional polymers have significant importance because of the high compatibilizing efficiency since the compatibilizer is created directly between the interfaces. In this chapter the interfacial reaction and morphology, the effect of reactive polymers on the polymer mixing process, the relationship between the flow field or process parameters, the compatibilizing efficiency of a reactive compatibilizer in different mixing techniques will be discussed. The concept of reactive compatibilizer, the characterization techniques used to monitor the compatibility of functional polymers, future perspectives and challenges in this field will also be discussed in this chapter.

Keywords Characterization · Grafting · Immiscible polymers · Polymer thermodynamics

A. A. Ramachandran · A. Reghunadhan · H. J. Maria
International and Inter University Centre for Nanoscience and Nanotechnology, Mahatma Gandhi University, Kottayam, Kerala, India

S. Thomas (✉)
International and Inter University Centre for Nanoscience and Nanotechnology, Mahatma Gandhi University, Kottayam, Kerala, India

School of Chemical Sciences, Mahatma Gandhi University, Kottayam, Kerala, India
e-mail: sabuthomas@mgu.ac.in

2.1 Introduction

Polymer mixtures is the combination of two or more polymers. Polymer mixing is an effective method to fabricate a new material with combined properties of both components. It is an efficient strategy to make a new material profitable other than synthesizing a new one. It can generally be said that polymer mixtures are physical mixtures of two or more polymers with chemical and physical interactions. Polymer mixing can be considered as a cost-effective method for the development of a material with specific properties according to customer requirements (Bahrami et al. 2015; Chiu 2017; Otero-Navas et al. 2017; Wang et al. 2017; Utracki 1982; Roman et al. 2017; Paul and Newman 1978; Brown 2003). Polymer mixtures can be classified into three types depending on the miscibility between the components, such as miscible, compatible and immiscible mixtures. Miscible mixtures are of a homogeneous nature and show properties of individual components (Lu and Weiss 1992), while immiscible mixtures are heterogeneous. The miscibility of polymer mixtures depends mainly on the chemical nature of the polymers, the interaction between the polymer components, the interfacial tension and the polarity of polymer components. Miscible mixtures will obtain negative free energy of mixture (Gibbs-Helmholtz equation - $\Delta G_m = \Delta H_m - T \cdot \Delta S_m$) (Zarrintaj et al. 2019). Some examples of miscible polymer mixtures are poly(styrene)/poly(phenylene oxide) (PS/PPO) and poly(styrene-acrylonitrile)/poly(methyl methacrylate) (PSAN/PMMA) (Thomas and Grohens 2014).

Compatible mixtures have a fine phase morphology and show better properties even though they are not completely miscible. Polymer mixture from acrylonitrile-butadiene-styrene (ABS)/poly(carbonate) (PC) involved in this category (Tjong and Meng 2000). Due to the large difference in polarity and viscosity between the individual polymer components and due to the absence of chemical interaction between individual polymer components, most mixtures are immiscible with a heterogeneous phase structure. The immiscible mixtures acquire clear interfaces due to the great interfacial adhesion between the components and the poor interfacial adhesion between the components. The real reason for the immiscibility based on thermodynamics sheds light on the insignificant entropy of the mixture (ΔS_m). Some examples include mixtures from poly(ethylene terephthalate)/poly(vinyl alcohol) (PET/PVA), poly(butylene terephthalate)/PS (PBT/PS), poly(propylene)/PS (PP/PS), PP/poly(ethylene) (PP/PE), PC/PP and PP/poly(trimethylene terephthalate) (PTT), etc. (Thomas and Grohens 2014; Arif et al. 2017; Mathew et al. 2018).

Four basic morphologies can be expected for miscible mixtures, such as co-continuous morphology, droplet/domain morphology, fiber-like morphology and lamellae morphology. Most mixtures exhibit co-continuous and domain morphologies. Co-continuous morphology can be defined as the coexistence of two or more continuous structures within the same amount, while the droplet/domain morphology means the dispersion of the minor phase (polymer phase with low concentration) on the major continuous phase (polymer phase of high concentration) (Pötschke and Paul 2003; Gergen et al. 1987).

2.2 Thermodynamics of Binary Polymer Mixing Systems

As already discussed, most polymer mixtures are thermodynamically immiscible and incompatible by nature. The miscibility of polymer mixtures can be predicted using thermodynamic relations through the Gibbs free energy of mixture (ΔG_m), i.e. miscible polymer mixtures satisfy the following equations:

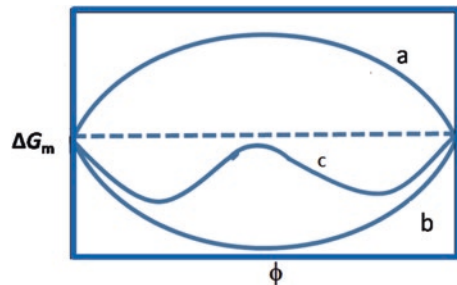
$$\Delta G_m = \Delta H_m - T\Delta S_m < 0 \quad (2.1)$$

$$\left(\frac{\partial^2 \Delta G_m}{\partial \Phi_i^2} \right)_{T,p>0} > 0 \quad (2.2)$$

where, ΔG_m is the free energy of the mixture *per* unit volume and ΔH_m and ΔS_m are enthalpy and entropy of the mixture, respectively, while Φ_i represents the volume fraction of the component, and p and T represent fixed pressure and temperature, respectively. Generally, the ΔS_m is very low due to the macromolecular size. The ΔG_m is thus more positive due to the important contribution of the positive ΔH_m . Miscible mixtures can be formed if the entropic contribution exceeds the enthalpic contribution. So, for the negative ΔG_m values, there must be excellent intermolecular interactions between the components (Paul and Barlow 1984; Robeson 2007). The general phase diagram showing the variation in ΔG_m for miscible, immiscible and partially miscible mixtures is given below in Fig. 2.1.

The mixtures of immiscible polymers do not satisfy Eqs. 2.1 and 2.2, and have positive ΔG_m values, which represents the curve 'a'. Miscible mixtures satisfy the above equations and represent as the curve 'b' in the phase diagram. The curve 'c' represents a partially miscible mixing system (Ajitha and Thomas 2020).

Fig. 2.1 Free energy of mixture for: (a) completely immiscible mixtures, (b) completely miscible mixtures and (c) partially miscible mixtures. Reproduced with permission from Ajitha and Thomas (2020)



2.3 Purpose of Compatibilization

Most polymer mixtures are thermodynamically immiscible and incompatible. Therefore, poor and inferior properties can be expected compared to individual components, and their applications are limited. The poor properties of incompatible mixtures are due to the great interfacial tension and the poor interfacial adhesion between the components. The immiscibility and incompatibility result in an unstabilized morphology, phase separation and poor interfacial adhesion between the polymer components, because of this, the mixtures show poor physical-mechanical properties. In general, the compatibilization method is used to overcome these problems and improve the applications of the mixtures. The compatibilization can be carried out using compatibilizers, which are interfacial agents that can be aligned along the interfaces between the two polymeric phases, thus reducing the interfacial tension. Thus, due to the interfacial activities of the compatibilizers, there are opportunities to improve the interfacial adhesion between the components, and therefore, to improve the compatibility between the components with the stabilized morphology. It can thus be said that compatibilizers play a fundamental role for improving the properties of immiscible and incompatible polymer mixtures by improving interfacial adhesion between polymer components.

Block, graft or random copolymers are generally used as compatibilizers for compatibilizing thermodynamically immiscible and incompatible mixtures (Bharati et al. 2017a, b). Immiscible and incompatible binary mixtures can be prepared, using a compatibilizer so that one segment is miscible or interacts with one phase of the mixture, while the other miscible segment interacts with the second phase of the mixture. As a result, compatibilizers are found in the interfaces of the mixtures and their interfacial activities result in better adhesion between the components by producing a useful product with improved properties (Bharati et al. 2017a, b).

2.4 Thermodynamic Theories

The compatibilization action of compatibilizers is similar to that of an emulsifier (Saleem and Baker 1990; Sinha Ray and Bousmina 2005; Utracki 2002; Wang et al. 2003). Noolandi and Hong (1982, 1984) studied the emulsifying effect of compatibilizers. Noolandi (1984) noted the importance of the copolymer concentration and molecular weight (Mw) in reducing the interfacial tension between the polymer components in the case of highly incompatible polymer mixtures. Leibler's theory means almost compatible systems. Leibler (1982) studied the interfacial properties of copolymer polymer mixtures and developed midfield formalism. Hong and Burns (1971) also developed the role of concentration and Mw of compatibilizers to

improve interfacial adhesion between polymer components in the polymer mixture. Hong and Burns (1971), Noolandi and Hong (1982, 1984) and Noolandi (1984) reported that as the concentration and Mw of the copolymers increases, the interfacial tension decreases. While at a particular concentration (critical micelle concentration - CMC) of copolymer produces interfacial saturation and particle size is leveled (interfacial saturation). No further changes in the interface can be observed with the addition of copolymers above CMC, but it leads to the formation of copolymer micelles in homopolymer phases.

According to Hong and Burns (1971), Noolandi and Hong (1982, 1984), Noolandi (1984), Thomas and Prud (1992) and George et al. (1995) for ternary systems of two polymers A and B with copolymer A-*b*-B (A/A-*b*-B/B), the reduction of interfacial tension can be expressed by the following equation:

$$\Delta\gamma \cong d\phi_c \left[1/2\chi + 1/Z_c - 1/Z_c \exp(Z_c\chi/2) \right] \quad (2.3)$$

where ϕ_c represents the bulk volume fraction of the copolymer, χ represents the Flory-Huggins interaction parameter between the two segments of the copolymer, d represents the width of half the height of copolymer profile and Z_c represents the degree of polymerization of the copolymer. According the above equation, the reduction or increase in particle size (ΔD) can be written as:

$$\Delta D \cong Kd\phi_c \left[1/2\chi + 1/Z_c - 1/Z_c \exp(Z_c\chi/2) \right] \quad (2.4)$$

where K is proportionality constant.

Figure 2.2 shows the mechanism of compatibilization of a copolymer A-*b*-B within an immiscible mixture, the yellow part of the copolymer has more affinity with the A polymer segment, while the blue part interacts selectively with the B polymer segment (Dal Lago et al. 2019; Ajitha and Thomas 2020).

During compatibilization, compatibilizers migrate to the interface between the components and interact with the polymer components. This action of compatibilizers helps reduce the dimensions of the dispersed phase, thus stabilizing the morphology of the mixture and improving the adhesion between the polymer components. Generally, graft, block copolymers and coupling agents are used as compatibilizers. Another important strategy for the compatibilization of immiscible mixtures involves the use of functional polymers, micro- and nanofillers and Janus nanoparticles (NPs). This chapter deals the role of functional polymers in the compatibilization of polymer mixtures.

2.5 Functional Polymers in Compatibilization

In compatibilization, the widely used functional polymers are maleic anhydride (MA) and glycidyl methacrylate (GMA). Compatibilizers of this type usually contain some polar groups in addition to the reactive functionalities. Compatibilization

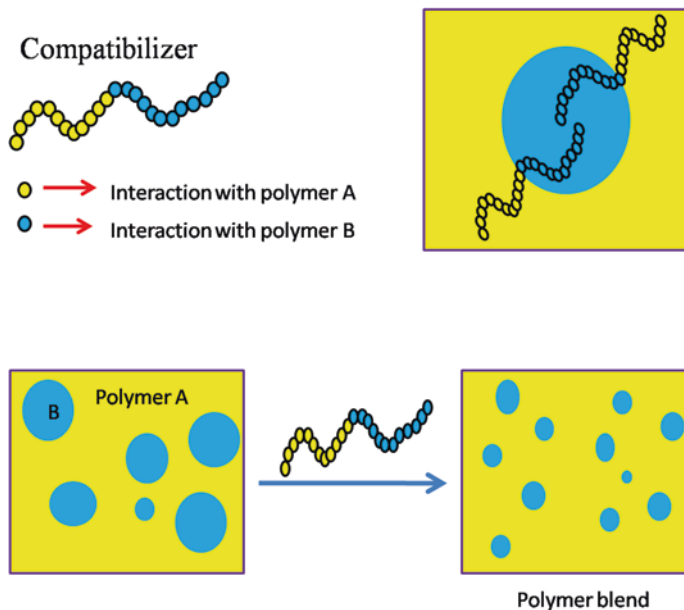
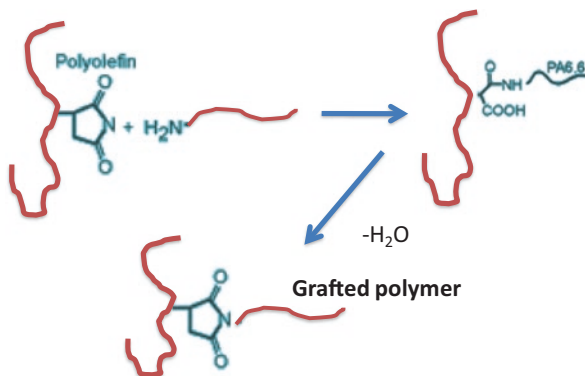


Fig. 2.2 Schematic representation of the compatibilization of a polymer mixture by block copolymers. Reproduced with permission from Ajitha and Thomas (2020)

Fig. 2.3 Schematic representation of a mixture system using compatibilizer



using functional polymers is given under *ex-situ* compatibilization conditions. Reactive rubbers are also considered compatibilizers. The compatibilized system having a reactive functional polymer as a compatibilizer can be represented in Fig. 2.3.

2.6 Characterization of Composites Involving Functional Polymers

Polymer composites and compatibilized mixtures can be characterized by several methods. Compatibilization usually introduces some kind of miscibility and interaction between the two polymers in a mixing system.

2.6.1 Structural Characterization

The compatible mixing system can be studied for the interfacial reaction by a series of techniques. Spectral studies, including nuclear magnetic resonance (NMR) and Fourier transform infrared (FTIR) spectra, are the most widely selected techniques. Special techniques including neutron reflectivity and forward recoil spectrometry (FRES), labeling of a functional polymer with a fluorescent group, etc.

Urethanes can, for example, be considered as a model compound to explain the process of reactive compatibilization. The -NHCOO and -NCO group into thermoplastic polyurethanes are reactive to most functional polymers. Urethanes react with acids, amines, anhydrides, epoxides, etc. Lu et al. (2002) used NMR spectra to control the reaction of urethanes with the functionalities mentioned above. The NMR spectra of the compatibilized systems showed a peak around 0.06 ppm, which was protected by the imide formed by the reaction between the urethane and the anhydride (Fig. 2.4).

Dal Lago et al. (2019) used FTIR spectroscopy for analyzing the changes in the PC/PET mixture system by adding a methylene diphenyl diisocyanate (MDI) compatibilizer. After extrusion using MDI, the FTIR spectra exhibited changes other than the previous ones. The vibrations around 2250 cm^{-1} and 1590 cm^{-1} due to the isocyanate and amide functionalities, both improved with the MDI content. Therefore, the effect of compatibilization for a binary mixture can be well understood by continuously monitoring the variations of reactive functionalities (Fig. 2.5).

2.6.2 Morphology

Morphology control is one of the most important properties when polymer mixtures and composites with superior properties are developed. Uncompatibilized mixtures show a clear interface and the particle size is larger (Kudva et al. 1999a). This means that the uncompatibilized mixing system follows the same structure and morphology of an immiscible system. This statement can be explained by considering a

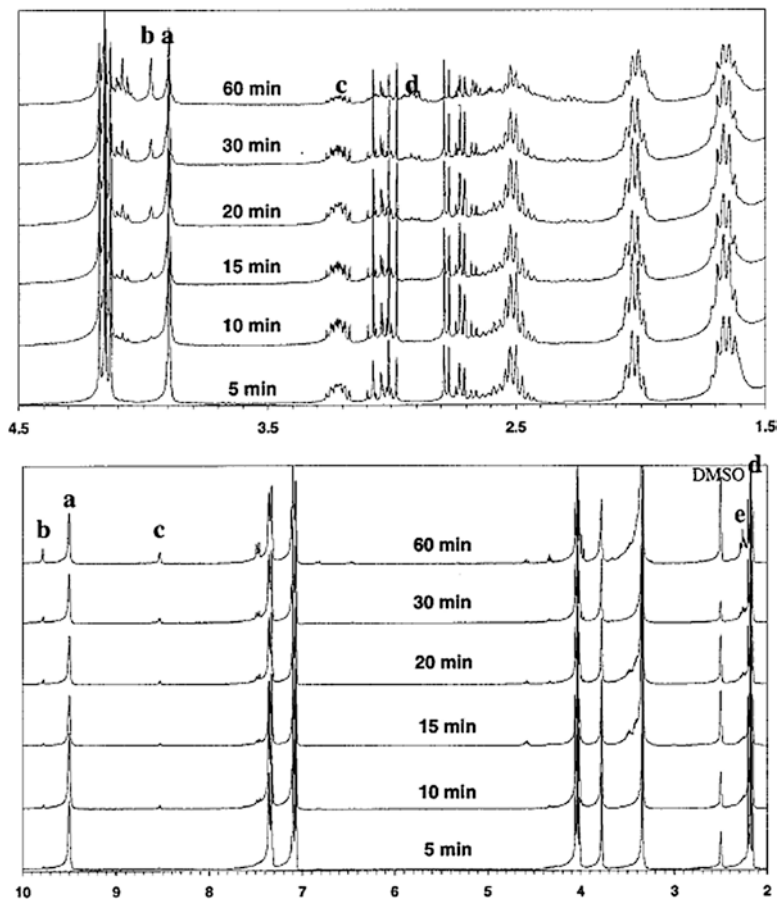


Fig. 2.4 Monitoring the reaction of urethane with a primary amine (a) and an acid (b) using ^1H NMR spectra. Reproduced with permission from Lu et al. (2002)

simple example of a binary mixing system formed from poly(amide) (PA) and PS. In this sense, Kudva et al. (1999a) showed that binary mixing systems had an average domain size of $30\ \mu\text{m}$, while the use of styrene-GMA as a compatibilizer, was shown to decrease the domain size and interfacial tension of the mixtures (Fig. 2.6). PA polymers are usually compatibilized by reactive functionalization and/or using reactive and functional polymers. In particular, the styrene-GMA pair is considered the most preferred compatibilizing agent for the immiscible polymer mixing system (Kudva et al. 1998). This compatibilizing pair has been used to compatibilizer mixtures made from PA/PS, PET/PS, PBT/PS, PBT/PPO, etc. (Hu et al. 1996; Liu et al. 1996).

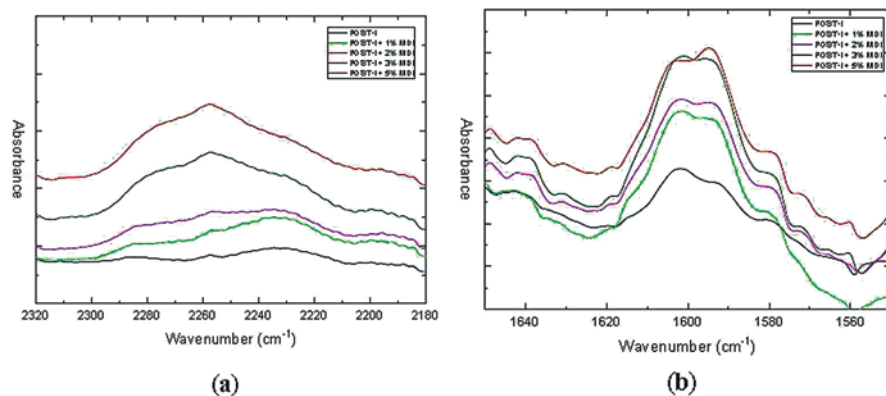


Fig. 2.5 PC/PET mixtures with and without the use of MDI as a compatibilizer. Reproduced with permission from Dal Lago et al. (2019)

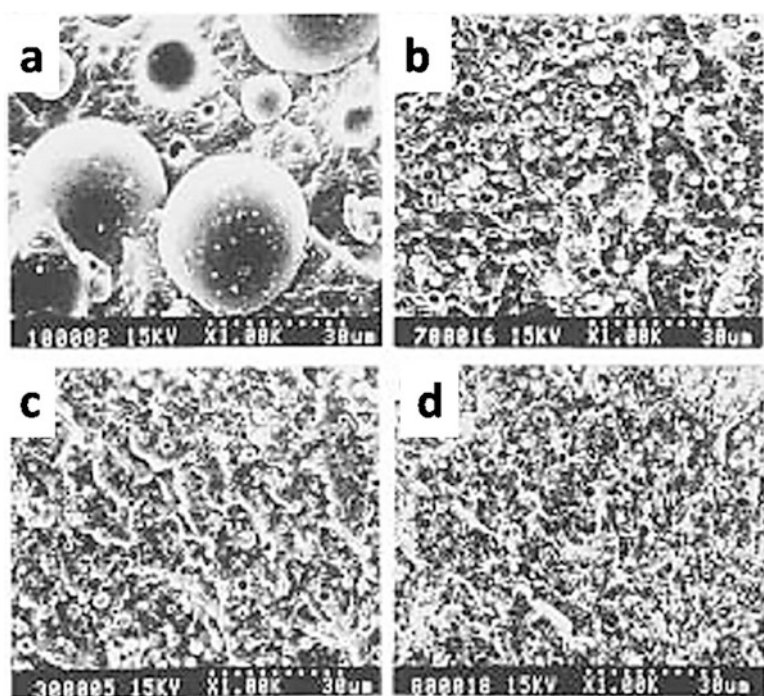
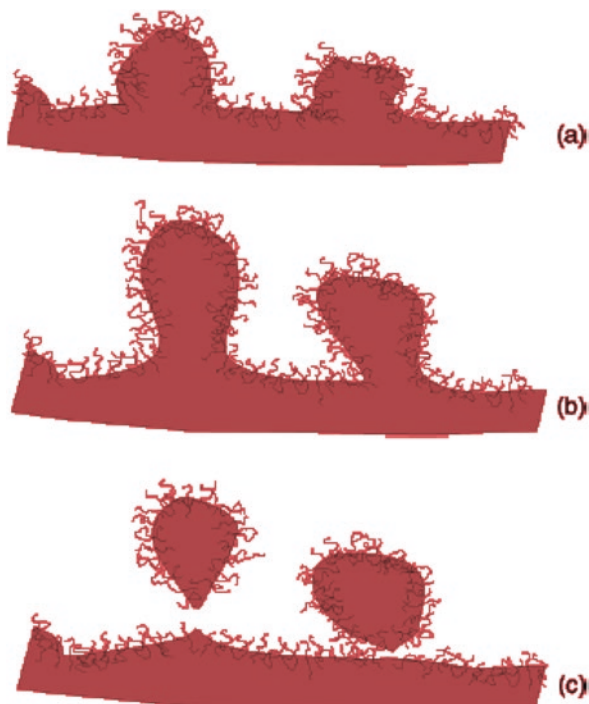


Fig. 2.6 Scanning electron microscopy (SEM) images of PA mixtures using styrene-GMA as a compatibilizer. Reproduced with permission from Kudva et al. (1999a)

Fig. 2.7 Different types of interfacial morphology developed during compatibilization using functional polymers: (a) interfacial roughness, (b) interfacial pinch-off and (c) microemulsion formation



On the other hand, the morphology change at the interface can be divided into three: (a) interfacial roughness, (b) interfacial pinch-off and (c) microemulsion formation (Fig. 2.7). For example, Larocca et al. (2005) used low Mw methyl methacrylate (MMA)/GMA/ethyl acrylate (EA) terpolymer (MGE) as a compatibilizing agent, which led to the formation of micelles and/or microemulsions in the PBT/styrene-acrylonitrile (SAN)/MGE mixture (Fig. 2.8).

Macosko et al. (2005) conducted a detailed investigation of the reactions of functional polymers at the interface. These authors explained that the interfacial reactions can be increased by selecting certain pairs for compatibilization. The common pairs for this purpose are acid/amine, acid/epoxy, acid/oxazoline, aliphatic amine/anhydride, aliphatic amine/epoxy, anhydride/aromatic amine, aromatic amine/epoxy and hydroxyl/(anhydride or acid) (Fig. 2.9) (Macosko et al. 2005).

2.7 New Challenges

The compatibility of a mixture made from naturally immiscible polymers is an important academic and technological challenge. An example of this is the compatibility of petroleum-based polymers with biobased polymers, in order to reduce the carbon footprint of the final material, while maintaining the outstanding

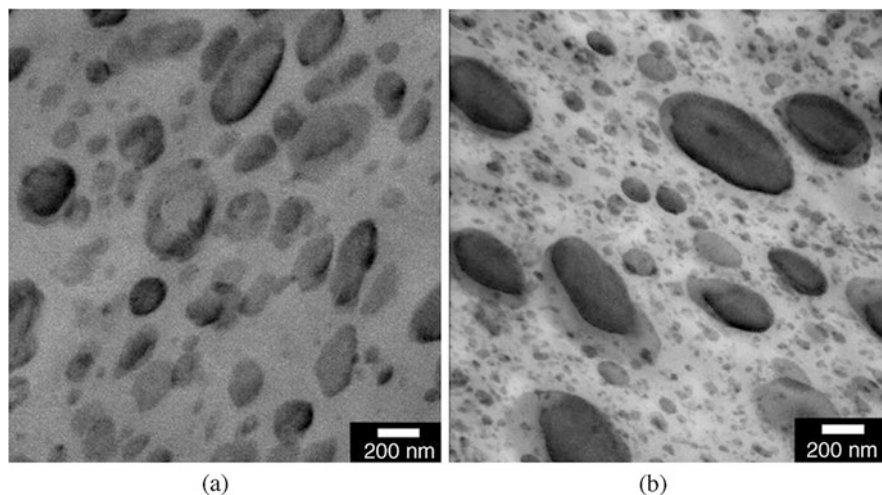


Fig. 2.8 Formation of microemions using MGE as a compatibilizing agent into the PBT/SAN mixture. Reproduced with permission from Larocca et al. (2005)

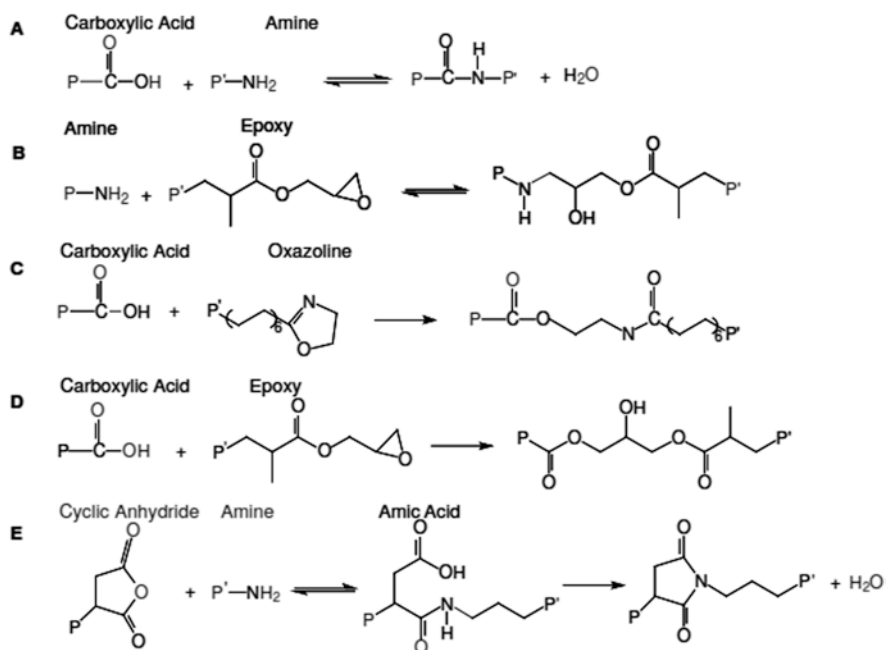


Fig. 2.9 Possible reactions between different functional groups. Reproduced with permission from Macosko et al. (2005)

thermomechanical properties of the final mixture. Another main challenge is with the recycled material, since in many cases, it is very difficult to predict the exact mixture of resins in any feed flow, and nowadays there is no ‘one-size-fits-all’ compatibilizer in the market for any mixture of materials. It is also mentioned from the literature that the optimal properties of the polymer mixtures are often based on an average dispersed-phase diameter less than several microns. Therefore, the stabilization of the dispersed-phase domain size against thickening is key to processing immiscible mixtures.

Among the compatibilization strategies tested so far, most involve a reduction in interfacial tension and/or steric hindrance against coarsening. The addition of block/graft copolymers normally leads to compatibilization, but this has not been commercialized, due in part to the very low CMC that prevents enough copolymer from reaching interface regions during melt processing. The addition of random copolymer leads to the encapsulation of the dispersed phase, and therefore, does not lead to compatibilization even in small-scale studies. There are some new approaches that can be studied to further expand the significance of compatibilizers. In one strategy, the gradient copolymers dispersed into homo polymer have much higher CMCs, and exhibit a broader interfacial coverage than block copolymers of the same composition, thus suggesting that gradient copolymers may be effective mixing compatibilizers. Other studies have been carried out with functional compatibilizers and are preferred in the compatibilization of nanomixtures (mixtures of

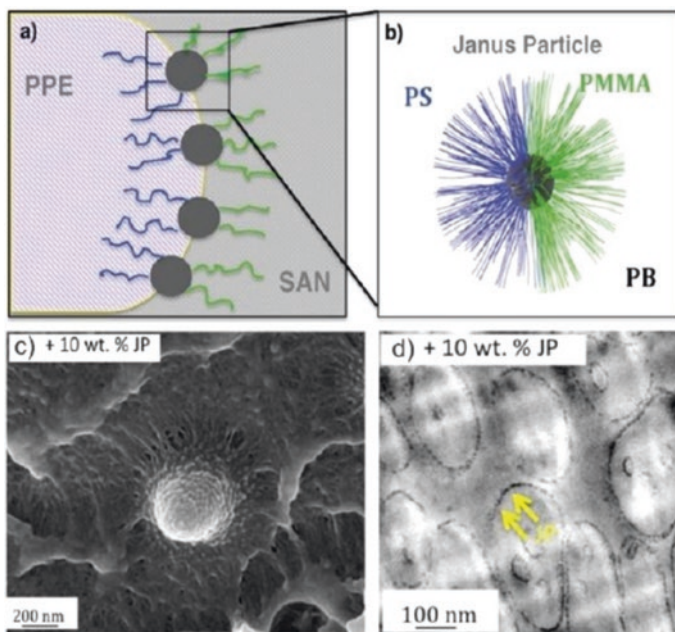


Fig. 2.10 Schematic illustration of SEM and transmission electron microscopy (TEM) images of Janus NPs at the interface. Reproduced with permission from Kirillova et al. (2019)

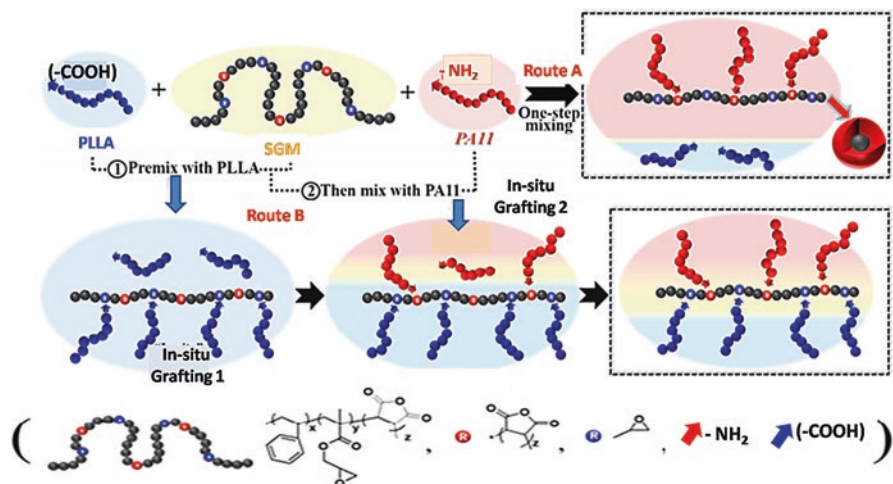


Fig. 2.11 Schematic representation of the compatibilization mechanism of PA11/PALLA. Reproduced with permission from Yang et al. (2019)

immiscible polymers in which the dispersed phase has particles with a size of 100 nm or less). In order to obtain nanostructured polymeric system, an attractive method is the inclusion of Janus NPs (J NPs), in which the surface is composed of hydrophilic groups and hydrophobic groups, resulting in asymmetric NPs able to act as surfactants in immiscible mixtures (Fig. 2.10) (Kirillova et al. 2019).

‘Dual-reactive compatibilization’ is another recent development in this area. This strategy uses a compatibilizer containing bi-functional groups. It has been shown that a compatibilizer containing two types of reactive groups shows greater compatibilization efficiency compared to the traditional compatibilizer with only one type of reactive groups. With this in mind, Yang et al. (2019) reported a series of poly(styrene-*co*-GMA-*co*-MA) ternary copolymers (SGM) containing both reactive epoxide groups and MA groups were synthesized and then incorporated into the immiscible poly(amide 11)/poly(L-lactic acid) (PA11/PLLA) mixture (Fig. 2.11) (Yang et al. 2019).

Another strategy in the reactive compatibilization is the use of thermo-oxidative synergistic maleation of the polymer. The synergistic action of maleation coupled with thermo-oxidation of the polymer backbone allows both improvements in hydrophilic/hydrophobic balance and availability of functional groups that can react during the reactive extrusion. Keeping this in view, Jubinville et al. (2019) investigated the maleation process of PA11, resulting in a multifunctional compatibilizer due to partial thermo-oxidation. The incorporation of PA11C into PA6/PBT mixtures promoted grafting reaction and resulted in better compatibilized mixtures (Jubinville et al. 2019).

2.8 Conclusion

Compatibility is a term related to the miscibility of the polymer. Several methods and theories have been developed to achieve the compatibilization process, which depend on the thermodynamics of polymer mixtures. The compatibilization process is generally performed to improve the interfacial adhesion between the immiscible polymers. Polymers or fillers having reactive functionalities are preferred for this purpose. Functional polymers are an important part in compatibilization, followed by *ex-situ* mechanisms. The addition of functional polymers leads to a chemical reaction which improves miscibility and properties. The reactions can be controlled using spectroscopic techniques in which one can have a detailed analysis of the scope of the compatibilization process by analyzing the variation of the functional groups. The change in morphology at the interface is generally controlled by microscopic techniques. This chapter covered the theories and techniques mentioned above in detail and examined the latest trends or strategies in the compatibilization process. The use of block copolymers, Janus particles and the development of nanostructures are recent trends in compatibilization.

Acknowledgments The authors declare no acknowledgments.

Conflicts of Interest The authors declare no conflict of interest.

References

- Ajitha, A. R., & Thomas, S. (2020). Chapter 1 Introduction: Polymer blends, thermodynamics, miscibility, phase separation, and compatibilization. In A. R. Ajitha & S. Thomas (Eds.), *Compatibilization of Polymer Blends: Micro and nano scale phase morphologies, inter-phase characterization and properties* (pp. 1–29). Pp: Elsevier. <https://doi.org/10.1016/b978-0-12-816006-0.00001-3>.
- Arif, P. M., Sarathchandran, C., Narayanan, A., Saiter, A., Terzano, R., Allegretta, I., Porfido, C., Kalarikkal, N., & Thomas, S. (2017). Multiwalled carbon nanotube promotes crystallisation while preserving co-continuous phase morphology of polycarbonate/polypropylene blend. *Polymer Testing*, *64*, 1–11. <https://doi.org/10.1016/j.polymertesting.2017.09.026>.
- Bahrami, R., Löbbling, T. I., Schmalz, H., Müller, A. H., & Altstädt, V. (2015). Micromechanics of “raspberry” morphology in PPE/SAN polymer blends compatibilized with linear ABC triblock terpolymers. *Polymer*, *80*, 52–63. <https://doi.org/10.1016/j.polymer.2015.10.039>.
- Bharati, A., Wübhenhorst, M., Moldenaers, P., & Cardinaels, R. (2017a). Dielectric properties of phase-separated blends containing a microcapacitor network of carbon nanotubes: Compatibilization by a random or block copolymer. *Macromolecules*, *50*(10), 3855–3867. <https://doi.org/10.1021/acs.macromol.6b02786>.
- Bharati, A., Cardinaels, R., Van der Donck, T., Seo, J. W., Wübhenhorst, M., & Moldenaers, P. (2017b). Tuning the phase separated morphology and resulting electrical conductivity of carbon nanotube filled PαMSAN/PMMA blends by compatibilization with a random or block copolymer. *Polymer*, *108*, 483–492. <https://doi.org/10.1016/j.polymer.2016.12.015>.

- Brown, S. B. (2003). Reactive compatibilization of polymer blends. In L. A. Utracki (Ed.), *Polymer blends handbook* (pp. 339–415). Dordrecht: Springer. https://doi.org/10.1007/0-306-48244-4_5.
- Chiu, F.-C. (2017). Poly (vinylidene fluoride)/polycarbonate blend-based nanocomposites with enhanced rigidity-Selective localization of carbon nanofillers and organoclay. *Polymer Testing*, 62, 115–123. <https://doi.org/10.1016/j.polymertesting.2017.06.018>.
- Dal Lago, E., Boaretti, C., Piovesan, F., Roso, M., Lorenzetti, A., & Modesti, M. (2019). The effect of different compatibilizers on the properties of a post-Industrial PC/PET blend. *Materials*, 12(1), 49. <https://doi.org/10.3390/ma12010049>.
- George, S., Joseph, R., Thomas, S., & Varughese, K. T. (1995). Blends of isotactic polypropylene and nitrile rubber: morphology, mechanical properties and compatibilization. *Polymer*, 36(23), 4405–4416. [https://doi.org/10.1016/0032-3861\(95\)96846-z](https://doi.org/10.1016/0032-3861(95)96846-z).
- Gergen, W. P., Lutz, R. G., & Davison, S. (1987). Hydrogenated block copolymers in thermoplastic elastomer IPNs. In C. H. Verlag (Ed.), *Thermoplastic elastomers: A comprehensive review* (pp. 507–540).
- Hong, S. D., & Burns, C. M. (1971). Compatibility of polystyrene and poly(methyl methacrylate) in benzene. Effects of molecular weight and temperature. *Journal of Applied Polymer Science*, 15(8), 1995–2006. <https://doi.org/10.1002/app.1971.070150817>.
- Hu, G.-H., Sun, Y.-J., & Lambla, M. (1996). Devolatilization: A critical sequential operation for *in situ* compatibilization of immiscible polymer blends by one-step reactive extrusion. *Polymer Engineering & Science*, 36(5), 676–684. <https://doi.org/10.1002/pen.10455>.
- Jubinville, D., Chang, B. P., Pin, J. M., Mohanty, A. K., & Misra, M. (2019). Synergistic thermo-oxidative maleation of PA11 as compatibilization strategy for PA6 and PBT blend. *Polymer*, 121594. <https://doi.org/10.1016/j.polymer.2019.121594>.
- Kirillova, A., Marschelke, C., & Synytska, A. (2019). Hybrid Janus particles: Challenges and opportunities for the design of active functional interfaces and surfaces. *ACS Applied Materials & Interfaces*, 11(10), 9643–9671. <https://doi.org/10.1021/acsami.8b17709>.
- Kudva, R. A., Keskkula, H., & Paul, D. R. (1998). Compatibilization of nylon 6/ABS blends using glycidyl methacrylate/methyl methacrylate copolymers. *Polymer*, 39(12), 2447–2460. [https://doi.org/10.1016/s0032-3861\(97\)00583-1](https://doi.org/10.1016/s0032-3861(97)00583-1).
- Kudva, R. A., Keskkula, H., & Paul, D. R. (1999a). Morphology and mechanical properties of compatibilized nylon 6/polyethylene blends. *Polymer*, 40(22), 6003–6021. [https://doi.org/10.1016/S0032-3861\(98\)00829-5](https://doi.org/10.1016/S0032-3861(98)00829-5).
- Larocca, N. M., Hage, E., Jr., & Pessan, L. A. (2005). Effect of reactive compatibilization on the properties of poly(butylene terephthalate)/acrylonitrile-ethylene-propylene-diene-styrene blends. *Journal of Polymer Science Part B: Polymer Physics*, 43(10), 1244–1259. <https://doi.org/10.1002/polb.20416>.
- Leibler, L. (1982). Theory of phase equilibria in mixtures of copolymers and homopolymers. 2. Interfaces near the consolute point. *Macromolecules*, 15(5), 1283–1290. <https://doi.org/10.1021/ma00233a014>.
- Liu, W.-B., Kuo, W.-F., Chiang, C.-J., & Chang, F.-C. (1996). *In situ* compatibilization of PBT/PPPO blends. *European Polymer Journal*, 32(1), 91–99. [https://doi.org/10.1016/0014-3057\(95\)00115-8](https://doi.org/10.1016/0014-3057(95)00115-8).
- Lu, X., & Weiss, R. A. (1992). Relationship between the glass transition temperature and the interaction parameter of miscible binary polymer blends. *Macromolecules*, 25(12), 3242–3246. <https://doi.org/10.1021/ma00038a033>.
- Lu, Q. W., Hoye, T. R., & Macosko, C. W. (2002). Reactivity of common functional groups with urethanes: models for reactive compatibilization of thermoplastic polyurethane blends. *Journal of Polymer Science Part A: Polymer Chemistry*, 40(14), 2310–2328. <https://doi.org/10.1002/pola.10310>.
- Macosko, C. W., Jeon, H. K., & Hoye, T. R. (2005). Reactions at polymer-polymer interfaces for blend compatibilization. *Progress in Polymer Science*, 30(8–9), 939–947. <https://doi.org/10.1016/j.progpolymsci.2005.06.003>.

- Mathew, L., Saha, P., Kalarikkal, N., Thomas, S., & Strankowski, M. (2018). Tuning of microstructure in engineered poly(trimethylene terephthalate) based blends with nano inclusion as multifunctional additive. *Polymer Testing*, 68, 395–404. <https://doi.org/10.1016/j.polymertesting.2018.03.052>.
- Noolandi, J. (1984). Recent advances in the theory of polymeric alloys. *Polymer Engineering & Science*, 24(2), 70–78. <https://doi.org/10.1002/pen.760240203>.
- Noolandi, J., & Hong, K. M. (1982). Interfacial properties of immiscible homopolymer blends in the presence of block copolymers. *Macromolecules*, 15(2), 482–492. <https://doi.org/10.1021/ma00230a054>.
- Noolandi, J., & Hong, K. M. (1984). Effect of block copolymers at a demixed homopolymer interface. *Macromolecules*, 17(8), 1531–1537. <https://doi.org/10.1021/ma00138a019>.
- Otero-Navas, I., Arjmand, M., & Sundararaj, U. (2017). Carbon nanotube induced double percolation in polymer blends: Morphology, rheology and broadband dielectric properties. *Polymer*, 114, 122–134. <https://doi.org/10.1016/j.polymer.2017.02.082>.
- Paul, D. R., & Barlow, J. W. (1984). A binary interaction model for miscibility of copolymers in blends. *Polymer*, 25(4), 487–494. [https://doi.org/10.1016/0032-3861\(84\)90207-6](https://doi.org/10.1016/0032-3861(84)90207-6).
- Paul, D. R., & Newman, S. (1978). Polymer blends. *Academic Press. Pag.*, 501. <https://doi.org/10.1016/c2012-0-01621-3>.
- Pötschke, P., & Paul, D. R. (2003). Formation of co-continuous structures in melt-mixed immiscible polymer blends. *Journal of Macromolecular Science, Part C: Polymer Reviews*, 43(1), 87–141. <https://doi.org/10.1081/mc-120018022>.
- Robeson, L. M. (2007). Polymer blends. A Comprehensive review. Available in: http://files.hanser.de/files/article/artk_lpr_9783446225695_0001.pdf.
- Roman, C., García-Morales, M., Gupta, J., & McNally, T. (2017). On the phase affinity of multi-walled carbon nanotubes in PMMA: LDPE immiscible polymer blends. *Polymer*, 118, 1–11. <https://doi.org/10.1016/j.polymer.2017.04.050>.
- Saleem, M., & Baker, W. E. (1990). *In situ* reactive compatibilization in polymer blends: effects of functional group concentrations. *Journal of applied polymer science*, 39(3), 655–678. <https://doi.org/10.1002/app.1990.070390316>.
- Sinha Ray, S., & Bousmina, M. (2005). Compatibilization efficiency of organoclay in an immiscible polycarbonate/poly(methyl methacrylate) blend. *Macromolecular rapid communications*, 26(6), 450–455. <https://doi.org/10.1002/marc.200400586>.
- Thomas, S., Grohens, Y., & Jyotishkumar, P. (Eds.). (2014). Characterization of polymer blends: Miscibility, morphology and interfaces. John Wiley & Sons. <https://doi.org/10.1002/9783527645602>
- Thomas, S., & Prud, R. E. (1992). Compatibilizing effect of block copolymers in heterogeneous polystyrene/poly(methyl methacrylate) blends. *Polymer*, 33(20), 4260–4268. [https://doi.org/10.1016/0032-3861\(92\)90266-y](https://doi.org/10.1016/0032-3861(92)90266-y).
- Tjong, S. C., & Meng, Y. Z. (2000). Effect of reactive compatibilizers on the mechanical properties of polycarbonate/poly (acrylonitrile-butadiene-styrene) blends. *European Polymer Journal*, 36(1), 123–129. [https://doi.org/10.1016/s0014-3057\(99\)00044-0](https://doi.org/10.1016/s0014-3057(99)00044-0).
- Utracki, L. A. (1982). Economics of polymer blends. *Polymer Engineering & Science*, 22(17), 1166–1175. <https://doi.org/10.1002/pen.760221717>.
- Utracki, L. A. (2002). Compatibilization of polymer blends. *The Canadian journal of Chemical Engineering*, 80(6), 1008–1016. <https://doi.org/10.1002/cjce.5450800601>.
- Wang, Y., Zhang, Q., & Fu, Q. (2003). Compatibilization of immiscible poly(propylene)/polystyrene blends using clay. *Macromolecular Rapid Communications*, 24(3), 231–235. <https://doi.org/10.1002/marc.200390026>.
- Wang, H., Fu, Z., Zhao, X., Li, Y., & Li, J. (2017). Reactive nanoparticles compatibilized immiscible polymer blends: synthesis of reactive SiO₂ with long poly (methyl methacrylate) chains

- and the in situ formation of janus SiO₂ nanoparticles anchored exclusively at the interface. *ACS Applied Materials & Interfaces*, 9(16), 14358–14370. <https://doi.org/10.1021/acsami.7b01728>.
- Yang, X., Wang, H., Chen, J., Fu, Z., Zhao, X., & Li, Y. (2019). Copolymers containing two types of reactive groups: New compatibilizer for immiscible PLLA/PA11 polymer blends. *Polymer*, 177, 139–148. <https://doi.org/10.1016/j.polymer.2019.05.074>.
- Zarrintaj, P., Jouyandeh, M., Ganjali, M. R., Hadavand, B. S., Mozafari, M., Sheiko, S. S., Vatankhah-Varnoosfaderani, M., Gutiérrez, T. J., & Saeb, M. R. (2019). Thermo-sensitive polymers in medicine: A review. *European Polymer Journal*, 117, 402–423. <https://doi.org/10.1016/j.eurpolymj.2019.05.024>.

Chapter 3

Compatibilization and Crosslinking in Biodegradable Thermoplastic Polyester Blends



M. Z. Ahmad Thirmizir, Z. A. Mohd Ishak, and M. S. Salim

Abstract Biodegradable polymers, especially bacterial synthesized polymers, have gained great attention and interest due to the concerns raised regarding the accumulation of petrochemical plastic wastes in the environment. It is known that biodegradable polymers have advantages such as being biocompatible, biodegradable, natural, renewable and have similar mechanical properties compared to conventional polymers. Poly(hydroxybutyrate) (PHBs) are biodegradable polyesters produced naturally by bacteria. PHBs are highly crystalline polyester, which are brittle and prone to thermal degradation during processing. In the past, attempts have been made to reduce the degree of the brittleness of the PHB by copolymerization with hydroxyhexanoate (HHx) or hydroxyvalerate (HVx) co-monomers. Among PHB copolymers: poly(3-hydroxybutyrate-*co*-3-hydroxyhexanoate) (PHB-*co*-HHx), poly(3-hydroxybutyrate-*co*-3-hydroxyvalerate) (PHBV) and poly(3-hydroxybutyrate-*co*-4-hydroxybutyrate) (P(3HB-*co*-4HB)) have improved the flexibility and mechanical properties more than other PHBs. This chapter aims to emphasize the potential on the compatibilization of biodegradable polymer blends with the presence of maleated compatibilizers derived from the host or guest polymers.

Keywords Biodegradability · Compatibilizer · Functionalization · Peroxide

M. Z. A. Thirmizir · Z. A. M. Ishak (✉)
Cluster for Polymer Composites, Science and Engineering Research Centre (SERC),
Universiti Sains Malaysia, Nibong Tebal, Pulau Pinang, Malaysia

School of Materials and Mineral Resources Engineering, Universiti Sains Malaysia,
Nibong Tebal, Pulau Pinang, Malaysia
e-mail: zarifin@usm.my

M. S. Salim
School of Materials and Mineral Resources Engineering, Universiti Sains Malaysia,
Nibong Tebal, Pulau Pinang, Malaysia

Abbreviations

3HH	3-hydroxyhexanoate
AAc	Acrylic acid
ABS	Acrylonitrile butadiene styrene
AIBN	2,2-azobis(isobutyronitrile)
ATP	Aliphatic thermoplastic polyester
BPO	Benzoyl peroxide
BTBV	<i>n</i> -butyl 4,4-di-(<i>t</i> -butyl peroxy) valerate
CTC	Charge transfer complex
DBP	di- <i>t</i> -butyl peroxide
DCP	Dicumyl peroxide
DG	Degree of grafting
DMA	Dynamic mechanical analysis
DMTA	Dynamic mechanical thermal analysis
DSC	Differential scanning calorimetry
ENR	Epoxidized natural rubber
EPDM	Ethylene propylene diene monomer
EVA	Ethylene vinyl acetate
FTIR	Fourier transform infrared
G'	Storage module
GMA	Glycidyl methacrylate
HA	Hyaluronan
HDPE	High-density polyethylene
HEMA	2-hydroxyethyl methacrylate
HHx	Hydroxyhexanoate
HVx	Hydroxyvalerate
LLDPE	Linear low-density polyethylene
LPO	Dilauroyl peroxide
MA	Maleic anhydride
MAPP	MA-grafted PP
MMA	Methyl methacrylate
Mw	Molecular weight
η^*	Complex viscosity
NBR	Butadiene-acrylonitrile rubber
NMR	Nuclear magnetic resonance
P(3HB)	Poly(3-hydroxybutyrate)
P(3HB- <i>co</i> -4HB)	Poly(3-hydroxybutyrate- <i>co</i> -4-hydroxybutyrate)
PBAT	Poly(butylene adipate- <i>co</i> -terephthalate)
PBES	Poly(butylenesuccinate- <i>co</i> -ethylene succinate)
PBS	Poly(butylene succinate)
PBSA	Poly(butylene succinate- <i>co</i> -adipate)
PBSL	Poly(butylene succinate- <i>co</i> -L-lactate)
PC	Poly(carbonate)
PCL	Poly(ϵ -caprolactone)

PDLLA	Poly(D,L-lactic acid)
PE	Poly(ethylene)
PEG	Poly(ethylene glycol)
PEO	Poly(ethylene oxide)
PES	Poly(ethylene succinate)
PET	Poly(ethylene terephthalate)
PGLA	Poly(glycolic acid- <i>co</i> -lactic acid)
PHB	Poly(hydroxybutyrate)
PHB- <i>co</i> -HHx	Poly(3-hydroxybutyrate- <i>co</i> -3-hydroxyhexanoate)
PHBHH	PHB- <i>co</i> -HHx
PHBV	Poly(3-hydroxybutyrate- <i>co</i> -3-hydroxyvalerate)
PLA	Poly(lactic acid)
PLA•	PLA macroradicals
PLLA	Poly(L-lactic acid)
PP	Poly(propylene)
PPO	Poly(phenylene oxide)
PVA	Poly(vinyl alcohol)
PVC	Poly(vinyl chloride)
REx	Reactive extrusion
RO•	Primary radicals
SEBS	Styrene-ethylene-butylene-styrene
St	Styrene
St•	Styryl macroradicals
T	Toughness
TBEC	OO-(<i>t</i> -butyl) O-(2-ethylhexyl) peroxy carbonate
TBEH	<i>t</i> -butyl peroxy-2-ethylhexanoate
TBPB	<i>t</i> -butyl peroxy benzoate
TBTH	<i>t</i> -butyl peroxy-3,5,5-trimethylhexanoate
T _g	Glass transition temperature
THF	Tetrahydrofuran
T _m	Melting temperature
TPS	Thermoplastic starch
UHMEPE	Ultra-high Mw polyethylene
UV	Ultraviolet
ε _b	Strain at break
σ	Tensile strength

3.1 Introduction

Biodegradable polymers, especially bacterial synthesized polymers, have gained significant attention in recent years, given the growing concerns regarding the accumulation of petrochemical plastics wastes in the environment (Zhang et al. 2012). It is well known that biodegradable polymers have advantages such as biocompatible,

biodegradable, natural, renewable, and having comparable mechanical properties compared to conventional polymers. Among the biodegradable polymers, biodegradable polyesters show an important role as biodegradable plastics due to their potentially hydrolysable ester bonds (Environment Australia 2012). As shown in Fig. 3.1, the biodegradable polyester family is divided into two main groups: aromatic (aromatic rings) and aliphatic (linear) polyesters.

The group of aliphatic thermoplastic polyester (ATP) is the most widely studied given its important diversity, synthetic versatility, variety of monomers and various routes ready for the polyester development (Vroman and Tighertz 2009). During the last decades, several types of ATP, such as poly(butylene succinate) (PBS), poly(lactic acid) (PLA), poly(hydroxybutyrate) (PHB) and its co-polyesters such as poly(hydroxybutyrate-*co*-hydroxyhexanoate) (PHB-*co*-HHx) and poly(3-hydroxybutyrate-*co*-3-hydroxyvalerate) (PHBV) have been studied in terms of single polymer, blends and their composite applications. However, some disadvantages of biodegradable polymers include brittleness and their susceptibility to thermal degradation during processing (Chen and Luo 2009), low toughness (T) and melt viscosity in PLA (Pradeep et al. 2017; Zhang et al. 2017), and low glass transition temperature ($T_g = -62\text{ }^\circ\text{C}$) and melting temperature ($T_m = 57\text{ }^\circ\text{C}$) in poly(ϵ -caprolactone) (PCL) (Abdul et al. 2013) have limited the processing and application of these polymers. The relatively high production cost of these polymers compared to conventional polymers is also an additional problem. However, to overcome these drawbacks, various strategies such as blending, compositing and copolymerization, are normally used. Among them, blending is the most preferred approach, since it is relatively easy to be carried out with lower costs compared to the copolymerization approach (Si et al. 2016). In addition, most commercially available plastic materials are polymer blends which have been used successfully for numerous applications.

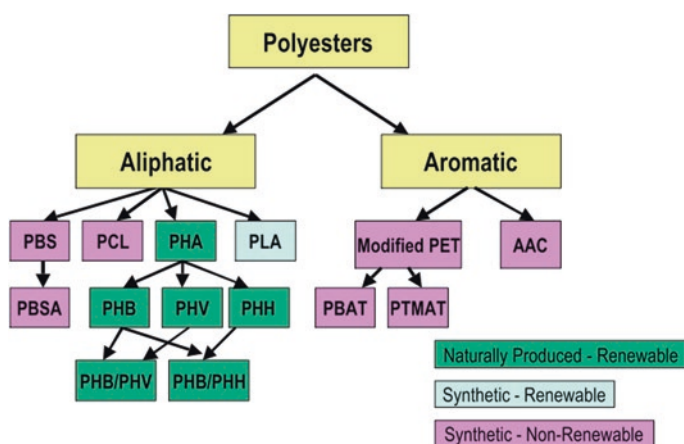


Fig. 3.1 Biodegradable polyester family. Reproduced with permission from Environment Australia (2012)

The blending of biodegradable polymer with other biodegradable polymers is favored due to the biodegradability of the blends which could be maintained, while improving the properties of the host polymer. According to Si et al. (2016), a number of studies on the blending of PLA with flexible biodegradable polyesters, such as PBS, PCL, poly(butylene succinate-*co*-L-lactate) (PBSL), poly(butylene-succinate-*co*-ethylene succinate) (PBES) and poly(ethylene succinate) (PES), have been published previously.

The key success of polymer blends is due to their good compatibility and miscibility between the components of the blend. The production of blends with an ideal physical-mechanical performance depends on the interfacial tension between the blends and the size of the dispersed phase droplets. Apart from that, a cohesive interfacial adhesion is also essential to allow the effective stress transfer from the continuous to the dispersed phase (Mani et al. 1999). This ideal condition could be achieved by adopting the compatibilization approach through the introduction of compatibilizer or by adding block or graft copolymers. The production of compatibilizer is relatively easier than the copolymerization process and also has a similar effect on improving the chemical and physical interactions, and phase dispersion between the blend's components. The compatibilizers can be derived by reacting with the host or *via* grafted polymers with suitable unsaturated polar molecule functional groups such as amines, anhydrides, epoxides, etc. (Pracella et al. 2010).

To the best of our knowledge, very limited compatibilizers commercially available specifically for biodegradable polymers have been produced. In previous studies, many attempts have been made to develop compatibilizer for biodegradable plastics, especially aliphatic thermoplastic polyesters such as glycidyl methacrylate (GMA)- or maleic anhydride (MA)-grafted compatibilizers (Tansiri and Potiyaraj 2015). According to Gardella et al. (2014), moieties such as acrylic acid (AAc), GMA, MA and oxazoline, are suitable to be grafted onto non-reactive polymers. MA is generally preferred, since it is relatively easy to handle, has low toxicity, and is not likely to be homopolymerized under standard free-radical melt-grafting conditions. In addition, the compatibilizer is expected to have a good miscibility when the components are combined, thus promoting chemical interactions with another, which improves the interfacial adhesion between them (Gardella et al. 2014).

3.2 Maleated Compatibilizer of Biodegradable Polymers

In the last year, the development of biodegradable polymers as an alternative to petroleum-based polymers has motivated researchers to develop MA-based compatibilizer in order to make the polymer more developed for industrial processing and applications. Compatibility by grafting with MA on several conventional polymers such as ethylene vinyl acetate (EVA-*g*-MA), linear low-density polyethylene (LLDPE-*g*-MA), polypropylene (PP-*g*-MA) and styrene-ethylene-butylene-styrene block copolymer (SEBS-*g*-MA) have been well established, and mainly investigated by previous researchers (Papadopoulou and Kalfoglou 2000).

Normally, a maleated compatibilizer is an additive used to improve interfacial adhesion or interaction between two or more blends and/or composite components. In polymer blend applications, the maleated compatibilizers are added to produce blends with good overall physical-mechanical behavior and can regulate interfacial tension to generate a smaller dispersed phase size and stronger interfacial adhesion, thus allowing the effective stress transfer between the phases of the blends (Mani et al. 1999). The compatibility of the blends is essential since most polymers are commonly immiscible and have little interfacial adhesion. Furthermore, it is known that the miscibility between polymers is determined by a balance of enthalpic and entropic contributions to the free energy of mixing (Fink 2013).

Notwithstanding, the quantity and the effectiveness of the compatibilizer in combination with the ratio of the components has a significant effect on the mechanical, morphological and thermal properties of the blends. According to Markham (1990), other factors may also affect the final properties of the blends such as the cooling rate, the mixing time, the rate of cooling, the shear rate and the temperature during the molding process. The compatibilizers can may also preserve or/and stabilize the morphology of the blends such as agglomeration, delamination, ‘skinning’ and other unwanted phase effects resulting from the blending process (Markham 1990).

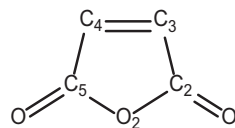
3.2.1 Preparation of Maleated Compatibilizer

As is already known, the miscibility between the components of a blend is determined by a balance of enthalpic and entropic of thermodynamic contributions to the free energy of mixing (Fink 2013). However, in reality, thermodynamically compatible blends are difficult to achieve, and in industrial practice, technological compatibility is more than adequate. In addition, technological compatibility can be achieved through chemical or mechanical approaches. As suggested by Fink (2013), technological compatibility of immiscible polymers blends can be achieved by incorporating a compatibilizer in advance or during the blending process.

3.2.1.1 MA Reactive Monomer

MA (furan-2,5-dione) is a well-known monomer for the development of compatibilizer and is commonly used for the modification of polyolefin (Mehrabzadeh 2009; Gao et al. 2012; Paolo et al. 2018). According to Musa (2016), the basic chemical structure of MA is fundamentally versatile where it has a five-member heterocyclic ring, comprising a double bond at the C3-C4 position and two carbonyl groups; one at the C2 position and the other at the C5 position, as shown in Fig. 3.2.

The C=C of MA is a powerful electron-accepting monomer due to the electron-deficient character of the double bond. The electronic deficiency originates from strong electron-withdrawing forces from the two C=O substituent groups (Musa 2016). Aside from that, the carboxylic acid groups are also known for their high

Fig. 3.2 Structure of the MA unit**Table 3.1** Physical properties of MA

Properties	MA
CAS number	108-31-6
EINECS number	203-571-6
Molecular formula	C ₄ H ₂ O ₃
Molecular weight (Mw) (g/mol)	98.06
Physical state	Solid
Color	Colorless to white
Odor	Irritation, choking
Density (g/cm ³)	1.48
Melting point (°C)	53.58
Boiling point (°C)	200
Vapor pressure (kPa)	0.033
Refractive index [<i>d</i> ₂₀ ²⁰ (solid)]	NA
Heat of formation (kJ/mol)	-470.4
Heat of fusion (kJ/mol)	12.26
Heat of sublimation (kJ/mol)	71.5 ± 5.0
Heat of combustion (kJ/mol)	-1391.2
Specific heat (liquid) (kJ/mol K)	-1.67
Heat of evaporation (kJ/mol)	54.8
Solubility in water	~400 g/L at 20 °C
pKa	NA
Biodegradation	Readily biodegradable

Source: Musa (2016)

reactivity coupled to two different acid dissociation constants (Musa 2016). The physical properties for MA chemical compounds are summarized in Table 3.1.

In addition, with respect to the economic point of view, MA is an attractive chemical compound, since it can be easily derived from butane gas and benzene that are readily available in world petroleum resources (Musa 2016).

3.2.1.2 Type of Grafting Reaction

Maleated compatibilizer can be produced by a grafting reaction of the polymer with MA functional groups in the presence of a peroxide radical initiator. As reported by Mani et al. (1999), many methods for producing compatibilizer through grafting reaction such as melt, solid-state, solution, solvents redox and suspension grafting in aqueous or organic solvents have been reported by previous studies. Table 3.2

Table 3.2 Advantages, disadvantages and application of free radical grafting

Technology	Advantages	Disadvantages	Main applications
Melt phase	Simple technology. No limit regarding melting point of backbone polymer.	Limited grafting level by short reaction time.	Grafted polyolefins; low Mw SEBS.
Solid state	High grafting possible. Grafting of PP without β -scission possible. Grafting of high Mw SEBS possible. Grafting of various monomers possible.	Grafting only on partially crystalline polymers or very high Mw polymers.	Grafted polyolefins; high Mw SEBS.
Solution	Very homogeneous grafting. High grafting levels. No degradation.	High production cost. Waste solvent.	Grafted polyolefins (gel-free).
Suspension/emulsion	Use of sticky polymers possible. High grafting levels.	High production cost.	Grafting of fibers. High grafting of acrylates onto crosslinked polyolefins.

Source: Raphel et al. (2018)

summarizes the advantages, disadvantages and applications of free radical grafting technologies.

The solid-state grafting, also known as mechanochemical grafting, is where the polymer is generally used as a powder and mixed with MA with a high concentration of initiator in the presence of an interfacial wetting agent, e.g. solvent of the polymer. The reaction is carried out in a low-shear mixer or stainless-steel reactor at a temperature ranging from 100–150 °C. Since the grafting reaction does not imply high temperature, degradation of the host polymer is very minimal. However, the homogeneity of the grafted product depends on the solvents used in the particle size of polymer powder and/or other co-monomer that are required to increase the degree of grafting (DG) of the polymer (Qiu and Hirotsu 2005). Solvents or water can further purify the maleated compatibilizer. Nonetheless, this technique only introduces the grafting reaction on the surface of the polymer powders, and the MA could not react with the polymer chain inside the powder particles (Ahmad Thirmizir 2011).

According to Qiu and Hirotsu (2005), the solution grafting process involves the dissolution of polymer in a suitable solvent at an elevated temperature followed by the addition of MA together with a peroxide radical initiator at a predetermined reaction time. The reaction must be carried out in a homogeneous chemical environment to allow a better interaction and reactivity between the polymer and other components. The resulting graft copolymer is further purified *via* a selective dissolution approach to obtain the compatibilizer with a relatively higher purity. The process is relatively complex and expensive, and it is difficult to eliminate by-products. Aside from that, it is not practical for large-scale production due to the large quantity of solvents recycling involved (Qiu and Hirotsu 2005).

The most practical method to produce compatibilizer is *via* melt grafting, also known as reactive extrusion (REx). The process involves grafting of MA onto polymer in the molten state with the presence of a free radical initiator. The functionalized polymer is further purified to remove unreacted MA and a radical initiator. In line with this, Ahmad Thirmizir (2011) obtained maleated PBS.

Normally, the effectiveness of the grafting process depends on the reactive components and the processing parameter applied. Previously, He et al. (2013) conducted an exhaustive study to investigate the effect of the concentration of reactive components and grafting parameters on the DG of maleated LDPE (LDPE-*g*-MA) *via* solution grafting in xylene solvent with the presence of dicumyl peroxide (DCP) radical initiator. Table 3.3 shows the studied parameters, and Fig. 3.3 summarizes the findings *via* an orthogonal experiment.

Following He et al. (2013) the concentration of reactive components (DCP and MA) can affect the DG of the compatibilizer (Fig. 3.3). These authors reported that there is a positive trend between the DG and the concentration of MA and DCP up to an optimal value before dropping with an additional increase in concentration and trends proportional to the reaction temperature. While the reaction time and total time for initiator dropped, thus showing an increasing pattern up to a plateau point where any additional increase does not affect the DG value.

A similar study done by Ahmad Thirmizir et al. (2011) also confirmed that the grafting reaction of MA with biodegradable aliphatic polyester (PBS) is affected by the concentration of MA, and this also affected the DG of the compatibilizer. As shown in Table 3.4, Ahmad Thirmizir et al. (2011) also reported that a maleated PBS at a constant mixing parameter and radical initiator concentration (DCP), as well as an increase of the MA concentration in the compatibilizer significantly increased the DG. In addition, as mentioned by Mani et al. (1999), increasing the MA concentration leads to an increase in the DG due to the better probabilities that free MA will bind to the polymer macro radical sites during the grafting reaction.

Chen et al. (2003) investigated the solution grafting of maleated PHB in chlorobenzene at a temperature of 130 °C with the presence of benzoyl peroxide (BPO) radical initiator. These authors reported the relationship between MA monomer concentrations on the DG. As illustrated in Fig. 3.4, the DG increased with increase in the MA concentration up to a maximum of 0.85%, at an MA concentration of 3% (w/v). Beyond 3% (w/v), the DG then decreased and gradually leveled off. According

Table 3.3 Reactive components concentration and grafting parameters for LDPE-*g*-MA compatibilizer

Factors levels	A (wt. %)	B (wt. %)	C (h)	D (°C)	E (min)
1	1	10	1	120	10
2	2	15	2	130	25
3	3	20	3	140	40
4	4	25	4	150	50

A: DCP concentration; B: MA concentration; C: reaction time; D: reaction temperature; E: total time for initiator dropping

Source: He et al. (2013)

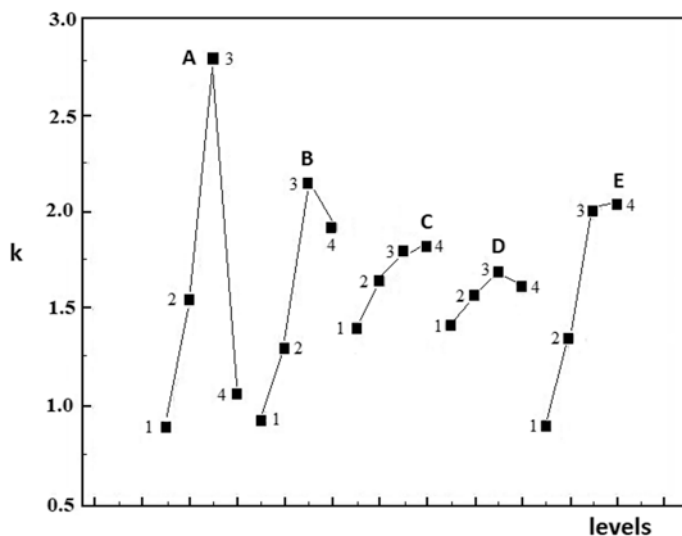


Fig. 3.3 The changing trend of test index (GD). A: DCP concentration, B: MA concentration, C: reaction time, D: reaction temperature and E: total time for initiator dropping. Reproduced with permission from He et al. (2013)

Table 3.4 Effect of MA content on the percentage of MA grafting onto PBS

PBS-g-MA compatibilizer	Content of MA (phr)	DG (%)
3pPBSgMA	3	0.91 ± 0.03
5pPBSgMA	5	1.07 ± 0.02
7pPBSgMA	7	2.14 ± 0.04
10pPBSgMA	10	2.32 ± 0.05

Source: Ahmad Thirmizir et al. (2011)

to Chen et al. (2003), under the solution grafting condition, it is difficult for the MA to homopolymerize given its special molecular structure. However, MA could bind to the PHB backbone in the form of single succinic anhydride rings. The DG is mostly influenced by the number of macroradicals initiated by a radical initiator. Here, as the concentration of MA increases, the chances of PHB macroradicals reacting with MA are higher. When the MA is excessive, unwanted reactions, such as the effect of the cage, easily occur, thus reducing the DG value (Chen et al. 2003).

Chen et al. (2003) also investigated the relationship between DG, MA concentration and Mw. These authors suggested from their results that the increase in the DG is not correlated with the Mw change, which shows that MA grafting is not produced at the ends of the polymer chains, but macro radical sites were formed along the polymer chain. However, in the melt grafting process conducted at relatively high temperature and high shearing rate, chain scission can occur. Meanwhile, our study on the production of maleated PBS and PHB-co-HHx via melt grafting at a temperature of 160 °C and a rotor speed of 50 rpm and a reaction of 5 min, showed that at a constant peroxide concentration, an increase in the MA concentration

Fig. 3.4 Grafting degree as a function of monomer concentration. Reaction conditions: BPO: 0.2% (w/v), chlorobenzene: 100 mL, PHB: 5 g, temperature: 130 °C and time: 4 h. Reproduced with permission from Chen et al. (2003)

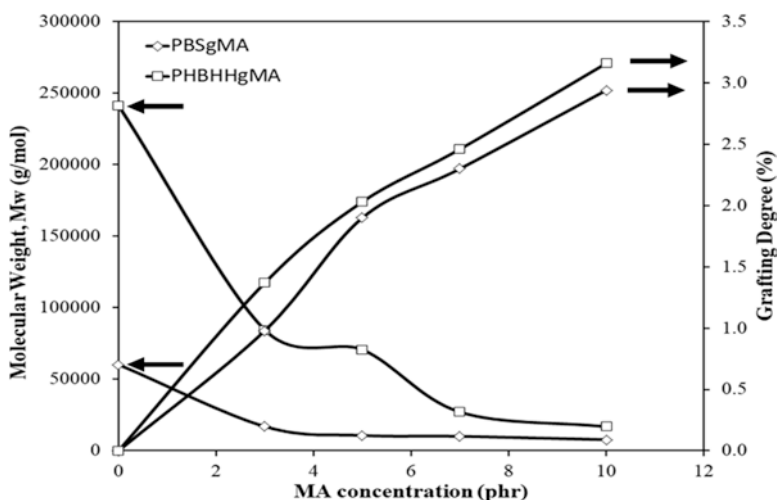
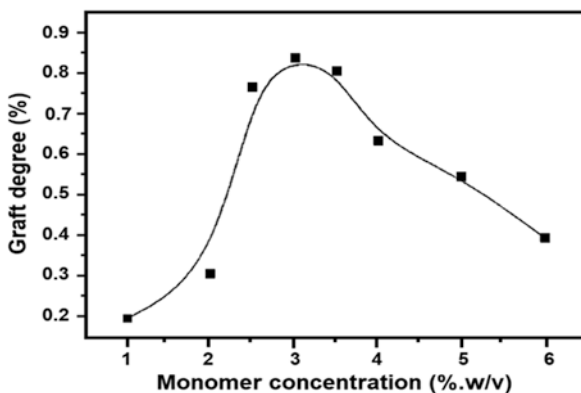


Fig. 3.5 Effect of the MA concentration on the grafting degree and Mw of PBS and PHB-*co*-HHx (PHBHH) (Own results from the authors)

resulted in an increase in the DG and reduction of Mw (Fig. 3.5) (Own results from the authors). Mani et al. (1999) also reported the occurrence of chain scission accompanying the grafting event showed a reduction of intrinsic viscosity of maleated PBS and poly(butylene succinate-*co*-adipate) (PBSA) compared to pure polymers with an increasing MA concentration.

3.2.1.3 Organic Peroxide Radical Initiator

In the grafting process, the reaction begins with the formation of free radicals *via* homolytic scission of the organic peroxide initiator (Ahmad Thirmizir 2011). The initiator has the ability to dehydrogenation to extract hydrogen atoms from α -carbon atoms in relation to the ester carbonyl group of that particular polyester in order to

form a polymeric macro-radical. While, simultaneously the polymeric macro-radical also undergoes a certain degree of degradation *via* β -scissoring to form an end of the radical chain and an end of the vinylidene chain. The ideal compatibilizer will also achieve an optimum DG and a minimal degree of degradation of the polymer chain (Ahmad Thirmizir et al. 2011). However, the grafting reaction is typically accompanied by a chain scission, which changes the rheological behavior of a polymer. Indeed, determining the optimum conditions of the grafting process is a very complex study. Actually, a great number of variables are involved, such as an additional sequence of the reagents, MA concentration, reaction temperature and time, rotor speed, type and concentration of peroxide, and type of stabilizers if added (Oromiehie et al. 2014).

In general, the grafting of MA onto the polymer chains is carried out *via* a reactive melt-blending technique in the presence of a peroxide initiator, such as BPO, DCP and *t*-butyl peroxide (Ahmad Thirmizir et al. 2011). Mani et al. (1999) in the study on the grafting of MA onto PLA *via* solution grafting comprehensively reported the effect of different types of radical initiators (2,2-azobis(isobutyronitrile) (AIBN), BPO, DCP and di-*t*-butyl peroxide (DBP)) on the DG and intrinsic viscosity. The condition of this grafting procedure included: toluene, DCP and MA concentration, 1 and 3% (w/w), respectively, temperature: 110 °C and a reaction time 4 hours. The results are shown in Table 3.5.

The maleated PLA obtained the highest DG with the addition of the BPO initiator due to the slow rate of initiator decomposition at that particular reaction temperature (Mani et al. 1999). As reported by Aldrich Chemical Company Inc. (2020), BPO has a 10-hour half-life temperature lower than DBP and DCP, and at 100 °C, the decomposition rate of BPO is considerably high, approx. $k_d = 5.0 \times 10^{-4}$. Takamura et al. (2008) reported the lifetime of several peroxides at 190 °C, where DCP peroxide had good stability at that temperature compared to other peroxides. Aside from that, the maleated PLA produced *via* solution grafting exhibited minimal chain scission/degradation even with different species of radical initiator (AIBN, BPO, DBP and DCP) compared to the one produced by the melt grafting procedure (Mani et al. 1999; Takamura et al. 2008).

In addition, the radical initiator concentration also affects the DG of MA onto a polymer backbone. Phua et al. (2013) in their study on grafting of MA onto PBS *via* melt grafting procedure, reported that the grafting efficiency increased as the DCP initiator concentration increased from 1 to 1.5 phr due to increased formation of

Table 3.5 Effect of peroxide radical initiator on the DG and the intrinsic viscosity of maleated PLA

No.	Initiator	DG (%)	Intrinsic viscosity (dL/g)
1	BPO	0.6	0.8305
2	DCP	0.27	0.8874
3	AIBN	0.20	0.9103
4	DBP	0.21	0.8744

Source: Mani et al. (1999)

radicals through the initiator decomposition reaction. Moreover, when the concentration of radicals was high, the probability of chain transfer to the polymer backbone was also high, resulting in a greater DG of the compatibilizer. Mani et al. (1999) also studied the effect of initiator (BPO for PLA and DCP for PBS) concentration on MA grafting onto the backbone of the polymer. These authors suggested that melt grafting showed an increase in the DG g with respect to the initiator concentration, which appeared to be quite linear. However, excess of radical initiator can promote termination or a combination reaction between polymer macroradicals due to the available free radical species, thus resulting in a decrease in the DG (Chen et al. 2003). As reported by Chen et al. (2003), the intrinsic viscosity of the compatibilized polymers was reduced by about 30% for PBS, 25% for PBSA and 12% for PLA compared to the unmodified polymer due to the chain scission reaction. The excess radical initiator may cause the polymer to depolymerize, and may also cause an acute reduction of Mw (Chen et al. 2003). Other than that, the presence of peroxide radical initiator could be due to the unwanted crosslinking reaction between the polymer chains, especially for the grafting reaction that was conducted at a high concentration of the initiator.

3.2.1.4 Purification of Compatibilizer

Another critical issue for manufacturing maleated compatibilizer is the purity of the compatibilizer itself. According to Bettini and Agnelli (2000), the MA residue could not be removed by self-evaporation during melt grafting if the reaction was carried out at a temperature below the boiling point of the MA (≈ 202 °C). The purification procedure is essential for producing good quality compatibilizers without the traces of any unreacted residues (Bettini and Agnelli 2000). Ahmad Thirmizir et al. (2011) demonstrated that the removal of ungrafted MA and unreacted DCP residues *via* solvent extraction improves the fiber-matrix interfacial adhesion. The residuals of the ungrafted MA and the unreacted DCP initiator present in the compatibilizers might interrupt the fiber-matrix interfacial adhesion since it could not form a complete bridging between the composite components (Ahmad Thirmizir 2011).

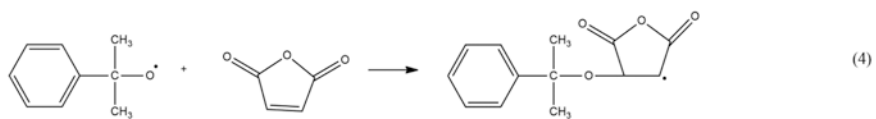
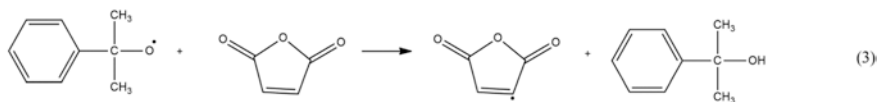
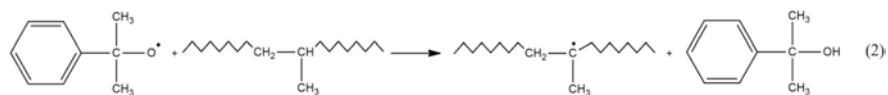
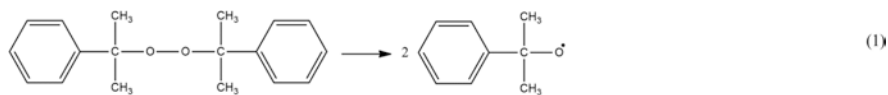
The high concentration of unreacted MA in the blends causes color fading, degassing, reduces ultraviolet (UV) resistance, release of unpleasant odors and the fogging of proximate surfaces (Martin 2019). In addition, Clasen et al. (2015) informed in its study about the thermoplastic starch (TPS)/PLA blends, that the grafting of MA onto polymer backbone restricts the segmental movement of the polymer chains. However, the presence of ungrafted MA in the blends act as a plasticizer and reduce stiffness of the blends. Here, the MA can act as a plasticizer or compatibilizer in the TPS/PLA blend depending on the concentration of the monomer used and residual of the unreacted monomer. MA as a plasticizer can reduce the rigidity of the blends by reducing the T_g and increasing the mobility of the polymer chain. Furthermore, the grafted MA reduces the crystallinity of the PLA-g-MA, which led to a reduction in the TPS/PLA blends module as a whole. Aside from that,

the balance degradation rate and degree of crosslinking are essentials for producing maleated compatibilizer with an optimal Mw distribution, low Mw degradation and a greater number of reactive sites (Raphel et al. 2018).

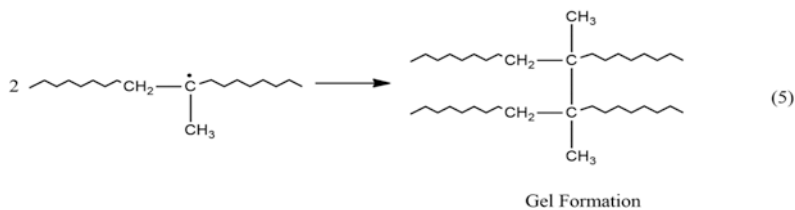
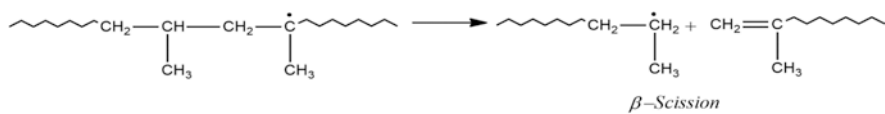
3.2.2 Reaction Mechanism of Maleated Compatibilizer

Free radical polymerization is the most commonly used functionalization technique for polyolefins in which organic peroxides are commonly used as initiators. Several formulations of MA-grafted PP (MAPP) are available in the plastics market depending on the processing method and end-use applications. The grafting reaction of MA onto PP by the melt grafting technique involves a reaction between the polymer melt with MA, in the presence of organic peroxides such as BPO, DCP, etc. As reported by Oromiehie et al. (2014), the organic peroxides are thermally unstable and undergo homolytic scission at the oxygen-oxygen bonds to form primary radicals. The radicals remove hydrogen atoms from the PP chains and form macroradicals to initiate the grafting process. As reviewed by Oromiehie et al. (2014) in other experiments, they found the mechanism of MA grafting onto PP can be divided into three stages: stage 1 - initiation, stage 2 - grafting and stage 3 - termination. The schematic reaction mechanism is shown from Eq. 1 to Eq. 21.

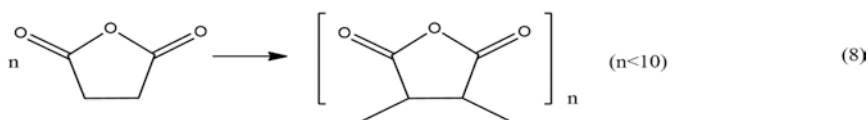
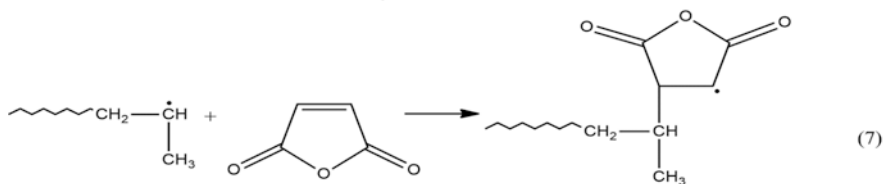
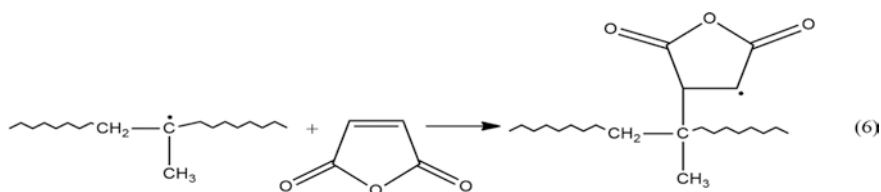
(i) Decomposition of a radical initiator:



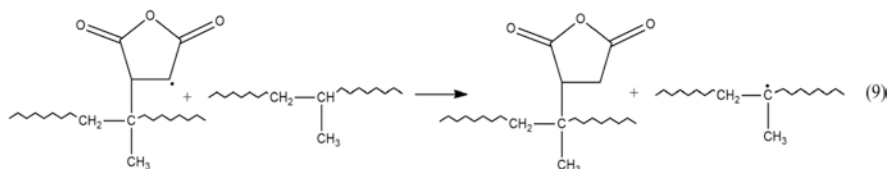
(ii) Some possible reaction for chain radical:



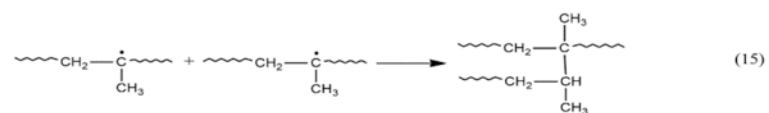
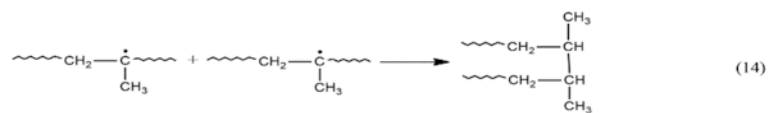
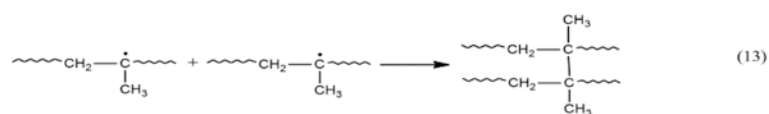
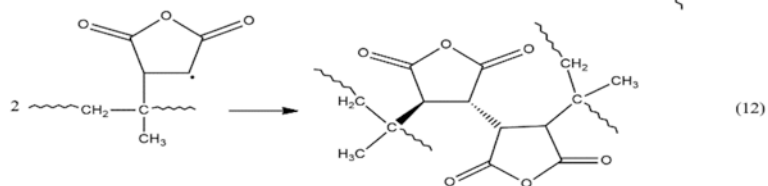
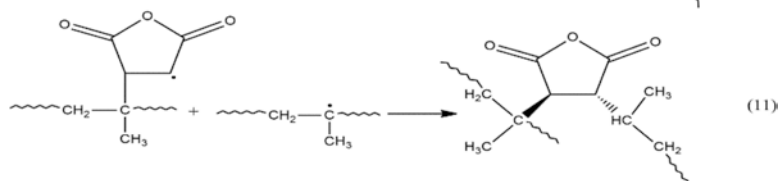
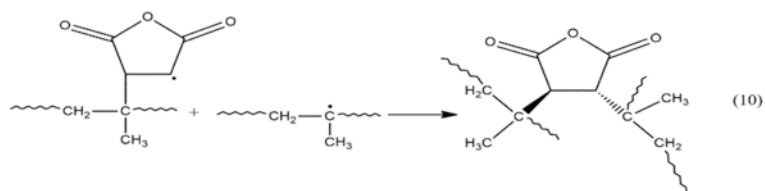
(iii) Grafting of MA



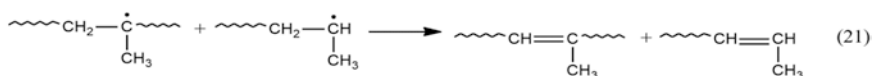
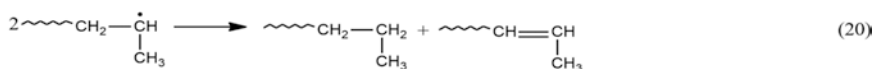
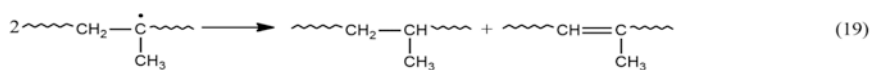
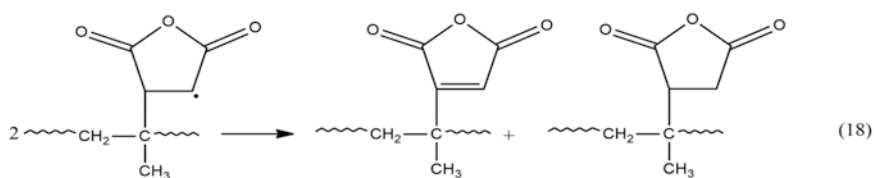
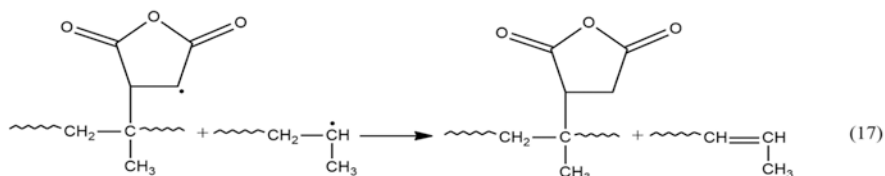
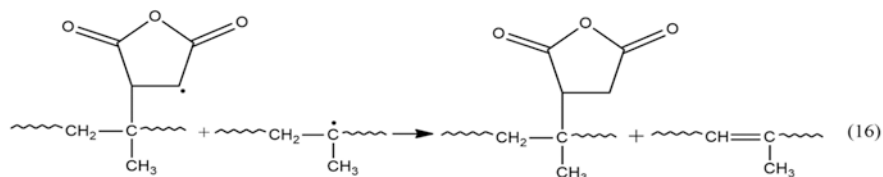
(iv) Chain transfer



(v) Termination by combination reaction



(vi) Termination by disproportioning



The grafting of MA onto PP was shown in Eqs. 6 and 7. Other than that, the homopolymerization of MA (Eq. 8) is possible to occur mainly at the high content of MA, while the chain transfer reaction was shown in eq. 9, and the different types of termination reactions included combinations and disproportionations, which were shown in equations from Eq. 10 to Eq. 15 and Eq. 16 to Eq. 21, respectively.

Mani et al. (1999) investigated the functionalization of PBS and PLA with MA, and suggested the mechanism of grafting reaction of MA onto polyester (Fig. 3.6).

According to Ahmad Thirmizir et al. (2013), the organic peroxide initiator formed a homolytic scission as a free radical. The reaction between a free radical and polyester resulted in the hydrogen abstraction of an α -carbon atom to the ester

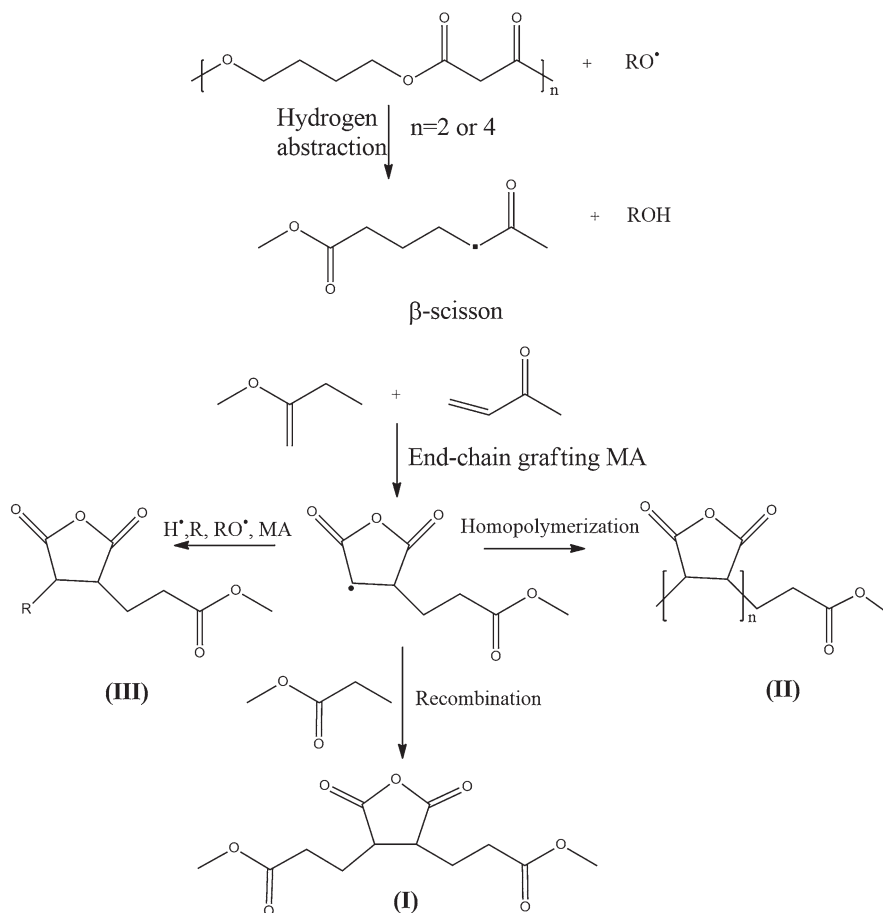


Fig. 3.6 Grafting reaction mechanism for MA grafting onto polyesters. Reproduced with permission from Mani et al. (1999)

carbonyl group of polyester to form a macroradical. Some of the macroradicals then suffered β -scission to form a radical chain end and a vinylidene chain end.

According to Mani et al. (1999), in solution grafting reactions, in the presence of organic peroxide, the additional reaction of the macroradicals is predominant before β -scission, but in the melt-grafting reaction, β -scission is predominant. Once the MA is grafted onto the polymer macroradical, several reactions such as chain transfer reaction, oligomerization, termination and some side reactions can occur. However, the materials made by Mani et al. (1999), no signs of homopolymerization or oligomerization of poly-MA were observed. Similar findings have been reported in previous studies in which the MA monomer has a poor homopolymerization tendency due to its unique structure consisting of 1,2-disubstituted double bonds and the reaction temperature is higher than the MA ceiling temperature

(Mantere 2015; Moghaddam et al. 2012; Muthuraj 2015). However, Mani et al. (1999) suggested based on evidence from Fourier transform infrared (FTIR) spectroscopy and nuclear magnetic resonance (NMR) analysis that the termination reaction of MA onto the polyester could occur *via* two routes: recombination and radical termination reactions to produce end products I and III as shown in Fig. 3.6. Some examples of biodegradable maleated polymers, mainly aliphatic polyesters, will be presented in Sect. 3.2.3.

3.2.3 Maleated Biodegradable Polymers: Some Examples

Rzayev (2011) used with successfully as a monomer in the grafting of biodegradable polymers such as PBS, PBSA, PCL and PLA. Functionalizing the biodegradable polymers with reactive groups is an effective strategy to produce commercial blends and composites suitable for end-user applications. In this section, some examples of maleated biodegradable will be further developed.

3.2.3.1 Maleated PBS

The grafting of MA onto PBS *via* the melt grafting technique was initially reported by Mani et al. (1999). In general, the mechanism of MA grafting onto PBS is similar to that of MA grafting onto polyolefins as presented in Fig. 3.6. Many researchers have reported on the production of maleated PBS and its copolymers for the application of polymer blends (Ramaswamy Mani and Bhattacharya 2008; Yin et al. 2015; Muthuraj et al. 2017) and composites (Ahmad Thirmizir et al. 2011; Phua et al. 2013).

In this sense, Mani and Bhattacharya (2008) reported the use of maleated PBS as a compatibilizer for PBS/starch blends. Here, the compatibilizer was produced using the melt grafting method in a twin-screw extruder. The results showed that the tensile strength (σ) values of the PBS/starch blends without PBS-*g*-MA compatibilizer decreased. For uncompatibilized blends, the increase in starch load decreased the σ values of the blends. At the higher concentration of starch approximately >50 wt.%, a tremendous reduction in σ values of about 60% was observed. Meanwhile, when PBS-*g*-MA was incorporated into the blends, the σ values increased for all blend's ratios. In contrast, the σ value decreased slightly at 30 wt.% starch content before increasing with an additional increase in starch content. At 70 wt.% starch content, the σ values were approximately similar to that of the pure PBS. As expected, the strain at break (ϵ_b) of the PBS/starch blends was severely reduced with the addition of starch. As reported by Mani and Bhattacharya (2008), at 10 wt.% starch content, only a slight reduction in ϵ_b values was observed, while at higher starch load, a tremendous decrease of ϵ_b values was reported. At concentrations of 30 wt.% or higher, the ϵ_b values of non-compatible and compatibilized blends was comparable (approx. Between 10 and 20% of ϵ_b). Starch is brittle

material with a modulus of approximately >1 GPa, and the addition of this into blends makes this material rigid.

Another study by Yin et al. (2015), also reported the consumption of maleated PBS as a compatibilizer in thermoplastic starch/PBS (TPS/PBS) blends. The maleated PBS was produced *via* the melt grafting technique with the presence of a DCP radical initiator. The formulation of maleated PBS was not mentioned in the paper. The TPS/PBS blends were produced in a twin-screw extruder, and then the blends were compression molded at 135 °C into test specimens and were characterized. The FTIR analysis of maleated PBS confirmed the presence of MA attributed to a weak peak at 1633 cm^{-1} , representing the symmetric stretching of the anhydride groups of MA. The $^1\text{H-NMR}$ analysis also confirmed the chemical interaction between MA and PBS, as indicated by the existence of new peaks at 2.74 and 3.52 ppm in the maleated PBS spectra. The mechanical properties in terms of σ and ϵ_b values for 40TPS/60PBS blends were significantly improved with the incorporation of maleated PBS. The TPS/PBS (40/60) blends showed good flexibility with an ϵ_b of about 20% higher compared to the pure blends. Most importantly, the σ values for TPS/PBS (40/60) blends increased almost twice with the same maleated PBS content. However, the tensile properties did not change, obviously, when maleated PBS content was increased even more from 5% to 10%. The result shows that maleated PBS has an excellent compatibilizing effect where it is thermodynamically miscible with PBS and could form a chemical interaction with TPS. With respect to thermal properties, the addition of maleated PBS reduced the crystallization temperature and degree of crystallinity of the TPS/PBS (40/60 wt.%) blends. The higher concentration maleated PBS resulted from the lower crystallization temperature and degree of crystallinity of the blends. It can also be specified that the maleated PBS could make the blends more ductile by promoting the migration of pure PBS molecular chain (Yin et al. 2015).

As reported by Yin et al. (2015) three T_g can be observed by dynamic mechanical analysis (DMA) and be associated with the glycerol-rich phase, the PBS phase and the starch-rich phase. The introduction of maleated PBS resulted in the DMA peaks approaching each other, indicating that PBS and TPS are partially compatible. In addition, the maleated PBS also improved the interfacial compatibilization through a plasticizing effect in the blending system.

Muthuraj (2015) reported the development of maleated PBS as a compatibilizer for poly(butylene adipate-*co*-terephthalate) (PBAT)/PBS blends. These authors investigated the effect of the concentration of DCP on the maleated PBS properties. The DG of maleated PBS increased with the increase of DCP concentrations, and the highest percentage of 2.56 was achieved at a concentration of 1.0 phr. The MA grafting efficiency of the batch and the continuous process were also compared, and the results showed that the batch-processed samples had a slightly higher grafting yield compared to the continuously processed samples. The grafting yield was slightly higher in the internal batch process, and can be attributed to a longer residence time and air contact of the reaction medium. Muthuraj (2015) reported from the differential scanning calorimetry (DSC) analysis that the crystallization and T_m of the maleated PBS decreased significantly and were lower compared to that of

pure PBS. It is believed that the presence of MA groups prevents the nucleation and lamella growth of PBS, thus leading to the formation of the imperfect crystalline structure.

3.2.3.2 Maleated PHB

Among the PHAs, PHB and its copolyesters are the most studied because they are relatively easier to produce and can yield a consistent quality of bioplastics (Avérous 2013). As for physical properties, PHBs are highly crystalline polyester, i.e. they are brittle and prone to thermal degradation during processing. In the past, attempts have been made to reduce the degree of the brittleness of the PHB by copolymerization with hydroxyhexanoate (HHx) or hydroxyvalerate (HVx) co-monomers. Among PHB copolymers, PHB-*co*-HHx, PHBV, poly(3-hydroxybutyrate-*co*-3-hydroxyhexanoate) (PHB-*co*-HHx) and poly(3-hydroxybutyrate-*co*-4-hydroxybutyrate) (P(3HB-*co*-4HB)) have improved flexibility and mechanical properties over other PHBs. In addition, they have properties comparable to those of conventional polymers such as poly(ethylene terephthalate) (PET), poly(ethylene) (PE) and PP. PHB-*co*-HHx become soft and flexible, with an increase in the 3-hydroxyhexanoate (3HH) co-monomer fraction. Doi et al. (1995) reported that an increase in the 3HH co-monomer from 0 to 17 mol% greatly increased the ϵ_b values from 6 to 850%, but the σ values decreased from 43 to 20 MPa. Another study done by Laycock et al. (2014) reported as the concentration of 3HH comonomer in the melt press P(3HB-*co*-3HH) copolymers increases from 2.5 to 9.5 mol%, the ϵ_b significantly increased from 6.7 to 43% and the σ tremendously reduced from 25.7 to 8.8 MPa.

Beyond that, its mechanical strength and T characteristics can be further improved by blending with ductile biodegradable polymers such as PBS and PCL. The blending approach is widely known for its use in conventional polymers, and is cost effective and relatively easy to be undertaken compared to the biological way. From the study by Thirmizir et al. (2017), it is known that the PBS/PHB-*co*-HHx blends are immiscible or immiscible limitedly, depending on the ratio of the components where it is expected to observe the morphology associated with phase separation. To overcome this drawback, several methods such as the addition of compatibilizer and/or the introduction of a crosslinking agent at the blending inter-phase can be employed. According to Chen et al. (2003), very limited studies on the graft copolymerization of PHB have been published. A study on the radiation grafting of 2-hydroxyethyl methacrylate (HEMA), AAc, acrylamide, methyl methacrylate (MMA) and styrene (St) onto PHB and its copolymer, found that grafted polymers are thermally stable and have a faster biodegradability rate (Chen et al. 2003). However, the graft copolymerization only modifies its surface properties and can produce long graft side chains by homopolymerization. These homopolymers can reside in the environment after PHB, which degrades completely and will damage the environment. Therefore, to avoid those drawbacks, Rzayev (2011) chose the MA monomer to be grafted to the PHB chains *via* free-radical polymerization due to its good reactivity and controllability reaction.

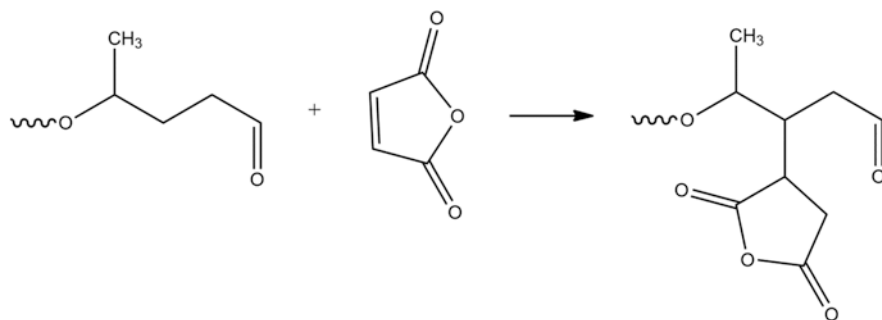


Fig. 3.7 Grafting of MA onto poly(3-hydroxybutyrate) (P(3HB)). Reproduced with permission from Rzayev (2011)

The grafting reaction is depicted in Fig. 3.7. As reported by Chen et al. (2003), grafting reaction of MA onto PHB chains was conducted in chlorobenzene with a solution temperature of about 130 °C using BPO as an initiator.

3.2.3.3 Maleated PLA

Gardella et al. (2014) studied PLA/PCL blends, and reported maleated PLA (PLA-*g*-MA) which was introduced to promote grafting between PCL and PLA-*g*-MA backbone and physical compatibility at the PLA-PLA-*g*-MA interface. The maleated PLA was produced by using the melt grafting technique employing a glass reactor with a mechanical stirrer placed in an aluminium block oven. Before the reaction process, MA, PLA and 2,5-dimethyl-2,5-di-*t*-butylperoxyhexane were purged with helium for 30 min and repeated at least three times, to ensure a moisture free atmosphere. The reaction was conducted at 180 °C under the stirring condition for a reaction time of 10 min. The peroxide content was 0.5 wt.%, and MA was 6 wt.%. The maleated PLA was then purified by dissolving in chloroform and precipitated into methanol. The blends were prepared by mixing different amounts of PCL, PLA and maleated PLA in the same reactor. The suggested reaction mechanism between PCL and maleated PLA is shown in Fig. 3.8.

Ma et al. (2014c) reported the production of maleated PLA *via* the melt grafting technique using a mini twin screw extruder. Before the grafting process, the PLA pellets were sprayed with a mixture of acetone dissolved in DCP, MA and St and allowed to dry. After that, the pre-treated PLA pellet was fed into the extruder, and the grafting reaction was conducted at 160–190 °C with a screw speed of 35 rpm. In this study, the DCP radical initiator and St co-monomer were used to promote the formation of free radical. St with an electron-donating feature can easily interact/ react with the electron-attracting monomers (i.e. MA *via* a charge transfer complex (CTC)) or through copolymerization (Ma et al. 2014b). St could activate MA to form an asymmetric structure and Π bonds of radical-anion. As a result, the interaction between macroradicals and MA monomers could be bridged by St, and a higher

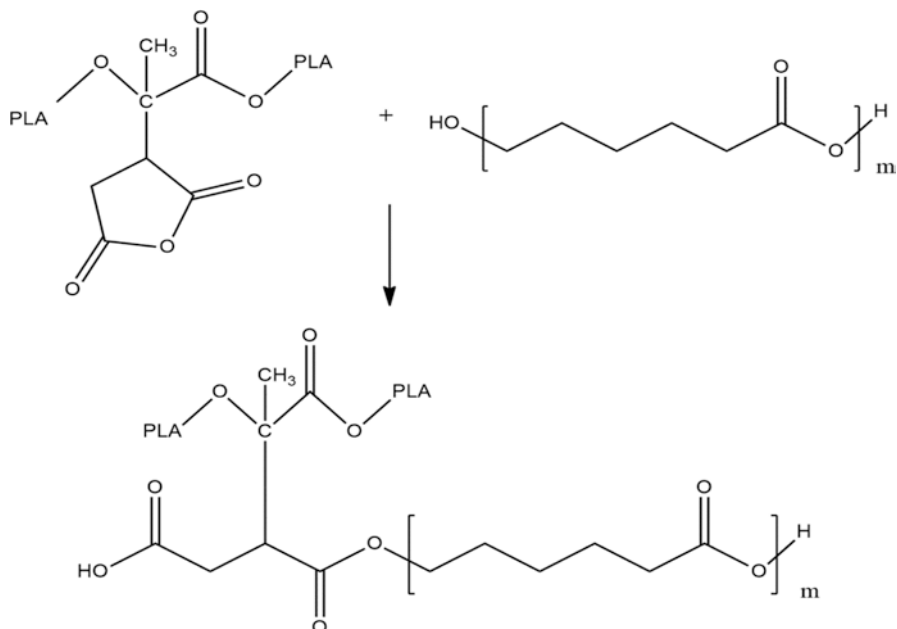


Fig. 3.8 Reaction scheme between PCL and PLA-g-MA. Reproduced with permission from Gardella et al. (2014)

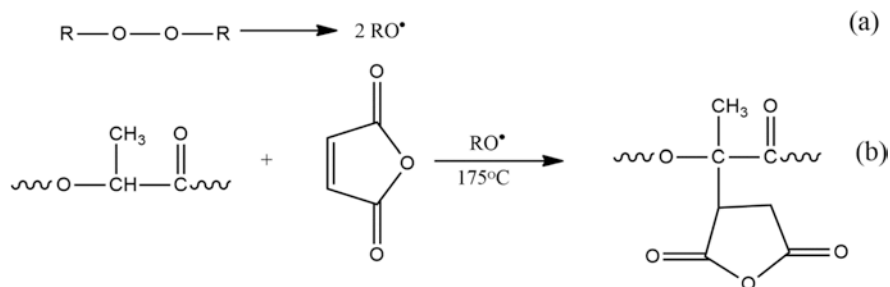


Fig. 3.9 Free radical grafting of MA onto PLA with the presence of DCP radical initiator. Reproduced with permission from Ma et al. (2014b)

DG could be achieved. The St co-monomer has been widely used for the production of maleated polyolefins, but for maleated aliphatic polyester, it is considerably rare. Keeping this in view, Ma et al. (2014b) reported that the use of the St co-monomer successfully increased the DG of MA onto PLA backbone and achieved an optimum at the St/MA ratio of 2/1. The St co-monomer is necessary in the maleated reaction due to the low MA reactivity towards the macro-radicals attributed to its structural symmetry and low electron density around the $-\text{CH}=\text{CH}-$ bond. The reaction mechanism of the free radical grafting of MA onto PLA with the presence of DCP radical initiator is shown in Fig. 3.9.

The grafting mechanism of MA onto PLA in the presence of St co-monomer is produced in two steps. As proposed by Ma et al. (2014b), first, the reaction begins with the decomposition of DCP to form primary radicals (RO^{\bullet}). This is followed by the initiation of PLA macroradicals (PLA^{\bullet}) by hydrogen abstraction. The PLA macroradicals then react with grafting monomers, and some of them involve inside reactions such as chain scission or recombination. Most of the PLA macroradicals would be used before reacting with MA due to the inert character of the MA towards the macroradicals. St reacts with PLA macroradicals, thus forming stable styryl macroradicals, which then copolymerize with MA. St then reacts with MA to form a CTC which can improve the electric asymmetry on the $-CH=CH-$ bond of MA. The CTC can increase the reactivity and DG of MA, which could be copolymerized with St in the presence of free radicals to form oligomer-radicals ($St-co-MA^{\bullet}$). The $St-co-MA^{\bullet}$ could also react with macroradicals (PLA^{\bullet}) by a combination reaction. Subsequently, more routes for MA to be grafted onto PLA chains are obtained, thus significantly increases the DG. However, the excess of St may result in the copolymerization of St and MA or the grafting of St rather than MA, which could reduce the DG (Ma et al. 2014b).

The maximum DG of MA was reported by Ma et al. (2014b) at a St/MA ratio of 2/1 in the PLA-g-MA/St system and not at a 1/1 ratio due to polymer chain structures. In the presence of primary radicals (RO^{\bullet}), the residual St may react with PLA macroradicals to produce relatively stable styryl macroradicals ($PLA-g-St^{\bullet}$) or copolymerize with MA to form short oligomer-radicals ($St-co-MA^{\bullet}$). The $PLA-g-St^{\bullet}$ could then react with short $St-co-MA^{\bullet}$, CTC or MA to form branched structures. Ma et al. (2014b) suggested that the grafting of short $St-co-MA^{\bullet}$ onto PLA chains causes the main reaction to occur at the St/MA ratio of around 2/1, as shown in Fig. 3.10.

As stated by Ma et al. (2014b), $St-co-MA$ is a random co-oligomer rather than a block co-oligomer, due to the strong free radical reactions. Ma et al. (2014b) also reported the effect of MA concentration on the DG at a constant St/MA/DCP ratio where the DG remained unchanged with the increase in the MA concentration. The DG also depends on the number of reactive species associated with the MA monomers and the DCP concentration. Another factor that affects the DG is the reaction temperature. In this sense, Ma et al. (2014b) reported that at a fix MA concentration of 4.5 phr and constant St/MA/DCP ratio of 2/1/0.1, the DG increased with temperature and achieved optimum at 180 °C. Beyond that, the DG was reduced.

3.2.3.4 Maleated PCL

PCL is a ductile biodegradable polyester commonly used to improve the brittleness of other biodegradable polymers, such as PBS (Can et al. 2014; Gumede et al. 2018), PHB (Barghini et al. 2010) and PLA (Gardella et al. 2014) through the blending approach. However, Gardella et al. (2014) indicated that PCL and PLA are thermodynamically incompatible and form blends with a multiphase structure and an inadequate interfacial bonding, which deteriorates their mechanical performance.

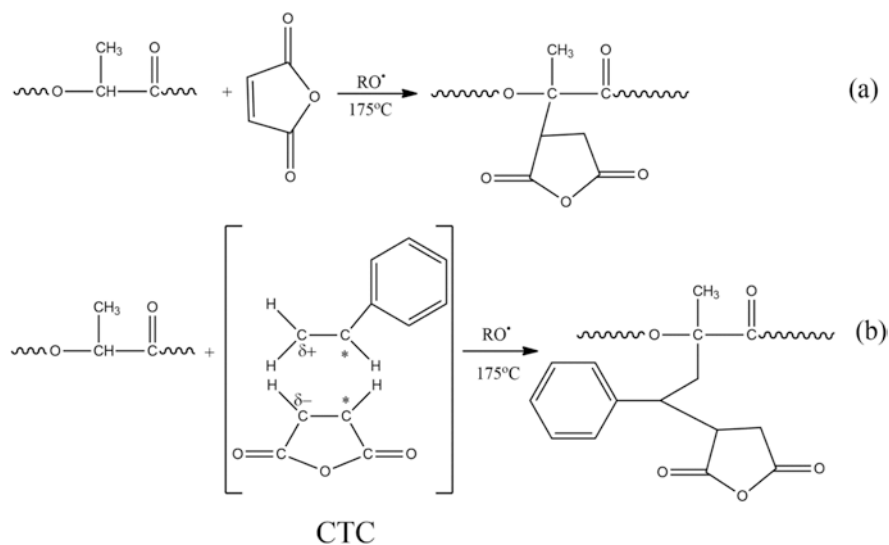


Fig. 3.10 The main grafting reactions proposed at low St/MA ratios ($R = C_9H_{11}$). Some possible side reactions are not present here. Reproduced with permission from Ma et al. (2014b)

Many studies have been carried out to improve the compatibility between them *via* compatibilization techniques, such as the incorporation of polymeric compatibilizers and reactive compatibilization approaches (Gutiérrez and Alvarez 2017 a,b,c; Herniou–Julien et al. 2019). Wu and Liao (2012) studied PCL/rice straw fiber blends and used maleated PCL as a compatibilizer. The maleated PCL was produced by the solution grafting technique using tetrahydrofuran (THF) as the solvent and BPO as the free radical initiator. The grafting reaction of MA onto PCL was carried out at a temperature of 40 ± 2 °C and a rotor speed of 60 rpm for 10 hours. The optimal DG was 1.02 wt.% with BPO and MA contents of 0.3 and 10 wt.%, respectively. The schematic reaction of MA onto PCL is shown in Fig. 3.11.

Wu and Liao (2012) assessed the maleated PCL by FTIR and ^{13}C -NMR to confirm the grafting reaction. The FTIR analysis exhibited the presence of two additional bands at 1786 and 1857 cm^{-1} , representing anhydride carboxyl groups in the modified PCL-*g*-MA. The presence of the bands represents free acid in the PCL-*g*-MA showing an effective MA grafting onto PCL (Wu and Liao 2012). Meanwhile, solid state ^{13}C -NMR analysis was conducted to confirm this finding. These authors observed six peaks, corresponding to carbon atoms in the unmodified PCL (1, $\delta = 64.3$ ppm; 2, $\delta = 28.9$ ppm; 3, $\delta = 25.8$ ppm; 4, $\delta = 25.1$ ppm; 5, $\delta = 34.4$ ppm; 6, $\delta = 172.9$ ppm). For PCL-*g*-MA, the additional peaks at (7, $\delta = 42.3$ ppm, 8, $\delta = 36.2$ ppm; 9, $-\text{C}=\text{O}$ $\delta = 174.3$ ppm) confirmed that MA was covalently grafted onto PCL (Wu and Liao 2012).

An overview on the REX of PCL/starch blends made by Kalambur and Rizvi (2006) was reported using maleated PCL as a compatibilizer in PCL/starch blend systems suggested by John et al. (1997). The maleated PCL was prepared by melt

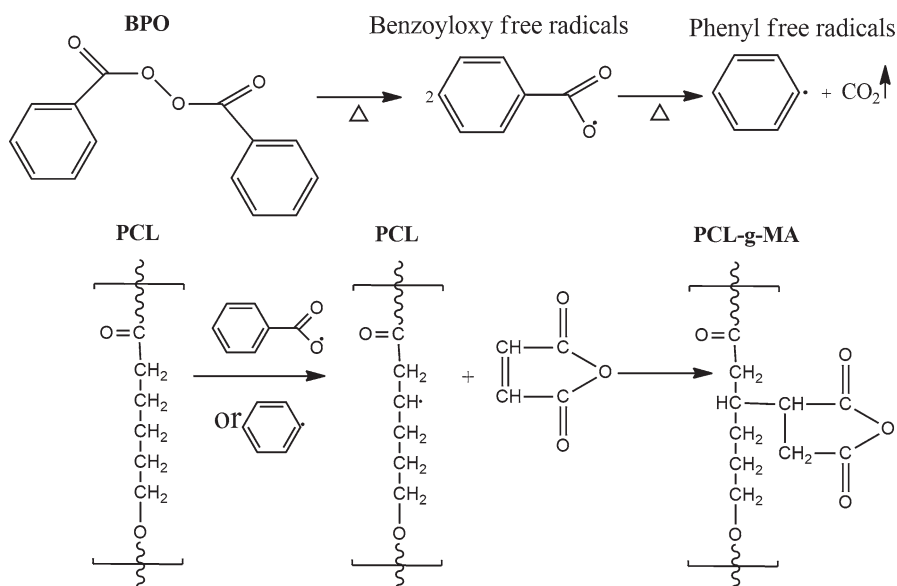


Fig. 3.11 The grafting reaction of MA onto PCL. Reproduced with permission from Wu and Liao (2012)

grafting of MA onto PCL in a batch mixer with a roller blades type rotor in a twin-screw extruder using DCP as an initiator. The results indicated that no crosslinking reaction occurred during the grafting process.

According to John et al. (1997), the reaction mechanism begins with the homolytic scission of peroxide, which produces radicals followed by hydrogen extraction of α - carbon atom relative to the carbonyl group. The second step involves the formation of radical on the PCL chain and some degree of β -scission due to the existence of organic peroxide. The third step involves the addition of a double bond to the radical from β -scission. In this case, the termination reaction can occur in three possibilities: homopolymerization, radical termination and recombination. Based on the FTIR and NMR analysis, the termination reaction and recombination reaction are favored and no traces of homopolymerization reaction products were detected in the compatibilizer. The reaction mechanism between the maleated PCL and the starch was further developed by Kalambur and Rizvi (2006) and the schematic reaction is shown in Fig. 3.12.

3.3 Free Radical Crosslinking of Biodegradable Polymer

During the last decade, stabilization of polymer blends by the crosslinking reaction has been widely practiced in many industries. Initially, the concept of a system of crosslinked blends was practiced in the production of thermoplastic vulcanizates for

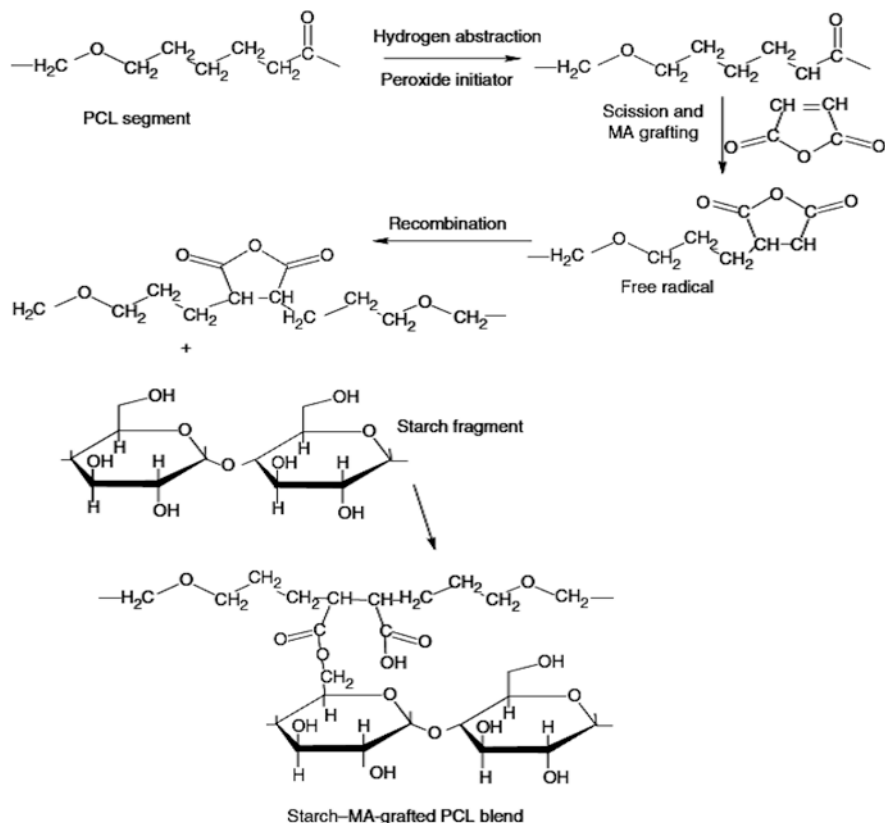


Fig. 3.12 Reaction mechanism of MA grafting onto PCL and reaction between maleated PCL and starch. Reproduced with permission from Kalambur and Rizvi (2006)

replacing pure elastomeric block copolymer which was relatively expensive and complicated to be produced. The blends were dynamically crosslinked using various crosslinking agents such as organic peroxides (e.g. 2,5-dimethyl-2,5 bis(*t*-butylperoxy) and DCP), phenolic curative (e.g. dimethyl alkyl phenol), sulphur and zinc oxide (Harrats and Groeninckx 2007). Various compatibilizers such as GMA-grafted ethylene propylene diene monomer (EPDM), MA-grafted EPDM and MA-grafted PP, have been to improve the interfacial adhesion between the rubber phase and thermoplastic matrix. As for the mechanical properties, thermoplastic vulcanizates show a full strain recovery compared to pure thermoplastics. They also have higher σ values compared to pure rubbers and are controlled by the size of the vulcanized rubber particles in the blends. As shown in the EPDM-PP blends in Fig. 3.13, the smaller the particle size, the higher the tensile stress of thermoplastic vulcanizate.

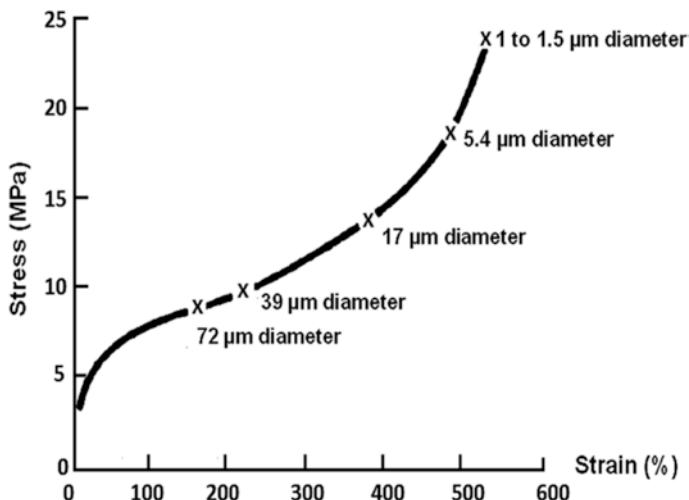


Fig. 3.13 Effect of vulcanized-rubber particle size on the mechanical properties of EPDM-PP thermoplastic vulcanizates. Reproduced with permission from Harrats and Groeninckx (2007)

3.3.1 Type of Peroxide Radical Crosslinking

Peroxide initiated crosslinking commonly produced by adding small amounts of peroxide during melt processing. Peroxides can be classified into seven types according to the chemical structures: diacyl peroxides, dialkyl peroxides, diperoxyketals, hydroperoxides, ketoneperoxides, peroxydicarbonates and peroxyesters (Takamura et al. 2008). In the context biodegradable polymers, various types of peroxides have been used in the crosslink or partial crosslink polymer blends, such as BPO, DCP, dilauroyl peroxide (LPO), *n*-butyl 4,4-di-(*t*-butyl peroxy) valerate (BTBV), OO-(*t*-butyl) O-(2-ethylhexyl) peroxy carbonate (TBEC), *t*-butyl peroxy benzoate (TBPB), *t*-butyl peroxy-2-ethylhexanoate (TBEH) and *t*-butyl peroxy-3,5,5-trimethylhexanoate (TBTH) (Takamura et al. 2008). Among these peroxides, DCP has been the most widely used peroxide crosslinking agent in the biodegradable polymer blends system (Semba et al. 2006; Mishra et al. 2007; Takamura et al. 2008; Deng and Thomas 2015).

Takamura et al. (2008) reported the use of various types of peroxides as crosslinking agents of PLA under REX conditions. The peroxides can be divided into three main groups according to their decomposition rates: group I: fast, group II: moderate and group III: slow, as shown in Table 3.6.

Table 3.6 Life time of peroxides at 190 °C

Group	Type	Name (purity)	Mw (g/mol)	Lifetime (s) ^b	Peroxide amounts (g/kg PLLA) ^c
I	Diacyl peroxides	LPO (98%)	399	2	324
		BPO (75% ^a)	242	5	257
	Peroxyesters	TBEH (97%)	216	11	177
II	Peroxyesters	TBEC (97%)	246	68	206
		TBTH (97%)	230	110	189
		TBPB (97%)	194	108	157
III	Diperoxyketals	BTBV (95%)	334	190	138
	Dialkyl peroxides	DCP (98%)	270	190	219

Source: Takamura et al. (2008)

^aMoisture content 25%

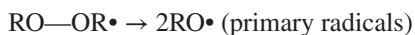
^bLifetime at 190 °C calculated using decomposition parameters (ΔE and A) from NOF Technical bulletin 2004. Lifetime (s) = $-\ln(\text{ratio of residual peroxide to initial peroxide})/A \exp(\Delta E/RT)$, where the ratio of residual peroxide to initial peroxide = 0.0001, $R = 831 \text{ J mol}^{-1} \text{ K}^{-1}$ (gas constant) and $T = 463 \text{ K}$

^cRadical content was fixed at one peroxide molecule *per* poly(L-lactic acid) (PLLA) molecule

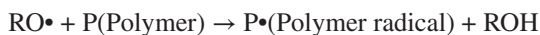
3.3.2 Crosslinking Reaction Mechanism

According to Takamura et al. (2008), crosslinking of polymers initiated with peroxides occurs through three key steps:

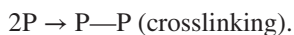
- (i) The generation of primary radicals derived from thermal decomposition of peroxides.



- (ii) Hydrogen abstraction from polymer chains by primary radicals to generate polymer radicals.



- (iii) The bimolecular recombination of polymer radicals to form carbon-carbon cross-links.



In contrast, Mishra et al. (2007) proposed the mechanism of crosslinking reaction from PCL/epoxidized natural rubber (ENR) (50/50) blends that occurred *via* two schemes: (1) formation of PCL macroradical and chain scission of its polymer chain (Fig. 3.14) and (2) inter-chain crosslinking between PCL and ENR at the interface (Fig. 3.15).

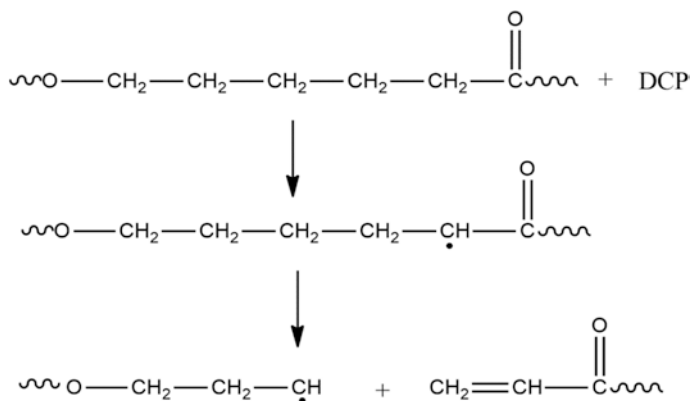


Fig. 3.14 Chain scission of PCL during crosslinking with DCP. Reproduced with permission from Mishra et al. (2007)

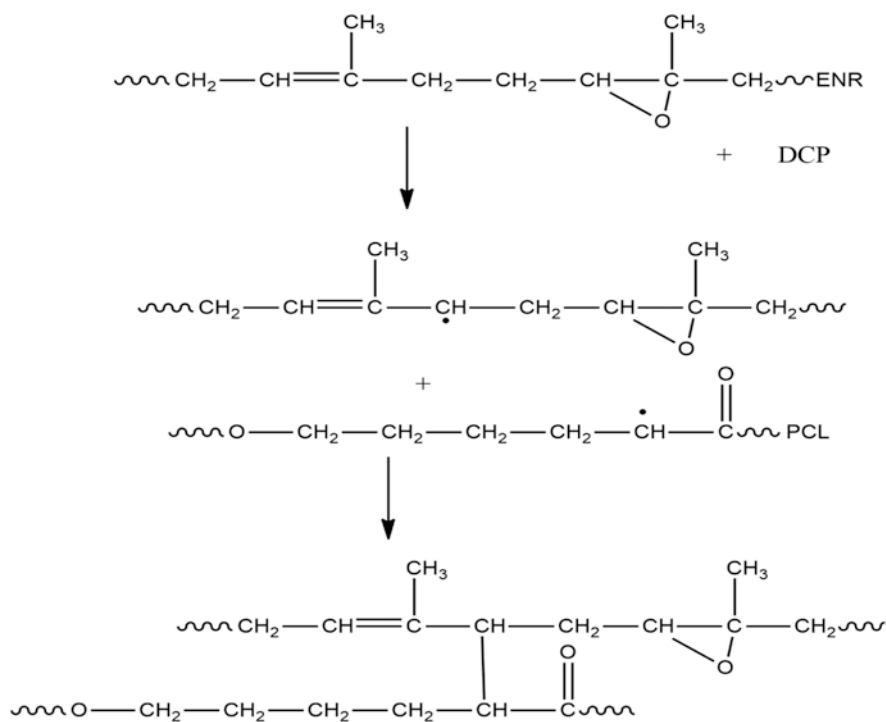


Fig. 3.15 Inter-chain crosslinking between PCL and ENR at the interfacial region with DCP. Reproduced with permission from Mishra et al. (2007)

On the other hand, Hu et al. (2018) produced crosslinked PBS/PLA blends by using BPO as a peroxide radical initiator in hot chloroform at a temperature of 65 °C as a blending solution. The reactive solution was blended for 120 min, and the blends were then dried for 48 h at 50 °C before compression molding at a temperature of 160 °C. The possible BPO-initiated crosslinking reaction mechanism of PLA/PBS is shown in Fig. 3.16.

3.3.3 Peroxides Concentration

Fei et al. (2004) and Takamura et al. (2008) reported the influence of the concentration peroxides on the degree of crosslinking of the partially crosslinked copolymer poly(L-lactic acid) (PLLA) and PHBV *via* the gel content, Mw analysis and thickness swelling. According to Fei et al. (2004), by varying the concentration of peroxide during processing, the degree of crosslinking of PHBV chains can be tailored to a suitable degree. By tailoring the Mw of PHBV *via* the grafting approach, the undesirable effect of heat processing on the melt viscosity and Mw of PHBV could be compensated, and the resulting material even shows better mechanical properties.

Generally, the crosslinking time can be estimated based on the half-life of the peroxide used at that particular grafting temperature. The grafting period is normally five times than the half-life of the peroxide (Fei et al. 2004). In addition, the crosslinking density can be controlled by the initial amount of peroxide at constant crosslinking parameters.

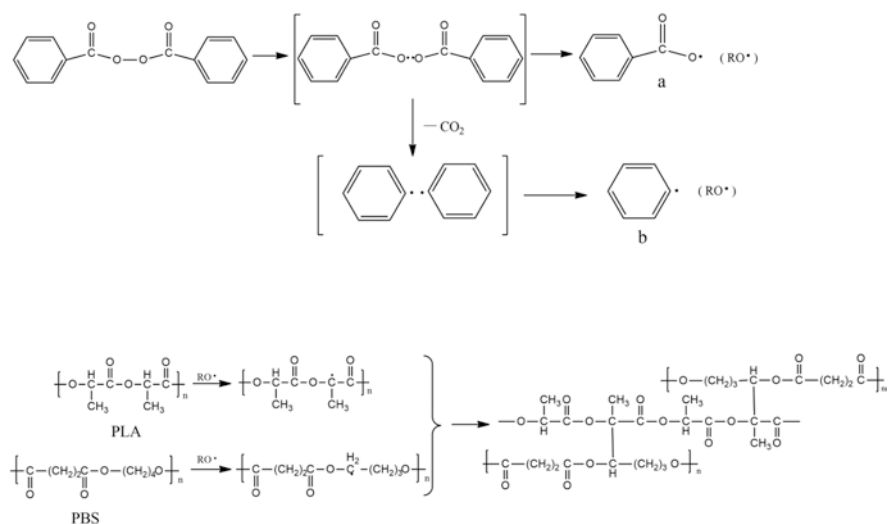


Fig. 3.16 Reaction mechanism of BPO-initiated PLA/PBS crosslinking. Reproduced with permission from Hu et al. (2018)

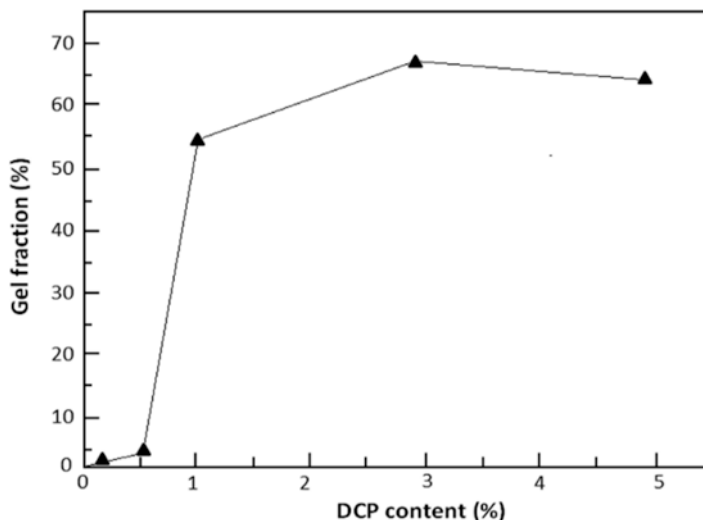


Fig. 3.17 Gel fraction based on DCP content for crosslinked PHBV. Reproduced with permission from Fei et al. (2004)

It can be seen in Fig. 3.17 that the gel fraction is almost zero at 0.17% DCP. Fei et al. (2004) suggested that mainly branched PHBV was produced under these conditions. When the DCP content was increased to 0.5%, the gel fraction of about 2% was obtained, and since the DCP content is increased to 1%, the gel fraction is about 55%. However, additional increases in the DCP content did not result in a significant increase in the gel fraction. Fei et al. (2004) also compared the gel fraction analysis between PHBV with LDPE, where the crosslinking efficiency of PHBV was much lower than that of LDPE when the peroxide concentration used reached between 3 and 5%. While at the lower peroxide concentration (1% of DCP), the crosslinking efficiency in PHBV is comparable to that in LDPE, thus suggesting that the ideal DCP content should be in a range between 0.5 and 1% in order to obtain an optimal degree of crosslinking of the PHBV. On the contrary, the gel swelling ratio decreased as the content of DCP increased, which explains why the crosslink density of the copolymer increased as the content of DCP increased (Fig. 3.18).

Peroxide radical crosslinking has also been used to improve the compatibility of biodegradable polymer blends *via* partial crosslinking of the components of the blend. Previous studies have reported the positive impact of partial crosslinking on the improvement of σ , ϵ_b and T of the blends (Dong et al. 2013; Ji et al. 2014; Ma et al. 2014a; Signori et al. 2015). In line with this, the incorporation of peroxides tends to promote the formation of chain branching, as well as crosslinking, thus increasing the degree of crystallinity, T and thermal behavior of the polymer blends. Indeed, the crosslinking reaction is also an effective approach to improve interfacial adhesion of the immiscible polymer blends by initiating the emerging of mixed chains (copolymers), which act as compatibilizers at the interphases (Signori et al. 2015).

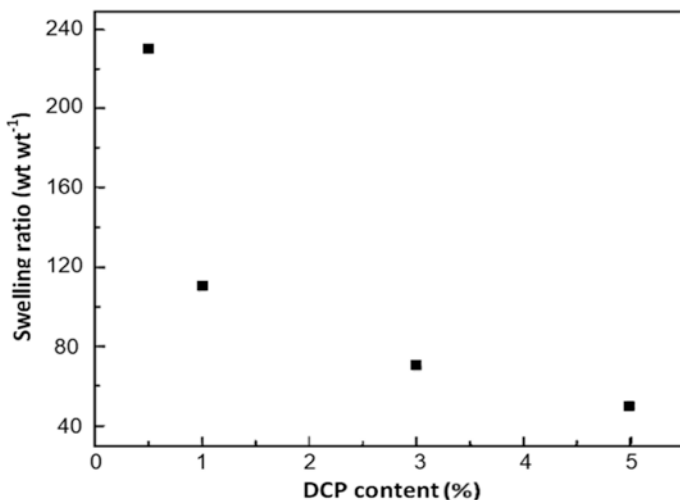


Fig. 3.18 Effect of DCP content on the swelling ratio of crosslinked PHBV obtained *via* chloroform extraction. Reproduced with permission from Fei et al. (2004)

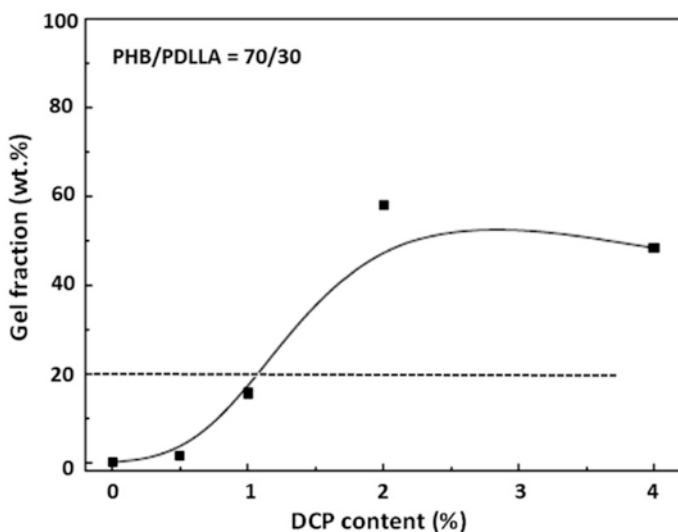


Fig. 3.19 Gel fraction of the crosslinked PHB/PDLLA (70/30) blends as a function of DCP content. Reproduced with permission from Dong et al. (2013)

The formation of branching or crosslinking of the polymer chains by heterogeneous and/or homogeneous radical coupling reactions are controlled by the concentration of peroxides used in the blending system.

Dong et al. (2013) reported the effect of peroxide (i.e. DCP concentration on the properties of PHB/poly(D,L-lactic acid) (PDLLA) blends). It can be seen from the result of the gel fraction (Fig. 3.19) that the gel fraction of the PHB/PDLLA (70/30) blends increased up to 2 wt.% before being leveled with an additional increase in DCP concentration. A similar observation was also reported by Signori et al. (2015) for PLA/PBAT/DCP crosslinked blends where the gel fraction of the blends increased with the peroxide content from 0 to 0.2 wt.%. Ji et al. (2014) also observed similar trends in which the gel fraction of partial crosslinked PLA/PBS blends increased when the DCP peroxide concentration increased from 0.1 to 0.5 phr. In addition, Dong et al. (2013) reported, at a low concentration of DCP (1%) the gel fraction obtained was considerably low, while with a 2% DCP content, the gel fraction was almost doubled. However, a slight drop in the gel fraction was observed at the high DCP concentration (4%). This was related to the domination of the chain scission reaction of the components of the blend's main chains instead of crosslink/branching reactions.

According to Dong et al. (2013), PHB/PDLLA blends with a DCP concentration greater than 1% were relatively more difficult to be processed due to the presence of a highly density portion from crosslinking which tended to increase the melt viscosity of the blends. Dong et al. (2013) reported that the incorporation of DCP into PHB/PDLLA (70/30) blends resulted in a large increase in the mixing torque: the higher the DCP content, the higher the mixing torque. This phenomenon was due to the formation of the crosslinking/branching structure by carbon-carbon crosslinks as a result of the recombination of polymer radicals (Takamura et al. 2008).

Regarding the rheology point of view, Dong et al. (2013) reported the effect of the DCP addition on the storage module (G') and the complex viscosity (η^*) of the PHB/PDLLA (70/30) blends (Figs. 3.20 and 3.21). The G' of the blends increased significantly after adding DCP, while the plots of G' vs frequency show a flatter curve in the low-frequency zone. The trends denote the presence of branched

Fig. 3.20 Storage module (G') of the PHB/PDLLA (70/30) blends as a function of DCP content. Reproduced with permission from Dong et al. (2013)

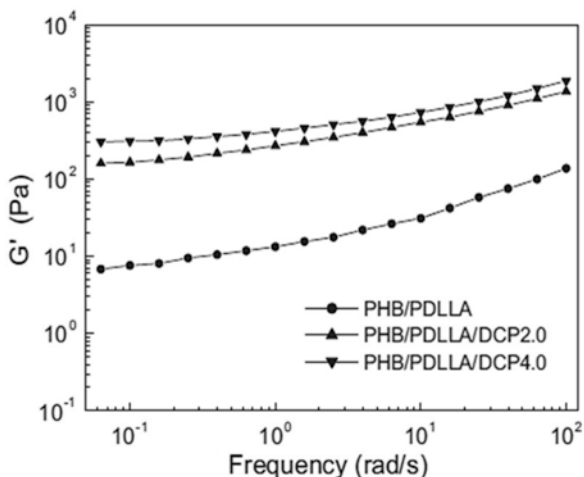
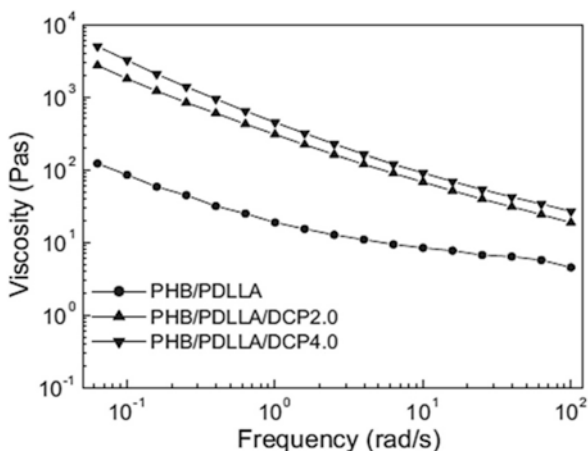


Fig. 3.21 Viscosity of the PHB/PDLLA (70/30) blends as a function of DCP content. Reproduced with permission from Dong et al. (2013)



structures and/or partial crosslinks in the blends. It can be seen from the η^* result that the partial crosslinking improved the melt strength of the blends. However, the η^* for the partially crosslinked PHB/PDLLA blends at the high frequency zone was not so high, thus indicating that the blends maintain good melt processability even after partial crosslinking. Signori et al. (2015) also found good processability for partial crosslinked PLA/PBAT blends up to the peroxide content of 0.2 wt.%.

3.4 Compatibilization of Blends

The polymer blend is a relatively easy and cost-effective approach to produce polymer products with beneficial combinations of valuable properties with respect to the single polymer properties (Raphel et al. 2018). Many of the polymer blends are immiscible and incompatible, and therefore, a compatibilization process either non-reactive or reactive is essential to ensure that the properties of desired blends can be achieved (Muthuraj 2015). Non-reactive compatibilization usually involves a process in which a prefabricated graft or block copolymers are used. On the other hand, reactive compatibilization is carried out *via* melt blending with the presence of compatibilizer can effectively form chemical interactions at the interfacial region of the components of the blend (Muthuraj 2015). This procedure is conducted by the addition of pre-produced polymers (block copolymer, graft copolymer, homopolymer, etc.) or by forming reactive compatibilizers *in-situ* to improve the interfacial adhesion, decrease the interfacial tension and the dispersed phase size and suppress the coalescence of the dispersed phase (Raphel et al. 2018).

3.4.1 Reactive Compatibilization of Biodegradable Blends

Reactive compatibilization is also known as REx if it is conducted in a continuous mixing system and reactive melt blending if it is conducted in a batch mixing system. Although REx has been well known for conventional polymer processing in the last decade, its application for processing of biodegradable polymer blends is a somewhat a new direction of scientific research. The reactive compatibilization of polymer blends can be produced *via* one step (*in-situ*) or two-step REx. In one-step REx, all components are introduced simultaneously during blending. Both the functionalization and reactive blending steps are carried out in the same extrusion process (Sun et al. 1996). The functionalization can be conducted in the first section of the extruder, followed by interfacial reaction compatibilizer and polymer blends. The process is also known as *in-situ* compatibilization. While in the multi-steps, usually two-step REx, it includes functionalization of the polymer with reactive agents normally with the presence of the free radical initiator in the first step and blend of functionalized polymers with other components through an extrusion process in the second step (Gutiérrez et al. 2017).

3.4.1.1 Single Step or *in-situ* Reactive Compatibilization

Finding the components of polymer blends that are thermodynamically correct with good miscibility is realistically challenging, since the incompatibility between the components tends to occur. The improvement of compatibility and adhesion between phases can be carried out by incorporating suitable interfacial agents, either block or graft copolymers, which is a relatively complicated and less economical process. Alternatively, these copolymers can be produced *in-situ* by a blending process through polymer-polymer graft reactions using functionalized polymers (Rzayev 2011). The incorporation of block copolymers or functionalized homopolymers, which can react to form copolymers *in-situ*, is an effective method for compatibilizing immiscible polymer blends and preventing coalescence (Fink 2013).

Sun et al. (1996) reported *in-situ* compatibilization based on the REx technological point of view, where the compatibilization and reactive melt blending are carried out in the same barrel. The authors also suggested two types of extruder and screw configuration, specifically for *in-situ* reactive compatibilization purposes, as shown in Fig. 3.22. For an extruder with type (a) screw configuration, e.g. the PP pellets, the monomers (GMA and St) and the peroxide are fed by the first hopper, while the poly(*p*-phenylene-2, 6-benzobisthiazole-diyl) (PBT) pellets are fed by the second hopper. In this configuration, the functionalization of the PP is produced almost completely in the first zone between the first and second hoppers, after which (in the second zone, from the second hopper to the matrix) the interfacial reaction between the functionalized PP and the PBT occurs. While in type (b) screw configuration, the devolatilization zone can be moved to the end of the first zone before the second

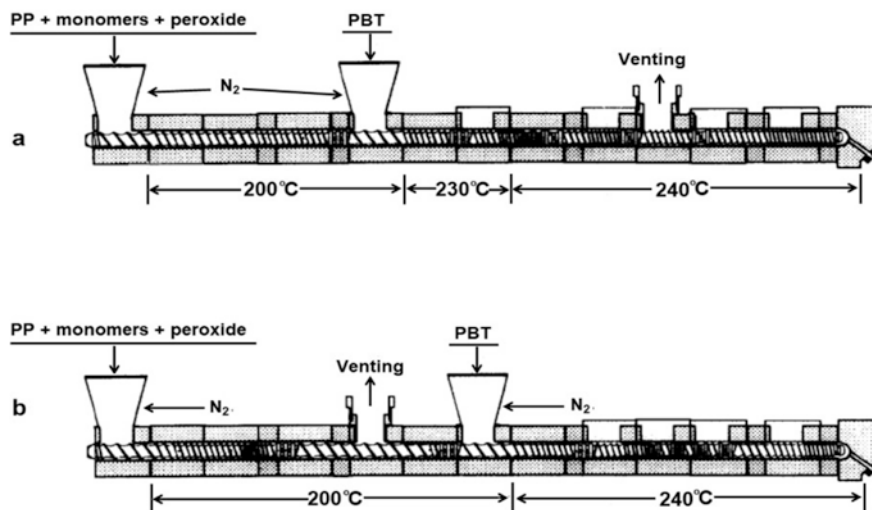
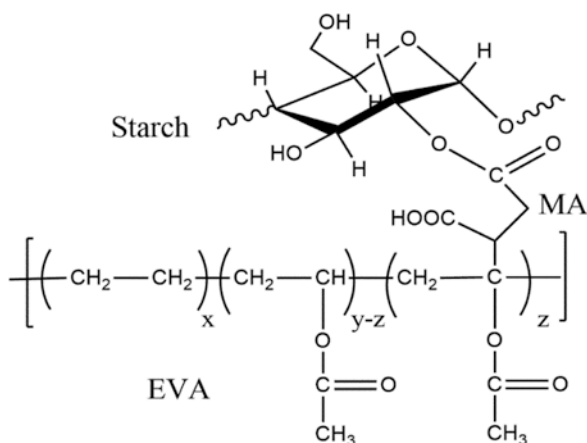


Fig. 3.22 The two screw configurations used for the *in situ* compatibilization of PP/PBT blends by one-step REX. Reproduced with permission from Sun et al. (1996)

Fig. 3.23 Grafting reaction between the EVA and starch *via* using MA to produce EVA-*g*-starch. Reproduced with permission from Ma et al. (2014c)



hopper. In addition, the devolatilization zone in the screw configuration (b) can also be extended more than in the configuration (a) in order to efficiently remove unreacted monomers and avoid any unwanted reaction between the unreacted monomer and the PBT.

Ma et al. (2014c) reported the preparation of PHB/EVA/starch ternary blends *via in-situ* grafting between EVA-*g*-starch and PHB. The EVA-*g*-starch was prepared separately in a twin-screw extruder at 135 °C and with a rotor speed of 100 rpm. The reactive compatibilization was conducted with the presence of MA, using BPO and

glycerol as a radical initiator and plasticizer, respectively. The possible MA-induced chemical interaction in the EVA-*g*-starch copolymer is shown in Fig. 3.23. The extruded PHB/EVA/starch blends were pelletized and compression-molded at 180 °C into the test specimens. In the grafting process between EVA and starch, the starch gelatinization occurs due to a combination of plasticizer elements, heat and shear during mixing, which resulted in the elimination of crystalline structure of starch (Ma et al. 2014c). However, the phase morphology of starch is usually thick due to its high Mw, hydrophilic nature and strong hydrogen bonds. In this grafting process, MA was introduced to alter the blends in a fine morphology, in order to produce better mechanical properties. The EVA-*g*-starch copolymers were generated *in-situ* at the interfaces to prevent the agglomeration of fine starch particles. As a result, a reduction in starch particle size in the blends by a factor of about 100 times was achieved. In addition, the PHB/EVA/starch ternary blends had a better affinity between starch and PHB due to the use of MA, thus reducing their particle size.

3.4.1.2 Two Steps or more Reactive Compatibilization

For example, Thirmizir et al. (2017) reported the use of maleated PHB-*co*-HHx (PHB-*co*-HHx-*g*-MA) as a compatibilizer for the PBS/PHB-*co*-HHx blend systems. The process was conducted *via* two steps REX. In the first step, the compatibilizer was produced by reactive melt grafting of MA onto PHB-*co*-HHx at 160 °C, using DCP as an initiator in a double-wing co-rotating internal mixer at 50 rpm rotor speed. The compatibilizer was also purified before use. For manufacturing blends, the 5 wt.% of PHB-*co*-HHx-*g*-MA was added to the PBS/PHB-*co*-HHx blends, and the reactive melt blending was conducted at 160 °C for 5 min. The blends were then compression molded at the same temperature and assessed using tensile and morphological analysis. The compatibilized blends had higher σ values in all the blend ratios compared to the uncompatibilized blends. The tensile modulus of the compatibilized blends was also higher than uncompatibilized blends. However, the ϵ_b values of the blends only experienced a significant increase effect at 20/80, 30/70 and 40/60 ratio from blends before remaining unchanged at 50/50 blend ratio. It is known that the incorporation of the PHB-*co*-HHx-*g*-MA compatibilizer helps promote a good interfacial interaction between both phases. As expected, the compatibilization between brittle and ductile polymers increased the ϵ_b values due to the improved stress transfer from the brittle phase to the ductile phase. The increase in the σ and T values denotes the improved mechanical properties. Therefore, these findings demonstrate that the addition of PHB-*co*-HHx-*g*-MA had a synergistic effect in improving the properties and morphologies of the blends towards a more cohesive and continuous structure (Thirmizir et al. 2017).

Persenaire et al. (2014) also investigated the reactive compatibilization of PLLA/PBS blends with the addition of maleated PBS and PLLA. These authors used reactive compatibilization of 2 steps, where the grafting process of the compatibilizers was prepared by REX using a twin-screw extruder at 120 °C and a low screw speed

of 30 rpm for developing PLLA-*g*-MA and PBS-*g*-MA. The compatibility of the blends was carried out separately in a batch mixer bench scale kneader at 190 °C with a reaction time sequence of 3 min at 30 rpm and 6 min at 60 rpm. The MA and the radical initiator Luperox® 101 concentrations were fixed at 3 wt.% and 0.5 wt.%, respectively, for both compatibilizers. The maleated compatibilizer was further purified to remove un-grafted MA and initiator. The grafted MA content was approximated to be 0.65 wt.% for PLLA-*g*-MA and 0.55 wt.% for PBS-*g*-MA. In addition, Persenaire et al. (2014) observed that the incorporation of 4 wt.% of PLLA-*g*-MA into PLLA/PBS blends 80/20 (w/w) exhibited the improvement of σ and ϵ_b values by 18% and 61%, respectively. With respect to the morphology of the blends, PLLA/PBS blends 80/20 (w/w) showed a dispersed phase morphology where the PBS drops were dispersed into the PLLA matrix, as shown in Fig. 3.24a. In contrast, the addition of PLLA-*g*-MA (4 wt.%) resulted in a drastic reduction in the size of the PBS drops, thus indicating a better dispersion of guest polymer. In fact, most of the drops were less than 1 μm in diameter, as shown in Fig. 3.24b. Furthermore, the polymer interface was improved as a result of the chemical interaction between both blend components.

Gardella et al. (2014) investigated the potential of PLA-*g*-MA as a compatibilizing agent for PLA/PCL blends. In this study, the maleated compatibilizer was prepared to be used in 2-step reactive compatibilization. The first step involved free radical grafting of MA onto PLA chains in the presence of 2,5-dimethyl-2,5-di-(*t*-butylperoxy)hexane peroxide initiator. The second step involved the compatibilization of the PLA/PCL blends with maleated PLA. As expected, the mechanical properties of the uncompatibilized blends were an average between the two polymers, depending on the ratio of the two components of blends. The module of the PLA/PCL blends was intermediate between those of PLA and PCL, while the ϵ_b did not significantly improve compared to that of pure PLA, indicating that there is no toughening effect of PCL. However, by incorporating maleated PLA, a direct relationship between the concentration of maleated PLA and the tensile modulus was

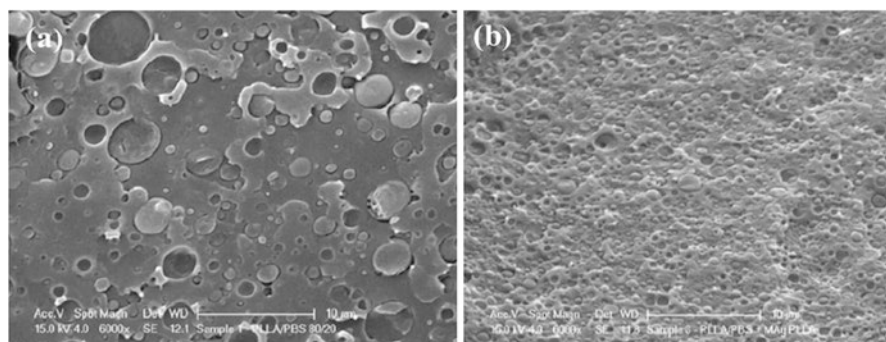


Fig. 3.24 SEM microphotographs of cryo-fractured surfaces of 80/20 (wt/wt) PLLA/PBS blends: (a) uncompatibilized and (b) PLLA-*g*-MA compatibilized. Reproduced with permission from Persenaire et al. (2014)

observed. In addition, ϵ_b values were significantly increased (650%) with the use of maleated PLA up to 7 wt.%, since at higher maleated PLA concentrations, ϵ_b values declined. According to Gardella et al. (2014) the increase in the tensile modulus and ϵ_b values of the PLA/PCL blends was related to the improved compatibility between the two phases. Nonetheless, at the high PLA-*g*-MA content, the loss of ductility obtained was observed.

3.4.2 Non-reactive Compatibilization of Biodegradable Blends

The method to improve the properties of the polymer with blending with other polymers has been well established in conventional polymers such as acrylonitrile butadiene styrene (ABS), poly(carbonate) (PC), polyolefins, etc. With respect to biodegradable polymers, modification as the toughening approach by adding elastomeric biodegradable polymer such as PCL has been reported in previous studies (Kalambur and Rizvi 2006; Barghini et al. 2010; Gardella et al. 2014). This type of non-reactive compatibilization is also effective for improving the T values by reducing the stiff characteristic of blends. However, it is generally unable to compensate for the reduction in strength of the blends due to two main factors, namely: (1) poor interfacial adhesion and (2) immiscibility between the components of the blend. To overcome these drawbacks and achieve more valuable properties, several methods have been introduced, e.g. the addition of block copolymers such as PCL-poly(ethylene glycol) (PEG) copolymer, PCL-PLA diblock, triblock and random copolymers and poly(ethylene oxide) (PEO)-poly(phenylene oxide) (PPO)-PEO triblock copolymer (Imre and Pukánszky 2013). In the immiscible blends, block-copolymer plays a role as a compatibilizer between the components of the blend, which reduces the interfacial tension between them (Muthuraj 2015). While, the incorporation of diblock-copolymer can improve the stability of the blend as it tends to segregate at the interface between the two components. In addition, the graft or block copolymer is designed to reduce the interfacial tension and create strong interfacial adhesion, which leads to reduced particle size of the dispersed phase and makes it more stable against coalescence during the melt processing (Karami et al. 2019).

According to Kim and Park (1999), a random or block copolymer of two or more biodegradable polymers can be produced by transesterification reaction using an appropriate catalyst (di-*n*-butyltin-dilaurate at 0.5 wt.%) at high temperature to accelerate the reaction. These authors demonstrated that the degree of transesterification between PBS and PTB increased linearly with increasing reaction time and the use of catalyst. The possible copolymer structure derived from the transesterification reaction between PBS and PBT is listed in Fig. 3.25. Kim and Park (1999) observed from the DSC and the dynamic mechanical thermal analysis (DMTA) that although the PBS/PBT blends were immiscible, with the introduction of the PBS-PBT copolyester, the degree of miscibility between both components was improved.

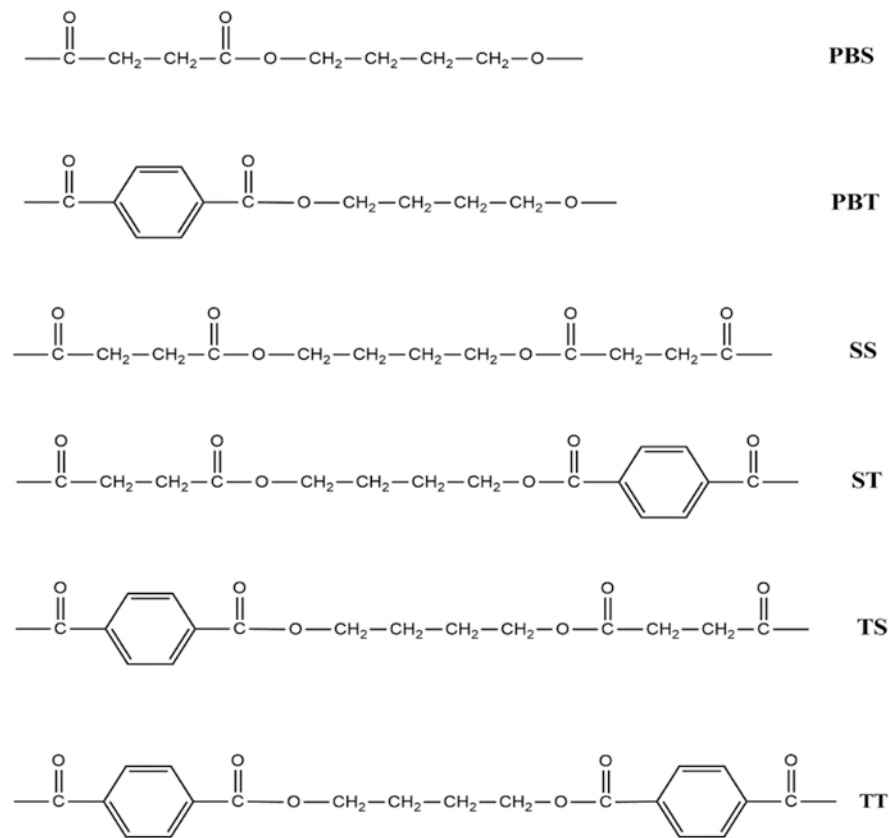


Fig. 3.25 Possible copolymer structures of the transesterification reaction between PBS and PBT. Reproduced with permission from Kim and Park (1999)

3.5 Crosslinking of Biodegradable Polymer Blends

Polymer blends are materials commonly used in the plastics industry for various applications, such as adhesives, coatings, composites, foams, molded products and many more. Many techniques can improve the blend properties. One of the simplest techniques is the introduction of organic peroxide crosslinking between blend components. The crosslinked blends are more compatible blends compared to simple blends due to improved interfacial adhesion between the components of the blend which can improve the mechanical properties of the blends as a whole (Mishra and Wonho 2011).

Keeping this in view, Mishra et al. (2007) reported on the development of PCL/ENR blends crosslinked with DCP as the peroxide crosslinking agent produced by the melt blending technique in an internal mixer at 160 °C for 8 min. The

crosslinking effect was improved the σ and ϵ_b values from the PCL/ENR (50/50) blends. It was believed that peroxide (DCP) introduced inter-chain crosslinking between PCL and ENR as presented in Fig. 3.15. Mishra et al. (2007) suggested that the compatibility of the interchain reaction *via* crosslinking of peroxide radical is similar to that of blends with the addition of block copolymers, which leads to an increased σ and ϵ_b values. While in a homopolymer system, the introduction of crosslinking normally increases the stiffness and causes a decrease in the ϵ_b values (Fei et al. 2004). Mishra et al. (2007) also reported that the crosslinked blends have a slightly lower modulus compared to uncrosslinked blends, possibly due to the alteration of at least one or more of the following factors: degree of crosslinking, entanglement network, number of binding molecules and crystallinity (Mishra et al. 2007).

Aside from that, many other studies have reported the use of peroxides as a crosslinking agent in the blend systems such as BPO (Hu et al. 2018) and DCP (Fei et al. 2004; Semba et al. 2006; Mishra et al. 2007; Dong et al. 2013; Ji et al. 2014). Dong et al. (2013) reported the introduction of partial crosslinking in PHB/PDLLA blends by using DCP as a free radical initiator *via* melt blending at 170 °C and a rotation speed of 40 rpm. The DCP was added after 4 min. of mixing, and the blends were processed for another 2 min. The formation of free radicals in the PHB and PDLLA chains was initiated by peroxide *via* a hydrogen absorption mechanism. The grafting of PHB/PDLLA blends was produced at the interface through a combination of free radicals on both components and also occurred in the PHB and PDLLA rich phases, separately (Dong et al. 2013). As a result, complex products such as branched/crosslinked PHB branched/crosslinked PDLLA, PHB-crosslinked-PDLLA network and PHB-g-PDLLA copolymers could be produced.

Following Dong et al. (2013) the melt blending technique also caused chain scissions due to the low thermal stability of the free radicals and PHB polymer. The

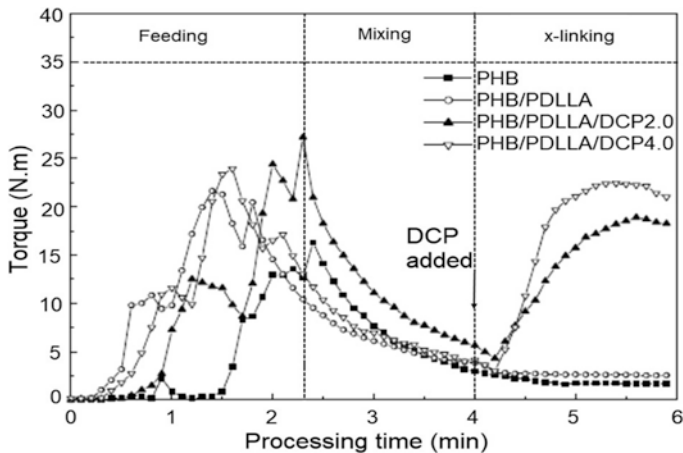


Fig. 3.26 Effect of DCP on the torque *vs* processing time during blending. Reproduced with permission from Dong et al. (2013)

crosslinking and chain scissions occurred through a six-member ring transition, which is difficult to avoid. The crosslinking and chain scission are two competitive reactions. These phenomena could be seen during the mixing process, where the torque value increases when the DCP is introduced until it reaches a maximum value and then dropping with a prolonged mixing time. This observation was also recorded by Dong et al. (2013) as indicated by the curves in the crosslinking zone (Fig. 3.26). Since the peroxide crosslinking only occurred somewhere of the blends. This is known as partial crosslinking systems.

Table 3.7 summarizes the properties of biodegradable blends crosslinked by peroxides that have been studied by previous researchers.

Table 3.7 Comparison of properties of biodegradable blends crosslinked by peroxides

Polymer Matrix		Peroxides		Preparation methods	Mechanical properties		References
Blends	Ratio	Type	Content (wt. %)		σ (MPa)	ϵ_b (%)	
PLA/PBAT	80/20	DCP	0.05	Internal mixed at 170 °C and 50 rpm. Compression molding at 170 °C and 10 MPa.	42.1	213	Semba et al. (2006)
			0.1		43.5	309	
			0.2		44.6	277	
			0.5		45.9	244	
			1.0		46.0	29	
PHBV/PBS	80/20	DCP	0.2	Internal mixed at 170 °C and 40 rpm. Compression molding at 170 °C and 10 MPa.	29.0	200	Ma et al. (2012)
			0.5		28.0	400	
			1.0		27.0	350	
PHB/PBS	80/20	DCP	0.5	Internal mixed at 170 °C and 40 rpm. Compression molding at 170 °C and 10 MPa.	40.0	4	Ma et al. (2012)
	70/30				38.0	11	
	50/50				37.0	15	
PLA/PBS	80/20	DCP	0.1	Internal mixed at 180 °C and 50 rpm. Compression molding at 180 °C and 10 MPa.	68.0	134	Ji et al. (2014)
			0.2		73.0	195	
			0.3		80.0	205	
			0.4		77.0	151	
			0.5		72.0	92	
PLA/PCL	70/30	DCP	0.1	Internal mixed at 180 °C and 60 rpm. Compression molding at 180 °C.	52.0	40	Semba et al. (2006)
			0.2		49.0	160	
			0.3		48.0	140	
PBS/PLA	20/80	BPO	0.1	Solution blending in chloroform at 65 °C. Compression molding at 160 °C.	16.0	76.0	Hu et al. (2018)
			0.3		16.3	97.3	
			0.5		18.1	157.3	
			0.7		17.8	247.9	
			1.0		16.8	399.9	
			1.5		15.3	223.9	
			2.0		15.4	159.9	

3.6 Crosslinked-Compatibilized of Biodegradable Blends

Compatibilization is a chemical process that was introduced to improve the adhesion between the phases of the blends, facilitate chain dispersion, reduce interfacial tension and stabilize the morphology of the blends (James et al. 2009). On the other hands, crosslinking in the context of polymer blends refers to *in-situ* free radical crosslinking which introduces partial crosslinking inter- and intra-components from blends. Crosslinking leads to a more cohesive interfacial interaction and phase distribution. In this chapter, the effect of phase compatibilization-crosslinking synergism is further discussed. Many studies on compatibilization of polymer blends *via* crosslinking have been focused on non-biodegradable polymers, as will be cited in the literatures below. In this section, we will demonstrate that such a technique can also be used to improve the properties of biodegradable blends.

In a review made by Koning et al. (1998) revealed the compatibilization reaction of polymer blends through a combination of peroxides and multifunctional chemicals. The peroxide is used to activate the reaction between a polymer and the functional groups of the chemical. The multifunctional chemical then bound to the polymer chains in graft or branch copolymers, which is the real compatibilizer. The combination of a peroxide and unsaturated monomers such as hydroxypropylmethacrylate, low Mw unsaturated rubber, MA, St, triallyl isocyanurate, and undefined silane is actually similar to the peroxide/co-agent systems that are commonly used for crosslinking of conventional polymers (e.g. EPDM, PE and PP). The main advantage of the crosslinked-compatibilized reaction is to increase the efficiency of the peroxide and the reaction rate. While for a single compatibilization reaction system, the crosslinking or compatibilization will experience a lack of chemical selectivity and the improvement of properties will not be pronounced.

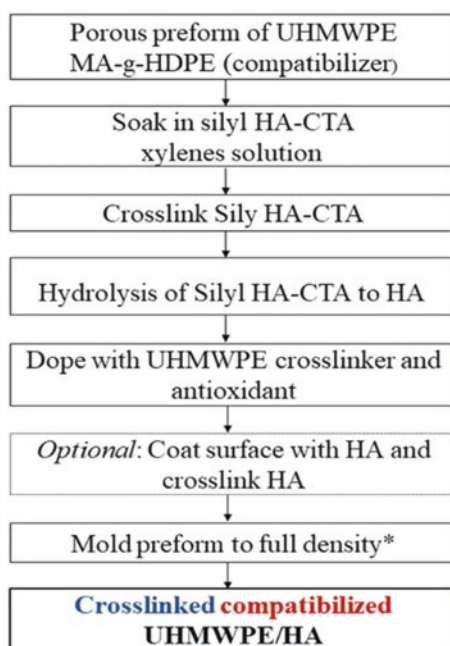
Xu et al. (1993), reported on the synergistic effect of crosslinking-compatibilization in poly(vinyl chloride) (PVC)/LDPE blends in the presence of butadiene-acrylonitrile rubber (NBR) unsaturated monomer as a compatibilizing agent and DCP organic peroxides as a crosslinking agent. A two-roll mixer produced the blends at 155 °C. In compatible PVC/LDPE blends, the NBR was added to shear forces during blending by increasing the melt viscosity of the LDPE and reducing the lubrication effect on PVC phase. As a result, the dispersion of the blends was improved as indicated by the reduction domain size of the dispersed phase. On the other hand, in the DCP-crosslinked PVC/LDPE blends, an increase in mechanical properties was recorded due to the formation of the co-crosslinked product. Without the NBR compatibilizer, the interphase area between two components was quite small, which made the co-crosslinking reaction at the interface region difficult, thus resulting in minimal improvements in the mechanical properties. In PVC/LDPE blends, crosslinked-compatibilized with DCP and NBR, provided a significant improvement in the σ and ϵ_b values. In this system, the possibility of a crosslinking agent residing in the interfacial area is greater due to the better phase dispersion which is promoted by the NBR compatibilizer. In addition, with the presence of DCP, a greater number of co-crosslinked products could be formed

to promote a more cohesive interfacial interaction. The phase morphology of the crosslinked-compatible blends shows an unclear interface and smaller domains, which indicates the successful synergism of crosslinked-compatible reaction between the blending system.

James et al. (2009) reported the crosslinked-compatible reaction between ultra-high Mw polyethylene (UHMWPE) and natural hyaluronan (HA) polysaccharide for biomaterial applications. These authors used MA-grafted high-density polyethylene (HDPE-g-MA) as a compatibilizer and DCP organic peroxide as a crosslinking agent. In this case, the anhydride group of MA reacted with the hydroxyl groups onto the HA to form ester bonds, while the hydrophobic chain portion of the compatibilizer diffused and entangles with the UHMWPE chains. Aside from that, HDPE-g-MA also helps improve the processability since the HDPE portion of the compatibilizer has a lower T_m compared to pure UHMWPE, which makes the molding process easier and spends less thermal energy compared to the molding of pure blends. To crosslink the compatible UHMWPE/HA, DCP was introduced as a crosslinking agent *via* dipping the compatible UHMWPE/HA preform in a DCP/antioxidant solution. This novel crosslinked-compatible process is simplified in Fig. 3.27.

James et al. (2009) also subjected the blends to a wear resistance test conducted in 90% bovine calf serum at 37 ± 1 °C, applying a load cycle with a maximum force of 330 N at a frequency of 1.6 Hz. The duration of the test was almost two million cycles. The authors found that the wear rates of crosslinked and crosslinked compatible UHMWPE/HA were non-significant compared to the control (50 kGy

Fig. 3.27 Crosslinked compatible UHMWPE/HA process. Reproduced with permission from James et al. (2009)



irradiated and stabilized PE GUR 1050) at 1.98 million cycles. Within the same cycles, the total wear of crosslinked compatibilized UHMWPE/HA was 5.54 mg, while the total wear of the control sample was 3.56 mg. The lower wear (mg) and wear rates (mg/million cycles) of crosslinked and crosslinked compatibilized blends, compared to pure blends, demonstrated the effectiveness of crosslinking-compatibilization reaction on the wear resistance properties of UHMWPE/HA blends.

3.7 Performance Evaluation

In this section, the evaluation of the performance of biodegradable polymer blends will be further discussed in terms of water performance or exposed to moisture, natural weathering, and biodegradation in the natural environment. The discussion will also cover the effect of the type of polymer, the blending system and type of additives used to alter or improve the properties of the blends.

3.7.1 Water Absorption

Some applications of biodegradable polymers involve a greater understanding of the durability and the possibility of the macroscopic properties. Functional groups, such as carboxylic acid, hydroxyl and lactide, as well as other hydrophilic molecules, can increase the level of moisture, which leads to higher degradation rates. Water absorption causes a severe alteration of the properties of biodegradable polymer blends, including chemical and physical modifications such as hydrolysis, interface debonding and plasticization (Hiljanen-Vainio et al. 1996).

In addition, water absorption is highly dependent on the morphology of polymer blends (Choi et al. 2002). In this case, the morphology cannot only affect water absorption based on crystallinity but also *via* the existence of microvoids or porosity (Drumright et al. 2000). The degree of crystallinity plays an important role in determining barrier properties, as well as the water absorption of the polymers. Berthé et al. (2010) revealed that crystallinity seemed to be the most influential factor rather than Mw to determine the water absorption properties of two different PLLA resins. These authors also found that PLLA resin with greater crystallinity induced less water absorption. According to Berthé et al. (2010), high crystallinity possibly reduced the mobility of the chain that could hinder the water diffusion into the polymer. Zhang et al. (1995) also investigated water absorption and hydrolytic degradation of PCL, PLA and PLA/PCL blends, and reported that highly crystalline PCL was more hydrophobic compared to amorphous PLA, which could explain the greater water absorption of PLA compared to PCL. Meanwhile, the water absorption of PLA/PCL (25/75 and 50/50) blends was between that of simple PCL and PLA. Interestingly, it was found that the PLA/PCL (75/25) blend exhibited greater

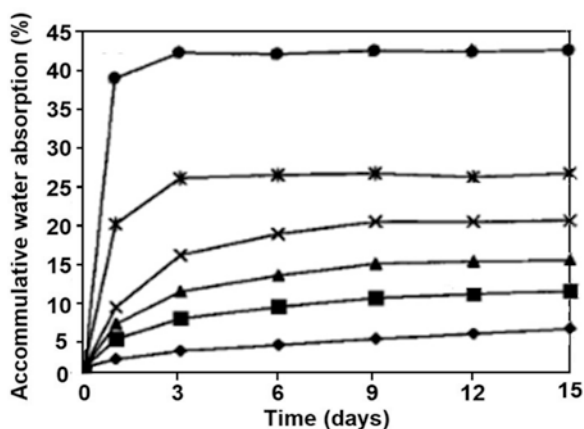
water absorption compared to the PLA component. Zhang et al. (1995) also stated that this was contributed by a higher content of the amorphous region and its two-phase nature of the blends. Realizing the importance of having a crystalline phase, some studies have focused on increasing the crystallinity of biodegradable blends (Bucci et al. 2007; Zhang and Thomas 2011). The incorporation of PHB, a highly crystalline biopolymer into the PLA matrix by melt blending, is a relatively easy approach to increase crystallinity and control the properties of the blends. Similar T_m values also allowed both polymers to be blended in the melt state. In the previous work of Arrieta et al. (2014), the PLA was melt blended with 25 w.% of PHB and showed an improved water resistance, the oxygen barrier and the reduction of the high transparency typical of PLA.

The presence of microvoids has also allowed water molecules to migrate into the blends and increase the rate of hydrolysis. Therefore, in some case, water absorption from biodegradable polymer blends is followed by hydrolysis that can also affect the absorption rate. Pitt et al. (1992) reported that the water absorption of the blends from poly(glycolic acid-*co*-lactic acid) (PGLA) and poly(vinyl alcohol) (PVA) increased rapidly at an early stage and then gradually decreased due to hydrolysis of PGLA in the blends. In contrast, Tsuji and Muramatsu (2001) not observed this behavior for PLLA/PVA blends. Rather, the water adsorption increased with immersion time and then reached saturation in 10 h, regardless of the blend ratio. This was due to the low hydrolysis rate of PLLA compared to that of PGLA.

It has also been reported that the hydrolysis rate constant (k) for PLLA and PGLA is $2.59 \times 10^{-3} \text{ day}^{-1}$ (Tsuji et al. 2000) and 7.44×10^{-2} (Cha and Pitt 1990), respectively. Hydrolysis of polymers is influenced by chemical structure (crosslinking, co-monomers) (Li and McCarthy 1999), crystallinity (Li and McCarthy 1999), Mw (Bastioli 2005), pH (Bastioli 2005), polydispersity (Lépine and Gilbert 2002), shape of the sample (Grizzi et al. 1995), temperature (Dell'Erba et al. 2001) and traces of catalysts (Sodergard and Stolt 2002).

On the other hand, blending biodegradable polymer with starch is a good way to balance cost-effective problems and obtain new material that has outstanding

Fig. 3.28 Water absorption of starch/PLA blends at different ratios depending on water soaking time. Reproduced with permission from Tianyi and Xiuzhi (2000)



properties (Ren et al. 2009). However, the starch is hydrophilic in nature due to the hydroxyl groups present in its structure. Tianyi and Xiuzhi (2000) studied the effects of the blend ratio of starch and PLA on the physical properties of the blends, including water absorption. Figure 3.28 shows the water absorption as a function of soaking time of PLA/starch blends at different ratios. Water absorption was increased sharply on day 1 and then stabilized on day 3 regardless of the blend ratio. According to Tianyi and Xiuzhi (2000), starch was mainly responsible for the water absorption of the blends. Tianyi and Xiuzhi (2000) also reported that the PLA formed a good continuous phase that covers the starch component at a lower starch content ($< 60\%$), resulting in less water absorption (Fig. 3.29). As the starch content increased to $>60\%$, the degree of the discontinuous phase of PLA increased considerably (Fig. 3.29). The water penetration into the blends could occur *via* voids and be absorbed by starch, resulting in greater water absorption values. A similar observation was reported in several studies of various biodegradable aliphatic polyester/starch blends (Lai et al. 2006; Yu et al. 2006; Liao and Wu 2009).

In the literature, a great effort has been made to modify the properties of starch-based blends in order to obtain blends with better dispersion, miscibility and morphology, as well as less water absorption. The increase in water resistivity is important because starch disintegrates in water and loses its properties when exposed to environmental humidity, since both amylose and amylopectin are swollen in the presence of water (Liao and Wu 2009). Zeng et al. (2011) also found that the incorporation of hydrophobic PBS significantly reduces the water sensitivity in TPS/PBS blends compared to TPS alone. This is understandable, since PBS is hydrophobic. Interestingly, Yin et al. (2015) obtained a further improvement in water resistance in maleated PBS-containing blends due to good dispersion, homogeneous microstructure of starch and well dispersion of starch particles hindering the diffusion of water molecules into TPS/PBS blends. Similarly, Wu (2003) found that at the same starch content, maleated PCL (PCL-*g*-MA/starch) blends showed

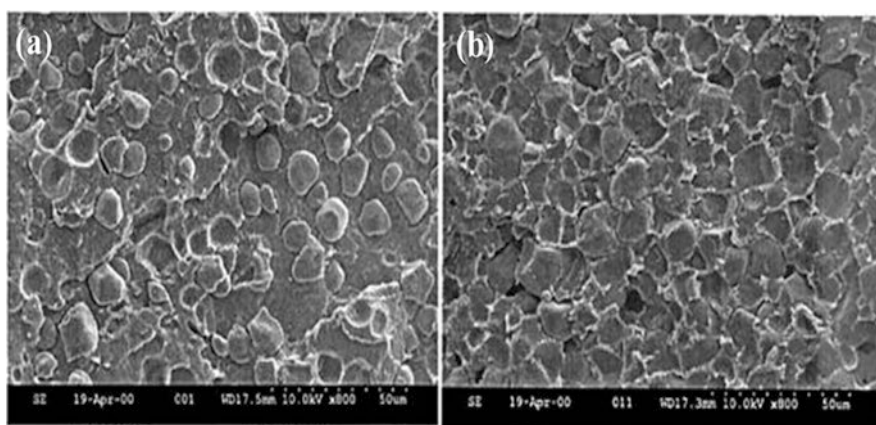


Fig. 3.29 Scanning electron microscopy of corn starch/PLA blends: (a) 20:80 and (b) 80:20. Reproduced with permission from Tianyi and Xiuzhi (2000)

moderately good water resistance compared to PCL/starch blends. The author deduced that this was due to a good miscibility between the components of the blend because of the presence of the carbonyl ester group in the blends.

3.7.2 Weathering

The weathering test is conducted within a specific time to measure the durability of the material towards the elements of environmental exposure. These elements are relative humidity/water, solar radiation, temperature and/or other environmental variables such as pollutants (dirt, dust, nitrogen oxides, sand and sulphur oxides) that can deteriorate the properties of the polymer, and polymer blends and composites (Li 2000; Falk et al. 2001; Matuana et al. 2002; Ariawan et al. 2017). Several studies have also reported that color fading, loss of mechanical properties, surface erosion and weight loss are the most common harmful effects on the polymeric materials that have been exposed to the weathering test (Lopez et al. 2006). Among all the weathering elements, it is important to analyze the solar radiation that induces photo-degradation of polymers, since it greatly influences the properties of polymers during their in-life service, especially in outdoor applications.

Solar radiation induces photo-degradation due to the absorption of UV radiation, which promotes chemical and physical alterations. The complex process of photo-degradation involves a sequence of reactions which produce radicals that progress as a sequence of chain mechanisms where peroxides are the oxidation initiators. The presence of a stabilizer and the material structure influences the properties of the final and stable end products. Fully formed products appear as an oxygen-containing structure caused by the collateral reactions (chain branching) or by the self-decaying of peroxy radicals (chain termination) as shown in Fig. 3.30.

On the other hand, few studies have reported on the degradation mechanism of biodegradable polymer blends. In most studies, comparisons between the blends and the original homopolymers in terms of stability have been made (Kaczmarek and Podgoorski 2004; Therias et al. 2010). In some cases, polymer blends with two or more components have less stable combinations (Waldman and De Paoli, 2008).

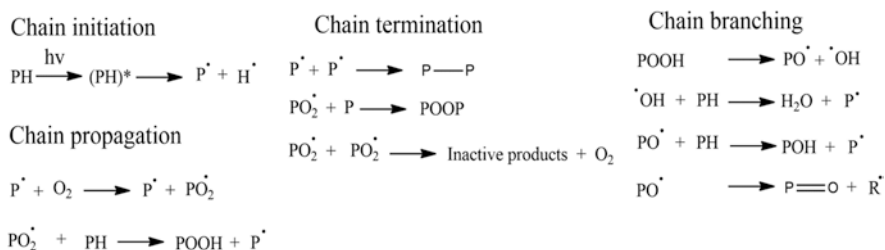


Fig. 3.30 Photodegradation of most polymers by exposure to UV rays. Reproduced with permission from Rosu and Visakh (2016)

The formation of free radicals in the less stable polymer degrades the more stable polymer. In most blends, the degradation rate of the blends was among that of the components of the blend. However, such a relationship is not obvious or direct due to several factors involved, and the mechanism of radical transport from one polymer to another is not simple. In addition, the photodegradation behavior of polymer blends is greatly influenced by the components of the blend which may deviate from the single polymer system due to chemical interactions between the different species in the blends during degradation and interactions between the degradation products. These chemical reactions can lead to an acceleration of the degradation rate (Kowalonek 2016) or a stabilizing effect (Botta et al. 2009; Fernandes et al. 2010). For example, Rivaton et al. (1998) studied the photolysis rate on PP/PBT

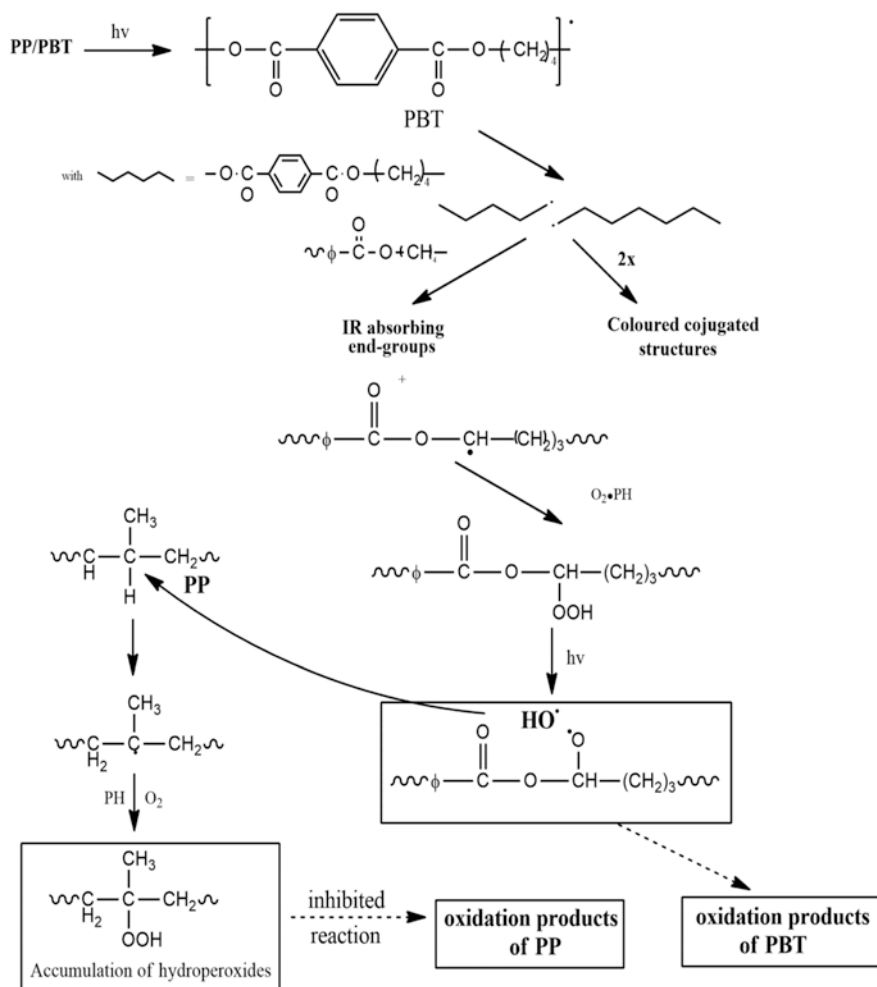


Fig. 3.31 Photolysis of PP/PBT blends. Reproduced with permission from Rivaton et al. (1998)

blends, and found that photo yellowing was more prevalent for the PP/PBT blend than PBT alone. These authors clarified that the appearance of a more extensive yellowing was due to the macroradicals formed by the photochemical hemolysis of the ester bonds in PBT that cannot extract hydrogen atoms from the PP chains. Figure 3.31 illustrates the mechanism of photolysis, as suggested by the authors. The mechanism includes cross-degradation of the polymer resulting in acceleration degradation of the blends.

However, in some polymer blends a stabilizing effect could occur. For example, Rivaton et al. (1998) studied polymer blends made from PP containing between 5 and 80% of PE exposed to UV radiation. A blend containing 5% PE endured the maximum degradation, and the degradation became less severe as the concentration of PE increased. This is in line with the performance of the individual polymers where PE had a better resistance since it does not contain susceptible tertiary hydrogens. In this case, the properties of the blends are the sum of the properties of their components. Meanwhile, Kaczmarek et al. (2011) suggested that the PEC/PVA blend is an example in which the blends have superior properties than the sum of the components. As confirmed by the authors, through spectroscopic analysis, they stated that intermolecular interactions between PEC and PVA explained the effect of mutual stabilization.

Among the various research works conducted on polymer blends, studies on biodegradable polymer blends under the weathering test are limited. With this in mind, Persenaire et al. (2014) investigated the weathering behavior of biodegradable polymers in a varied blending ratio of PLLA/PBS with and without the use of MA as a compatibilizer. These authors found that the addition of PBS to PLLA accelerated the degradation of the blend. In addition, PBS demonstrates a higher degradation rate than PLLA. As a consequence, its dispersion in the PLLA matrix improved the PLLA degradability. When considering the PLLA/PBS blend at a 80/20 (w/w) composition as the optimal ratio of polymer blends, the authors deduced that PBS tends to promote the degradation of PLLA in the presence of compatibilizer. Meanwhile, uncompatibilized blends seem less degradable compared to pure PLLA. This phenomenon was attributed to the existence of homogeneously dispersed carboxylic acids produced by PBS degradation, which preferred the hydrolysis of the PLLA matrix.

It can thus be concluded that the prediction of the degradation of polymer blends is not directly related to the behavior of the pure component. The composition of the blend and the possible presence of a compatibilizer can strongly affect the degradation behavior of a polymer blend. The degradation means of the pure components may differ from the blends since interactions can occur between the different components in the blends during degradation or between the degradation products. Therefore, the additive rule cannot be used for the degradation of polymer blends. Apparently, the degradation rate of a polymer blend may be greater, intermediate or lower than that of the pure components. The chemical and physical changes of degraded blends are comparable to those that occur in the single polymer. The possible changes in carbonyl index, the hydroxyl/hydroperoxide index, the optical

density of the material can be determined by deterioration of the mechanical properties, IR, UV-Vis, gel content and cloud point determination (Wypych 2008).

3.7.3 Biodegradability

Most conventional polymers are petroleum based, have good resistance against biological degradation (biodegradation), and therefore, exist in the environment for many years (Muniyasamy et al. 2016). This problem has motivated researchers to develop biobased and biodegradable polymers (Gutiérrez 2018a; Toro-Márquez et al. 2018; Gutiérrez et al. 2019; Herniou-Julien et al. 2019). In addition, these polymers have mechanical properties comparable to conventional polymers and have been used as eco-friendly materials in various industries such as automotive, medical, packaging, pharmaceutical and consumer products (Gutiérrez 2018b; Gutiérrez and Alvarez 2017d). They are also widely used for single-use applications and short-term applications, such as food packaging, trash bags, mulch films, personal products and some home care products (Muniyasamy et al. 2016; Merino et al. 2018a, b; 2019a, b).

However, these biodegradable polymers have several drawbacks, such as poor mechanical properties and resistance to environmental degradation, as well as low thermal resistance. For that reason, several approaches have been imposed to modify biodegradable polymers using blending, compatibilization, crosslinking and a combination of them to improve the chemical, thermal and physical properties. Other than that, the lifetime of a biodegradable polymer can be tailored by incorporating additives (e.g. antioxidants, antioxidants, plasticizers and other chemicals) (Gutiérrez 2018c, d; Gutiérrez and Alvarez 2018; Gutiérrez, Herniou-Julien et al. 2018).

Consequently, further studies should be carried out to understand the influence of the modification of chemical, thermal, physical and mechanical properties on the biodegradability and degradation performance of biodegradable polymers in natural environments. Therefore, it is necessary to carry out an exhaustive study on the degradation and biodegradation mechanisms of these polymers to ensure their safe use in various end-use applications. Several international norms and standards can be adopted and used to test the biodegradability properties of biodegradable polymers in a natural environment. The biodegradation rate can also be measured through loss of mechanical properties, morphology variations and weight reduction under different environmental conditions (Muniyasamy et al. 2016). Several standards can be also used as guidelines for biodegradation analysis, such as ASTM D5338–15, biodegradation under composting conditions and ASTM D5988–12, biodegradation under soil burial condition.

Biodegradation can be described as the decomposition of materials by the action of microorganisms, which involve the recycling of carbon, the mineralization of organic compounds and the production of biomass (Lucas et al. 2008). Biodegradation occurs in three steps: biodeterioration, biofragmentation and

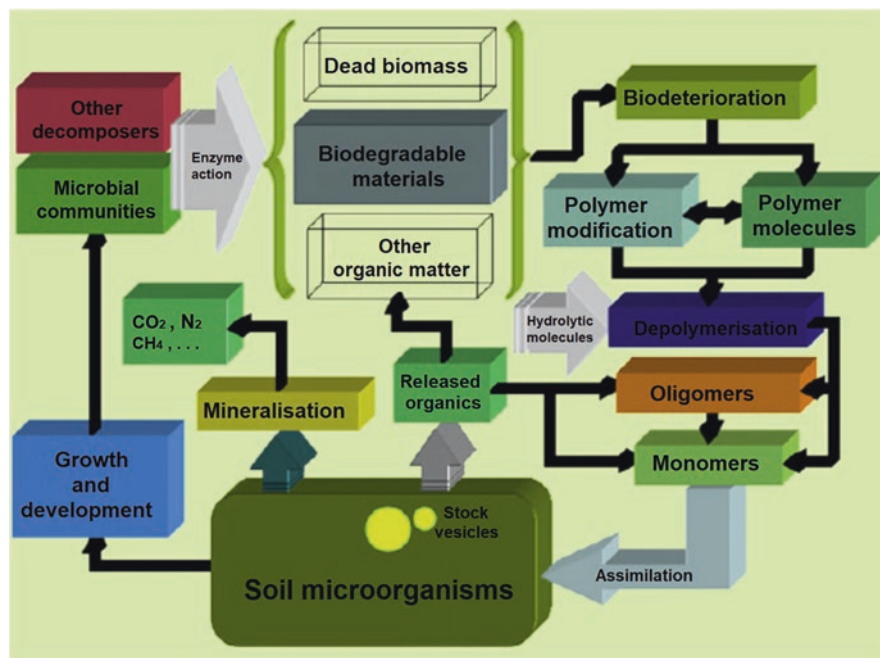


Fig. 3.32 Polymer biodegradation process. Reproduced with permission from Lucas et al. (2008)

assimilation, without neglecting the participation of abiotic factors (Fig. 3.32). The biodegradation of polymeric materials involves several steps, so the process can be stopped at each stage, as shown in Fig. 3.34.

According to Lucas et al. (2008), the biodegradation process involves several stages. Starting with biodeterioration *via* the combined reaction of microbes, other decomposing organisms or/and abiotic factors, biodegradable plastics become small pieces. This is followed by depolymerization by microorganism-secreted catalytic agents (e.g. free radicals and enzymes) that can reduce the polymer molecules into oligomers, dimers and monomers. Certain molecules are identified by microbial cell receptors and can cross the plasmic membrane. The other molecules remain in the extracellular environment and may be object to different changes. Next is assimilation, where in the cytoplasm, the transported molecules are integrated by microbial metabolism to produce storage vesicles, energy and new biomass. The last stage is mineralization, where some simple and complex metabolites can be excreted and reach the extracellular environment (e.g. aldehydes, antibiotics, organic acids, terpenes, etc.). Simple molecules such as CH_4 , CO_2 , H_2O , N_2 and various salts from intracellular metabolites are completely oxidized and released into the environment.

In addition, polymeric products exposed to outdoor conditions (i.e. aging, burying and weathering) may experience abiotic degradation that will deteriorate the chemical, light, mechanical and thermal properties of polymers.

Keeping this in view, Muniyasamy et al. (2016) reported the biodegradation of PHBV, PLA and PLA/PHBV blends under composting and soil burial conditions according to ASTM D5338–15 and ASTM D5988–12, respectively. The degree of biodegradation was calculated as a percentage of the overall theoretical CO₂. For biodegradation under control composting condition, the test was conducted for 200 days. According to the results, no significant amount of CO₂ emission was observed for both pure PHBV and PLA during the first 32 days of compost incubation. After the initial phase, the blends reached 70% biodegradation rate in 120 days and a slight static phase that achieved a 92% biodegradation in 200 days. This slow biodegradation could be due to the crystalline and brittle nature of the PLA. While the delayed degradation of PHBV could be due to an approx. 12% valeric acid content present in the degradation of PHBV polymer.

On the other hand, Muniyasamy et al. (2016) reported that the PLA/PHBV blends showed about 20% biodegradability in the first 32 days because the blending process could break the crystalline structure of the PLA, as well as the surface-enriched heterogeneous phase in one constituent. In terms of physical degradation, all samples (PHBV, PLA and PLA/PHBV blends) began to experience fragmentation after 32 days. The size of fragmented samples became smaller over time and apparently could not be detected in the composting medium after 45 days, thus indicating that the composting environment conditions were adequate for the primary degradation (i.e. fragmentation/disintegration) to occur.

Regarding biodegradation under the soil burial environment, the pure PHBV and PLA/PHBV blends exhibited about 30% biodegradability after 120 days while pure PLA showed no significant biodegradability even after 200 days of exposition. Following Muniyasamy et al. (2016) results indicated the pure PHBV and PLA/PHBV blends have a better degree of biodegradability under the soil burial environment compared to pure PLA. The PLA had a better biodegradation capability under industrial composting conditions than in soil burial because the PLA requires environment temperature in order to trigger hydrolytic degradation of its Mw before allowing the action of microbial degradation (thermophilic bacteria and fungi).

Lucas et al. (2008) mentioned that another way in which the polymer can undergo chemical degradation during biodegradation in the compost or in the soil environment is by hydrolysis. Polymers containing hydrolysable functional groups, such as amide, anhydride, carbamide, ester and ether can be hydrolyzed. However, the degradation reaction depends on some parameters such as pH, temperature, time and water activity. The crystalline fraction could prevent the diffusion of oxygen and water, thus limiting hydrolytic degradation. While amorphous domains which disorganize molecular regions are prone to oxidative and hydrolytic degradations. Lucas et al. (2008) proposed the schematic reaction of the PLA hydrolysis under acidic and alkaline condition as examples of abiotic degradation *via* chemical degradation, as shown in Figs. 3.33 and 3.34, respectively.

These biodegradation conditions require adequate controls of moisture content, pH and temperature, and a specific thermophilic microorganism, which is only available in an industrial composting facility to adequately test the biodegradation of plastic materials. In addition, the biodegradation of polymer blends depends

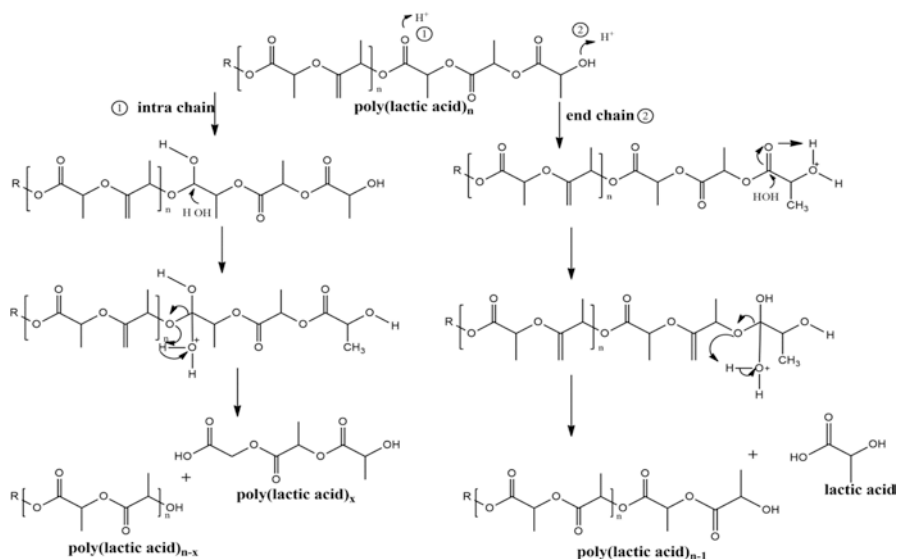


Fig. 3.33 PLA hydrolysis under acidic conditions. Reproduced with permission from Lucas et al. (2008)

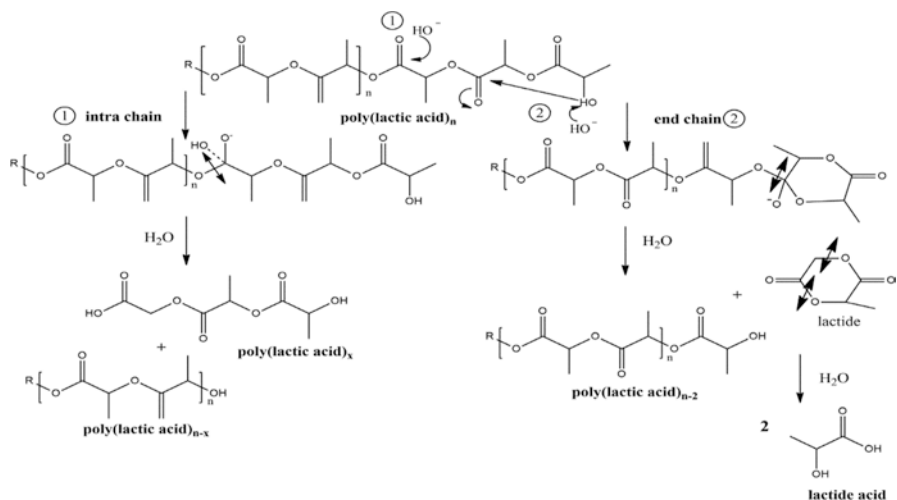


Fig. 3.34 PLA hydrolysis under alkaline conditions. Reproduced with permission from Lucas et al. (2008)

largely on the ratio of the components and the type of polymer blend. For example, Zhang and Thomas (2011) observed that the PHB/PLA blends and the components of the blends experienced a different degradation mechanism. In this sense, the PHB is mainly degraded by the reaction of several enzymes on the surface, while the

degradation of the PLA begins with non-enzymatic hydrolysis, which depends largely on the ambient temperature.

In another study by Liu et al. (2019) reported the species of soil bacteria responsible for the biodegradation of PHB, PLA and their blends. In this accelerated biodegradation test, the soil bacteria were collected and cultured several times, approximately three times in the generation of bacterial culture (Gen III) until a stable bacterial community was achieved before the biodegradation test. The bacteria were then inoculated into a vial filled with several nonwoven samples and grown for 15 days on a shaker at 150 rpm at room temperature. As expected, the morphological observation revealed that the incubation of nonwoven blends for 15 days with the soil bacterial resulted in severe degradation with different changes, such as the presence of pores and microcracks on the nonwoven samples. In line with this, the CO₂ evolved during the 15 day of incubation period also exhibited an increasing percentage of biodegradation over time.

Liu et al. (2019) in order to identify bacterial species that may be responsible in the biodegradation process, extracted the Gen III bacteria DNA and then subjected to pyrosequencing analysis. From the sequencing analysis, the relative abundance of marker gene sequences in the samples was associated with members of the genera *Citrobacter*, *Lysinibacillus* (phylum Firmicutes) and *Pseudomonas* (phylum Proteobacteria), which demonstrates that these newly identified bacterial species can play an important role in the biodegradation of PHB/PLA-blended nonwovens (Liu et al. 2019). Several species belong to the genus *Citrobacter*, such as *C. amalonaticus*, *C. freundii* and *C. koseri*, which have been reported to use polyhydroxyl compounds as the sole carbon source (Liu et al. 2019).

According to Shah et al. (2008), the biodegradation rate of polymer blends is mainly controlled by the degradation of the most susceptible biodegradation components with respect to the type of presence of bacteria and the environmental condition. Table 3.8 shows a list of microorganisms that could degrade biodegradable polyesters.

To date, limited studies have reported on the biodegradability of biodegradable polymer blends and the effect of the compatibilizer and crosslinking agent on the biodegradation rate. With this in mind, a slower biodegradation for compatibilized blends in another mixing systems (biodegradable/non-biodegradable polymer blends) such as PC/PLA (Lee et al. 2011), PHB/PP (Sadi et al. 2013) and PBS/PP (Bionelle/CPP) blends (Zainuddin et al. 1999) have been informed.

As reported by Zainuddin et al. (1999), the addition of Modic compatibilizer into PBS/PP blends improved the dispersion of the dispersed phase into finer droplets, thus allowing the microbes to attack randomly and penetrate the blends as a whole matrix. However, the biodegradability of the compatibilized blends seems to depend on the ratio of the blends. At the 25/75 blend ratio, the biodegradability was considerably lower is due to the PBS droplets since they were protected from microbial attacks and degradation by the surrounding PP layer as the interfacial interaction between the components of blend. On the contrary, the degradation rates appear to increase exponentially up to 75% PBS content due to the changes in the morphology of the blends and the presence of higher PBS-rich area.

Table 3.8 Different degrading microorganisms of biodegradable polyesters

Plastic	Microorganism
Poly(3-hydroxybutyrate-co-3-mercaptopropanoate)	<i>Schlegelella thermodepolymerans</i>
Poly(3-hydroxybutyrate-co-3-mercaptopropionate)	<i>Pseudomonas indica</i> K2
P(3HB)	<i>Alcaligenes faecalis</i>
P(3HB)	<i>Caenibacterium thermophilum</i> <i>Schlegelella thermodepolymerans</i>
P(3HB)	<i>Pseudomonas lemoignei</i>
P(3HB) PHBV	<i>Streptomyces sp.</i> SNG9
Poly(hydroxybutyrate-co-3-hydroxypropionate)	<i>Ralstonia pikeitii</i> T1
Poly(hydroxybutyrate-co-3-hydroxypropionate)	<i>Acidovorax sp.</i> TP4
P(3HB) poly(3-hydroxypropionate) poly(4-hydroxybutyrate)	<i>Alcaligenes faecalis</i>
PES poly(ethylene adipate)	<i>Comamonas acidovorans</i> <i>Pseudomonas stutzeri</i>
PHBV	<i>Clostridium acetobutylicum</i> <i>Clostridium acetobutylicum</i> <i>Clostridium botulinum</i> <i>Clostridium botulinum</i>
PCL	<i>Clostridium acetobutylicum</i> <i>Clostridium botulinum</i>
PCL	<i>Fusarium solani</i>
PLA	<i>Amycolatopsis sp.</i> <i>Bacillus brevis</i> <i>Fusarium moniliforme</i> <i>Penicillium Roquefort</i> <i>Rhizopus delemer</i>

Source: Shah et al. (2008)

Hu et al. (2018) investigated the effect of BPO as a crosslinking agent on the biodegradable properties of PBS/PLA blends. In this study, the biodegradation rate was determined by the enzymatic degradation of proteinase K from the *Tritirachium album*. The hydrophobic interaction of proteinase K is well known to be the main cause of degradation of PLA. Aside from that, it could reside on the surface of PLA and be able to change its conformation to create the catalytic site to hydrolyze PLA around the enzyme molecules. Hu et al. (2018) reported that the BPO-crosslinked PBS/PLA blends showed a better resistance to enzymatic degradation of proteinase K than pure PLA. It is known that PBS is relatively less susceptible to degradation of proteinase K than PLA and that the incorporation of PBS in the blends reduces the degradation rate of the blends. In addition, the introduction of peroxide crosslinking can change the structure of the blends and limit degradation by proteinase K (Hu et al. 2018). Along with the degradation, the surface morphology of PBS/PLA/BPO blends changed from the filament to the segments and finally to the particles as structures. It can also be concluded from the work of Hu et al. (2018) that the uncrosslinked PLA fraction was degraded first and left the crosslinked PLA/PBS

filaments in the blends. Then, the fragments of crosslinked PLA began to degrade, causing the filaments to change to segments and eventually to particles. The remaining particles or fragments could be associated with the PBS and a portion of non-degraded crosslinked PLA. The results obtained in this study were useful to tailor the biodegradation characteristic of the new biodegradable polymers and can also be used to understand the biodegradation mechanisms in new polymers or mixing systems.

3.8 Conclusions

In recent decades, biodegradable polymers have been developed, along with many published studies on biodegradable polymers. The research in this field is focused on strategies to improve the mechanical, thermal and biodegradable properties of polymers through many approaches, such as compatibilization, copolymerization, crosslinking and addition of reinforcement or functional additives.

In terms of compatibilizer, maleated compatibilizers have been the most studied and are well established in the polymer industry. It has also been demonstrated that the incorporation of maleated compatibilizers improves the mechanical properties of binary and ternary biodegradable polymer blends. The maleated compatibilizer also reduces the interfacial energy, which results in a reduction of the size of the dispersed phase. It is known that the presence of active chemical sites on the MA (i.e. the double bond and the carboxylic acid group) is a powerful electron-accepting monomer and reactive. The most extensive method to produce compatibilizer is by the melt grafting technique, which involves the grafting of MA onto polymer in a molten state with the presence of a free radical initiator. MA has been used successfully as a monomer to graft onto biodegradable polymers such as PBS, PBSA, PCL and PLA to produce maleated compatibilizer.

Other than that, crosslinking by means of radical peroxides is an interesting strategy that has been widely used to stabilize and improve the properties of biodegradable polymer blends due to its simplicity and efficiency. Among these peroxides, DCP is the most widely used peroxide crosslinking agent in the biodegradable polymer blend system. The use of peroxides promotes the formation of chain branches, as well as crosslinking, which increases the T_g , the modulated crystalline content and the thermal behavior of polymer blends. The crosslinking reaction is also an effective means to improve interfacial adhesion in immiscible polymer blends by initiating the appearance of mixed chains (copolymers), which act as compatibilizers at the interfaces. The formation of chain branching or crosslinking by heterogeneous and/or homogeneous radical coupling reactions also depends on the concentration of peroxides and the reaction temperature used.

In addition, reactive compatibilization, either by incorporating a maleated compatibilizer or peroxide-induced crosslinking, can be performed in one step (*in-situ*) or two-step extrusion, depending on the available processing equipment and the system of blends and additives used. In addition to the compatibilization and

crosslinking approaches, the combination of the crosslinked-compatibilization approach seems to be more effective for improving the mechanical properties such as σ , ϵ_b and T of the biodegradable polymer blends. The synergistic effect of crosslinking and compatibilization is produced due to the presence of a compatibilizer, which reduces the interfacial energy and forms a better interfacial adhesion which in turn helps the guest polymer to be well dispersed, thus providing larger interface area between the components of the blend. When the peroxide radical crosslinking agent is added, the higher number of crosslinking will be formed at the interface region, thus resulting in a significant increase in the properties of the blends.

Finally, the performance of biodegradable blends depends on the moisture or water exposure. Likewise, the biodegradation rate of polymers in the natural environment depends largely on the characteristics of the components of the blend and how they interact with environmental factors. Additions of compatibilizer or crosslinking agent have improved the resistance of the blends to environmental degradation. However, due to limited studies on the effect of compatibilizer and crosslinking agent on the performance of biodegradable polymer blends and natural degradation, a comprehensive study is necessary to understand the degradation mechanism and its safe use in many applications. International norms and standards should be used to test the degradation properties of biodegradable polymers in the natural environment in order to allow these materials to be used safely in consumer products.

Acknowledgement The authors gratefully acknowledge the financial support by the Long Term Research Grant Scheme (Account No: 1001/PKT/6725002) from the Ministry of Education Malaysia and Short Term Research Grant (Account No: 304.PBAHAN.60312042) from the Universiti Sains Malaysia (USM). Thanks for the research facilities by the Cluster for Polymer Composites, Science and Engineering Research Centre, Universiti Sains Malaysia. The authors would also like to express their gratitude to all researchers that make this book chapter possible.

Conflicts of Interest The authors declare no conflict of interest.

References

- Abdul, R. H., Wahab, M. S., & Wahit, M. U. (2013). Improvement of mechanical properties of polycaprolactone (PCL) by Addition of nano-montmorillonite (MMT) and hydroxyapatite (HA). *Applied Mechanics and Materials*, 315(2013), 815–819. <https://doi.org/10.4028/www.scientific.net/amm.315.815>.
- Ahmad Thirmezir, M. Z. (2011). *Characterization of kenaf bast fibre filled poly(butylene succinate) composites : Mechanical, water absorption and weathering*. Universiti Sains Malaysia.
- Thirmezir, M. A., Ishak, Z. M., Taib, R. M., Rahim, S., & Jani, S. M. (2011). Kenaf-bast-fiber-filled biodegradable poly(butylene succinate) composites: Effects of fiber loading, fiber length, and maleated poly(butylene succinate) on the flexural and impact properties. *Journal of Applied Polymer Science*, 122(5), 3055–3063. <https://doi.org/10.1002/app.34046>.
- Sigmaaldrich.com. (n.d.). Applications: free radical initiators. Retrieved June 26, 2020, from https://www.sigmaaldrich.com/content/dam/sigma-aldrich/docs/Aldrich/General_Information/thermal_initiators.pdf?utm_source=redirect&utm_medium=promotional&utm_campaign=insite_thermal_initiators

- Arrieta, M. P., Samper, M. D., López, J., & Jiménez, A. (2014). Combined effect of poly(hydroxybutyrate) and plasticizers on polylactic acid properties for film intended for food packaging. *Journal of Polymers and the Environment*, 22(4), 460–470. <https://doi.org/10.1007/s10924-014-0654-y>.
- Barghini, A., Ivanova, V. I., Imam, S. H., & Chiellini, E. (2010). Poly(ϵ -caprolactone) (PCL) and poly(hydroxy-butyrates) (PHB) blends containing seaweed fibers: Morphology and thermal-mechanical properties. *Journal of Polymer Science, Part A: Polymer Chemistry*, 48(23), 5282–5288. <https://doi.org/10.1002/pola.24327>.
- Bastioli, C. (2005). Handbook of biodegradable polymers. Rapra Technology Limited. Available in: [http://appliedchem.unideb.hu/biodegradabilis/bastioli%20c.%20\(ed\)%20-%20handbook%20of%20biodegradable%20polymers%20-%20\(rapra%202005\).pdf](http://appliedchem.unideb.hu/biodegradabilis/bastioli%20c.%20(ed)%20-%20handbook%20of%20biodegradable%20polymers%20-%20(rapra%202005).pdf)
- Berthé, V., Ferry, L., Bénézet, J. C., & Bergeret, A. (2010). Ageing of different biodegradable polyesters blends mechanical and hygrothermal behavior. *Polymer Degradation and Stability*, 95(3), 262–269. <https://doi.org/10.1016/j.polymerdegradstab.2009.11.008>.
- Botta, L., Dintcheva, N. T., & La Mantia, F. P. (2009). The role of organoclay and matrix type in photo-oxidation of polyolefin/clay nanocomposite films. *Polymer Degradation and Stability*, 94(4), 712–718. <https://doi.org/10.1016/j.polymerdegradstab.2008.12.017>.
- Bucci, D. Z., Tavares, L. B. B., & Sell, I. (2007). Biodegradation and physical evaluation of PHB packaging. *Polymer Testing*, 26(7), 908–915. <https://doi.org/10.1016/j.polymeresting.2007.06.013>.
- Can, E., Bucak, S., Kinaci, E., Çalikoğlu, A. C., & Köse, G. T. (2014). Polybutylene succinate (PBS)-polycaprolactone (PCL) blends compatibilized with poly(ethylene oxide)-*block*-poly(propylene oxide)-*block*-poly(ethylene oxide) (PEO-PPO-PEO) copolymer for biomaterial applications. *Polymer - Plastics Technology and Engineering*, 53(11), 1178–1193. <https://doi.org/10.1080/03602559.2014.886119>.
- Cha, Y., & Pitt, C. G. (1990). The biodegradability of polyester blends. *Biomaterials*, 11(2), 108–112. [https://doi.org/10.1016/0142-9612\(90\)90124-9](https://doi.org/10.1016/0142-9612(90)90124-9).
- Chen, C., Peng, S., Fei, B., Zhuang, Y., Dong, L., Feng, Z., Chen, S., & Xia, H. (2003). Synthesis and characterization of maleated poly(3-hydroxybutyrate). *Journal of Applied Polymer Science*, 88(3), 659–668. <https://doi.org/10.1002/app.11771>.
- Chen, G.-Q., & Luo, R.-C. (2009). Polyhydroxyalkanoate blends and composites polyhydroxy-alkanoate blends and composites. In L. Yu (Ed.), *Biodegradable polymer blends and composites from renewable resources* (pp. 239–286). New Jersey: John Wiley & Sons. <https://doi.org/10.1002/9780470391501.ch11>.
- Choi, N. S., Kim, C. H., Cho, K. Y., & Park, J. K. (2002). Morphology and hydrolysis of PCL/PLLA blends compatibilized with P(LLA-*co*- ϵ CL) or P(LLA-*b*- ϵ CL). *Journal of Applied Polymer Science*, 86(8), 1892–1898. <https://doi.org/10.1002/app.11134>.
- Dell'Erba, R., Groeninckx, G., Maglio, G., Malinconico, M., & Migliozzi, A. (2001). Immiscible polymer blends of semicrystalline biocompatible components: Thermal properties and phase morphology analysis of PLLA/PCL blends. *Polymer*, 42(18), 7831–7840. [https://doi.org/10.1016/s0032-3861\(01\)00269-5](https://doi.org/10.1016/s0032-3861(01)00269-5).
- Deng, Y., & Thomas, N. L. (2015). Blending poly(butylene succinate) with poly(lactic acid): Ductility and phase inversion effects. *European Polymer Journal*, 71, 534–546. <https://doi.org/10.1016/j.eurpolymj.2015.08.029>.
- Doi, Y., Kitamura, S., & Abe, H. (1995). Microbial synthesis and characterization of poly(3-hydroxybutyrate-*co*-3-hydroxyhexanoate). *Macromolecules*, 28(14), 4822–4828. <https://doi.org/10.1021/ma00118a007>.
- Dong, W., Ma, P., Wang, S., Chen, M., Cai, X., & Zhang, Y. (2013). Effect of partial crosslinking on morphology and properties of the poly(β -hydroxybutyrate)/poly(D,L-lactic acid) blends. *Polymer Degradation and Stability*, 98(9), 1549–1555. <https://doi.org/10.1016/j.polymerdegradstab.2013.06.033>.
- Drumright, R. E., Gruber, P. R., & Henton, D. E. (2000). Polylactic acid technology. *Advanced Materials*, 12(23), 1841–1846. [https://doi.org/10.1002/1521-4095\(200012\)12:23<1841::aid-adma1841>3.0.co;2-e](https://doi.org/10.1002/1521-4095(200012)12:23<1841::aid-adma1841>3.0.co;2-e).

- Environment Australia. (2012). Biodegradable plastics – Developments and environmental impacts. Melbourne. Available in: <http://www.europeanplasticfilms.eu/docs/australianreportonbiodegradableplastics.pdf>
- Fei, B., Chen, C., Chen, S., Peng, S., Zhuang, Y., An, Y., & Dong, L. (2004). Crosslinking of poly[(3-hydroxybutyrate)-co-(3-hydroxyvalerate)] using dicumyl peroxide as initiator. *Polymer International*, 53(7), 937–943. <https://doi.org/10.1002/pi.1477>.
- Fernandes, L. L., Freitas, C. A., Demarquette, N. R., & Fechine, G. J. M. (2010). Photodegradation of thermodegraded polypropylene/high-impact polystyrene blends: Mechanical properties. *Journal of Applied Polymer Science*, 120(2), 770–779. <https://doi.org/10.1002/app>.
- Fink, J. K. (2013). *Reactive polymers fundamentals and applications: A concise guide to industrial polymers* (Second ed., p. 576). William Andrew. <https://doi.org/10.1016/c2012-0-02516-1>.
- Gao, H., Xie, Y., Ou, R., & Wang, Q. (2012). Grafting effects of polypropylene/polyethylene blends with maleic anhydride on the properties of the resulting wood-plastic composites. *Composites Part A: Applied Science and Manufacturing*, 43(1), 150–157. <https://doi.org/10.1016/j.compositesa.2011.10.001>.
- Gardella, L., Calabrese, M., & Monticelli, O. (2014). PLA maleation: An easy and effective method to modify the properties of PLA/PCL immiscible blends. *Colloid and Polymer Science*, 292(9), 2391–2398. <https://doi.org/10.1007/s00396-014-3328-3>.
- Grizzi, I., Garreau, H., Li, S., & Vert, M. (1995). Hydrolytic degradation of devices based on poly(dl-lactic acid) size-dependence. *Biomaterials*, 16(4), 305–311. [https://doi.org/10.1016/0142-9612\(95\)93258-f](https://doi.org/10.1016/0142-9612(95)93258-f).
- Gumede, T. P., Luyt, A. S., & Müller, A. J. (2018). Review on PCL, PBS, and PCL/PBS blends containing carbon nanotubes. *Express Polymer Letters*, 12(6), 505–529. <https://doi.org/10.3144/expresspolymlett.2018.43>.
- Gutiérrez, T. J., & Alvarez, V. A. (2017a). Data on physicochemical properties of active films derived from plantain flour/PCL blends developed under reactive extrusion conditions. *Data in Brief*, 15, 445–448. <https://doi.org/10.1016/j.dib.2017.09.071>.
- Gutiérrez, T. J., & Alvarez, V. A. (2017b). Eco-friendly films prepared from plantain flour/PCL blends under reactive extrusion conditions using zirconium octanoate as a catalyst. *Carbohydrate Polymers*, 178, 260–269. <https://doi.org/10.1016/j.carbpol.2017.09.026>.
- Gutiérrez, T. J., & Alvarez, V. A. (2017c). Properties of native and oxidized corn starch/polystyrene blends under conditions of reactive extrusion using zinc octanoate as a catalyst. *Reactive and Functional Polymers*, 112, 33–44. <https://doi.org/10.1016/j.reactfunctpolym.2017.01.002>.
- Gutiérrez, T. J., & Alvarez, V. A. (2017d). Films made by blending poly(ϵ -caprolactone) with starch and flour from sagu rhizome grown at the Venezuelan Amazons. *Journal Polymers and the Environment*, 25(3), 701–716. <https://doi.org/10.1007/s10924-016-0861-9>.
- Gutiérrez, T. J., & Alvarez, V. A. (2018). Bionanocomposite films developed from corn starch and natural and modified nano-clays with or without added blueberry extract. *Food Hydrocolloids*, 77, 407–420. <https://doi.org/10.1016/j.foodhyd.2017.10.017>.
- Gutiérrez, T. J. (2018a). Chapter 9. Biodegradability and compostability of food nanopackaging materials. In G. Cirillo, M. A. Kozłowski, & U. G. Spizzirri (Eds.), *Composite materials for food packaging* (pp. 269–296). EE.UU. ISBN: 978-1-119-16020-5: WILEY-Scrivener Publisher. <https://doi.org/10.1002/9781119160243.ch9>.
- Gutiérrez, T. J. (2018b). Biological macromolecule composite films made from sagu starch and flour/poly(ϵ -caprolactone) blends processed by blending/thermo molding. *Journal Polymers and the Environment*, 26(9), 3902–3912. <https://doi.org/10.1007/s10924-018-1268-6>.
- Gutiérrez, T. J. (2018c). Active and intelligent films made from starchy sources/blackberry pulp. *Journal Polymers and the Environment*, 26(6), 2374–2391. <https://doi.org/10.1007/s10924-017-1134-y>.
- Gutiérrez, T. J. (2018d). Are modified pumpkin flour/plum flour nanocomposite films biodegradable and compostable? *Food Hydrocolloids*, 83, 397–410. <https://doi.org/10.1016/j.foodhyd.2018.05.035>.

- Gutiérrez, T. J., Guarás, M. P., & Alvarez, V. A. (2017). Chapter 9. Reactive extrusion for the production of starch-based biopackaging. In M. A. Masuelli (Ed.), *Biopackaging* (pp. 287–315). Miami, EE.UU.. ISBN: 978-1-4987-4968-8; Editorial CRC Press Taylor & Francis Group. <https://doi.org/10.1201/9781315152349-9>.
- Gutiérrez, T. J., Herniou-Julien, C., Álvarez, K., & Alvarez, V. A. (2018). Structural properties and *in vitro* digestibility of edible and pH-sensitive films made from guinea arrowroot starch and wastes from wine manufacture. *Carbohydrate Polymers*, *184*, 135–143. <https://doi.org/10.1016/j.carbpol.2017.12.039>.
- Gutiérrez, T. J., Toro-Márquez, L. A., Merino, D., & Mendieta, J. R. (2019). Hydrogen-bonding interactions and compostability of bionanocomposite films prepared from corn starch and nano-fillers with and without added Jamaica flower extract. *Food Hydrocolloids*, *89*, 283–293. <https://doi.org/10.1016/j.foodhyd.2018.10.058>.
- Harrats, C., & Groeninckx, G. (2007). Reactive processing of polymer blend using reactive compatibilization and dynamic crosslinking: Phase morphology control and microstructure – Property relations. In F. Ciardelli & S. Penczek (Eds.), *Modification and blending of synthetic and natural macromolecules* (pp. 155–199). Dordrecht: Kluwer Academic Publishers. https://doi.org/10.1007/978-1-4020-2735-2_9.
- He, X., Zheng, S., Huang, G., & Rong, Y. (2013). Solution grafting of maleic anhydride on low-density polyethylene: Effect on crystallization behavior. *Journal of Macromolecular Science, Part B: Physics*, *52*(9), 1265–1282. <https://doi.org/10.1080/00222348.2013.764217>.
- Hiljanen-Vainio, M., Varpomaa, P., Seppälä, J., & Törmälä, P. (1996). Modification of poly(L-lactides) by blending: mechanical and hydrolytic behavior. *Macromolecular Chemistry and Physics*, *197*(4), 1503–1523. <https://doi.org/10.1002/macp.1996.021970427>.
- Herniou-Julien, C., Mendieta, J. R., & Gutiérrez, T. J. (2019). Characterization of biodegradable/non-compostable films made from cellulose acetate/corn starch blends processed under reactive extrusion conditions. *Food Hydrocolloids*, *89*, 67–79. <https://doi.org/10.1016/j.foodhyd.2018.10.024>.
- Hu, X., Su, T., Li, P., & Wang, Z. (2018). Blending modification of PBS/PLA and its enzymatic degradation. *Polymer Bulletin*, *75*(2), 533–546. <https://doi.org/10.1007/s00289-017-2054-7>.
- Imre, B., & Pukánszky, B. (2013). Compatibilization in bio-based and biodegradable polymer blends. *European Polymer Journal*, *49*(6), 1215–1233. <https://doi.org/10.1016/j.eurpolymj.2013.01.019>.
- James, S. P., Kurkowski Rachael, O., Zhang, M., & Schwartz, H. (2009). UHMWPE/hyaluronan microcomposite biomaterials. In S. M. Kurtz (Ed.), *UHMWPE biomaterials handbook: Ultra High Molecular Weight Polyethylene in Total joint replacement and medical devices* (2nd ed., pp. 259–276). London: Academic. <https://doi.org/10.1016/b978-0-12-374721-1.00018-3>.
- Ji, D., Liu, Z., Lan, X., Wu, F., Xie, B., & Yang, M. (2014). Morphology, rheology, crystallization behavior, and mechanical properties of poly(lactic acid)/poly(butylene succinate)/dicumyl peroxide reactive blends. *Journal of Applied Polymer Science*, *131*(3), 1–8. <https://doi.org/10.1002/app.39580>.
- John, J., Tang, J., Yang, Z., & Bhattacharya, M. (1997). Synthesis and characterization of anhydride-functional polycaprolactone. *Journal of Polymer Science, Part A: Polymer Chemistry*, *35*(6), 1139–1148. [https://doi.org/10.1002/\(sici\)1099-0518\(19970430\)35:6<1139::aid-pola17>3.0.co;2-7](https://doi.org/10.1002/(sici)1099-0518(19970430)35:6<1139::aid-pola17>3.0.co;2-7).
- Kaczmarek, H., Dabrowska, A., & Vukovic-Kwiatkowska, I. (2011). Accelerated weathering of pectin/poly(vinyl alcohol) blends studied by spectroscopic methods halina. *Journal of Applied Polymer Science*, *122*(3), 1936–1945. <https://doi.org/10.1002/app.34298>.
- Kaczmarek, H., & Podgoorski, A. (2004). Photostability of poly(vinyl chloride)/poly(vinyl alcohol) blends. *Molecular Crystals and Liquid Crystals*, *416*(3), 479–484. <https://doi.org/10.1080/15421400490482916>.
- Kalambur, S., & Rizvi, S. S. H. (2006). An overview of starch-based plastic blends from reactive extrusion. *Journal of Plastic Film and Sheeting*, *22*(1), 39–58. <https://doi.org/10.1177/8756087906062729>.

- Karami, S., Nazockdast, H., Ahmadi, Z., Rabolt, J. F., Noda, I., & Chase, D. B. (2019). Microstructure effects on the rheology of nanoclay-filled PHB/LDPE blends. *Polymer Composites*, 40(10), 4125–4134. <https://doi.org/10.1002/pc.25273>.
- Kim, Y. J., & Park, O. O. (1999). Miscibility and biodegradability of poly(butylene succinate)/poly(butylene terephthalate) blends. *Journal of Environmental Polymer Degradation*, 7(1), 53–66. <https://doi.org/10.1023/a:1021846219775>.
- Koning, D., Pagnouille, & Jerome. (1998). Strategies for compatibilization of polymer blends. *Progress in Polymer Science*, 23(97), 707–757. [https://doi.org/10.1016/s0079-6700\(97\)00054-3](https://doi.org/10.1016/s0079-6700(97)00054-3).
- Kowalonek, J. (2016). Surface studies of UV-irradiated poly(vinyl chloride)/poly(methyl methacrylate) blends. *Polymer Degradation and Stability*, 133, 367–377. <https://doi.org/10.1016/j.polyimdegradstab.2016.09.016>.
- Lai, S. M., Don, T. M., & Huang, Y. C. (2006). Preparation and properties of biodegradable thermoplastic starch/poly(hydroxy butyrate) blends. *Journal of Applied Polymer Science*, 100(3), 2371–2379. <https://doi.org/10.1002/app.23085>.
- Laycock, B., Halley, P., Pratt, S., Werker, A., & Lant, P. (2014). The chemomechanical properties of microbial polyhydroxyalkanoates. *Progress in Polymer Science*, 39(2), 397–442. <https://doi.org/10.1016/j.progpolymsci.2013.06.008>.
- Lee, J. B., Lee, Y. K., Choi, G. D., Na, S. W., Park, T. S., & Kim, W. N. (2011). Compatibilizing effects for improving mechanical properties of biodegradable poly(lactic acid) and polycarbonate blends. *Polymer Degradation and Stability*, 96(4), 553–560. <https://doi.org/10.1016/j.polyimdegradstab.2010.12.019>.
- Lépine, L., & Gilbert, R. (2002). Thermal degradation of polyacrylic acid in dilute aqueous solution. *Polymer Degradation and Stability*, 75(2), 337–345. [https://doi.org/10.1016/s0141-3910\(01\)00236-1](https://doi.org/10.1016/s0141-3910(01)00236-1).
- Li, S., & McCarthy, S. (1999). Influence of crystallinity and stereochemistry on the enzymatic degradation of poly(lactide)s. *Macromolecules*, 32(13), 4454–4456. <https://doi.org/10.1021/ma990117b>.
- Liao, H. T., & Wu, C. S. (2009). Preparation and characterization of ternary blends composed of polylactide, poly(ϵ -caprolactone) and starch. *Materials Science and Engineering A*, 515(1–2), 207–214. <https://doi.org/10.1016/j.msea.2009.03.003>.
- Liu, Y., Zhan, Z., Ye, H., Lin, X., Yan, Y., & Zhang, Y. (2019). Accelerated biodegradation of PLA/PHB-blended nonwovens by a microbial community. *RSC Advances*, 9(18), 10386–10394. <https://doi.org/10.1039/c8ra10591j>.
- Martin, L. W. (2019). Overview of Maleic-Anhydride-Grafted Polyolefin Coupling Agents. Retrieved April 14, 2019, from http://www.temp.speautomotive.com/SPEA_CD/SPEA2012/pdf/TP/TP9.pdf
- Lucas, N., Bienaime, C., Belloy, C., Queneudec, M., Silvestre, F., & Nava-Saucedo, J.-E. (2008). Polymer biodegradation: Mechanisms and estimation techniques – A review. *Chemosphere*, 73(4), 429–442. <https://doi.org/10.1016/j.chemosphere.2008.06.064>.
- Ma, P., Xu, P., Chen, M., Dong, W., Cai, X., Schmit, P., Spoelstra, A. B., & Lemstra, P. J. (2014c). Structure-property relationships of reactively compatibilized PHB/EVA/starch blends. *Carbohydrate Polymers*, 108(1), 299–306. <https://doi.org/10.1016/j.carbpol.2014.02.058>.
- Ma, P., Cai, X., Wang, W., Duan, F., Shi, D., & Lemstra, P. J. (2014a). Crystallization behavior of partially crosslinked poly(β -hydroxyalkanoates)/poly(butylene succinate) blends. *Journal of Applied Polymer Science*, 131(21), 1–8. <https://doi.org/10.1002/app.41020>.
- Ma, P., Hristova-Bogaerds, D. G., Lemstra, P. J., Zhang, Y., & Wang, S. (2012). Toughening of PHBV/PBS and PHB/PBS blends via in situ compatibilization using dicumyl peroxide as a free-radical grafting initiator. *Macromolecular Materials and Engineering*, 297(5), 402–410. <https://doi.org/10.1002/mame.201100224>.
- Ma, P., Jiang, L., Ye, T., Dong, W., & Chen, M. (2014b). Melt free-radical grafting of maleic anhydride onto biodegradable poly(lactic acid) by using styrene as a comonomer. *Polymers*, 6(5), 1528–1543. <https://doi.org/10.3390/polym6051528>.

- Mani, R., Bhattacharya, M., & Tang, J. (1999). Functionalization of polyesters with maleic anhydride by reactive extrusion. *Journal of Polymer Science: Part A: Polymer Chemistry*, 37(11), 1693–1702. [https://doi.org/10.1002/\(sici\)1099-0518\(19990601\)37:11<1693::aid-pola15>3.0.co;2-y](https://doi.org/10.1002/(sici)1099-0518(19990601)37:11<1693::aid-pola15>3.0.co;2-y).
- Mani, R., & Bhattacharya, M. (2008). Properties of injection moulded blends of starch and modified biodegradable polyesters. *European Polymer Journal*, 37(3), 515–526. [https://doi.org/10.1016/s0014-3057\(00\)00155-5](https://doi.org/10.1016/s0014-3057(00)00155-5).
- Mantere, L. (2015). *Functional polyethylene as a compatibilizer in blends of recycled polyethylenes and polyamides*. Tampere University of technology.
- Markham, R. L. (1990). Introduction to compatibilization of polymer blends. *Advances in Polymer Technology*, 10(3), 231–236. <https://doi.org/10.1002/adv.1990.060100307>.
- Mehrabzadeh, M. (2009). Maleic anhydride grafting onto HDPE by in situ reactive extrusion and its effect on intercalation and mechanical properties of HDPE/clay nanocomposites. *Iranian Polymer Journal*, 18(10), 833–842. Available in: <http://194.225.115.91/manuscripts/ipj-2009-10-4941.pdf>
- Merino, D., Gutiérrez, T. J., & Alvarez, V. A. (2019a). Potential agricultural mulch films based on native and phosphorylated corn starch with and without surface functionalization with chitosan. *Journal Polymers and the Environment*, 27(1), 97–105. <https://doi.org/10.1007/s10924-018-1325-1>.
- Merino, D., Gutiérrez, T. J., & Alvarez, V. A. (2019b). Structural and thermal properties of agricultural mulch films based on native and oxidized corn starch nanocomposites. *Starch-Stärke*, 71(7–8), 1800341. <https://doi.org/10.1002/star.201800341>.
- Merino, D., Gutiérrez, T. J., Mansilla, A. Y., Casalengué, C. A., & Alvarez, V. A. (2018a). Critical evaluation of starch-based antibacterial nanocomposites as agricultural mulch films: Study on their interactions with water and light. *ACS Sustainable Chemistry & Engineering*, 6(11), 15662–15672. <https://doi.org/10.1021/acssuschemeng.8b04162>.
- Merino, D., Mansilla, A. Y., Gutiérrez, T. J., Casalengué, C. A., & Alvarez, V. A. (2018b). Chitosan coated-phosphorylated starch films: Water interaction, transparency and antibacterial properties. *Reactive and Functional Polymers*, 131, 445–453. <https://doi.org/10.1016/j.reactfunctpolym.2018.08.012>.
- Mishra, J. K., Chang, Y. W., & Kim, D. K. (2007). Green thermoplastic elastomer based on polycaprolactone/epoxidized natural rubber blend as a heat shrinkable material. *Materials Letters*, 61(17), 3551–3554. <https://doi.org/10.1016/j.matlet.2006.11.119>.
- Mishra, J. K., & Wonho, Y. C. (2011). The effect of peroxide crosslinking on thermal, mechanical, and rheological properties of polycaprolactone/epoxidized natural rubber blends. *Polymer Bulletin*, 66(5), 673–681. <https://doi.org/10.1007/s00289-010-0376-9>.
- Moghaddam, L., Rintoul, L., Halley, P. J., George, G. A., & Fredericks, P. M. (2012). In-situ monitoring by fibre-optic NIR spectroscopy and rheometry of maleic anhydride grafting to polypropylene in a laboratory scale reactive extruder. *Polymer Testing*, 31(1), 155–163. <https://doi.org/10.1016/j.polymertesting.2011.10.002>.
- Muniyasamy, S., Ofosu, O., John, M. J., & Anandjiwala, R. D. (2016). Mineralization of poly(lactic acid) (PLA), poly(3-hydroxybutyrate-co-valerate) (PHBV) and PLA/PHBV blend in compost and soil environments. *Journal of Renewable Materials*, 4(2), 133–145. <https://doi.org/10.7569/jrm.2016.634104>.
- Musa, O. M. (Ed.). (2016). *Handbook of maleic anhydride based materials - synthesis, properties and applications* (Pp) (Vol. 638). New Jersey: Springer International Publishing. <https://doi.org/10.1007/978-3-319-29454-4>.
- Muthuraj, R. (2015). Biodegradable polymer blends and their biocomposites: Compatibilization and performance evaluation. Retrieved from chrome-extension://ngpampappnmepgilofohad-hhmbhlaek/captured.html?back=1
- Muthuraj, R., Misra, M., & Mohanty, A. K. (2017). Biocomposite consisting of miscanthus fiber and biodegradable binary blend matrix: Compatibilization and performance evaluation. *RSC Advances*, 7(44), 27538–27548. <https://doi.org/10.1039/c6ra27987b>.

- Oromiehie, A., Ebadi-Dehaghani, H., & Mirbagheri, S. (2014). Chemical modification of polypropylene by maleic anhydride: Melt grafting, characterization and mechanism. *International Journal of Chemical Engineering and Applications*, 5(2), 117–122. <https://doi.org/10.7763/ijcea.2014.v5.363>.
- Paolo, F., Mantia, L., Ceraulo, M., Mistretta, M. C., Botta, L., & Morreale, M. (2018). Compatibilization of polypropylene/polyamide 6 blend fibers using photo-oxidized polypropylene. *Materials*, 12(1), 81. <https://doi.org/10.3390/ma12010081>.
- Papadopoulou, C. P., & Kalfoglou, N. K. (2000). Comparison of compatibilizer effectiveness for PET/PP blends: Their mechanical, thermal and morphology characterization. *Polymer*, 41(7), 2543–2555. [https://doi.org/10.1016/s0032-3861\(99\)00442-5](https://doi.org/10.1016/s0032-3861(99)00442-5).
- Persenaire, O., Quintana, R., Lemmouchi, Y., Sampson, J., Martin, S., Bonnaud, L., & Dubois, P. (2014). Reactive compatibilization of poly(l-lactide)/poly(butylene succinate) blends through polyester maleation: From materials to properties. *Polymer International*, 63(9), 1724–1731. <https://doi.org/10.1002/pi.4700>.
- Phua, Y. J., Chow, W. S., & Mohd Ishak, Z. A. (2013). Reactive processing of maleic anhydride-grafted poly(butylene succinate) and the compatibilizing effect on poly(butylene succinate) nanocomposites. *Express Polymer Letters*, 7(4), 340–354. <https://doi.org/10.3144/expresspolymlett.2013.31>.
- Pitt, G. G., Cha, Y., Shah, S. S., & Zhu, K. J. (1992). Blends of PVA and PGLA: Control of the permeability and degradability of hydrogels by blending. *Journal of Controlled Release*, 19(1–3), 189–199. [https://doi.org/10.1016/0168-3659\(92\)90076-4](https://doi.org/10.1016/0168-3659(92)90076-4).
- Pracella, M., Haque, M., & Alvarez, V. (2010). Functionalization, compatibilization and properties of polyolefin composites with natural fibers. *Polymers*, 2, 554–574. <https://doi.org/10.3390/polym2040554>.
- Pradeep, S. A., Kharbas, H., Turng, L. S., Avalos, A., Lawrence, J. G., & Pilla, S. (2017). Investigation of thermal and thermomechanical properties of biodegradable PLA/PBSA composites processed via supercritical fluid-assisted foam injection molding. *Polymers*, 9(1), 22. <https://doi.org/10.3390/polym9010022>.
- Qiu, W., & Hirotsu, T. (2005). A new method to prepare maleic anhydride grafted poly(propylene). *Macromolecular Chemistry and Physics*, 206(24), 2470–2482. <https://doi.org/10.1002/macp.200500375>.
- Raphel, I., Wilms, J., & Piester, F. (2018). Industrial production and use of grafted polyolefin. In G. Beyer & C. Hopmann (Eds.), *Reactive extrusion: Principles and applications* (pp. 449–496). Weinheim: WILEY-VCH. <https://doi.org/10.1016/b978-0-12-814509-8.00015-4>.
- Ren, J., Fu, H., Ren, T., & Yuan, W. (2009). Preparation, characterization and properties of binary and ternary blends with thermoplastic starch, poly(lactic acid) and poly(butylene adipate-co-terephthalate). *Carbohydrate Polymers*, 77(3), 576–582. <https://doi.org/10.1016/j.carbpol.2009.01.024>.
- Rivaton, A., Serre, F., & Gardette, J. L. (1998). Oxidative and photooxidative degradations of PP/PBT blends. *Polymer Degradation and Stability*, 62(1), 127–143. [https://doi.org/10.1016/s0141-3910\(97\)00271-1](https://doi.org/10.1016/s0141-3910(97)00271-1).
- Rosu, D., & Visakh, P. M. (Eds.). (2016). *Photochemical behavior of multicomponent polymeric-based materials* (p. 405). Springer International: Publishing. <https://doi.org/10.1007/978-3-319-25196-7>.
- Rzayev, Z. M. O. (2011). Graft copolymers of maleic anhydride and its isostructural analogues: High performance engineering materials. *International Review of Chemical Engineering*, 3(2), 153–215. <https://doi.org/10.15866/ireamt.v2i5.7001>.
- Sadi, R. K., Fechine, G. J. M., & Demarquette, N. R. (2013). Effect of prior photodegradation on the biodegradation of polypropylene/poly(3-hydroxybutyrate) blends. *Polymer Engineering & Science*, 53(10), 2109–2013. <https://doi.org/10.1002/pen.23471>.
- Semba, T., Kitagawa, K., Ishiaku, U. S., & Hamada, H. (2006). The effect of crosslinking on the mechanical properties of polylactic acid/polycaprolactone blends. *Journal of Applied Polymer Science*, 101(3), 1816–1825. <https://doi.org/10.1002/app.23589>.

- Shah, A. A., Hasan, F., Hameed, A., & Ahmed, S. (2008). Biological degradation of plastics: A comprehensive review. *Biotechnology Advances*, 26(3), 246–265. <https://doi.org/10.1016/j.biotechadv.2007.12.005>.
- Si, P., Luo, F., & Luo, F. (2016). Miscibility, morphology and crystallization behavior of poly(butylene succinate-co-butylene adipate)/poly(vinyl phenol)/poly(L-lactic acid) blends. *Polymers*, 8(12), 421. <https://doi.org/10.3390/polym8120421>.
- Signori, F., Boggioni, A., Righetti, M. C., Rondán, C. E., Bronco, S., & Ciardelli, F. (2015). Evidences of transesterification, chain branching and cross-linking in a biopolyester commercial blend upon reaction with dicumyl peroxide in the melt. *Macromolecular Materials and Engineering*, 300(2), 153–160. <https://doi.org/10.1002/mame.201400187>.
- Sodergard, A., & Stolt, M. (2002). Properties of lactic acid based polymers and their correlation with composition. *Progress in Polymer Science*, 27(6), 1123–1163. [https://doi.org/10.1016/s0079-6700\(02\)00012-6](https://doi.org/10.1016/s0079-6700(02)00012-6).
- Sun, Y. J., Hu, G. H., Lambla, M., & Kotlar, H. K. (1996). In situ compatibilization of polypropylene and poly(butylene terephthalate) polymer blends by one-step reactive extrusion. *Polymer*, 37(18), 4119–4127. [https://doi.org/10.1016/0032-3861\(96\)00229-7](https://doi.org/10.1016/0032-3861(96)00229-7).
- Takamura, M., Nakamura, T., Takahashi, T., & Koyama, K. (2008). Effect of type of peroxide on cross-linking of poly(L-lactide). *Polymer Degradation and Stability*, 93(10), 1909–1916. <https://doi.org/10.1016/j.polymdegradstab.2008.07.001>.
- Tansiri, V., & Potiyaraj, P. (2015). Compatibilization efficiency of reactively modified poly(butylene succinate) as a compatibilizer for poly(butylene succinate) composites. *Advanced Materials Research*, 1119, 288–291. <https://doi.org/10.4028/www.scientific.net/amr.1119.288>.
- Therias, S., Tzankova Dintcheva, N., Gardette, J. L., & La Mantia, F. P. (2010). Photooxidative behaviour of polyethylene/polyamide-6 blends. *Polymer Degradation and Stability*, 95(4), 522–526. <https://doi.org/10.1016/j.polymdegradstab.2009.12.017>.
- Thirmizir, M. Z. A., Hazahar, M. D., & Mohd Ishak, Z. A. (2017). Mechanical and morphological properties of poly(butylene succinate)/poly(hydroxybutyrate-co-hydroxyhexanoate) polymer blends: Effect of blend ratio and maleated compatibiliser. *Key Engineering Materials*, 737(2003), 313–319. <https://doi.org/10.4028/www.scientific.net/kem.737.313>.
- Tianyi, K., & Xiuzhi, S. (2000). Physical properties of poly(lactic acid) and starch composites with various blending ratios. *Cereal Chemistry*, 77(6), 761–768. <https://doi.org/10.1094/chem.2000.77.6.761>.
- Toro-Márquez, L. A., Merino, D., & Gutiérrez, T. J. (2018). Bionanocomposite films prepared from corn starch with and without nanopackaged Jamaica (*Hibiscus sabdariffa*) flower extract. *Food and Bioprocess Technology*, 11(11), 1955–1973. <https://doi.org/10.1007/s11947-018-2160-z>.
- Tsuji, H., Mizuno, A., & Ikada, Y. (2000). Properties and morphology of poly(L-lactide). III. Effects of initial crystallinity on long-term *in vitro* hydrolysis of high molecular weight poly(L-lactide) film in phosphate-buffered solution. *Journal of Applied Polymer Science*, 77(7), 1452–1464. [https://doi.org/10.1002/1097-4628\(20000815\)77:7%3c1452::aid-app7%3e3.0.co;2-s](https://doi.org/10.1002/1097-4628(20000815)77:7%3c1452::aid-app7%3e3.0.co;2-s).
- Tsuji, H., & Muramatsu, H. (2001). Blends of aliphatic polyesters. IV. Morphology, swelling behavior, and surface and bulk properties of blends from hydrophobic poly(L-lactide) and hydrophilic poly(vinyl alcohol). *Journal of Applied Polymer Science*, 81(9), 2151–2160. <https://doi.org/10.1002/app.1651>.
- Vroman, I., & Tighzert, L. (2009). Biodegradable polymers. *Materials*, 2(2), 307–344. <https://doi.org/10.3390/ma2020307>.
- Waldman, W. R., & De Paoli, M. A. (2008). Photodegradation of polypropylene/polystyrene blends: Styrene-butadiene-styrene compatibilisation effect. *Polymer Degradation and Stability*, 93(1), 273–280. <https://doi.org/10.1016/j.polymdegradstab.2007.09.003>.
- Wu, C. S. (2003). Physical properties and biodegradability of maleated-polycaprolactone/starch composite. *Polymer Degradation and Stability*, 80(1), 127–134. [https://doi.org/10.1016/s0141-3910\(02\)00393-2](https://doi.org/10.1016/s0141-3910(02)00393-2).

- Wu, C. S., & Liao, H. T. (2012). Polycaprolactone-based green renewable eco-composites made from rice straw fiber: Characterization and assessment of mechanical and thermal properties. *Industrial and Engineering Chemistry Research*, 51(8), 3329–3337. <https://doi.org/10.1021/ie202002p>.
- Wypych, G. (2008). *Handbook of material weathering* (4th ed.). Toronto: ChemTec Publishing. [https://doi.org/10.1016/1352-2310\(96\)90058-8](https://doi.org/10.1016/1352-2310(96)90058-8).
- Xu, C., Fang, Z., & Zhong, J. (1993). Study on compatibilization-crosslinking synergism in PVC/LDPE blends. *Die Angewandte Makromolekulare Chemie*, 212(1), 45–52. <https://doi.org/10.1002/apmc.1993.052120105>.
- Yin, Q., Chen, F., Zhang, H., & Liu, C. (2015). Fabrication and characterisation of thermoplastic starch/poly(butylene succinate) blends with maleated poly(butylene succinate) as compatibiliser. *Plastics, Rubber and Composites*, 44(9), 362–367. <https://doi.org/10.1179/1743289815y.0000000031>.
- Yu, L., Dean, K., & Li, L. (2006). Polymer blends and composites from renewable resources. *Progress in Polymer Science*, 31(6), 576–602. <https://doi.org/10.1016/j.progpolymsci.2006.03.002>.
- Zainuddin, Sudradjat, A., Razzak, M. T., Yoshii, F., & Makuuchi, K. (1999). Polyblend CPP and Bionolle with PP-g-MAH as compatibilizer: I. compatibility. *Journal of Applied Polymer Science*, 72(10), 1277–1282. [https://doi.org/10.1002/\(sici\)1097-4628\(19990606\)72:10<1277::aid-app6>3.0.co;2-%23](https://doi.org/10.1002/(sici)1097-4628(19990606)72:10<1277::aid-app6>3.0.co;2-%23).
- Zeng, J. B., Jiao, L., Li, Y. D., Srinivasan, M., Li, T., & Wang, Y. Z. (2011). Bio-based blends of starch and poly(butylene succinate) with improved miscibility, mechanical properties, and reduced water absorption. *Carbohydrate Polymers*, 83(2), 762–768. <https://doi.org/10.1016/j.carbpol.2010.08.051>.
- Zhang, B., Sun, B., Bian, X., Li, G., & Chen, X. (2017). High melt strength and high toughness PLLA/PBS blends by copolymerization and in situ reactive compatibilization. *Industrial and Engineering Chemistry Research*, 56(1), 52–62. <https://doi.org/10.1021/acs.iecr.6b03151>.
- Zhang, K., Mohanty, A. K., & Misra, M. (2012). Fully biodegradable and biorenewable ternary blends from polylactide, poly(3-hydroxybutyrate-co-hydroxyvalerate) and poly(butylene succinate) with balanced properties. *ACS Applied Materials and Interfaces*, 4(6), 3091–3101. <https://doi.org/10.1021/am3004522>.
- Zhang, L., Xiong, C., & Deng, X. (1995). Biodegradable polyester blends for biomedical application. *Journal of Applied Polymer Science*, 56(1), 103–112. <https://doi.org/10.1002/app.1995.070560114>.
- Zhang, M., & Thomas, N. L. (2011). Blending polylactic acid with polyhydroxybutyrate: The effect on thermal, mechanical, and biodegradation properties. *Advances in Polymer Technology*, 30(2), 67–79. <https://doi.org/10.1002/adv.20235>.

Chapter 4

Crosslinked Polymer Hydrogels



Reem K. Farag and Salma Hani

Abstract The use of synthetic crosslinked polymer gels has increased in recent years, due to their unique characteristics such as high mechanical strength, service life and water and oil swelling, as well as being biocompatible. They have been studied as promising candidates in various fields such as cardiac and oil sobrieties, contact lenses, cosmetics, drug delivery, tissue engineering, wound dressing, among others. This chapter provides general information on polymer gels, including definition, classification, preparation methods and applications.

Keywords Gel applications · Hydrophilic polymer · Hydrophobic polymer · Swelling

4.1 Introduction

Polymers are macromolecules made from small parts called monomers linked to each other. The behavior of the polymer depends on several factors as inter- and intramolecular interactions such as van Der Waals forces, hydrophobic association, electrostatic interactions and hydrogen bonds (Zhang et al. 2015a, b). However, the hydrophobic interactions and the hydrogen bonds result in an efficient polymer-polymer attraction which causes the association between polymers (Dai et al. 2015). Polymers can be divided into biopolymers and synthetic polymers. The biopolymers are macromolecules manufactured by the living organisms such as cellulose, DNA, peptides, proteins, etc. (Wang and Heilshorn 2015). These biopolymers are responsible in the organism for performing biological functions such as homeostasis and molecular motions. The synthetic polymers are chemical compounds that are man-made such as

R. K. Farag (✉)

Department of Application, Egyptian Petroleum Research Institute (EPRI),
Nasr City, Cairo, Egypt

S. Hani

Faculty of biotechnology, October University for Modern Science and Arts, Cairo, Egypt

nylon, poly(acrylamide) (PAAm), poly(ethylene glycol) (PEG), poly(vinyl chloride) (PVC), etc., which are used in different industrial purposes (Chin et al. 2017).

Crosslinked polymer gels are three-dimensional (3D) hydrophilic polymeric structures that can absorb huge volumes of water and other biological fluids and can even preserve them under pressure sometimes (Tomadoni et al. 2019). In addition, they have a high-water content, and with physical properties such as high flexibility similar to soft tissues. Crosslinked polymers are made to tolerate strong chemicals or eventually be disintegrated and dissolved (Peppas et al. 2000). The dissolution process can be carried out by altering the environmental conditions such as ionization of the solution, pH or temperature (Shimba et al. 2017).

4.1.1 Crosslinking Process

Crosslinking is a process in polymer chemistry that results in a network structure that depends on a multidimensional extension of a chain polymer by a crosslink which is a bond that could be ionic or covalent that works by linking a polymer to other (Sun et al. 2018). This crosslinking process changes the liquid polymer to a gel or solid by restricting the movement capacity of the polymer chains individually, thus increasing the molecular weight (Mw) of the polymer (Lin et al. 2015; Gutiérrez and González 2017; Gutiérrez et al. 2016b; Gutiérrez et al. 2015a; Gutiérrez et al. 2016a; Gutiérrez et al. 2015b). The resulting crosslinked polymers have an essential elastic characteristic which gives the polymer the ability to stretch and return to its original structure. However, by increasing the number of crosslink, they become less elastic and could be prone to be fragile (Rosales et al. 2017). But, by using sulfur curing or vulcanization, depending on the insertion of short sulfur chains that work on bonding the polymer chains in the rubber can give it more strength and durability (Maitra and Shukla 2014), are also resistant to heat and wear, as well as being mechanically strong, non-soluble in aqueous fluids, since crosslinking form strong covalent bonds, which results in solvent insoluble materials. They can, however, absorb a larger solvent content, for this reason they are called gels (Billah et al. 2018). Crosslinking has been implemented to improve the mechanical strength, insolubility, rigidity and stiffness of polymers, thus allowing polymers to be considered potential candidates in various fields, including agricultural, biomedical, environmental and industrial (Griffith et al. 2018). Therefore, by controlling the type of crosslinker and the required concentration, promising crosslinked polymers with desired properties of pore size, thermal degradation, particle size and swelling are generated (Vining et al. 2019). There are two types of crosslinking which are chemical crosslinking, including (1) free-radical radiation, ultraviolet-visible (UV) radiation, condensation and (2) polymerization of small molecules, in addition to the physical and biological crosslinking (Feng et al. 2016).

4.1.2 *Forms of Crosslinked Polymers*

Over the last two decades, natural and synthetic crosslinked polymers have been potentially used in several applications, since both types have advantages and disadvantages (Fortman et al. 2018). The natural polymers have low thermal stability, more solubility and no strength, so in order to improve these characteristics it is necessary (Gong et al. 2016). Crosslinking processes are classified into two types: the *in-situ* crosslinking and the post-crosslinking (Akhtar et al. 2016). In order to synthesize the *in-situ* hydrogels, there are two methods: the first method depends on the polymerization of the small molecules in the presence of crosslinkers and initiators (Desai et al. 2015), while the second method depends on the direct crosslinking of the monomers, either naturally or synthetically, to obtain a polymer chain (Takashima et al. 2017). In general, the synthetic polymers are hydrophobic and tougher compared to natural polymers, which results in high durability in hydrogels, but slow degradation (Foster et al. 2015). However, the post-crosslinking process depends on crosslinking after polymerization (Akhtar et al. 2016).

Crosslinked polymers are categorized into different types based on several parameters, such as ionic charge, mechanical and structural properties and preparation method (Slaughter et al. 2009). According to the crosslinking mechanisms, the crosslinked polymers can be divided into three types: the chemical, biological and physical crosslinked polymers (Pakulska et al. 2015). The crosslinking of the polymers may be reversible or irreversible with respect to the nature of the crosslinking (Ghobril and Grinstaff 2015). The chemical method produces irreversible polymers. However, physical and biological methods lead to reversible crosslinked polymers through the application of electricity, light, magnetic field, pH change, pressure or stress (Sawada et al. 2019).

4.1.2.1 **Physically Crosslinked Polymers**

The physical crosslinked polymers are crosslinked by physical forces such as electrostatic forces, hydrogen bonds and hydrophobic interactions (Nystrom et al. 1996). This type of hydrogels can form reversible stable 3D gel structures from polymer solutions, and this occurs by changing some external stimulus such as concentration, ionic strength, pH and temperature (Hennink and Van nostrum 2012). According to Kjoniksen et al. (1998), an example of this hydrogels is the ethyl hydroxyl ethyl cellulose (EHEC) in the existence of an ionic surfactant which forms a thermo reversible gel at elevated temperatures.

4.1.2.2 **Chemically Crosslinked Polymers**

The chemically crosslinked polymers are also known as continuous or chemical gels. They are responsible for primary forces such as covalent bonding through chemical reactions in order to achieve the crosslinking of the macromolecules in solution (Wang and Heilshorn 2015). They are efficient to obtain and have high mechanical strength and heat resistance. When the chemical crosslinked polymers

form a covalent bond, a permanent 3D network is formed. An example of these polymers are hydrogels made from HEC in the presence of a divinyl sulfone crosslinker (Ouyang et al. 2016). Two common methods are used for preparing chemically crosslinked polymers: the first method is the 3D polymerization which depends on the polymerization of hydrophilic molecules as vinyl monomers in the presence of multifunctional crosslinkers (Cao et al. 2015). However, the drawback of this method is the significant amount of the unreacted monomers which can be toxic and require extensive purification methods (Wu et al. 2018). The second method depends on the direct crosslinking of the hydrophilic polymers so that extensive purification procedures could be avoided due to the small available amounts of the toxic molecules in the system (Mahou et al. 2015). Polymers that are water soluble, including PAAm, PEG, poly(vinyl alcohol) (PVA) and polysaccharides are the main systems used for applications in the biomedical and pharmaceutical fields, due to their biocompatibility and non-toxicity (Caló and Khutoryanskiy 2015).

4.1.2.3 Biological Crosslinked Polymers

The biological crosslinking method is an evolving technique that depends on the use of biomolecules to achieve the crosslinking, such as opposite charged peptides, complementary oligonucleotides, in addition to heparin growth factors (Sadler et al. 2019). While, the opposite charged peptides and the polymers can form connections that allow the formation of the biological crosslink (Contessi et al. 2019). In addition, this method aids the polymer is not solubilized in organic solvents or aqueous solutions. However, this type of crosslinking is perceived as not strong enough as the chemical crosslinking techniques (Chaudhuri et al. 2016).

4.2 Methods of Synthesis of Crosslinked Polymers

Several different strategies for crosslinking the polymers can be used depending on the nature of the polymer, which could be through the polymerization of the small molecules by condensation or by forming a covalent bond between the polymeric chains through the irradiation, which is done by using high-energy ionizing radiation, such as electron beam, and gamma and X-ray (Hassan and Peppas 2000). However, the gamma irradiation is considered more economical, since it uses low doses about 80 kGy and less for large parts that have high density, while for small parts the electron beam is mainly used such as in the production of cables and wires (Maitra and Shukla 2014). It could also be through the vulcanization of sulfur which depend on chemical reactions by introducing different chemicals accompanied by heating and, in some cases, with pressure. Thus, in all the cases, the chemical structure of the polymer will be altered during the crosslinking process.

Conventional polymerization techniques, such as the condensation and the free-radical polymerizations, are mainly used for chemically crosslinked polymers (Das et al. 2018). These techniques produce a degradable or a non-degradable

crosslinked polymer which depends on the formation of the bond (Li et al. 2017). In addition, the crosslinked polymers that could be obtained from these techniques do not impose any difficulty during their application, i.e. due to their robust crosslinking ability provided by the primary forces, while crosslinked polymers that are achieved by physical crosslinking can cause some difficulties throughout its application due to its fragile crosslinking provided by secondary forces (Li et al. 2016). For this reason, chemical crosslinking is more preferred.

4.2.1 Free-Radical Polymerization

Free radical polymerization is one of the most widely used synthetic methods worldwide to produce crosslinked polymers, both by academics and industrialists. It is used to generate a substantial amount of the crosslinked polymers produced globally, comprising 45% of the industrial synthetic plastics and 40% of the manufactured rubber, which is equivalent to an amount of 100 and 4.6 million tons, respectively (Kade and Tirrell 2014). It is widely used due to the favorable properties provided over other polymerization methods. First, it is found to be highly reactive, which results in crosslinked polymers of high Mws and ‘crosslinking density’ (Pan et al. 2015). Second, this method supports several functional groups and takes place in soft environments (Lansalot et al. 2016). It is thus considered an effortless approach to the synthesis of crosslinking polymers. Free-radical polymerization is carried out in the existence of an initiator and heat. Mainly, acrylic acids and small acrylate-based molecules are synthesized and polymerized using this method. Free radical polymerization is further categorized as homopolymer, copolymer, semi-interpenetrating network and interpenetrating network (Sutirman et al. 2016). The homopolymers are crosslinked polymers of a type of hydrophilic small molecules units, while the copolymers are the result of crosslinking between two different monomers, where at least one is hydrophilic in order to be swellable. The interpenetrating and the semi-interpenetrating networks are produced due to the formation of a swelling network first and then to the formation of a second intermeshing network system.

4.2.1.1 Homopolymer

It refers to the polymer network that originates from the polymerization of a single monomer species in the presence of a crosslinker and an initiator. Crosslinked homopolymers are used in various applications such as contact lenses and drug delivery systems. For example, homopolymerization of *N*-acryloylglycinamide through free radical polymerization using the initiator 2,2'-azobisisobutyronitrile (AIBN) and the crosslinker *N,N'*-methylenebisacrylamide (MBAm), produced a hydrogel (Liu et al. 2014). *N*-vinyl-2-pyrrolidone can also be homopolymerized in the presence of a radical initiator AIBN and a crosslinker MBAm to create a pH-responsive hydrogel for the *in vitro* delivery of propranolol hydrochloride (Shantha and Harding 2002).

4.2.1.2 Copolymer

The copolymers are crosslinked polymers that are synthesized by polymerization of at least two different monomers with somewhere around a hydrophilic compound. Depending on the structure of the polymer chain, the copolymers are categorized into block, random and alternating copolymers. According to Zhou et al. (2016) a recent report portrays the synthesis of pH-temperature double stimuli-responsive hydrogel for medication drug release. In this study, PEG was reacted with methyl ether methacrylate to achieve methacrylate ended PEG, which copolymerized with *N,N'*-dimethylaminoethyl methacrylate. The solution of the copolymer was then mixed with α -cyclodextrin (α -CD) to form a pH-thermo double touch hydrogel, thus allowing the arrival of a model drug 5-fluorouracil to be adequately controlled by pH and temperature (Bi and Liang 2016).

4.2.1.3 Semi-Inter Penetrating Network (Semi-IPN)

It refers to a crosslinked polymer generated from the combination of two independent synthetic or natural polymer compounds, comprised in the form of a network. In addition, in the semi-IPN polymer, one of the compounds is usually a crosslinked polymer, while the other is a non-crosslinked polymer (Zhang et al. 2009). Due to the absence of the restricting interpenetrating elastic network, the semi-IPNs can effectively reserve fast kinetic response rates to pH or temperature, while offering the advantages as modified pore size and slow drug release.

4.2.1.4 Interpenetrating Polymer Systems (IPNs)

It refers to the combination of two polymers or more of which are synthesized immediately in the presence of the other polymer (Muniz and Geuskens 2001). This is achieved by the immersing a pre-polymerized crosslinked polymer in a solution of small molecules and an initiator. This method can overcome the thermodynamic incompatibility due to the permanent interlocking of the networks, which causes the structure stable (Zhang and Zhuo 2000). The main advantages of this polymer networks are that dense crosslinked polymers can be produced which are characterized to have a robust mechanical strength, and is more competent for drug delivery compared to the conventional gels. IPN's pore sizes and the surface chemistry can be controlled in order to tune the drug release (Yin et al. 2007). IPNs can also moderate the effect of environmental changes on the crosslinked polymers, thus minimizing the drug burst release during oral delivery, due to their ability to prevent the swelling of the interpenetrating phases with respect to the elasticity (Rana et al. 2015).

4.2.2 Condensation Polymerization

Condensation polymers are identified as any type of polymers formed through the condensation reaction by the combination of small molecules, and obtaining water or methanol as byproducts (Kumru et al. 2017). Condensation polymerization is used to produce some of the main polymers, such as poly(amide)s, poly(carbonate)s and poly(ester)s. It also plays a special role in the history of polymer science, while the first genuinely synthetic polymer, Bakelite, was developed in 1907, as a condensation product of phenol and formaldehyde (Kade and Tirrell 2014). The polymers produced by this method can be degradable or non-degradable depending on the groups formed during the polymerization process (Kabiri et al. 2011). This polymerization method is performed in the existence of heat, catalyst or both. In addition, the polymers resulting from this method generally have low Mw (Wang et al. 2018a, b). The polymerizations are divided into two groups, which are the condensation and the addition, while a step growth method with the condensation polymerization has also been used by Song et al. (2016). However, not all condensation reactions use a step growth method. Nonetheless, the step growth mechanism is still considered the most widely used method for the condensation of polymers for materials of industrial importance (Jain et al. 2016).

4.2.3 Bulk Polymerization

This technique of polymerization generates crosslinked polymers by using one or more types of monomers (Wu et al. 2018). This variety of the types of monomers permits the production of crosslinked polymers with the desired properties for different applications. This technique typically requires the addition of a small amount of a crosslinking agent during the polymer production. The polymerization of the monomers is usually initiated with the help of chemical catalysts or UV radiation. In addition, the choice of the main initiator depends on the types of solvents and monomers that is used. The resulting crosslinked polymer can be generated in various forms comprising emulsions, films, membranes, particles or rods.

4.2.4 Ultraviolet (UV) Radiation

UV radiation is considered an economical route to achieve a crosslinked polymer compared to condensation and free radical polymerization techniques. In addition, the polymerization of the crosslinked polymer through this technique is perceived as safe, it also has the least amount of effect on the properties of the crosslinked polymer and does not require the addition of any chemical compound such as initiators, solvents and surfactants. Thus, it allows the crosslinked polymer to retain its proper swelling, mechanical strength and biocompatibility properties (Wang et al. 2016).

4.3 Properties of Crosslinked Polymers

Much of the crosslinked polymer chains are chemically or physically linked, and therefore, are considered as a molecule, regardless of size. For this reason, the Mw of the crosslinked polymer is not perceived and are occasionally called macromolecules or infinitely large molecules (Niu et al. 2019). Minor changes in environmental conditions can cause reversible and fast alterations in the crosslinked polymers. The changes in the environmental parameters, including electrical signal, enzyme presence, pH or temperature, can cause a change to the physical structure of the crosslinked polymers (Rao et al. 2016). The changes that are produced can take place at macroscopic levels, since they change the size and water content of the crosslinked polymer (Deng et al. 2011). The alteration in the ion concentrations inside the crosslinked polymer in relation to the external solution could change, the pH and the volume of the solvent. In addition, the response of the crosslinked polymers with acidic or basic functional groups to the external environment depends on the degree of ionization of the functional group (Rana et al. 2015).

4.3.1 Biocompatibility

Crosslinked polymers to be used in various applications in the biomedical field must be biocompatible and non-toxic. For this reason, before being applied the crosslinked hydrogels must pass the cytotoxicity and *in-vivo* toxicity tests in order to be applied (Nawaz et al. 2018). The biocompatibility is the ability of the material to respond appropriately in the host during a specific application. In addition, biocompatibility consists of two basic elements: biosafety and biofunctionality (Kirschning et al. 2018). The biosafety is the performance of an adequate response from the host with the absence of carcinogens, cytotoxicity and mutagenesis. However, it is not only based on the systemic response but also on the local response of the neighboring tissues (Ibáñez-Fonseca et al. 2018), while the biofunctionality is the polymer's ability to perform the intended and required tasks. This is mainly important for tissue engineering, since the nature of tissue construction is to continuously interact with the body through cell regeneration and healing processes (Szafulewa et al. 2018). However, if the requirements are not met, this means that the gel could be fouled or that there are injuries and scars to the connected tissues (Molpeceres et al. 2018). In addition, the toxic chemicals such as emulsifiers, initiators, solvents, stabilizers and unreacted monomers that are used in the polymerization of the synthesis of crosslinked polymers could interact with the body if the conversion is not performed 100% correctly. This presents a challenge for biocompatibility *in vivo*. These chemicals are toxic to host cells if they are filtered to encapsulated cells or tissues (Choi et al. 2015).

4.3.2 Degree of Crosslinking (DC)

The DC of the polymers is often measured using the swelling experiment, where the crosslinked terpolymer sample is placed in a solvent which is usually water at suitable temperature conditions (Nam et al. 2016). The DC is assessed by measuring the changes that occur in the mass or the volume of the crosslinked polymer. It should be noted that more crosslinked hydrogels have less swelling capacity. The DC will be calculated according to Flory (1953), where the sample is weighed dry then placed in the solvent for 24 hours and subsequently weighed at different time intervals.

4.3.3 Mechanical Properties

The mechanical properties of crosslinked polymers vary and can be tailored depending on the nature of the material. To achieve a gel with a higher toughness, the DC could be increased (Najdahmadi et al. 2018). A stronger gel can be acquired by increasing the DC, while decreasing the DC leads to a more brittle gel structure. The mechanical properties of crosslinked polymers have a great role in the biomedical and pharmaceutical fields, as they can be used for tendon and ligament repair, as well as they could be used as a matrix for the delivery of drugs, tissue engineering, and cartilage replacement and wound dressing material (Ahmadi et al. 2015; Chai et al. 2017). It is worth noting that crosslinked polymers can maintain their physical texture during the delivery of therapeutic medications (Benjamin 2017).

4.3.4 Swelling Characteristics

Crosslinked polymers are networks that can be swollen in a fluid medium. The liquids that are absorbed function as a selective medium or filter to allow the entry of some solute molecules, while the network of polymers act as a matrix that holds the liquid together (Bukhari et al. 2015). Crosslinked polymers can contain up to a thousand times of their weight in liquids (Wang et al. 2018a, b). The nature of the water in the polymer can establish a complete infiltration of the nutrients into and the cell products out of the gel. When a dry crosslinked polymer absorbs water, the first molecules of water move towards the matrix working to hydrate the most polar hydrophilic groups. Since the polar groups are primarily linked, these results cause swelling of polymer bonds, exposing the hydrophobic groups, which also interact with the water molecules, which leads to secondary water binding. As a result, the network absorbs additional water due to the osmotic driving force of the network system to be diluted (Wang et al. 2018a, b). This swelling is opposed by the covalent or physical crosslinking, thus generating an elastic network withdrawal force.

Finally, the crosslinked polymer reaches the swelling equilibrium level. The extra water that is absorbed after the saturation of the polar and the hydrophobic groups will be defined as bulk water and acts as a filling to the space between the network chains and the pores (Zhu et al. 2019). Gradually, as the swelling of the networks increases, if the crosslinks are degradable, the gel will begin to dissolve at rates that depend on its structure (Chen et al. 2018).

4.4 Application of Crosslinked Polymers

4.4.1 *Anti-Biological Crosslinked Polymers*

Infections caused by pathogenic organisms such as bacteria, parasites and viruses are a major health problem despite the expansion in the medical field and health care. Conventional techniques for the treatment of the microbial agent as antibiotics usually lead to the development of resistance to the antibiotics (Anjum et al. 2016). Recent studies have found a new method to treat the microbial agents by using the anti-biological crosslinked polymers (Jones et al. 2015). The crosslinked polymers work on the rupture of the cell membranes of the microbial agent, resulting in the leakage of the cytoplasmic content and cell death (Tian et al. 2018). Several types of anti-biological crosslinked polymers have been developed in the recent years (Konwar et al. 2016). According to Echazú et al. (2017), crosslinked polymers based on chitosan containing varying concentrations of benzoyl have demonstrated high antibacterial and antifungal activity. The elevation of antimicrobial activity was associated with the increase in crosslinking concentration. Some researchers have also produced cellulose-based crosslinked polymers exhibiting high biocompatibility, mechanical strength, swelling property and antimicrobial activity against *Saccharomyces cerevisiae*, thus showing the possibility of using crosslinked polymers as an antimicrobial candidate (Nordström and Malmsten 2017; Hu et al. 2018). It has also been reported that crosslinked polymers based on peptides show a significant antibacterial effect. In this sense, Rinehart et al. (2016), reported the development of a β -hairpin crosslinked polymer that had an anti-biological effect. Although the anti-biological crosslinked polymers have demonstrated remarkable activity against microbes. However, it was found that the interaction between the polymer and the cell membrane was nonspecific, thus causing in most cases the death of the mammalian cells (Picone et al. 2019). The solution that was proposed in order to use the crosslinked polymer as an antimicrobial agent, was to combine the crosslinked polymer with the antibiotics, in order to decrease the associated toxicity (Gallagher et al. 2016). Some researchers have also proposed another type of NP-loaded composite polymers which could be used in various applications such as wound dressing and against microbes (Mishra et al. 2018).

4.4.2 Artificial Muscles

The first generation of the crosslinked polymer has been used to mimic the neuromuscular and neurosensory systems (Miyamae et al. 2015). The muscles work by converting chemical reactions into mechanical actions. The artificial muscles that have been generated from the crosslinked polymers are comprised of an elastomer layer present between two layers of crosslinked polymers, while the elastomer layer acts as a di-electric, while the crosslinked polymer layers behave as a conductor (Iwaso et al. 2016). Metallic cables are used in order to connect the two layers of the crosslinked polymer to a power source. Upon the application of the voltage, the mobile electrons in the metal and the mobile ions present in the crosslinked polymer will move away or approach each other (Chandler 2018). Furthermore, accumulation of the mobile ions occurs between the elastomer and the polymer, simultaneously (Shi et al. 2016). In addition, due to the opposite polarities of the crosslinked polymers and the elastomer layers, this leads to a reduction in the thickness and an elevation in the elastomer layer. However, this could be avoided by generating a softer crosslinked polymer to prevent the deformation of the elastomer layer (Lee et al. 2016). Different designs of the artificial muscles could be generated depending on the electromechanical coupling which is based on the geometry of the layers (Fig. 4.1) (Dicker et al. 2017).

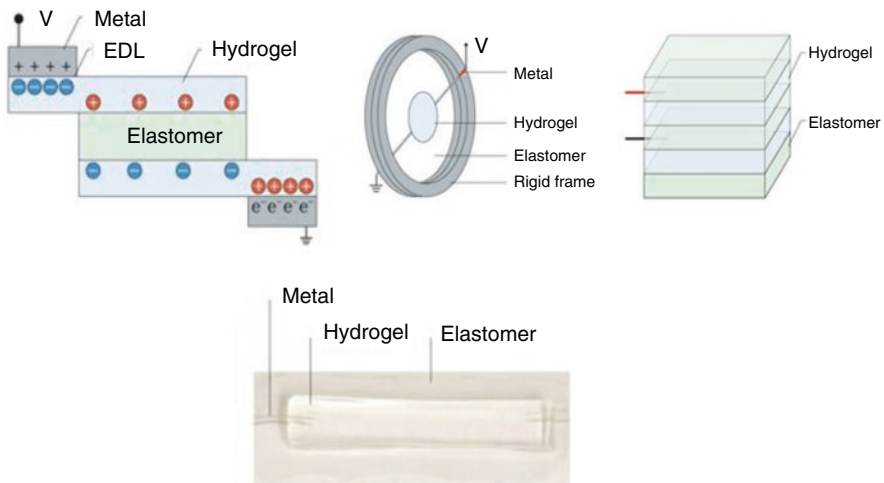


Fig. 4.1 Crosslinked polymer hydrogels for artificial muscle applications. Adapted with permission from Yang and Suo (2018)

4.4.3 Cancer Research

Crosslinked polymers have been implemented in many applications, including the cancer research (Song et al. 2015). Although most drugs are hydrophobic and this reduces their efficacy to be loaded and released from a crosslinked polymer (Pires et al. 2018). Two solutions to improve the release and loading of the drug from the polymer have been proposed, which are introducing a hydrophobic compound into the crosslinked polymer and incorporating nanoparticles (NP) which will act as an encapsulation for the hydrophobic domain (Norouzi et al. 2016). Recent studies have established that the crosslinked polymer nanostructures can help the development of novel devices for various medical and industrial applications (Baek et al. 2018). The nanocomposite crosslinked polymers are robust and have a greater capacity for controlled drug release (Pellá et al. 2018). This polymer structure allows a better quality of life by intra-peritoneal administration of the chemotherapy drug for the cancer patient (Jamal et al. 2018). According to Fisher et al. (2018), hyaluronic acid (HA)-based crosslinked polymers have been studied for their effect on the invasion of breast cancer cells, and the results have shown that upon increasing the crosslink density, the invasion of cancer cells from breast decreases. This study proves that the crosslinked polymers could be a promising candidate in cancer treatments (Huang and Huang 2018).

4.4.4 Contact Lenses and Ocular Implants

The production of contact lenses is one of the most widely used applications of crosslinked polymers, while one of the main properties of the crosslinked polymers is their ability to be perfectly tailored to the global ocular curvature (Schafer et al. 2018). In addition, they allow the oxygen to permeate the cornea by diffusing into the lens. One of the methods used in the contact lens production industry is the Lathe cutting technique, in which the lenses would be molded from 'buttons' of solid dehydrated crosslinked polymers (Fig. 4.2) (Caló and Khutoryanskiy 2015). According to Maulvi et al. (2016), the crosslinked poly(2-hydroxyethyl methacrylate) (PHEMA) polymers have been used for producing contact lenses, due to their mechanical properties and biocompatibility. In addition, a significant number of companies have developed a range of crosslinked polymer contact lenses compounds comprising different types of monomers in order to acquire a contact lens that holds the highest amount of water content and mechanical properties, thus allowing the lens to resist the eyelid strength with an increased oxygen permeation (Pitt et al. 2015). Furthermore, with these applicable contact lenses, this has increased the researches in the field of ophthalmic drug delivery, due to their ability to increase the residence time of the drug in the precorneal region that is provided due to the geometric barrier of the lenses to the medicine upon the diffusion out of the gel matrix to the tear film (Wolffsohn et al. 2015).

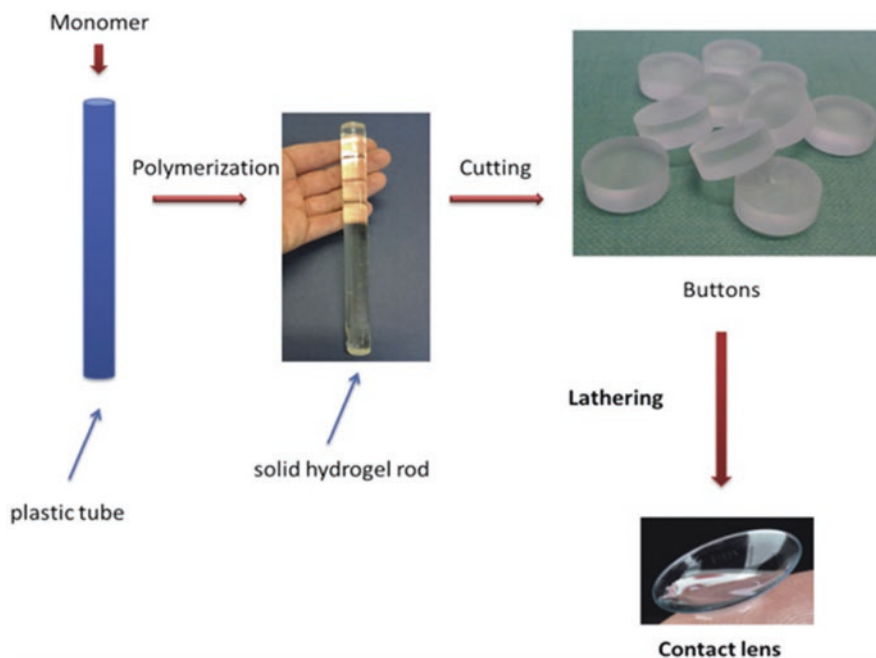


Fig. 4.2 Schematic representation of Lathe cutting technique for the production of contact lenses. Adapted with permission from Caló and Khutoryanskiy (2015)

4.4.5 Drug Delivery

Crosslinked polymers right after their discovery were used in antibiotics and anti-cancer drug delivery researches (Deen and Loh 2018). They have been seen as a potential solution to achieve a sustainable and targetable drug release at appropriate and specific sites, while working on increase the influence of the drug and decrease its side effects simultaneously (Xing et al. 2015). Crosslinked polymers have a porous system, which could eventually be controlled by the compactness of the crosslink or by altering the swelling affinity of the polymer in the environment (Sharma et al. 2018). Due to this porous property, this aids the crosslinked polymer gels release the drugs, which is achieved by monitoring the diffusion coefficient of the drugs (Fig. 4.3) (Wang et al. 2016). Crosslinked polymers when used through topical transdermal application, comprise many advantages, since they prevent liver metabolism, and therefore, increase the drug effectiveness and bioavailability (Culver et al. 2017). Due to the swelling property of the crosslinked polymers, they promise to be used in transdermal drug delivery, since the crosslinked polymer are similar to living tissues which can be effortlessly removed compared to ointments or patches (Dimatteo et al. 2018). In addition, crosslinked polymers comprising gentamycin have been shown to be more efficient in the treatment of skin infections compared to parenteral delivery of the gentamycin which causes severe disorders (García-Astrain and Avérous 2018).

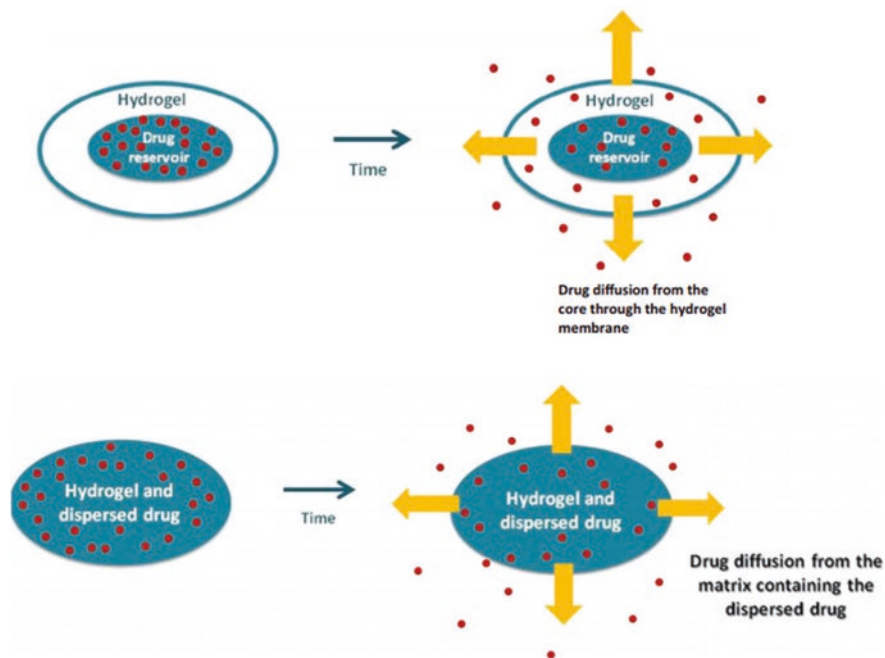


Fig. 4.3 Schematic representation of the release of a drug through a crosslinked polymeric membrane and a matrix. Adapted with permission from Li and Mooney (2016)

4.4.6 Gene Delivery

Crosslinked polymers have been proposed as a promising candidate for gene delivery, since they can reserve the activity of the viral and non-viral vectors, and protect them from the immune system attack (Yang et al. 2016). Crosslinked hydrogels can be injectable, in addition to being biologically sensitive, so it has great promise in the field of gene delivery (Nurunnabi et al. 2015). On the other hand, the crosslinked polymers implemented in the gene delivery require advanced strength for the prolonged transgene expression to occur (Nguyen et al. 2017). According to Zhang et al. (2017), lentivirus gene therapy is generated from crosslinked fibrin polymers comprising hydroxyapatite NPs that have the ability to interact with the lentivirus and the fibrin, this interaction leads to the stabilization of the crosslinked polymer and subsequently improved the vector release and cell infiltration rate. Therefore, with the appropriate biomaterial system and vector, gene delivery could be improved, thus improving transgenic expression (Xiang et al. 2017).

4.4.7 Oil Sorbers

Crosslinking with chemical covalent bonds linking the crystalline and amorphous domains is responsible for the 3D network structure that characterizes these materials. This drastically improves a large number of low-, room- and especially high temperature properties, such as abrasion, chemical and stress- cracking resistance impact, heat deformation, tensile strength and viscous deformation, and also adds new useful properties, such as shape memory. The elasticity and swelling properties are attributed to the presence of chemical or physical crosslinks within the polymer chains. Many authors have reviewed the advances in crosslinking technology for oil sorbers. For example, Jang and Kim (2000) studied the copolymerization of styrene monomer with several long-chain alkyl acrylate monomers such as, 2-ethylhexyl acrylate (EHA), lauryl acrylate (LA), lauryl methacrylate (LMA) and stearyl acrylate (SA). These acrylates with long chain alkyl groups are generally known as hydrophobic materials. Therefore, a highly absorbent property of oil can be obtained by controlling the composition and the crosslinking density of the copolymer.

Jang and Kim (2000) conducted a detailed study on the swelling properties of the crosslinked copolymers. The influence of the synthetic variables (amount of crosslinking agent and initiator, monomer feed ratio, polymerization temperature and type of acrylate monomer) of the crosslinked copolymers on the oil absorption capacity was examined.

Atta and Arndt (2005) synthesized new oil- absorbing polymers containing alkyl acrylate *via* different types of chemical crosslinkers and irradiation techniques. These authors conducted a detailed study on the swelling properties of the crosslinked 1-octene-isodecyl acrylate copolymers. The crosslinking polymerizations were carried out in the presence of different concentrations of ethylene glycol diacrylate (EGDA) and ethylene glycol dimethacrylate (EGDMA) crosslinkers *via* catalytic initiation and electron beam irradiation at a dose rate of 80 kGy. More oil sorption capacities were performed upon using longer alkyl acrylate, reaching a maximum of 20.5 and 38.8 g of crude oil/g of sample, respectively. In addition, crosslinked reactive macromonomers based on octadecyl acrylate (ODA) and polyisobutylene modified with maleic anhydride and cinnamoyloxy ethyl methacrylate (CEMA) moieties were prepared and oil sorption was evaluated. Farag et al. (2011) also synthesized linear and crosslinked copolymers with different compositions of 1-hexadecene and trimethylolpropane distearate monoacrylate monomers, and evaluated the oil absorption. Different concentrations of EGDA and EGDMA crosslinkers were varied from 0.5 to 2%. These authors concluded that the oil absorbency and swelling rate were mainly influenced by the DC and the hydrophobicity of the copolymer units. Keeping this in view, El-Ghazawy and Farag (2014) prepared a series of comb-like crosslinked dodecyl acrylate-*co*-ODA-*co*-vinyl acetate terpolymers (DOVs) with four different feed ratios of vinyl acetate while remaining constant the other monomer ratios. Crosslinking was carried out using trimethylolpropane triacrylate (hexafunctional) or divinyl benzene (tetrafunctional). The structure-performance relationship was discussed, especially with respect to crosslinker

type, crystallinity and feed ratio. These authors found that the highest oil absorption of crosslinked DOVs was 43.22 g of oil/g of sample after 20 min. of immersion. Lauren et al. (2014) illustrated an example system of thermally crosslinked octene-styrene-divinylbenzene (OS-DVB) copolymers. In the molecular models, the DC was ranged from 0 to 100%, and the resulting structural and thermal properties were examined. The simulations reveal an increase in the free volume with higher DCs.

On the other hand, Abdel-Azim et al. (2007) synthesized porous crosslinked copolymers for the sorption of oil spills by CEMA copolymerized with different monomer feed ratios of ODA and crosslinked using AIBN as a initiator and *N,N',N''*-trisacryloyl melanine (AM) or *N,N',N''*-trismethacryloylmelanine (MM) as cross-linkers. These authors observed that the sol fraction values of the CEMA/ODA crosslinked copolymer were lower when MM was used instead of AM, and the thermal stability of the crosslinked network increased as the ODA concentration increased and also in the presence of MM crosslinker, as a consequence of a higher crosslinking density. In addition, SEM results showed micropores that were formed as the ODA content increased. Similarly, the flexibility of the network was improved by incorporating MM instead of AM.

El-Ghazawy et al. (2014) prepared linear and branched polyesters by transesterification of methyl recinoleate without or with diethylene glycol, pentaerithritol or trimethylol propane for different durations. Mws of the synthesized polyesters were determined using gel permeation chromatography and hydroxyl number. As an example, Fig. 4.4 represents the crude oil sorption by the crosslinked polymethyl recinoleates.

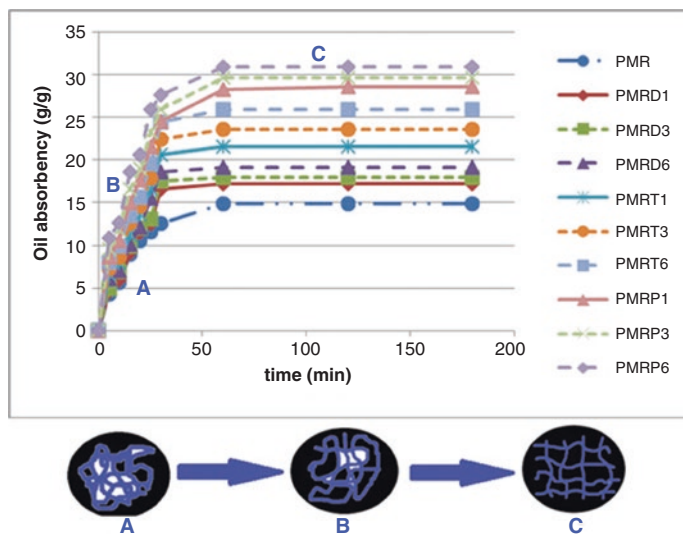


Fig. 4.4 Crude oil sorption by crosslinked polymethyl recinoleates. Reproduced with permission from El-Ghazawy et al. (2014)

4.4.8 Plastic Replacement

Plastics are synthetic polymers, which are considered easy to manufacture, as well as being economical and efficient, although they are not ecological. Previously, crosslinked gels were not perceived as suitable alternatives to plastics (Kondo et al. 2015). However, it was discovered that when the crosslinked polymer binds to clays, they retain properties as robust and can be easily molded, in addition to having the ability to self-heal when cut, thus allowing them to be a potential substitute for plastics (Cuadri et al. 2018).

4.4.9 Prevention of Soil Erosion

Crosslinked polymers have been applicable in the field of the environment for more than a decade, while the soluble crosslinked polymers have been used to reduce the soil erosion and improve the water infiltration from fine agricultural soils (Hotta et al. 2016). According to Guilherme et al. (2015), the soluble crosslinked PAAm polymers are dissolved in the irrigation water to form a thin slimy film that would protect the soil surface of the wash floor. As the irrigation water causes erosion to bare soils, and by the presence of a thin film that could hydrate the soil and allow irrigation water to permeate easily (Cheng et al. 2018). Several investigations have been carried out on different types of soils using the crosslinked PAAm polymer, which are suitable for soil degradation and erosion (Kabir et al. 2017). It has also been shown that the use of anionic soluble crosslinked PAAm polymer is more efficient than cationic crosslinked PAAm polymers in reducing soil erosion (Neethu et al. 2018).

4.4.10 Wound Dressing

The treatment that is applicable for damaged skin and the diabetic ulcers. These polymers are used in prosthetic skin engineering and have a high value, since it implies many requirements for patients that are generally not met (Hamedi et al. 2018). Thus, wound dressing is considered the potential new way to restore damaged skin tissues and diabetic ulcers with the applicability of high biocompatible bioactive compounds (Mohamad et al. 2018). Crosslinked polymers can retain the water and the injected drug for an enough time. Attributing to this ability, they were applied to contain wound exudates (Qu et al. 2018). According to Kamoun et al. (2017), the sodium alginate and the gelatin crosslinked polymers have been used to protect and cover the wounds from any bacterial infections. Zhang et al. (2015a, b) found that gelatin and HA crosslinked polymers are promising compounds for the treatment of skin regeneration.

4.5 Conclusions

This chapter gave a general description of the crosslinked polymer hydrogels, forms of the polymers (biological, chemical and physical), processes and methods for preparation (free-radical polymerization, condensation polymerization, bulk polymerization and ultra-violet radiation). In addition, the chapter shows the swelling, mechanical and biocompatible properties of crosslinked polymers. An emphasis on different applications of hydrophilic networks mentioned in literature is provided. Finally, the chapter shows several workers have successfully use oil sorbers with their different categories in cleaning oil spills for hydrophobic networks applications.

Acknowledgments This chapter was supported by Egyptian petroleum research institute.

Conflicts of Interest The authors declare no conflict of interest.

References

- Abdel-Azim, A. A., Mahmoud, A., Atta, A. M., Witold, B., & El-Kafrawy, A. F. (2007). Synthesis and characterization of porous crosslinked copolymers for oil spill sorption. *E-Polymer*, 7(1), 1371–1383. <https://doi.org/10.1515/epoly.2007.7.1.1371>.
- Ahmadi, F., Oveisi, Z., Samani, S. M., & Amoozgar, Z. (2015). Chitosan based hydrogels: Characteristics and pharmaceutical applications. *Research in Pharmaceutical Sciences*, 10(1), 1–16. PMID: 26430453.
- Akhtar, M. F., Hanif, M., & Ranjha, N. M. (2016). Methods of synthesis of hydrogels... a review. *Saudi Pharmaceutical Journal*, 24(5), 554–559. <https://doi.org/10.1016/j.jsps.2015.03.022>.
- Anjum, S., Arora, A., Alam, M. S., & Gupta, B. (2016). Development of antimicrobial and scar preventive chitosan hydrogel wound dressings. *International Journal of Pharmaceutics*, 508(1–2), 92–101. <https://doi.org/10.1016/j.ijpharm.2016.05.013>.
- Atta, A. M., & Arndt, K. F. (2005). Swelling of high oil-absorptive network based on 1-octene and isodecyl acrylate copolymers. *Journal of Polymer Research*, 12(2), 77–88. <https://doi.org/10.1007/s10965-004-2025-1>.
- Baek, J., Fan, Y., Jeong, S. H., Lee, H. Y., Jung, H. D., Kim, H. E., & Jang, T. S. (2018). Facile strategy involving low-temperature chemical cross-linking to enhance the physical and biological properties of hyaluronic acid hydrogel. *Carbohydrate Polymers*, 202, 545–553. <https://doi.org/10.1039/c2sm06463d>.
- Benjamin, C. (2017). *Adhesion characteristics and swelling response of stimuli-responsive hydrogels*. The University of Wisconsin-Madison.
- Bi, X., & Liang, A. (2016). In situ-forming cross-linking hydrogel systems: Chemistry and biomedical applications. In Emerging concepts in analysis and applications of hydrogels. <https://doi.org/10.5772/63954>.
- Billah, S. M. R., Mondal, M. I. H., Somoal, S. H., & Pervez, M. N. (2018). Cellulose-based hydrogel for industrial applications. In M. Mondal (Ed.), *Cellulose-based superabsorbent hydrogels* (Polymers and polymeric composites: A reference series). Cham: Springer. https://doi.org/10.1007/978-3-319-76573-0_63-1.
- Bukhari, S. M. H., Khan, S., Rehanullah, M., & Ranjha, N. M. (2015). Synthesis and characterization of chemically cross-linked acrylic acid/gelatin hydrogels: Effect of pH and composition on swelling and drug release. *International Journal of Polymer Science*, 2015, 1–15. <https://doi.org/10.1155/2015/187961>.

- Caló, E., & Khutoryanskiy, V. V. (2015). Biomedical applications of hydrogels: A review of patents and commercial products. *European Polymer Journal*, *65*, 252–267. <https://doi.org/10.1016/j.eurpolymj.2014.11.024>.
- Cao, L., Cao, B., Lu, C., Wang, G., Yu, L., & Ding, J. (2015). An injectable hydrogel formed by in situ cross-linking of glycol chitosan and multi-benzaldehyde functionalized PEG analogues for cartilage tissue engineering. *Journal of Materials Chemistry B*, *3*(7), 1268–1280. <https://doi.org/10.1039/c4tb01705f>.
- Chai, Q., Jiao, Y., & Yu, X. (2017). Hydrogels for biomedical applications: Their characteristics and the mechanisms behind them. *Gels*, *3*(1), 6. <https://doi.org/10.3390/gels3010006>.
- Chandler, D. L. (2018). Biomedical materials learn to heal themselves: Self-healing polymers, hydrogels, and artificial muscles are mimicking nature's repair mechanisms. *IEEE Pulse*, *9*(3), 10–14. <https://doi.org/10.1109/mpul.2018.2814241>.
- Chaudhuri, O., Gu, L., Klumpers, D., Darnell, M., Bencherif, S. A., Weaver, J. C., & Mooney, D. J. (2016). Hydrogels with tunable stress relaxation regulate stem cell fate and activity. *Nature Materials*, *15*(3), 326–334. <https://doi.org/10.1038/nmat4489>.
- Chen, M., Coasne, B., Guyer, R., Derome, D., & Carmeliet, J. (2018). Role of hydrogen bonding in hysteresis observed in sorption-induced swelling of soft nanoporous polymers. *Nature Communications*, *9*(1), 3507. <https://doi.org/10.1038/s41467-018-05897-9>.
- Cheng, D., Liu, Y., Yang, G., & Zhang, A. (2018). Water and fertilizer integrated hydrogel derived from the polymerization of acrylic acid and urea as a slow release N fertilizer and water retention in agriculture. *Journal of Agricultural and Food Chemistry*, *66*(23), 5762–5769. <https://doi.org/10.1021/acs.jafc.8b00872>.
- Chin, S. Y., Poh, Y. C., Kohler, A. C., Compton, J. T., Hsu, L. L., Lau, K. M., & Sia, S. K. (2017). Additive manufacturing of hydrogel-based materials for next-generation implantable medical devices. *Science Robotics*, *2*(2), eaah6451. <https://doi.org/10.1126/scirobotics.aah6451>.
- Choi, M., Humar, M., Kim, S., & Yun, S. H. (2015). Step index optical fiber made of biocompatible hydrogels. *Advanced Materials*, *27*(27), 4081–4086. <https://doi.org/10.1002/adma.201501603>.
- Contessi Negrini, N., Tarsini, P., Tanzi, M. C., & Farè, S. (2019). Chemically crosslinked gelatin hydrogels as scaffolding materials for adipose tissue engineering. *Journal of Applied Polymer Science*, *136*(8), 47104. <https://doi.org/10.1002/app.47104>.
- Cuadri, A. A., Romero, A., Bengochea, C., & Guerrero, A. (2018). The effect of carboxyl group content on water uptake capacity and tensile properties of functionalized soy protein-based superabsorbent plastics. *Journal of Polymers and the Environment*, *26*(7), 2934–2944. <https://doi.org/10.1007/s10924-018-1183-x>.
- Culver, H. R., Clegg, J. R., & Peppas, N. A. (2017). Analyte-responsive hydrogels: Intelligent materials for biosensing and drug delivery. *Accounts of Chemical Research*, *50*(2), 170–178. <https://doi.org/10.1021/acs.accounts.6b00533>.
- Dai, X., Zhang, Y., Gao, L., Bai, T., Wang, W., Cui, Y., & Liu, W. (2015). A mechanically strong, highly stable, thermoplastic, and self-healable supramolecular polymer hydrogel. *Advanced Materials*, *27*(23), 3566–3571. <https://doi.org/10.1002/adma.201500534>.
- Das, D., Pham, T. T. H., & Noh, I. (2018). Characterizations of hyaluronate-based terpolymeric hydrogel synthesized via free radical polymerization mechanism for biomedical applications. *Colloids and Surfaces B: Biointerfaces*, *170*, 64–75. <https://doi.org/10.1016/j.colsurfb.2018.05.059>.
- Deen, G., & Loh, X. (2018). Stimuli-responsive cationic hydrogels in drug delivery applications. *Gels*, *4*(1), 13. <https://doi.org/10.3390/gels4010013>.
- Deng, G., Tang, C., Li, F., Jiang, H., & Chen, Y. (2011). Covalent cross-linked polymer gels with reversible sol–gel transition and self-healing properties. *Macromolecules*, *43*(3), 1191–1194. <https://doi.org/10.1021/ma9022197>.
- Desai, R. M., Koshy, S. T., Hilderbrand, S. A., Mooney, D. J., & Joshi, N. S. (2015). Versatile click alginate hydrogels crosslinked via tetrazine–norbornene chemistry. *Biomaterials*, *50*, 30–37. <https://doi.org/10.1016/j.biomaterials.2015.01.048>.

- Dicker, M. P., Baker, A. B., Iredale, R. J., Naficy, S., Bond, I. P., Faul, C. F., & Weaver, P. M. (2017). Light-triggered soft artificial muscles: Molecular-level amplification of actuation control signals. *Scientific Reports*, 7(1), 9197. <https://doi.org/10.1038/s41598-017-08777-2>.
- Dimatteo, R., Darling, N. J., & Segura, T. (2018). *In situ* forming injectable hydrogels for drug delivery and wound repair. *Advanced Drug Delivery Reviews*, 127, 167–184. <https://doi.org/10.1016/j.addr.2018.03.007>.
- Echazú, M. I. A., Olivetti, C. E., Anesini, C., Pérez, C. J., Alvarez, G. S., & Desimone, M. F. (2017). Development and evaluation of thymol-chitosan hydrogels with antimicrobial-antioxidant activity for oral local delivery. *Materials Science and Engineering: C*, 81, 588–596. <https://doi.org/10.1016/j.msec.2017.08.059>.
- El-Ghazawy, R. A., & Farag, R. K. (2014). Comb-like crosslinked alkyl acrylates-vinyl acetate terpolymers for oil sorption. *Journal of Polymer Research*, 21(7), 1–11. <https://doi.org/10.1007/s10965-014-0509-1>.
- El-Ghazawy, R. A. M., Farag, R. K., Elsaheed, S. M., Abdel-Halim, E. D. A., Yossef, M. A., & Toyor, W. E. (2014). Castor oil based organogels: I. synthesis, swelling, and network parameters. *Journal of Dispersion Science and Technology*, 35(3), 350–357. <https://doi.org/10.1080/001932691.2013.788450>.
- Farag, R. K., El-Saeed, S. M., & Maysour, N. E. (2011). Swelling and network parameters of 1-hexadecene-co-trimethylolpropane distearate monoacrylate sorbers. *Journal of Dispersion Science and Technology*, 32(3), 395–406. <https://doi.org/10.1080/001932691003662415>.
- Feng, Q., Wei, K., Lin, S., Xu, Z., Sun, Y., Shi, P., & Bian, L. (2016). Mechanically resilient, injectable, and bioadhesive supramolecular gelatin hydrogels crosslinked by weak host-guest interactions assist cell infiltration and *in situ* tissue regeneration. *Biomaterials*, 101, 217–228. <https://doi.org/10.1016/j.biomaterials.2016.05.043>.
- Fisher, S. A., Tam, R. Y., Fokina, A., Mahmoodi, M. M., Distefano, M. D., & Shoichet, M. S. (2018). Photo-immobilized EGF chemical gradients differentially impact breast cancer cell invasion and drug response in defined 3D hydrogels. *Biomaterials*, 178, 751–766. <https://doi.org/10.1016/j.biomaterials.2018.01.032>.
- Flory, P. J. (1953). *Principles of polymer chemistry*. Cornell University Press.
- Fortman, D. J., Brutman, J. P., De Hoe, G. X., Snyder, R. L., Dichtel, W. R., & Hillmyer, M. A. (2018). Approaches to sustainable and continually recyclable cross-linked polymers. *ACS Sustainable Chemistry & Engineering*, 6(9), 11145–11159. <https://doi.org/10.1021/acscchemeng.8b02355>.
- Foster, J. A., Parker, R. M., Belenguer, A. M., Kishi, N., Sutton, S., Abell, C., & Nitschke, J. R. (2015). Differentially addressable cavities within metal-organic cage-cross-linked polymeric hydrogels. *Journal of the American Chemical Society*, 137(30), 9722–9729. <https://doi.org/10.1021/jacs.5b05507>.
- Gallagher, A. G., Alorabi, J. A., Wellings, D. A., Lace, R., Horsburgh, M. J., & Williams, R. L. (2016). A novel peptide hydrogel for an antimicrobial bandage contact lens. *Advanced Healthcare Materials*, 5(16), 2013–2018. <https://doi.org/10.1002/adhm.201600258>.
- García-Astrain, C., & Avérous, L. (2018). Synthesis and evaluation of functional alginate hydrogels based on click chemistry for drug delivery applications. *Carbohydrate Polymers*, 190, 271–280. <https://doi.org/10.1016/j.carbpol.2018.02.086>.
- Ghobril, C., & Grinstaff, M. W. (2015). The chemistry and engineering of polymeric hydrogel adhesives for wound closure: A tutorial. *Chemical Society Reviews*, 44(7), 1820–1835. <https://doi.org/10.1039/c4cs00332b>.
- Gong, Z., Zhang, G., Zeng, X., Li, J., Li, G., Huang, W., & Wong, C. (2016). High-strength, tough, fatigue resistant, and self-healing hydrogel based on dual physically cross-linked network. *ACS Applied Materials & Interfaces*, 8(36), 24030–24037. <https://doi.org/10.1021/acsmi.6b05627>.
- Griffith, L. G., Imperiali, B., Cook, C. D., Ahrens, C. C., Renggli, K., & Macias, J. L. V. (2018). *U.S. Patent Application No. 15/543,866*.
- Guilherme, M. R., Aouada, F. A., Fajardo, A. R., Martins, A. F., Paulino, A. T., Davi, M. F., & Muniz, E. C. (2015). Superabsorbent hydrogels based on polysaccharides for application in agriculture as soil conditioner and nutrient carrier: A review. *European Polymer Journal*, 72, 365–385. <https://doi.org/10.1016/j.eurpolymj.2015.04.017>.

- Gutiérrez, T. J., & González, G. (2017). Effect of cross-linking with *Aloe vera* gel on surface and physicochemical properties of edible films made from plantain flour. *Food Biophysics*, 12(1), 11–22. <https://doi.org/10.1007/s11483-016-9458-z>.
- Gutiérrez, T. J., Morales, N. J., Pérez, E., Tapia, M. S., & Famá, L. (2015a). Physico-chemical properties of edible films derived from native and phosphated cush-cush yam and cassava starches. *Food Packaging and Shelf Life*, 3, 1–8. <https://doi.org/10.1016/j.foodhyd.2014.09.002>.
- Gutiérrez, T. J., Tapia, M. S., Pérez, E., & Famá, L. (2015b). Structural and mechanical properties of edible films made from native and modified cush-cush yam and cassava starch. *Food Hydrocolloids*, 45, 211–217. <https://doi.org/10.1016/j.foodhyd.2014.11.017>.
- Gutiérrez, T. J., Suniaga, J., Monsalve, A., & García, N. L. (2016a). Influence of beet flour on the relationship surface-properties of edible and intelligent films made from native and modified plantain flour. *Food Hydrocolloids*, 54(Part B), 234–244. <https://doi.org/10.1016/j.foodhyd.2015.10.012>.
- Gutiérrez, T. J., Guzmán, R., Medina Jaramillo, C., & Famá, L. (2016b). Effect of beet flour on films made from biological macromolecules: Native and modified plantain flour. *International Journal of Biological Macromolecules*, 82, 395–403. <https://doi.org/10.1016/j.ijbiomac.2015.10.020>.
- Hamed, H., Moradi, S., Hudson, S. M., & Tonelli, A. E. (2018). Chitosan based hydrogels and their applications for drug delivery in wound dressings: A review. *Carbohydrate Polymers*, 199, 445–460. <https://doi.org/10.1016/j.carbpol.2018.06.114>.
- Hassan, C. M., & Peppas, N. A. (2000). Structure and applications of poly(vinyl alcohol) hydrogels produced by conventional crosslinking or by freezing/thawing methods. In *Biopolymers-PVA hydrogels, anionic polymerisation nanocomposites* (Advances in polymer science) (Vol. 153). Berlin/Heidelberg: Springer. https://doi.org/10.1007/3-540-46414-x_2.
- Hennink, W. E., & van Nostrum, C. F. (2012). Novel crosslinking methods to design hydrogels. *Advanced Drug Delivery Reviews*, 64, 223–236. <https://doi.org/10.1016/j.addr.2012.09.009>.
- Hotta, M., Kennedy, J., Higginbotham, C., & Morris, N. (2016). Development of seed coating agent with ι-carrageenan hydrogel for sustainable agriculture. *Journal of the Institute of Chemistry of Ireland*, 2, 36–37.
- Hu, B., Ow, C., Chee, P. L., Leow, W. R., Liu, X., Wu, Y. L., & Chen, X. (2018). Supramolecular hydrogels for antimicrobial therapy. *Chemical Society Reviews*, 47(18), 6917–6929. <https://doi.org/10.1039/c8cs00128f>.
- Huang, G., & Huang, H. (2018). Hyaluronic acid-based biopharmaceutical delivery and tumor-targeted drug delivery system. *Journal of Controlled Release*, 278, 122–126. <https://doi.org/10.1016/j.jconrel.2018.04.015>.
- Ibáñez-Fonseca, A., Ramos, T. L., González de Torre, I., Sánchez-Abarca, L. I., Muntión, S., Arias, F. J., & Rodríguez-Cabello, J. C. (2018). Biocompatibility of two model elastinlike recombinamer based hydrogels formed through physical or chemical crosslinking for various applications in tissue engineering and regenerative medicine. *Journal of Tissue Engineering and Regenerative Medicine*, 12(3), e1450–e1460. <https://doi.org/10.1002/term.2562>.
- Iwasa, K., Takashima, Y., & Harada, A. (2016). Fast response dry-type artificial molecular muscles with [c2]daisy chains. *Nature Chemistry*, 8(6), 625–632. <https://doi.org/10.1038/nchem.2513>.
- Jain, A., Balasubramanian, R., & Srinivasan, M. P. (2016). Hydrothermal conversion of biomass waste to activated carbon with high porosity: A review. *Chemical Engineering Journal*, 283, 789–805. <https://doi.org/10.1016/j.cej.2015.08.014>.
- Jamal, A., Shahzadi, L., Ahtaz, S., Zahid, S., Chaudhry, A. A., Rehman, I., & Yar, M. (2018). Identification of anti-cancer potential of doxazocin: Loading into chitosan based biodegradable hydrogels for on-site delivery to treat cervical cancer. *Materials Science and Engineering: C*, 82, 102–109. <https://doi.org/10.1016/j.msec.2017.08.054>.
- Jang, J., & Kim, B. (2000). Studies of crosslinked styrene-alkyl acrylate copolymers for oil absorbency application. II. Effects of polymerization conditions on oil absorbency. *Journal of Applied Polymer Science*, 77(4), 914–920. [https://doi.org/10.1002/\(sici\)1097-4628\(20000725\)77:4<914::aid-app27>3.0.co;2-7](https://doi.org/10.1002/(sici)1097-4628(20000725)77:4<914::aid-app27>3.0.co;2-7).

- Jones, D. S., McCoy, C. P., Andrews, G. P., McCrory, R. M., & Gorman, S. P. (2015). Hydrogel antimicrobial capture coatings for endotracheal tubes: A pharmaceutical strategy designed to prevent ventilator-associated pneumonia. *Molecular Pharmaceutics*, 12(8), 2928–2936. <https://doi.org/10.1021/acs.molpharmaceut.5b00208>.
- Kabir, M. H., Ahmed, K., & Furukawa, H. (2017). A low cost sensor based agriculture monitoring system using polymeric hydrogel. *Journal of the Electrochemical Society*, 164(5), B3107–B3112. <https://doi.org/10.1149/2.0171705jes>.
- Kabiri, K., Omidian, H., Zohuriaan-Mehr, M. J., & Doroudiani, S. (2011). Superabsorbent hydrogel composites and nanocomposites: A review. *Polymer Composites*, 32(2), 277–289. <https://doi.org/10.1002/pc.21046>.
- Kade, M., & Tirrell, M. (2014). Free radical and condensation polymerizations. In W. F. Reed & A. M. Alb (Eds.), *Monitoring polymerization reactions: From fundamentals to applications* (pp. 1–28). Wiley. <https://doi.org/10.1002/9781118733813>.
- Kamoun, E. A., Kenawy, E. R. S., & Chen, X. (2017). A review on polymeric hydrogel membranes for wound dressing applications: PVA-based hydrogel dressings. *Journal of Advanced Research*, 8(3), 217–233. <https://doi.org/10.1016/j.jare.2017.01.005>.
- Kirschning, A., Dibbert, N., & Dräger, G. (2018). Chemical functionalization of polysaccharides—Towards biocompatible hydrogels for biomedical applications. *Chemistry—A European Journal*, 24(6), 1231–1240. <https://doi.org/10.1002/chem.201701906>.
- Kondo, S., Hiroi, T., Han, Y. S., Kim, T. H., Shibayama, M., Chung, U. I., & Sakai, T. (2015). Reliable hydrogel with mechanical “fuse link” in an aqueous environment. *Advanced Materials*, 27(45), 7407–7411. <https://doi.org/10.1002/adma.201503130>.
- Konwar, A., Kalita, S., Kotoky, J., & Chowdhury, D. (2016). Chitosan–iron oxide coated graphene oxide nanocomposite hydrogel: A robust and soft antimicrobial biofilm. *ACS Applied Materials & Interfaces*, 8(32), 20625–20634. <https://doi.org/10.1021/acsami.6b07510>.
- Kumru, B., Shalom, M., Antonietti, M., & Schmidt, B. V. (2017). Reinforced hydrogels via carbon nitride initiated polymerization. *Macromolecules*, 50(5), 1862–1869. <https://doi.org/10.1021/acs.macromol.6b02691>.
- Lansalot, M., Rieger, J., & D’Agosto, F. (2016). Polymerization induced self-assembly: The contribution of controlled radical polymerization to the formation of self-stabilized polymer particles of various morphologies. In L. Billon & O. Borisov (Eds.), *Macromolecular self-assembly* (pp. 33–82). Pp: Wiley. <https://doi.org/10.1021/ma070442w>.
- Lauren, J. A., Justin, E. H., & Coray, M. C. (2014). Virtual synthesis of thermally cross-linked copolymers from a novel implementation of polymatic. *The Journal of Physical Chemistry. B*, 118(7), 1916–1924. <https://doi.org/10.1021/jp409664d>.
- Lee, S. H., Kim, T. H., Lima, M. D., Baughman, R. H., & Kim, S. J. (2016). Biothermal sensing of a torsional artificial muscle. *Nanoscale*, 8(6), 3248–3253. <https://doi.org/10.1039/c5nr07195j>.
- Li, J., & Mooney, D. J. (2016). Designing hydrogels for controlled drug delivery. *Nature Reviews Materials*, 1(12), 16071. <https://doi.org/10.1038/natrevmats.2016.71>.
- Li, Q. F., Du, X., Jin, L., Hou, M., Wang, Z., & Hao, J. (2016). Highly luminescent hydrogels synthesized by covalent grafting of lanthanide complexes onto PNIPAM via one-pot free radical polymerization. *Journal of Materials Chemistry C*, 4(15), 3195–3201. <https://doi.org/10.1039/c6tc00336b>.
- Li, Z., Tang, M., Dai, J., Wang, T., Wang, Z., Bai, W., & Bai, R. (2017). Preparation of covalent pseudo-two-dimensional polymers in water by free radical polymerization. *Macromolecules*, 50(11), 4292–4299. <https://doi.org/10.1021/acs.macromol.7b00668>.
- Lin, P., Ma, S., Wang, X., & Zhou, F. (2015). Molecularly engineered dual crosslinked hydrogel with ultrahigh mechanical strength, toughness, and good self-recovery. *Advanced Materials*, 27(12), 2054–2059. <https://doi.org/10.1002/adma.201405022>.
- Liu, F., Seuring, J., & Agarwal, S. (2014). A non-ionic thermophilic hydrogel with positive thermo-sensitivity in water and electrolyte solution. *Macromolecular Chemistry and Physics*, 215(15), 1466–1472. <https://doi.org/10.1002/macp.201400155>.
- Mahou, R., Borcard, F., Crivelli, V., Montanari, E., Passemard, S., Noverraz, F., & Wandrey, C. (2015). Tuning the properties of hydrogel microspheres by adding chemical cross-linking functionality to sodium alginate. *Chemistry of Materials*, 27(12), 4380–4389. <https://doi.org/10.1021/acs.chemmater.5b01098>.

- Maitra, J., & Shukla, V. K. (2014). Cross-linking in hydrogels-a review. *American Journal of Polymer Science*, 4(2), 25–31. <https://doi.org/10.5923/jj.ajps.20140402.01>.
- Maulvi, F. A., Lakdawala, D. H., Shaikh, A. A., Desai, A. R., Choksi, H. H., Vaidya, R. J., & Shah, D. O. (2016). *In vitro* and *in vivo* evaluation of novel implantation technology in hydrogel contact lenses for controlled drug delivery. *Journal of Controlled Release*, 226, 47–56. <https://doi.org/10.1016/j.jconrel.2016.02.012>.
- Mishra, S., Rani, P., Sen, G., & Dey, K. P. (2018). Preparation, properties and application of hydrogels: A review. In V. Thakur & M. Thakur (Eds.), *Hydrogels* (Gels horizons: From science to smart materials). Singapore: Springer. <https://doi.org/10.4172/2254-609x.100013>.
- Miyamae, K., Nakahata, M., Takashima, Y., & Harada, A. (2015). Self-healing, expansion–contraction, and shape-memory properties of a preorganized supramolecular hydrogel through host–guest interactions. *Angewandte Chemie International Edition*, 54(31), 8984–8987. <https://doi.org/10.1002/anie.201502957>.
- Mohamad, N., Loh, E. Y. X., Fauzi, M. B., Ng, M. H., & Amin, M. C. I. M. (2018). *In vivo* evaluation of bacterial cellulose/acrylic acid wound dressing hydrogel containing keratinocytes and fibroblasts for burn wounds. *Drug Delivery and Translational Research*, 9(2), 444–452. <https://doi.org/10.1007/s13346-017-0475-3>.
- Molpeceres, C., Marquez, A., Lauzurica, S., Gómez-Fontela, M., Muñoz, D., & Morales, M. (2018). Laser direct writing of biocompatible hydrogels using a blister assisted approach with thick polyimide layers (Conference Presentation). In *Laser-based Micro-and Nanoprocessing XII* (Vol. 10520, p. 1052000). International Society for Optics and Photonics.
- Muniz, E. C., & Geuskens, G. (2001). Polyacrylamide hydrogels and semi-interpenetrating networks (IPNs) with poly(N-isopropylacrylamide): Mechanical properties by measure of compressive elastic modulus. *Journal of Materials Science: Materials in Medicine*, 12(10–12), 879–881. <https://doi.org/10.1023/a:1012863705484>.
- Najdahmadi, A., Lakey, J. R., & Botvinick, E. (2018). Structural characteristics and diffusion coefficient of alginate hydrogels used for cell based drug delivery. *MRS Advances*, 3(40), 2399–2408. <https://doi.org/10.1557/adv.2018.455>.
- Nam, C., Zimudzi, T. J., Geise, G. M., & Hickner, M. A. (2016). Increased hydrogel swelling induced by absorption of small molecules. *ACS Applied Materials & Interfaces*, 8(22), 14263–14270. <https://doi.org/10.1021/acsami.6b02069>.
- Nawaz, S., Khan, S., Farooq, U., Haider, M. S., Ranjha, N. M., Rasul, A., & Hameed, R. (2018). Biocompatible hydrogels for the controlled delivery of anti-hypertensive agent: Development, characterization and *in vitro* evaluation. *Designed Monomers and Polymers*, 21(1), 18–32. <https://doi.org/10.1080/15685551.2018.1445416>.
- Neethu, T. M., Dubey, P. K., & Kaswala, A. R. (2018). Prospects and applications of hydrogel technology in agriculture. *International Journal of Current Microbiology and Applied Sciences*, 7(5), 3155–3162. <https://doi.org/10.20546/ijcmas.2018.705.369>.
- Nguyen, L. H., Gao, M., Lin, J., Wu, W., Wang, J., & Chew, S. Y. (2017). Three-dimensional aligned nanofibers-hydrogel scaffold for controlled non-viral drug/gene delivery to direct axon regeneration in spinal cord injury treatment. *Scientific Reports*, 7, 42212. <https://doi.org/10.1038/srep42212>.
- Niu, Y., Xia, Q., Li, N., Wang, Z., & Yu, L. L. (2019). Gelling and bile acid binding properties of gelatin-alginate gels with interpenetrating polymer networks by double cross-linking. *Food Chemistry*, 270, 223–228. <https://doi.org/10.1016/j.foodchem.2018.07.105>.
- Nordström, R., & Malmsten, M. (2017). Delivery systems for antimicrobial peptides. *Advances in Colloid and Interface Science*, 242, 17–34. <https://doi.org/10.1016/j.cis.2017.01.005>.
- Norouzi, M., Nazari, B., & Miller, D. W. (2016). Injectable hydrogel-based drug delivery systems for local cancer therapy. *Drug Discovery Today*, 21(11), 1835–1849. <https://doi.org/10.1016/j.drudis.2016.07.006>.
- Nurunnabi, M., Parvez, K., Nafiujjaman, M., Revuri, V., Khan, H. A., Feng, X., & Lee, Y. K. (2015). Bioapplication of graphene oxide derivatives: Drug/gene delivery, imaging, polymeric modification, toxicology, therapeutics and challenges. *RSC Advances*, 5(52), 42141–42161. <https://doi.org/10.1039/c5ra04756k>.

- Nystrom, B., Kjøniksen, A. L., & Lindman, B. (1996). Effects of temperature, surfactant, and salt on the rheological behavior in semidilute aqueous systems of a nonionic cellulose ether. *Langmuir*, 12(13), 3233–3240. <https://doi.org/10.1021/la960029+>.
- Ouyang, L., Highley, C. B., Rodell, C. B., Sun, W., & Burdick, J. A. (2016). 3D printing of shear-thinning hyaluronic acid hydrogels with secondary cross-linking. *ACS Biomaterials Science & Engineering*, 2(10), 1743–1751. <https://doi.org/10.1021/acsbomaterials.6b00158>.
- Pakulska, M. M., Vulic, K., Tam, R. Y., & Shoichet, M. S. (2015). Hybrid crosslinked methylcellulose hydrogel: A predictable and tunable platform for local drug delivery. *Advanced Materials*, 27(34), 5002–5008. <https://doi.org/10.1002/adma.201502767>.
- Pan, X., Lamson, M., Yan, J., & Matyjaszewski, K. (2015). Photoinduced metal-free atom transfer radical polymerization of acrylonitrile. *ACS Macro Letters*, 4(2), 192–196. <https://doi.org/10.1021/mz500834g>.
- Pellá, M. G., Lima-Tenório, M. K., Tenório-Neto, E. T., Guilherme, M. R., Muniz, E. C., & Rubira, A. F. (2018). Chitosan-based hydrogels: From preparation to biomedical applications. *Carbohydrate Polymers*, 196, 233–245. <https://doi.org/10.1016/j.carbpol.2018.05.033>.
- Peppas, N. A., Bures, P., Leobandung, W., & Ichikawa, H. (2000). Hydrogels in pharmaceutical formulations. *European Journal of Pharmaceutics and Biopharmaceutics*, 50(1), 27–46. [https://doi.org/10.1016/s0939-6411\(00\)00090-4](https://doi.org/10.1016/s0939-6411(00)00090-4).
- Picone, P., Sabatino, M. A., Ajovalasit, A., Giacomazza, D., Dispenza, C., & Di Carlo, M. (2019). Biocompatibility, hemocompatibility and antimicrobial properties of xyloglucan-based hydrogel film for wound healing application. *International Journal of Biological Macromolecules*, 121, 784–795. <https://doi.org/10.1016/j.ijbiomac.2018.10.078>.
- Pires, R. A., Abul-Hajja, Y. M., Reis, R. L., Ulijn, R. V., & Pashkuleva, I. (2018). Hydrogel nanomaterials for cancer diagnosis and therapy. In T. Raghu, R. Singh, G. Laverty, & R. Donnelly (Eds.), *Hydrogels: Design, synthesis and application in drug delivery and regenerative medicine* (pp. 170–183). CRC Press. ISBN 9781498748612. <https://doi.org/10.1201/9781315152226-10>.
- Pitt, W. G., Zhao, Y., Jack, D. R., Perez, K. X., Jones, P. W., Marelli, R., & Pruitt, J. D. (2015). Extended elution of phospholipid from silicone hydrogel contact lenses. *Journal of Biomaterials Science, Polymer Edition*, 26(4), 224–234. <https://doi.org/10.1080/09205063.2014.994947>.
- Qu, J., Zhao, X., Liang, Y., Zhang, T., Ma, P. X., & Guo, B. (2018). Antibacterial adhesive injectable hydrogels with rapid self-healing, extensibility and compressibility as wound dressing for joints skin wound healing. *Biomaterials*, 183, 185–199. <https://doi.org/10.1016/j.biomaterials.2018.08.044>.
- Rana, P., Ganarajan, G., & Kothiyal, P. (2015). Review on preparation and properties hydrogel formulation. *World Journal of Pharmacy and Pharmaceutical Sciences*, 4(12), 1069–1080. Available in: <https://pdfs.semanticscholar.org/d9ac/ef6d09c60149d9beeff1978753df8c7aafe0.pdf>.
- Rao, Y. L., Chortos, A., Pfattner, R., Lissel, F., Chiu, Y. C., Feig, V., & He, M. (2016). Stretchable self-healing polymeric dielectrics cross-linked through metal–ligand coordination. *Journal of the American Chemical Society*, 138(18), 6020–6027. <https://doi.org/10.1021/jacs.6b0242>.
- Rinehart, S. J., Campbell, T., Burke, K. J., Garcia, B., Mlynarski, A., Brain, S. J., & Keleher, J. J. (2016). Synthesis and characterization of a chitosan/PVA antimicrobial hydrogel nanocomposite for responsive wound management materials. *Journal of Microbial Biochemical Technology*, 8(2), 065–070. <https://doi.org/10.4172/1948-5948.1000264>.
- Rosales, A. M., Vega, S. L., DelRio, F. W., Burdick, J. A., & Anseth, K. S. (2017). Hydrogels with reversible mechanics to probe dynamic cell microenvironments. *Angewandte Chemie International Edition*, 56(40), 12132–12136. <https://doi.org/10.1002/anie.201705684>.
- Sadtler, K., Wolf, M. T., Ganguly, S., Moad, C. A., Chung, L., Majumdar, S., & Elisseeff, J. H. (2019). Divergent immune responses to synthetic and biological scaffolds. *Biomaterials*, 192, 405–415. <https://doi.org/10.1016/j.biomaterials.2018.11.002>.
- Sawada, J., Aoki, D., Otsuka, H., & Takata, T. (2019). A guiding principle for toughening cross-linked polymers: Synthesis and application of mobilitycontrolling rotaxane crosslinkers. *Angewandte Chemie. Int. Ed.*, 58(9), 2765–2768. <https://doi.org/10.1002/anie.201813439>.

- Schafer, J., Reindel, W., Steffen, R., Mosehauer, G., & Chinn, J. (2018). Use of a novel extended blink test to evaluate the performance of two polyvinylpyrrolidone-containing, silicone hydrogel contact lenses. *Clinical Ophthalmology (Auckland, NZ)*, *12*, 819–825. <https://doi.org/10.2147/oph.s162233>.
- Shantha, K. L., & Harding, D. R. K. (2002). Synthesis and evaluation of sucrose-containing polymeric hydrogels for oral drug delivery. *Journal of Applied Polymer Science*, *84*(14), 2597–2604. <https://doi.org/10.1002/app.10378>.
- Sharma, M., Jingjunjiao, L., & Seyfoddin, A. (2018). Thermosensitive hydrogels for drug delivery and tissue engineering. In T. R. R. Singh, G. Laverty, & R. Donnelly (Eds.), *Hydrogels: Design, synthesis and application in drug delivery and regenerative medicine* (pp. 184–207). CRC Press. <https://doi.org/10.1201/9781315152226>.
- Shi, Z., Gao, X., Ullah, M. W., Li, S., Wang, Q., & Yang, G. (2016). Electroconductive natural polymer-based hydrogels. *Biomaterials*, *111*, 40–54. <https://doi.org/10.1016/j.biomaterials.2016.09.020>.
- Shimba, K., Miyamoto, Y., & Yagi, T. (2017). Hydrogel-supported bilayers for studying membrane protein functions. In: *Biomedical Engineering International Conference (BMEiCON), 2017 10th* (pp. 1–4). IEEE.
- Slaughter, B. V., Khurshid, S. S., Fisher, O. Z., Khademhosseini, A., & Peppas, N. A. (2009). Hydrogels in regenerative medicine. *Advanced Materials*, *21*(32–33), 3307–3329. <https://doi.org/10.1002/adma.200802106>.
- Song, J., Im, K., Hwang, S., Hur, J., Nam, J., Ahn, G. O., & Park, N. (2015). DNA hydrogel delivery vehicle for light-triggered and synergistic cancer therapy. *Nanoscale*, *7*(21), 9433–9437. <https://doi.org/10.1039/c5nr00858a>.
- Song, S. C., Lee, S. M., Kim, C. W., & Park, M. R. (2016). *U.S. Patent No. 9,526,699*. Washington, DC: U.S. Patent and Trademark Office.
- Sun, M., Bai, R., Yang, X., Song, J., Qin, M., Suo, Z., & He, X. (2018). Hydrogel interferometry for ultrasensitive and highly selective chemical detection. *Advanced Materials*, *30*(46), 1804916. <https://doi.org/10.1002/adma.201804916>.
- Sutirman, Z. A., Sanagi, M. M., Karim, K. J. A., & Ibrahim, W. A. W. (2016). Preparation of methacrylamide-functionalized crosslinked chitosan by free radical polymerization for the removal of lead ions. *Carbohydrate Polymers*, *151*, 1091–1099. <https://doi.org/10.1016/j.carbpol.2016.06.076>.
- Szafulera, K., Wach, R. A., Olejnik, A. K., Rosiak, J. M., & Ulański, P. (2018). Radiation synthesis of biocompatible hydrogels of dextran methacrylate. *Radiation Physics and Chemistry*, *142*, 115–120. <https://doi.org/10.1016/j.radphyschem.2017.01.004>.
- Takashima, Y., Sawa, Y., Iwaso, K., Nakahata, M., Yamaguchi, H., & Harada, A. (2017). Supramolecular materials cross-linked by host–guest inclusion complexes: The effect of side chain molecules on mechanical properties. *Macromolecules*, *50*(8), 3254–3261. <https://doi.org/10.1021/acs.macromol.7b00266>.
- Tian, R., Qiu, X., Yuan, P., Lei, K., Wang, L., Bai, Y., & Chen, X. (2018). Fabrication of self-healing hydrogels with on-demand antimicrobial activity and sustained biomolecule release for infected skin regeneration. *ACS Applied Materials & Interfaces*, *10*(20), 17018–17027. <https://doi.org/10.1002/ami.201700434>.
- Tomadoni, B., Casalagué, C., & Alvarez, V. A. (2019). Biopolymer-based hydrogels for agriculture applications: Swelling behavior and slow release of agrochemicals. In T. J. Gutiérrez (Ed.), *Polymers for Agri-food applications* (pp. 99–125). Cham: Springer. https://doi.org/10.1007/978-3-030-19416-1_7.
- Vining, K. H., Stafford, A., & Mooney, D. J. (2019). Sequential modes of crosslinking tune viscoelasticity of cell-instructive hydrogels. *Biomaterials*, *188*, 187–197. <https://doi.org/10.1016/j.biomaterials.2018.10.013>.
- Wang, H., & Heilshorn, S. C. (2015). Adaptable hydrogel networks with reversible linkages for tissue engineering. *Advanced Materials*, *27*(25), 3717–3736. <https://doi.org/10.1002/adma.201501558>.

- Wang, X., Wang, C., Zhang, Q., & Cheng, Y. (2016). Near infrared light-responsive and injectable supramolecular hydrogels for on-demand drug delivery. *Chemical Communications*, 52(5), 978–981. <https://doi.org/10.1039/c5cc08391e>.
- Wang, L., Shi, X., Wu, Y., Zhang, J., Zhu, Y., & Wang, J. (2018a). A multifunctional supramolecular hydrogel: Preparation, properties and molecular assembly. *Soft Matter*, 14(4), 566–573. <https://doi.org/10.1039/c7sm02358h>.
- Wang, Y., He, G., Li, Z., Hua, J., Wu, M., Gong, J., & Huang, L. (2018b). Novel biological hydrogel: Swelling behaviors study in salt solutions with different ionic valence number. *Polymers*, 10(2), 112. <https://doi.org/10.3390/polym10020112>.
- Wolffsohn, J. S., Mroczkowska, S., Hunt, O. A., Bilkhu, P., Drew, T., & Sheppard, A. (2015). Crossover evaluation of silicone hydrogel daily disposable contact lenses. *Optometry and Vision Science*, 92(11), 1063–1068. <https://doi.org/10.1097/OPX.0000000000000706>.
- Wu, S. W., Liu, X., Miller, A. L., II, Cheng, Y. S., Yeh, M. L., & Lu, L. (2018). Strengthening injectable thermo-sensitive NIPAAm-g-chitosan hydrogels using chemical cross-linking of disulfide bonds as scaffolds for tissue engineering. *Carbohydrate Polymers*, 192, 308–316. <https://doi.org/10.1016/j.carbpol.2018.03.047>.
- Xiang, Y., Oo, N. N. L., Lee, J. P., Li, Z., & Loh, X. J. (2017). Recent development of synthetic nonviral systems for sustained gene delivery. *Drug Discovery Today*, 22(9), 1318–1335. <https://doi.org/10.1016/j.drudis.2017.04.001>.
- Xing, J. F., Zheng, M. L., & Duan, X. M. (2015). Two-photon polymerization microfabrication of hydrogels: An advanced 3D printing technology for tissue engineering and drug delivery. *Chemical Society Reviews*, 44(15), 5031–5039. <https://doi.org/10.1039/c5cs00278h>.
- Yang, Y., Zhao, H., Jia, Y., Guo, Q., Qu, Y., Su, J., & Qian, Z. (2016). A novel gene delivery composite system based on biodegradable folate-poly(ester amine) polymer and thermosensitive hydrogel for sustained gene release. *Scientific Reports*, 6, 21402. <https://doi.org/10.1038/srep21402>.
- Yin, L., Fei, L., Cui, F., Tang, C., & Yin, C. (2007). Superporous hydrogels containing poly(acrylic acid-co-acrylamide)/O-carboxymethyl chitosan interpenetrating polymer networks. *Biomaterials*, 28(6), 1258–1266. <https://doi.org/10.1016/j.biomaterials.2006.11.008>.
- Zhang, X., & Zhuo, R. (2000). Synthesis of temperature-sensitive poly(*N*-isopropylacrylamide) hydrogel with improved surface property. *Journal of Colloid and Interface Science*, 223(2), 311–313. <https://doi.org/10.1006/jcis.1999.6654>.
- Zhang, J. T., Bhat, R., & Jandt, K. D. (2009). Temperature-sensitive PVA/PNIPAAm semi-IPN hydrogels with enhanced responsive properties. *Acta Biomaterialia*, 5(1), 488–497. <https://doi.org/10.1016/j.actbio.2008.06.012>.
- Zhang, S., Ermann, J., Succi, M. D., Zhou, A., Hamilton, M. J., Cao, B., & Traverso, G. (2015a). An inflammation-targeting hydrogel for local drug delivery in inflammatory bowel disease. *Science Translational Medicine*, 7(300), 300ra128–300ra128. <https://doi.org/10.1126/scitranslmed.aaa5657>.
- Zhang, D., Zhou, W., Wei, B., Wang, X., Tang, R., Nie, J., & Wang, J. (2015b). Carboxyl-modified poly(vinyl alcohol)-crosslinked chitosan hydrogel films for potential wound dressing. *Carbohydrate Polymers*, 125, 189–199. <https://doi.org/10.1016/j.carbpol.2015.02.034>.
- Zhang, J., Sen, A., Cho, E., Lee, J. S., & Webb, K. (2017). Poloxamine/fibrin hybrid hydrogels for non-viral gene delivery. *Journal of Tissue Engineering and Regenerative Medicine*, 11(1), 246–255. <https://doi.org/10.1002/term.1906>.
- Zhou, M., Liu, K., & Qian, X. (2016). A facile preparation of pH-temperature dual stimuli-responsive supramolecular hydrogel and its controllable drug release. *Journal of Applied Polymer Science*, 133(15). <https://doi.org/10.1002/app.43279>.
- Zhu, K., Yu, D., Chen, X., & Song, G. (2019). Preparation, characterization and controlled-release property of Fe³⁺ cross-linked hydrogels based on peach gum polysaccharide. *Food Hydrocolloids*, 87, 260–269. <https://doi.org/10.1016/j.foodhyd.2018.08.019>.

Chapter 5

Crosslinking of Polymers: Rubber Vulcanization



**Gordana Marković, Milena Marinović-Cincović,
Suzana Samaržija-Jovanović, Vojislav Jovanović,
and Jaroslava Budinski-Simendić**

Abstract Crosslinking is a process whereby the polymer segments from different polymer chains are interconnected by covalent (and sometimes ionic) linkages. Crosslinks can be formed either during the polymer synthesis process, or additionally by reaction leading to the connection of already finished macromolecules. The crosslinking agent is necessary for the crosslinking of the finished polymer. Given the great length of the macromolecules, only a small amount of crosslinking agent is necessary to produce huge spatially arranged macromolecules. The increase in the degree of branching and polymerization and the growth of the polymer are observed at the beginning of the crosslinking reaction. The branched polymer gradually passes into an infinite structure that is represented by the network of polymers. The polymer with a small number of crosslinking sites contains part of the soluble portion (sol) and part of the insoluble portion (gel). The portion of soluble (extractible) polymer is decreased along with the growth of crosslinking density. Crosslinking of polymers leads, on the one hand, to the reduction of solubility and fusibility and, on the other hand, the increase of thermal stability and resistance to chemicals. The most frequently used crosslinking reaction in technological practice is the rubber vulcanization. Formerly, the plastic material is changed during vulcanization in highly elastic vulcanized rubber. Vulcanization resides in the reaction of elemental sulphur, organic sulphur compounds or organic peroxides with linear polymer chains, when crosslinks are forming. The most important and at the same time the oldest vulcanizing agent of polydiene rubbers is sulphur. Polymers can also

G. Marković (✉)
Tigar, Pirot, Serbia

M. Marinović-Cincović
Institute of Nuclear Science Vinča, University of Belgrade, Belgrade, Serbia

S. Samaržija-Jovanović · V. Jovanović
Faculty of Natural Sciences and Mathematics, University of Priština-Kosovska Mitrovica,
Kosovska Mitrovica, Serbia

J. Budinski-Simendić
Faculty of Technology, University of Novi Sad, Novi Sad, Serbia

construct crosslinks by peroxides. The main objective of this chapter was to analyze the crosslinking processes associated with vulcanization reactions between rubber macromolecules, as well as the types of crosslinking and the determination of crosslinking density.

Keywords Crosslinking density · Fillers

5.1 Introduction

A crosslink is a bond that links one polymer chain to another. These links can take the form of covalent or ionic bonds and the polymers can be natural or synthetic polymers (such as carbohydrate polymers and proteins) (Gutiérrez et al. 2015a; Gutiérrez and González 2017). In polymer chemistry, ‘crosslinking’ usually refers to the use of crosslinks to promote a change in the physical properties of polymers (Marković et al. 2016). The resulting modification of the mechanical properties depends strongly on the crosslinking density. Low crosslink densities decrease the viscosities of molten polymers. Intermediate crosslink densities transform gummy polymers into materials that have elastomeric properties and potentially high strengths. Very high crosslinking densities can cause materials to become very rigid or glassy, such as phenol-formaldehyde materials.

Crosslinks can be formed by chemical reactions that are initiated by heat, pressure, pH change or radiation. For example, mixing of an unpolymerized or partially polymerized resin with specific chemicals called crosslinking reagents results in a chemical reaction that forms crosslinks (Gutiérrez et al. 2015b; Gutiérrez 2018). Crosslinking can also be induced in materials that are normally thermoplastic through exposure to a radiation source, such as electron beam exposure, gamma radiation or UV light (Gutiérrez and González 2016; Gutiérrez 2017a). For example, electron beam processing has been used for crosslinking of type C polyethylene (Cleland 1983; Drobny 2010). Other types of crosslinked polyethylene are made by the addition of peroxide during extrusion (type A) or by the addition of a crosslinking agent (e.g. vinylsilane) and a catalyst during extrusion and then performing a post-extrusion curing (Gutiérrez and Alvarez 2017a, b, c; Merino et al. 2018, 2019).

5.2 Vulcanization

Vulcanization (curing, crosslinking) is one of the most important processes for rubber technologies. During vulcanization, the rubber compound changes to an elastic final product: vulcanized rubber. This is done by consecutive and parallel changes of chemical and physical nature. The essence of vulcanization is the creation of crosslinks between rubber macromolecules in which a three-dimensional network of rubber matrix is formed. The part of the vulcanizing network are also physical

bonds such as hydrogen bonds and polar or dispersive interactions between individual macromolecules, which are created during the preparation or processing of the relevant rubber compound. The rest of ingredients participating in rubber compound are in original or changed form, chemically connected, dispersed or soluble (Kruželák et al. 2016).

For the formation of chemical bonds between rubber macromolecules, different vulcanizing chemical agents such as sulphur, peroxides, metal oxides, resins, quinones and others are used more frequently. These can react with suitable rubber functional groups and create crosslinks between them during the process (Flory 1953). Curing can also be caused by the different types of radiation influence, which is satisfactory for the generation of reactive forms of rubber macromolecules (Vasile and Butnaru 2017). Microwave energy or ultrasound can also lead to cure (Baig and Varma 2012). Vulcanization is required for most rubber processing methods, but is not necessary for some types of thermoplastic rubbers (Drobný 2007).

Vulcanization occurs in the presence of vulcanizing agents formally divided into three stages: first stage (induction period), gets to reciprocal interaction of elements of used vulcanization systems and the crosslinks are even not created or only a little (Joseph et al. 2015). The length of the cross links depends on the type of vulcanization system and the temperature. In the case of sulphur vulcanization, it is affected by the presence of accelerators, and eventually by vulcanizing retarders or pre-cure inhibitors. Second stage (main stage of the vulcanization process) (Fig. 5.1), the rapid curing of rubber macromolecules and the vulcanizate formation are given. For

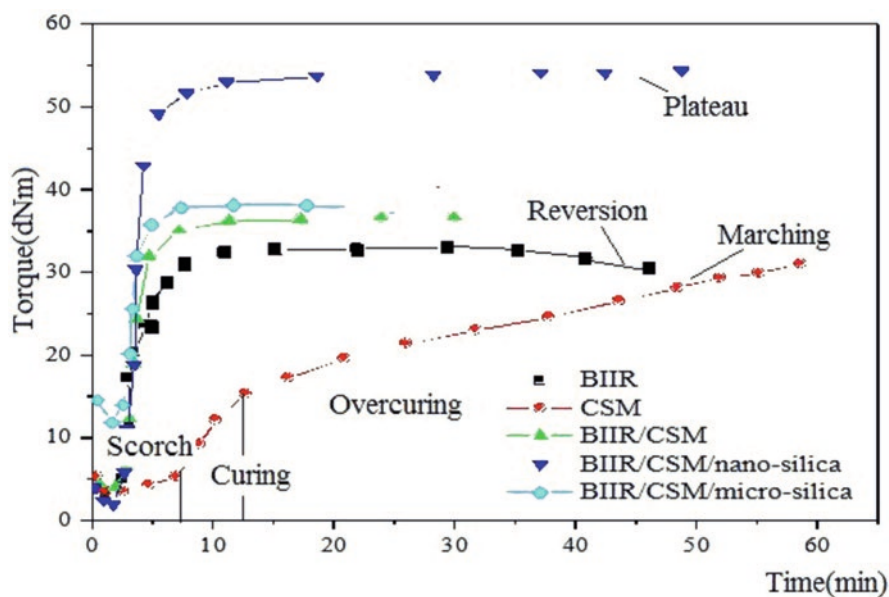


Fig. 5.1 Typical rheological curves for vulcanization processes using different network precursors. Reproduced with permission from the authors

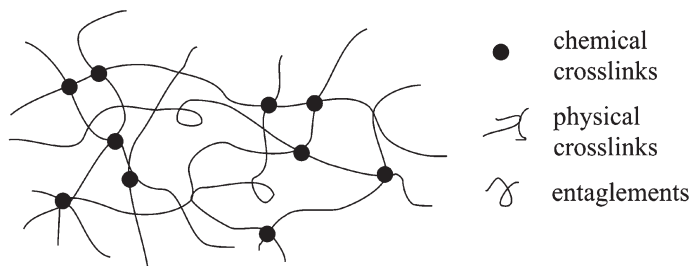


Fig. 5.2 General scheme of vulcanized network

this reason, the vulcanization rate is directly related to this stage. Finally, in the third stage, the restructuring of crosslinks created, and the modification of rubber chains can be applied. At this stage, the decrease in the number of crosslinks (reverse) can also be connected, thus showing changes in the properties of the final vulcanized product. The scorch time (t_{s2}), the optimal vulcanization time (t_{c90}), the difference (ΔM) between maximum (M_{max}) and minimum torque (M_{min}), the cure rate index (CRI) and, eventually, reverse rate are the properties most frequently evaluated during the vulcanization processes, which are followed through the so-called curves of vulcanization obtained by different types of rheometers.

The number of created crosslinks (Fig. 5.2) between rubber macromolecules (characterized by crosslink density - ν) and their chemical structure depend mainly on the content and activity of the vulcanization agent, the temperature and the vulcanization time. The temperature at which vulcanization is performed mainly influences the cure rate. Therefore, vulcanization reactions tend to have a similar tendency to chemical reactions governed by the Arrhenius equations (Marinović-Cincović et al. 2013). With the vulcanization time, the crosslink content is initially increased non-linear and after the optimal achievement of vulcanization may decrease (reverse). At the same time, the properties of the vulcanization compounds are altered, but its dependence with the vulcanization time is different. Some of vulcanizing properties can reach optimal values even before achieving optimum vulcanization.

There are different types of crosslinks such as: covalent, polysulfidic, mono- and di-sulfidic, carbon-carbon bonds and ionic (Fig. 5.3), and they are dependent on: sulphur content, accelerator type, accelerator/sulphur ratio and cure time. In general, a high accelerator/sulphur ratio and longer curing time increase the number of mono and di-sulfidic linkages. Mono- and disulfidic crosslinks have better resistance to solvent, heat, setting and reversion, but generally are more rigid, therefore, they have lower stress (σ) and cracking resistance. Polysulfidic crosslinks have better σ , softer and crack resistance, but less resistance to setting, heat and solvent. Rubbers have an optimum ν range for practical use.

Sulphur curing systems for highly unsaturated general-purpose synthetic rubber compounds based on natural rubber, polyisoprene and butadiene can be classified as (Lien et al. 2008):

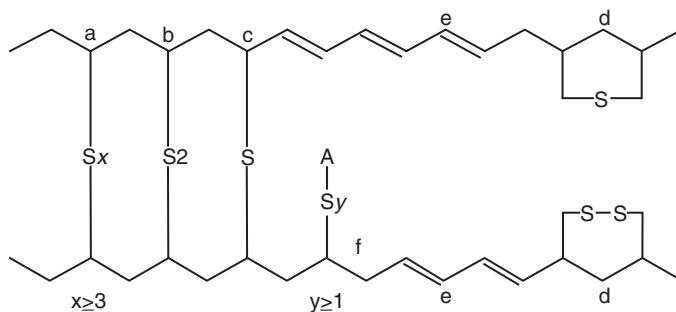


Fig. 5.3 Typical chemical bonds formed in sulphur vulcanized rubber: (a) polysulfid cross-links, (b) disulfid cross links, (c) monosulfid cross-links, (d) intra-chain cyclic monosulfides and intra-chain cyclic disulfides, (e) conjugated diene and conjugated triene and (f) fendent sulfidic group terminated by moiety X derived from the accelerator. Reproduced with permission from Jovanović and Samaržija-Jovanović (2013)

- Conventional curing system: when a relatively high dose of sulphur (above 1.5 phr) and a low dose of accelerators (0.5 to 1.0 phr) are used.
- Efficient vulcanization curing system (EV): when a low dose of sulphur (below 0.4–0.5 phr) and a high dose of accelerators (2.5 to 5.0 phr) are used.
- Semi-efficient vulcanization curing system: when sulphur and accelerator concentrations are between those of conventional vulcanizing system and the EV system.

Vulcanization temperature has a significant effect on crosslink structure (Stojčeva-Radovanović and Marković 2001). Optimum properties are obtained when curing is done at the lowest possible temperature. However, to increase productivity, higher temperatures are frequently used. The modulus decreases with increase in cure temperature irrespective of type of accelerator used, which could be recovered to a great extent by increasing dosages of accelerators.

5.2.1 Methods for Determining Polysulfidic, Mono- and Disulfidic Crosslinks

The sulphur crosslinks can be a mixture of polysulfide (S atoms >3), disulfide and monosulfide crosslinks. Its distribution varies according to the curing system used. Chemical probes can be used to determine the type of crosslinks. The sulphur-sulphur bonds in the polysulfidic crosslinks are more susceptible to nucleophilic attack by thiolate ions. The proportion of polysulfidic crosslinks is determined using piperidine-propane-2-thiol, which can cleave only the polysulfidic crosslinks (Casassa et al. 1986). The test sample extracted with benzene is placed under nitrogen and then treated with a 0.2 M solution of propane-2-thiol dissolved in 0.4 M piperidine in heptane solvent at 25 °C for 6 days to break only the polysulfidic

crosslinks. A comparison of original ν and the value obtained after the probe treatment can provide the concentration of the polysulfidic crosslinks. The same sample can be further treated with 1 M hexane-1-thiol in piperidine for 48 h to cleave disulfidic (and polysulfidic crosslinks) and the ν is determined. This gives the crosslink proportions of crosslinked C-C monosulfidic bonds. Therefore, the determination of ν before and after the treatment of the sample with specified probes allows the assessment of mono-, di- and polysulfidic concentrations of crosslinks in a vulcanized test sample. Tri-, tetra- and higher sulfides could not be separated by this method proposed by Casassa et al. (1986) because their chemical reactivity is similar.

Table 5.1 shows the typical rubber compound formulations from brominated copolymer isobutylene isoprene and chlorosulphonated polyethylene (BIIR/CSM) rubber mixtures consisting of 10 or more ingredients, which are added to improve physical properties, affect vulcanization, prevent long-term deterioration and improve processability.

These ingredients are given in amounts based on a total of 100 parts of the rubber (parts *per* hundred of rubber).

On the other hand, the values of Young's modulus (E), maximum stress (σ_{\max}), strain at break (ϵ_b) and average molecular weight of rubber (M_c) are proportional at low rubber density (ρ) values, and its relation is given by the following equation:

$$\sigma = \frac{\rho}{M_c} \cdot RTA(\lambda - \lambda^2) \quad (5.1)$$

where σ is stress, λ is the relative extension, R is the gas constant, T is the absolute temperature, A is the cross-sectional area of the test sample in a non-deformable state.

Table 5.1 Formulations from brominated copolymer isobutylene isoprene/chlorosulfonated polyethylene rubber composites reinforced with nano- and micro-silica

Sample	BIIR	CSM	SiO ₂ (15 nm)	SiO ₂ (28 μ m)
C1	100	0	0	0
C2	0	100	0	0
C3	50	50	0	0
C4	50	50	10	0
C5	50	50	20	0
C6	50	50	30	0
C7	50	50	40	0
C8	50	50	50	0
C9	50	50	0	10
C10	50	50	0	20
C11	50	50	0	30
C12	50	50	0	40
C13	50	50	0	50

However, the σ values cease to increase proportionally to high ρ values. In this sense, once an optimal condition is reached between the σ and ρ values, an increase in the ρ values leads to a reduction in the σ values, thus demonstrating a fragile behavior of the highly crosslinked materials. Other factors affecting σ are the rubber structure and the crosslinking structure. Most synthetic rubber vulcanizates have lower σ than natural rubber vulcanizates, because they cannot crystallize in their macromolecules by different types of structural units (*cis*-, *trans*-, 1,4-, 1,2-) or more co-monomer units (e.g. butadiene, styrene, acrylonitrile and others). In addition, the vulcanizates with polysulfide crosslinks have higher σ values than vulcanizates with monosulfide, eventually carbon-carbon crosslinks. Initially, the ϵ_b values have a proportional relationship with the ρ values. However, then is asymptotically approached to minimum value. Vulcanized hardness also increases by the vulcanization time as well as the ρ values. The highest structural strength is associated with soft vulcanized conditions. After vulcanization, the optimal achievement of this characteristic along with time decreases. The change in ϵ_b values is similar to the change in the E values, it is proportional to ρ and the relative ϵ_b in the three coordinates. After optimal vulcanization (maximum ν value) the vulcanization time decreases.

5.2.2 Cross-Link Density (ν)

The density of the network and the M_c are the most used properties for the characterization of the network, and they can be determined using Eq. 5.2:

$$\nu = \frac{\rho}{M_c} \quad (5.2)$$

where ν is the crosslink density, ρ is the rubber density, and M_c is the molecular weight of rubber segments between two crosslinks.

Sometimes, the vulcanizing network is also characterized by the number of crosslinks created in the vulcanizing volume unit. This property can also be calculated from the density of the network, assuming that crosslinks are created between two rubber segments:

$$n = \frac{\nu}{2} \quad (5.3)$$

where n is the number of crosslinks *per* unit of vulcanized volume, ν is its crosslink density.

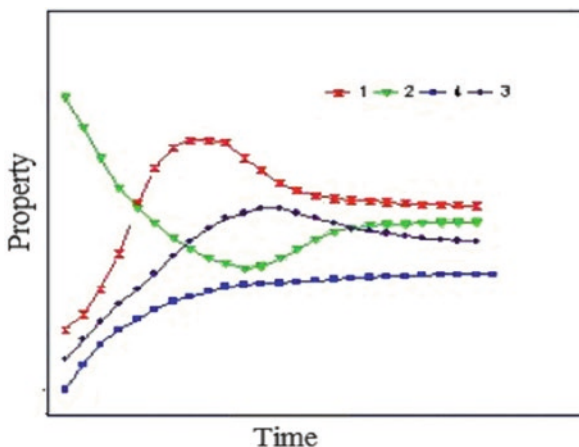
Several types of methods have been used to determine the characteristics of the vulcanized network (Marković et al. 2014). In particular, chemical methods can only be used when the curing mechanism of the crosslinking system is well known, and the reaction products can be quantitatively determined. The number of

crosslinks (n) can be calculated in this case on the basis of the material balance of the appropriate chemical equation related to curing.

5.2.3 Effects of Cross-Link Density on Mechanical Properties

The mechanical properties of a vulcanized rubber depend largely on the vulcanization time and ν . The ν effect on the properties of the compound is shown in Fig. 5.4. Properties such as static modulus, dynamic modulus and hardness increase as ν increases. The fracture properties such as σ and tear strength pass through a maximum value as the ν increases and then decreases. M_c is related to the σ of the vulcanized rubber. The practical value of M_c is between 8000 and 10,000 g/mol. The effects of different particle sizes and silica content on the mechanical properties of hybrid materials based on BIIR/CSM rubber mixtures can also be observed in Fig. 5.5. For this last case, both the micro- (MPs) and nanoparticles (NPs) were used as fillers, thus increasing the σ values to the filler contents of 40 phr and 30 phr, respectively (Fig. 5.5a). However, the σ values decrease to higher contents than those indicated. This fact may be associated with a better dispersion of the fillers at low contents, and a tendency towards agglomeration of the fillers at higher contents. In this way, a better dispersion of the particles improves the silica-rubber interactions, and a tendency to agglomerate the particles is a result of the greater particle-particle interactions, thus leading to fragile materials with lower σ values. Meanwhile, the use of silica NPs increased σ values compared to rubber materials containing silica MPs. This is due to the large surface area of the silica NPs, which make it possible to improve the interactions between the NPs and the rubber matrix. Therefore, better particle-matrix interactions increase the σ values. In contrast, the incorporation of the fillers generally decreases the ϵ_b values, since their presence relatively reduces the amount of resistant material available in the system. It can be seen (Fig. 5.5b),

Fig. 5.4 Variations of the mechanical properties of rubber composites during vulcanization. Line 1: stress (σ), line 2: strain at break (ϵ_b), line 3: hardness and line 4: elasticity. Reproduced with permission from the authors



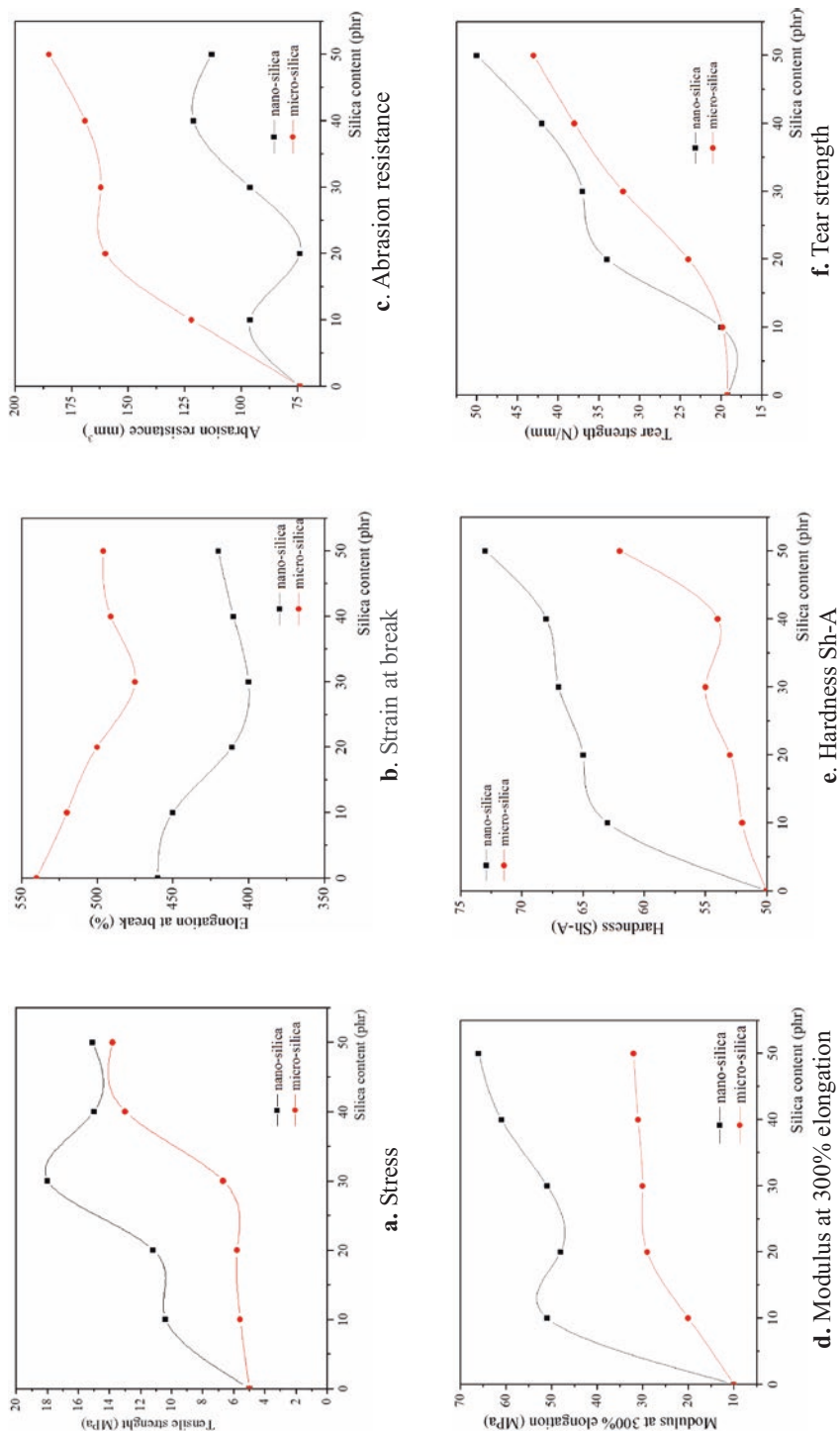


Fig. 5.5 Mechanical properties of brominated copolymer isobutylene isoprene/chlorosulfonated polyethylene rubber composites reinforced with nano- and micro-silica. Reproduced with permission from Marković et al. (2012)

however, clearly that the incorporation of silica micro- and nanoparticle fillers in BIIR/CSM rubber composites (50/50) up to 30 phr increased ϵ_b values. It should be noted that the ϵ_b values of the composites containing silica NPs showed lower ϵ_b values compared to the composites containing silica microparticles. These two properties, σ and ϵ_b , are also related to the nature and number of crosslinks.

Abrasion resistance is defined as the ability of the crosslinked material to resist the progressive removal of the material from its surface, as a result of the mechanical action of rubbing or scraping, or the action of some erosive nature. Abrasion resistance values are increased by loading silica filler (Fig. 5.5c). This suggests that the silica NPs harden and the rubber matrix.

Theoretically, the content of the fillers in the polymer composites, when increased, could significantly increase the σ and E values. In line with this, BIIR/CSM rubber composites containing silica NPs had higher E values than BIIR/CSM rubber composites containing silica MPs (Fig. 5.5d). This has been associated with a larger matrix-filler contact area (Gutiérrez et al. 2017; Collazo-Bigliardi et al. 2018).

Higher hardness values have also been used as indicators of the degree of crosslinking of the material. Higher hardness values have been observed from BIIR/CSM rubber composites containing silica NPs compared to analogue materials containing silica MPs, maintaining the same content of the filler (Fig. 5.5e). This is supported by the ν values (Table 5.2). The hardness as well as E show an increasing tendency with the increase of the filler content, due to the reduction of the mobility of the rubber chains. This also agrees with the previous discussion on the effect of a larger area of matrix-filler interactions.

Table 5.2 Rheological properties of brominated copolymer isobutylene isoprene and chlorosulphonated polyethylene (BIIR/CSM) rubber mixtures reinforced with nano- and micro-silica. Reproduced with permission from the authors

Samples	Ratio	ML (1 + 4) at 373 K	M_{\min} (dNm)	M_{\max} (dNm)	t_{s2} (min)	t_{c90} (min)	CRI (min ⁻¹)
BIIR/CSM/SiO ₂	100/0/0	25	2	34	2.35	6.39	25
BIIR/CSM/SiO ₂	0/100/0	33	3	32	6.52	50.15	2
BIIR/CSM/SiO ₂	50/50/0	29	3	38	2.29	6.06	17
BIIR/CSM/nm SiO ₂	50/50/10	31	5	38	2.30	5.23	30
BIIR/CSM/nm SiO ₂	50/50/20	32	5	39	1.57	4.45	34
BIIR/CSM/nm SiO ₂	50/50/30	34	7	42	2.12	5.43	30
BIIR/CSM/nm SiO ₂	50/50/40	40	9	47	1.52	4.30	35
BIIR/CSM/nm SiO ₂	50/50/50	56	12	54	2.10	4.46	30
BIIR/CSM/ μ m SiO ₂	50/50/10	29	5	39	2.21	5.01	36
BIIR/CSM/ μ m SiO ₂	50/50/20	30	5	40	2.19	4.45	44
BIIR/CSM/ μ m SiO ₂	50/50/30	30	4	41	2.07	4.09	50
BIIR/CSM/ μ m SiO ₂	50/50/40	37	5	41	2.08	3.57	50
BIIR/CSM/ μ m SiO ₂	50/50/50	38	3	39	2.09	4.03	52

ML (1 + 4): Mooney viscosity at 373K, M_{\max} : maximum torque, M_{\min} : minimum torque, t_{s2} : time up to 2 units of torque increase above the minimum and t_{c90} : torque at 90% of full torque development

Tear resistance is defined as the force required to obtain a test piece of tear crosslinked materials. Higher tear resistance values are also increased in the BIIR/CSM rubber composites containing the silica NPs compared to the BIIR/CSM rubber composites containing the MPs, maintaining the same content of the filler (Fig. 5.5f).

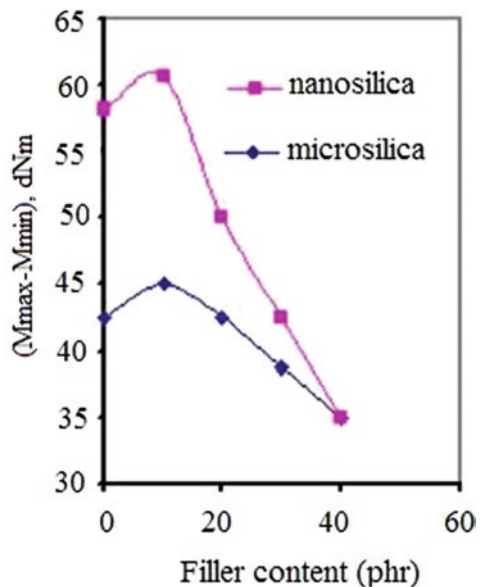
5.2.4 Determination of Cross-Link Density (ν): Rheological Method

It is known that the torque difference can be indirectly related to the ν of the mixtures (Fig. 5.6). The values of each curing time represent the state or degree of vulcanization (Marković et al. 2008a, Marković et al. 2008b). Consequently, the degree of crosslinking in rubber mixtures can be determined using rheological data. Typical rheological properties of BIIR/CSM rubber mixtures are shown in Table 5.2. The CRI can be calculated following Eq. 5.4 (Jovanović et al. 2018).

$$CRI = \frac{100}{(t_{c90} - t_{s2})} \cdot 100 \quad (5.4)$$

The M_{\min} can be increased slightly because of the addition of the fillers, thus increasing the M_{\max} values (the ν and chain entanglement are increased) (Table 5.2). These results are attributed to the fact that the nano-silica filler affects ν by reacting with the chemical ingredients of the formulation, thus leading to a torque.

Fig. 5.6 Variation of ΔM ($M_{\max} - M_{\min}$) for BIIR/CSM rubber mixtures containing silica particles. Reproduced with permission from Marković et al. (2012)



The silica NPs have a larger surface area to interact with the rubber matrix, which leads to an increase in torque and CRI values, while t_{s2} and the t_{c90} are diminished with the addition of fillers. In addition, the added silica NPs into the rubber mixtures increase the mixing time compared to the rubber mixtures containing silica MPs. This is due to the greater hydrogen bonding interactions between the silica NPs and the rubber matrix. The incorporation of the fillers in the rubber matrices also increases the mixing time, resulting in an increase in heat due to the friction of the fillers. The increase in the content of the fillers also increases the viscosity of the mixtures, so the heat generated accelerates crosslinking. The ΔM can thus be taken as the extension of ν in the rubber phase.

5.2.5 Determination of Cross-Link Density (ν): Stress (σ)-Strain (ϵ) Method

M_c can be calculated under low deformations (<100%) (Fig. 5.7) from the experimentally determined E (for tensile deformation) using Eq. 5.5:

$$E = \frac{3\rho RT}{2M_c} \quad (5.5)$$

or G (for shear deformation):

$$E = 3G \quad (5.6)$$

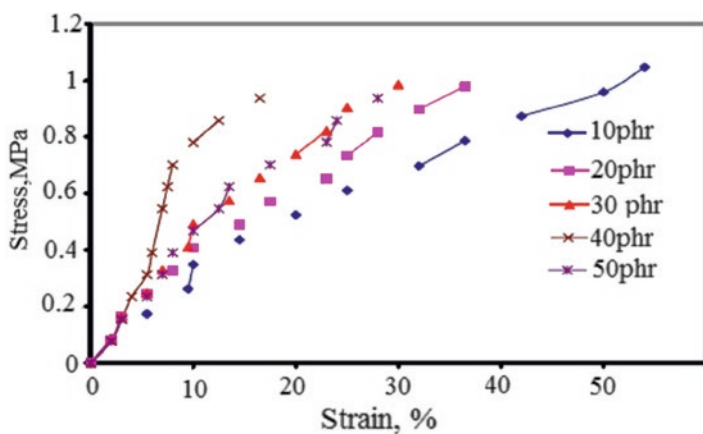


Fig. 5.7 Determination of the cross-link density (ν) by the stress (σ)-strain (ϵ) method. Reproduced with permission from Stojčeva-Radovanović and Marković (2001)

where E is Young's modulus, G is the shear modulus, ρ is the rubber density, R is the gas constant, T is the absolute temperature and M_c is the molecular weight of rubber segments between two crosslinks.

The Mooney-Rivlin equation (Eq. 5.7) is used very frequently for the determination of the constants C_1 and C_2 , thus allowing the calculation for the determination of the ν values, and eventually also determination of the M_c values, since that these measurements can be conducted under high deformations. In this sense, C_1 can be determined graphically from the linearized form of the Mooney-Rivlin's equation (Eq. 5.8).

$$\frac{\sigma}{2(\lambda - \lambda^{-2})} = C_1 - C_2 \cdot \lambda^{-1} \quad (5.7)$$

$$C_1 = \frac{1}{2} \nu \cdot RT = \frac{\rho RT}{2M_c} \quad (5.8)$$

where σ is the stress, λ is the relative elongation, and C_1 and C_2 are constants.

Some observations of σ - ϵ method. The linearity plot may be affected by the uncertainty in the initial length value when the $\lambda^{-1} > 0.95$. The C_1 constant is normally derived from measurements in the range $0.5 > \lambda^{-1} > 0.95$. To ensure that the equilibrium is reached, the σ - ϵ measurements must be carried out at a low ϵ rate for automated tests. The C_1 values obtained do not depend largely on the extension rate up to 30 mm/min for a 100 mm test length (Marković et al. 2016).

5.2.6 Determination of Cross-Link Density (ν): Solvent Swelling Method

ν of a vulcanized rubber can be measured using the solvent swelling method (Jovanović et al. 2016; Stojčeva-Radovanović, & Marković, 2001; Stojčeva-Radovanovic et al. 2002). A good should be used such that the crosslinked rubber can absorb and swell as much as possible until the retraction forces in the network balance the swelling forces. The rubber test piece is normally allowed to swell in the dark at room temperature until equilibrium is reached.

The swelling of a rubber by a liquid is a mixing process. According to the Gibbs equation (Eq. 5.9) two substances are mixed when the free energy of mixing (ΔG) is negative:

$$\Delta G = \Delta H - T\Delta S \quad (5.9)$$

where ΔH is the enthalpy change, T is the absolute temperature and ΔS is the entropy change.

Mixing processes are thus favored by the minimum or negative ΔH values, or ΔS variations (Flory 1953). The Flory-Huggins interaction parameter (χ) can be calculated for the rubber mixtures in a benzene solvent using Eq. 5.10:

$$x = \left[\nu V \left(v_s^{1/3} - 0.5v_s \right) + \ln(1 - v_s) + v_s \right] / v_s^2 \quad (5.10)$$

Since ν can be determined from the swelling data (Marković et al. 2002). M_c can then be calculated using the following equation:

$$M_c = -2V_s \rho_r \left(V_r \right)^{1/3} / \ln(1 - V_r) + V_r + 2\chi^2 V_s^2 \quad (5.11)$$

where M_c is the molecular weight of the polymer between two crosslinks, ρ_r is rubber density, V_s is the molar volume of benzene solvent, V_r is the volume fraction of swollen rubber sample and χ is the filler-polymer (Flory-Huggins) interaction parameter.

The percentage of swelling volume can also be calculated using the following equations:

$$R_v = 1 + \left[(w - w_0) - 1 \right] \frac{\rho_r}{\rho_s} \quad (5.12)$$

$$R_w = \frac{w}{w_0} \quad (5.13)$$

$$v_s = \frac{1}{R_v} \quad (5.14)$$

where R_v is the ratio of the swelling volume with respect to the non-swollen (original) volume of the samples, w and w_0 are the weights of the samples before and after swelling, respectively, ρ_r and ρ_s are densities of the rubber and the solvent, respectively, R_w is the ratio of the swelling weight with respect to the non-swollen (original) volume of the samples and v_2 is the volume fraction of the sample in the swollen gel.

The influence of the filler fraction on the values of the characteristic parameters of the network such as R_v , R_w , V_r , χ , and E can be obtained by measuring σ - ϵ (Marković et al. 2017). The ν , M_c and ρ_r values of systems reinforced with nano- and micro-silica particles are given in Table 5.3.

The R_v , R_w , v_2 , E , ν , and w parameters are clearly increased with the increase in the filler content except for M_c values, which are diminished. Higher R_v , R_w , v_2 , E , ν , and w values of for rubber composites containing silica NPs are obtained as compared to analogue composites containing silica MPs. This fact can be explained due to the restriction of swelling, thus causing an increase in the V_r values, which in turn affect the increase in the ν values.

Table 5.3 The characteristic network parameters of the brominated copolymer isobutylene isoprene/chlorosulfonated polyethylene rubber composites reinforced with nano- and micro-silica particles. Reproduced with permission from the authors

Samples	Ratios	R_v	R_w	V_r	χ	$E \cdot 10^5$ (MPa)	$\nu \cdot 10^2$ (mol/m ³)	M_c (g/ mol)	ρ (g/ cm ³)
BIIR/CSM/ SiO ₂	100/0/0	2.557	2.150	0.2881	0.8665	1.21	2.8	1478	1.002
BIIR/CSM/ SiO ₂	0/100/0	2.576	2.150	0.3444	0.7883	1.15	3.1	1582	1.045
BIIR/CSM/ SiO ₂	50/50/0	2.533	2.120	0.3911	0.6858	1.50	5.1	1874	1.096
BIIR/CSM/ nm SiO ₂	50/50/10	2.472	2.003	0.3882	0.6835	1.30	5.3	1827	1.107
BIIR/CSM/ nm SiO ₂	50/50/20	2.421	1.992	0.3956	0.6894	1.41	5.8	1841	1.116
BIIR/CSM/ nm SiO ₂	50/50/30	2.387	1.960	0.4021	0.6939	1.92	6.2	905	1.136
BIIR/CSM/ nm SiO ₂	50/50/40	2.352	1.900	0.4197	0.7066	1.58	6.4	1772	1.166
BIIR/CSM/ nm SiO ₂	50/50/50	2.229	1.840	0.4486	0.7287	1.71	6.9	1524	1.189
BIIR/CSM/ μm SiO ₂	50/50/10	2.502	2.100	0.3997	0.6921	1.26	5.1	1815	1.100
BIIR/CSM/ μm SiO ₂	50/50/20	2.480	2.080	0.4032	0.6945	1.26	5.1	2514	1.116
BIIR/CSM/ μm SiO ₂	50/50/30	2.392	1.990	0.4181	0.7053	1.42	5.2	1002	1.135
BIIR/CSM/ μm SiO ₂	50/50/40	2.365	1.950	0.4229	0.7089	1.31	5.3	2917	1.168
BIIR/CSM/ μm SiO ₂	50/50/50	2.314	1.880	0.4322	0.7163	1.44	5.8	3435	1.216

5.2.7 Effect of Crosslinking on Glass Transition Temperature (T_g)

Crosslinking reduces the mobility of the rubber molecules, which leads to a significant increase in the T_g values (Marković et al. 2009; Gutiérrez 2017b, 2018). This effect depends on the types of crosslinks (Marković et al. 2013b; Marković et al. 2013a). The impact of crosslinks formed by sulphur on mobility of T_g is greater compared to those formed by peroxide or other crosslinking agents. Finally, other methods are also used to characterize the vulcanized network, e.g. sol-gel analysis, ultrasonic, small-angle neutron scattering (SANS) in swollen crosslinked gels and also methods based on the ¹H and ¹³C nuclear magnetic resonance (NMR) spectroscopy of swollen and non-swollen vulcanized composites.

5.3 Conclusion

The crosslink density (ν) of vulcanized rubbers can be determined using the simple solvent swelling method. When a filler is used in the rubber formulation, an appropriate correction must be made so as not to overestimate the ν values. Additional analyzes can be performed to quantify covalent and ionic crosslinks, as well as mono-, di- and polysulfidic crosslinks in vulcanized rubbers. Excessive intraparticle crosslinking in a latex system may not contribute to the desired mechanical properties of vulcanized rubber. There are many other methods to measure the ν values vulcanized rubber such as solvent freezing point depression, nuclear magnetic resonance (NMR) signal line width, transverse relaxation decay and longitudinal relaxation in rotating frame techniques, but the latter were not discussed in this chapter.

Acknowledgments The authors are thankful to the Ministry of Education, Science and Technological Development of the Republic of Serbia for financial support (Projects Numbers 45022, and 45020).

Conflicts of Interest The authors declare no conflict of interest.

References

- Baig, R. B. N., & Varma, R. S. (2012). Alternative energy input: Mechanochemical, microwave and ultrasound-assisted organic synthesis. *Chemical Society Reviews*, 41(4), 1559–1584. <https://doi.org/10.1039/c1cs15204a>.
- Casassa, E. Z., Sarquis, A. M., & Van Dyke, C. (1986). The gelation of polyvinyl alcohol with borax: A novel class participation experiment involving the preparation and properties of a “slime.”. *Journal of Chemical Education*, 63(1), 57. <https://doi.org/10.1021/ed063p57>.
- Cleland, M. R. (1983). Radiation processing: Basic concepts and practical aspects. *Journal of Industrial Irradiation Technology*, 1(3), 191–218.
- Collazo-Bigliardi, S., Ortega-Toro, R., & Chiralt, A. (2018). Properties of micro- and nano-reinforced biopolymers for food applications. In T. J. Gutiérrez (Ed.), *Polymers for food applications* (pp. 61–99). Cham: Springer. https://doi.org/10.1007/978-3-319-94625-2_4.
- Drobny, J. G. (Ed.). (2007). *Handbook of thermoplastic elastomers* (p. 736). Norwich: William Andrew. isbn:978-0-8155-1549-4.
- Drobny, J. G. (Ed.). (2010). *Radiation technology for polymers. Second Edition*. CRC Press. Pp. 307. eBook ISBN 9780429148019. <https://doi.org/10.1201/b10304>
- Flory, P. J. (1953). *Principles of polymer chemistry*. Ithaca/New York: Cornell University Press.
- Gutiérrez, T. J. (2017a). Effects of exposure to pulsed light on molecular aspects of edible films made from cassava and taro starch. *Innovative Food Science & Emerging Technologies*, 41, 387–396. <https://doi.org/10.1016/j.ifset.2017.04.014>.
- Gutiérrez, T. J. (2017b). Surface and nutraceutical properties of edible films made from starchy sources with and without added blackberry pulp. *Carbohydrate Polymers*, 165, 169–179. <https://doi.org/10.1016/j.carbpol.2017.02.016>.
- Gutiérrez, T. J. (2018). Active and intelligent films made from starchy sources/blackberry pulp. *Journal of Polymers and the Environment*, 26(6), 2374–2391. <https://doi.org/10.1007/s10924-017-1134-y>.

- Gutiérrez, T. J., & Alvarez, V. A. (2017a). Data on physicochemical properties of active films derived from plantain flour/PCL blends developed under reactive extrusion conditions. *Data in Brief*, 15, 445–448. <https://doi.org/10.1016/j.dib.2017.09.071>.
- Gutiérrez, T. J., & Alvarez, V. A. (2017b). Eco-friendly films prepared from plantain flour/PCL blends under reactive extrusion conditions using zirconium octanoate as a catalyst. *Carbohydrate Polymers*, 178, 260–269. <https://doi.org/10.1016/j.carbpol.2017.09.026>.
- Gutiérrez, T. J., & Alvarez, V. A. (2017c). Properties of native and oxidized corn starch/polystyrene blends under conditions of reactive extrusion using zinc octanoate as a catalyst. *Reactive and Functional Polymers*, 112, 33–44. <https://doi.org/10.1016/j.reactfunctpolym.2017.01.002>.
- Gutiérrez, T. J., & González, G. (2016). Effects of exposure to pulsed light on surface and structural properties of edible films made from cassava and taro starch. *Food and Bioprocess Technology*, 9(11), 1812–1824. <https://doi.org/10.1007/s11947-016-1765-3>.
- Gutiérrez, T. J., & González, G. (2017). Effect of cross-linking with *Aloe vera* gel on surface and physicochemical properties of edible films made from plantain flour. *Food Biophysics*, 12(1), 11–22. <https://doi.org/10.1007/s11483-016-9458-z>.
- Gutiérrez, T. J., González Seligra, P., Medina Jaramillo, C., Famá, L., & Goyanes, S. (2017). Chapter 14. Effect of filler properties on the antioxidant response of thermoplastic starch composites. In V. K. Thakur, M. K. Thakur, & M. R. Kessler (Eds.), *Handbook of composites from renewable materials* (pp. 337–370). EE.UU: WILEY-Scrivener Publisher. <https://doi.org/10.1002/9781119441632.ch14>. isbn:978-1-119-22362-7.
- Gutiérrez, T. J., Morales, N. J., Pérez, E., Tapia, M. S., & Famá, L. (2015a). Physico-chemical properties of edible films derived from native and phosphated cush-cush yam and cassava starches. *Food Packaging and Shelf Life*, 3, 1–8. <https://doi.org/10.1016/j.fpsl.2014.09.002>.
- Gutiérrez, T. J., Tapia, M. S., Pérez, E., & Famá, L. (2015b). Edible films based on native and phosphated 80: 20 waxy: Normal corn starch. *Starch-Stärke*, 67(1–2), 90–97. <https://doi.org/10.1002/star.201400164>.
- Joseph, A., George, B., Madhusoodanan, K., & Alex, R. (2015). Current status of Sulphur vulcanization and devulcanization chemistry: Process of vulcanization. *Rubber Sci*, 28(1), 82–121.
- Jovanović, S., Samaržija-Jovanović, S., Marković, G., Jovanović, V., Adamović, T., & Marinović-Cincović, M. (2016). Mechanical properties and thermal aging behaviour of polyisoprene/polybutadiene/styrene-butadiene rubber ternary blend reinforced with carbon black. *Composites Part B: Engineering*, 98, 126–133. <https://doi.org/10.1016/j.compositesb.2016.04.060>.
- Jovanović, S., Samaržija-Jovanović, S., Marković, G., Jovanović, V., Adamović, T., & Marinović-Cincović, M. (2018). Ternary NR/BR/SBR rubber blend nanocomposites. *Journal of Thermoplastic Composite Materials*, 31(2), 265–287. <https://doi.org/10.1177/0892705717697778>.
- Jovanović, V., & Samaržija-Jovanović, S. (2013). *Nanokompoziti na osnovu različitih prekursora mreža*. Beograd: Akademiska misao.
- Kruželák, J., Sýkora, R., & Hudec, I. (2016). Sulphur and peroxide vulcanisation of rubber compounds-overview. *Chemical Papers*, 70(12), 1533–1555. <https://doi.org/10.1515/chempap-2016-0093>.
- Lien, S.-M. M., Te Li, W.-T., & Huang, T.-J. J. (2008). Genipin-crosslinked gelatin scaffolds for articular cartilage tissue engineering with a novel crosslinking method. *Materials Science and Engineering: C*, 28(1), 36–43. <https://doi.org/10.1016/j.msec.2006.12.015>.
- Marinović-Cincović, M., Janković, B., Jovanović, V., Samaržija-Jovanović, S., & Marković, G. (2013). The kinetic and thermodynamic analyses of non-isothermal degradation process of acrylonitrile-butadiene and ethylene-propylene-diene rubbers. *Composites Part B: Engineering*, 45(1), 321–332. <https://doi.org/10.1016/j.compositesb.2012.08.006>.
- Marković, G., Marinović-Cincović, M., Jovanović, V., Samaržija-Jovanović, S., & Budinski-Simendić, J. (2016). Polymer characterization (II). In S. A. Méndez-Vilas A (Ed.), *Polymer science: Research advances, practical applications and educational aspects* (pp. 397–403). Formatex Research Center. Retrieved from <http://www.formatex.org/polymerscience1/>.

- Marković, G., Radovanović, B., Cincović-Marinović, M., & Budinski-Simendić, J. (2008a). Swelling properties of cross linking systems based on wood flour filled polyisoprene and chlorosulfonated polyethylene rubber blends. *Svet Polimera*, 11(3), 77–80.
- Marković, G., Marinović-Cincović, M., Jovanović, V., Samaržija-Jovanović, S., & Budinski-Simendić, J. (2014). Modeling of non-linear viscoelastic behavior of filled rubbers. In D. Ponnamma & S. Thomas (Eds.), *Non-linear viscoelasticity of rubber composites and nanocomposites*, *Advances in Polymer Science* (Vol. 264). Cham: Springer. https://doi.org/10.1007/978-3-319-08702-3_8.
- Marković, G., Marinović-Cincović, M., Jovanović, V., Samaržija-Jovanović, S., & Budinski-Simendić, J. (2013a). NR/CSM/biogenic silica rubber blend composites. *Composites Part B: Engineering*, 55, 368–373. <https://doi.org/10.1016/j.compositesb.2013.06.045>.
- Marković, G., Marinović-Cincović, M., Jovanović, V., Samaržija-Jovanović, S., & Budinski-Simendić, J. (2017). Chlorosulfonated rubber-based nanoblends: Preparation, characterization and applications. In G. Marković & P. M. Visakh (Eds.), *Rubber nano blends* (pp. 105–153). Springer. https://doi.org/10.1007/978-3-319-48720-5_5.
- Marković, G., Marinović-Cincović, M., Jovanović, V., Samaržija-Jovanović, S., & Budinski-Simendić, J. (2012). Hybrid materials based on brominated copolymer isobutylene isoprene/chlorosulfonated polyethylene rubber blends reinforced by nano and micro silica. *Journal of Elastomers and Plastics*, 44(4), 335–351. <https://doi.org/10.1177/0095244311428895>.
- Marković, G., Marinović-Cincović, M., Radovanović, B., & Budinski-Simendić, J. (2008b). NR/CSM rubber blends reinforced by silica and carbon black. *Svet Polimera*, 11(5), 179–182.
- Marković, G., Radovanović, B., Marinović-Cincović, M., & Budinski-Simendić, J. (2009). The effect of accelerators on curing characteristics and properties of natural rubber/chlorosulfonated polyethylene rubber blend. *Materials and Manufacturing Processes*, 24(10–11), 1224–1228. <https://doi.org/10.1080/10426910902967087>.
- Marković, G., Veljković, O., Marinović-Cincović, M., Jovanović, V., Samaržija-Jovanović, S., & Budinski-Simendić, J. (2013b). Composites based on waste rubber powder and rubber blends: BR/CSM. *Composites Part B: Engineering*, 45(1), 178–184. <https://doi.org/10.1016/j.compositesb.2012.08.013>.
- Marković, G. S., Stojčeva-Radovanović, B., Marinović-Cincović, M., Babić, D., & N. J. (2002). Parameters of dry and swelling network of nano- and micro filled crosslinked systems based on butadiene acrylonitrile and chlorosulfonated polyethylene rubbers. *Svet Polimera*, 5(4), 171–176.
- Merino, D., Gutiérrez, T. J., & Alvarez, V. A. (2019). Potential agricultural mulch films based on native and phosphorylated corn starch with and without surface functionalization with chitosan. *Journal of Polymers and the Environment*, 27(1), 97–105. <https://doi.org/10.1007/s10924-018-1325-1>.
- Merino, D., Mansilla, A. Y., Gutiérrez, T. J., Casalengué, C. A., & Alvarez, V. A. (2018). Chitosan coated-phosphorylated starch films: Water interaction, transparency and antibacterial properties. *Reactive and Functional Polymers*, 131, 445–453. <https://doi.org/10.1016/j.reactfunctpolym.2018.08.012>.
- Stojčeva-Radovanović, B., & Marković, G. S. (2001). Testing of the influence of medium on changes in the physical and mechanical properties of NR/CSM compounds. *Hemijaska Industrija*, 55(11), 514–518.
- Stojčeva-Radovanović, B., Marković, G., Marinović-Cincović, M., Babić, D., & Nedeljković, J. (2002). Effect of fillers on parameters of dry and swollen polymer matrix networks. *Hemijaska Industrija*, 56(10), 415–421. <https://doi.org/10.2298/hemind0210415s>.
- Vasile, C., & Butnaru, E. (2017). Chapter 5. Radiation chemistry of organic solids. In S. Yongxia & A. G. Chmielewski (Eds.), *Applications of ionizing radiation in materials processing* (pp. 117–141). Warszawa: Institute of Nuclear Chemistry and Technology. Available in: <http://www.ichtj.waw.pl/ichtj/publ/monogr/sun2017/sun-chapter5.pdf>.

Chapter 6

Cross-Linkable Bio and Mineral Fillers for Reactive Polymer Composites: Processing and Characterization



Jelena D. Rusmirović, Tihomir M. Kovačević, Saša J. Brzić,
and Aleksandar D. Marinković

Abstract It has been found that polymer composites possess advanced mechanical and thermal performances after being loaded with functional/reactive bio or mineral fillers. The high bonding strength between the polymer matrix and the fillers represents a crucial factor for obtaining a good reinforcement in the composite materials. Many techniques have been developed for chemical functionalization of the filler surface to improve its bonding strength, compatibility and dispersibility within polymer matrices, and also to prevent deterioration of the structure. Thus, reactive cross-linkable groups showing high reactivity toward the target functional groups of the polymer matrix have been attached to the filler surface. However, the introduction of reactive residues onto the filler surface, such as vinyl and epoxy functionalized molecules, provides polymerizable centers convenient for copolymerization with corresponding groups in monomer chains. This chapter aims to present a comprehensive review of various chemical modification techniques applied to obtain reactive cross-linkable bio and mineral fillers suitable for copolymerization with polymer matrices. It also covers the analysis of the processing and reinforcement properties of reactive polymer/modified filler-based composites.

Keywords Composite materials · Polymerizable fillers. · Reactive composites. · Reinforcement.

J. D. Rusmirović (✉) · T. M. Kovačević · S. J. Brzić
Department for Materials and Protection, Military Technical Institute, Belgrade, Serbia
e-mail: jrusmirovic@tmf.bg.ac.rs

A. D. Marinković
Department of Organic Chemistry, Faculty of Technology and Metallurgy, University of
Belgrade, Belgrade, Serbia

6.1 Introduction

Today, polymer composites have been the focus of researchers mainly due to their excellent mechanical, dynamic-mechanical and thermal properties (Gun'ko 2019). The addition of inorganic/organic fillers to the polymers reduces the cost of the final product and extends its range of application, such as aerospace, automotive, biomedical, constructions, etc. (Toro-Márquez et al. 2018; Gutiérrez et al. 2019; Oğuz et al. 2019). Depending on the desired characteristics (brittleness, elasticity or ductility), thermosetting or thermoplastic polymers can be used as a matrix in composite production (Đurđević et al. 2017; Rusmirović et al. 2017b; Gun'ko 2019). In addition, various processing techniques such as the solution blending method, melt-compounding, *in situ* polymerization, etc. are generally used for fillers compounding into the polymer matrices and the preparation of the hybrid composites.

To date, a fairly large number of researches on the influence of inorganic and organic fillers on mechanical characteristics of polymers are presented in the literature (Gutiérrez et al. 2017a) Some of them are related to composites based on the silica (SiO₂) (Rusmirović et al. 2017b), alumina (Kovačević et al. 2018; Drah et al. 2019; 2020), carbon nanotubes (Tasić et al. 2016), cellulose (Rusmirović 2016; Rusmirović et al. 2017a; Rusmirović et al. 2018c; Herniou-Julien et al. 2019), and lignin (Gutiérrez et al. 2017b; Rusmirović et al. 2018a; Rusmirović et al. 2019).

It is important, however, to choose compatible polymers and fillers for the composite preparation, i.e. the adhesion and ease of incorporation and distribution of the filler throughout the polymer matrix (Akpan et al. 2019; Merino et al. 2018, 2019). Most commonly used fillers have a hydrophilic surface which limits their use in non-polar hydrophobic polymers. This obstacle can be solved using surface compatibilization to achieve uniform homogenization of fillers into the polymer matrices and, therefore, desired properties. Chemical modification using non-reactive or reactive modifying agents stands out as one of the most promising methods for surface compatibilization of fillers with polymers (Kango et al. 2013; Çakir et al. 2015; Rančić et al. 2015; Soleimani and Zamani 2017). Functionalized surface fillers can react chemically with the polymer matrix showing weak aggregation and homogenous dispersion (Rusmirović et al. 2018c; Oğuz et al. 2019). The introduction of cross-linkable vinyl or epoxide groups onto a bio- or inorganic filler surface makes them suitable for copolymerization with unsaturated polyester or epoxy resins.

This chapter presents a comprehensive review of several chemical modification techniques applied to obtain reactive cross-linkable bio and inorganic fillers (aluminum oxide, cellulose, lignin and silicon dioxide) suitable for copolymerization with thermosetting polymer matrices with the main focus on processing and reinforcement properties of reactive polymer/modified filler composites.

6.2 Polymer Composites

As the development of materials and the needs of end users have increased rapidly, composite materials have attracted a lot of attention due to their excellent properties and immense fields of application. The composites are products made from two or more constituents with unique physical and chemical properties, which when combined, give materials with characteristics quite different from the individual components. Composite materials are basically classified by the continuous phase (matrix) into ceramic, metal and polymer composites. In recent decades, interest in the field of polymer matrix composites (PMC) has increased, as they provide easy to process and have tunable the product's properties. The use of PMC instead of pure polymers allows better dimensional control/less shrinkage, which is of essential importance in the automotive or aerospace industry. In addition, the construction industry has used wood polymer composites as a natural wood replacement due to lower water absorption and reduced price (Bayer et al. 2016).

PMCs are composed of short/continuous fibers or nano/micro filler particles which are dispersed uniformly in a continuous polymeric matrix. The incorporation of bio or mineral reinforcements into polymeric matrix causes the obtaining materials with superior properties for a wide variety of applications. The analysis of these properties shows that they depend on (1) the properties of the particular components; (2) the ratio and amount of constitutive phases; (3) the orientation of embedded reinforcements; the bonding strength established between the matrix and the reinforcements and (4) the size, shape and distribution of the reinforcements (Bagherpour 2012). Each of the materials involved in the composite structure must have appropriate characteristics and function both individually and collectively to achieve the desired superior properties of end-product. Fillers contribute high stress (σ) and Young's module (E) values to the composite and provides resistance to bending and breaking under the applied load. The main role of the polymer matrix is to distribute stress among the filler particles. The polymer matrix also provides protection against filler abrasion and exposure to moisture or other environmental conditions (Mohammad 2007).

The combination of type and amount/particle size of filler particles leads to obtaining the composite material with targeted properties. Generally, the finer the particle size, the better physical properties of the composites are obtained. The addition of a greater amount of filler can lead to decreasing of physical properties due to the increase of the discontinuity/heterogeneity of polymeric network/system by the formation of filler agglomerates as a weak spot in the composite structure (Rusmirović et al. 2016; Kovačević et al. 2017; Kovačević et al. 2019). According to these observations, the optimization of the mentioned parameters is the most important aspect in composite preparation process.

6.3 Polymer Matrices

The continuous phase of PMC can be thermoplastic or thermosetting polymers. Thermosetting polymers are usually in form of a resin, polymerizes completely when heated in the process known as curing (Chung 2017). One of the main advantages of thermosets is easy processability in terms of applied temperature, which is relatively low (about 200 °C) depending on the type of polymer. The most commonly used thermosetting polymers for PMC are epoxy, unsaturated polyester, phenolic and polyurethane resins. Epoxy and unsaturated polyester resin (UPR) have been widely used in countless fields such as coating, marine, automotive, aerospace and construction, due to its high strength, high chemical and corrosion resistance, low cost, etc. (Tomić et al. 2014; Dittanet et al. 2017; Lin et al. 2017). However, both the epoxy and the UPR manifest an inherently brittle nature and poor thermal characteristics which disable its use in high performance applications (Abenojar et al. 2017; Kovačević et al. 2017; Drah et al. 2019). The mechanical, thermal, dynamic-mechanical and fire-resistant properties of aforementioned polymers can be significantly improved by introducing various reinforcements within their structure. The most commonly used materials for this purpose are: SiO₂, cellulose, lignin, ceramics (alumina, clay), glass fibers, carbon nanotubes, chalk, some polymeric waste etc. (Tomić et al. 2014; Đurđević et al. 2017; Kovačević et al. 2017; Rusmirović et al. 2017a; Rusmirović et al. 2017b; Kovačević et al. 2018; Rusmirović et al. 2018a; Drah et al. 2019; Kovačević et al. 2019). The use of waste materials has an additional benefit in terms of preservation of resources due to the expected shortage of non-renewable raw materials, as well as the promotion of the application of the green and circular economy (Kovačević 2018).

There are some drawbacks related to the achievement of great miscibility/compatibility between the polymer matrix and the incorporated reinforcements, which are mainly due to the hydrophilic nature of the reinforcements towards the hydrophobic polymer matrices. To achieve good interactions between the reinforcements and the polymer matrix, reflected in satisfactory wetting and adhesion, it is necessary that additional actions come into play. These actions involve surface modification/functionalization through the reaction between modifying agent and an infinity of hydroxyl groups within the structure of the reinforcements (Drah et al. 2019).

6.4 Bio and Mineral Reinforcement in PMC

Filler particles, inorganic or organic, are designed to improve polymer matrix the strength and thermal properties, as well as to reduce polymerization shrinkage and swelling (Khalil et al. 2015). Non-modified fillers strengthen the polymer matrices because of their hardness in relation to the matrix (Khalil et al. 2015), while modified/reactive fillers also include copolymerization with polymer chains which increase the crosslinking density (ν) values (Rusmirović et al. 2018c). The strength

of the composites also depends on the filler diameter, the interparticle spacing/porosity and the volume fraction of the composite (Tasić et al. 2016; Rusmirović et al. 2017b; Rusmirović et al. 2018c).

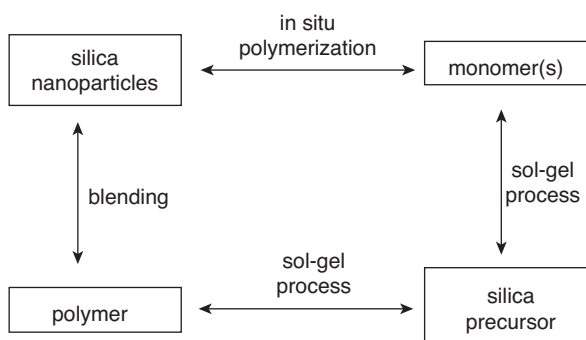
Inorganic fillers are usually pure crystalline oxides of aluminum, silicon, zirconia, titanium etc. with a defined chemical composition. Also, several minerals such as calcium carbonate, dolomite, wollastonite, talc, and crystalline SiO_2 meet the requirements for use as a polymer reinforcement, due to its inert nature and low cost and easy production that only requires a particle size reduction (Rothon 2002).

6.4.1 SiO_2 Filler

Among the numerous inorganic-organic hybrid materials, the SiO_2 -polymer based composites are the most described in the literature (Rusmirović 2016). This can be attributed to the various types of SiO_2 morphology, abundance in natural sources, various synthesis/preparation techniques, which makes SiO_2 applicable in polymers as a reinforcement (Spange 2000). Depending on the morphology and performed synthesis technique, SiO_2 particles are commonly used as fillers in the production of paints, adhesives and binders from rubber and polymers. The processing techniques used for the preparation of the SiO_2 /polymer composites can be classified as mixing or sol-gel technique and *in situ* polymerization (Rusmirović 2016). The three general approaches to the preparation of SiO_2 -polymer composites are shown in Fig. 6.1.

Although the SiO_2 loading in polymer matrices causes the improvement of the mechanical properties, achieving a high compatibility of the SiO_2 with the matrix plays an important role in the design of composites. The significant difference between the properties of the polymer and SiO_2 can lead to phase separation due to the hydrophilicity of SiO_2 caused by surface silanol/hydroxyl groups. The formation of hydrogen bonding between silanol groups causes the aggregate formation (Fig. 6.2) (Nordström et al. 2010).

Fig. 6.1 Three general approaches to prepare SiO_2 -polymer composites. Reproduced with permission from Rusmirović (2016)



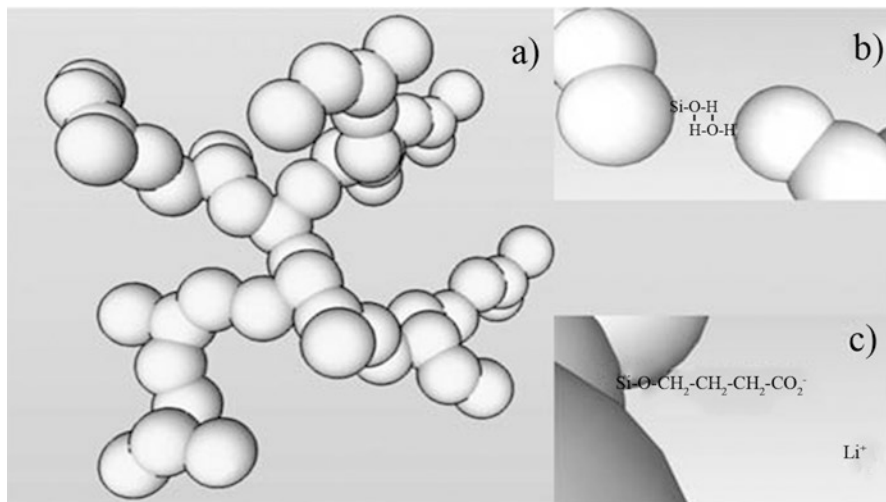


Fig. 6.2 Schematic figure of the fumed silica structure (a), formation of aggregates on the nano-SiO₂ surface by (b) hydrogen bonds and (c) alkyl functionalities. Reproduced with permission from Nordström et al. (2010)

6.4.2 Alumina Filler

Alumina or aluminum oxide is an amphoteric oxide that exists in nature as the minerals of corundum (Al₂O₃), diaspore (Al₂O₃·H₂O), gibbsite (Al₂O₃·3H₂O), and more commonly as bauxite, which is an impure form of gibbsite. Alumina exists in numerous crystalline structures. The metastable phases, usually called ‘transition alumina’, can be irretrievably translated into α-Al₂O₃ by appropriate thermal or hydroxylation treatments. The crystal structure of alumina comprises hexagonal and octahedral sites (Mallakpour and Khadem 2014).

Al₂O₃ has favorable physical and chemical properties such as high strength, hardness, *E* and excellent resistance to chemical environments. Because of that, Al₂O₃ has wide applications in structural composites (Soleimani and Zamani 2017; Drah et al. 2019). Drah et al. (2019) demonstrated that the significant increase in mechanical properties can be achieved by incorporating a pristine Al₂O₃ filler into the UPR resin with respect to the pure polymer. However, its applications are somewhat limited due to low toughness and lower thermal resistance (Miranda-Hernández et al. 2006).

6.4.3 Cellulose Filler

In addition to the mineral fillers that exist in nature or that can be produced by easy synthesis procedures, natural materials such as cellulose, lignin and tannins are commonly used in the production of polymer composites. Cellulose represents renewable, biodegradable, low-weight and non-toxic biopolymer that are

abundantly found in nature, thus acting as structural building blocks that confer its mechanical properties to superior plant cells (Dufresne 2012). The basic chemical structure of cellulose (Fig. 6.3) represents a dimer cellobiose that appears as a repeated segment (β -D-anhydroglucopyranose units (AGU) linked together by β -1,4-glycosidic bonds in both crystalline and amorphous regions (Rusmirović et al. 2018b). There are three different AGU units in the cellulose molecules: reducing and non-reducing end-groups, and internal glucose rings (Rusmirović et al. 2018b). Reducing end-group contains free hemiacetal or aldehyde at the position C1, while the non-reducing groups contains free hydroxyl groups at the position C4 (Dufresne 2012; Rusmirović et al. 2018b). The internal glucose rings are joined at positions C1 and C4 (Dufresne 2012; Rusmirović et al. 2018b). In addition, each internal AGU has three hydroxyl groups at the positions C2, C3 and C6 that represent all possible sites for the chemical modification of cellulose. At the C6 position there is a primary hydroxyl group, while the hydroxyl groups at the C2 and C3 positions are secondary. The hydroxyl group at the C6 position is the most reactive (Dufresne 2012; Rusmirović et al. 2018b). Depending on the size, the cellulose can be microcrystalline or nanocrystalline. Nanocellulose (NC), in the form of nanocrystals, whiskers, rods, nanofibrils or nanofibers, refers to cellulose fibers or crystals that have at least one dimension within the nanometric size range. NC has been evaluated in recent research as a reinforcing phase in nanocomposites based on different synthetic or nature polymer matrices such as acrylic latex (Pu et al. 2007), polyvinyl alcohol (Roohani et al. 2008), polyurethane (Cao et al. 2007), polyethylene (Junior de Menezes et al. 2009), rubber (Pasquini et al. 2010), polyester (Rančić et al. 2015; Rusmirović et al. 2017a; Rusmirović et al. 2018c; Rusmirović et al. 2018b) and thermoplastic starch (Table 6.1) (Zainuddin et al. 2013). It can be concluded by comparing the mechanical properties of cellulose nanocrystals with respect to properties of other commercial reinforcing agents that cellulose nanocrystals have great potential as a reinforcing material (Durán et al. 2011).

NC has a hydrophilic and polar nature which causes moisture absorption and also disables homogenous dispersion in synthetic hydrophobic polymers (Rusmirović et al. 2018b). This problem can be overcome by modifying it, either by coating the NC using surfactants or by chemically modifying the surface with hydrophobic groups (Rusmirović et al. 2018b). Coating the NC using surfactants is the easiest method, but it requires a very high amount of surfactants which causes problems in composite applications (Rusmirović et al. 2018b).

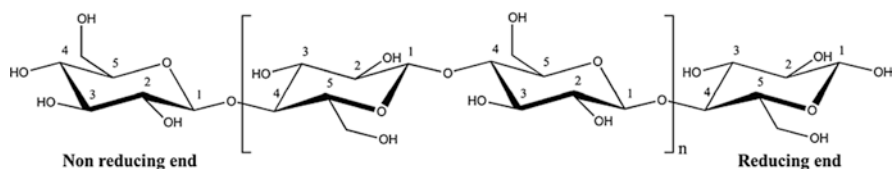


Fig. 6.3 Chemical structure of cellulose. Reproduced with permission from Rusmirović et al. (2018b)

Table 6.1 Properties of cellulose based materials. Reproduced with permission from Moon et al. (2011) and Rusmirović et al. (2018b)

Materials	E_A (GPa)	E_T (GPa)	σ_{max} (GPa)	ϵ_b (%)
Wood fiber	14–27	–	0.3–1.4	4–23
Plant fiber	5–45	–	0.3–0.8	1.3–8
Microcrystalline cellulose	25 ± 4	–	–	–
Cellulose nanocrystals	57, 105	–	–	–
Plant wood	–	18–50	–	–
Treated cellulose nanocrystals	143	–	–	–
Acid treated	151 ± 29	–	–	–
TEMPO treated ^a	145 ± 31	–	–	–
Bacterial nanocellulose	78 ± 17	–	–	–
Bacterial nanocellulose	114	–	–	–

E_A , E_T = Young's modulus in axial direction and transverse direction, respectively; σ_{max} = maximum stress; ϵ_b = strain at break

^a2,2,6,6-tetramethylpiperidine 1-oxyl radical

6.4.4 Lignin Filler

Many researches are focused on lignin as a reinforcement or flame retardant additive in polymer matrices (Thakur et al. 2014; Prieur et al. 2016; Rusmirović et al. 2018a). Lignin is an aromatic biopolymer structured from three types of polyphenols: coniferyl alcohol, sinapyl alcohol and *p*-coumaryl alcohol (Fig. 6.4) (Faruk and Sain 2016; Rusmirović et al. 2018a).

Lignin changes the permeability and thermal stability of the plant, and serves as a structural material that adds strength and rigidity to plant tissue (Faruk and Sain 2016). There are numerous common methods to produce commercial grade lignin, such as kraft or sulphite pulping, as well as soda, organosolv, hydrothermal and dilute acid processes that give different types of lignin with a wide range of chemical characteristics (Faruk and Sain 2016). It is essential that researchers understand the changes on the chemistry properties of lignin by applying different processing methods and how to predict the characteristics of the lignins obtained (Faruk and Sain 2016).

Lignin with its highly branched and aromatic structure, and a large number of functional groups such as hydroxyl, represents a valuable biobased candidate for thermosets, thermoplastics and composites. Lignin has been used as filler, matrix or coupling agent with various thermoplastic, thermosetting or biopolymers (Schorr et al. 2014; Faruk and Sain 2016; Rusmirović et al. 2018a). Lignin fibers possess excellent mechanical properties shown in work of Hosseini et al. (2017) who estimated the average strength of the aligned nanofibers. The results obtained for the average value of 12 samples show a reasonable agreement with the theoretical data (Table 6.2).

Even, the significant improvement of the mechanical and thermal properties of the polymers is achieved by loading the pristine inorganic/organic bio and mineral fillers, it is still necessary to increase the degree of the interaction between the filler and the polymer matrix. The introduction of functionality of the inorganic/organic

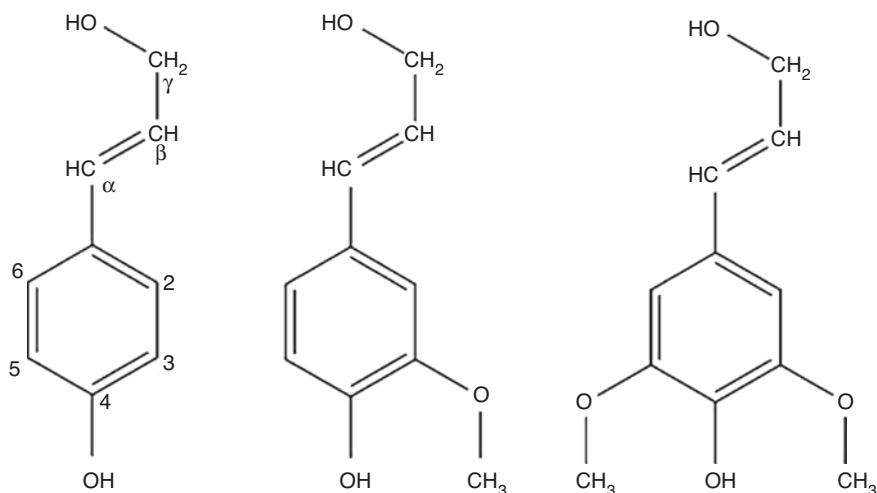


Fig. 6.4 Molecular structures of coniferyl alcohol (left), sinapyl alcohol (middle) and *p*-coumaryl alcohol (right). Reproduced with permission from Faruk and Sain (2016)

Table 6.2 Experimental and theoretical strength results for the nanofibrous lignin. Reproduced with permission from Hosseini et al. (2017)

Materials	Gauge length (mm)	Experimental strength (MPa) (CV%)	Theoretical strength (MPa) (CV%)
Single nanofiber	5	37.5 (28.7)	37.4 (30.5)
Aligned nanofiber mat	40	14.2 (4.6)	12.5
Nanofiber yarn		None	19.1–189.5 MPa According to the critical length

$\eta = 41.5$ (MPa) and $\beta = 3.7$. β = Shape factor, η = Scale parameter, and CV = Coefficient of variance

fillers at the molecular level is a very effective way to design new reactive materials with novel functionalities which provide better connectivity and covalent/induced dipole/hydrogen interactions with the polymer matrix (Rusmirović 2016; Rusmirović et al. 2018b, c).

6.5 Compatibilization Between Polymer Matrix and Reinforcements

As mentioned earlier, the use of surface modifiers is the best approach to reduce the surface tension between the reinforcement and the matrix, resulting in the improvement of final properties of the polymers. The most common mechanism of how

modifiers work is the reaction between the functional groups within the modifier and the reinforcing structure, while the loose organic parts from the modifier are inserted into the free space between the macromolecule chains in the polymer matrix (Chung 2017). If these organic tails contain reactive groups, they can chemically interact with similar groups from the polymer matrix, even during the curing process. In addition, the modification of the reinforcing surface changes the intensity of the interactions between the particles/fibers themselves, especially if its surface is charged. In this case, a competition occurs between electrostatic repulsion and the establishment of intermolecular hydrogen bonds, resulting in the prevention of filler agglomerates (Almasi et al. 2015).

6.6 Chemical Modification of the Bio and Mineral Fillers

The key parameter in the production of hybrid composite materials is the achievement of the desired design of the polymer matrix and fillers as well. Commonly, the way to design filler/polymer surface is chemical modification. Generally, the chemical modification represents the chemical bonding of the modifier/coupling agents or polymeric chains on the filler surface. By an appropriate surface or molecular modification of fillers it is possible to distribute them uniformly throughout the polymer matrix, resulting in establishment of a better interaction between the reinforcement and the matrix. In this way, the significant improvement of the properties of the polymeric material is achieved with the simultaneous decrease in the price of the final product (Radoman et al. 2015b). After appropriate surface modification, the filler particles become hydrophobic, which decreases their surface tension and leads to better miscibility and compatibility with the hydrophobic polymer matrix (Radoman et al. 2015a). In addition, surface functionalization causes changes in the surface charge which is manifested by the competition between electrostatic reflection of the particles themselves and the formation of intramolecular hydrogen bonds (Bagwe et al. 2006; Rusmirović 2016).

6.6.1 Chemical Modification of SiO₂ Fillers

Although nano-SiO₂ particles have unique advantages such as special optical, electrical, magnetic, mechanical and thermal properties (Chuang et al. 2018). However, due to the large specific surface area, which favors the creation of agglomerates, it is difficult to uniformly disperse the nano-SiO₂ throughout polymer matrices. For this reason, the use of coupling agents to overcome these inconveniences is the best available technique covered in literature and practice. In this sense, silane coupling agents are used successfully for the modification of innumerable reinforcements with available hydroxyl groups within its structure (Abdelmouleh et al. 2005; Kargarzadeh et al. 2015; Rusmirović et al. 2017a; Yue et al. 2018; Drah et al. 2019).

The schematic illustration of the chemical bond of organosilane on the surface of SiO_2 is shown in Fig. 6.5.

The organosilanes have a bifunctional structure suitable for use in the treatment of natural fiber and inorganic fillers, since both have reactive hydroxyl groups onto the surface (Rusmirović et al. 2017b; 2016). Table 6.3 shows the most commonly used silanes as coupling agents: amino, vinyl, acryl, methacrylate and azido (Xie et al. 2010). According to data from the literature, aminosilanes are the most suitable for the modification of natural fibers in combination with thermoplastic and thermosetting polymers (Abdelmouleh et al. 2005; Drah et al. 2019). Methacrylate treated fillers show high reactivity towards UPRs, azides are extensively used for modification of inorganic fillers to react with thermoplastic matrices, while vinyl and acryl need peroxide based initiators to establish the bond between the matrix and the reinforcements (Xie et al. 2010).

The chemical structure of organosilanes can be presented through the general formula RSiX_3 , where X represents different groups, such as chloride, ethoxy or methoxy. R represents organic reactive or non-reactive chains that can optionally have a similar structure and properties as those of the polymeric matrix (Ranjan 2008). The chloride, ethoxy or methoxy functional groups react with the hydroxyl groups of SiO_2 surface, while organic chains (marked with R) react with the polymer matrix chains. Commonly used organosilanes for SiO_2 surface functionalization are (3-aminopropyl)trimethoxysilane 97% (APTMS), 3-(trimethoxysilyl)propyl methacrylate (TMSPM), *tris*(2-methoxyethoxy)(vinyl)silane (TMEVS), among others (Rusmirović 2016). The procedure for its attachment onto the filler surface, known as grafting, allows the introduction of suitable hydrophobic segments for establishing the best compatibility with the polymer matrix. In this way, the potential for obtaining high performance building nanocomposites increases significantly. It has also been shown that by grafting the interfacial interactions are improved, which causes the appearance of entanglements of the SiO_2 surface loose segments and the polymer matrix chains. Thus, by changing the grafted monomers and the grafting conditions, the potential of tailoring the desired structure is provided, i.e. achieving the best correlation between the structures and properties of the nanocomposites (Rusmirović 2016).

Reinforcements treated by coupling agents can improve the targeted properties of various types of polymer matrices. For example, the modification of nano- SiO_2 by the KH-560 and SEA-171 coupling agents increase the interfacial bonding between the

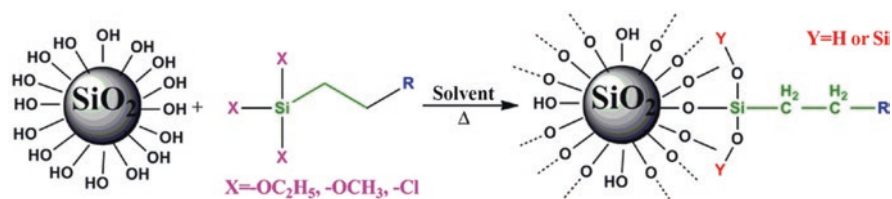


Fig. 6.5 Surface functionalization of the SiO_2 surface via organosilanes. Reproduced with permission from Ranjan (2008)

Table 6.3 Silanes used for natural fiber/polymer composites: Molecular formulas, functionalities and target polymer matrices. Reproduced with permission from Xie et al. (2010)

Molecular formulas	Functionality	Abbreviations	Target matrix
$(\text{RO})_3\text{Si}-(\text{CH}_2)_3-\text{NH}_2$	Amino	APS	Epoxy Polyethylene Butyl rubber Polyacrylate PVC
$(\text{RO})_3\text{Si}-\text{CH}=\text{CH}_2$	Vinyl	VTS	Polyethylene Polypropylene Polyacrylate
$(\text{RO})_3\text{Si}-(\text{CH}_2)_3-\text{OC}(\text{CH}_3)\text{C}=\text{CH}_2$	Methacryl	MPS	Polyethylene Polyester
$(\text{RO})_3\text{Si}-(\text{CH}_2)_3-\text{SH}$	Mercapto	MRPS	Natural rubber PVC
$(\text{RO})_3\text{Si}-(\text{CH}_2)_3-\text{O}-\text{CH}_2\text{CHCH}_2\text{O}$	Glycidoxy	GPS	Epoxy Butyl rubber Polysulfide
$\text{R}_2-\text{Si}-\text{Cl}_2$	Chlorine	DCS	Polyethylene PVC
VTS grafted plastics	Vinyl	VSPP	Polypropylene Polyethylene
$(\text{RO})_3-\text{Si}-\text{R}''-\text{N}_3$	Azido	ATS	Polypropylene Polyethylene Polystyrene
$(\text{RO})_3\text{Si}-(\text{CH}_2)_{15}\text{CH}_3$	Alkyl	HDS	Polyethylene Natural rubber

R = -methyl or ethyl and R'' = $-\text{C}_6\text{H}_4-\text{SO}_2-$

filler and the cyanate ester (CE) resin, thus improving the thermal and friction properties of the composites (Chuang et al. 2018). After the surface treatment of nano-SiO₂ by SEA-171, the thermal decomposition temperature of the 3.0 wt.% nano-SiO₂/CE composites increases by 75 °C, the frictional coefficient is reduced by 25% and the wear resistance increases by 77%, with respect to the pure CE (Chuang et al. 2018).

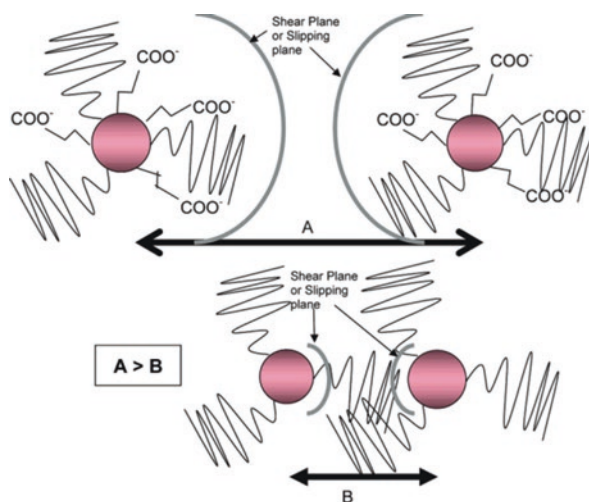
In order to obtain the best efficacy of the filler modification, it is necessary to optimize the process parameters, mainly the amount of coupling agent and the temperature. Xu et al. (2014) found that 5 wt.% of 3-aminopropyltriethoxysilane (KH-550) or 3-methacryloxypropyltrimethoxysilane (KH-570) at 75 °C provides optimal results in relation to a certain number of hydroxyl groups of nano-SiO₂ surface. In contrast, a too high concentration of the modifier can then cause adhesion of the modifier onto the nano-SiO₂ surface. On the contrary, the reaction of the silane coupling agent and the nano-SiO₂ is hindered by the steric phenomena exhibited by the modifier length chain (Xu et al. 2014). Similar results have been obtained by Soleimani and Zamani (2017) by varying the amount of trimethoxyvinylsilane (TMVS) during the modification of alumina nanoparticles (NPs). It can also be observed that the hydrophobicity of the alumina surface increases as the amount of modifier increases up to 10 wt.%. Similarly, a greater increase in the amount of

TMVS has the same as in the case of $\text{SiO}_2/\text{KH-550}$ (KH-570) (Soleimani and Zamani 2017).

Bagwe et al. (2006) presented a systematic study of the design of the surface modification of SiO_2 NPs involving an optimal balance of the use of inert and active surface functional groups to achieve a minimal aggregation of particles. The surface modification was performed by co-hydrolysis with tetraethyl orthosilicate (TEOS) and various organosilanes (Bagwe et al. 2006). The schematic illustration of the SiO_2 agglomeration prevention mechanisms is shown in Fig. 6.6 (Bagwe et al. 2006). Different functional groups, such as carboxylate, amine, amine/phosphonate, poly(ethylene glycol), octadecyl, and carboxylate/octadecyl groups were introduced onto the SiO_2 surface. SiO_2 particles modified with only octadecyl groups had a significantly lower sliding plane with octadecyl moieties outside the sliding plane (Bagwe et al. 2006). Therefore, there are strong hydrophobic interactions between particles caused an agglomeration. The introduction of carboxylate/octadecyl groups caused an increase of sliding plane border where octadecyl moieties are inside in sliding plane (Bagwe et al. 2006). Thus, the stable suspension of SiO_2 particles into polymer was obtained.

Composite coatings based on alkyd resins and vinyl and methacryloyl silane modified SiO_2 particles made by Rusmirovic et al. (2016) showed improved mechanical and anticorrosive properties in both wet and salt chamber compared to the bare alkyd resins. The crosslinking of the TMEVS modified SiO_2 particles with thermosetting polymer matrix (UPR) is shown in Fig. 6.7. The crosslinking of UPR-based composites with vinyl modified SiO_2 particles was produced *via* chemical reaction through unsaturated sites on polymer chains and vinyl silane moieties (Rusmirović et al. 2016). The schematic illustration of the preparation and intermolecular interactions for TMEVS, TMSPM and APTMS/biodiesel (BD) crosslinked SiO_2 /polyester nanocomposites is shown in Fig. 6.8 (Rusmirović et al. 2016). The determined morphological, mechanical, dynamic-mechanical properties of these

Fig. 6.6 Prevention of SiO_2 agglomeration *via* electrostatic reflection and steric stabilization. Reproduced with permission from Bagwe et al. (2006)



composites reflected the influence of the vinyl SiO_2 functionalization on the dispersibility, the extent of intermolecular interactions, and electronic and steric interference to the reactivity of the vinyl group (Rusmirović et al. 2016). The extent of the interactions depended on the nature of SiO_2 functional groups and the UPR chains. High intensity π,π -stacking attractive interactions between the vinyl and terephthaloyl moieties contributed to the effective network of the system obtained (Rusmirović et al. 2016), while low intensity non-covalent interactions such as van der Waals, London dispersive forces, and dipolar interactions have a minor contribution to order and physical crosslinking. The modified SiO_2 reinforced composites exhibited higher mechanical properties than the pure cured UPR matrix because the hydrophobicity of SiO_2 surface and higher reactivity contributed to a higher ν value (Fig. 6.8).

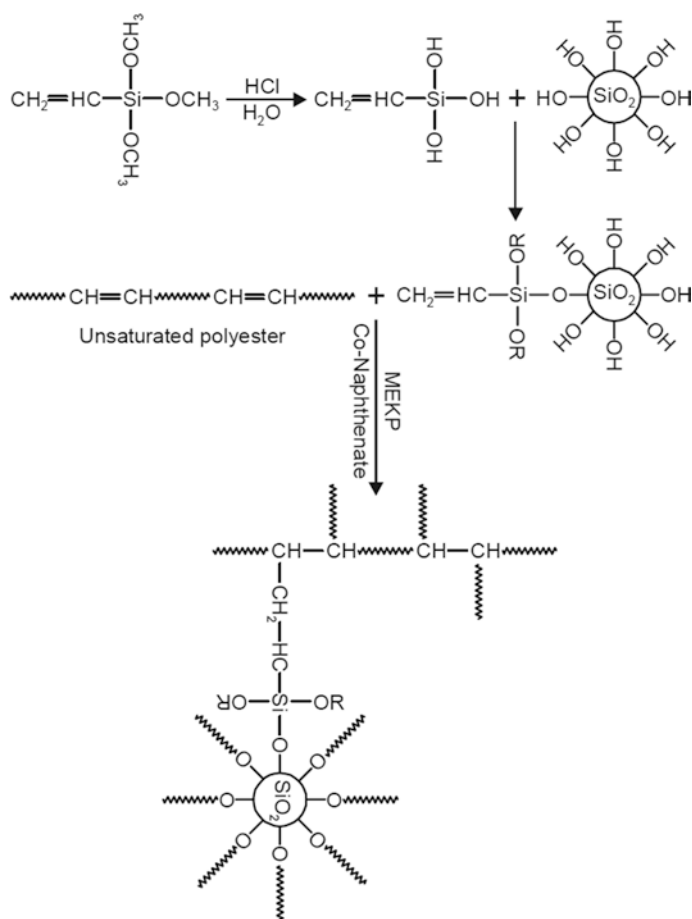


Fig. 6.7 Schematic illustration of crosslinking of the SiO_2 vinyl surface groups with unsaturated polyester resin. Reproduced with permission from Çakir et al. (2015). *MEKP: methyl ethyl ketone peroxide

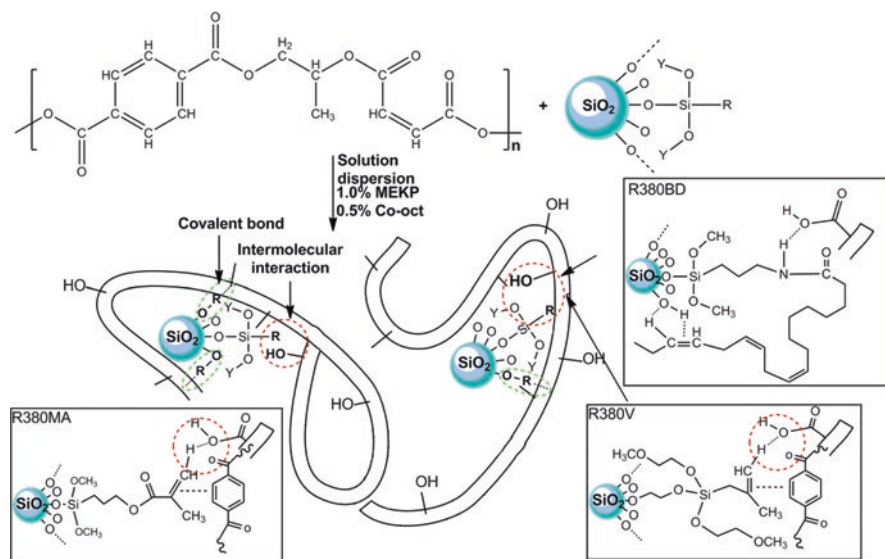


Fig. 6.8 Preparation of nanocomposites with proposed reinforcement interactions between modified silica nanofiller and polyester matrix. Reproduced with permission from Rusmirović et al. (2016)

6.6.2 Chemical Modification of Alumina Fillers

The hydrophilic nature of alumina NPs leads to high moisture absorption, formation of agglomerates and incompatibility with hydrophobic segments of polymeric matrices. These disadvantages can often be overcome by modifying the alumina NPs, using silane a coupling agent. The structures obtained allow the establishment of a large bond with polymeric matrices, especially with those containing double bond segments.

Jin et al. (2007) prepared the nanocomposites based on ethylene-vinyl acetate (EVA) and modified nano-Al₂O₃. Maximum stress (σ_{\max}), strain at break (ϵ_b) and viscosity values of EVA/Al₂O₃ nanocomposites were significantly improved with respect to pure EVA (Jin et al. 2007). Zunjarrao and Singh (2006) investigated the effects of particle size and silane treatment on the fracture toughness for epoxy resin reinforced with aluminum particles of 20–100 nm was greater than that reinforced with particles of 3–4.5 μm . However, agglomeration problems can limit the improvement achieved in the fracture toughness of the composites with nanometer size particles (Bracone et al. 2016). Mallakpour and Dinari (2013) reported the modification of Al₂O₃ using KH550 as a coupling agent. The results obtained indicated that Al₂O₃ NPs formed aggregates of several hundred nanometers in diameter. On the contrary, KH550-modified Al₂O₃ NPs were finely dispersed into the polymer matrix (Mallakpour and Dinari 2013).

Drah et al. (2019) functionalized two types of alumina particles: commercial alumina ($\alpha\text{-Al}_2\text{O}_3$) and alumina doped with ferrous oxide ($\text{Fe@Al}_2\text{O}_3$), and its application in strengthening of the UPR matrix was studied. The functionalization of both alumina particles was performed by APTMS (one-step modification) and successive modification with APTMS in the first step followed by methyl ester of linseed oil fatty acids (LOFAs used as a BD) in the second step (Fig. 6.9) (Drah et al. 2019). The mechanical and dynamic-mechanical properties, and the curing kinetics from pure UPR resin and its composites containing 1 wt.% of filler was also measured by Drah et al. (2019) using the Fourier transform infrared (FTIR) technique. Curing kinetics was traced out by monitoring of characteristic peak of styrene at 909 cm^{-1} (Fig. 6.10), while the obtained data was processed using Beer's law. Drah et al. (2019) also reported the auto-acceleration of the curing reaction when the incorporation of pristine alumina particles ($\text{Fe@Al}_2\text{O}_3$) was done, thus obtaining higher values for styrene consumption, meanwhile the lowest conversion value of styrene was observed for alumina modified with APTMS due to the inhibitory effect exhibited by the amine functionalities of APTMS, which potentially participates in the radical transfer reactions with peroxy (initiator) or alkyl radicals (chain transfer radical - propagation). On the contrary, the modified APTMS-LOFA alumina depletes a greater amount of styrene due to its reactivity (six ethylenic bonds within the LOFA structure) which is manifested in reduced intensity of the characteristic peak of styrene, regardless of steric hindrance in reactivity caused by the LOFA conformational structure (Drah et al. 2019). The potential of the unsaturations presented is enough to break the steric impact of the flexible/coiled LOFA structure, as a consequence a higher final value of styrene consumption was observed. Drah et al. (2019) suggested that the reactivity of the system can thus be designed by modifying the properties of the filler surface.

6.6.3 *Chemical Modification of Biofillers: Cellulose and Lignin*

The hydrophilic nature of cellulose-based fillers limits their use in hydrophobic and polar matrices. Numerous functional groups (hydroxyl) onto the cellulose structure represent a unique basis for surface modification and hydrophilic-hydrophobic balance (Popović et al. 2020). The increased availability of cellulose crystal segments represents the main objective of chemical functionalization to use cellulose as a reinforcement in polymer composites. It has been demonstrated from the literature that the introduction of long alkyl chains onto the surface of cellulose fiber causes dispersion in the low-density poly(ethylene) matrix (Dufresne 2010).

The hydroxyl group at the C6 atom linked through the methylene group to the cellulose core has been shown to have the highest reactivity. As described in the literature, during the first stage of cellulose modification, only the surface is modified, while the dimensions and crystallinity of the cellulose remain unchanged. With the increase in modification time, diffusion mechanisms control the rate, which

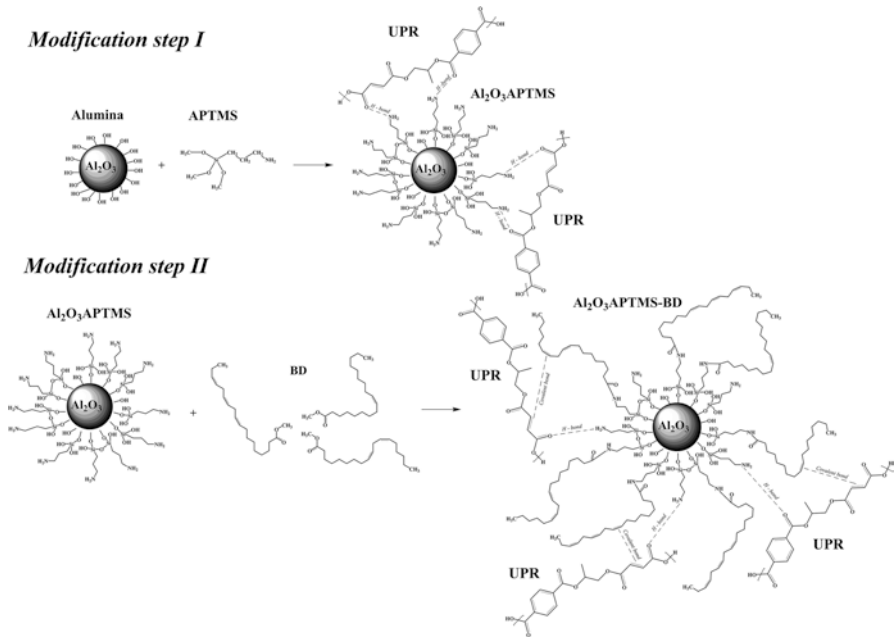


Fig. 6.9 Alumina particle modification pathways along with interactions between modified fillers and UPR resin. Reproduced with permission from Drah et al. (2019)

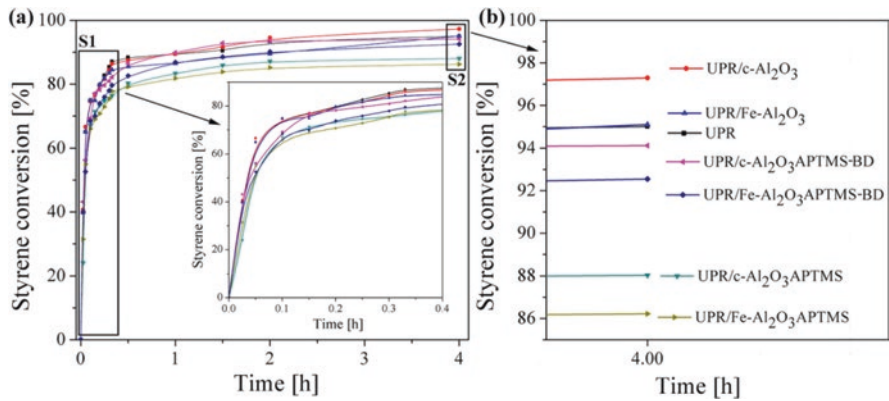


Fig. 6.10 Styrene conversion during curing determined by the FTIR method. Reproduced with permission from Drah et al. (2019)

leads to cellulose with higher levels of modification, smaller dimensions, lower crystallinity and improved stability in low polar solvents (Çetin et al. 2009). Accordingly, it is important to provide modification conditions which give a high degree of substitution of hydroxyl groups with modifying agent. The methods of chemical modification can be classified into the following groups (Dufresne 2013):

1. Substitution of hydroxyl groups with small molecules (red arrows in Fig. 6.11)
2. Polymer grafting based on the ‘grafting onto’ strategy with different coupling agents (blue arrows in Fig. 6.11)
3. Polymer grafting based on the ‘grafting from’ approach with a radical polymerization involving ring opening polymerization (ROP), atom transfer radical polymerization (ATRP) or single-electron transfer living radical polymerization (SET-LP) (yellow arrows in Fig. 6.11).

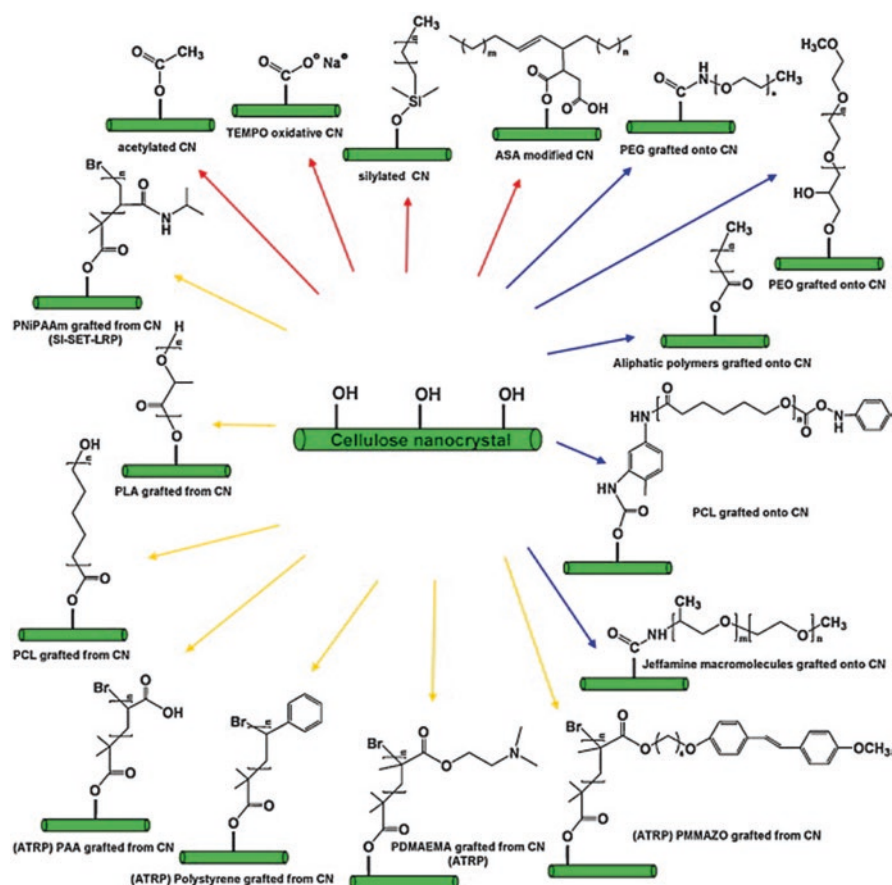


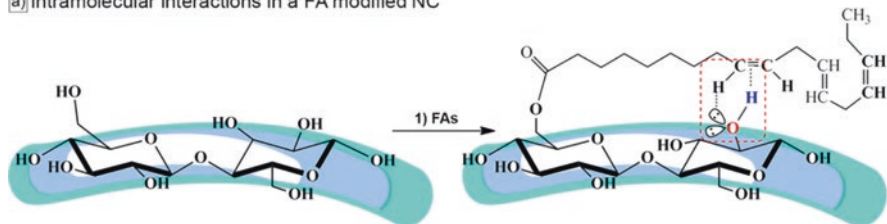
Fig. 6.11 Common surface covalent chemical modifications of cellulose nanocrystals. PEG: poly(ethylene glycol), PEO: poly(ethylene oxide), PLA: poly(lactic acid), PAA: poly(acrylic acid), PNIPAAm: poly(*N*-isopropylacrylamide) and PDMAEMA: poly(*N,N*-dimethylaminoethyl methacrylate). Reproduced with permission from Dufresne (2013)

Chemical modification using different coupling agents such as acid anhydrides, polymeric isocyanates, triazines, silanes, amines, etc., stands out as one of the most effective way to reduce cellulose hydrophilicity and agglomeration in non-polar matrices (Dufresne 2013; Rusmirović 2016). In addition, the chemical modification reduces the degree of crystallinity and the size of the cellulose crystals, which contributes to a homogeneous dispersion of the cellulose into the polymers. In addition to the synthetic coupling agents that are used in cellulose functionalization, today, great researches efforts are focused on the development of natural modifying agents, such as vegetable oils, fatty acids isolated from vegetable oils and their derivatives.

The carboxylic groups from fatty acids provides the appropriate conditions for their anchorage onto filler's surface, thus producing the carboxylic salts (Dearmitt and Rothon 2014). The fatty acids can be coupling (unsaturated) or non-coupling (saturated) modifiers depending on the nature of alkyl chains. Saturated acids are relative inexpensive and abundant, which makes them good candidates for the surface treatment of calcium carbonate and other basic/amphoteric fillers (Jeon et al. 2018). They have relatively non-reactive short chains to become entanglements with macromolecules from the polymer matrix, but provide a better dispersity of the fillers into the polymer. In addition, the material with greater strain (ϵ) and toughness values can be obtained by incorporating reinforcements modified with saturated fatty acids into the polymer matrix (Dearmitt and Rothon 2014). On the contrary, unsaturated fatty acids contain one or more ethylenic segments within their structure able to react with polymer matrices. Commercially available products from this group are based on unsaturated oligomeric carboxylic acids (Scofield 2003). The use of unsaturated fatty acids is best suited with unsaturated polyester resins or some elastomers where the curing reaction is initiated using a peroxide-based system *via* a radical polymerization mechanism (Rusmirović et al. 2017a, 2018c; Drah et al. 2019).

Rusmirović et al. (2016, 2017a, 2018c) investigated the potential application of unsaturated fatty acid (FA) modified nanocellulose (m-NC) to improve the polymerization properties of unsaturated polyester/m-NC nanocomposites (UPR/m-NC). These authors used two methods for NC modification: 1) direct esterification with oleic acid, linseed or sunflower oil FAs or 2) esterification/amidation with maleic acid/ethylene diamine (MA/EDA) bridging group followed amidation with methyl ester of FAs (Rusmirović et al. 2018c). They found that m-NC loading in polyester caused an increase of the crosslinking rate in the first 90 min (Rusmirović et al. 2018c). The highest conversion rate in the first 90 min was observed for composites based on linseed oil FA-modified nanocellulose (Rusmirović et al. 2018c). The schematic summary of the NC modification with FAs directly and *via* MA/EDA bridge group, as well as crosslinking with unsaturated polyester are shown in Figs. 6.12 and 6.13. Rusmirović et al. (2018c) also suggested different types of intermolecular interactions, such as O-H/O-H and N-H/O-H hydrogen bonds between polyester chains and m-NC (Fig. 6.13). Oleic acid residues contain unsaturated double bonds at the C9 atom, which are suitable for copolymerization with unsaturated polyester chains and participation in a formation of weak induced dipole/hydrogen bonds. The modification of cellulose with FAs through MA/EDA bridging group caused an additional contribution for N-H/O hydrogen bonding formation with polyester chains.

a) Intramolecular interactions in a FA modified NC



b) Intramolecular interactions in MEFA modified NC via cross linker

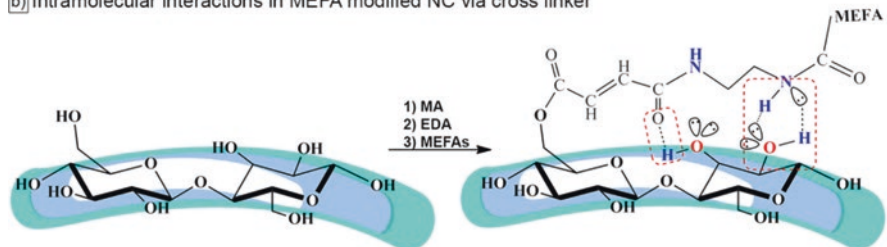


Fig. 6.12 Schematic summary of the NC modification with FAs (a) directly and (b) through a crosslinking agent. Reproduced with permission from Rusmirović et al. (2018c)

Lignin is a biobased filler obtained from biomass, which has had a growing interest. The common way to increase the reactivity of lignin for composite applications is chemical modification. The main methods of modification, such as hydroxymethylation, phenolation, partially depolymerization (Qin et al. 2014), epoxidation (Malutan et al. 2008) and phosphorilation (Rusmirović et al. 2018a; Rusmirović et al. 2019) have been reported in the literature. For example, Qin et al. (2014) used partially depolymerized kraft lignin with greater solubility in organic solvents for its modification with succinic anhydride, for its subsequent application as an reactive curing agent for epoxy resins (Fig. 6.14). They found that the solid LPCA could be used together with other liquid curing agents such as glycerol tris(succinate mono-ester) (GTA) or commercial hexahydrophthalic anhydride (HHPA) to cure epoxy resins (Qin et al. 2014). The combination based on LPCA and GTA or HHPA was adequate to adjust the viscosity of the resin systems. This study demonstrates that partially depolymerized lignin can serve as a raw material in the preparation of the curing agent and be used for epoxy applications (Qin et al. 2014).

6.7 Mechanical and Dynamic-Mechanical Properties of the Cross-Linkable Bio and Mineral Filler-Based Polymer Composites

There are many studies that confirm the positive influence of the modified cross-linkable bio and mineral fillers on the mechanical and dynamic-mechanical properties of the polymer-based composites (Brzić et al. 2016). This section focuses on a

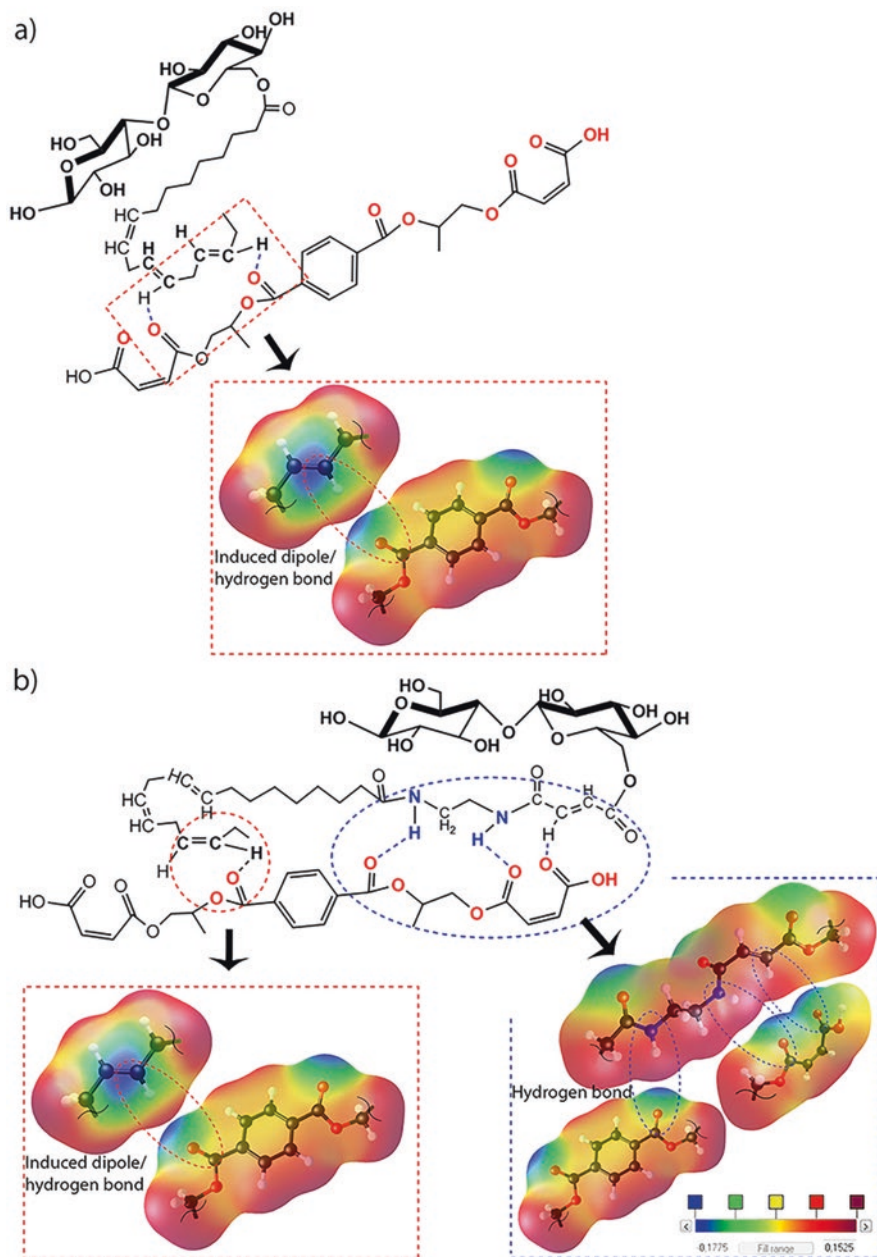


Fig. 6.13 Schematic illustration of the possible intermolecular interaction between UPR and m-NC particles. Reproduced with permission from Rusmirović et al. (2018c)

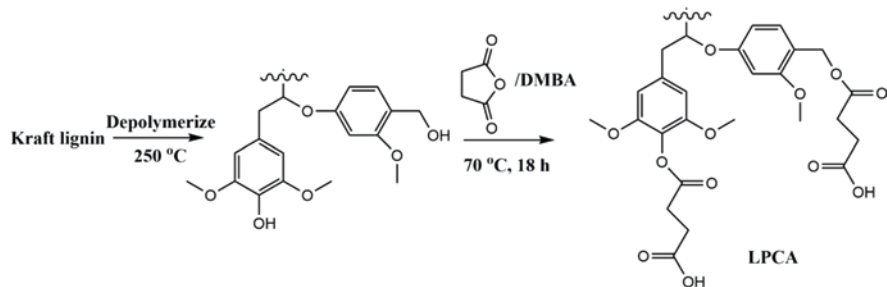


Fig. 6.14 Schematic preparation of partially depolymerized lignin (PDL) and lignin polycarboxylic acid (LPCA) from kraft lignin. Reproduced with permission from Qin et al. (2014). DMBA: dimethylbenzylamine and LPCA: lignin-derived polycarboxylic acids

review of the literature based on the methods of chemical modification having the best potential to improve the mechanical and dynamic mechanical properties of polymer composites.

Rusmirović et al. (2016) investigated the mechanical properties of the UPR based nanocomposites containing SiO₂ NPs (trade name AEROSIL® 380) modified using vinyl (V) and methacryloylsilane (MAS) as coupling agents, and LOFA. Two types of UPR were synthesized from polyethylene terephthalate (PET) wastes: UPR1 *via* classic method and UPR2 *via* azeotropic removal of ethylene glycol (Rusmirović et al. 2016). They found that the chemical modification of SiO₂ NPs prevents the formation of the aggregates into the polymer matrix (Rusmirović et al. 2016). An increase relative in σ_{\max} values were also observed: 147, 100 and 129% (UPR1) and 95, 74 and 81% (UPR2) for V, MAS and LOFA, respectively, containing 1 wt.% filler of the modified SiO₂ NPs as compared to pure analogue UPR resins (Rusmirović et al. 2016). The highest σ_{\max} and ϵ_b values were recorded for composite materials compared to pure crosslinked UPR1. These results may be associated with TMEVS configuration. The side chains with 1,2-dimethoxyethyl groups are short and oriented so that they cannot cause steric hindrance and hide active sites on the surface of modified SiO₂ NPs (Rusmirović et al. 2016).

Kanimozhi et al. (2014) evaluated the effect of reinforcement of rice husk ashes functionalized with vinyl silane contained into unsaturated polyester composites. They confirmed that the reinforced composites exhibited higher thermal and mechanical properties than pure UPR. The APTMS-BD and TMSPM modifiers managed to occupy a twisted conformation, due to the flexibility of the unsaturated fatty acid residue, thus resulting in the interaction between the functional groups of the surface by forming a closed structure which prevented the availability of active vinyl sites.

Drah et al. (2019) demonstrated that c-Al₂O₃ and Fe@Al₂O₃ increased the values of mechanical properties in terms of σ_{\max} , ϵ_b , E and Vickers hardness (VH) for composite UPR matrices containing up to 1.0 wt.% of fillers compared to the pure matrix. Drah et al. (2019) also observed the appearance of agglomerates at higher filler contents (> 1.0 wt.%), which led to the loss of mechanical properties. These

authors also reported that the surface modification of the fillers did not significantly improve the σ_{\max} values between them (Drah et al. 2019). This fact is generally due to the steric/repulsion interactions which disables the effective approach of the reactive species of the fillers. This phenomenon can be overcome with the introduction of BD into the APTMS modified alumina structure since the appearance of innumerable ethylenic bonds in a flexible BD structure suitable for efficient participation in crosslinking reactions (Rusmirović et al. 2017a). This suggests that covalent bonds created between double bonds BD and UPR resin provide a transfer of load from the polymer matrix to the filler particles (Muthu and Dendere 2014).

Rusmirović et al. (2018c) also evaluated the mechanical properties of the modified nanocellulose composites containing FA as a plasticizer and MA/EDA as crosslinking agents. As expected, the incorporation of FA increased the ϵ values for the composite systems compared to the pure UPR matrix. This can be explained due to the introduction of soft and flexible segments of oleic acid and sunflower oil fatty acids, which can exert an appropriate plasticizing effect by dipole/induced dipole interactions. In contrast, the incorporation of MA/EDA caused a greater increase in σ_{\max} values.

6.8 Conclusions and Remarks

The global industrial and technological growth demands the development of sophisticated materials with improved mechanical, rheological and thermal properties. The proper combination of two types of materials with different physical-mechanical properties in a composite structure can be a promising technique to meet excessive engineering demands. Hybrid polymer compounds reinforced with bio or inorganic fillers represent the new generation of lightweight and mechanically strong materials that can be applied in advanced industries such as aerospace, automotive, biomedical, construction, among others. Homogeneous dispersion and the achievement of chemical and physical interactions between the fillers and polymer chains stand out as one of the most important parameters in the design of the composites. Terminal-free groups on the commonly used filler surface, such as the hydroxyl groups on the surface of silica, alumina, cellulose and lignin, create hydrogen bonds between the filler particles to a greater extent, and with the electronegative polymer atoms to a lesser extent. This interconnection of filler particles causes the agglomeration and alteration of the mechanical properties when the filler contents exceed the optimal limits. The use of the filler's surface groups for the chemical reaction with molecules containing cross-linkable reactive moieties increases their influence on the mechanical and dynamic-mechanical properties of the polymers. The development of a new type of modified cross-linkable bio and inorganic fillers with reactive surface groups offers new possibilities for the design of functional hybrid materials with unique physicochemical properties. In addition, the use of bio-renewable sources as modifiers, reinforcements and raw material to produce polymer matrices gives new values to the final products respecting the principles of the circular and green economy.

Acknowledgments This research is financed by the Ministry of Education, Science and Technological Development of the Republic of Serbia as a part of the project OI 172057 and TR34033 and III45019.

Conflicts of Interest The authors declare no conflict of interest.

References

- Abdelmouleh, M., Boufi, S., Belgacem, M. N., Dufresne, A., & Gandini, A. (2005). Modification of cellulose fibers with functionalized silanes: Effect of the fiber treatment on the mechanical performances of cellulose-thermoset composites. *Journal of Applied Polymer Science*, 98(3), 974–984. <https://doi.org/10.1002/app.22133>.
- Abenojar, J., Tutor, J., Ballesteros, Y., del Real, J. C., & Martínez, M. A. (2017). Erosion-wear, mechanical and thermal properties of silica filled epoxy nanocomposites. *Composites. Part B, Engineering*, 120, 42–53. <https://doi.org/10.1016/j.compositesb.2017.03.047>.
- Akpan, E. I., Shen, X., Wetzel, B., & Friedrich, K. (2019). Design and synthesis of polymer nanocomposites. In K. Pielichowski & T. M. Majka (Eds.), *Polymer composites with functionalized nanoparticles: Synthesis, properties, and applications* (pp. 47–83). Pp: Elsevier. <https://doi.org/10.1016/b978-0-12-814064-2.00002-0>.
- Almasi, H., Ghanbarzadeh, B., Dehghannya, J., Entezami, A. A., & Asl, A. K. (2015). Novel nanocomposites based on fatty acid modified cellulose nanofibers/poly(lactic acid): Morphological and physical properties. *Food Packaging and Shelf Life*, 5, 21–31. <https://doi.org/10.1016/j.fpsl.2015.04.003>.
- Bagherpour, S. (2012). Fibre reinforced polyester composites. In H. Saleh (Ed.), *Polyester* (pp. 135–166). Pp: InTech. <https://doi.org/10.5772/48697>.
- Bagwe, R. P., Hilliard, L. R., & Tan, W. (2006). Surface modification of silica nanoparticles to reduce aggregation and nonspecific binding. *Langmuir*, 22(9), 4357–4362. <https://doi.org/10.1021/la052797j>.
- Bayer, J., Granda, L. A., Méndez, J. A., Pèlach, M. A., Vilaseca, F., & Mutjé, P. (2016). Cellulose polymer composites (WPC). In M. Fan and F. Fu (Eds.), *Advanced High Strength Nature Fibre Composites in Construction* (pp. 115–139). ISBN: 978-0-08-100411-1: Woodhead Publishing. <https://doi.org/10.1016/b978-0-08-100411-1.00005-4>.
- Bracone, M., Merino, D., González, J., Alvarez, V. A., & Gutiérrez, T. J. (2016). Chapter 6. Nanopackaging from natural fillers and biopolymers for the development of active and intelligent films. In S. Ikram & S. Ahmed (Eds.), *Natural polymers: Derivatives, blends and composites* (pp. 119–155). New York.. EE.UU. ISBN: 978-1-63485-831-1: Editorial Nova Science Publishers.
- Brzić, S., Bogosavljević, M., Ušćumlić, G., & Jelisavac, L. (2016). Effect of tris(2,3-epoxypropyl) isocyanurate on dynamic modulus of CTBN-based composite rocket propellant. *Scientific Technical Review*, 68(4), 18–27. <https://doi.org/10.5937/str1602018b>.
- Çakir, M., Simsek, R., & Çelik, A. A. (2015). Effect of surface modification of fumed-silica on mechanical properties of unsaturated polyester composites. *Asian J. Chem*, 27(11), 4120–41204.
- Cao, X., Dong, H., & Li, C. M. (2007). New nanocomposite materials reinforced with cellulose nanocrystals in waterborne polyurethane. *Biomacromolecules*, 8(3), 899–904. <https://doi.org/10.1021/bm0610368>.
- Çetin, N. S., Tingaut, P., Özmen, N., Henry, N., Harper, D., Dadmun, M., & Giles, S. (2009). Acetylation of cellulose nanowhiskers with vinyl acetate under moderate conditions. *Macromolecular Bioscience*, 9(10), 997–1003. <https://doi.org/10.1002/mabi.200900073>.
- Chuang, W., Geng-Sheng, J., Lei, P., Bao-lin, Z., Ke-Zhi, L., & Jun-long, W. (2018). Influences of surface modification of nano-silica by silane coupling agents on the thermal and frictional properties of cyanate ester resin. *Results Physics*, 9, 886–896. <https://doi.org/10.1016/j.rinp.2018.03.056>.

- Chung, D. D. L. (2017). Polymer-matrix composites: Structure and processing. In D. D. L. Chung (Ed.), *Carbon composites: Composites with carbon fibers, nanofibers and nanotubes* (pp. 161–217). Pp: Butterworth-Heinemann. <https://doi.org/10.1016/b978-0-12-804459-9.00003-8>.
- Dearmitt, C., & Rothon, R. (2014). Surface modifiers for use with particulate fillers. In S. Palsule (Ed.), *Polymers and polymeric composites: A reference series* (pp. 1–22). Berlin, Heidelberg: Springer. https://doi.org/10.1007/978-3-642-37179-0_8-2.
- Dittanet, P., Pearson, R. A., & Kongkachuichay, P. (2017). Thermo-mechanical behaviors and moisture absorption of silica nanoparticle reinforcement in epoxy resins. *International Journal of Adhesion and Adhesives*, 78, 74–82. <https://doi.org/10.1016/j.ijadhadh.2017.06.006>.
- Drah, A., Kovačević, T., Rusmirović, J., Tomić, N., Brzić, S., Bogosavljačić, M., & Marinković, A. (2019). Effect of surface activation of alumina particles on the performances of thermosetting-based composite materials. *Journal of Composite Materials*, 53(19). <https://doi.org/10.1177/0021998319839133>.
- Drah, A., Tomić, N. Z., Kovačević, T., Djokić, V., Tomić, M., Heinemann, R. J., Marinković, A. (2020) Structurally and surface-modified alumina particles as a reinforcement in polyester-based composites with an improved toughness. *Mechanics of Composite Materials*, 56, 249–260. <https://doi.org/10.1007/s11029-020-09877-3>.
- Dufresne, A. (2010). Processing of polymer nanocomposites reinforced with polysaccharide nanocrystals. *Molecules*, 15(6), 4111–4128. <https://doi.org/10.3390/molecules15064111>.
- Dufresne, A. (2012). Chemical modification of nanocellulose. In: Nanocellulose: From nature to high performance tailored materials. De Gruyter. Pp. 147–192. <https://doi.org/10.1515/9783110254600.147>.
- Dufresne, A. (2013). Nanocellulose: A new ageless bionanomaterial. *Materials Today*, 16(6), 220–227. <https://doi.org/10.1016/j.mattod.2013.06.004>.
- Durán, N., Lemes, A., Durán, M., Freer, J., & Baeza, J. (2011). A minireview of cellulose nanocrystals and its potential integration as co-products in biethanol production. *Journal of the Chilean Chemical Society*, 56(2), 672–677. <https://doi.org/10.4067/S0717-97072011000200011>.
- Durđević, V., Kovačević, T., Rusmirović, J., Božić, A., Tomić, N., Nešić, J., & Brzić, S. (2017). Application of the waste polymeric material from processing of optical lenses as a reinforcement in unsaturated polyester based on waste PET. 4th Sci. Conference Politeh, 2017, 29–34.
- Faruk, O., & Sain, M. (2016). Lignin in polymer composites, William Andrew, Pp. 350. <https://doi.org/10.1016/c2014-0-01101-x>.
- Gun'ko, V. M. (2019). Polymer composites with functionalized silica. In K. Pielichowski & T. M. Majka (Eds.), *Polymer composites with functionalized nanoparticles: Synthesis, properties, and applications* (pp. 119–148). Elsevier. <https://doi.org/10.1016/b978-0-12-814064-2.00004-4>.
- Gutiérrez, T. J., Alvarez, V. A., & V. A. (2017a). Cellulosic materials as natural fillers in starch-containing matrix-based films: A review. *Polymer Bulletin*, 74(6), 2401–2430. <https://doi.org/10.1007/s00289-016-1814-0>.
- Gutiérrez, T. J., González Seligra, P., Medina Jaramillo, C., Famá, L., & Goyanes, S. (2017b). Chapter 14. Effect of filler properties on the antioxidant response of thermoplastic starch composites. In V. K. Thakur, M. K. Thakur, & M. R. Kessler (Eds.), *Handbook of composites from renewable materials* (pp. 337–370). WILEY-Scrivener Publisher. EE.UU. ISBN: 978-1-119-22362-7. <https://doi.org/10.1002/9781119441632.ch14>.
- Gutiérrez, T. J., Toro-Márquez, L. A., Merino, D., & Mendieta, J. R. (2019). Hydrogen-bonding interactions and compostability of bionanocomposite films prepared from corn starch and nano-fillers with and without added Jamaica flower extract. *Food Hydrocolloids*, 89, 283–293. <https://doi.org/10.1016/j.foodhyd.2018.10.058>.
- Herniou--Julien, C., Mendieta, J. R., & Gutiérrez, T. J. (2019). Characterization of biodegradable/non-compostable films made from cellulose acetate/corn starch blends processed under reactive extrusion conditions. *Food Hydrocolloids*, 89, 67–79. <https://doi.org/10.1016/j.foodhyd.2018.10.024>.

- Hosseini, S. A., Lin, L., & Ko, F. (2017). Investigation of the mechanical properties of lignin nanofibrous structures using statistical modeling. *Textile Research Journal*, 88(17), 1943–1953. <https://doi.org/10.1177/0040517517715080>.
- Jeon, C. W., Park, S., Bang, J.-H., Chae, S., Song, K., & Lee, S.-W. (2018). Nonpolar surface modification using fatty acids and its effect on calcite from mineral carbonation of desulfurized gypsum. *Coatings*, 8(1), 43. <https://doi.org/10.3390/coatings8010043>.
- Jin, B., Zhang, W., Sun, G., & Gu, H.-B. (2007). Fabrication and characterization of ethylenevinyl acetate copolymer Al₂O₃ nanocomposites. *Journal of Ceramic Processing Research*, 8(5), 336–340. Available in: http://jcpr.kbs-lab.co.kr/file/jcpr_vol.8_2007/jcpr8-5/vol.8,no.5,pp.336~340_2007.pdf.
- Junior de Menezes, A., Siqueira, G., Curvelo, A. A. S., & Dufresne, A. (2009). Extrusion and characterization of functionalized cellulose whiskers reinforced polyethylene nanocomposites. *Polymer*, 50(19), 4552–4563. <https://doi.org/10.1016/j.polymer.2009.07.038>.
- Kango, S., Kalia, S., Celli, A., Njuguna, J., Habibi, Y., & Kumar, R. (2013). Surface modification of inorganic nanoparticles for development of organic-inorganic nanocomposites-A review. *Progress in Polymer Science*, 38(8), 1232–1261. <https://doi.org/10.1016/j.progpolymsci.2013.02.003>.
- Kanimozhi, K., Prabunathan, P., Selvaraj, V., & Alagar, M. (2014). Vinyl silane-functionalized rice husk ash-reinforced unsaturated polyester nanocomposites. *RSC Advances*, 4(35), 18157–18163. <https://doi.org/10.1039/c4ra01125b>.
- Kargarzadeh, H., Sheltami, R. M., Ahmad, I., Abdullah, I., & Dufresne, A. (2015). Cellulose nanocrystal: A promising toughening agent for unsaturated polyester nanocomposite. *Polymer*, 56, 346–357. <https://doi.org/10.1016/j.polymer.2014.11.054>.
- Khalil, H. P. S. A., Dungani, R., Hossain, M. S., Suraya, N. L. M., Aprilia, S., Astimar, A. A., Hayawin, Z. N., & Davoudpour, Y. (2015). Mechanical properties of oil palm biocomposites enhanced with micro to nanobiofillers. In M. Misra, J. K. Pandey, & A. K. Mohanty (Eds.), *Biocomposites: Design and mechanical performance* (pp. 401–435). Woodhead Publishing. <https://doi.org/10.1016/b978-1-78242-373-7.00026-3>.
- Kovačević, T., Drah, A., Božić, A., Stamenović, M., Rusmirović, J., Tomić, N., Alivojvodić, V., & Marinković, A. (2018). The surface modification of alumina particles for its application in unsaturated polyester resins. 26th Int. Conf. Ecol. Truth Environ. Res. 338–342.
- Kovačević, T., Rusmirović, J., Tomić, N., Marinović-Cincović, M., Kamberović, Ž., Tomić, M., & Marinković, A. (2017). New composites based on waste PET and non-metallic fraction from waste printed circuit boards: Mechanical and thermal properties. *Composites. Part B, Engineering*, 127, 1–14. <https://doi.org/10.1016/j.compositesb.2017.06.020>.
- Kovačević, T., Rusmirović, J., Tomić, N., Mladenović, G., Milošević, M., Mitrović, N., & Marinković, A. (2019). Effects of oxidized/treated non-metallic fillers obtained from waste printed circuit boards on mechanical properties and shrinkage of unsaturated polyester-based composites. *Polymer Composites*, 40(3), 1170–1186. <https://doi.org/10.1002/pc.24827>.
- Kovačević, T. M. (2018). The influence of modified micro-particles from nonmetallic fraction of waste printed circuit boards on mechanical and thermal properties of polyester resin synthesized from waste poly(ethylene terephthalate). University of Belgrade; 160.
- Lin, J., Zhong, B., Jia, Z., Hu, D., Ding, Y., Luo, Y., & Demin, Y. (2017). In-situ fabrication of halloysite nanotubes/silica nano hybrid and its application in unsaturated polyester resin. *Applied Surface Science*, 407, 130–136. <https://doi.org/10.1016/j.apsusc.2017.02.149>.
- Mallakpour, S., & Dinari, M. (2013). Investigating the nanostructure and thermal properties of chiral poly(amide-imide)/Al₂O₃ compatibilized with 3-aminopropyltriethoxysilane. *Materials Research Bulletin*, 48(10), 3865–3872. <https://doi.org/10.1016/j.materresbull.2013.05.095>.
- Mallakpour, S., & Khadem, E. (2014). Recent development in the synthesis of polymer nanocomposites based on nano-alumina. *Progress in Polymer Science*, 51, 74–93. <https://doi.org/10.1016/j.progpolymsci.2015.07.004>.
- Malutan, T., Nicu, R., & Popa, V. I. (2008). Lignin modification by epoxidation. *BioResources*, 3(4), 1371–1376. Available in: https://ojs.cnr.ncsu.edu/index.php/biores/article/view/biores_03_4_1371_malutan_np_lignin_mod_epoxidation/289.

- Merino, D., Gutiérrez, T. J., & Alvarez, V. A. (2019). Structural and thermal properties of agricultural mulch films based on native and oxidized corn starch nanocomposites. *Starch-Stärke*, 71(7–8), 1800341. <https://doi.org/10.1002/star.201800341>.
- Merino, D., Gutiérrez, T. J., Mansilla, A. Y., Casalagué, C., & Alvarez, V. A. (2018). Critical evaluation of starch-based antibacterial nanocomposites as agricultural mulch films: Study on their interactions with water and light. *ACS Sustainable Chemistry & Engineering*, 6(11), 15662–15672. <https://doi.org/10.1021/acssuschemeng.8b04162>.
- Miranda-Hernández, J. G., Moreno-Guerrero, S., Soto-Guzmán, A. B., & Rocha-Rangel, E. (2006). Processing research production and characterization of. *Al₂O₃-Cu composite materials.*, 7(4), 311–314.
- Mohammad, N. A. B. (2007). Synthesis, characterization and properties of of the new unsaturated polyester resins for composite applications, 39. Available in: http://eprints.usm.my/29361/1/Synthesis_characterization_and_properties_of_the_new_unsaturated_polyester_resins_for_composite_applications.pdf
- Moon, R. J., Martini, A., Nairn, J., Simonsen, J., & Youngblood, J. (2011). Cellulose nanomaterials review: Structure, properties and nanocomposites. *Chemical Society Reviews*, 40(7), 3941–3994. <https://doi.org/10.1039/c0cs00108b>.
- Muthu, J., & Dendere, C. (2014). Functionalized multiwall carbon nanotubes strengthened GRP hybrid composites: Improved properties with optimum fiber content. *Composites. Part B, Engineering*, 67, 84–94. <https://doi.org/10.1016/j.compositesb.2014.06.012>.
- Nordström, J., Matic, A., Sun, J., Forsyth, M., & MacFarlane, D. R. (2010). Aggregation, ageing and transport properties of surface modified fumed silica dispersions. *Soft Matter*, 6(10), 2293. <https://doi.org/10.1039/b921488g>.
- Oğuz, O., Monfared Zanjani, J. S., Soytaş, S. H., & Menceloğlu, Y. Z. (2019). Specific interactions and self-organization in polymer/functionalized nanoparticle systems. In K. Pielichowski & T. M. Majka (Eds.), *Polymer composites with functionalized nanoparticles: Synthesis, properties, and applications* (pp. 85–117). Elsevier. <https://doi.org/10.1016/b978-0-12-814064-2.00003-2>.
- Pasquini, D., Teixeira, E de M, Curvelo, AA da S, Belgacem, M. N., & Dufresne, A. (2010). Extraction of cellulose whiskers from cassava bagasse and their applications as reinforcing agent in natural rubber. *Industrial Crops and Products*, 32(3), 486–490. <https://doi.org/10.1016/j.indcrop.2010.06.022>.
- Prieur, B., Meub, M., Wittemann, M., Klein, R., Bellayer, S., Fontaine, G., & Bourbigot, B. (2016). Phosphorylation of lignin to flame retard acrylonitrile butadiene styrene (ABS). *Polymer Degradation and Stability*, 127, 32–43. <https://doi.org/10.1016/j.polymdegradstab.2016.01.015>.
- Popović A., Rusmirović J.D., Veličković Z., Radovanović Ž., Ristić M., Pavlović V., Marinković A., (2020). Novel amino-functionalized lignin microspheres: High performance biosorbent with enhanced capacity for heavy metal ion removal. *International Journal of Biological Macromolecules*, 156, 1160–1173. <https://doi.org/10.1016/j.ijbiomac.2019.11.152>
- Pu, Y., Zhang, J., Elder, T., Deng, Y., Gatenholm, P., & Ragauskas, A. J. (2007). Investigation into nanocellulosics versus acacia reinforced acrylic films. *Composites. Part B, Engineering*, 38(3), 360–366. <https://doi.org/10.1016/j.compositesb.2006.07.008>.
- Qin, J., Wolcott, M., & Zhang, J. (2014). Use of polycarboxylic acid derived from partially depolymerized lignin as a curing agent for epoxy application. *ACS Sustainable Chemistry & Engineering*, 2(2), 188–193. <https://doi.org/10.1021/sc400227v>.
- Radoman, T., Terzić, N., Spasojević, P., Džunuzović, J. V., Marinković, A., Jeremić, K., & Džunuzović, E. S. (2015a). Synthesis and characterization of the surface modified titanium dioxide/epoxy nanocomposites. *Advance Technology*, 4(1), 7–15. <https://doi.org/10.5937/savteh1501007r>.
- Radoman, T. S., Trifković, K., Palija, T., Marinković, A. D., Bugarski, B., & Džunuzović, E. S. (2015b). Effect of surface modified TiO₂ nanoparticles on thermal, barrier and mechanical properties of long oil alkyd resin-based coatings. *Express Polym. Letters*, 9(10), 916–931. <https://doi.org/10.3144/expresspolymlett.2015.83>.

- Rančić, M., Rusmirović, J., Popović, I., & Marinković, A. (2015). Isolation and chemical modification of nanocellulose nanocrystals for reinforcement of nanocomposites. *Wood Technol. Prod. Des.* 2nd Int. Sci. Conf. Ohrid, Macedonia; 327–355.
- Ranjan, R. (2008). Surface modification of silica nanoparticles. The University of Akron, 150.
- Roohani, M., Habibi, Y., Belgacem, N. M., Ebrahim, G., Karimi, A. N., & Dufresne, A. (2008). Cellulose whiskers reinforced polyvinyl alcohol copolymers nanocomposites. *European Polymer Journal*, 44(8), 2489–2498. <https://doi.org/10.1016/j.eurpolymj.2008.05.024>.
- Rothon, R. N. (2002). Particulate fillers for polymers. Rapra Technology Limited; 12(9):161. Available in: <http://www.polymerjournals.com/pdfdownload/844670.pdf>
- Rusmirović, J., Božić, A., Stamenović, M., Spasojević, P., Rančić, M., Stojiljković, I., & Marinković, A. (2016). Alkyd nanocomposite coatings based on waste PET glycolyzates and modified silica nanoparticles. *Zašt. Material*, 57(1), 47–54. <https://doi.org/10.5937/zasmat1601047r>.
- Rusmirović, J., Daničić, D., Kovačević, T., Bogosavljević, M., Brzić, S., Marinković, A., & Stevanović, T. (2018a). Phosphorylated kraft lignin based flame retardant: Efficient method for improvement of lignin flame retardancy and mechanical action in polyester. 8th Int. Sci. Conf. Defensive Technol. 538–543.
- Rusmirović, J. D. (2016). Dynamic-mechanical and thermal properties of composites based on unsaturated polyester resins and modified silicon-dioxide and cellulose nanoparticles. University of Belgrade; 186.
- Rusmirović, J. D., Ivanović, J. Z., Pavlović, V. B., Rakić, V. M., Rančić, M. P., Đokić, V., & Marinković, A. (2017a). Novel modified nanocellulose applicable as reinforcement in high-performance nanocomposites. *Carbohydrate Polymers*, 164, 64–74. <https://doi.org/10.1016/j.carbpol.2017.01.086>.
- Rusmirović, J. D., Radoman, T., Džunuzović, E. S., Džunuzović, J. V., Markovski, J., Spasojević, P., & Marinković, A. (2017b). Effect of the modified silica nanofiller on the mechanical properties of unsaturated polyester resins based on recycled polyethylene terephthalate. *Polymer Composites*, 38(3), 538–554. <https://doi.org/10.1002/pc.23613>.
- Rusmirović, J. D., Rančić, M. P., & Marinković, A. D. (2018b). Processing and characterization of modified nanocellulose/polyester composites. In T. Stevanović (Ed.), *Chemistry of Lignocellulosics: Current Trends* (pp. 167–213). Taylor & Francis Group, CRC Press. <https://doi.org/10.1201/b20936-8>.
- Rusmirović, J. D., Rančić, M. P., Pavlović, V. B., Rakić, V. M., Stevanović, S., Djonlagić, J., & Marinković, A. (2018c). Cross-linkable modified nanocellulose/polyester resin-based composites: Effect of unsaturated fatty acid nanocellulose modification on material performances. *Macromolecular Materials and Engineering*, 303(8), 1700648. <https://doi.org/10.1002/mame.201700648>.
- Rusmirović, J. D., Trifković, K. T., Bugarski, B., Pavlović, V. B., Džunuzović, J., Tomić, M., & Marinković, A. (2016). High performances unsaturated polyester based nanocomposites: Effect of vinyl modified nanosilica on mechanical properties. *Express Polym. Letters*, 10(2), 139–159. <https://doi.org/10.3144/expresspolymlett.2016.14>.
- Rusmirović, J. D., Lukić, V., Kovačević, T., Bogosavljević, M., Brzić, S., Marinković, A., & Stevanović, T. (2019) Fireproof phosphorylated kraft lignin/polyester based composites: Green material for rocket propellant thermal protection systems. *Scientific and Technical Review*, 69(1), 16–22. <https://doi.org/10.5937/str1901016r>.
- Schorr, D., Niokhor, P., & Stevanović, T. (2014). Evaluation of industrial lignins for biocomposites production. *Industrial Crops and Products*, 52, 65–73. <https://doi.org/10.1016/j.indcrop.2013.10.014>.
- Scofield, J. D. (2003). A novel coupling agent technology. *Polymers and Polymer Composites*, 11(2), 67–75. <https://doi.org/10.1177/096739110301100201>.
- Soleimani, E., & Zamani, N. (2017). Surface modification of alumina nanoparticles: A dispersion study in organic media. *Acta Chimica Slovenica*, 64(3), 644–653. <https://doi.org/10.17344/acsi.2017.3459>.
- Spange, S. (2000). Silica surface modification by cationic polymerization and carbenium intermediates. *Progress in Polymer Science*, 25(6), 781–849. [https://doi.org/10.1016/S0079-6700\(00\)00014-9](https://doi.org/10.1016/S0079-6700(00)00014-9).

- Tasić, A., Rusmirović, J. D., Nikolić, J., Božić, A., Pavlović, V., Marinković, A., & Uskoković, P. (2016). Effect of the vinyl modification of multi-walled carbon nanotubes on the performances of waste poly(ethylene terephthalate)-based nanocomposites. *Journal of Composite Materials*, 51(4), 1–15. <https://doi.org/10.1177/0021998316648757>.
- Thakur, V. K., Thakur, M. K., Raghavan, P., & Kessler, M. R. (2014). Progress in green polymer composites from lignin for multifunctional applications: A review. *ACS Sustainable Chemistry & Engineering*, 2(5), 1072–1092. <https://doi.org/10.1021/sc500087z>.
- Tomić, M. D., Dunjić, B., Likić, V., Bajat, J., Rogan, J., & Djonlagić, J. (2014). The use of nano-clay in preparation of epoxy anticorrosive coatings. *Progress in Organic Coatings*, 77(2), 518–527. <https://doi.org/10.1016/j.porgcoat.2013.11.017>.
- Toro-Márquez, L. A., Merino, D., & Gutiérrez, T. J. (2018). Bionanocomposite films prepared from corn starch with and without nanopackaged Jamaica (*Hibiscus sabdariffa*) flower extract. *Food and Bioprocess Technology*, 11(11), 1955–1973. <https://doi.org/10.1007/s11947-018-2160-z>.
- Xie, Y., Hill, C. A. S., Xiao, Z., Militz, H., & Mai, C. (2010). Silane coupling agents used for natural fiber/polymer composites: A review. *Composites. Part A, Applied Science and Manufacturing*, 41(7), 806–819. <https://doi.org/10.1016/j.compositesa.2010.03.005>.
- Xu, M., Cao, Y., & Gao, S. (2014). Surface modification of nano-silica with silane coupling agent. *Key Engineering Materials*, 636, 23–27. <https://doi.org/10.4028/www.scientific.net/kem.636.23>.
- Yue, L., Maiorana, A., Khelifa, F., Patel, A., Raquez, J. M., Bonnaud, L., Gross, R., Dubois, P., & Manas-Zloczower, I. (2018). Surface-modified cellulose nanocrystals for biobased epoxy nanocomposites. *Polymer*, 134, 155–162. <https://doi.org/10.1016/j.polymer.2017.11.051>.
- Zainuddin, S. Y. Z., Ahmad, I., Kargarzadeh, H., Abdullah, I., & Dufresne, A. (2013). Potential of using multiscale kenaf fibers as reinforcing filler in cassava starch-kenaf biocomposites. *Carbohydrate Polymers*, 92(2), 2299–2305. <https://doi.org/10.1016/j.carbpol.2012.11.106>.
- Zunjarrao, S. C., & Singh, R. P. (2006). Characterization of the fracture behavior of epoxy reinforced with nanometer and micrometer sized aluminum particles. *Composites Science and Technology*, 66(13), 2296–2305. <https://doi.org/10.1016/j.compscitech.2005.12.001>.

Chapter 7

Functional Crosslinked Hydrogels



Saminu M. Magami

Abstract In this chapter, the science, technology and applications of functional hydrogels are considered. A brief discussion on fundamental network properties, such as fractal dimensions, network relaxation and stiffness, are given. A large number of synthesis approaches for the manufacture of functional hydrogels are discussed here. The key synthesis approaches which underpin a series of hydrogel variants and their applications are also discussed. An overview of the composition, structure, functionality, characterization and application of a range of functional hydrogels is offered in this chapter, as well as relevant rheological approaches in the synthesis and characterization of these materials are discussed here, paying particular attention to the gelation, sol-gel transitions and multiwave mechanical spectroscopy.

Keywords Applications · Characterization · Critical gel · Crosslinking

7.1 Introduction

The behavior of functional hydrogels arises from their (micro) structure, which is a three-dimensional (3D) network, created by the chemical and physical crosslinking of monomers/polymers. There are several applications of functional hydrogels, and therefore, any information that can lead to (or promote) an understanding of its fundamental structure, synthesis routes and characterization pathways is essential. Functional hydrogels are often classified from the extent and type of crosslinking, the mechanical properties, the network characteristics, the point of view of their constituent materials and the presence of entanglements and other physical forces. These essential factors control the micro- and macro-behavior of functional

S. M. Magami (✉)
Newton-le-Willows, UK

Department of Chemistry, Maitama Sule University, Kano, Nigeria

hydrogels. The structure of functional hydrogels has defined characteristics. This can also be dynamic, depending on the conditions that the material is subject. As a basis for the application of the hydrogel, essential properties such as insolubility, optical clarity, rigidity/stiffness, stimuli responsiveness, swelling and viscoelasticity (tendency or resistance to deformation) are often considered and targeted during synthesis (Tomadoni et al. 2019). The swelling of the material is based on properties such as crosslinking, hydrophilicity and mesh size. The hydrophilicity of the hydrogel network arises due to the presence of hydrophilic functional groups such as amido, amino, carbonyl, carboxylic, hydroxyl, phosphonic and sulfonic functional groups.

7.2 Fundamentals of Hydrogel Structure

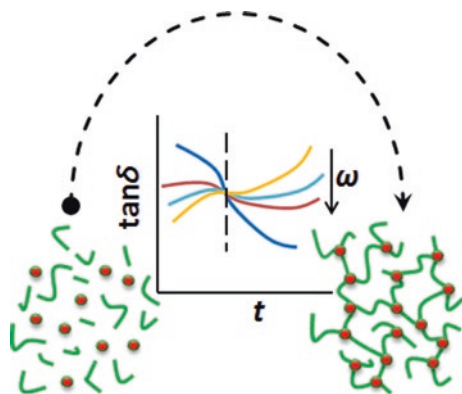
The structure of the hydrogel is an important property that defines its application. The structure can be made using hydrophilic or hydrophobic components. The hydrophilic nature of the selected materials used to fabricate the structure makes it possible for hydrogels to incorporate water (Laftah et al. 2011). A controlled use of hydrophobic components can thus be used in the manufacturing steps to tailor binding/incorporation of water into the hydrogel structure. The crosslinking of the materials contained in the hydrogel prevents its polymeric structure from dissolving. When such a material is placed in a fluid, swelling is observed, which can cause the final structural geometry to be much larger than the original size (Akhtar et al. 2016).

Water is the main component in a hydrogel, this allows it to perform several functions and interact with internal or external stimuli. The physical properties of the material depend on how water is retained on the surface and within the material. Water can exhibit different characteristics due to the existence of different states in the hydrogel. Thus, different melting points of water can be observed. Free water melts at 0 °C (Liu and Yao 2001). Secondary water melts at a lower temperature and bound water does not freeze. The relative amounts of water that are maintained in the various states can vary significantly as the swelling extent of the hydrogel structure varies (Quinn et al. 1988).

7.2.1 *The Critical Gel and the Gel Point*

The critical gel also called the incipient gel, is the material at the gel point. The gel point marks the transition point where the starting material changes from a fluid (often viscoelastic liquid) into a viscoelastic solid (Winter 1987). Thus, the gel point marks the beginning of the formation of crosslinked networks in the material, i.e. the gel point is an intermediate state between the liquid and solid states. This is also the critical point in the reaction of the material as it undergoes the phase transition. It is widely considered that at the gel point, the molecular weight (Mw) of the

Fig. 7.1 Illustration of the gel point of a hydrogel material, showing the transition from the liquid to the solid state. Reproduced with permission from Magami and Williams (2019a)



system begins to diverge (Magami and Williams 2018). Therefore, this provides a window through which the molecular flexibility of the formed network clusters can be observed and defined (Chiou et al. 1996). Figure 7.1 shows a rheological intersection point where the convergence and subsequent divergence of $\tan\delta$ is observed during the creation of typical hydrogel materials. This intersection point represents the rheological gel point of the material. The time (during creation or synthesis) corresponding to the intersection point is the gel time.

The critical state of the gel also marks the stage at which the mechanical properties of the hydrogel are formed. Thus, at this stage, the material is characterized by properties such as fractal dimensions, mesh size, relaxation exponent and stiffness (Magami and Williams 2019). The relaxation exponent describes the critical microstructure of the gel and provides an understanding of the dynamics of the macromolecular chains and crosslinks that are formed (or begin to be formed) at the gel point. This can be calculated using Eq. 7.1. The stiffness of the critical gel, given in Eq. 7.2, describes how ‘soft’ or ‘hard’, in viscoelastic representation, is the critical gel (Chiou et al. 1996). The fractal dimension of the critical gel, given in Eq. 7.3, describes how open/closed or branched the clusters of networks are formed. The value of the fractal dimensions ranges between one and three, which describes the types of sparse/open and dense network, respectively. Therefore, this defines the spatial distribution of macromolecules and crosslinks in the material (Muthukumar 1989).

$$\tan \delta = \tan(n\pi / 2) \quad (7.1)$$

$$G'(\omega) = ST(1-n)\cos(n\pi / 2)\omega^n \quad (7.2)$$

$$n = d(d+2-2D_f) / 2(d+2-D_f) \quad (7.3)$$

where: d is the space-dimension of the material, D_f is the fractal dimension, G' is storage modulus, n is the relaxation exponent, S provides the stiffness value, T is the gamma function and ω is the oscillation frequency. For hydrogels, the value of d is considered to be 3.

7.2.2 *Microstructure*

In addition to the micromechanical properties of the functional hydrogel, which defines the polymer backbone, the characteristics of the liquid component surrounding the network are also critical. The degree of linking up of the macromolecular chains in the hydrogel also defines their microstructure. A polymer network, in which both ends of the polymer chains are connected as crosslinks, with all the crosslinks connected to the polymer network, is an ideal end-linked polymer network and has the highest strength (Patel et al. 1992). The presence of defects in the polymer network, such as loops and dangling ends, reduces the strength of the gel and makes it softer.

The microstructure of the polymer backbone also influences the gel response in the application of a stress/force. The polymer chains are reorganized when a stress is applied, and by removing the stress, the polymer tends to return to its original form (Borzacchiello and Ambrosio 2009). The relaxation time depends on the crosslinking density/Mw/structure of the polymer matrix, as well as the viscosity of the liquid component present. However, not all hydrogels when deformed fully recover their original state. Despite this, the materials act as viscoelastic solids dissipating a certain amount of the energy (Llorente and Mark 1979).

The microstructure can also be described from the point of view of how the pores/clusters are interconnected in the hydrogel. The physical dimensions of the network clusters can dictate the opportunities or limitations that the hydrogel can possess when considered for different applications. Physical restrictions on the hydrogel microstructure can affect the distribution, migration and movement of incorporated molecules (Nair 2016). When spatial arrangements in the microstructure can hinder the subsequent loading of releasable molecules, studies have shown that the hydrogel microstructure can often be designed with a sacrificial component which can allow a defined microstructure. This sacrificial component can then be removed by processes such as targeted enzymatic degradation. The removal of the sacrificial material then improves the porosity of the microstructure and paves the way for the loading of desirable materials (Namba et al. 2009).

7.3 **Crosslinking in Functional Hydrogels**

The design of hydrogels can be achieved using chemical or physical crosslinking, or a combination of both approaches. In the first, chemical crosslinks are formed when the side functional groups of the polymer chains react with the functional groups in the crosslinking agent to form the strong covalent bonds (Hennink and van Nostrum 2012). This ensures the chemical stability and mechanical strength of the formed hydrogels. However, the physical crosslinking physical is the result from the association of adjacent polymer chains through relatively weak forces, such as hydrogen (H) bonds, van der Waals forces and physical entanglements or electrostatic

attractions (Singhal and Gupta 2016). The crosslinking in hydrogels may arise from formulations containing predominantly hydrophilic components or those containing a significant proportion of hydrophobic components.

Hydrogel materials can be assembled from predominantly hydrophobic starting materials such as hydrophobically modified chitosan (Cs) biopolymers (Valencia et al. 2019). When this is reacted with dodecyl groups, in the presence of a β -glycerophosphate disodium salt, a hydrogel material can be observed. Through this preparation procedure, it has been shown that the extents of the reactions and the properties of the crosslinked hydrogel, such as the size of the pores, could be tailored by a combination of hydrophilic and hydrophobic starting materials (Dashtimoghdam et al. 2014). This approach can also be used to create a balance of covalent and non-covalent forces that are required for specific gelation processes. In some cases, the starting material must be modified in order to adapt the hydrogel synthesis. For example, Cs is a very hydrophilic material. This hydrophilicity often needs to be modified using functionalization techniques, such as grafting the biopolymer with several side chains *via* Schiff-base reactions with salicylaldehyde or dodecyl aldehyde materials, followed by reductive amination procedures (Abdulganiyu et al. 2017). Figure 7.2 provides an illustration of a range of molecular interactions that are involved in the gelation of a Cs, hydrophobically modified Cs chains, β -glycerophosphate groups, in a thermoresponsive material. In this, the ionic forces can be seen at play, in addition to the chemical crosslinkers which are formed through functional group interactions.

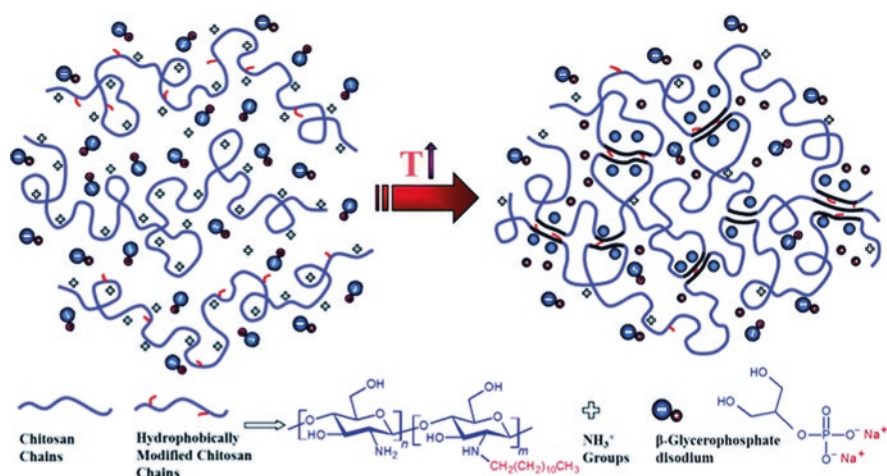


Fig. 7.2 Interactions involved in the formation of a chitosan-based hydrogel. Reproduced with permission from Dashtimoghdam et al. (2014)

7.3.1 Covalently Crosslinked Hydrogels

Hydrogels, when crosslinked by covalent bonds are obtained materials with improved mechanical properties. Due to the strength of covalent crosslinks, the relative movement of macromolecular chains is limited or impeded in the gels. In contrast, hydrogel networks formed from physical interactions are more dynamic. This is because molecular diffusion is very possible in physically crosslinked hydrogels. In the design of hydrogels with target mechanical strength, therefore, care must be taken to ensure that the flexibility, rigidity and stiffness of the final hydrogel is controlled. This can be done using a balanced or near-balanced stoichiometry of reactant species. In covalently crosslinked hydrogels, the growing macromolecular chains arising from the reaction of monomers, dimers, oligomers, polymers and crosslinkers are reacted covalently, which leads to the formation of an interconnected micro-molecular structure (Magami 2020). Figure 7.3 depicts covalent reactions, crosslinking and branching in a hydrogel formulated using monomeric acrylic acid (AA) and crosslinkable *N,N'*-methylenebisacrylamide. All these reactions/interactions lead to the creation of a 3D material.

7.3.2 Ionically Crosslinked Hydrogels

Functional hydrogels can be manufactured when metal cations are incorporated into suitable polymerization matrices (Koochi et al. 2011). This leads to the formation of 3D network clusters which arise due to the chelation of the macromolecular chains by the incorporated metal ion(s) (Higham et al. 2014). An important factor to be considered in the ionic crosslinking of hydrogels is the solubility of the chosen metal specie (Magami and Williams 2019b). Effective crosslinking in aqueous systems can be achieved using cationic species including Ca^{2+} , Mg^{2+} , Cu^{3+} and Fe^{3+} (Bai et al. 2011a). The reactivity of the starting material can be dictated by the type of metal salt chosen. A limitation often associated with the preparation of ionically crosslinked hydrogels is the solubility of some of the metal salts (Ma and Elisseff 2005). Metal oxides and metal hydroxides often have limited solubility in water-based hydrogels, due to the chemistry of their dissociation and their tendency to precipitate. Recent studies have shown that it is possible to calculate the solubility of metal hydroxides, oxide-hydroxides and oxides as a function of the equilibrium pH of the solutions, while considering the formation of several anionic and cationic species of metal ions (Scholz and Kahlert 2015). This can serve as a guide in the selection of starting metal-based compounds when formulating hydrogels. When the metal-based compound has undesirable hydrolysis tendencies, the Pechini process is often considered (Pechini 1967). This process allows the formation of metal-polymer bonds during *in situ* polymerization of suitable polymeric systems. With this technique, coatings, complexes, fibers, films and gels of transition metals and non-transition metals can be synthesized (Dimesso 2018).

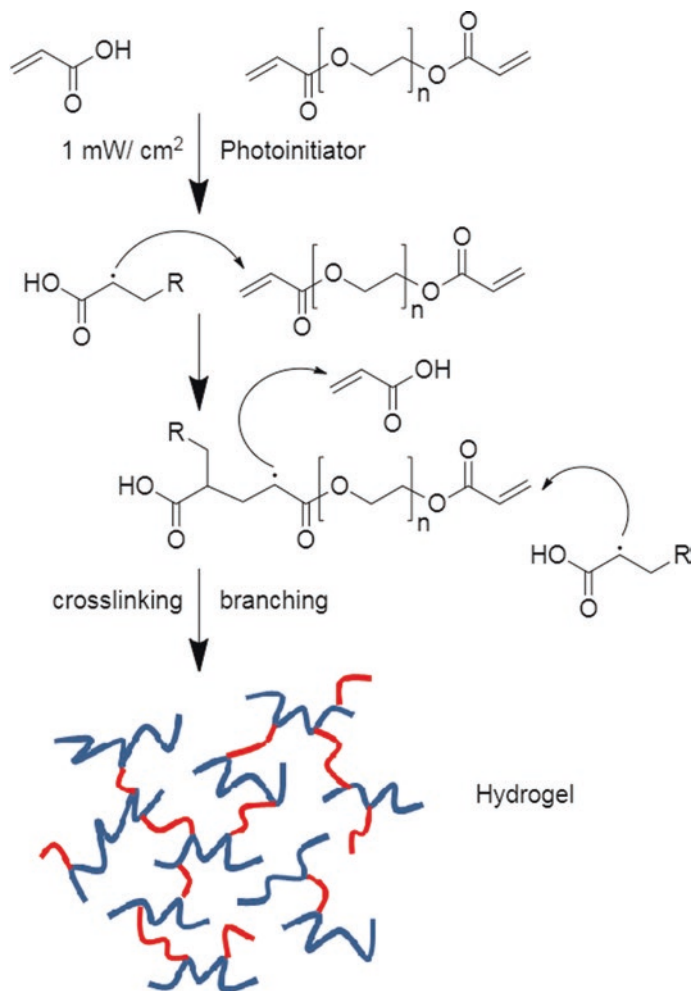


Fig. 7.3 Reactions involved during the polymerization and crosslinking reaction between AA and *N,N'*-methylenebisacrylamide. Reproduced with permission from Magami and Williams (2019a)

7.3.3 Entanglement in Hydrogels

Hydrogel networks can be formed through the physical entanglement of macromolecular chains. The entanglement in polymers and gels is often described in a too simplified manner, because the dynamics of entangled polymers require an approach where the macromolecular movement and relaxation of chains must be obtained in real space at different length and time scales (Abadi et al. 2018). One way to differentiate entangled bonds in hydrogels from covalently maintained networks is the

stress relaxation in the former. Stress relaxation can occur in entangled hydrogels due to relatively weaker forces holding the network together. When the material is strained, the generated stress is dissipated over time, i.e. the stress relaxation in entangled hydrogels is produced through a reptation mechanism, where a strain applied causes macromolecular chains to diffuse and glide pass each other in ‘tubes’ created by neighboring chains (Wyss 2016).

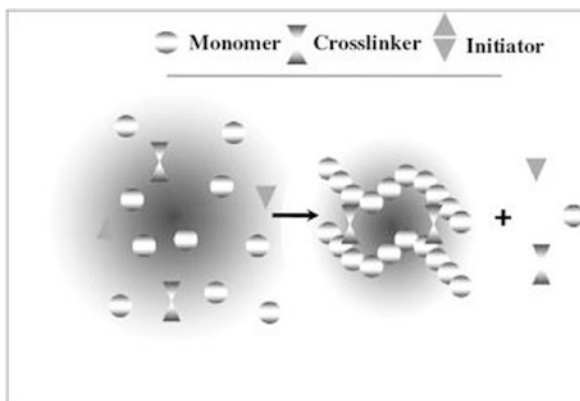
The entanglement in hydrogels can offer the advantage of producing materials *in situ*. In stimulus-sensitive hydrogels, in typical biomedical applications, entanglement chains can form as a response to changes in the environment, such as temperature (Zarrintaj et al. 2019). Entangled hydrogels can offer ease of degradation. This may be particularly important for *in vivo* applications where subsequent biodegradability is an essential characteristic/requirement (Khan et al. 2015).

7.4 Composition of Functional Hydrogels

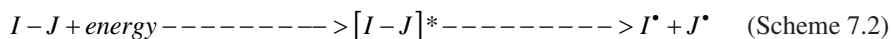
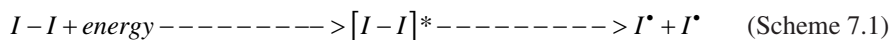
Functional hydrogels are assembled using a variety of starting materials, including crosslinking agents, initiators and monomers (Xu et al. 2018). A hydrogel, depending on the target application, may contain other components derived from materials such as drugs, inorganic salts, pharmaceutical agents and soil conditioners. Figure 7.4 shows the relationship between maintaining the hydrogel starting components.

Initiators: the role of the initiator molecules is to initiate the polymerization/crosslinking reactions which will ultimately lead to the formation of the hydrogel. Three main mechanistic routes have been indicated by which molecules that absorb energy from light can generate free radicals or ions and potentially initiate a polymerization reaction. The first route is by homolytic dissociation of a bond of an

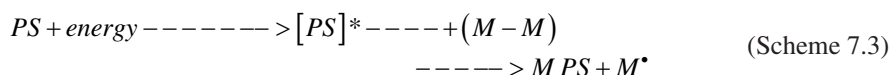
Fig. 7.4 Illustration of key hydrogel starting materials in a typical polymerization set up. Reproduced with permission from Ahmed (2015)



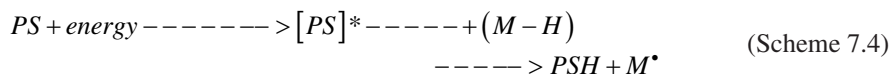
excited molecule in the absorption of photons (Gruber 1992). The example given in Scheme 7.1 involves a symmetric initiator molecule while the one given in Scheme 7.2 involves an asymmetric molecule.



The second pathway is by the transfer of energy, from a molecule that had absorbed light energy, (but not enough to cause dissociation of bonds) to another molecule (Yagci et al. 2010). In Scheme 7.3, M-M acts as the energy receptor molecule.



The third mechanism is by hydrogen abstraction from a hydrogen atom-donating molecule (McGinnes 1982). In Scheme 7.4, M-H acts as the hydrogen donor. This is shown in Scheme 7.4.



Salts and Other Ionizable Species in addition to the functions that salts can play at the start of polymerization reactions, they can also be incorporated into hydrogels in order to help determine how water is maintained in the microstructure of the hydrogel. The hydration enthalpy of ionizable species varies from one composition to another and governs the amount of water that can be maintained in the hydration sphere of the relevant ion. Thus, the appropriate salt(s) can be selected to tailor the target application. Figure 7.5 shows how water can interact with a range of anions and cations. The hydration enthalpy values of various anions and cations are given in Tables 7.1 and 7.2, respectively.

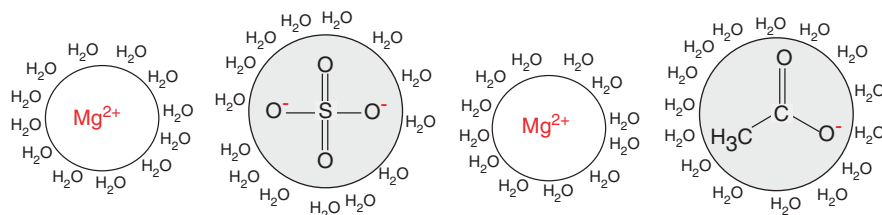


Fig. 7.5 Illustration of the interaction that can exist between water and various ionic species in a functional hydrogel

Table 7.1 Hydration enthalpy of a selection of cations

Ion	H ⁺	Na ⁺	NH ₄ ⁺	K ⁺	Mg ²⁺	Ca ²⁺	Zn ²⁺	Fe ²⁺	Sn ²⁺	Al ³⁺
ΔH (kJ/mol)	-1130	-444	-361	-307	-2003	-1657	-2046	-1946	-1554	-4446

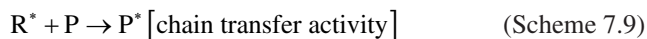
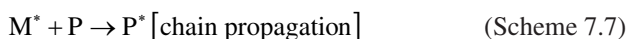
Table 7.2 Hydration enthalpy of a selection of anions

Ion	OH ⁻	F ⁻	Cl ⁻	Br ⁻	I ⁻	NO ₃ ⁻	CH ₃ COO ⁻
ΔH (KJ/mol)	-460	-483	-340	-309	-296	-314	-425

7.5 Routes for the Synthesis of Hydrogels

The synthesis of hydrogels can be achieved by a chain growth polymerization reaction, by a ring opening polymerization (ROP) reaction and by a step growth polymerization reaction. The most common method of polymerization by which hydrogels are produced is that of free-radical chain growth polymerization. This is mainly because of the unsaturated nature of monomers used in the typical hydrogel synthesis. The technique involves the use of free radicals from initiators that are generated by exposure to ultraviolet (UV) or gamma radiation and/or thermal initiators together with monomers and crosslinking agents. Free-radical polymerization reactions, carried out using UV and gamma irradiation, are known as radiation induced polymerization reactions.

The main steps involved in free-radical polymerization reactions are initiation, propagation, termination and chain transfer (Magami and Abdulganiyyu 2017). These are illustrated in Schemes 7.5, 7.6, 7.7, 7.8, 7.9.



where * represents a free radical, $h\nu$ denotes the energy of the incident radiation, M represents the monomer, P is the polymer chain, PI is the photoinitiator and R^* is any free radical. Free radical polymerization of hydrogels, as is the case with other polymeric materials, is affected by several factors, including dissolved oxygen in the reaction mixture, as well as the type of crosslinker, photoinitiator and monomer, in addition to the concentration of these species. The oxygen inhibition of the reaction can take many forms, including the quenching of the excited states and the formation of a peroxy radical. The formation of peroxy radicals is a problem, since the radical cannot attack vinyl functional groups and maintain propagation (Ligon et al. 2014).

During the induction period, cleavage of the intramolecular bond is likely to occur. In the initiation stage, the generated radicals attack the monomer molecules (Matyjaszewski et al. 1998). Chain propagation and crosslinking are established and continue beyond the gel point. These processes lead to the formation of networks, macromolecular advancement and development, as well as the increase of viscoelastic properties. The crosslinking reaction and network branching continue until the network is fully formed. This is typically indicated when the elastic modulus has reached a plateau state.

7.6 Characteristics of Functional Hydrogels

Once the hydrogel has been produced, subsequent treatments and use require knowledge of the actual water content, the degree to which the polymerization has taken place, the number of crosslinks, the structure of the polymer network and the thermal properties and other characteristics of the hydrogel. Various analytical techniques have been used to answer questions related to the arrangement and location of the pendant groups, the degradation of the hydrogels, the degree of polymerization/crosslinking and conversion of monomers, the structure of the generated polymer and the thermal behavior.

7.6.1 Swelling Characteristics

The swelling characteristics of hydrogels allow them to increase their volume up to several times their original size, by absorbing and accommodating liquid component into their microstructure (Mathur et al. 1998). The swelling of the hydrogel depends mainly on the degree of crosslinking in the gel, but also increases by the hydrophilicity of the polymer matrix. These two factors dictate the equilibrium swelling point (Hoffman 2012). A higher extent of crosslinking results in smaller pores and a lower equilibrium swelling point. This will be relevant to most hydrogel applications, since water will usually have a key role in the desired function. Therefore, the amount of water in the matrix is an integral property of the application. Swelling with ionic hydrogels such as those based on poly(acrylic acid) (PAA) and/or poly(acrylamide) is observed. The carboxylic acid moiety of PAA is ionized in an environment of increased pH, which increases swelling. The opposite is observed in poly(acrylamide)-based compositions, where the decrease in the pH increases the swelling properties (Brannon-Peppas and Peppas 1991).

The volume fraction of a swollen hydrogel is a measure of the water retention capacity of the hydrogel, i.e. the amount of water that the hydrogel can contain with maximum swelling. The volume fraction compares the volume of the non-swollen hydrogel with the volume of the swollen hydrogel (Lin and Metters 2006). It is, therefore, an inverse relationship of the equilibrium volume swelling ratio, given by Eq. 7.4. The volume fraction can be determined using Eq. 7.4.

$$V_f = \frac{V_u}{V_s} = \frac{1}{\left[1 + \frac{\rho_1}{\rho_2}(Q-1)\right]} \quad (7.4)$$

where Q is the equilibrium mass swelling ratio, V_f is the volume fraction, V_s is the equilibrium swollen material, V_u is the volume of the pre-swelled hydrogel, ρ_1 is the density of the underlining polymer material and ρ_2 is the density of the medium.

7.6.2 *Optical Properties*

Optical clarity and freedom from color are basic requirements for hydrogels that are prepared for use in double glazed units (Oh and Myungjin 2009). In many cases, the hydrogel material in the double-glazed assembly confers fire resistance property to the unit. The monomer and other precursors are carefully selected so that none absorb light in the visible region of the electromagnetic spectrum. In addition, materials that change color or lose their transparency in moderate temperature changes cannot be used in the synthesis stages.

In biomedical applications, the use of hydrogels in the (re)filling of lenses requires meeting strict refractive index requirements. It is known that in the natural lens, the refractive index gradually decreases from the center of the lens to the equator. When (re)filling of lenses is required across a natural lens, and a hydrogel with uniform refractive index is used, an undesirable optical aberration may arise (Ding et al. 2006). Therefore, this provides a challenge in the formulation and application of functional hydrogels for these applications. The transport of oxygen to the lens is critically important. The microporosity of many hydrogel matrices is suitable for this purpose, and thereby, allows enough diffusion of oxygen over the lens. A simple and fast method for the manufacture of contact lens is given as an illustration in Fig. 7.6.

7.6.3 *Mechanical Properties*

The mechanical properties of functional hydrogels are some of the key reasons for their varied applications. Hydrogels are often evaluated and described using terms such as compressive strength, fracture energies, fracture strains, tensile strength and toughness (Ma et al. 2016). Thus, an understanding of the mechanical properties of hydrogels is very important and provides information about their underlining structure and how such a structure is or may be paramount in a chosen application.

The tensile strength of hydrogels is tested when the material is subjected to a constant or varied force, under stress conditions. The corresponding response of the material is then defined by how it yields to the applied forces or by how it elongates

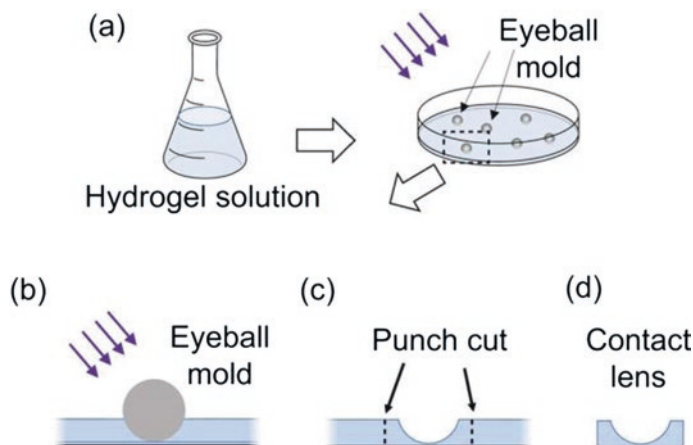


Fig. 7.6 Schematic illustration of the manufacture of hydrogel contact lens, using Petri dish and steel balls as eyeball molds. Reproduced with permission from Childs et al. (2016)

or by how it deflects physically (Drury et al. 2004). The work required to cause these changes in the material is then estimated, having known its pre-test dimensions. Similar information is obtained from compression tests. However, in this case, the material is subjected to the applied forces under compression conditions (Stammen et al. 2001).

The mechanical properties of a hydrogel can be tuned by varying the composition and the amount of constituent starting materials. However, care must be taken during the synthesis to ensure that other essential properties, such as clarity, extent of swelling and porosity, are not compromised. Figure 7.7 shows that the composition of the starting materials in bio-ionic liquids conjugated with gelatin and methacryloyl/poly(ethylene glycol) diacrylate can be tailored during the visible light crosslinking reactions (Noshadi et al. 2017). In this sense, by increasing the final concentration of polymer, as well as the polymer/bio-ionic liquid ratio, the compressive moduli of the resulting hydrogels increased. This also shows that the increase in polymer concentration affects the elastic moduli of the various materials in similar extents, when the tests were conducted in tension mode. Clearly, in this example, the extents of the crosslinking reactions and network formation were improved as a result of the increase in the number of reactive polymer groups.

7.6.4 Stimulus Response

The stimuli-responsive nature of many hydrogels allows their applications in sensors and actuators. This paves the way for their applications in various technologies. There are many examples of electrical-signal-responsive, pH-responsive, solvent-sensitive and thermo-responsive hydrogels (Ahn et al. 2008; Zarrantaj et al. 2019).

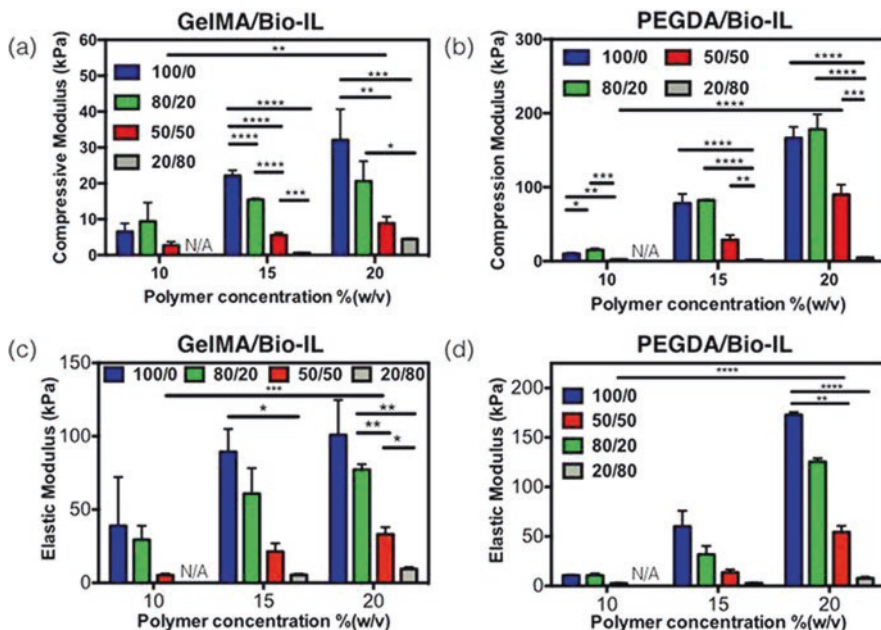


Fig. 7.7 Compressive modulus of various hydrogel compositions depending on the polymer concentration. Reproduced with permission from Noshadi et al. (2017)

In all these cases, when the stimuli are applied or removed, changes in the hydrogel material occur. These changes are typically reversible and can lead to chemical, mechanical or physical alterations in the material. A temperature-induced phase change is used (below) to provide a general description of the stimuli-responsiveness in hydrogels.

Certain hydrogels may exhibit temperature dependent light transmittance. Figure 7.8 shows a temperature vs light transmittance relationship at 450 nm for an AA-based hydrogel, where the hydrogel exhibits a temperature dependent light transmittance. In this sense, the hydrophilic/hydrophobic nature of the polymer's backbone plays a central role, which leads to optical transitions where the hydrogel is seen as clear or as cloudy, depending on the prevalence of hydrophilic or hydrophobic interactions (Magami 2017). Below a certain temperature (the critical temperature), the hydrogel remains clear and transparent, suggesting that hydrophilic interactions, such as H-bonding between water and polar functional groups that are present in the matrix, such as $-\text{COOH}$ and $-\text{C}=\text{O}$, are dominant. As the temperature changes (usually increased), these hydrophilic interactions are reduced, allowing any cation that may be present (such as Ca^{2+} , Mg^{2+} , Al^{3+}) to form a complex with the ionic macromolecules that are present (such as poly(carboxylate) ions). When such complexation occurs, the composition of the hydrogel becomes more hydrophobic in nature, which leads to precipitation or phase separation, resulting in cloudiness. In addition, Magami (2017) showed that when the concentration of

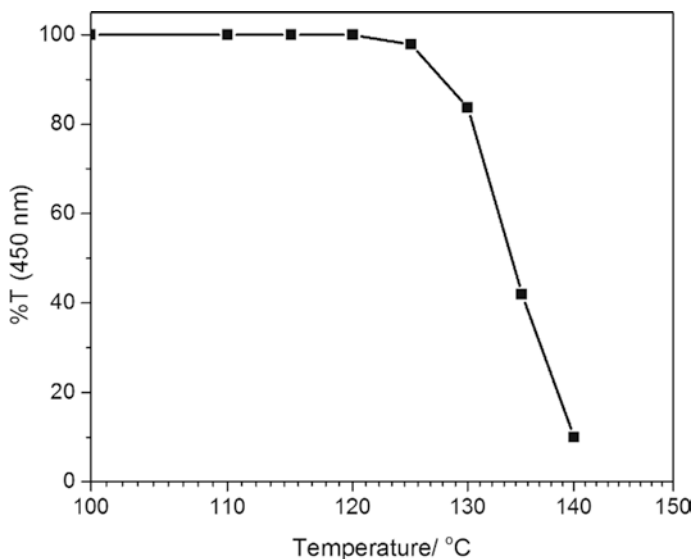


Fig. 7.8 Temperature vs light transmittance (showing 450 nm) of AA-based hydrogels. Reproduced with permission from Magami (2017)

β -acryloxypropionic acid is increased, the optical clarity of the hydrogel at the test temperature increases markedly, reaching a 100% light transmittance. Thus, the carboxyl groups in the hydrogel material can form strong H-bonds with water molecules in both ionized and protonated form. When strong enthalpic interactions occur in these hydrogels, the criterion of lower critical solution temperature (LCST) is met (Ruel-Gariépy and Leroux 2004; Shen et al. 2019).

The LCST phenomena in acrylate hydrogels can be dictated by varying a series of parameters such as ionic strength, pH, nature of anion and cation, and by copolymerizing with hydrophobic or hydrophilic (ionic, non-ionic) monomer. Thus, simple changes to the polymer backbone can significantly affect the degree to which the ionic interactions are formed, broken or sustained. The LCST of hydrogels can also be influenced by changing the polymer backbone through copolymerization. For example, 2-carboxyethyl acrylate (higher pKa value) can be copolymerized with AA to achieve hydrogels. The difference in pKa value between the two monomers is enough to affect the pH of the solution formulations. At elevated temperatures, the carboxyl groups of poly(carboxyethyl acrylate) (PCEA) would remain protonated, which would lead to a reduction in hydrophobic complexation by any ionic species that might be present, by maintaining their hydrophilic interactions with water molecules *via* H-bonding. Thus, intramolecular H-bonding and the intermolecular bonding between cations and carboxylate groups of either the PAA or the PCEA species that are attached to the polymer backbone play a role in the LCST phenomenon (Magami 2017).

7.7 Characterization Methods

There are several characterization techniques which are applicable to the characterization of functional hydrogels. Often, the choice of the characterization technique is influenced by the required application of the material. Typically, hydrogels are characterized in different stages: during synthesis and post-preparation. During synthesis, crosslinking, structure development and transparency can be monitored. It may be important, post-preparation, to differentiate the type of network that is characteristic of the test material. For example, a mechanical spectrum or viscoelastic spectrum from a test material could reveal whether it is simply a dense polymer or if it is composed of entangled network or chemical crosslinks.

7.7.1 Spectroscopic Analysis Methods

Spectroscopic analysis methods provide insight into the structure and composition of polymers, through the excitations of electrons or atom groups, when irradiated with a source of electromagnetic radiation. In addition, the spectroscopic analysis of residual materials in the hydrogel can be vital in understanding how they can affect performance properties. For example, the presence of residual initiator molecules/fragments may affect the long-term stability and aging characteristics of the hydrogel material.

Generally, an infrared spectrophotometer is used to analyze the transmitted light after the molecules in a polymer sample have absorbed radiation in the infrared region of an electromagnetic spectrum. The radiation absorption by molecules in this region causes bending, stretching and molecular vibrations occurring at different frequencies that are unique to the nature of the bonds and atoms present (Stuart 2015). UV-visible spectroscopy has also been widely used to study the structure-performance properties of hydrogels. While this is typically relevant for optical applications of hydrogels, the technique has proven useful for obtaining the absorbance spectra of components of functional hydrogels (Hebeish et al. 2013). In this way, the conversion of reactive species in the hydrogels can be monitored and evaluated.

Raman spectroscopy is another technique that can be used to identify chemical bonds and subsequently analyze the composition of functional hydrogels (Pastorczak et al. 2009). A notable advantage that Raman spectroscopy has over other spectroscopic techniques is that Raman spectroscopy is not affected by water. This technique can thus be used to analyze hydrogels in their swollen form. Raman micro-spectroscopy can be used to evaluate differences in the 3D structure of

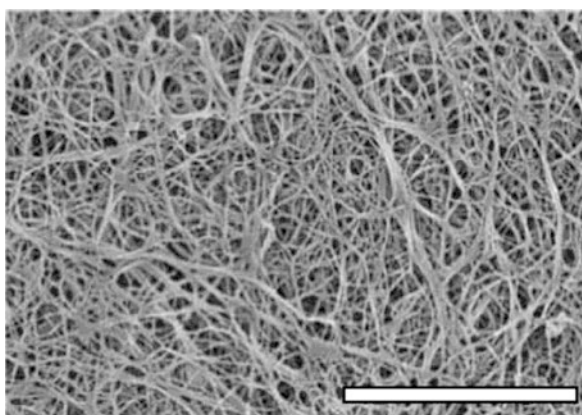
different hydrogels (Hwang and Lyubovitsky 2013). This can be valuable in assessing the effects of different formulations on the final hydrogel product.

7.7.2 Microscopic Analysis Methods

Microscopy can allow obtaining valuable information on hydrogel materials (Liao et al. 2008). These include pore sizes, porosity, network homogeneity or inhomogeneity. Figure 7.9 shows a microscopic image of a collagen hydrogel network. In this sense, an interconnected network mesh can be observed, as a representation of the crosslinked network in the material. To perform scanning electron microscopic (SEM) analysis in hydrogels, test samples are commonly immersed in water to swell. This is usually carried out at room temperature. After equilibrium swelling in water is achieved, the test samples are then dehydrated using the lyophilization technique. The cross-section of the samples is then coated with a thin layer of gold or platinum before making the measurements. Using an SEM instrument, an accelerating voltage (kV) of the electrons is then used. The voltage used depends on the topographic information sought. To obtain deeper information from the material, a higher energy of the accelerating electrons may be required. However, very high energy electrons penetrate deeper into the sample and decrease the yield of secondary electrons, thus lowering surface detail/resolution. In addition, the use of high energy electrons can cause damage to the test samples. This can be disadvantageous particularly when analyzing biological samples.

When SEM images are combined with X-ray diffraction (XRD) spectroscopy, the elements on the surface of the hydrogel can be mapped and evaluated (Bai et al.

Fig. 7.9 SEM of a collagen gel network, with a 5 μm scale bar. Reproduced with permission from Holder et al. (2018)



2011b). A map of the distribution of the various elements on the surface of the hydrogel can determine the distribution of materials, such as enzymes, pharmaceuticals and salts, in the hydrogel. When the mapping of high density elements is required, higher acceleration voltages may be preferred, in order to improve the X-ray performance (Niranjan et al. 2013).

7.7.3 Methods of Rheological Analysis

Hydrogels belong to the group of viscoelastic polymers. They may also exhibit some degree of elasticity in their swollen state, along with limited flow properties (Liu et al. 2015). This elastic behavior of the hydrogels depends not only on the water content but also on the type of polymerization that has taken place in the formation of the polymer networks, the cross-link density and the presence of any impurities. However, this degree of elasticity, translated as a degree of swelling, can be affected by a number of factors, such as the crosslinking density, the polymerization conditions and the presence of comonomers or insoluble inorganic species (Vural et al. 2010). An increase in the degree of swelling of hydrogel inversely affects the mechanical and flow properties of the composition.

The viscoelastic properties of hydrogels are commonly evaluated by rheological measurements. In this context, test specimens are typically subjected to stress-strain conditions. The response of the specimens to the applied forces is often expressed using a series of parameters, including loss modulus (G''), phase angle (δ), G' and tangent delta (Anseth et al. 1996). The G' describes the elastic behavior of the material, through its ability to conserve the energy applied. However, G'' describes the flow tendency of the material, through its ability to dissipate the applied energy. The

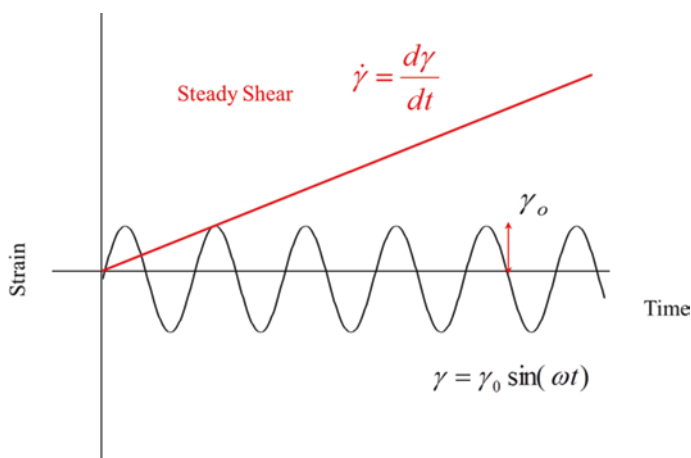


Fig. 7.10 Small amplitude diagram, showing strain-time relationship

tangent delta combines the effects of the storage module and the loss module, in the same way that the δ does. In addition, these describe the in-phase or out-of-phase time relationship between the applied stress and the resulting strain, or vice-versa. The strain-time relationship is given in Fig. 7.10. In this sense, a small amplitude shear diagram is illustrated, where t is the oscillation time and γ_o is the strain amplitude. Constant shear is then given as the rate of change of strain over time. The applied sinusoidal strain and the generated stress are further described by the relationships given in Eqs. 7.5 and 7.6, where τ is the shear stress. The implications of the stress-strain relationship in hydrogels can be directly related to the effect of creep and the frequency response of the material (McKeen 2009).

$$\gamma = \gamma_o \sin(\omega t) \quad (7.5)$$

$$\tau = \tau_o \sin(\omega t + \delta) \quad (7.6)$$

7.7.4 Sol-Gel Transition and the Gel Point

Rheological methods are often used in determining the gel point of hydrogels, thus leading to an understanding of the sol-gel transition. Common techniques used for the gelation study of functional hydrogels are given in Table 7.3. The Chirp method and the multi-wave technique are more commonly used, compared to the other two techniques, when the gel point of the critical gel is identified. When the determination of the gel point becomes difficult, the strain approximation approach can be used as a complementary method. This monitors changes in strain during the gel synthesis and considers the point of sharp decline in strain as the gel point. The moduli crossover technique is a less accurate method of determining the gel point compared to the other techniques, especially when stoichiometric imbalance is a factor in the reaction. This technique considers the time corresponding to the crossover point of G' and G'' during the synthesis steps (Magami and Williams 2019).

The multi-wave technique is highly accurate even where the relaxation exponent value is $n < 0.5$ or $n > 0.5$. It could be carried out using stress or strain time sweeps in a method considered as the Fourier transform mechanical spectroscopy (Hawkins et al. 2008). To maximize data quality, frequency ranges are carefully selected. These depend largely on the viscosity and reactivity of the test material, in addition to the mutation of the rheological data (Williams and Williams 1997). Sinewaves with different frequency values are shown in Fig. 7.11, with their combined image in Fig. 7.12. In the multi-wave techniques, a limitation may be the use of sinewaves with low frequency values. This is because the low frequencies correspond to long experimental times. This also means that the interval between observed data points is long to allow the material to change. Even at the gel point, the material typically experiences a characteristic stress relaxation. One way to ensure that the rheological data generated is significant/meaningful is to ensure that the mutation number

Table 7.3 Typical methods used to establish the gel point of functional hydrogels

Typical methods	Brief notes	Reference
Chirp(s) technique	ω increases or decreases over time. Quick acquisition of data compared to multi-wave technique. Time and frequency resolution are effectively achieved. Stress amplitude or strain amplitude of the individual frequencies do not require adding up.	Geri et al. (2018)
Multiwave rheometry	Fundamental and additional oscillation frequencies are required. These are kept constant while the material is subjected to controlled stress or strain at each frequency. Thus, cross-over of modules can be observed and compared as a function of frequency.	Jiao et al. (2012)
Strain decrease method	The point of intersection is controlled during the sharp decrease in strain. Method is less precise compared to Fourier transform methods, and therefore, is largely a complementary technique.	Bonino et al. (2011)
Moduli crossover technique	Relatively easy technique. Only valid for systems where the value of relaxation exponent $n = 0.5$. Data can be obtained from measurement at single frequency of oscillation.	Ishida and Allen (1996)

criteria is met (Mours and Winter 1994). A mutation number value of <1 often indicates that rheological data points are collected within reasonable time intervals and that the test sample does not change significantly in the range of the data points.

As the structure develops in the possible gel and the crosslinks are formed, a crossover point is observed in the multi-wave plots of loss tangent δ ($\tan \delta$) vs time. This crossover point is the gel point of the material, where the G' and the G'' have the same variation of the power law with respect to the ω . This is the so-called Winter-Chambon criteria (Chambon et al. 1986).

7.7.5 Other Characterization Methods

Thermal analysis techniques, such as thermogravimetric analysis (TGA) and differential scanning calorimetry (DSC) can be quite useful in the characterization of functional hydrogels (Thermal Analysis of Polymers 2009). In addition to the thermal stability that can be determined using TGA, the water bonding in the hydrogel network can be determined. Slightly bound water is easily lost during controlled heating, while tightly bound water is usually retained but is lost after excessive heating of the sample. On the other hand, DSC can be used to determine the influence of crosslinking on transition temperatures in hydrogels (Neto et al. 2005). However,

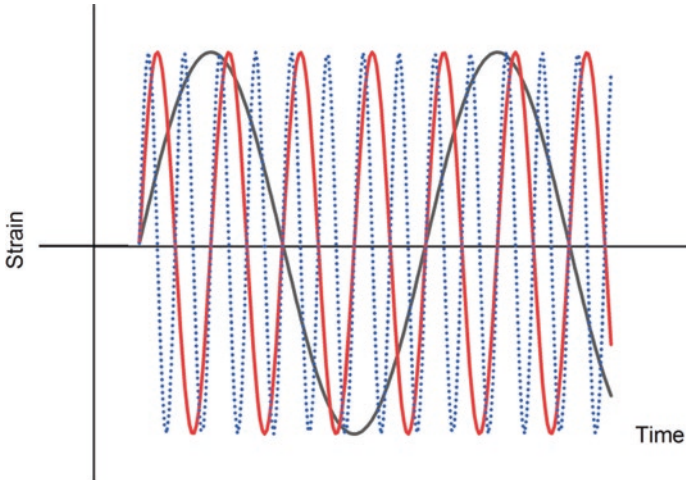
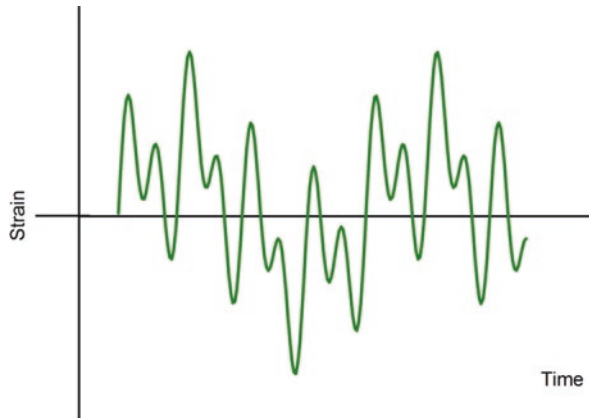


Fig. 7.11 Sinewaves with different frequency values, having the same strain amplitude value

Fig. 7.12 Sinewaves from Fig. 7.11 combined into a single wave screen



in highly crosslinked hydrogels, transition temperatures are very difficult to be observed. When the network of the hydrogel material is highly dense, it is unlikely, if not impossible, that despite heating of the material, stiff crosslinks and rigid network clusters impede mechanical movements (Wu and Freeman 2009).

7.7.6 *Practical Notes*

1. If there is enough material, it is good practice to conduct the analysis of hydrogel samples in duplicate or triplicate. This can ensure confidence in that the statistical significance of the effects in structure-property relationship is determined.
2. It is not good practice to allow hydrogels to dry before lyophilizing them prior to microscopic evaluation. This can cause shrinkage in pore sizes.
3. Performing DSC experiments in a sealed pan can cause damage to the instrument, as pressure may build-up due to the water vapor formation as the heating temperature increases.
4. Moisture loss or moisture absorption can affect mechanical characterization data. Where relevant, tests should be performed in a controlled humidity environment.
5. Mutation in the test sample may occur during the rheological evaluation. Ensure that the mutation number values are $\ll 1$, thus meeting the so-called mutation number criteria.
6. If available and relevant, the use of an *in situ* rheological measurement is desirable. This can be critical for slightly crosslinked hydrogels or those with entangled network. The preparation of this type of hydrogels can be a challenge for obtaining the sample size that can match the test plate geometry. In addition, sample loading procedures may apply undesirable stress on the test material.
7. In the case of studying the gelation of low viscosity systems, the torque amplitudes in the first curing stages will be much lower than in the more conventional '100% solids' systems with the risk of a poor signal/noise ratio. This can affect the quality of the rheological data. It can, however, be overcome with a controlled stress instrument which has a magnetic bearing, which allows testing with lower torque amplitudes.
8. The cohesive nature of the hydrogel is increased by the high crosslink density.

7.8 Applications of Functional Hydrogels

The unique properties of hydrogels have made them useful in various fields of science and technology, including agriculture, architecture and biomedicine.

7.8.1 *Healthcare and Biomedical Applications*

In today's healthcare, functional hydrogels have been shown to be widely used due to their intrinsic properties. These include biocompatibility, biodegradability, flexibility, optical clarity, permeability, swelling ability, thermal stability and transparency. With this in mind, synthetic or natural polymers or blends are used (Rosiak

and Yoshii 1999). The use of hydrogels in tissue engineering can be achieved using a variety of strategies. Figure 7.13 shows a simplified process involved in the use of polymeric hydrogel scaffolds in tissue formation or tissue regeneration. Often, tissues are explanted from the subject and then preferentially infused, modified and engineered though *in vitro* techniques. These can then be implanted into the individual, thus exposing them to mechanical and molecular environments. When necessary, engineered scaffolds can be further developed in suitable bioreactors, in order to generate an artificial organ before implantation (Khan et al. 2015).

Soft contact lenses made from hydrogels have been synthesized so that the gel can deliver the necessary antibiotics to the eye and can also provide visual corrections (Kopecek 2009). Other biomedical applications of hydrogels include wound dressing for burns, supports for tissue engineering and biodegradable drug delivery systems capable of delivering anti-nausea/vomiting drugs, oral insulin and vitamins. The delivery of pharmaceutical products or the scaffolding application of hydrogels is largely determined by its network structure. Often, the hydrogels are required to be slightly crosslinked. This can thus lead to a greater tendency to swelling and less flexibility (Sun et al. 2011).

Biocompatibility: hydrogels in biomedical applications in most cases are designed to be in contact with mammalian tissue. Therefore, this requires that they are biocompatible. When this is not achieved, cytotoxicity then arises. In many cases, it is the choice and the concentration of constituent materials in the hydrogel that determine whether they are biocompatible or not. Often, half maximal inhibitory concentration (IC_{50}) tests are designed and used to study the biocompatibility of hydrogels. IC_{50} is thus used to measure the degree to which specific biological functions are effectively inhibited by the substance under investigation.

Hydrogels based on β -sheet peptides have now emerged widely for biomedical applications. Keeping this in view, the sequence design of the peptide material and the concentration of the peptide in the hydrogel are key factors in the material's

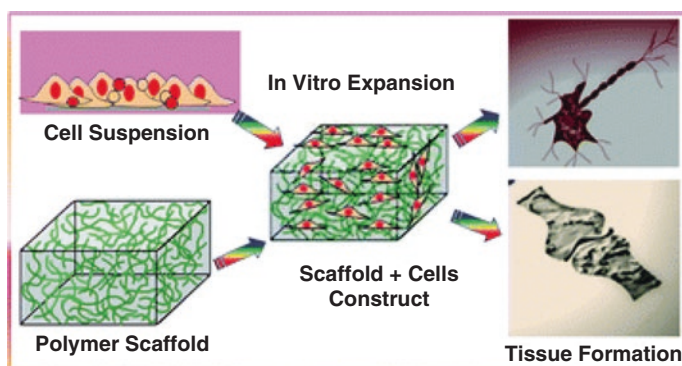


Fig. 7.13 Illustration of the processes involved in the use of hydrogel scaffolds in tissue engineering. Reproduced with permission from Khan et al. (2015)

biocompatibility. It has recently been shown that functional hydrogels that are of peptide and inorganic compound hybrids can be successfully manufactured to possess great potential for tissue scaffolding engineering. For example, hydrogel networks can be formed successfully by combining graphene with selected peptide materials. In this context, Wychowaniec (2017) reported that cytotoxicity of the hybrid hydrogels were desirable and that the material possessed essential tissue injectability properties, in addition to being biocompatible. These hybrid hydrogels were proposed as a versatile platform for culturing cells in three-dimensions (Wychowaniec 2017).

Biodegradability: when functional hydrogels used in biomedical applications (e.g. as tissue scaffolds) are biodegradable, this ensures that their application is temporary in nature. Such biodegradable materials often continue to exist and fulfill their function until they are degraded and replaced by new biological tissues. Many biodegradable functional hydrogels are made from polymers that are themselves biodegradable. Typical examples include cellulose, Cs, collagen and poly(lactic acid) (PLA) (Gutiérrez 2017). Due to their biodegradability, the mechanical properties of hydrogels are degraded, which leads to a decrease in crosslinking, elasticity and stiffness over time. It is essential for these changes in the hydrogel occur at a rate equal or similar to the rate of formation of new tissues.

It has been shown that cellulose-based hydrogels are biodegradable, in addition to their biocompatibility. Among the list of biodegradable cellulose-based starting materials, carboxymethyl cellulose, hydroxyethyl cellulose and hydroxymethyl cellulose are widely used as monomers in hydrogel syntheses (Sarkar 1979). A challenge is to find a suitable biodegradable crosslinker for use during synthesis. Often, the salt molecules used in the preparations can act as chelating agents, leading to gelation and network formation. Another strategy is to use two or more cellulosic starting materials, with gelation achieved through physical entanglement of growing polymer chains. In line with this, hydrophobic interactions are key in the gelation process, which arise from the methoxy chains that are present in the growing cellulosic polymer chains. These interactions depend on temperature and occur faster when processing temperatures increase (Sannino et al. 2009).

Other safety aspects: physically crosslinked hydrogels in particular are typically not considered for use in biological environments (e.g. in tissue scaffolding or visual correction applications), since the crosslinking in these materials is largely reversible, it is often difficult to control the nature and rate at which the entangled chains are unraveled (te Nijenhuis 2007). Examples of safety checks that are carried out in relation to the biomedical application of hydrogels are given in Table 7.5. The ways in which untangling of macromolecular chains in physically crosslinked hydrogels can be monitored include observing changes in their tendency to flow (increase) and assessing changes (loss or decrease) in viscoelasticity and other mechanical properties, due to application of stress or changes occurring in storage-influenced conditions, such as temperature. Thus, the degradation mechanisms of physically crosslinked hydrogels are largely uncontrollable.

Table 7.4 Examples of biodegradable hydrogels used in tissue scaffolds

Hydrogel	Function	Biodegradability	References
Dextran hydrogels	Wound healing	Largely influenced by the immobilization of vascular endothelial growth factors	Sun et al. (2011)
PLA- <i>b</i> -poly(ethylene glycol)- <i>b</i> -PLA end capped with acrylate groups	Tissue engineering cartilage	Biodegradability tailored by reaction and reactivity of the starting materials	Bryant and Anseth (2003)

Table 7.5 Examples of safety controls that are carried out in relation to the biomedical application of hydrogels

Hydrogel	Application	Safety verification	Safety comment	References
Bukamid – poly(acrylamide) based hydrogel.	Management of conditions related to urinary incontinence.	Post-operative assessments, at 3 and 12 months, followed by specified annual checks.	Administered Bukamid was found to be durable, effective and safe.	Pai and Al-Singary (2015)
Bukamid – poly(acrylamide) based hydrogel.	Female stress management and stress-predominant mixed incontinence.	24 months follow-up assessments.	There were no security problems after the evaluations.	Toozs-Hobson et al. (2012)
Raindrop corneal inlay.	Improvement of near vision in conditions related to emmetropic presbyopia.	12 months of safety and efficacy checks.	Patients satisfied with the overview. Only a small effect on distance visual sharpness.	Garza et al. (2013)

7.8.2 Fire Resistance Glazing Applications

Polymeric hydrogels have found applications in fire-resistant glazing assemblies. Usually, they are used as interlayers between glass sheets, in doors, partitions and windows. Their typical high-water content makes them suitable for these applications. When exposed to fire/flames, the hydrogel releases water in a controlled manner. In this way, the high specific heat capacity of water plays an advantage, by minimizing the increase in temperature on the glass surface. In this sense, the way in which water is bound to the internal structures of the hydrogel material is important. The water in hydrogels can thus be considered as strongly bound water or freely bound water. After exposure of the hydrogel at elevated temperatures, the latter is released first, followed by the former.

The composition of the hydrogel plays a very important role in the fire resistance application. The more hydrophilic the hydrogel backbone, the stronger would be the binding of the water molecules. In typical preparation procedures, water-solubilized

prepolymer formulations are created and then poured between the sealed double-glazing glass sheets. This formulation is then cured thermally or using UV light to give the resultant hydrogel. Specific examples are given Table 7.6. The properties of the fully formed hydrogel must be adequate so that they can be adhered to the glass and can withstand fire exposure for a specified period of time, thus providing the required insulating and fire resisting/retarding properties.

The fire resistance mechanism: char formation, free radical trapping, fuel dilution, heat absorption and thermal barrier are the key mechanisms through which intumescent fire-resistant compositions, including functional hydrogels. When a double-glazed unit, containing a formulation of hydrogels with dissolved salts, is exposed to flames and heat, water is released in a controlled manner once the first sheet of glass breaks through thermal shock. The dissolved salts then combined with the polymeric components of the gel to form an inorganic salt-carbonaceous composition that acts as an insulator, while adhering to the other glass sheet. This process of retarding fire is known as intumescence fire retardation. Fire tests are conducted in order to monitor the degree to which the hydrogel intumescence. This adds to the fire resistance monitoring of the structural components and the fire reaction of the flammable components in the material (Hull 2008). For fire resistant glass, the test panels are mounted onto a furnace in a vertical orientation. The furnace is then heated in a controlled manner so that it follows the temperature-time curve shown in Fig. 7.14. EN 1363–1 is a standard for testing fire resistance in materials intended for use in buildings. During the tests, the temperature on the fire-less side of the glass (cold side) rises and is monitored using thermocouple thermometers. The pressure inside the furnace is also controlled. The inherent

Table 7.6 Examples of functional hydrogels, monomer used in synthesis and curing method, relevant for the application of materials in fire-resistant glazing units

Technologies	Monomer* (example)	Curing methods	References
Fire-resistant glazing unit comprising about 40–85% by weight of water.	AA	Thermal curing, with typical reaction temperatures between 35 ° C and 90 ° C.	Crook and Ali (2016)
Fire-resistant glazing unit consisting about 40–90% by weight of water. A gel stabilizing agent, such as a tin compound, is an essential part of the formulation.	AA	UV-induced polymerization, by using a photo-initiator such as 2-hydroxy-2-methyl-1-phenylpropane-1-one.	Oh and Myungjin (2009)
Fire-resistant glazing unit comprising about 70–90% by weight of water.	Acrylamide	Cured at room temperature based on the use of highly soluble persulfate initiators such as ammonium persulfate or peroxidosulfate.	Ortmans and Hassiepen (1989)

*Other components are likely polymerizable and gel-forming

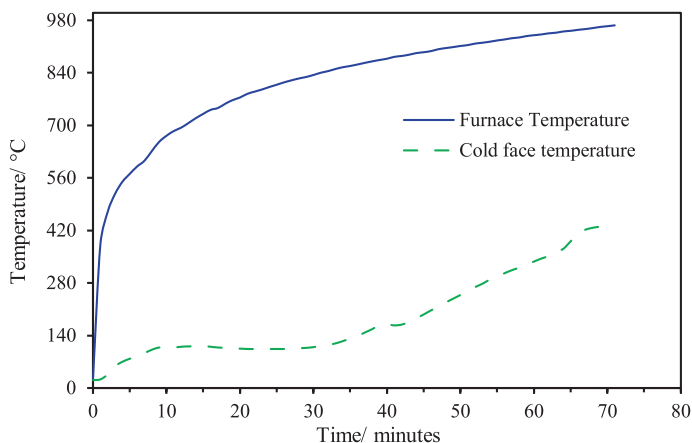


Fig. 7.14 Temperature-time relationship during a fire test, showing a required furnace temperature curve and a hypothetical cold face temperature

fire-resistant property of the hydrogel ensures that the temperature on the cold side of the glass is significantly lower than in the furnace.

7.8.3 *Personal Care/Hygiene Application*

The ability of hydrogels to absorb large amount of water and retain this water in their microstructure is the reason they have found application for personal care and hygiene fields. A key application of acrylate hydrogels is the manufacture of nappies. By absorbing moisture in large quantities, they help the user to keep the dry skin, with such practice promoting comfort and hygiene. In addition, this practice helps prevent skin irritation and contamination. In order for such nappies to be suitable and fit for purpose and to be free from leakages, the design of the hydrogel network must be carefully considered. An ideal level of crosslinking must be achieved to allow the hydrogel material in the nappies to accommodate/retain desirable amounts of fluid. On the other hand, a balance of viscoelasticity (rigidity, softness, stiffness, etc.) is required to ensure that such nappies are comfortable for their users. With increasing awareness for the creation and use of environmentally friendly materials, the generation of biodegradable hydrogel-based healthcare products is becoming increasingly popular. One strategy is to use biodegradable starting materials during the manufacturing stages. For this, cellulose and its many derivatives have found application. This development is thus likely to result in a continuous decrease in the use of acrylate-based starting materials.

7.9 Remark Conclusions

A general description of the structure, composition, synthesis routes, properties and applications of functional hydrogels has been given in this chapter. The fundamental gel point of the critical gels was defined, and relevant gelation models were given, paying attention to the multi-wave mechanical technique. This technique provides a good basis for determining the properties of critical gels, such as network relaxation exponent, stiffness and fractal dimensions. Despite the availability of rigorous gelation models, the gelation of many hydrogels has not yet been tested or confirmed. Many reports on functional hydrogels refer to biomedical applications of such materials. Although inventions (patents) show the relevance of the use of functional hydrogels in fire-resistant applications, very little work has been reported through scientific journals. Despite this, it is expected that the outline given in this chapter provides a background of the science that supports the applications of hydrogels in fire-resistant applications.

Acknowledgments The author acknowledges the helpful discussions provided by Emeritus Professor Jim Guthrie (University of Leeds).

Conflicts of Interest The author declares no conflict of interest.

References

- Abadi, M., Serag, M. F., & Habuchi, S. (2018). Entangled polymer dynamics beyond reptation. *Nature Communications*, 9(1), 5098. <https://doi.org/10.1038/s41467-018-07546-7>.
- Abdulganiyu, U., Magami, S. M., & Aminu, M. (2017). Graft copolymerization and characterization of styrene with chitosan via radical polymerization. *ChemSearch Journal*, 8(1), 56–63. <https://doi.org/10.4314/csaj.v8i1.8>.
- Ahmed, E. M. (2015). Hydrogel: Preparation, characterization, and applications: A review. *Journal of Advanced Research*, 6(2), 105–121. <https://doi.org/10.1016/j.jare.2013.07.006>.
- Ahn, S., Kasi, R. M., Kim, S.-C., Sharma, N., & Zhou, Y. (2008). Stimuli-responsive polymer gels. *Soft Matter*, 4(6), 1151–1157. <https://doi.org/10.1039/B714376A>.
- Akhtar, M. F., Hanif, M., & Ranjha, N. M. (2016). Methods of synthesis of hydrogels ... a review. *Saudi Pharmaceutical Journal*, 24(5), 554–559. <https://doi.org/10.1016/j.jsps.2015.03.022>.
- Anseth, K. S., Bowman, C. N., & Brannon-Peppas, L. (1996). Mechanical properties of hydrogels and their experimental determination. *Biomaterials*, 17(17), 1647–1657. [https://doi.org/10.1016/0142-9612\(96\)87644-7](https://doi.org/10.1016/0142-9612(96)87644-7).
- Bai, H., Li, C., Wang, X., & Shi, G. (2011a). On the gelation of graphene oxide. *The Journal of Physical Chemistry C*, 115(13), 5545–5551. <https://doi.org/10.1021/jp1120299>.
- Bai, H., Sheng, K., Zhang, P., Li, C., & Shi, G. (2011b). Graphene oxide/conducting polymer composite hydrogels. *Journal of Materials Chemistry*, 21(46), 18653–18658. <https://doi.org/10.1039/c1jm13918e>.
- Bonino, C. A., Samorezov, J. E., Jeon, O., Alsberg, E., & Khan, S. A. (2011). Real-time in situ rheology of alginate hydrogel photocrosslinking. *Soft Matter*, 7(24), 11510–11517. <https://doi.org/10.1039/c1sm06109g>.

- Borzacchiello, A., & Ambrosio, L. (2009). Structure-property relationships in hydrogels. In *Hydrogels: Biological properties and applications* (pp. 9–20). https://doi.org/10.1007/978-88-470-1104-5_2.
- Brannon-Peppas, L., & Peppas, N. A. (1991). Equilibrium swelling behavior of pH-sensitive hydrogels. *Chemical Engineering Science*, 46(3), 715–722. [https://doi.org/10.1016/0009-2509\(91\)80177-z](https://doi.org/10.1016/0009-2509(91)80177-z).
- Bryant, S. J., & Anseth, K. S. (2003). Controlling the spatial distribution of ECM components in degradable PEG hydrogels for tissue engineering cartilage. *Journal of Biomedical Materials Research Part A*, 64A(1), 70–79. <https://doi.org/10.1002/jbm.a.10319>.
- Chambon, F., Petrovic, Z. S., MacKnight, W. J., & Winter, H. H. (1986). Rheology of model polyurethanes at the gel point. *Macromolecules*, 19(8), 2146–2149. <https://doi.org/10.1021/ma00162a007>.
- Childs, A., Li, H., Lewittes, D. M., Dong, B., Liu, W., Shu, X., Sun, C., & Zhang, H. F. (2016). Fabricating customized hydrogel contact lens. *Scientific Reports*, 6, 34905. <https://doi.org/10.1038/srep34905>.
- Chiou, B.-S., English, R. J., & Khan, S. A. (1996). Rheology and photo-cross-linking of thiol–ene polymers. *Macromolecules*, 29(16), 5368–5374. <https://doi.org/10.1021/ma960383e>.
- Crook, V., & Ali, M. I. (2016). Fire resistant glazing unit. U.S. Patent Application No. 14/912,939. Available in: <https://patents.google.com/patent/us20160200077a1/en>
- Dashtimoghadam, E., Mirzadeh, H., Taromi, F. A., & Nyström, B. (2014). Thermoresponsive biopolymer hydrogels with tunable gel characteristics. *RSC Advances*, 4(74), 39386–39393. <https://doi.org/10.1039/c4ra05246c>.
- Dimesso, L. (2018). Pechini processes: An alternate approach of the sol-gel method, preparation, properties, and applications. In: *Handbook of sol-gel science and technology* (2nd ed.). Klein, L., Aparicio, M. & Jitianu, A. (Eds.). Springer International Publishing. https://doi.org/10.1007/978-3-319-32101-1_123.
- Ding, L., Blackwell, R., Künzler, J. F., & Knox, W. H. (2006). Large refractive index change in silicone-based and non-silicone-based hydrogel polymers induced by femtosecond laser micro-machining. *Optics Express*, 14(24), 11901–11909. <https://doi.org/10.1364/oe.14.011901>.
- Drury, J. L., Dennis, R. G., & Mooney, D. J. (2004). The tensile properties of alginate hydrogels. *Biomaterials*, 25(16), 3187–3199. <https://doi.org/10.1016/j.biomaterials.2003.10.002>.
- Garza, E., Gomez, S., Chayet, A., & Dishler, J. (2013). One-year safety and efficacy results of a hydrogel inlay to improve near vision in patients with emmetropic presbyopia. *Journal of Refractive Surgery*, 29, 166–172. <https://doi.org/10.3928/1081597x-20130129-01>.
- Geri, M., Keshavarz, B., Divoux, T., Clasen, C., Curtis, D. J., & McKinley, G. H. (2018). Time-resolved mechanical spectroscopy of soft materials via optimally windowed chirps. *Physical Review X*, 8(4), 41042. <https://doi.org/10.1103/physrevx.8.041042>.
- Gruber, H. F. (1992). Photoinitiators for free radical polymerization. *Progress in Polymer Science*, 17(6), 953–1044. [https://doi.org/10.1016/0079-6700\(92\)90006-k](https://doi.org/10.1016/0079-6700(92)90006-k).
- Gutiérrez, T. J. (2017). Chapter 8. Chitosan applications for the food industry. In S. Ahmed & S. Ikram (Eds.), *Chitosan: Derivatives, composites and applications* (pp. 183–232). WILEY-Scrivener Publisher. EE.UU. ISBN: 978-1-119-36350-7. <https://doi.org/10.1002/9781119364849.ch8>.
- Hawkins, K., Lawrence, M., Williams, P. R., & Williams, R. L. (2008). A study of gelatin gelation by Fourier transform mechanical spectroscopy. *Journal of Non-Newtonian Fluid Mechanics*, 148(1), 127–133. <https://doi.org/10.1016/j.jnnfm.2007.05.016>.
- Hebeish, A., Hashem, M., El-Hady, M. M. A., & Sharaf, S. (2013). Development of CMC hydrogels loaded with silver nano-particles for medical applications. *Carbohydrate Polymers*, 92(1), 407–413. <https://doi.org/10.1016/j.carbpol.2012.08.094>.
- Hennink, W. E., & van Nostrum, C. F. (2012). Novel crosslinking methods to design hydrogels. *Advanced Drug Delivery Reviews*, 64, 223–236. <https://doi.org/10.1016/j.addr.2012.09.009>.

- Higham, A. K., Bonino, C. A., Raghavan, S. R., & Khan, S. A. (2014). Photo-activated ionic gelation of alginate hydrogel: Real-time rheological monitoring of the two-step crosslinking mechanism. *Soft Matter*, *10*(27), 4990–5002. <https://doi.org/10.1039/c4sm00411f>.
- Hoffman, A. S. (2012). Hydrogels for biomedical applications. *Advanced Drug Delivery Reviews*, *64*, 18–23. <https://doi.org/10.1016/j.addr.2012.09.010>.
- Holder, A. J., Badiei, N., Hawkins, K., Wright, C., Williams, P. R., & Curtis, D. J. (2018). Control of collagen gel mechanical properties through manipulation of gelation conditions near the sol-gel transition. *Soft Matter*, *14*(4), 574–580. <https://doi.org/10.1039/c7sm01933e>.
- Hull, T. R. (2008). 11 - Challenges in fire testing: Reaction to fire tests and assessment of fire toxicity. In A. R. Horrocks & D. B. T.-A. in F. R. M. Price (Eds.), *Woodhead Publishing Series in Textiles*. Pp. 255–290. <https://doi.org/10.1533/9781845694701.2.255>
- Hwang, Y. J., & Lyubovitsky, J. G. (2013). The structural analysis of three-dimensional fibrous collagen hydrogels by raman microspectroscopy. *Biopolymers*, *99*(6), 349–356. <https://doi.org/10.1002/bip.22183>.
- Ishida, H., & Allen, D. J. (1996). Physical and mechanical characterization of near-zero shrinkage polybenzoxazines. *Journal of Polymer Science: Part B Polymer Physics*, *34*(6), 1019–1030. [https://doi.org/10.1002/\(sici\)1099-0488\(19960430\)34:6<1019::aid-polb1>3.0.co;2-t](https://doi.org/10.1002/(sici)1099-0488(19960430)34:6<1019::aid-polb1>3.0.co;2-t).
- Jiao, Y., Gyawali, D., Stark, J. M., Akcora, P., Nair, P., Tran, R. T., & Yang, J. (2012). A rheological study of biodegradable injectable PEGMC/HA composite scaffolds. *Soft Matter*, *8*(5), 1499–1507. <https://doi.org/10.1039/c1sm05786c>.
- Khan, F., Tanaka, M., & Ahmad, S. R. (2015). Fabrication of polymeric biomaterials: A strategy for tissue engineering and medical devices. *Journal of Materials Chemistry B*, *3*(42), 8224–8249. <https://doi.org/10.1039/c5tb01370d>.
- Koohi, A. D., Moghaddam, A. Z., Sefti, M. V., & Moghadam, A. M. (2011). Swelling and gelation time behavior of sulfonated polyacrylamide/chromium triacetate hydrogels. *Journal of Macromolecular Science, Part B*, *50*(10), 1905–1920. <https://doi.org/10.1080/00222348.2010.549419>.
- Kopecek, J. (2009). Hydrogels: From soft contact lenses and implants to self-assembled nanomaterials. *Journal of Polymer Science Part A: Polymer Chemistry*, *47*(22), 5929–5946. <https://doi.org/10.1002/pola.23607>.
- Laftah, W. A., Hashim, S., & Ibrahim, A. N. (2011). Polymer hydrogels: A review. *Polymer-Plastics Technology and Engineering*, *50*(14), 1475–1486. <https://doi.org/10.1080/03602559.2011.593082>.
- Liao, H., Munoz-Pinto, D., Qu, X., Hou, Y., Grunlan, M. A., & Hahn, M. S. (2008). Influence of hydrogel mechanical properties and mesh size on vocal fold fibroblast extracellular matrix production and phenotype. *Acta Biomaterialia*, *4*(5), 1161–1171. <https://doi.org/10.1016/j.actbio.2008.04.013>.
- Ligon, S. C., Husár, B., Wutzel, H., Holman, R., & Liska, R. (2014). Strategies to reduce oxygen inhibition in photoinduced polymerization. *Chemical Reviews*, *114*(1), 557–589. <https://doi.org/10.1021/cr3005197>.
- Lin, C.-C., & Metters, A. T. (2006). Hydrogels in controlled release formulations: Network design and mathematical modeling. *Advanced Drug Delivery Reviews*, *58*(12), 1379–1408. <https://doi.org/10.1016/j.addr.2006.09.004>.
- Liu, W. G., & Yao, K. D. (2001). What causes the unfrozen water in polymers: Hydrogen bonds between water and polymer chains? *Polymer*, *42*(8), 3943–3947. [https://doi.org/10.1016/S0032-3861\(00\)00726-6](https://doi.org/10.1016/S0032-3861(00)00726-6).
- Liu, Z., Toh, W., & Ng, T. Y. (2015). Advances in mechanics of soft materials: A review of large deformation behavior of hydrogels. *International Journal of Applied Mechanics*, *07*(05), 1530001. <https://doi.org/10.1142/s1758825115300011>.
- Lorente, M. A., & Mark, J. E. (1979). Model networks of end-linked polydimethylsiloxane chains. IV. Elastomeric properties of the tetrafunctional networks prepared at different degrees of dilution. *The Journal of Chemical Physics*, *71*(2), 682–689. <https://doi.org/10.1063/1.438354>.
- Ma, P. X., & Elisseeff, J. (Eds.) (2005). *Scaffolding in tissue engineering* (1st ed.). CRC Press. ISBN: 9780429121272. <https://doi.org/10.1201/9781420027563>.

- Ma, S., Yu, B., Pei, X., & Zhou, F. (2016). Structural hydrogels. *Polymer*, 98, 516–535. <https://doi.org/10.1016/j.polymer.2016.06.053>.
- Magami, S. M. (2017). In situ viscoelasticity and in situ thermo-responsiveness in acrylic acid-based soft hydrogels. *{IOP} Conference Series: Materials Science and Engineering*, 264, 12019. <https://doi.org/10.1088/1757-899x/264/1/012019>.
- Magami, S. M., & Abdulganiyyu, U. (2017). Raft approach to the copolymerisation of methyl methacrylate based polymeric micelles. *Bayero Journal of Pure and Applied Sciences*, 10(1), 197–204. <https://doi.org/10.4314/bajopas.v10i1.28>.
- Magami, S. M., & Williams, R. L. (2018). Gelation studies on acrylic acid-based hydrogels via in situ photo-crosslinking and rheology. *Journal of Applied Polymer Science*, 135(38), 46691. <https://doi.org/10.1002/app.46691>.
- Magami, S. M., & Williams, R. L. (2019a). Roles of the molecular weight of n-ethylene glycol diacrylates and UV irradiance on the mechanical properties at the gel point of acrylic acid based hydrogels. *Journal of Applied Polymer Science*, 136(23), 47606. <https://doi.org/10.1002/app.47606>.
- Magami, S. M., & Williams, R. L. (2019b). Gelation via actionic chelation/crosslinking of acrylic acid-based polymers. *Polymer International*, 68(12), 1980–1991. <https://doi.org/10.1002/pi.5910>.
- Magami, S. M. (2020). Comparative gelation of acrylic acid and acrylamide in diacrylate and dimethacrylate crosslinked matrices. *Polymer Bulletin*, <https://doi.org/10.1007/s00289-020-03147-x>.
- Mathur, A. M., Hammonds, K. F., Klier, J., & Scranton, A. B. (1998). Equilibrium swelling of poly(methacrylic acid-g-ethylene glycol) hydrogels: Effect of swelling medium and synthesis conditions. *Journal of Controlled Release*, 54(2), 177–184. [https://doi.org/10.1016/S0168-3659\(97\)00186-7](https://doi.org/10.1016/S0168-3659(97)00186-7).
- Matyjaszewski, K., Coca, S., Gaynor, S. G., Wei, M., & Woodworth, B. E. (1998). Controlled radical polymerization in the presence of oxygen. *Macromolecules*, 31(17), 5967–5969. <https://doi.org/10.1021/ma9808528>.
- McGinnes, V. D. (1982). *Photoinitiated polymerisation by aromatic carbonyl and alkyl-phenyl ketone compounds in developments in polymer photochemistry*. London: Applied Science Publishers.
- McKeen, L. W. (2009). Chapter 1- introduction to plastics and elastomers. In L. W. McKeen (Ed.), *The effect of creep and other time related factors on plastics and elastomers* (pp. 1–31). Pp: Second Edition. <https://doi.org/10.1016/b978-0-8155-1585-2.50003-0>.
- Mours, M., & Winter, H. H. (1994). Time-resolved rheometry. *Rheologica Acta*, 33(5), 385–397. <https://doi.org/10.1007/bf00366581>.
- Muthukumar, M. (1989). Screening effect on viscoelasticity near the gel point. *Macromolecules*, 22(12), 4656–4658. <https://doi.org/10.1021/ma00202a050>.
- Nair, L. S. (2016). *Injectable hydrogels for regenerative engineering*. London: Imperial College Press.
- Namba, R. M., Cole, A. A., Bjugstad, K. B., & Mahoney, M. J. (2009). Development of porous PEG hydrogels that enable efficient, uniform cell-seeding and permit early neural process extension. *Acta Biomaterialia*, 5(6), 1884–1897. <https://doi.org/10.1016/j.actbio.2009.01.036>.
- Neto, C. G. T., Giacometti, J. A., Job, A. E., Ferreira, F. C., Fonseca, J. L. C., & Pereira, M. R. (2005). Thermal analysis of chitosan based networks. *Carbohydrate Polymers*, 62(2), 97–103. <https://doi.org/10.1016/j.carbpol.2005.02.022>.
- Niranjan, R., Koushik, C., Saravanan, S., Moorthi, A., Vairamani, M., & Selvamurugan, N. (2013). A novel injectable temperature-sensitive zinc doped chitosan/β-glycerophosphate hydrogel for bone tissue engineering. *International Journal of Biological Macromolecules*, 54, 24–29. <https://doi.org/10.1016/j.ijbiomac.2012.11.026>.
- Noshadi, I., Walker, B. W., Portillo-Lara, R., Shirzaei Sani, E., Gomes, N., Aziziyan, M. R., & Annabi, N. (2017). Engineering biodegradable and biocompatible bio-ionic liquid conjugated hydrogels with tunable conductivity and mechanical properties. *Scientific Reports*, 7(1), 4345. <https://doi.org/10.1038/s41598-017-04280-w>.

- Oh, J., & Myungjin, C. (2009). *Patent No. US8663788B2*. Available in: <https://patents.google.com/patent/us8663788>
- Ortmans, G., & Hassiepen, M. (1989). Fire-resistant glazing and method of making same. U.S. Patent No. 4,830,913. Washington, DC: U.S. Patent and Trademark Office. Available in: <https://patents.google.com/patent/us4830913a/en>
- Pai, A., & Al-Singary, W. (2015). Durability, safety and efficacy of polyacrylamide hydrogel (Bulkamid®) in the management of stress and mixed urinary incontinence: Three year follow up outcomes. *Central European Journal of Urology*, 68(4), 428–433. <https://doi.org/10.5173/cej.2015.647>.
- Pastorczyk, M., Kozanecki, M., & Ulanski, J. (2009). Water-polymer interactions in PVME hydrogels - Raman spectroscopy studies. *Polymer*, 50(19), 4535–4542. <https://doi.org/10.1016/j.polymer.2009.07.048>.
- Patel, S. K., Malone, S., Cohen, C., Gillmor, J. R., & Colby, R. H. (1992). Elastic modulus and equilibrium swelling of poly(dimethylsiloxane) networks. *Macromolecules*, 25(20), 5241–5251. <https://doi.org/10.1021/ma00046a021>.
- Pechini, M. P. (1967). *Patent No. 3330697*.
- Quinn, F. X., Kampff, E., Smyth, G., & McBrierty, V. J. (1988). Water in hydrogels. 1. A study of water in poly(*N*-vinyl-2-pyrrolidone/methyl methacrylate) copolymer. *Macromolecules*, 21(11), 3191–3198. <https://doi.org/10.1021/ma00189a012>.
- Rosiak, J. M., & Yoshii, F. (1999). Hydrogels and their medical applications. *Nuclear Instruments and Methods in Physics Research Section B: Beam Interactions with Materials and Atoms*, 151(1), 56–64. [https://doi.org/10.1016/s0168-583x\(99\)00118-4](https://doi.org/10.1016/s0168-583x(99)00118-4).
- Ruel-Gariépy, E., & Leroux, J.-C. (2004). In situ-forming hydrogels—Review of temperature-sensitive systems. *European Journal of Pharmaceutics and Biopharmaceutics*, 58(2), 409–426. <https://doi.org/10.1016/j.ejpb.2004.03.019>.
- Sannino, A., Demitri, C., & Madaghiele, M. (2009). Biodegradable cellulose-based hydrogels: Design and applications. *Materials*, 2(2), 353–373. <https://doi.org/10.3390/ma2020353>.
- Sarkar, N. (1979). Thermal gelation properties of methyl and hydroxypropyl methylcellulose. *Journal of Applied Polymer Science*, 24(4), 1073–1087. <https://doi.org/10.1002/app.1979.070240420>.
- Scholz, F., & Kahlert, H. (2015). The calculation of the solubility of metal hydroxides, oxide-hydroxides, and oxides, and their visualisation in logarithmic diagrams. *ChemTexts*, 1(1), 7. <https://doi.org/10.1007/s40828-015-0006-0>.
- Shen, Y., Zhu, H., Wang, Y., Cui, H., & Sun, R. (2019). Applications and implications of environmental-responsive polymers toward agrochemicals. In T. Gutiérrez (Ed.), *Polymers for Agriculture applications* (pp. 67–90). Cham: Springer. https://doi.org/10.1007/978-3-030-19416-1_5.
- Singhal, R., & Gupta, K. (2016). A review: Tailor-made hydrogel structures (classifications and synthesis parameters). *Polymer-Plastics Technology and Engineering*, 55(1), 54–70. <https://doi.org/10.1080/03602559.2015.1050520>.
- Stammen, J. A., Williams, S., Ku, D. N., & Guldberg, R. E. (2001). Mechanical properties of a novel PVA hydrogel in shear and unconfined compression. *Biomaterials*, 22(8), 799–806. [https://doi.org/10.1016/s0142-9612\(00\)00242-8](https://doi.org/10.1016/s0142-9612(00)00242-8).
- Stuart, B. (2015). Infrared spectroscopy. In *Kirk-Othmer Encyclopedia of chemical technology* (pp. 1–18). <https://doi.org/10.1002/0471238961.0914061810151405.a01.pub3>.
- Sun, G., Shen, Y.-I., Kusuma, S., Fox-Talbot, K., Steenberg, C. J., & Gerecht, S. (2011). Functional neovascularization of biodegradable dextran hydrogels with multiple angiogenic growth factors. *Biomaterials*, 32(1), 95–106. <https://doi.org/10.1016/j.biomaterials.2010.08.091>.
- te Nijenhuis, K. (2007). On the nature of crosslinks in thermoreversible gels. *Polymer Bulletin*, 58(1), 27–42. <https://doi.org/10.1007/s00289-006-0610-7>.
- Menczel, J. D., & Prime, R. B. (2009). *Thermal analysis of polymers*. (1st ed.). <https://doi.org/10.1002/9780470423837>.
- Tomadoni, B., Casalongué, C., & Alvarez, V. A. (2019). Biopolymer-based hydrogels for agriculture applications: Swelling behavior and slow release of agrochemicals. In T. Gutiérrez

- (Ed.), *Polymers for Agri-food applications* (pp. 99–125). Cham: Springer. https://doi.org/10.1007/978-3-030-19416-1_7.
- Toozs-Hobson, P., Al-Singary, W., Fynes, M., Tegerstedt, G., & Lose, G. (2012). Two-year follow-up of an open-label multicenter study of polyacrylamide hydrogel (Bulkamid®) for female stress and stress-predominant mixed incontinence. *International Urogynecology Journal*, 23(10), 1373–1378. <https://doi.org/10.1007/s00192-012-1761-8>.
- Valencia, G. A., Zare, E. N., Makvandi, P., & Gutiérrez, T. J. (2019). Self-Assembled carbohydrate polymers for food applications: A review. *Comprehensive Reviews in Food Science and Food Safety*, 18(6), 2009–2024. <https://doi.org/10.1111/1541-4337.12499>.
- Vural, S., Dikovics, K. B., & Kalyon, D. M. (2010). Cross-link density, viscoelasticity and swelling of hydrogels as affected by dispersion of multi-walled carbon nanotubes. *Soft Matter*, 6(16), 3870–3875. <https://doi.org/10.1039/c0sm00099j>.
- Williams, P. R., & Williams, R. L. (1997). Gel-point studies in reacting systems by shear wave dispersion measurements. *Journal of Non-Newtonian Fluid Mechanics*, 68(2), 311–322. [https://doi.org/10.1016/s0377-0257\(96\)01510-8](https://doi.org/10.1016/s0377-0257(96)01510-8).
- Winter, H. H. (1987). Can the gel point of a cross-linking polymer be detected by the $G' - G''$ crossover? *Polymer Engineering & Science*, 27(22), 1698–1702. <https://doi.org/10.1002/pen.760272209>.
- Wu, Y.-H., & Freeman, B. D. (2009). Structure, water sorption, and transport properties of cross-linked N-vinyl-2-pyrrolidone/N,N'-methylenebisacrylamide films. *Journal of Membrane Science*, 344(1), 182–189. <https://doi.org/10.1016/j.memsci.2009.07.050>.
- Wychowanec, J. K. (2017). *Designing nanostructured peptide hydrogels containing graphene oxide and its derivatives for tissue engineering and biomedical applications* (The University of Manchester). Available in: https://www.research.manchester.ac.uk/portal/files/64900745/full_text.pdf p 120.
- Wyss, H. M. (2016). Rheology of soft materials. In A. Fernandez-Nieves & A. M. Puertas (Eds.), *Fluids, colloids and soft materials* (pp. 149–163). <https://doi.org/10.1002/9781119220510.ch9>.
- Xu, J., Liu, X., Ren, X., & Gao, G. (2018). The role of chemical and physical crosslinking in different deformation stages of hybrid hydrogels. *European Polymer Journal*, 100, 86–95. <https://doi.org/10.1016/j.eurpolymj.2018.01.020>.
- Yagci, Y., Jockusch, S., & Turro, N. J. (2010). Photoinitiated polymerization: Advances, challenges, and opportunities. *Macromolecules*, 43(15), 6245–6260. <https://doi.org/10.1021/ma1007545>.
- Zarrintaj, P., Jouyandeh, M., Ganjali, M. R., Hadavand, B. S., Mozafari, M., Sheiko, S. S., Vatankeh-Varnoosfaderani, M., Gutiérrez, T. J., & Saeb, M. R. (2019). Thermo-sensitive polymers in medicine: A review. *European Polymer Journal*, 117, 402–423. <https://doi.org/10.1016/j.eurpolymj.2019.05.024>.

Chapter 8

Grafting Polymers



Sonal Choudhary, Kashma Sharma, Vishal Sharma, and Vijay Kumar

Abstract In recent decades, a series of strategies have been reported for modifying surface properties of natural and synthetic polymers. Among the strategies for the modification of polymers, grafting is considered the most ideal technique. Several monomers with specific physicochemical and surface characteristics can be grafted onto the polymers. Therefore, graft copolymerization is an attractive technique for providing several active sites into a polymer. Graft copolymerization began with a chemical process, such as photo-irradiation, among others, which were widely discussed in this chapter, as well as the most important control parameters on graft copolymerization were reviewed. The grafted polymers resulting *via* grafting have a brilliant scope and their progression is truly infinite. In this chapter, some of the essential applications and current challenges on copolymers were also realized. Finally, an outlook of future work that would benefit the field was addressed.

Keywords Backbone · Copolymers · Free radicals · Monomers · Polymerization · Surface modification

8.1 Introduction

Grafting is an attractive approach to impart a variety of functional groups onto a polymer. Thus, many amendment practices have been shown to increase the inherent properties of the conventional polymer backbone under required conditions (Ito and Nagai 2007; Goddard and Hotchkiss 2007; Muth et al. 2000). By introducing new reactive sites, the surface morphology of polymers can be tailored to improve certain properties for developing essential products. The incorporation of such

S. Choudhary · K. Sharma · V. Sharma (✉)
Institute of Forensic Science & Criminology, Panjab University, Chandigarh, India
e-mail: vsharma@pu.ac.in

V. Kumar
Department of Physics, National Institute of Technology Srinagar, Jammu and Kashmir, India

reaction sites makes them hydrophilic or hydrophobic, and provide chemical and thermal stability to the acid-base attack (Lv et al. 2008; Kalia and Kaith 2008a). This method modifies the structure-property relationship such as chemical reactivity, elasticity, glass transition temperature (T_g), melting temperature (T_m), permeability and solubility by combining natural and synthetic polymers through graft copolymerization based on the specific requirements (Moreira et al. 1997; Fares et al. 2003; Kaith and Kalia 2008a, b).

Graft copolymerization modifies the vinyl monomers in the biopolymer backbone to incorporate favorable properties, while maintaining their required properties such as biodegradability, saline retention/water and thickening (Zohourian 2005). In this chapter, different grafting methods are analyzed. The two common grafting methods that can be used: (1) single-step grafting, which involves the use of a single monomer and (2) grafting side-by-side, which can occur with the immediate use of two monomers to acquire the essential property (Bhattacharya and Misra 2004). In the first part of this chapter, the different grafting techniques and the key factors, which regulate the grafting have been discussed.

8.2 Polysaccharides

Polysaccharides encompass various advantages over the synthetic polymers, since they are natural biopolymers having characteristics such as bioadhesivity, biocompatibility, biodegradability and nontoxicity, together with their wide availability. On the other hand, simple carbohydrate polymers can also act as defensive substances such as antigenic and immunogenic polysaccharides. Usually, they are of low cost, which is intended for their gradually increasing use in the formation of products for cosmetics, food and biomedical applications. Polysaccharides can also be used as chelators, emulsifiers, encapsulants, flocculants, stabilizers and thickeners (Lapasin and Pricl 1995). These properties making them suitable for applications such as adhesives, fibers, films, hydrogels, melt processing plastics, drug delivery agents and emulsifiers (Haag et al. 2004; Shi et al. 2007; Reis et al. 2006; Liu et al. 2007; Nakauma et al. 2008; Pillai et al. 2009; Bastos et al. 2009). Polysaccharides are also eco-friendly and renewable materials. The hydroxyl groups present on the surface of natural polysaccharides are the main reactive sites for modification to obtain the desirable properties (Jayakumar et al. 2007). Cellulose, chitin, chitosan (Cs) and starch have been modified by many distinctive reactions of hydroxyl groups, such as esterification, etherification, urethane formation, crosslinking with polyfunctional reagents and can also be widely grafted with various vinyl monomers under different reaction conditions (Peniche et al. 2008; Pillai et al. 2009).

Graft copolymer consists of a preformed polymeric backbone with other polymeric chains of different chemical nature linked at many points. According to Stannett (1981) 'graft copolymers comprises of a polysaccharide/polymer

backbone linked through covalent bonds to the side chains'. The grafting method can be used for the modification of chemical and physical properties of polymeric materials. These can be achieved by ionizing or ultraviolet (UV) radiation, or chemical initiators (Chapiro and Jendrychowska-Bonamoury 1980). A copolymer is usually defined when different monomer units are linked themselves in sequence onto the polymeric backbone according to their comparative reactivities. The copolymers are of different types, which can be alternate, random, block and graft copolymers. A random copolymer can be differentiated by the binding of random monomer due to an alternate copolymer, the monomer units are present in an ordered form. Block copolymers consist of the sections of different terminally grouped monomers and the graft copolymers are those to which polymeric chains are attached by covalently linked side chains at different sites on the backbone (Stannett 1981). The side by side addition of binary monomers is called mosaic grafting. Alferey and Bandel (1951) introduced the first graft copolymer of vinyl acetate in the presence of styrene and vinylidene chloride. The graft copolymerization of several natural polymers such as casein, silk and soya protein have been reported (Freddi and Tsukada 1996; Kaith et al. 2011; Liu et al. 2004). The grafting with vinyl monomers with different side chain generates active sites onto the polymer backbone which in turn effectively change its chain bulkiness, flexibility and polarity. This technique can be reviewed as an influential tool to improve the functional and physicochemical properties that are appropriate for technological applications (Arai 1973; Maclaren and Milligan 1981).

8.3 Grafting Techniques

There is a high amount of conventional methods for the preparation of graft copolymers such as biochemical (ensymatic), chemical, photochemical and physical (plasma-induced) techniques, which are reliable.

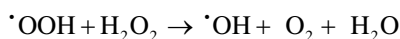
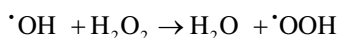
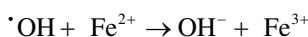
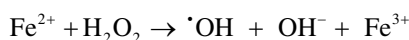
8.3.1 Chemical Methods

The chemical graft copolymerization can be performed laterally with the help of free-radical generators such as ammonium persulfate (APS), azobisisobutyronitrile (AIBN), ceric ammonium nitrate (CAN), dibenzoyl peroxide, potassium permanganate (KMnO_4), potassium persulfate (KPS - $\text{K}_2\text{S}_2\text{O}_8$) and Fenton's reagent like redox systems to initiate free radicals on the backbone (Shah et al. 1994; Zahran and Mahmoud 2003; Shih-Tong Hsu and Ting-Chung Pan 2007; Kumari et al. 2010). Several researchers have reported that Lewis acids, strong bases and metal carbonyls can also act as redox initiators for chemical grafting.

8.3.1.1 Initiators for Chemical Grafting

8.3.1.1.1 Ferrous Ammonium Sulfate (FAS)/Hydrogen Peroxide (H₂O₂) Initiation

Fenton's reagent (Fe²⁺/H₂O₂) is an economical and easily accessible redox initiator. For example, Fenton's reagent has been used as a redox initiator in the graft copolymerization of methyl methacrylate (MMA) onto Cs, or the graft copolymerization of cellulose sawdust and acrylonitrile (AN)/acrylamide (AM) (Richards 1961a; Lagos and Reyes 1988; Wang et al. 2001; Wang et al. 2002). Rice husk and methacrylic acid (MAA) can also be copolymerized by using Fenton's reagent (Hsu and Pan 2007), while the psyllium mucilage (a medically important natural polymer) was also grafted with acrylic acid (AA) using FAS/H₂O₂ as a redox initiator and glutaraldehyde as a crosslinker (Kumari et al. 2010). Graft copolymerization of AN onto sodium alginate (NaAlg) was also done by Shah et al. (1994) in the presence of FAS/H₂O₂ as redox initiator. The H₂O₂ molecules counter ferrous (Fe²⁺) ions, and therefore, ferric (Fe³⁺) ions and primary hydroxyl radicals are formed as given below:



The use of new redox systems has been reported for the fusion of the anticipated properties by graft copolymerization of various vinyl monomers, such as MMA onto cellulosic fabrics through the potassium peroxydiphosphate-metal ion-cellulose thiocarbonate redox initiator system (Zahran and Mahmoud 2003) or AA-copolymerized flax fibers with AA using citric acid/Mn⁴⁺ redox system (Zahran and Rehan 2006).

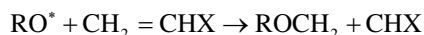
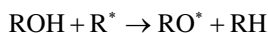
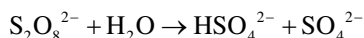
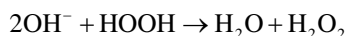
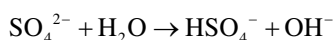
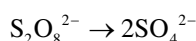
8.3.1.1.2 Ceric Ion Initiation

Ceric ion-based graft copolymerization offers many advantages due to its high grafting efficacy with less homopolymer formation. Alcohols, aldehydes, amines, glycols and thiols can act as organic reducing agents when they are reacted with nitrate and sulfate-based salts, which form operational redox systems. The generation of ceric ions and transient free radical species occurs due to their oxidation-reduction reaction which is proficient competent for initiating vinyl polymerization. The oxidation of ceric ions continues *via* a single electron transfer by forming macroradicals on the reducing agents (Mino and Kaizerman 1958). For example, the

poly(acrylamide) (PAM) grafting onto the silica surface was performed by Tsubokawa et al. (1989) by the reaction of a ceric ion with alcoholic hydroxyl, amino or mercapto groups through redox polymerization. Styrene polymerization was investigated by Iwakura et al. (1965) in an oil-soluble ceric salt-alcohol redox system on cellulose polymers for free radical graft copolymerization.

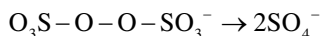
8.3.1.1.3 Persulfates

Graft polymerization commonly use APS, KPS or ferrous as initiators. The heating of the aqueous solution of persulphate decomposes into sulfate radical together with free radical species as follows (Xie et al. 2002).



where R-OH = polysaccharide and R = free radical species.

Persulfate ion is the main source for the creation of active sites, and this helps oxidation of various inorganic and organic molecules and free radical initiates. The sulfate-free radical (SO^+) is formed by a simple O-O bond scission (Walling 1957).



The sulfate free radical can oxidize and polymerize organic substances at high temperature (Merz and Waters 1947; Ikada et al. 1974). For example, Khalil et al. (1993) grafted corn starch was grafted with AM by using KPS as initiator, while Retuert and Yazdani-Pedram (1993) used KPS as a redox initiator for graft copolymerization of Cs. Previously, Yazdani-Pedram et al. (1992) observed that the effectiveness of KPS as an initiator can be radically improved by consuming FAS as a reducing agent in the graft copolymerization of MMA onto chitin.

KPS is a water-soluble free radical initiator. With this in mind, Liu and Sun (2008) reported the free radical graft polymerization process to functionalize the cotton cellulose surface. In line with this, Retuert and Yazdani-Pedram (1993) also used organic (ammonium oxalate - $(\text{NH}_4)_2\text{C}_4\text{H}_4\text{O}_6$ and ammonium tartrate - $(\text{NH}_4)_2\text{C}_2\text{O}_4\text{H}_2\text{O}$) and inorganic co-catalysts (CuCl_2 and MnCl_2) in combination

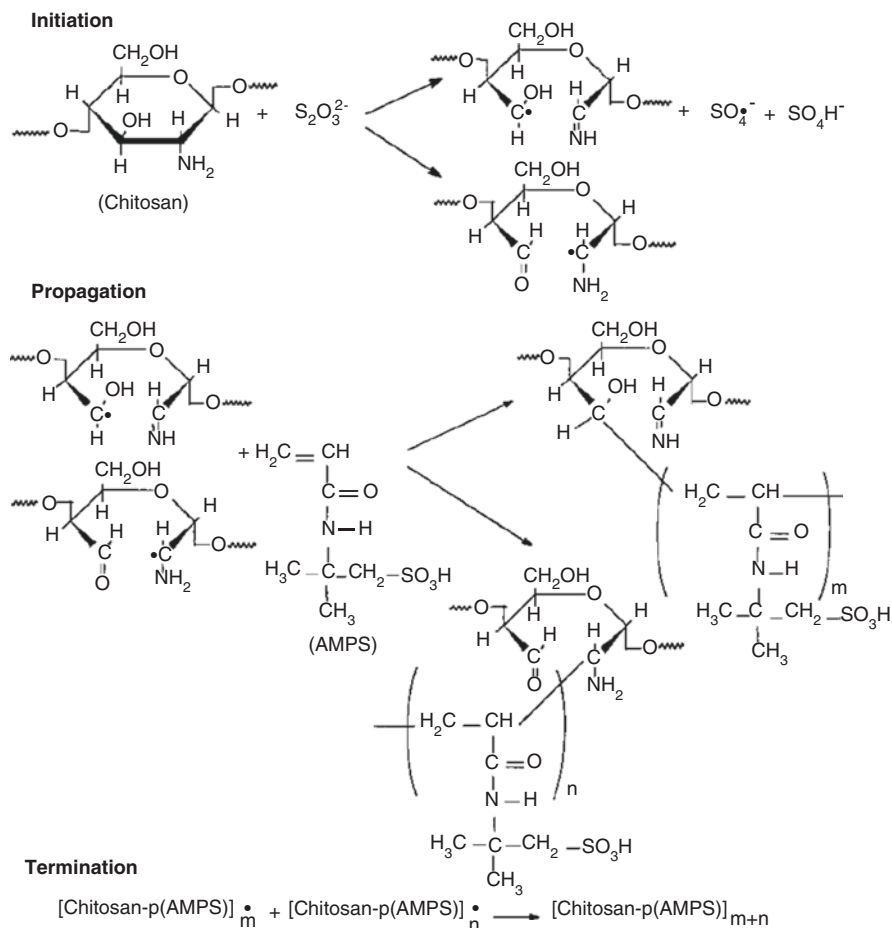


Fig. 8.1 Mechanism of the graft copolymerization of AMPS onto Cs. Reproduced with permission from Najjar et al. (2000)

with MMA and methyl acrylate (MA) by using KPS only as a redox initiator for graft copolymerization onto Cs. Najjar et al. (2000) also successfully grafted 2-acrylamido-2-methylpropane-sulfonic acid (AMPS) onto Cs through the use of KPS as a redox initiator in a homogeneous solution (Fig. 8.1).

The chemical modification of starch through vinyl graft copolymerization is an influential method for improving starch properties. Several authors have used a binary redox initiator pair such as CAN and KPS for grafting MMA onto sago starch as a new backbone (Fig. 8.2) (Mostafa 1995; Fakhru'L- Razi et al. 2001). Persulfate/ascorbic acid have also been used by Singh et al. (2006b) as the initiator for MMA grafting onto guar gum under atmospheric oxygen at 35 °C (Fig. 8.3).

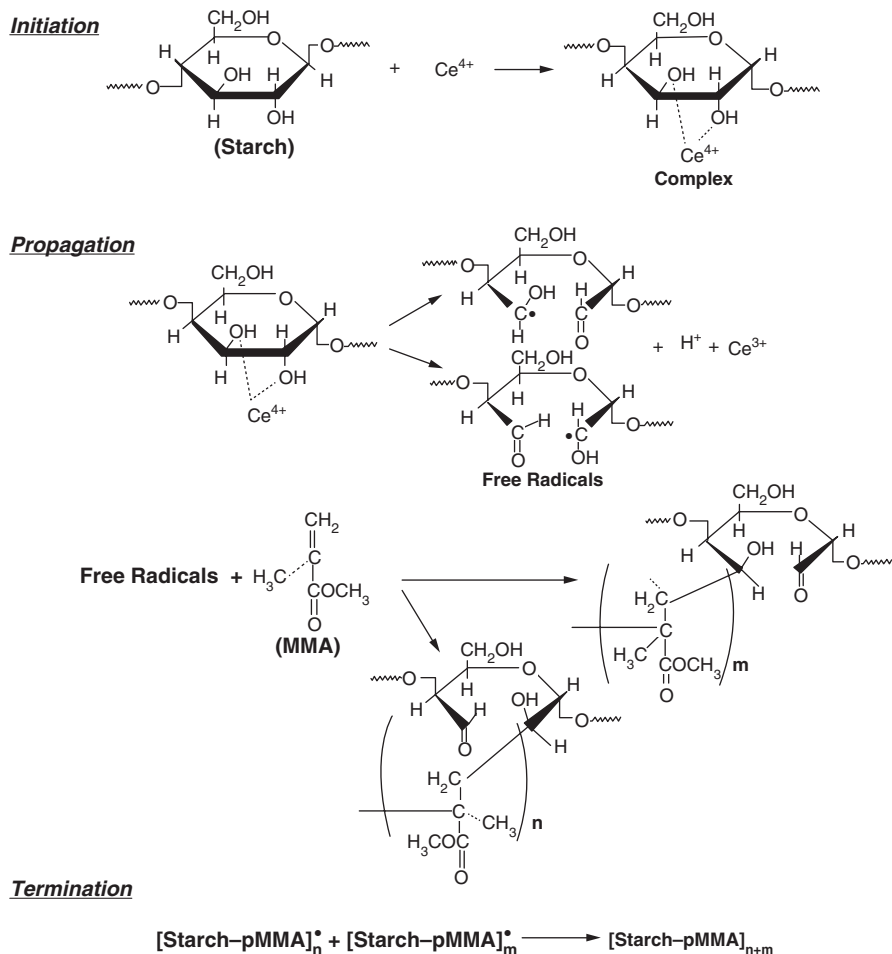


Fig. 8.2 Reaction mechanism for poly(methyl methacrylate) (PMMA) grafting onto sago starch using CAN as an initiator. Reproduced with permission from Fakhru'L- Razi et al. (2001)

8.3.1.1.4 Ceric Ammonium Nitrate (CAN)

Zhang et al. (2003a) proposed that electrically neutral and the zwitterionic interfacial molecular structures improves biocompatibility of these materials. This could be achieved by directly grafting zwitterionic vinyl monomer (*N,N*-dimethyl-*N*-methacryloyloxyethyl-*N*-(3-sulfopropyl) ammonium - DMMSA) on the surface of the cellulose membrane in the presence of CAN. Huang and Xu (2010) also used zwitterionic vinyl monomer to graft the poly(urethane) (PU) membrane surface by using [2-(methacryloyloxy)ethyl]-dimethyl-(3-sulfopropyl)-ammonium hydroxide

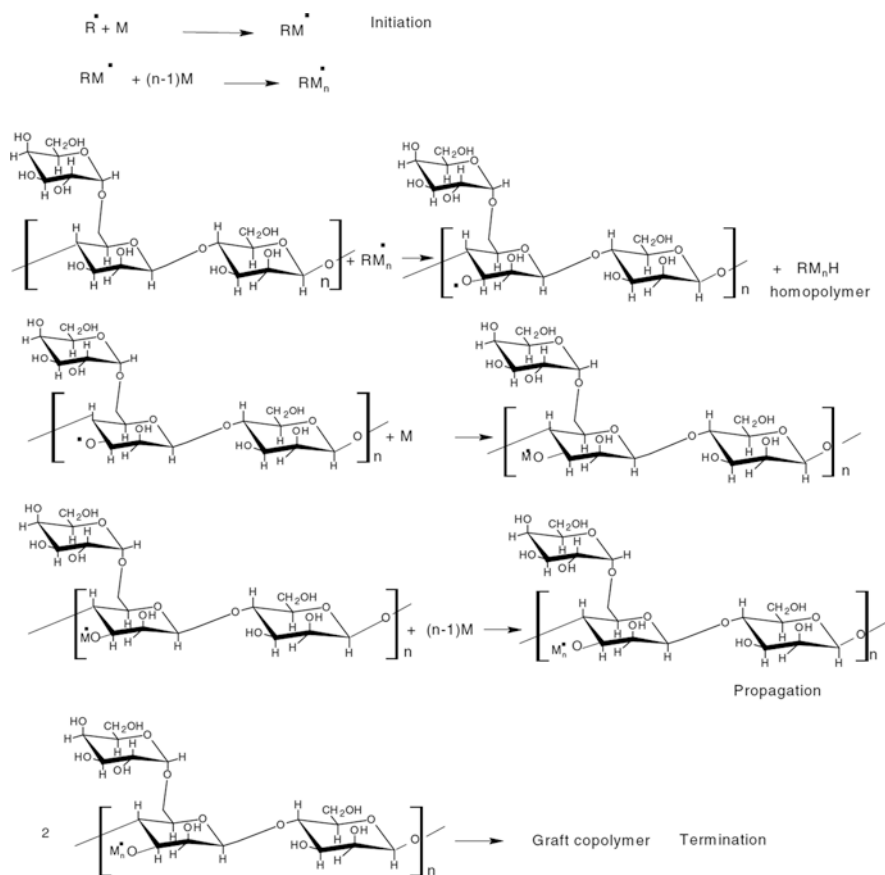


Fig. 8.3 Graft copolymerization initiated by primary radicals given by redox initiator. Reproduced with permission from Singh et al. (2006b)

(MEDSA) and N,N' -methylene bis-acrylamide (MBA) as crosslinking agents *via* Ce^{4+} ions-induced graft copolymerization on the PU membrane through the poly(ethylene glycol) (PEG) reactive species, which allowed graft copolymerization. The progress of grafting has been depicted in Fig. 8.4 (Huang and Xu 2010). First, the PU surface was activated by diisocyanates, and PEG was then grafted onto PU surfaces by the reaction of hydroxyl groups with isocyanate. In the last step, the stable activated surface was achieved by the graft copolymerization (Fig. 8.4) (Huang and Xu 2010).

Zhang et al. (2006b) investigated the grafting of zwitterionic DMMSA monomer onto Cs using CAN as an initiator in acetic acid solution. In the same lines, Caner et al. (1998) reported the efficient copolymerization of Cs on poly(4-vinylpyridine) by using a ceric ion initiator under homogeneous conditions in 1% acetic acid solution. A similar study was carried out by Liu et al. (1993) for graft copolymerization of MA onto potato starch by using CAN as initiator.

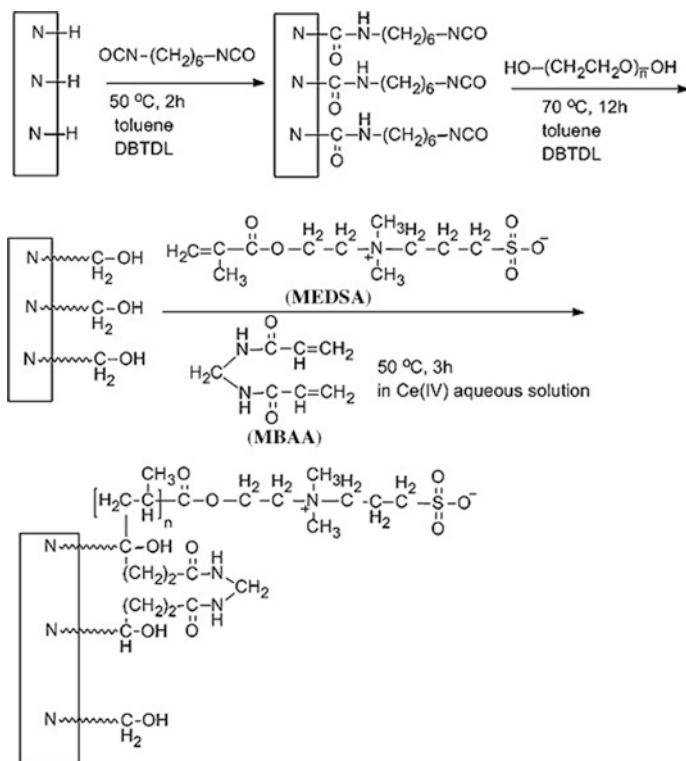


Fig. 8.4 Procedure of grafting MEDSA onto PU membrane surface. Reproduced with permission from Huang and Xu (2010)

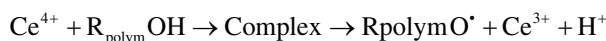
8.3.1.2 Types of Reaction Mechanisms for Chemical Grafting

8.3.1.2.1 Free-Radical Grafting

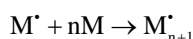
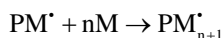
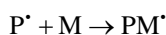
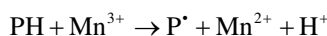
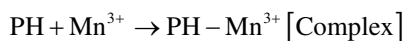
In this grafting process, initiator generated free radicals are moved to the substrate to react with the monomer to build the graft copolymers by direct or indirect methods (Mishra et al. 1984). When H_2O_2 , KPS, Fe^{3+} , Cu^{2+} , etc. are used instead of H_2O_2 in combination with sodium bisulphite, the thiosulphate can be produced as reducing agent in the same electron transfer reaction. In this sense, Bajpai et al. (1990), studied the chain reaction mechanism of peroxydisulphate/ascorbic acid catalyzed by Ag^{2+} , which generated the sulphate ion radicals, which act as chain carriers. Pradhan et al. (1982) also indicated that the formation of metal ions leads to the generation of free-radical sites, which may be necessary for grafting. In addition, peroxide groups can be grafted from cellulose and poly(vinyl alcohol) substrates by treating with H_2O_2 , thus having the ability to initiate thermal photografting onto the vinyl monomer (Kubota and Ogiwara 1978; Ogiwara et al. 1979).

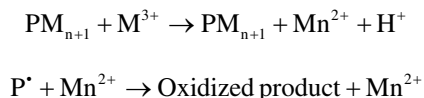
On the other hand, the use of diazonium salts in the grafting processes using AA, MAA and *N*-vinylpyrrolidone monomers, initiates the chain reaction mechanism and avoids the formation of homopolymers (Richards 1961b; Simionescu and Opera 1972). There is another reaction mechanism in which Ce^{4+} ions initiate the grafting of cellulose by forming complexes at C2 and C3 carbons of the anhydroglucose unit of cellulose. In this redox system, the cerium salt (Ce^{4+}) act as a predominant oxidizing agent, since cellulose itself functions as a reducing element. The dynamic centers were generated onto the cellulosic chain and no changes in the allocation of essential elements for the formation of the cellulose graft copolymer. In addition, the acid medium or dimethyl sulfoxide (DMSO) improves the chelation of Ce^{4+} ions with the -OH groups of C2 and C3 carbons of the anhydroglucose unit of cellulose. The electron transfer is produced from cellulose, and the Ce^{4+} ions form Ce^{3+} ions, which are disassociated from the chelate. The anhydroglucose ring scissions occur between C2 and C3 carbons, thus forming a short-living radical (Halab-Kessira and Ricard 1999; Lin et al. 2005; Nada et al. 2008; Tosh and Routray 2011).

Another mechanism for free-radical grafting is oxidation induced by transition metals (e.g. Ce^{4+} , Cr^{6+} , V^{5+} , Co^{3+}), in which are generated macroradicals on the polymeric backbone. In this regard, the grafting efficiency is affected by the redox potential of the metal ions. The low oxidation potential is associated with the greater grafting efficiency. The formation of transition chelates between metal ions and polymers can, for example, occur through the OH- groups of the polymer main chains to form complexes with ceric ions, which are further decomposed to generate free radicals through an electron transfer.



The permanganate ion (MnO_4^{-}) under acidic medium dissolves and form Mn^{3+} ions by means of Mn^{4+} . These Mn^{3+} ions are very reactive to initiate graft copolymerization and homopolymerization (Mohrana et al. 1991).





As can be concluded from the above reactions, the high potential of the metal ions causes them to react with the monomers and leads to high homopolymerization. Thus, to avoid this result, preference should be given to the metal ions with low oxidation potential or metal chelates. The role of metal chelates is shown in Fig. 8.5 (Misra et al. 1980).

It is clear from the previous results that heating breaks the metal-oxygen bond, which decomposes even more in the free radical species responsible for graft copolymerization and homopolymerization. This also through an electron transfer process. Few compounds can generate free radical species in the heating effect are azo compounds, hydroperoxides, peroxides and peroxide diphosphate, etc. (Bhattacharya and Misra 2004). In this perspective, Tsubokawa et al. (1999) reported that the azo groups from the organic pigment promoted the copolymerization of vinyl monomers by means of an irradiation grafting mechanism (Fig. 8.6).

On the other hand, the grafting efficiency of the polymer backbone can be improved by a pretreatment method such as diazotization, ozonation and xanthation (Kubota and Ogiwara 1980).

8.3.1.2.2 Grafting Through ‘Living Polymerization’

The term ‘living polymerization’ was introduced by Szwarc (1956) because the chain ends remain lively until killed. Prior to this, Flory (1953) explored some properties that were linked related with alkoxide-initiated living polymerization on ethylene oxide. This author found that there was a successful growth at the chain ends, and the concentration of initiator determined the molecular weight (Mw). Living polymerization technique provides high degree control over the structural design of the polymer chains. The anionic polymerization of styrene, dienes and ethylene oxide requires initiator and monomer for a biddable living polymerization. The more complex routes are necessary to retard the chain transfer and termination. Living polymerization uses initiators, catalysts and chain-end stabilizers. In this method, the initiator promotes the chain end growth by bonding themselves to the non-growing chain end. The catalyst act as Lewis acid and base and is essential for initiation and propagation, but does not run out. It is essential to achieve Mw control, that the initiation step is faster than or proceeds at the same rate as chain reaction mechanism proceeds. If the propagation rate is faster than the initiation rate, the formation of the first chain is longer than the last formation of chains. The living polymerization system works best if there is a high monomer concentration. The living polymerization is given by the following types:

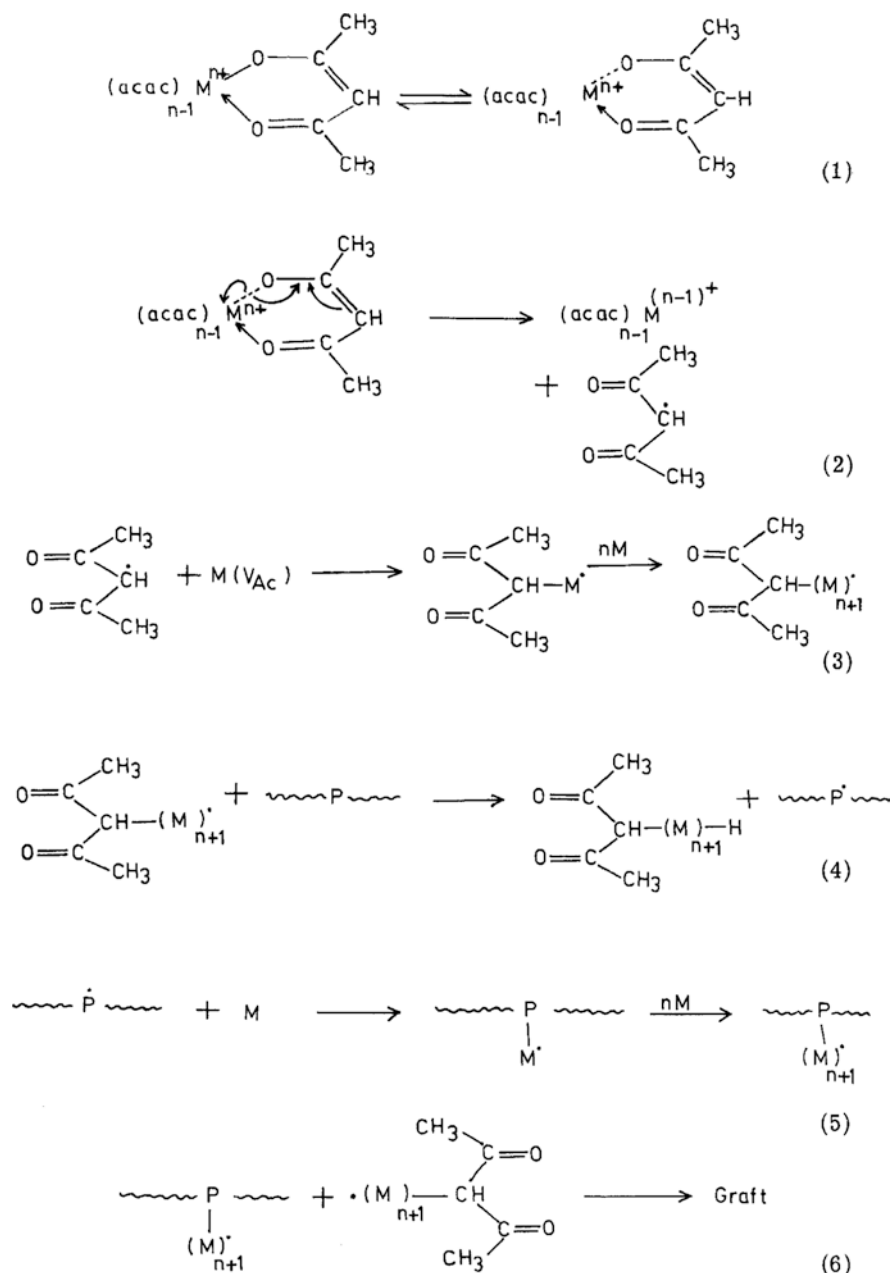


Fig. 8.5 Schematic representation of metal chelates initiated for graft copolymerization. Reproduced with permission from Misra et al. (1980)

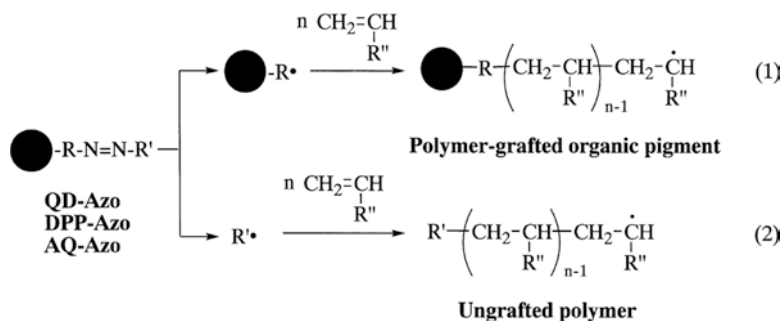


Fig. 8.6 Organic pigments (AQ: anthraquinone, DPP: diketopyrrolopyrrole, QD: quinacridone) promoted copolymerization of vinyly monomers through the irradiation grafting mechanism. Reproduced with permission from Tsubokawa et al. (1999)

8.3.1.2.3 Living Anionic Polymerizations

The various classes of monomers, such as acrylates, butadiene, hexamethylcyclotrisiloxane, lactones, methacrylate and styrene, which give rise to living anionic polymerization reactions. The monomers from styrene and substituted styrene with non-base sensitive groups have been studied to the maximum for living polymerization (Szwarc 1968). Teyssié et al. (1990) studied butyl lithium and sodium naphthalene as exceptional initiators for initiation process, and explained that living polymerization works very effectively when there is a subsequent accumulation of lithium chloride counterparts at each chain end, which allows living polymerization at temperatures up to -20°C . The previous study was further elucidated by Reetz et al. (1988). These authors revealed that by simply replacing the counterion of lithium to tetrabutylammonium, there is a significant increase in the chain end stability.

8.3.1.2.4 Living Cationic Polymerizations

Living cationic polymerization is more multifaceted than its anionic equivalent. The electron-rich monomers initiated by the carbenium ion chain ends with a robust protic acid that readily allocate beta-protons to start a new chain, resulting in a lower Mw (Kennedy and Marechal 1982), while the initiators mediated by tertiary esters (Faust and Kennedy 1986), ethers (Mishra and Kennedy 1987) through extra BCl_3 act as a catalyst, which provides true living polymers. The additional use of Lewis acid gives the best results. The addition of a smaller amount of external electron donor in tertiary chloride initiators is responsible for living polymers. This polymerization process of propylene oxide and epichlorohydrin can also be initiated with a strong alcohol and acid catalyst (Penczek 1988; Kaszas et al. 1990).

8.3.1.2.5 Living Covalent Polymerizations

The number of electrophiles and nucleophiles initiated and propagated by the action of a responsive covalent end group with monomer are classified as living covalent polymerizations. The living covalent polymerization of oxazolines was initiated by methyl iodide. The polymerization mechanism changes when oxazolines are polymerized by the tosylate rather than alkyl iodide. The nucleophilic I⁻ (iodide ion) is highly capable to exposing the ring and redeveloping an alkyl-iodide end group (Saegusa et al. 1973).

8.3.1.2.6 Living Free-Radical Polymerizations

Currently, there is no true living free-radical polymerization. Several researchers have worked on this problem and resulted in an operational technique with the purpose to generate a free radical-capped agent that will not initiate new chains, but that can react with the free-radical chain ends and provide block and end-functional polymers (Bledzki et al. 1983; Otsu et al. 1989). The polymerization process is restarted when this capped polymer is heated with a fresh monomer and is abundantly worked to provide block and end-functionalized polymers. Solomon et al. (1986) described the use of nitroxides as capping radicals in living free-radical polymerization mechanism. On the other hand, Sonmez et al. (2003) investigated the AM grafting *via* ATRP in which the initiation occurred through the formation of radicals in a redox reaction of *N*-chloro sulfonamide groups with copper (I) bromide (Fig. 8.7).

This ATRP-mediated precise living radical polymerization method helps to increase the versatility of macromonomers by increasing the number of monomers and making them available for the processing of macromonomers. Carlmark and Malmstroem (2002) modified the filter paper by immobilizing 2-bromoisobutyryl bromide by reaction with the OH⁻ group from cellulose backbone. These authors performed an additional graft by immersing the modified filter paper into the reaction mixture containing CuBr, MA, tris(2-(dimethylamino)ethyl)amine (Me₆-TREN) as initiators and ethyl acetate (Fig. 8.8) (Carlmark and Malmstroem, 2002).

Several initiators have been used for living free-radical polymerization, which are formed from the terminator of the initiator-transfer agent, better known as inferters. With this in mind, Peng and Cheng (2001) investigated the use of a photoinferter in order to graft the poly(*N*-isopropylacrylamide) and poly(MAA) (PMAA) on porous PE membranes. These authors found that, under the effect of UV radiation, xanthone was converted into xanthone ketyl radical by abstracting hydrogen atom (Peng and Cheng 2001). Thus, this newly formed radical modified the PMAA chains grafted with terminal xanthone ketyl groups and terminated the chain reaction, which also generated free radical species that showed more PMAA grafting.

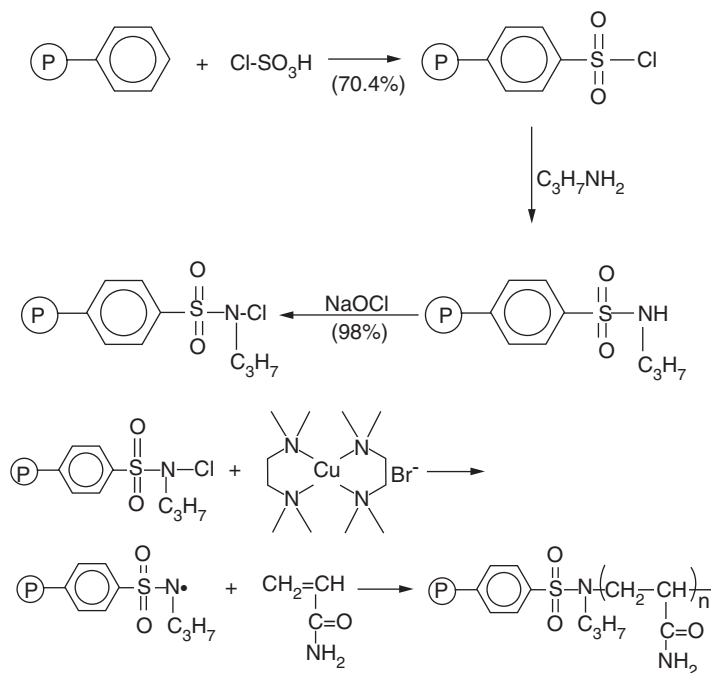


Fig. 8.7 Proposed mechanism for grafting of PAM onto functional poly(styrene-divinylbenzene) resin *via* ATRP. Reproduced with permission from Sonmez et al. (2003)

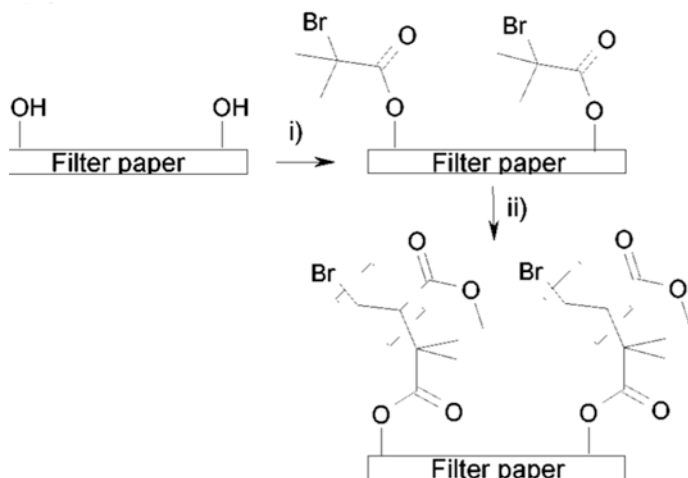


Fig. 8.8 Synthetic pathway for the preparation of the PM-grafted filter papers. Conditions: (i) 2-bromoisobutyryl bromide, 4-(dimethylamino) pyridine (DMAP), CH_2Cl_2 , triethylamine and (ii) CuBr, ethyl 2-bromoisobutyrate, MA, $\text{Me}_6\text{-TREN}$. Reproduced with permission from Carlmark and Malmstrom (2002)

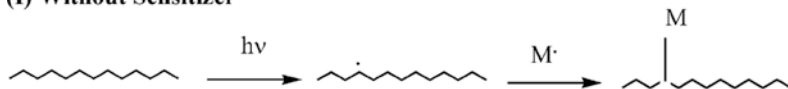
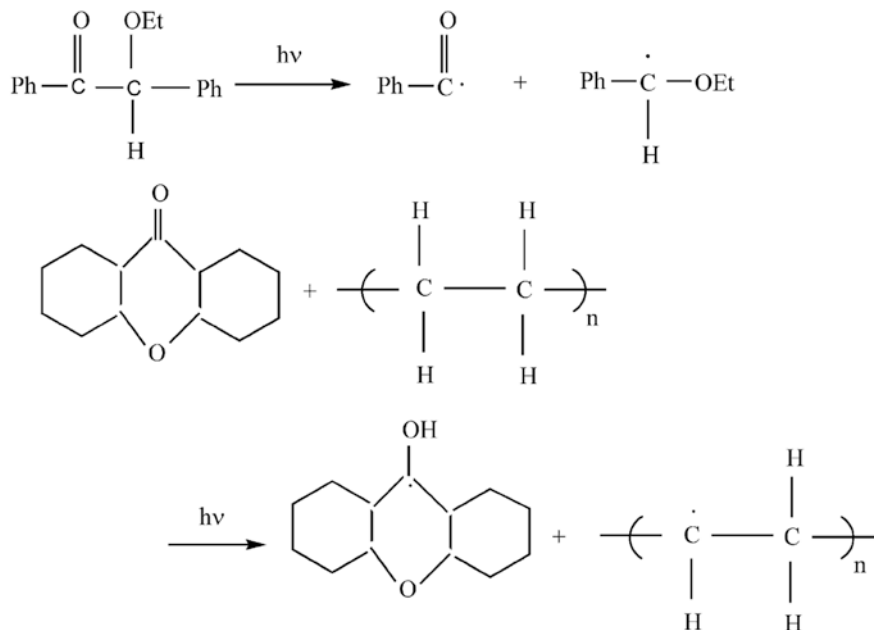
(I) Without Sensitizer**(II) With sensitizer**

Fig. 8.9 Mechanism for the method of photochemical grafting. Reproduced with permission from Bhattacharyya and Misra (2004)

8.3.2 Physical Methods

This grafting method is initiated by the excitation of macromolecules by adsorbed radiation, and then reactive free radicals are produced. Sometimes, the reactive free radical is not generated through the breaking of the bond by radiation absorption, therefore, photosensitizers such as acrylate azo dyes, aromatic ketones or metal ions must be added to promote the process. The photochemical grafting can thus be processed with/without a sensitizer (Bellobono et al. 1981; Peng and Cheng 2001; Kubota et al. 2001). Grafting polymerization without sensitizer generates active sites on the backbone which counters the monomer free radical species to modify the surface properties of the base polymer. In contrast, the sensitizer initiates free radicals which pass-through diffusion, so that they produce radical sites essential for grafting by extracting hydrogen atoms from the base polymer (Fig. 8.9) (Bhattacharyya and Maldas 1983).

Photopolymerization can control the the Mw distribution (MWD or polydispersity index - $PDI = \text{weight-average apparent molecular weight } (M_w) / \text{number-average apparent molecular weight } (M_n)$) by varying the intensity of the radiation. The spatial control of photopolymerization helps in the confinement to local regions. The initiation of primary radicals by the method of photochemical production occurs at a very low temperature, i.e. is independent of temperature. Therefore, branching of the macromolecule *via* chain transfer is absent (Fox et al. 1958). The photopolymerization offers the activation of certain monomers at low temperature, i.e. they are polymerized at varying ceiling temperatures (Dainton and Ivin 1958). The first technique used to polymerize vinyl monomers through photopolymerization was to discover the monomer to sunlight. This polymerization method played an important role in the development of polymer chemistry.

8.3.2.1 Plasma Radiation-Induced Grafting

Plasma radiation-induced grafting has gained a lot of attention in recent years. This grafting mechanism offers the same possibilities that ionizing radiation through the slow discharge (Yamaguchi et al. 1994; Wenzel et al. 2000). The central process in the plasma-induced grafting includes electron-induced excitation, ionization and dissociation. The polymer molecule under plasma radiations forms macromolecule radicals. The accelerated electrons from breaks the chemical bonds in the polymer structure which initiate the graft copolymerization. This is a competent technique to amend the surface chemistry and morphology of various polymeric materials by treating them in the presence of specific gases, such as Ar, H, N and O (Inagaki 1996). Depending on the nature of the gases, the active species generated can trigger and alter the polymer chemistry (Gupta et al. 2001; Gupta et al. 2008; Shen et al. 2008). The plasma treatment is restrained to the depth of a few nanometers below the surface of the polymeric material. This interesting aspect provides the options to produce a wide spectrum of surface chemistry with the desired composition material. By controlling the external factors in plasma-induced grafting, the desired functionality and morphology of the surface can be produced (Gupta et al. 2000b).

8.3.2.2 Irradiation-Induced Grafting

The graft copolymerization with high energy radiation is a highly competent method to generate free radicals and does not cause any additional contamination related to chemical initiators (Khalek and Mahmoud 2011). In this sense, different fields are using a series of cationic starches (Khalil and Aly 2001), which can be formed by the reaction of unsaturated monomer (ethylene) having cationic groups under the influence of gamma irradiation (Carr 1994). In addition to this, the simultaneous radiation grafting method also helps in the production of corn starch copolymers from binary monomers of AM/dimethyl diallyl ammonium chloride (AM/DMDAAC) (Lv et al. 2013). Other water-soluble vinyl monomers, such as AA and

AM, can for example also be grafted by a preirradiation method onto isotactic poly(propylene) (PP) (Mehta et al. 1990). The gamma-irradiated graft polymerization of jute (unbleached) surface with *n*-butyl methacrylate and phosphoric acids can act as adsorbent remove heavy metals from industrial wastewater (Hossain et al. 2014). Singh and Vashishtha (2008) also used gamma-irradiation induced graft copolymerization to modify the sterculia gum polysaccharide with AA and 2-hydroxyethylmethacrylate (HEMA) to develop crosslinked hydrogels destined for the controlled release of ornidazole (antidiarrheal model drug) through the non-Fickian diffusion mechanism. Singh and Kumar (2008) also developed hydrogels based on psyllium mucilage-NVP crosslinked under gamma radiation with the aim of obtaining drug delivery devices. The binary monomers of AA and vinyl-imidazole (VI) were also grafted by Naguib et al. (2003) onto PP films using gamma-radiation, resulting in improved dye and moisture absorption capacity. Similarly, Mahmoud and Abdel (2012) grafted different natural polymers such as tara gum using AA, and were irradiated in the presence of a crosslinking agent (MBA). Simultaneous grafting of starch and natural rubber latex by irradiating with gamma radiation, and initiated by a cobalt-60 source was also reported by Iskandar (2011).

On the other hand, high-energy radiation induced by the graft sometimes interferes with the mechanical properties of the polymers, but the deterioration of the mechanical properties when using the UV irradiation technique is slight. Shanmugapriya et al. (2011) grafted AA onto Cs using the CAN and nitric acid (HNO₃) redox system.

8.3.2.3 Microwave (MW) Energy-Induced Initiation

The MW-assisted graft copolymerization is more attractive and eco-ecological. This type of grafting limits the use of lethal solvents, decreases the response time confirmed by the high product yield and has less formation of side products. MW radiation causes the cleavage of polar bonds by selective excitation, which further generates free radicals on the polymeric backbone (Mishra et al. 2014).

This type of grafting is given without any radical initiators or catalysts. With this in mind, Singh et al. (2004a, b) grafted the poly(acrylonitrile) (PAN) onto guar gum in the presence of water under MW radiation. The maximum percent grafting (%G) was approx. 188% for 1.66 min, and was obtained under controlled reaction conditions (Singh et al. 2004a, b). The grafting of linear low-density poly(ethylene) (LLDPE) films were also performed using AM, resulting in higher yield, and the grafting was produced in a very short time (Gupta et al. 2000a). Mishra and Sen (2011) also studied the MW radiation time and monomer (MMA) concentration on guar gum, and observed that highest %G was achieved by applying MW radiation. NaAlg was also modified by Akin and Isiklan (2016) using AIBN and *N,N'*-dimethylacrylamide (DMAAm) as initiator and monomer, respectively, under MW radiation conditions.

MW-induced grafting also has advantageous properties, including the formation of active sites, which are obtained by cleavage the O-H bonds, which are required to

achieve the growth chain (Gabriel et al. 1998; Mishra et al. 2011). Some examples are given in Table 8.1.

Liu et al. (2005) discussed the MW-assisted copolymerization of caprolactone and Cs by using phthaloyl. Cs was used as a precursor and Sn(Oct)₂ as a catalyst without using any solvent (Fig. 8.10). The Cs-*g*-poly(ϵ -caprolactone) (PCL) copolymer obtained with increased hydrophobic units and free amino groups was intended as degradable amphoteric material with potential for various biomedical applications.

8.3.3 *Enzymatic Methods*

This technique is quite innovative and involves the use of an enzyme for initiating the grafting. Enzymatic copolymerization has gained a lot of attention since grafting occurs without disrupting the backbone. However, medium reaction conditions and a very precise surface modification. Enzymatic modification against natural products has been used for various industrial applications (Chen et al. 2000). For example, Kumar et al. (1999) grafted the chlorogenic acid (hydrophilic compound and phenolic substrate) onto Cs in presence of tyrosinase under basic conditions in order to obtain a water-soluble copolymer. The phenolic substrate was converted into O-quinone which reacted further with the Cs amino group to form a graft copolymer with the help of the enzyme tyrosinase (Kumar et al. 1999).

8.4 Graft Copolymerization Using Different Monomers

To date, several grafting strategies have been explored to transform the various chemical and physical properties of natural polymers, such as:

8.4.1 *Grafting of Acrylic Acid Monomers*

Grafting with vinyl monomers such as AA and ethyl methacrylate (EMA) on starch was done by Taghizadeh and Mehrdad (2006) in an aqueous media in the presence of CAN to prepare a crosslinked network of starch-*g*-poly(acrylic acid) (St-*g*-PAA) and starch-*g*-poly(ethyl methacrylate) (St-*g*-PEMA) copolymers. Jenkins and Hudson (2001) also fabricated the 'grafting-from' approach through which AA was grafted onto the pre-existing base polymer through a free radical mechanism. The free radicals formed on polymer backbone lead to the covalent reaction of the vinyl monomer and propagates a new polymer chain. This chain propagation attributes the formation of new properties of the backbone polymer. The free radical grafting of vinyl and acrylic monomers onto cellulose is shown in Fig. 8.11 (Roy et al. 2009).

Table 8.1 Different polysaccharides and their grafted chains under MW radiation in presence and in absence of catalysts or initiators

Polysaccharide	Grafted chains	Initiators	MW radiation conditions	Solvent	References
Gum acacia	PANI	APS	500 W for 40 s.	Water	Tiwari and Singh (2008)
NaAlg	PAM	–	900 W for 3 min.	Water	Sen (2010)
	PMMA	CAN	800 W for min.	Water	Rani et al. (2013)
	DMAAm	AIBN	500 W	Water	Akin and Isiklan (2016)
Artemisia seed gum	AA	APS	180 W for 3 min.	Water	Zhang (2007)
Cellulose	AA and AM	KPS/STS and MBA	360 W for 8 min.	Water	Bao-Xiu et al. (2006)
	AA, ispAM, MA	CAN/KPS	–	HNO ₃	Matahwa (2007)
Saccharum spontaneum fiber	MMA	FAS/KPS	1200 W for 90 s.	Water	Kaith (2009)
Flax fiber	MMA	–	210 W for 30 min.	Water	Kaith and Kalia (2008a, b) Kalia and Kaith (2008a, b)
	MMA/EA	–	210 W for 30 min.	Water	Kaith and Kalia (2007)
	MMA/AA	–	210 W for 30 min.	Water	Kaith and Kalia (2007)
Cs	AA	Ce ⁴⁺ /MBA	260 W for 30 min.	Water	Huacai et al. (2006)
	AN	–	960 W for 1.5 min.	Water	Singh et al. (2005)
	AM	–	960 W for 1.16 min.	Water	Singh et al. (2006c)
	MMA	–	960 W for 2 min.	Water	Singh et al. (2006d)
PhthaloylCs	CL	Sn ²⁺ octoate	450 W for 12.5 min.	Neat	Liu et al. (2005)
Chitin wishkers	CL	Sn ²⁺ octoate	255 W for 3 min.	Neat	Feng et al. (2009)
Guar gum	AM	–	840 W for 0.33 min.	Water	Singh et al. (2004b)
	AN	–	1200 W for 1.66 min.	Water	Singh et al. (2004a)
	EA	–	1200 W for 15 s	Water	Singh et al. (2009)

(continued)

Table 8.1 (continued)

Polysaccharide	Grafted chains	Initiators	MW radiation conditions	Solvent	References
Cassia marginata	MMA	–	480 W for 40 s.	Water	Singh et al. (2008)
	AN	–	960 W for 80 s.	Water	Singh et al. (2007a)
	AM	–	480 W for 50 s.	Water	Singh et al. (2010a)
Cassia siamea	AN	–	800 W for 120 s.	Water	Singh and Tripathi (2006)
Cassia javanica	AA	–	640 W for 40 s.	Water	Singh et al. (b)
Starch	CAP	Sn(II)-2-ethylhexanoate	3 min.	Pure	Koroskenyi and McCarthy (2002)
Potato starch	AN	APS	1200 W for 70 s.	Water	Singh et al. (b)
	AM	KPS	720 W for 60 s.	Water	Singh et al. (2006a)
Corn starch	SA	KPS/PEGD	80–90 W for 10 min.	Water	Zheng et al. (2005)
Carboxymethyl starch	AM	CAN	900 W for 3 min.	Water	Sen and Pal (2009)
Agar&Carageenan	VP	KPS	1200 W for 120 s.	Water	Prasad et al. (2006)
Xathan gum	AM	APS	1200 W for 100 s.	Water	Kumar et al. (2009)
Xyloglucan	AN	CAN/HNO ₃	150 W for 120 s.	Water	Mishra et al. (2008)
Gellan gum	AM	CAN	480 W for 60 s.	Water	Vijan et al. (2012)
	DMAEMA	APS/MBA	80 W for 60 s.	Water	Karthika and Vishalakshi (2015)
	Poly(itaconic acid)	BPO	20–80 W for 10–60 s.	Water	Karthika and Vishalakshi (2014)
Locust bean gum	AM	CAN	480 W for 60 s.	Water	Kaity et al. (2013)
Neem gum	AM	CAN	100 W for 30 s.	Water	Malviya et al. (2019)
Agar	AM	CAN	800 W for 3 min.	Water	Mishra et al. (2011)
	HEMA	CAN	800 W for 3 min.	Water	Sen et al. (2013)

(continued)

Table 8.1 (continued)

Polysaccharide	Grafted chains	Initiators	MW radiation conditions	Solvent	References
	PAM	CAN	800 W for 3 min.	Water	Rani et al. (2014)
Gum ghatti	PAM	CAN	800 W for 3 min.	Water	Rani et al. (2012)
Psyllium mucilage	PMMA	CAN	700 W	Water	Mishra et al. (2014)
Soya peptone	PAM	CAN	700 W	Water	Mahto et al. (2014)
Aegle marmelos	AM	APS	1000 W	Water	Setia and Kumar (2014)

BPO: Benzoyl peroxide, CAN: Cerium(IV) ammonium nitrate, EA: Ethylacrylate, PDMAEMA: Poly(dimethylamino)ethylmethacrylate, Sn(Oct)₂: Tin octoate, STS: Sodium thiosulphate

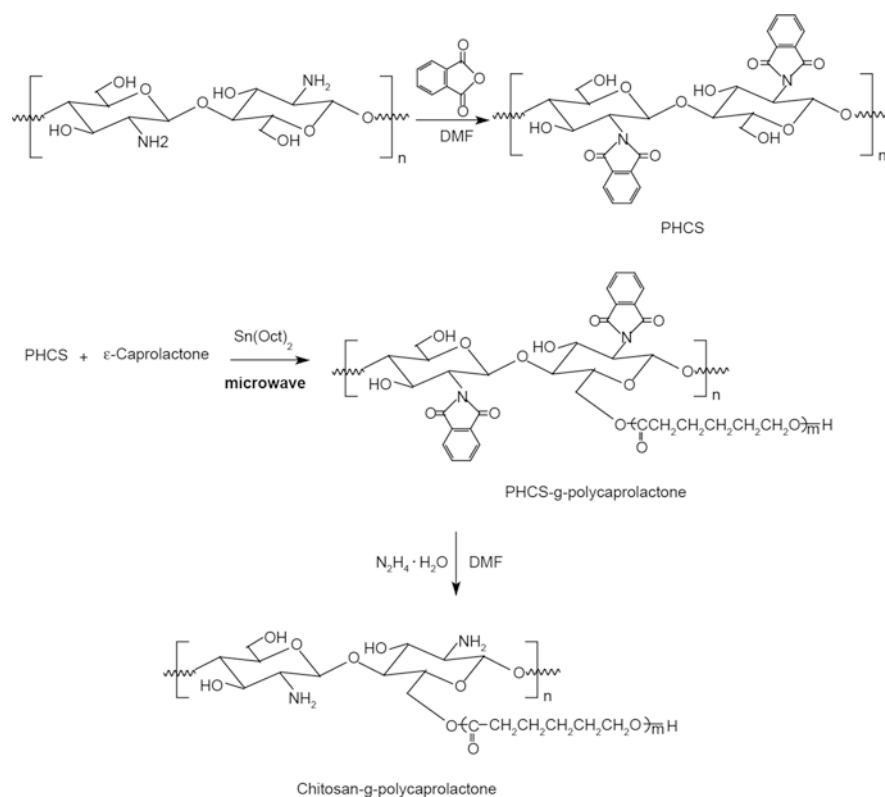


Fig. 8.10 MW-assisted grafting of PCL onto Cs. Reproduced with permission from Liu et al. (2005)

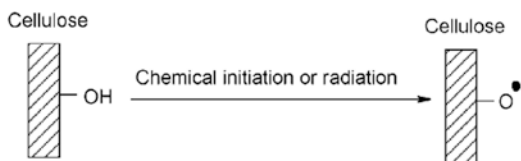
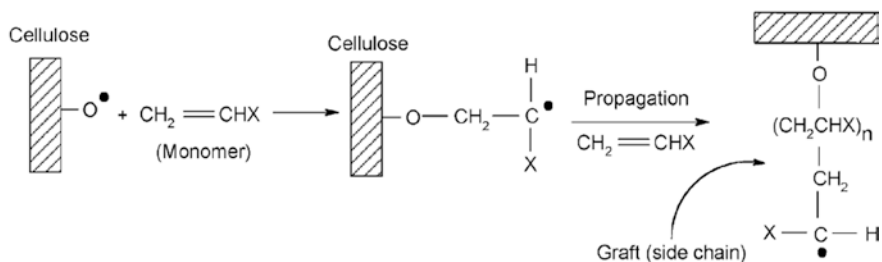
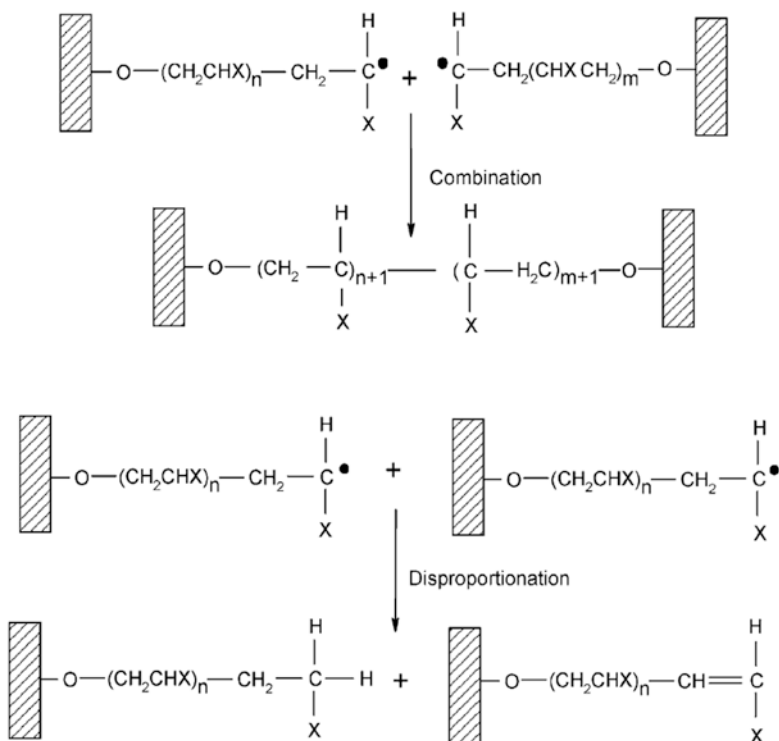
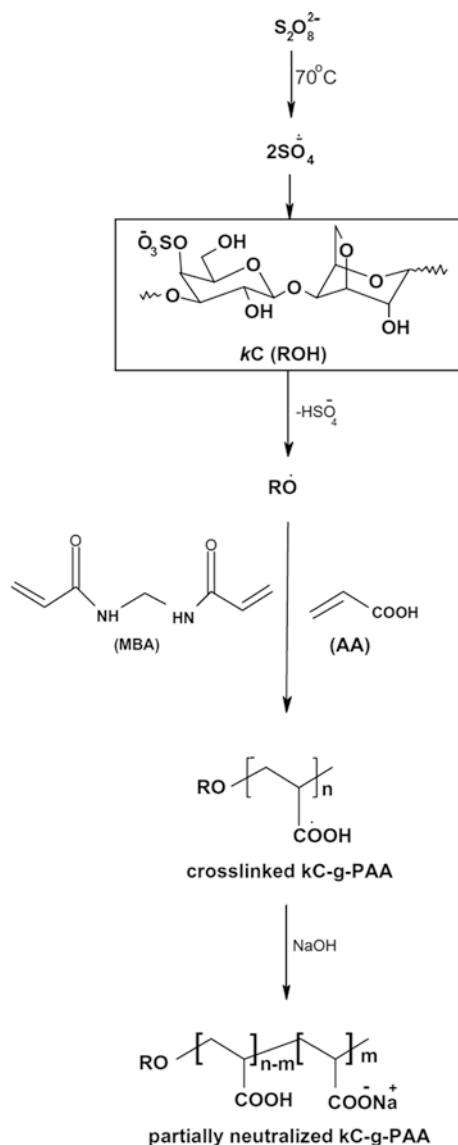
Initiation*Propagation**Termination*

Fig. 8.11 Graphical representation of free radical grafting of vinyl and AA monomers onto cellulose. Reproduced with permission from Roy et al. (2009)

In another study, Athawale and Lele (1998) prepared a crosslinked network hydrogel by grafting vinyl or AA monomer on granular corn starch under a nitrogen atmosphere, thus obtaining a maximum water absorption rate of 250 g/g. Pourjavadi et al. (2004) also synthesized chemically crosslinked superabsorbent hydrogel *via* graft copolymerization of AA onto kappa-carrageenan (kC) using MBA as a crosslinking agent and APS as a free radical initiator (Fig. 8.12).

Fig. 8.12 Grafting of AA onto kC. Reproduced with permission from Pourjavadi et al. (2004)



The Psyllium mucilage was also modified by grafting with AA, using KPS as an initiator and hexamethylenetetramine (HMTA) as a crosslinking agent (Kaith and Kumar 2007). Deshpande (1986) also prepared AA-*g*-Cs copolymers, using CAN and HNO₃ redox system irradiated with UV radiation. In the same lines, Mandal and Ray (2014) synthesized interpenetrating network (IPN) from Cs crosslinked with AA, sodium acrylate and hydroxyethyl methacrylate *via* radical grafting.

8.4.2 Grafting of Acrylonitrile Monomers

Grafting is the method to providing valuable properties to the polymer backbone for the use in designated areas. This can be done by initiating free radicals on the polymer backbone for polymerization of acrylic or vinyl monomers. AN has been the most commonly used vinyl monomer for grafting due to its higher grafting efficiency (Fanta and Doane 1986). For example, Fanta et al. (1987) reported the grafting of AN onto wheat straw using the ferrous sulfate (FeSO₄)/H₂O₂ mixture as an initiator system, resulting in a PAN yield from 30 to 35% *via* polymerization of the wheat straw-*g*-PAN network. In addition, the final product formed had both water absorption and coagulation properties (Fanta et al. 1987).

On the other hand, the phenoxy radical accelerates the manufacturing process of the graft copolymer to the AN monomer, due to the generation of free radical donors to the neighboring molecule (Kislenko and Berlin 1996; Kislenko and Oliinyk 2003). In this manner, the grafted chain commonly grows depending on the reaction conditions provided. The termination is the last step where the free radical AN is associated and forms a graft copolymer. For example, Farag and Al-Afaleq (2002) grafted the AN monomer onto the delignified cellulose in order to obtain water adsorbing materials. Bhatt et al. (2011) also explored and described the different properties of the copolymer made from AN monomer grafted onto cellulose obtained from *Lantana camara*, and using ceric ions as initiator. This type of reaction has been very useful for increasing ductile strength and Young's module of AN-grafted polymer materials (Mishra et al. 2001).

On the other hand, Khullar et al. (2008) grafted the AN monomer onto cellulose obtained from bamboo (*Dendrocalamus strictus*), concluding that this reaction can be initiated efficiently with CAN, resulting in a %G for optimized samples up to 210.3% and a grafting efficiency up to 97%. Predominantly, the grafting of AN monomer onto starch offers the possibility to execute additional chemical modifications and combining new components for numerous applications, such as additives for paper and textiles, adhesives, drug delivery devices, improved oil recovery, sanitary products, wastewater treatment, etc. (Peniche et al. 2008; Shanmugapriya et al. 2011).

8.4.3 Grafting of Acrylamide Monomers

The concentration of the monomer, the initiators and the catalyst are the main factors affect the grafting of vinyl monomers. For this reason, the number of grafted monomers can be regulated by these variables. In this sense, Reyes et al. (1966) considered the graft copolymerization of AN and AA onto starch using ceric ion, resulting in a maximum grafting efficiency of 87% for AN and 43.8% for AA. Although the monomer content of the grafted AN number was higher than that of grafted AA.

Lv et al. (2013) used KPS as an initiator to give rise to AM grafting onto corn starch. As a result, the highest graft capacity was obtained using AM, while the lowest graft capacity was obtained using the AA monomer, and intermediate graft capacity values were obtained using the AN and MAA monomers. In this reaction mechanism, persulfate ions when heated decompose to form sulfate ion radicals. These radicals, in turn, can act as macroinitiators and react with water molecules to produce hydroxy (OH^\cdot) radicals. These macroradicals initiated the chain propagation reaction on the starch backbone. Successive accumulation of monomer molecules in the initiated chain eventually formed the starch graft copolymer. Therefore, the chemical modification is another approach to expand the properties of starch, thus improving its range of application. The starch graft copolymer with binary monomers such as AM/DMDAAC binary monomers was the first to be prepared under the radiation grafting method. This method provided a higher ratio of grafting and efficiency of binary monomers at absorbed doses of 2 kGy and 3 kGy using a 6:9.8:4.2 (w/w/w) ratio of starch/AM/DMDAAC as shown in Fig. 8.13 (Lv et al. 2013).

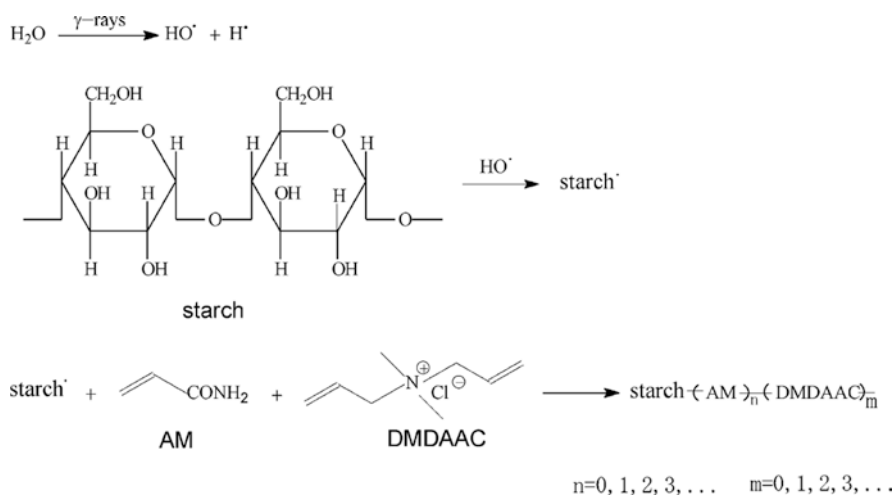


Fig. 8.13 The gamma radiation-initiated graft copolymerization of AM and DMDAAC onto corn starch. Reproduced with permission from Xiaohua et al. (2013)

Kumar et al. (2009) prepared two graft copolymers based on xanthan and PAM through the MW radiation-irradiated method and the other ceric ion-induced graft copolymerization method. These authors concluded that the MW radiation increased %G in a shorter time and increased with the increase in the MW power compared to the ceric ion-induced grafting. In addition, Kumar et al. (2009) used these graft copolymers to study the mechanism of drug release and observed the controlled drug release with a modified polymer matrix compared to the xanthan gum (XG) matrix.

On the other hand, Vijan et al. (2012) reported the MW radiation-irradiated free radical polymerization of AM-g-gellan gum copolymer, using CAN as a redox initiator. These authors incorporated an antidiabetic drug such as metformin hydrochloride (MTF) into copolymerized gum together with the excipients for sustained drug release. The controlled drug release from this polymer was obtained by varying different parameters such as the AM and CAN concentration, MW irradiation time, among others. This led to the slow MTF release up to 8 h (Vijan et al. 2012).

Giri et al. (2015) studied the graft copolymerization of AM in an aqueous medium onto locust bean gum by the MW radiation-assisted method using KPS as an initiator. The AM-g-locust bean gum copolymer was also used as a sustained release matrix for antihypertensive drugs such as atenolol and carvedilol. Their results revealed that with greater grafting efficiency, the rate of drug release increased. The PAM-g-XG matrix tablets containing atenolol showed 85% of the drug release up to 24 h in simulated gastric fluid followed by simulated intestinal fluid without enzymes. It should be noted that the base locust bean gum matrix reached 99% release of the drug only in 12 h. In contrast, Mundargi et al. (2007) reported that the PAM-g-XG extended the drug's release time by increasing the grafting ratio of the polymer matrix.

8.5 Factors Affecting the Grafting

Factors affecting graft copolymerization such as additives, backbone nature, initiator role, monomer, temperature, among others, will be discussed in the following sections:

8.5.1 Additives

Additives are a consideration factor when studying the grafting mechanism because the amount of graft copolymerization depends on the action of the additives such as acids, metal ions and organic-inorganic salts. The presence of additives increases the grafting efficiency by promoting the reaction mechanism of monomer/backbone, and sometimes, decreases the grafting efficiency. Zahran and Zohdy (1986) observed that alkali treatment could improve grafting yield, and also found that the addition

of sulfuric acid (H_2SO_4) or alkali controlled grafting yield when sisal fiber was cografted with ethyl acrylate and styrene. As a result, a reduction in fiber sorption capacity was observed. In turn, the adsorbed monomer concentration also decreased (Zahran and Zohdy 1986). These influenced the grafting efficiency by affecting the backbone, the initiator concentration and the solvent. In addition to this, when the fibers were subjected to a combined treatment, the intracrystallite swelling by acid allowed sodium hydroxide (NaOH) permeation, thus leading better grafting onto cellulose. In addition, this can also result in a greater order with greater crystallinity. H_2SO_4 also increases the grafting yield when MMA was grafted onto cellulose in the presence of a Ce^{4+} initiated system (Zahran and Zohdy 1986; Misra et al. 1991; Misra et al. 1993). While, acids, (Dworjanyn et al. 1993; Chaplin et al. 1996), inorganic salts (Taher et al. 1996), multifunctional acrylates, (Ang et al. 1983) and organic materials, such as urea (Dworjanyn and Garnett 1988) increase grafting efficiency when copolymerized under ionizing radiation.

According to Zu et al. (2007) the addition of sodium acetate and sodium chloride using the immediate radiation technique also affected the grafting yield. When AN was grafted onto nylon, the introduction of 1% amine FeSO_4 improved the grafting six times more than that without the additive. Zinc chloride also played an important role in the progressive increase in grafting yield (Zu et al. 2007).

8.5.2 Backbone Nature

The backbone nature has its unique role in the graft copolymerization, since it includes the covalent bond of a monomer onto the surface of the base polymeric backbone (Ibrahim and Nada 1985). Keeping this in view, Taghizadeh and Mehrdad (2006) explained the role of backbone on %G by varying its concentration within the range of 0.2–2.6 g/50 cm³ for St-g-PAA and 0.1–1 g/30 cm³ for St-g-PEMA. The results showed an increase in %G with an increase in starch concentration and was calculated largest in [starch] = 1.4 g/50 cm³ for starch-g-PAA and [starch] = 0.5 g/30 cm³ for starch-g-PEMA and then remained almost constant. Following Das et al. (1990) the optimal backbone concentration at which the %G was highest was observed. This may occur since at a higher concentration the primary radicals react with the starch molecules to generate macroradicals and beyond this the grafting was constant.

Pandey et al. (2003) also synthesized the XG-g-AA copolymer using potassium monopersulfate (PMS)/ Fe^{2+} redox pair at 35 °C. The higher %G could be attributed to a greater number of grafting sites present and the adequate presence of gum molecules at the reaction site. Although delayed grafting may result from 1) an increase in the viscosity of the reaction medium due to the increase in concentration of gum molecules which obstructs the path of the free radical species and 2) with an increase in the XG concentration, new free radicals generated can act together and lead to termination (Pandey et al. 2003).

8.5.3 Initiator Role

All chemical grafting reactions involve the use of initiator, and its concentration, nature, solubility and function should be considered. According to Gupta et al. (2002) an increase in the concentration of the initiator (CAN in the presence of nitric acid) can efficiently increase the graft copolymerization rate. Bardhan et al. (1977) also studied the grafting of AM monomer onto methyl cellulose using KPS as and initiator. These authors observed that the maximum graft increased rapidly with the use of an initiator concentration of 3.7×10^{-4} moles/L at 40 °C (Bardhan et al. 1977). In another study, Retuert and Yazdani-Pedram (1993) used different organic $((\text{NH}_4)_2\text{C}_4\text{H}_4\text{O}_6$ and $(\text{NH}_4)_2\text{C}_2\text{O}_4\text{H}_2\text{O}$) and inorganic ($\text{CuCl}_2 \cdot 2\text{H}_2\text{O}$ and MnCl_2) cocatalysts for graft copolymerization of MMA and MA onto Cs using KPS as initiator. These authors observed that MnCl_2 increased the grafting of MMA and MA onto Cs compared to the use of KPS alone (Retuert and Yazdani-Pedram 1993). This was explained due to the greater reducing capacity of Mn^{2+} ions to reach higher oxidation states. Retuert and Yazdani-Pedram (1993) also found that CuCl_2 decreased %G. Cu^{2+} ions with low reducing capacity could decrease the intrinsic capacity of polysaccharide reduction, while $(\text{NH}_4)_2\text{C}_4\text{H}_4\text{O}_6$ and $(\text{NH}_4)_2\text{C}_2\text{O}_4\text{H}_2\text{O}$ acted as strong organic reducing agents, which stimulated the formation of active sites for grafting by rapid adsorption on the backbone (Retuert and Yazdani-Pedram 1993). Nishioka and Kosai (1981) also evaluated two initiators (AIBN and APS). These authors reported that the greatest %G (87.3%) was for the reactions given using the APS and AN as initiator and copolymer, respectively. In contrast, grafting of MMA onto Cs was 52%, using APS as initiator. Meanwhile, the grafting of MMA and AN was 10 and 48%, respectively, using AIBN as initiator. Thus, APS is a better initiator compared to AIBN (Nishioka and Kosai 1981).

8.5.4 Monomer

As with other factors, the reactivity of the monomer is also an important factor. The grafting of hydrophobic monomers such as AN, butadiene, MMA, styrene and vinyl acetate onto cellulose substrates can improve the adhesion of the grafted materials to hydrophobic fibers (Zhang and Chen 2002). Pandey et al. (2003) also found that %G was increased using an AA concentration of 5.0×10^{-2} mol/dm, but an additional increase in concentration deteriorated the grafting parameters. The mechanism responsible for the chain termination process was the gelation mechanism, which restricted the polymer chain and there was no new formation of grafting sites (Pandey et al. 2003).

Abdel Ghaffar et al. (2016) individually prepared hydrogels from carboxymethyl cellulose (CMC) grafted by AM and MAA monomers using the radiation grafting technique. These authors observed that %G and grafting ratio increased with the

increasing monomer concentration for poly(CMC-*g*-AM) and poly(CMC-*g*-MAA) hydrogels.

Following Shah et al. (1995) the %G ratio and grafting efficiency can be improved by changing the NaAlg concentration, e.g. increasing the NaAlg concentration progressively decreased %G and increasing graft efficiency. This could happen because the Mw of the grafted polymer increases as the NaAlg concentration increases, which increases the grafting efficiency and decreases the %G. In addition to this, the increase in the backbone concentration decreased the rate of graft copolymerization. Similar results were observed by Li et al. (1988) for copolymerization by grafting butyl acrylate onto gelatin.

On the other hand, Bhattacharya et al. (1998) reported the grafting order of substituted acrylamide onto cellulose acetate as follows: AM > methyl acrylamide > *N,N*-dimethyl acrylamide. These authors indicated that methylacrylamide contained a methyl group which slowed the mobility of the monomer on the polymer chain, thus improving the grafting, while *N,N*-dimethyl acrylamide with two methyl groups was more reactive and caused steric hindrance between the monomer and the backbone, which delayed the grafting yield (Bhattacharya et al. 1998). Similar results were previously observed by various authors (Varma and Narashinan 1972; Bhattacharya et al. 1998; Bhattacharya and Misra 2004) for the study of substituted acrylates. These authors also reported that the graft polymerization sequence mediated by Ce⁴⁺ onto cellulose was as follows: MA > ethyl acrylate > butyl acrylate > MMA (Bhattacharya and Misra 2004). This order was given due to the steric and polar effects. In addition to this, radical stability plays an important role for determining the %G, i.e. the more reactive the monomer is, the more stable the polymer radical is. Misra et al. (1982) described the modification for grafting of vinyl acetate (2.6%) and ethyl acrylate (60.8%) onto wool in terms of their reactivity, while Reyes et al. (1966) observed a grafting yield of 87% for AN and 43.8% for AA.

8.5.5 Temperature

Temperature conditions have been studied by different authors with the aim of obtaining a relationship with the maximum %G (Schwab et al. 1962; Hebeish and Mehta 1969; Hebeish and Mehta 1968; Heikal and El-Kalyubi 1982; Sharma et al. 2003; Khullar et al. 2008). A higher %G can be greatly improved by a higher rate of initiator dissociation, mobility and diffusion of the monomer associated with a varied temperature range. For example, Taghizadeh and Mehrdad (2006) copolymerized AA and EMA onto starch in aqueous solution using CAN as a redox system under N₂ atmosphere. The temperature range was varied from 25–65 °C for starch-*g*-PAA and 25–55 °C for starch-*g*-PEMA by keeping other variable constants. As a result of this study, the maximum %G was observed between 40 °C and 45 °C, and then decreased (Taghizadeh and Mehrdad 2006).

8.6 Applications

The graft copolymers have found tremendous application in various fields of science and technology ranging from agriculture to biomedical. Various industries, such as cosmetics, food, paper, plastics, textile, etc., have used grafted polymers.

8.6.1 *Agroindustrial Inputs*

In recent decades, the intrinsic soil fertility has deteriorated due to the incessant refinement and poor nutrient renewal, among other restriction factors (Gupta et al. 2013). Nitrogen and phosphorus from fertilizers are leached into the environment, causing economic and resource losses, as well as damage to the environment (Mucheru-Muna et al. 2014). In recent times, there has been a greater use of grafted polymer hydrogels in agricultural production. For example, the PAM-grafted cellulose hydrogel was evaluated by Naderi and Danesh-Shahraki (2013) for slow and controlled fertilizer release.

8.6.2 *Controlled Drug Release*

Natural grafted polymers have been used to formulate different types of drug delivery systems. These grafted polymers and their derivatives have been widely used for the controlled release of drugs in the biomedical and pharmaceutical field. In particular, polysaccharides from natural gums such as arabinose, galactose, glucose, mannose, rhamnose and xylose grafted have had wide applications in this field. Grafted polymers can improve their performance for drug delivery applications (Kaith and Jindal 2017).

8.6.3 *Environmental Remediation*

Grafted polymers have been used, e.g. for the remediation of wastewater containing dyes and heavy metals. In this sense, dyes discharged into water sources from the textile industry are undesirable and this can remain in the water even at concentrations as low as parts *per million* (ppm). These dyes are harmful, carcinogenic and deadly chemicals, even at a very low concentration (Mittal et al. 2015). To overcome these problems, several methods such as activated carbon adsorption, coagulation, ion exchange and membrane technology have been widely used (Ong et al. 2007). Among all these strategies, adsorption is a reliable, highly efficient, simply and economical design with ease of operation. The discoloration of the dye prior to

discharges has been mandatory by several countries and environmental regulations (Grau 1991; Ramakrishna and Viraraghavan 1997; Nigam et al. 2000). Most researchers have begun treating this type of effluent with natural flocculant materials. Among them, polysaccharides are the most promising material for efficient wastewater treatment. The grafted fibers generally increase the adsorption sites and also increases the sorption capacity for target metal ions and dyes. Abdel-Halim and Al-Hoqbani (2015) found that dyeing and removal of metal ions increase with increasing grafting of the PAA-*g*-cellulose copolymer synthesized for the methylene blue and lead ion removal. However, an additional graft reduced the sorption capacity due to greater firmness in the polymeric backbone.

8.7 Conclusion

This chapter shows that graft copolymerization is an idiosyncratic method among other techniques to modify and control the inherent properties of polymers. Grafting is an imperative technique to introduce desirable properties into the main polymer backbone, and therefore, can be used in various applications. In this chapter, the various systematic grafting techniques, factors affecting the grafting and applications of grafted copolymer were outlined. It can be concluded that the grafted copolymer is a competent and innovative technique and has a wide range of applications, such as adsorption, drug delivery, wastewater treatment and also in agriculture and serving for the service of humanity. Although grafting techniques are over 75 years old, despite a great deal of inventive research, a large-scale commercial exploitation of the method has not been developed. Providentially, the grafting process is now rapidly increasing through electron beam curing processes which can be achieved in a fraction of a seconds, and is a one-step procedure that produces products without further purification. Despite the various advantages of grafting, research takes a step towards 'biodegradability'. It can solve some of the environmental pollution problems caused by components that resist biodegradation.

Acknowledgements One of the authors (Kashma) is thankful to the University Grants Commission (UGC), New Delhi, India, for support through Post-Doctoral Fellowship for Women [F.15-1/2017/PDFWM-2017-18-HIM-51703(SA-II)]. Vishal Sharma is thankful for the financial support to the Department of Science and Technology (DST) (Govt. of India) through sanction no. EMR/2016/001103 and PURSE-II grant.

Conflicts of Interest The authors declare no conflict of interest.

References

- Abdel Ghaffar, A. M., El-Arnaouty, M. B., Abdel Baky, A. A., & Shama, S. A. (2016). Radiation-induced grafting of acrylamide and methacrylic acid individually onto carboxymethyl cellulose for removal of hazardous water pollutants. *Designed Monomers and Polymers*, 19(8), 706–718. <https://doi.org/10.1080/15685551.2016.1209630>.

- Abdel-Halim, E.S., & Al-Hoqbani, A.A. (2015). Utilization of poly(acrylic acid)/cellulose graft copolymer for dye and heavy metal removal. *Bio Resour.* 10(2), 3112–3130. Available in: https://ojs.cnr.ncsu.edu/index.php/biores/article/view/biores_10_2_3112_abdel-halim_utilization_poly_acrylic_acid
- Akın, A., & Işıkhan, N. (2016). Microwave assisted synthesis and characterization of sodium alginate-graft-poly(N,N'-dimethylacrylamide). *International Journal of Biological Macromolecules*, 82, 530–540. <https://doi.org/10.1016/j.ijbiomac.2015.10.050>.
- Alferey, T., & Bandel, D. (1951). Paper presented in 118th American Chemical Society Annual Fall Meeting, through Mark HF. Rec. Chem. Progr, vol 12. Chicago, p 139.
- Ang, C. H., Garnett, J. L., Levoll, R., & Long, M. A. (1983). Novel additives for enhancing UV and radiation grafting of monomers to polymers and use of these copolymers as ion exchange resins. In F. E. Bailey, E. J. Vandenberg, A. Blumstein, M. J. Bowden, J. C. Arthur, J. Lal, & R. M. Ottenbrite (Eds.), *Initiation of polymerization* (ACS symposium series) (Vol. 212, pp. 209–223). <https://doi.org/10.1021/bk-1983-0212.ch016>.
- Arai, K. (1973). In R. Ceresa (Ed.), *Block and graft copolymerization* (Vol. 1, p. 193). London: Wiley.
- Athawale, V. D., & Lele, V. (1998). Graft copolymerization onto starch. II. Grafting of acrylic acid and preparation of its hydrogels. *Carbohydrate Polymers*, 35(1–2), 21–27. [https://doi.org/10.1016/s0144-8617\(97\)00138-0](https://doi.org/10.1016/s0144-8617(97)00138-0).
- Bajpai, U. D. N., Jain, A., & Ray, S. (1990). Grafting of polyacrylamide on to guar gum using $K_2S_2O_8$ ascorbic acid redox system. *Journal of Applied Polymer Science*, 39(11–12), 2187–2204. <https://doi.org/10.1002/app.1990.070391101>.
- Bao-Xiu, Z., Peng, W., Tong, Z., Chun-yun, C., & Jing, S. (2006). Preparation and adsorption performance of a cellulosic-adsorbent resin for copper (II). *Journal of Applied Polymer Science*, 99(6), 2951–2956. <https://doi.org/10.1002/app.22986>.
- Bardhan, K., Mukhopadhyay, S., & Chatterjee, S. R. (1977). Grafting of acrylamide onto methyl cellulose by persulfate ion. *Journal of Polymer Science: Polymer Chemistry Edition*, 15(1), 141–148. <https://doi.org/10.1002/pol.1977.170150114>.
- Bastos, D. C., Santos, A. E. F., Silva, M. L. V., & Simao, R. A. (2009). Hydrophobic corn starch thermoplastic films produced by plasma treatment. *Ultramicroscopy*, 109(8), 1089–1093. <https://doi.org/10.1016/j.ultramic.2009.03.031>.
- Bellobono, I. R., Calgari, S., Leonari, M. C., Selli, E., & Paglia, E. D. (1981). Photochemical grafting of acrylated azo dyes onto polymeric surfaces. IV. Grafting of 4-(N-ethyl-N-2-acryloxyethyl)amino-4'-nitro-azobenzene onto cellulose. *Applied Macromolecular Chemistry and Physics*, 100(1), 135–146. <https://doi.org/10.1002/apmc.1981.051000109>.
- Bhatt, N., Gupta, P.K., & Naithani, S. (2011). Ceric-induced grafting of acrylonitrile onto alpha cellulose isolated from *Lantana camara*. *Cellulose Chemistry and Technology*, 45(5–6), 321–327. Available in: [http://www.cellulosechemtechnol.ro/pdf/cct45,5-6\(2011\)/p.321-327.pdf](http://www.cellulosechemtechnol.ro/pdf/cct45,5-6(2011)/p.321-327.pdf).
- Bhattacharya, A., Das, A., & De, A. (1998). Structural influence on grafting of acrylamide based monomers on cellulose acetate. *Indian Journal of Chemical Technology*. 5(3), 135–138. Available in: <http://nopr.niscair.res.in/handle/123456789/30829>
- Bhattacharya, A., & Misra, B. N. (2004). Grafting: A versatile means to modify polymers techniques, factors and applications. *Progress in Polymer Science*, 29(8), 767–814. <https://doi.org/10.1016/j.progpolymsci.2004.05.002>.
- Bhattacharyya, S. N., & Maldas, D. (1983). Graft copolymerization on to cellulose. *Progress in Polymer Science*, 10(2–3), 171–270. [https://doi.org/10.1016/0079-6700\(84\)90002-9](https://doi.org/10.1016/0079-6700(84)90002-9).
- Bledzki, A., Braun, D., & Titzschkau, K. (1983). Polymerization initiation with substituted ethane, 6. Polymerization of methyl methacrylate with various tetraphenylethanes. *Macromolecular Chemistry*, 184–745.
- Caner, H. A., Hasipoglu, H. A., Yilmaz, O. S., & Yilmaz, E. L. (1998). Graft copolymerization of 4-vinylpyridine on to chitosan-I. By ceric ion initiation. *European Polymer Journal*, 34(3–4), 493–497.
- Carlmark, A., & Malmstroem, E. (2002). Atom transfer radical polymerization from cellulose fibers at ambient temperature. *Journal of the American Chemical Society*, 124(6), 900–901. <https://doi.org/10.1021/ja016582h>.

- Carr, M. E. (1994). Preparation of cationic starch containing quaternary ammonium substituents by reactive twin-screw extrusion processing. *Journal of Applied Polymer Science*, 54(12), 1855–1861. <https://doi.org/10.1002/app.1994.070541208>.
- Chapiro, A., & Jendrychowska-Bonamoury, A. M. (1980). Synthesis of permselective membranes by radiation induced grafting of hydrophilic monomers into poly(tetrafluoroethylene) films. *Polymer Engineering and Science*, 20(3), 202–205. <https://doi.org/10.1002/pen.760200306>.
- Chaplin, R. P., Dworjanyan, P. A., Gamage, N. J. W., Garnett, J. L., Jankiewicz, S. V., Khan, M. A., & Sangster, D. F. (1996). The role of partitioning of reagents in grafting and curing reactions initiated by ionizing radiation and UV. *Radiation Physics and Chemistry*, 47(3), 435–437. [https://doi.org/10.1016/0969-806x\(95\)00133-i](https://doi.org/10.1016/0969-806x(95)00133-i).
- Chen, T., Kumar, G., Harries, M. T., Smith, P. J., & Payne, G. F. (2000). Enzymatic grafting of hexyloxyphenol onto chitosan to alter surface and rheological properties. *Biotechnology and Bioengineering*, 70(5), 564–573. [https://doi.org/10.1002/1097-0290\(20001205\)70:5<564::aid-bit11>3.0.co;2-w](https://doi.org/10.1002/1097-0290(20001205)70:5<564::aid-bit11>3.0.co;2-w).
- Dainton, F. S., & Ivin, K. J. (1958). Some thermodynamic and kinetic aspects of addition polymerisation. *Quarterly Reviews Chemical Society*, 12(1), 61–92. <https://doi.org/10.1039/qr9581200061>.
- Das, N. R., Nayak, N. C., Das, H. K., Mishra, S. N., & Singh, B. C. (1990). Influence of dimethyl sulfoxide on the kinetics of the graft copolymerization of acrylonitrile onto the jute fibers initiated by ceric ion. *Journal of Applied Polymer Science*, 39(5), 1079–1086. <https://doi.org/10.1002/app.1990.070390505>.
- Deshpande, M. (1986). Enzymatic degradation of chitin and its biological applications. *Journal of Scientific and Industrial Research*, 45, 273–281.
- Dworjanyan, P. A., & Garnett, J. L. (1988). Synergistic effects of urea with polyfunctional acrylates for enhancing the photografting of styrene to polypropylene. *Journal of Polymer Science Part C: Polymer Letters*, 26(3), 135–138. <https://doi.org/10.1002/pol.1988.140260302>.
- Dworjanyan, P. A., Garnett, J. L., Khan, M. A., Maojun, X., Meng-Ping, Q., & Nho, Y. C. (1993). Novel additives for accelerating radiation grafting and curing reactions. *Radiation Physics and Chemistry*, 42(1–3), 31–40. [https://doi.org/10.1016/0969-806x\(93\)90198-4](https://doi.org/10.1016/0969-806x(93)90198-4).
- Fakhru'L-Razi, A., Qudsieh, I. Y., Yunus, W. M., Ahmad, M. B., & Rahman, M. Z. (2001). Graft copolymerization of methyl methacrylate onto sago starch using ceric ammonium nitrate and potassium persulfate as redox initiator systems. *Journal of Applied Polymer Science*, 82(6), 1375–1381. <https://doi.org/10.1002/app.1974>.
- Fanta, G. F., Burr, R. C., & Doane, W. M. (1987). Graft polymerization of acrylonitrile onto wheat straw. *Journal of Applied Polymer Science*, 33(3), 899–906. <https://doi.org/10.1002/app.1987.070330318>.
- Fanta, G. F., & Doane, W. M. (1986). In Wurzburg-OB (Ed.), *Modified starches: Properties and uses* (pp. 149–178). Boca Raton, FL: CRC Press.
- Farag, S., & Al-Afaleq, E. I. (2002). Preparation and characterization of saponified delignified cellulose polyacrylonitrile-graft copolymer. *Carbohydrate Polymers*, 48(1), 1–5. [https://doi.org/10.1016/s0144-8617\(01\)00193-x](https://doi.org/10.1016/s0144-8617(01)00193-x).
- Fares, M. M., El-faqeeh, A. S., & Osman, M. E. (2003). Graft copolymerization onto starch—I. synthesis and optimization of starch grafted with N-tert-butylacrylamide copolymer and its hydrogels. *Journal of Polymer Research*, 10, 119–125. <https://doi.org/10.1023/a:1024928722345>.
- Faust, R., & Kennedy, J. P. (1986). Living carbocationic polymerization. *Polymer Bulletin*, 15(4), 317–323. <https://doi.org/10.1007/bf00254850>.
- Feng, L., Zhou, Z., Dufresne, A., Huang, J., Wei, M. L., & An, L. (2009). Structure and properties of new thermoforming bionanocomposites based on chitin whisker-graft-polycaprolactone. *Journal of Applied Polymer Science*, 112(5), 2830–2837. <https://doi.org/10.1002/app.29731>.
- Flory, P. J. (1953). *Principles of polymer chemistry*. Ithaca, NY: Cornell Univ. Press.
- Fox, T. G., Goode, W. E., Gartch, S., Hugget, C. H., Kincaid, J. F., Spell, A., & Stroupe, J. D. (1958). Temperature dependence of the stereospecificity in the free radical polymer-

- ization of methyl methacrylate. *Journal of Polymer Science*, 31(122), 173–177. <https://doi.org/10.1002/pol.1958.1203112218>.
- Freddi, G., & Tsukada, T. (1996). In J. C. Salamone (Ed.), *Silk fibers (grafting), polymeric materials, encyclopedia*. S (pp. 7734–7744). Boca Raton: CRC Press Inc.
- Gabriel, C., Grant, E., & Halstead, B. J. (1998). Dielectric parameters relevant to microwave dielectric heating. *Chemical Society Reviews*, 27(3), 213–224. <https://doi.org/10.1039/a827213z>.
- Giri, T. K., Pure, S., & Tripathi, D. K. (2015). Synthesis of graft copolymers of acrylamide for locust bean gum using microwave energy: Swelling behavior, flocculation characteristics and acute toxicity study. *Polímeros*, 25(2), 168–174. <https://doi.org/10.1590/0104-1428.1717>.
- Goddard, J. M., & Hotchkiss, J. H. (2007). Polymer surface modification for the attachment of bioactive compounds. *Progress in Polymer Science*, 32(7), 698–725. <https://doi.org/10.1016/j.progpolymsci.2007.04.002>.
- Grau, P. (1991). Textile industry wastewaters treatment. *Water Science and Technology*, 24(1), 97–103. <https://doi.org/10.2166/wst.1991.0015>.
- Gupta, B., Anjum, N., & Gupta, A. P. (2000a). Influence of solvents on radiation-induced graft copolymerization of acrylamide into polyethylene films. *Journal of Applied Polymer Science*, 77(6), 1401–1404. [https://doi.org/10.1002/1097-4628\(20000808\)77:6<1401::aid-app28>3.0.co;2-t](https://doi.org/10.1002/1097-4628(20000808)77:6<1401::aid-app28>3.0.co;2-t).
- Gupta, B., Hilborn, J. G., Bisson, I., & Frey, P. (2001). Plasma-induced graft polymerization of acrylic acid onto poly(ethylene terephthalate) films. *Journal of Applied Polymer Science*, 81(12), 2993–3001. <https://doi.org/10.1002/app.1749>.
- Gupta, B., Hilborn, J. G., Hollenstein, C. H., Plummer, C. J., Houriet, R., & Xanthopoulos, N. (2000b). Surface modification of polyester films by RF plasma. *Journal of Applied Polymer Science*, 78(5), 1083–1091. [https://doi.org/10.1002/1097-4628\(20001031\)78:5<1083::aid-app170>3.0.co;2-5](https://doi.org/10.1002/1097-4628(20001031)78:5<1083::aid-app170>3.0.co;2-5).
- Gupta, K. C., Sahoo, S., & Khandekar, K. (2002). Graft copolymerization of ethyl acrylate onto cellulose using ceric ammonium nitrate as initiator in aqueous medium. *Biomacromolecules*, 3(5), 1087–1094. <https://doi.org/10.1021/bm020060s>.
- Gupta, V. K., Agarwal, S., Singh, P., & Pathania, D. (2013). Acrylic acid grafted cellulosic *Luffa cylindrical* fiber for the removal of dye and metal ions. *Carbohydrate Polymers*, 98(1), 1214–1221. <https://doi.org/10.1016/j.carbpol.2013.07.019>.
- Haag, A. P., Maier, R. M., Combie, J., & Geesey, G. G. (2004). Bacterially derived biopolymers as wood adhesives. *International Journal of Adhesion and Adhesives*, 24(6), 495–502. <https://doi.org/10.1016/j.ijadhadh.2004.01.004>.
- Halab-Kessira, L., & Ricard, A. (1999). Use of the trial and error method for the optimization of the graft copolymerization of a cationic monomer onto cellulose. *European Polymer Journal*, 35(6), 1065–1071. [https://doi.org/10.1016/s0014-3057\(98\)00182-7](https://doi.org/10.1016/s0014-3057(98)00182-7).
- Hebeish, A., & Mehta, P. C. (1969). Grafting of vinyl monomers and their binary mixtures to cellulose, using ce iv as initiator. *Cellulose Chemistry and Technology*, 3, 469–475.
- Hebeish, A., & Mehta, P. C. (1968). Cerium-initiated grafting of acrylonitrile onto cellulosic materials. *Journal of Applied Polymer Science*, 12(7), 1625–1647. <https://doi.org/10.1002/app.1968.070120712>.
- Heikal, S. O., & El-Kalyubi, S. F. (1982). Graft copolymerization of acrylonitrile onto bagasse and wood pulp. *Journal of Applied Polymer Science*, 27(8), 3027–3041. <https://doi.org/10.1002/app.1982.070270826>.
- Hossain, M. M., Moniruzzaman, M., Khan, M. A., Shahjahan, M., Alam, M. Z., & Jamal, M. S. (2014). Preparation of selective ion adsorbent by gamma radiation induced graft copolymerization of n-butyl methacrylate & phosphoric acid on jute fiber. *Ind J Advanc Chem Sci.*, 2(2), 146–150. Available in: <https://www.ijacskros.com/artcles/ijacs-m62.pdf>.
- Hsu, S. T., & Pan, T. C. (2007). Adsorption of paraquat using methacrylic acid-modified rice husk. *Bioresource Technology*, 98(18), 3617–3621. <https://doi.org/10.1016/j.biortech.2006.11.060>.
- Huacai, G., Wan, P., & Dengke, L. (2006). Graft copolymerization of chitosan with acrylic acid under microwave irradiation and its water absorbency. *Carbohydrate Polymers*, 66(3), 372–378. <https://doi.org/10.1016/j.carbpol.2006.03.017>.

- Huang, J., & Xu, W. (2010). Zwitterionic monomer graft copolymerization onto polyurethane surface through a PEG spacer. *Applied Surface Science*, 256(12), 3921–3927. <https://doi.org/10.1016/j.apsusc.2010.01.051>.
- Ibrahim, A. A., & Nada, A. M. (1985). Grafting of acrylamide onto cotton linters. *Acta polymerica*, 36(6), 342–343. <https://doi.org/10.1002/actp.1985.010360611>.
- Ikada, Y., Nishizaki, Y., & Sakurada, I. (1974). Reaction of poly(vinyl alcohol) with potassium persulfate and graft copolymerization. *J Polym Sci: Polymer Chemistry Edition*, 12(8), 1829–1839. <https://doi.org/10.1002/pol.1974.170120823>.
- Inagaki, N. (1996). *Plasma surface modification and plasma polymerization Technomic*. PA: Lancaster.
- Iskandar, S. (2011). Graft copolymerization of methyl methacrylate monomer onto starch and natural rubber latex initiated by gamma irradiation. *Atom Indonesia*, 22(37), 24–28.
- Ito, M., & Nagai, K. (2007). Degradation behaviour and application of recycled PVC sheet made of floor sheet for railway vehicle. *Polymer Degradation and Stability*, 92(9), 1692–1699. <https://doi.org/10.1016/j.polymdegradstab.2007.06.005>.
- Iwakura, Y., Kurosaki, T., & Imai, Y. (1965). Graft copolymerization onto cellulose by the ceric ion method. *J Polym Sci Part A: General Papers*, 3(3), 1185–1193. <https://doi.org/10.1002/pol.1965.100030326>.
- Jayakumar, R., New, N., Tokura, S., & Tamura, H. (2007). Sulfated chitin and chitosan as novel biomaterials. *International Journal of Biological Macromolecules*, 40(3), 175–181. <https://doi.org/10.1016/j.ijbiomac.2006.06.021>.
- Jenkins, D. W., & Hudson, S. M. (2001). Review of vinyl graft copolymerization featuring recent advances toward controlled radical-based reactions and illustrated with chitin/chitosan trunk polymers. *Chemical Reviews*, 101(11), 3245–3274. <https://doi.org/10.1021/cr000257f>.
- Kaith, B. S., & Jindal, R. (2017). Controlled biofertilizer release kinetics and moisture retention in gum xanthan-based IPN. *Iranian Polymer Journal*, 26(8), 563–577. <https://doi.org/10.1007/s13726-017-0539-8>.
- Kaith, B. S., Jindal, R., & Bhatia, J. K. (2011). Morphological and thermal evaluation of soy protein concentrate on graft copolymerization with ethylmethacrylate. *Journal of Applied Polymer Science*, 120(4), 2183–2190. <https://doi.org/10.1002/app.33448>.
- Kaith, B.S., Jindal, R., Jana, A. K., & Maiti, M. (2009). Ferrous-persulphate induced graft copolymerization of monomer mixtures onto *Saccharum spontaneum* L. natural fibre. *Iranian Polymer Journal*, 18(10), 789–800. Available in: <https://www.sid.ir/en/journal/ViewPaper.aspx?ID=159868>
- Kaith, B. S., & Kalia, S. (2007). Synthesis and characterization of graft copolymer of flax fiber with binary vinyl monomers. *International Journal of Polymer Analysis and Characterization*, 12(5), 401–412. <https://doi.org/10.1080/10236660701543676>.
- Kaith, B. S., & Kalia, S. (2008a). A study of crystallinity of graft copolymers of flax fiber with binary vinyl monomers. *E-Polymers*, 8(1), 1–6. <https://doi.org/10.1515/epoly.2008.8.1.11>.
- Kaith, B. S., & Kalia, S. (2008b). Graftcopolymerization of MMA onto flax under different reaction conditions: A comparative study. *eXPRESS Polymer Letters*, 2(2), 93–100. <https://doi.org/10.3144/expresspolymlett.2008.13>.
- Kaith, B.S., & Kumar, K. (2007). Preparation of psyllium mucilage and acrylic acid based hydrogels and their application in selective absorption of water from different oil/water emulsions. *Iranian Polymer Journal*, 16(8), 529–538. Available in: <https://www.sid.ir/en/journal/viewpaper.aspx?id=93303>
- Kaity, S., Isaac, J., Kumar, P. M., Bose, A., Wong, T. W., & Ghosh, A. (2013). Microwave assisted synthesis of acrylamide grafted locust bean gum and its application in drug delivery. *Carbohydrate Polymers*, 98(1), 1083–1094. <https://doi.org/10.1016/j.carbpol.2013.07.037>.
- Kalia, S., & Kaith, B. S. (2008a). Mechanical properties of phenolic composites reinforced with flax-gcopolymers prepared under different reaction conditions-a comparative study. *E-Journal of Chemistry*, 5(1), 177–184. <https://doi.org/10.1155/2008/538397>.

- Kalia, S., & Kaith, B. S. (2008b). Microwave enhanced synthesis of flax-g-poly(MMA) for use in phenolic composites as reinforcement. *European Journal of Chemistry*, 5(1), 163–168. <https://doi.org/10.1155/2008/392932>.
- Karthika, J. S., & Vishalakshi, B. (2014). Microwave-assisted synthesis and characterization of poly(itaconic acid) grafted gellan gum. *International Journal of Polymer Analysis and Characterization*, 19(2), 95–106. <https://doi.org/10.1080/1023666x.2014.872815>.
- Karthika, J. S., & Vishalakshi, B. (2015). Novel stimuli responsive gellan gum-graft-poly(DMAEMA) hydrogel as adsorbent for anionic dye. *International Journal of Biological Macromolecules*, 81, 648–655. <https://doi.org/10.1016/j.ijbiomac.2015.08.064>.
- Kaszas, G., Puskas, J. E., Chen, C. C., & Kennedy, J. P. (1990). Electron pair donors in carbocationic polymerization. 2. Mechanism of living carbocationic polymerizations and the role of in situ and external electron pair donors. *Macromolecules*, 23(17), 3909–3915. <https://doi.org/10.1021/ma00219a008>.
- Kennedy, J. P., & Marechal, E. (1982). *Carbocationic polymerization*. New York: Wiley.
- Khalek, M. A. A., & Mahmoud, G. A. (2011). Flocculation studies of fine coal using acrylamide and acrylic acid graft copolymer by gamma irradiation. *Aust J Basic and Appl Sci*, 5(11), 271–278. Available in: https://pdfs.semanticscholar.org/b28d/f72b0df285cfff3565146dd37e75f7d67de6.pdf?_ga=2.95077913.462508867.1576429955-1730570640.1549554737
- Khalil, M. I., & Aly, A. A. (2001). Preparation and evaluation of some cationic starch derivatives as flocculants. *Starch-Stärke*, 53(2), 84–89. [https://doi.org/10.1002/1521-379x\(200102\)53:2<84::aid-star84>3.0.co;2-n](https://doi.org/10.1002/1521-379x(200102)53:2<84::aid-star84>3.0.co;2-n).
- Khalil, M. I., Mostafa, K. M., & Hebeish, A. (1993). Graft polymerization of acrylamide onto maize starch using potassium persulfate as initiator. *Appl Macromol Chem Physic.*, 213(1), 43–54. <https://doi.org/10.1002/apmc.1993.052130106>.
- Khullar, R., Varshney, V. K., Naithani, S., & Soni, P. L. (2008). Grafting of acrylonitrile onto cellulose material derived from bamboo (*Dendrocalamus strictus*). *Express Polymer Letters*, 2(1), 12–18. <https://doi.org/10.3144/expresspolymlett.2008.3>.
- Kislenko, V. N., & Berlin, A. A. (1996). Kinetics of interaction between water-soluble derivatives of lignin and hydrogen peroxide. *European Polymer Journal*, 32(8), 1023–1029. [https://doi.org/10.1016/0014-3057\(96\)00002-x](https://doi.org/10.1016/0014-3057(96)00002-x).
- Kislenko, V. N., & Oliynyk, L. P. (2003). Kinetics of hydrogen peroxide decomposition in guaiacol solution, catalyzed by hexacyanoferrate (II). *Russian Journal of General Chemistry*, 73(1), 114–118. <https://doi.org/10.1023/a:1023490805897>.
- Koroskenyi, B., & McCarthy, S. P. (2002). Microwave-assisted solvent-free or aqueous-based synthesis of biodegradable polymers. *Journal of Polymers and the Environment*, 10(3), 93–104. <https://doi.org/10.1023/A:1021120113910>.
- Kubota, H., & Ogiwara, Y. (1978). Formation of peroxides on cellulose derivatives. *Journal of Applied Polymer Science*, 22(12), 3363–3370. <https://doi.org/10.1002/app.1978.070221202>.
- Kubota, H., & Ogiwara, Y. (1980). Cellulose peroxides derived from carboxylated cellulose and hydrogen peroxide. *Journal of Applied Polymer Science*, 25(4), 683–689. <https://doi.org/10.1002/app.1980.070250414>.
- Kubota, H., Suka, I. G., Kuroda, S., & Kondo, T. (2001). Introduction of stimuli-responsive polymers into regenerated cellulose film by means of photografting. *European Polymer Journal*, 37(7), 1367–1372. [https://doi.org/10.1016/s0014-3057\(00\)00257-3](https://doi.org/10.1016/s0014-3057(00)00257-3).
- Kumar, A., Singh, K., & Ahuja, M. (2009). Xanthan-g-poly(acrylamide): Microwave-assisted synthesis, characterization and *in vitro* release behavior. *Carbohydrate Polymers*, 76(2), 261–267. <https://doi.org/10.1016/j.carbpol.2008.10.014>.
- Kumar, G., Smith, P. J., & Payne, G. F. (1999). Enzymatic grafting of a natural product onto chitosan to confer water solubility under basic conditions. *Biotechnology and Bioengineering*, 63(2), 154–165. [https://doi.org/10.1002/\(sici\)1097-0290\(19990420\)63:2<154::aid-bit4>3.0.co;2-r](https://doi.org/10.1002/(sici)1097-0290(19990420)63:2<154::aid-bit4>3.0.co;2-r).
- Kumari, A., Kaith, B. S., Singha, A. S., & Kalia, S. (2010). Synthesis, characterization and salt resistance swelling behavior of psy-g-poly (AA) hydrogel. *Advanced Materials Letters*, 1(2), 123–128. <https://doi.org/10.5185/amlett.2010.6129>.

- Lagos, A., & Reyes, J. (1988). Grafting onto chitosan. I. Graft copolymerization of methyl methacrylate onto chitosan with Fenton's reagent (Fe^{2+} - H_2O_2) as a redox initiator. *J Polym Sci Part A: Polym Chem.*, 26(4), 985–991. <https://doi.org/10.1002/pola.1988.080260403>.
- Lapasin, R., & Pricl, S. (1995). *Rheology of industrial polysaccharides: Theory and applications*. New York, NY: Aspen Publishers.
- Li, Z. C., Fu, Z. F., Huang, M. Z., & Lian, N. (1988). Graft copolymerization of butyl acrylate onto gelatin in the presence of ceric ion. *J Macromol Sci Chem.*, 25(12), 1487–1513. <https://doi.org/10.1080/10601328808055084>.
- Lin, O. H., Kumar, R. N., Rozman, H. D., & Noor, M. A. (2005). Grafting of sodium carboxymethylcellulose (CMC) with glycidyl methacrylate and development of UV curable coatings from CMC-g-GMA induced by cationic photo-initiators. *Carbohydrate Polymers*, 59(1), 57–69. <https://doi.org/10.1016/j.carbpol.2004.08.027>.
- Liu, L., Li, Y., Fang, Y. E., & Chen, L. (2005). Microwave-assisted graft copolymerization of ϵ -caprolactone onto chitosan via the phthaloyl protection method. *Carbohydrate Polymers*, 60(3), 351–356. <https://doi.org/10.1016/j.carbpol.2005.01.009>.
- Liu, L. S., Fishman, M. L., & Hicks, K. B. (2007). Pectin in controlled drug delivery - a review. *Cellulose*, 14, 15–24. <https://doi.org/10.1007/s10570-006-9095-7>.
- Liu, M., Cheng, R., Wu, J., & Ma, C. (1993). Graft copolymerization of methyl acrylate onto potato starch initiated by ceric ammonium nitrate. *J Polym Sci Part A: Polym Chem.*, 31(13), 3181–3186. <https://doi.org/10.1002/pola.1993.080311302>.
- Liu, S., & Sun, G. (2008). Radical graft functional modification of cellulose with allyl monomers: Chemistry and structure characterization. *Carbohydrate polymers.*, 71(4), 614–625. <https://doi.org/10.1016/j.carbpol.2007.07.006>.
- Liu, Y., Li, J., & Yang, L. (2004). Graft copolymerization of methyl methacrylate onto casein initiated by potassium ditelluratocuprate(III). *Journal of Macromolecular Science, Part A Pure and Applied Chemistry*, 41(3), 305–316. <https://doi.org/10.1081/ma-120028209>.
- Lv, J., Ma, J., Huang Fu, P., Yang, S., & Gong, Y. (2008). Surface modification with both phosphorylcholine and stearyl groups to adjust hydrophilicity and hydrophobicity. *Applied Surface Science*, 255(2), 498–501. <https://doi.org/10.1016/j.apsusc.2008.06.149>.
- Lv, X., Song, W., Ti, Y., Qu, L., Zhao, Z., & Zheng, H. (2013). Gamma radiation-induced grafting of acrylamide and dimethyl diallyl ammonium chloride onto starch. *Carbohydrate Polymers*, 92(1), 388–393. <https://doi.org/10.1016/j.carbpol.2012.10.002>.
- Maclaren, J. A., & Milligan, B. (1981). *Wool science. The chemical reactivity of wool fiber* (p. 235). Marrickville, NSW: Science Press.
- Mahmoud, G. A., & Abdel, K. (2012). Development of graft copolymer flocculant based on acrylamide and acrylic acid for the dewatering of coal. *Bas. Appl. Sci.*, 5, 629–633.
- Mahto, D., Rani, P., Mishra, S., & Sen, G. (2014). Microwave assisted synthesis of polyacrylamide grafted soya peptone and its application as water soluble adhesive. *Industrial Crops and Products*, 58, 251–258. <https://doi.org/10.1016/j.indcrop.2014.04.013>.
- Malviya, R., Sharma, P. K., & Dubey, S. K. (2019). Microwave-assisted preparation of biodegradable, hemocompatible, and antimicrobial neem gum-grafted poly(acrylamide) hydrogel using (3) 2 factorial design. *Emergent Materials.*, 2, 95–112. <https://doi.org/10.1007/s42247-019-00022-y>.
- Mandal, B., & Ray, S. K. (2014). Swelling, diffusion, network parameters and adsorption properties of IPN hydrogel of chitosan and acrylic copolymer. *Materials Science and Engineering: C*, 44, 132–143. <https://doi.org/10.1016/j.msec.2014.08.021>.
- Matahwa, H., Ramiah, V., Jarrett, W. L., Mcleary, J. B., & Sanderson, R. D. (2007). Microwave assisted graft copolymerization of n-isopropyl acrylamide and methyl acrylate on cellulose: Solid state NMR analysis and CaCO_3 crystallization. *Macromolecular Symposia*, 255(1), 50–56. <https://doi.org/10.1002/masy.200750906>.
- Mehta, I. K., Kumar, S., Chauhan, G. S., & Misra, B. N. (1990). Grafting onto isotactic polypropylene. III. Gamma rays induced graft copolymerization of water soluble vinyl mono-

- mers. *Journal of Applied Polymer Science*, 41(5–6), 1171–1180. <https://doi.org/10.1002/app.1990.070410526>.
- Merz, J.H., & Waters, W.A. (1947). Discussions of the Faraday Society, pubs.rsc.org.
- Mino, G., & Kaizerman, S. (1958). A new method for the preparation of graft copolymers. Polymerization initiated by ceric ion redox systems. *Journal of Polymer Science*, 31(122), 242–243. <https://doi.org/10.1002/pol.1958.1203112248>.
- Mishra, A., Clark, J. H., Vij, A., & Daswal, S. (2008). Synthesis of graft copolymers of xyloglucan and acrylonitrile. *Polymers for Advanced Technologies*, 19(2), 99–104. <https://doi.org/10.1002/pat.973>.
- Mishra, B. N., Mehta, I. K., & Khetrapal, R. C. (1984). Grafting onto cellulose. VIII. Graft copolymerization of poly(ethylacrylate) onto cellulose by use of redox initiators. Comparison of initiator reactivities. *Journal of Polymer Science: Polymer Chemistry Edition*, 22(11), 2767–2775. <https://doi.org/10.1002/pol.1984.170221103>.
- Mishra, M. K., & Kennedy, J. P. (1987). Living carbocationic polymerization. VII. Living polymerization of isobutylene by tertiary alkyl (or aryl) methyl ether/boron trichloride complexes. *Journal of Macromolecular Science – Chemistry*, 24(8), 933–948. <https://doi.org/10.1080/00222338708076927>.
- Mishra, S., Misra, M., Tripathy, S. S., Nayak, S. K., & Mohanty, A. K. (2001). Graft copolymerization of acrylonitrile on chemically modified sisal fibers. *Macromolecular Materials and Engineering*, 286(2), 107–113. [https://doi.org/10.1002/1439-2054\(20010201\)286:2<107::aid-mame107>3.0.co;2-0](https://doi.org/10.1002/1439-2054(20010201)286:2<107::aid-mame107>3.0.co;2-0).
- Mishra, S., & Sen, G. (2011). Microwave initiated synthesis of polymethylmethacrylate grafted guar (GG-g-PMMA), characterizations and applications. *International Journal of Biological Macromolecules*, 48(4), 688–694. <https://doi.org/10.1016/j.ijbiomac.2011.02.013>.
- Mishra, S., Sen, G., Rani, G. U., & Sinha, S. (2011). Microwave assisted synthesis of polyacrylamide grafted agar (Ag-g-PAM) and its application as flocculant for wastewater treatment. *International Journal of Biological Macromolecules*, 49(4), 591–598. <https://doi.org/10.1016/j.ijbiomac.2011.06.015>.
- Mishra, S., Sinha, S., Dey, K. P., & Sen, G. (2014). Synthesis, characterization and applications of polymethylmethacrylate grafted psyllium as flocculant. *Carbohydrate Polymers*, 99, 462–468. <https://doi.org/10.1016/j.carbpol.2013.08.047>.
- Misra, B. N., Chauhan, G. S., & Rawat, B. R. (1991). Grafting onto wool. XXVIII. Effects of acids on gamma-radiation induced graft copolymerization of ethylmethacrylate onto wool fiber. *Journal of Applied Polymer Science*, 42(12), 3223–3227. <https://doi.org/10.1002/app.1991.070421215>.
- Misra, B. N., Jassal, J. K., Dogra, R., & Sood, D. S. (1980). Grafting onto cellulose. VI. Graft copolymerization of vinyl acetate by use of metal chelates as initiators. *Journal of Macromolecular Science – Chemistry*, 14(7), 1061–1070. <https://doi.org/10.1080/00222338008056730>.
- Misra, B. N., Mehta, I. K., Rathore, M. P., & Lakhanpal, S. (1993). Effect of L(-)threonine, 5-hydroxytryptophane, and 5-hydroxytryptamine on the ceric-ion-initiated grafting of methyl acrylate onto cellulose. *Journal of Applied Polymer Science*, 49(11), 1979–1984. <https://doi.org/10.1002/app.1993.070491114>.
- Misra, B. N., Sharma, R. K., & Mehta, I. K. (1982). Grafting onto wool. XV. Graft copolymerization of MA and MMA by use of Mn(acac)₃ as initiator. *Journal of Macromolecular Science – Chemistry*, 17(3), 489–500. <https://doi.org/10.1080/00222338208056486>.
- Mittal, H., Maity, A., & Ray, S. S. (2015). Effective removal of cationic dyes from aqueous solution using gum ghatti-based biodegradable hydrogel. *International Journal of Biological Macromolecules*, 79, 8–20. <https://doi.org/10.1016/j.ijbiomac.2015.04.045>.
- Moharana, S., Mishra, S. B., & Tripathy, S. S. (1991). Chemical modification of jute fibers. I. Permanganate-initiated graft copolymerization methyl methacrylate onto jute fibers. *Journal of Applied Polymer Science*, 40(3–4), 345–357. <https://doi.org/10.1002/app.1990.070400304>.

- Moreira, A. C. E., Oliveira, M. G., & Soares, B. G. (1997). Thermal degradation studies of poly(EVAL-g-methylmethacrylate). *Polymer Degradation and Stability*, 58(1–2), 181–185. [https://doi.org/10.1016/s0141-3910\(97\)00044-x](https://doi.org/10.1016/s0141-3910(97)00044-x).
- Mostafa, K. M. (1995). Graft polymerization of acrylic acid onto starch using potassium permanganate acid (redox system). *Journal of Applied Polymer Science*, 56(2), 263–269. <https://doi.org/10.1002/app.1995.070560217>.
- Mucheru-Muna, M., Mugendi, D., Pypers, P., Mugwe, J., Kung'u, J., Vanlauwe, B., & Merckx, R. (2014). Enhancing maize productivity and profitability using organic inputs and mineral fertilizer in Central Kenya small-hold farms. *Experimental Agriculture*, 50(2), 250–269. <https://doi.org/10.1017/s0014479713000525>.
- Mundargi, R. C., Patil, S. A., & Aminabhavi, T. M. (2007). Evaluation of acrylamide-grafted-xanthan gum copolymer matrix tablets for oral controlled delivery of antihypertensive drugs. *Carbohydrate Polymers*, 69(1), 130–141. <https://doi.org/10.1016/j.carbpol.2006.09.007>.
- Muth, O., Hirth, T., & Vogel, H. (2000). Polymer modification by supercritical impregnation. *Journal of Supercritical Fluids*, 17(1), 65–72. [https://doi.org/10.1016/s0896-8446\(99\)00042-x](https://doi.org/10.1016/s0896-8446(99)00042-x).
- Nada, A.M., Alkady, M.Y., & Fekry, H.M. (2008). Synthesis and characterization of grafted cellulose for use in water and metal ions sorption. *Bio Resour.* 3(1), 46–59. Available in: https://ojs.cnr.ncsu.edu/index.php/biores/article/view/biores_03_1_0046_nada_af_graftedcellulose/90
- Naguib, H. F., Aly, R. O., Sabaa, M. W., & Mokhtar, S. M. (2003). Gamma radiation induced graft copolymerization of vinylimidazole-acrylic acid onto polypropylene films. *Polymer Testing*, 22(7), 825–830. [https://doi.org/10.1016/S0142-9418\(03\)00018-7](https://doi.org/10.1016/S0142-9418(03)00018-7).
- Najjar, A. M. K., Yunus, W. M. Z. W., Ahmad, M. B., & Rahman, M. Z. A. (2000). Preparation and characterization of poly(2-acrylamido-2-methylpropane-sulfonic acid) grafted chitosan using potassium persulfate as redox initiator. *Journal of Applied Polymer Science*, 77(10), 2314–2318. [https://doi.org/10.1002/1097-4628\(20000906\)77:10<2314::aid-app25>3.0.co;2-7](https://doi.org/10.1002/1097-4628(20000906)77:10<2314::aid-app25>3.0.co;2-7).
- Nakauma, M., Funami, T., Noda, S., Ishihara, S., Al-Assaf, S., Nishinari, K., & Phillips, G. O. (2008). Comparison of sugar beet pectin, soybean soluble polysaccharide, and gum arabic as food emulsifiers. 1. Effect of concentration, pH, and salts on the emulsifying properties. *Food Hydrocolloids*, 22(7), 1254–1267. <https://doi.org/10.1016/j.foodhyd.2007.09.004>.
- Nigam, P., Armour, G., Banat, I. M., Singh, D., & Marchant, R. (2000). Physical removal of textile dyes from effluents and solid-state fermentation of dye-adsorbed agricultural residues. *Bioresource Technology*, 72(3), 219–226. [https://doi.org/10.1016/S0960-8524\(99\)00123-6](https://doi.org/10.1016/S0960-8524(99)00123-6).
- Nishioka, N., & Kosai, K. (1981). Homogeneous graft copolymerization of vinyl monomers onto cellulose in a dimethyl sulfoxide–paraformaldehyde solvent system. I. Acrylonitrile and methyl methacrylate. *Polymer Journal*, 13(12), 1125–1133. <https://doi.org/10.1295/polymj.13.1125>.
- Ogiwara, Y., Umasaka, T., & Kubota, H. (1979). Formation of peroxide on aldehyde cellulose and its ability to initiate graft copolymerization. *Journal of Applied Polymer Science*, 23(3), 837–845. <https://doi.org/10.1002/app.1979.070230318>.
- Ong, S. T., Lee, C. K., & Zainal, Z. (2007). Removal of basic and reactive dyes using ethylenediamine modified rice hull. *Bioresource Technology*, 98(15), 2792–2799. <https://doi.org/10.1016/j.biortech.2006.05.011>.
- Otsu, T., Matsunaga, T., Kuriyama, A., & Yoshioka, M. (1989). Living radical polymerization through the use of iniferters: Controlled synthesis of polymers. *European Polymer Journal*, 25(7–8), 643–650. [https://doi.org/10.1016/0014-3057\(89\)90023-2](https://doi.org/10.1016/0014-3057(89)90023-2).
- Pandey, P. K., Banerjee, J., Taunk, K., & Behari, K. (2003). Graft copolymerization of acrylic acid onto xanthum gum using a potassium monopersulfate/Fe²⁺ redox pair. *Journal of Applied Polymer Science*, 89(5), 1341–1346. <https://doi.org/10.1002/app.12302>.
- Penczek, S. (1988). *Polym. Prepr. Am. Chem. Soc. Div. Polym. Chem*, 29(2), 38.
- Peng, T., & Cheng, Y. L. (2001). PNIPAAm and PMAA co-grafted porous PE membranes: Living radical co-grafting mechanism and multi-stimuli responsive permeability. *Polymer*, 42(5), 2091–2100. [https://doi.org/10.1016/s0032-3861\(00\)00369-4](https://doi.org/10.1016/s0032-3861(00)00369-4).
- Peniche, C., Argüelles-Monal, W., & Goycoolea, F. M. (2008). Chitin and chitosan: Major sources, properties and applications. In M. N. Belgacem & A. Gandini (Eds.), *Monomers, polymers and composites from renewable resources* (pp. 517–542). Elsevier Science. <https://doi.org/10.1016/b978-0-08-045316-3.00025-9>.

- Pillai, C. K. S., Paul, W., & Sharma, C. P. (2009). Chitin and chitosan polymers: Chemistry, solubility and fiber formation. *Progress in Polymer Science*, 34(7), 641–678. <https://doi.org/10.1016/j.progpolymsci.2009.04.001>.
- Pourjavadi, A., Harzandi, A. M., & Hosseinzadeh, H. (2004). Modified carrageenan 3. Synthesis of a novel polysaccharide-based superabsorbent hydrogel via graft copolymerization of acrylic acid onto kappa-carrageenan in air. *European Polymer Journal*, 40(7), 1363–1370. <https://doi.org/10.1016/j.eurpolymj.2004.02.016>.
- Pradhan, A. K., Pati, N. C., & Nayak, P. L. (1982). Grafting vinyl monomers onto nylon 6. IV. Graft copolymerization of methyl methacrylate onto nylon 6 using the V⁵⁺-thiourea redox system. *Journal of Applied Polymer Science*, 27(5), 1839–1843. <https://doi.org/10.1002/app.1982.070270540>.
- Prasad, K., Mehta, G., Meena, R., & Siddhanta, A. K. (2006). Hydrogel-forming agar-graft-PVP and k-carrageenan-graft-PVP blends: Rapid synthesis and characterization. *Journal of Applied Polymer Science*, 102(4), 3654–3663. <https://doi.org/10.1002/app.24145>.
- Ramakrishna, K. R., & Viraraghavan, T. (1997). Dye removal using low cost adsorbents. *Water Science and Technology*, 36(2–3), 189–196. [https://doi.org/10.1016/s0273-1223\(97\)00387-9](https://doi.org/10.1016/s0273-1223(97)00387-9).
- Rani, G. U., Konreddy, A. K., Mishra, S., & Sen, G. (2014). Synthesis and applications of polyacrylamide grafted agar as a matrix for controlled drug release of 5-ASA. *International Journal of Biological Macromolecules*, 65, 375–382. <https://doi.org/10.1016/j.ijbiomac.2014.01.034>.
- Rani, P., Mishra, S., & Sen, G. (2013). Microwave based synthesis of polymethyl methacrylate grafted sodium alginate: Its application as flocculant. *Carbohydrate Polymers*, 91(2), 686–692. <https://doi.org/10.1016/j.carbpol.2012.08.023>.
- Rani, P., Sen, G., Mishra, S., & Jha, U. (2012). Microwave assisted synthesis of polyacrylamide grafted gum ghatti and its application as flocculant. *Carbohydrate Polymers*, 89(1), 275–281. <https://doi.org/10.1016/j.carbpol.2012.03.009>.
- Reetz, M. T., Knauf, T., Minet, U., & Bingel, C. (1988). Metal-free carbanion salts as initiators for the anionic polymerization of acrylic and methacrylic acid esters. *Angewandte Chemie International Edition in English*, 27(10), 1373–1374. <https://doi.org/10.1002/anie.198813731>.
- Reis, A. V., Guilherme, M. R., Cavalcanti, O. A., Rubira, A. F., & Muniz, E. C. (2006). Synthesis and characterization of pH-responsive hydrogels based on chemically modified Arabic gum polysaccharide. *Polymer*, 47(6), 2023–2029. <https://doi.org/10.1016/j.polymer.2006.01.058>.
- Retuert, J., & Yazdani-Pedram, M. (1993). Cocatalyst effect in potassium persulfate initiated grafting onto chitosan. *Polymer Bulletin*, 31(5), 559–562. <https://doi.org/10.1007/bf00297892>.
- Reyes, Z., Rist, C. E., & Russell, C. R. (1966). Grafting vinyl monomers to starch by ceric ion. I. Acrylonitrile and acrylamide. *Journal of Polymer Science Part A-1: Polymer Chemistry*, 4(5), 1031–1043. <https://doi.org/10.1002/pol.1966.150040506>.
- Richards, G. N. (1961a). Diazonium derivatives of cellulose as initiators of graft polymerization. *Journal of Applied Polymer Science*, 5(17), 553–557. <https://doi.org/10.1002/app.1961.070051709>.
- Richards, G. N. (1961b). Initiation of graft polymerization on cellulose by hydroxyl radicals and by ceric salts. *Journal of Applied Polymer Science*, 5(17), 539–544. <https://doi.org/10.1002/app.1961.070051707>.
- Roy, D., Semsarilar, M., Guthrie, J. T., & Perrier, S. (2009). Cellulose modification by polymer grafting: A review. *Chemical Society Reviews*, 38(7), 2046–2064. <https://doi.org/10.1039/b808639g>.
- Saegusa, T., Ikeda, H., & Fujii, H. (1973). Isomerization polymerization of 2-oxazoline. V. Kinetic studies on the polymerization of 2-oxazoline. *Macromolecules*, 6(3), 315–319. <https://doi.org/10.1021/ma60033a002>.
- Schwab, E., Stannett, V., Rakowitz, D. H., & Magrane, J. K. (1962). Paper grafted with vinyl monomers using the ceric ion method. *Tappi*, 45(5), 390–400.
- Sen, G., & Pal, S. (2009). Microwave initiated synthesis of polyacrylamide grafted carboxymethylstarch (CMS-g-PAM): Application as a novel matrix for sustained drug release. *International Journal of Biological Macromolecules*, 45(1), 48–55. <https://doi.org/10.1016/j.ijbiomac.2009.03.012>.

- Sen, G., Rani, G. U., & Mishra, S. (2013). Microwave assisted synthesis of poly(2-hydroxyethylmethacrylate) grafted agar (Ag-gP (HEMA)) and its application as a flocculant for wastewater treatment. *Frontiers of Chemical Science and Engineering*, 7(3), 312–321. <https://doi.org/10.1007/s11705-013-1344-3>.
- Sen, G., Singh, R. P., & Pal, S. (2010). Microwave-initiated synthesis of polyacrylamide grafted sodium alginate: Synthesis and characterization. *Journal of Applied Polymer Science*, 115(1), 63–71. <https://doi.org/10.1002/app.30596>.
- Setia, A., & Kumar, R. (2014). Microwave assisted synthesis and optimization of *Aegle marmelos*-g-poly(acrylamide): Release kinetics studies. *International Journal of Biological Macromolecules*, 65, 462–470. <https://doi.org/10.1016/j.ijbiomac.2014.02.006>.
- Shah, S. B., Patel, C. P., & Trivedi, H. C. (1994). Fenton's reagent-initiated graft copolymerization of acrylonitrile onto sodium alginate. *Journal of Applied Polymer Science*, 51(8), 1421–1426. <https://doi.org/10.1002/app.1994.070510809>.
- Shah, S. B., Patel, C. P., & Trivedi, H. C. (1995). Ceric-induced grafting of acrylate monomers onto sodium alginate. *Carbohydrate Polymers*, 26(1), 61–67. [https://doi.org/10.1016/0144-8617\(95\)98836-6](https://doi.org/10.1016/0144-8617(95)98836-6).
- Shanmugapriya, A., Srividhya, A., Ramya, R., & Sudha, P. N. (2011). Graft copolymerization of chitosan with acrylic acid used in waste water treatment. *International Journal of Environmental Sciences*, 1(7), 2086–2095. Available in: <http://www.indianjournals.com/ijor.aspx?target=ijor:ijes&volume=1&issue=7&article=059>
- Sharma, B. R., Kumar, V., & Soni, P. L. (2003). Graft copolymerization of acrylonitrile onto *Cassia tora* gum with ceric ammonium nitrate–nitric acid as a redox initiator. *Journal of Applied Polymer Science*, 90(1), 129–136. <https://doi.org/10.1002/app.12593>.
- Shen, H., Hu, X., Bei, J., & Wang, S. (2008). The immobilization of basic fibroblast growth factor on plasma-treated poly(lactide-co-glycolide). *Biomaterials*, 29(15), 2388–2399. <https://doi.org/10.1016/j.biomaterials.2008.02.008>.
- Shi, R., Zhang, Z., Liu, Q., Han, Y., Zhang, L., Chen, D., & Tian, W. (2007). Characterization of citric acid/glycerol co-plasticized thermoplastic starch prepared by melt blending. *Carbohydrate Polymers*, 69(4), 748–755. <https://doi.org/10.1016/j.carbpol.2007.02.010>.
- Simionescu, C. I., & Oprea, S. (1972). Researches in the field of the grafting on cellulose with acrylic and methacrylic derivatives. *Journal of Polymer Science Part C: Polymer Symposia*, 37(1), 251–263. <https://doi.org/10.1002/polc.5070370115>.
- Singh, B., & Kumar, S. (2008). Synthesis and characterization of psyllium-NVP based drug delivery system through radiation crosslinking polymerization. *Nuclear Instruments and Methods in Physics Research Section B: Beam Interactions with Materials and Atoms*, 266(15), 3417–3430. <https://doi.org/10.1016/j.nimb.2008.04.022>.
- Singh, B., & Vashishtha, M. (2008). Development of novel hydrogels by modification of sterculia gum through radiation cross-linking polymerization for use in drug delivery. *Nuclear Instruments and Methods in Physics Research Section B: Beam Interactions with Materials and Atoms*, 266(9), 2009–2020. <https://doi.org/10.1016/j.nimb.2008.03.086>.
- Singh, V., & Tripathi, D. N. (2006). Microwave promoted grafting of acrylonitrile onto *Cassia siamea* seed gum. *Journal of Applied Polymer Science*, 101(4), 2384–2390. <https://doi.org/10.1002/app.23878>.
- Singh, V., Kumari, P. L., Tiwari, A., & Pandey, S. (2010a). Alumina-supported microwave synthesis of *Cassia marginata* seed gum-graft-polyacrylamide. *Journal of Applied Polymer Science*, 117(6), 3630–3638. <https://doi.org/10.1002/app.32273>.
- Singh, V., Kumari, P. L., Tiwari, A., & Sharma, A. K. (2007a). Alumina supported synthesis of *Cassia marginata* gum-g-poly (acrylonitrile) under microwave irradiation. *Polymers for Advanced Technologies*, 18(5), 379–385. <https://doi.org/10.1002/pat.899>.
- Singh, V., Sharma, A. K., & Maurya, S. (2009). Efficient cadmium (II) removal from aqueous solution using microwave synthesized guar gum-graft-poly(ethylacrylate). *Industrial & Engineering Chemistry Research*, 48(10), 4688–4696. <https://doi.org/10.1021/ie801416z>.

- Singh, V., Sharma, A. K., Kumari, P., & Tiwari, S. (2008). Efficient chromium (VI) adsorption by *Cassia marginata* seed gum functionalized with poly(methylmethacrylate) using microwave irradiation. *Industrial & Engineering Chemistry Research*, 47(15), 5267–5276. <https://doi.org/10.1021/ie070467j>.
- Singh, V., Singh, S. K., & Maurya, S. (2010b). Microwave induced poly(acrylic acid) modification of *Cassia javanica* seed gum for efficient hg(II) removal from solution. *Chemical Engineering Journal*, 160(1), 129–137. <https://doi.org/10.1016/j.cej.2010.03.020>.
- Singh, V., Tiwari, A., Pandey, S., & Singh, S. K. (2007b). Peroxydisulfate initiated synthesis of potato starch-graft-poly(acrylonitrile) under microwave irradiation. *Express Polymer Letters*, 1(1), 51–58. <https://doi.org/10.3144/expresspolymlett.2007.10>.
- Singh, V., Tiwari, A., Pandey, S., & Singh, S. K. (2006a). Microwave-accelerated synthesis and characterization of potato starch-g-poly(acrylamide). *Starch-Starke*, 58(10), 536–543. <https://doi.org/10.1002/star.200600520>.
- Singh, V., Tiwari, A., Shukla, P., Singh, S. P., & Sanghi, R. (2006b). Grafting of methylmethacrylate on to the plant seed galactomannans using potassium persulphate/ascorbic acid redox pair. *Reactive and Functional Polymers*, 66(11), 1306–1318. <https://doi.org/10.1016/j.reactfunctpolym.2006.03.013>.
- Singh, V., Tiwari, A., Tripathi, D. N., & Sanghi, R. (2004a). Grafting of polyacrylonitrile onto guar gum under microwave irradiation. *Journal of Applied Polymer Science*, 92(3), 1569–1575. <https://doi.org/10.1002/app.20099>.
- Singh, V., Tiwari, A., Tripathi, D. N., & Sanghi, R. (2004b). Microwave assisted synthesis of guar-g-polyacrylamide. *Carbohydrate Polymers*, 58(1), 1–6. <https://doi.org/10.1016/j.carbpol.2004.04.010>.
- Singh, V., Tiwari, A., Tripathi, D. N., & Sanghi, R. (2006c). Microwave enhanced synthesis of chitosan-graft-polyacrylamide. *Polymer*, 47(1), 254–260. <https://doi.org/10.1016/j.polymer.2005.10.101>.
- Singh, V., Tripathi, D. N., Tiwari, A., & Sanghi, R. (2005). Microwave promoted synthesis of chitosan-graft-poly(acrylonitrile). *Journal of Applied Polymer Science*, 95(4), 820–825. <https://doi.org/10.1002/app.21245>.
- Singh, V., Tripathi, D. N., Tiwari, A., & Sanghi, R. (2006d). Microwave synthesized chitosan-graft-poly(methylmethacrylate): An efficient Zn²⁺ ion binder. *Carbohydrate Polymers*, 65(1), 35–41. <https://doi.org/10.1016/j.carbpol.2005.12.002>.
- Solomon, D. H., Rizzardo, E., & Cacioli, P. (1986). U.S. Patent 4 581 429.
- Sonmez, H. B., Senkal, B. F., Sherrington, D. C., & Bıcak, N. (2003). Atom transfer radical graft polymerization of acrylamide from *N*-chlorosulfonamidated polystyrene resin, and use of the resin in selective mercury removal. *Reactive and Functional Polymers*, 55(1), 1–8. [https://doi.org/10.1016/s1381-5148\(02\)00193-1](https://doi.org/10.1016/s1381-5148(02)00193-1).
- Stannett, V. (1981). Grafting. *Radiation Physics and Chemistry*, 18(1–2), 215–222.
- Szwarc, M., Levy, M., & Milkovich, R. (1956). Polymerization initiated by electron transfer to monomer. A new method of formation of block polymers I. *Journal of the American Chemical Society*, 78(11), 2656–2657. <https://doi.org/10.1021/ja01592a101>.
- Szwarc, R. (1968). *Carbanion, living polymers and Electron transfer processes*. New York: Interscience.
- Taghizadeh, M. T., & Mehrdad, A. (2006). Kinetic study of graft polymerization of acrylic acid and ethyl methacrylate onto starch by ceric ammonium nitrate. *Iranian journal of chemistry and chemical engineering*, 25(1), 1–12.
- Taher, N. H., Dessouki, A. M., Khalil, F. H., & El-Arnaouty, M. B. (1996). Preparation and properties of cationic membranes obtained by radiation grafting of vinyl monomers onto poly(tetrafluoroethylene-perfluoropropylvinyl ether) (PFA) films. *Polymer International*, 41(4), 383–389. [https://doi.org/10.1002/\(sici\)1097-0126\(199612\)41:4<383::aid-pi622>3.0.co;2-2](https://doi.org/10.1002/(sici)1097-0126(199612)41:4<383::aid-pi622>3.0.co;2-2).
- Teysseyé, P. H., Fayt, R., Hautekeer, J. P., Jacobs, C., Jerome, R., Leemans, L., & Varshney, S. K. (1990, February). New prospects for “living” anionic polymerization of (meth) acrylic

- esters. *Makromolekulare Chemie. Macromolecular Symposia*, 32(1), 61–73. <https://doi.org/10.1002/masy.19900320107>.
- Tiwari, A., & Singh, V. (2008). Microwave-induced synthesis of electrical conducting gum acacia-graft-polyaniline. *Carbohydrate Polymers*, 74(3), 427–434. <https://doi.org/10.1016/j.carbpol.2008.03.015>.
- Tosh, B., & Routray, C. R. (2011). Homogeneous grafting of PMMA onto cellulose in presence of Ce^{4+} as initiator. *In. J. Chem. Techno.*, 18(3), 234–243.
- Tsubokawa, N., Kobayashi, M., & Ogasawara, T. (1999). Graft polymerization of vinyl monomers initiated by azo groups introduced onto organic pigment surface. *Progress in Organic Coatings*, 36(1–2), 39–44. [https://doi.org/10.1016/s0300-9440\(98\)00083-6](https://doi.org/10.1016/s0300-9440(98)00083-6).
- Tsubokawa, N., Maruyama, K., Sone, Y., & Shimomura, M. (1989). Graft polymerization of acrylamide from ultrafine silica particles by use of a redox system consisting of ceric ion and reducing groups on the surface. *Polymer Journal*, 21(6), 475–481. <https://doi.org/10.1295/polymj.21.475>.
- Varma, D. S., & Narashinan, V. (1972). Thermal behavior of graft copolymers of cotton cellulose and acrylate monomers. *Journal of Applied Polymer Science*, 16(1972), 3325–3339. <https://doi.org/10.1002/app.1972.070161222>.
- Vijan, V., Kaity, S., Biswas, S., Isaac, J., & Ghosh, A. (2012). Microwave assisted synthesis and characterization of acrylamide grafted gellan, application in drug delivery. *Carbohydrate Polymers*, 90(1), 496–506. <https://doi.org/10.1016/j.carbpol.2012.05.071>.
- Walling, C. (1957). *Free radicals in solution*. New York: John Wiley and Sons. Inc.
- Wang, G., Song, Z., Lin, Z., & Wang, L. (2002). Preparation for graft copolymers of sawdust/vinyl monomers and their application for removal of dye. *Journal of Applied Polymer Science*, 83(11), 2390–2396. <https://doi.org/10.1002/app.10303>.
- Wang, G. H., Song, Z. Q., & Wang, L. S. (2001). Study on the preparation of grafted copolymer of acrylonitrile/wood powder and adsorption properties of its hydrolysate. *Chemistry and Industry of Forest Products*, 21(2), 9–15.
- Wenzel, A., Yanagishita, H., Kitamoto, D., Endo, A., Haraya, K., Nakane, T., Hanai, N., Matsuda, H., Kamuswet, H., & Paul, D. (2000). Effects of preparation condition of photoinduced graft filling-polymerized membranes on pervaporation performance. *Journal of Membrane Science*, 179(1–2), 69–77. [https://doi.org/10.1016/s0376-7388\(00\)00502-0](https://doi.org/10.1016/s0376-7388(00)00502-0).
- Xie, W., Xu, P., Wang, W., & Liu, Q. (2002). Preparation and antibacterial activity of a water-soluble chitosan derivative. *Carbohydrate Polymers*, 50(1), 35–40. [https://doi.org/10.1016/S0144-8617\(01\)00370-8](https://doi.org/10.1016/S0144-8617(01)00370-8).
- Yamaguchi, T., Yamahara, S., Nakao, S. I., & Kimura, S. (1994). Preparation of pervaporation membranes for removal of dissolved organics from water by plasma-graft filling polymerization. *Journal of Membrane Science*, 95(1), 39–49. [https://doi.org/10.1016/0376-7388\(94\)85027-5](https://doi.org/10.1016/0376-7388(94)85027-5).
- Yazdani-Pedram, M., Lagos, A., Campos, N., & Retuert, J. (1992). Comparison of redox initiators reactivities in the grafting of methyl methacrylate onto chitin. *International Journal of Polymeric Materials*, 18(1–2), 25–37. <https://doi.org/10.1080/00914039208034811>.
- Zahran, A. H., & Zohdy, M. H. (1986). Effect of radiation chemical treatment on sisal fibers I. radiation induced grafting of ethyl acrylate. *Journal of Applied Polymer Science*, 31(6), 1925–1934. <https://doi.org/10.1002/app.1986.070310633>.
- Zahran, M. K., & Mahmoud, R. I. (2003). Peroxydiphosphate–metal ion–cellulose thiocarbonate redox system-induced graft copolymerization of vinyl monomers onto cotton fabric. *Journal of Applied Polymer Science*, 87(12), 1879–1889. <https://doi.org/10.1002/app.11542>.
- Zahran, M. K., & Rehan, M. F. (2006). Grafting of acrylic acid onto flax fibers using Mn(IV)-citric acid redox system. *Journal of Applied Polymer Science*, 102(3), 3028–3036. <https://doi.org/10.1002/app.24690>.
- Zhang, J., Yuan, J., Yuan, Y., Shen, J., & Lin, S. (2003a). Chemical modification of cellulose membranes with sulfo ammonium zwitterionic vinyl monomer to improve hemocompatibility. *Colloids and Surfaces B: Biointerfaces*, 30(3), 249–257. [https://doi.org/10.1016/s0927-7765\(03\)00069-9](https://doi.org/10.1016/s0927-7765(03)00069-9).

- Zhang, J., Yuan, Y., Shen, J., & Lin, S. (2003b). Synthesis and characterization of chitosan grafted poly(*N,N*-dimethyl-*N*-methacryloxyethyl-*N*-(3-sulfopropyl) ammonium) initiated by ceric (IV) ion. *European Polymer Journal*, 39(4), 847–850. [https://doi.org/10.1016/S0014-3057\(02\)00286-0](https://doi.org/10.1016/S0014-3057(02)00286-0).
- Zhang, J., Zhang, S., Yuan, K., & Wang, Y. (2007). Graft copolymerization of artemisia seed gum with acrylic acid under microwave and its water absorbency. *Journal of Macromolecular Science, Part A: Pure and Applied Chemistry*, 44(8), 881–885. <https://doi.org/10.1080/10601320701407003>.
- Zhang, L. M., & Chen, L. Q. (2002). Water-soluble grafted polysaccharides containing sulfobetaine groups: Synthesis and characterization of graft copolymers of hydroxyethyl cellulose with 3-dimethyl (methacryloyloxyethyl) ammonium propane sulfonate. *Journal of Applied Polymer Science*, 83(13), 2755–2761. <https://doi.org/10.1002/app.10191>.
- Zheng, T., Wang, P., Zhang, Z., & Zhao, B. (2005). Microwave irradiation copolymerization of super absorbents from corn starch and sodium acrylate. *Journal of Applied Polymer Science*, 95(2), 264–269. <https://doi.org/10.1002/app.21265>.
- Zohuriaan, M. M. (2005). Advances in chitin and chitosan modification through graft copolymerization. 14(3), 235–265. Available in: <https://www.sid.ir/en/journal/viewpaper.aspx?id=33941>
- Zu, J., Hu, Z., Wang, W., Zhang, J., Pino, E. S., Gu, J., & Tong, L. (2007). The effect of additives on radiation-induced grafting of AA and SSS onto HDPE. *Journal of Radioanalytical and Nuclear Chemistry*, 273(2), 479. <https://doi.org/10.1007/s10967-007-6816-9>.

Chapter 9

Grafting Functional Groups onto Biodegradable Thermoplastic Polyesters



Casparus J. R. Verbeek and Chanelle Gavin

Abstract A general awareness of the environmental impacts of plastics has caused behavioral changes in the public sector. This in turn has led to research related to biodegradable or sustainable alternatives to petrochemical plastics. Biodegradable polymers have been around for years (e.g. poly(ϵ -caprolactone) (PCL), poly(butylene succinate) (PBS) and poly(lactic acid) (PLA)). However, these have recently become an affordable alternative. PLA and poly(butylene adipate-*co*-terephthalate) (PBAT) are two polyesters that have gained significant research interest as biodegradable alternatives, especially for the preparation of natural or biobased polymer blends. Nonetheless, the lack of miscibility in some polymer blends limits their usefulness unless a compatibilizing agent is used. A very common strategy is to graft a functional monomer into the polymer backbone, of which maleic anhydride (MA) is the most common, but not the only one. This chapter explores the use of grafting functional groups onto polyesters in light of the well-established field of free radical grafting of polyolefins to achieve materials that are effective at compatibilizing biodegradable or compostable blends.

Keywords Blend · Compatibilizer · Polyester · Reactive extrusion

9.1 Introduction

The global polymer market typically grows approx. 7% annually and exceeded US \$60 billion in 2016 (Smith and Verbeek 2018). The polymer industry is mature in many aspects, but research is being done to manipulate material properties for

C. J. R. Verbeek (✉)

Plastics Centre of Excellence, Faculty of Engineering, University of Auckland,
Auckland, New Zealand

e-mail: johan.verbeek@auckland.ac.nz

C. Gavin

School of Engineering, University of Waikato, Hamilton, New Zealand

© The Editor(s) (if applicable) and The Author(s), under exclusive license
to Springer Nature Switzerland AG 2020

T. J. Gutiérrez (ed.), *Reactive and Functional Polymers Volume Two*,
https://doi.org/10.1007/978-3-030-45135-6_9

specific applications. The last few years have seen a rapid increase in the development of sustainable polymer materials, as well as those derived from natural resources. Globally, the market for biodegradable resins is expected to reach more than US \$16 billion by 2022 (Smith and Verbeek 2018).

The widespread application of biodegradable polymers as commodity materials has been slow, mainly due to the higher cost of the resin compared to petroleum-based alternatives. For example, poly(lactic acid) (PLA) and poly(butylene adipate-*co*-terephthalate) (PBAT) generally sold for more than 3 USD/kg and poly(*ε*-caprolactone) (PCL) can be up to 20 USD/kg, compared to commodity polymers such as poly(ethylene) (PE) and poly(propylene) (PP) which are in the region of about 1 USD/kg (Smith and Verbeek 2018).

The processing and subsequent properties of biobased polymers can also be a challenge. They sometimes have narrow processing windows and mechanical properties that are often not suitable for the purpose with a lack of balance between stiffness, strength and toughness (or impact strength). This has significantly slowed their widespread adoption and it is generally concluded that commercialization would require inexpensive techniques to modify these materials (Raquez et al. 2008b).

As a result, research into polymer blends to achieve property and price advantages is continuously expanding. Achieving good mechanical properties in particular depends largely on the ability to manipulate and control interfacial properties and creating the correct morphology (Mani et al. 1999; Raquez et al. 2008b). However, this must be balanced against blend's biodegradability and careful consideration may offer a strategy to modify biodegradation rates for specific applications (Raquez et al. 2008b).

Biodegradable polyesters, such as PCL and PLA, are good examples of polymers that have been modified by melt blending with a focus on the dispersion of one in the another, using functional polymers as interfacial modifiers or incorporating block and random copolymers (Mani et al. 1999; Gutiérrez and Alvarez 2017a,b,c; Gutiérrez 2018).

Grafting is a convenient way to prepare these functional polymers and a variety of methods are available in melt, solid or solution states. The most convenient method is the melt or reactive extrusion (REx) for which free radical grafting of maleic anhydride (MA) onto polyolefins is probably the most widespread industrial application (Gutiérrez et al. 2017).

This chapter considers the free radical grafting of biodegradable polyesters for their application in polymer blends. More specifically, it reviews the common biodegradable polyesters used today, the functional groups used for grafting, and the mechanisms by which grafting occurs. It also considers the equipment used for producing these materials and how grafting affects the properties of the newly formed functional material. A significant amount of research has been done to examine MA grafting onto polyolefins, however, fewer studies focus on grafting functional groups onto polyesters (John et al. 1997a).

9.2 Reactive Extrusion

One of the main objectives of grafting polymers through REX is an improvement in the material properties by introducing chemical groups which alter the polymer's characteristics, such as adhesion and reactivity with other polymers (Herniou--Julien et al. 2019; Morais et al. 2019). Free-radical grafting functional groups onto polyolefins *via* REX has gained widespread industrial applications and several functional PP and PE grades are commercially sold. The general consensus is that the reaction pathway for grafting depends on the polymer's molecular structure, and therefore, some variations between grafting efficiencies can occur for different polymers. In addition, by using a peroxide as initiator, crosslinking and other side reactions occur at the same time (Fang et al. 2008).

One of the most used monomers for grafting is MA. However, there are many other functional groups available, such as carboxylic acids, epoxy groups, vinylsilanes and other anhydrides (Raquez et al. 2008b; Wenfei et al. 2010; Fink 2013; Xijun et al. 2013). The modified polyolefins are characterized by a change in polarity, adhesion and greater miscibility compared to polar polymers (Kučera et al. 2017). When carboxylic acids are used, the acid is sometimes neutralized using hydroxides or metal oxides, which further changes the properties and uses of the grafted polymer (Krivoguz et al. 2003).

On the other hand, the development of functional polyesters is a more challenging issue and has hardly been explored compared to polyolefins (Morais et al. 2019). Functional biodegradable polyesters can be prepared by ring opening polymerization or polycondensation starting from functional monomers, but it is a rather expensive proposition and depends largely on the scale. However, the technologies available to functionalize polyolefins could be adapted here and would minimize the economic impact of changing raw materials (Signori et al. 2011).

The general concept of grafting is not new, and dates back to the early nineteenth century after the development of oil-resistant butadiene-acrylonitrile synthetic rubbers and the modification of natural rubber in its latex state (White and Sasaki 2003). During the 1960s, an effort was made to develop continuous extrusion processes for free radical grafting using peroxides (White and Sasaki 2003). One of the first patents on the use of twin-screw extrusion for grafting was filed in 1972, for grafting anhydrides and carboxylic acids onto polyolefins. Since then, twin-screw extruders have been dominant (White and Sasaki 2003).

REX is thus also an attractive route for processing biodegradable plastics, since it improves the commercial viability and profitability of these materials (Fink 2013). Because of these characteristics, REX is often used for a variety of chemical reactions to:

- Produce high molecular weight (M_w) polymers.
- Controlled degradation and crosslinking of polymers.
- Functionalization of commodity polymers.
- Interchain copolymer formation.

Table 9.1 Benefits and challenges of REX

Benefits	Challenges
Solvent free	Intimate reagent mixing mandatory
Quick preparation	High reaction temperatures are required
Simple product isolation	Side reactions, e.g. degradation
Continuous process	Crosslinking or discoloration
Economic	

Compared to other methods, such as solution polymerization, the benefits and challenges of REX, can be summarized in Table 9.1. REX is considered one of the most practical and profitable methods, since it achieves a better degree of mixing, is solvent-free, has a shorter production time, and is suitable for mass production (Signori et al. 2011; Standau et al. 2019).

Part of the benefits of using REX is that it allows multiple feed, venting and provides a high intensity distributive and dispersive mixture. Grafting is thus achieved using one of the following methods:

- The free-radical initiator the polar monomer and the polymer are added simultaneously.
- The polymer can be melted in a mixer (low pressure system) before being injected into the extruder.
- The polymer is fed first, and then the free-radical initiator and the polar monomer are fed separately at different points along the barrel.

One of the major applications of graft copolymers is their use as compatibilizers in polymer blends, which is a widely used method to tailor the properties of materials. Several studies have been devoted to the issue and to the challenge for obtaining adequately dispersed blends using various combinations of polymers, including polyesters such as PCL and PLA. Achieving a good dispersion of one phase in another is essential, since the properties of the final material depends largely on the characteristics of the interface (Nocita et al. 2017). The properties of synthetic and natural polymer blends can also be improved with compatibilizers, e.g. using MA-grafted PBAT as a compatibilizer has resulted in fine domain sizes and good dispersion of the soy protein concentrate in PBAT (Chen and Zhang 2010).

The compatibility of modified polymer compositions with a polar material can be controlled by the selection of the monomer, the level of grafting and the blend processing conditions. Tailoring the compatibility of blends with modified polymer compositions leads to better processability and improved physical properties of the resulting blend.

It is recognized that the miscibility between polymers is determined by a balance of enthalpic (ΔH_m) and entropic (ΔS_m) contributions to the free energy of mixing (ΔG_m). While for small molecules the energy is high enough to ensure miscibility, for polymers the entropy is almost zero, which makes enthalpy decisive for determining miscibility (Zarrintaj et al. 2019).

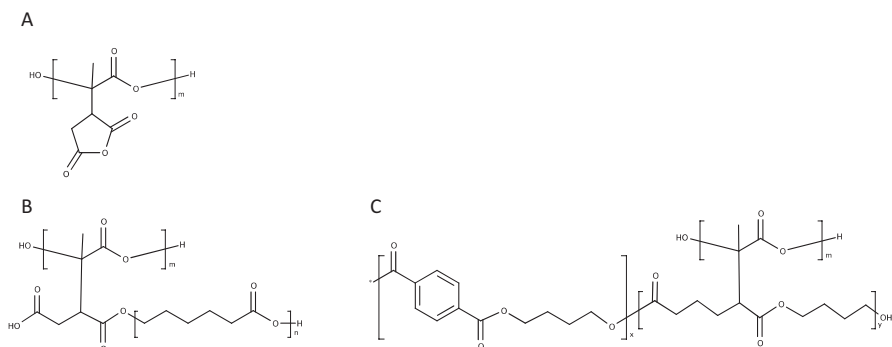


Fig. 9.1 (A) MA grafted onto PLA, (B) PLA crosslinked with PCL and (C) PBAT crosslinked with PLA. Reproduced with permission from Al-Itry et al. (2012)

For spontaneous mixing, ΔG_m must be negative, which means that the mixture is exothermic ($\Delta H_m < 0$, enthalpy of mixing) and will mix spontaneously, while for endothermic mixtures miscibility will only occur at high temperatures (Fink 2013). However, thermodynamic miscibility may not be required and compatibility, where the blend has useful properties, may be sufficient. This can be achieved by:

- Addition of a compatibilizer before or during processing.
- Adjustment of viscosity ratios to allow formation of a desired phase morphology.
- *In situ* formation of a compatibilizer.
- Introduction of crosslinks in one of the phases.

One approach to compatibilization is the addition of a block copolymer having segments with chemical structures or solubility parameters similar to those of the polymers that are blended. In general, this is extremely efficient, although it is rarely used for commercial applications. Another less costly approach is reactive composition, by which the compatibilizer is formed at the interface (Fink 2013). For example, PBAT and PLA or PCL and PLA can be reactively combined in the presence of a free radical initiator (dicumyl peroxide - DCP) and/or MA, which produce a compatible blend as is shown in Fig. 9.1 (Gardella et al. 2014; Ma et al. 2014).

9.3 Biodegradable Polyesters

Biodegradable and/or biobased polymers often struggle to compete in the market, currently dominated by low-cost petrochemical polymers. Despite this, the new biobased materials continue to receive academic and industrial interest. However, the redesign of products and materials requires the adaptation of processes currently tailored for polyolefin materials. Biodegradable aliphatic polyesters such as PLA, poly(butylene succinate) (PBS), poly(butylene succinate-co-adipate) are a

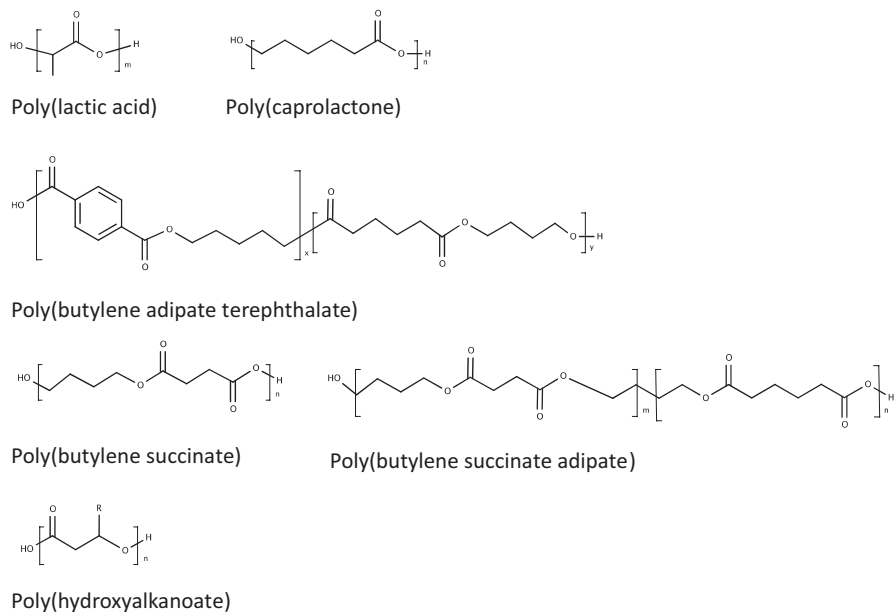


Fig. 9.2 Common biopolyesters

promising group of materials based on their performance, renewability and constant cost reduction (Fig. 9.2) (Signori et al. 2011; Morais et al. 2019).

The reason for grafting these polyesters is to modify properties such as impact resistance or melt strength, or to functionalize them to then be used as blend compatibilizers. An important limitation of PCL is the lack of functional groups, which limits its compatibility with other polymers (Riva et al. 2005). In addition, polyesters such as PBAT, PCL, PLA, poly(ester amide) (PEA), poly(hydroxybutyrate-co-valerate) (PHBV) and poly(hydroxy-ester ether) (PHEE) to be blended with starch, these polymers require some degree of functionality (Nabar et al. 2005). A similar behavior was observed by Wu (2015) for biopolyester/collagen blends, where better adhesion between collagen and polyhydroxyalkanoate (PHA) was observed after grafting PHA with MA.

9.3.1 Poly(Butylene Adipate-Co-Terephthalate) (PBAT)

Among the biodegradable polyesters mentioned, PBAT has attracted significant attention in the literature. PBAT is an aliphatic-aromatic polyester and has a high strain at break (ϵ_b) and is very suitable for packaging and agricultural films (Hayes et al. 2019; Merino et al. 2019). PBAT is a synthetic biodegradable polymer, based on adipic acid, butanediol and terephthalic acid. It is often used to improve the biodegradability of blends and composites or to improve the properties in other

biobased materials. However, it requires the addition of a compatibilizer to ensure optimal properties. PBAT is most commonly grafted with MA using REX in the presence of a peroxide initiator (Nabar et al. 2005; Raquez et al. 2008a; Chen and Zhang 2009; Wu 2012a, b; Adrar et al. 2017; Kashani Rahimi et al. 2017; Liu et al. 2017; Muthuraj et al. 2017; Fourati et al. 2018).

9.3.2 Poly(*Butylene Succinate*) (PBS)

PBS is a very promising biodegradable polyester, synthesized *via* polycondensation of 1,4-butanediol with succinic acid (SA), and can be derived from fossil or renewable resources. PBS has mechanical properties similar to those of PE, as well as has very good processing behavior (Chikh et al. 2016). However, it has a low melt strength and a relatively low Young's modulus (YM) value (Calderon et al. 2019a).

PBS is often used in blends, but requires modification. For example, PBS has been blended with poly(L-lactic acid) (PLLA) and other polymers to improve mechanical properties and processing performance (Phua et al. 2013; Persenaire et al. 2014; Wu et al. 2014; Liu et al. 2015; Yin et al. 2015; Zhu et al. 2017; Picard et al. 2019). Generally, by adding grafted PBS (MAH-*g*-PBS) into blends or composites, a significant improvement in tensile and flexural strength can be expected over the corresponding uncompatibilized material (Signori et al. 2011; Muthuraj et al. 2015).

9.3.3 Poly(*caprolactone*) (PCL)

PCL is a synthetic aliphatic polyester which is generally considered biodegradable by enzymatic activity. It has good processability and high ϵ_b values, but low YM and tensile strength (σ_m) values. However, its high cost limits its applications. For this reason, PCL is often also mixed with other economical biodegradable polymers (Guaras et al. 2016). Several authors have described the grafting of PCL using MA, in the presence of peroxides and when used in blends having greatly improved the mechanical properties (Nitz et al. 2001; Wu 2003; Nabar et al., 2005; Morais et al. 2019). Some authors have also shown that the degree of grafting is higher than some conventional polymers and other biodegradable polyesters (Morais et al. 2019).

9.3.4 Poly(*Lactic Acid*) (PLA)

PLA is a thermoplastic aliphatic polyester derived from renewable biomass and is undoubtedly the most commercially successful biobased polymer. PLA is often used in compatibilized blends, either to improve the properties of the other polymer, or to try to overcome some of its own limitations, such as low melt strength and low

impact strength (Gardella et al. 2014; Persenaire et al. 2014; Dawidziuk et al. 2018). PLA's reactivity for radical grafting is somewhat limited due to the low activity of MA towards the macro-radicals resulting from PLA's structural symmetry, but can be improved in the presence of electron-donating co-monomers (Ku Marsilla and Verbeek 2015b). As with other polyesters, there is an optimum concentration of radicals, which depends on the peroxide/monomer ratio and there are also other side reactions, such as chain scission and crosslinking, which can occur (Mani et al. 1999; Fink 2013).

9.3.5 *Poly(hydroxyalkanoate)s (PHA)*

This class of biodegradable thermoplastic polyesters are serious competitors for replacing petrochemical equivalents. PHAs are produced by bacterial fermentation as intracellular compounds. However, PHA-based materials are very expensive and this still limits their widespread industrial applications. PHA is often blended with other polymers to reduce cost. For example, poly(3-hydroxybutyrate-*co*-3-hydroxyhexanoate) (PHBHH) can be blended with PBAT or PBS, showing the beneficial effect of adding maleated PHBHH to the blend (Chikh et al. 2016; Thirmizir et al. 2017). On the other hand, the REx of poly(3-hydroxybutyrate) (PHB) and a peroxide can be used to alter the crystallization behavior to improve melt spinning (Fink 2013).

9.4 Factors Affecting Grafting

Graft copolymerization is a common technique to modify a polymer's properties with minimal degradation. The type and extent of the changes depend on many factors, the most important being the polymer type, the reagent concentration, the type of monomer, the mixing and processing parameters (Mani et al. 1999; Maharana et al. 2015). However, the efficiency of grafting cannot be improved by increasing only the concentration of the radical initiator or the monomer. Equally important is the proper mixing, and often, the inclusion of comonomers. In fact, grafting without a radical initiator is also possible and can be formed by shear-induced chain scission (Fink 2013).

In order to obtain a high grafting efficiency together with an effective suppression of the side reactions, it is necessary to transform the macroradicals on the backbone as much as possible into graft sites. In general, within reasonable limits, higher reaction temperatures, higher initiator levels and lower yield rates result in higher grafting efficiency (John et al. 1997a, Fink 2013).

Grafting is somewhat complicated by side reactions such as backbiting depolymerization, or hydrolysis, which leads to an undesirable Mw reduction, as shown for many systems such as MA-grafted PLA. However, this could be mitigated by

some additives (chain extenders) that allow the relinking of chains. In addition, branching and/or crosslinking can also occur and depend on the same variables controlling grafting (Standau et al. 2019).

As the name suggests, melt-grafting is performed above the melting point of the polymer in question, typically in melt mixers or extruders. The method is quite generic, since it requires mixing the reagents before processing or melting the polymer first, followed by the addition of the reagent. This could be achieved using side feeders during extrusion. An important step for all polyesters is sufficient drying before processing to prevent degradation during melt processing (Mohanty and Nayak 2010; Muthuraj et al. 2015; Liu et al. 2017). Unreacted monomers and decomposition products can be removed by vacuum.

9.4.1 Initiators

Free radicals can be generated by several compounds. The selection of a grafting initiator during REx is mainly based on the initiator's half-life and solubility in the polymer (Fink 2013; Kučera et al. 2017). Peroxides are commonly used as initiators in graft copolymerization and can be divided into seven groups, providing a range of reactivity: diacyl peroxides, dialkyl peroxides, diperoxyketals, hydroperoxides, ketoneperoxides, peroxydicarbonates and peroxyesters (Takamura et al. 2008). Of these, diacyl peroxides such as benzoyl peroxide (BPO) and di-*t*-butyl peroxide (DTBP) are the most commonly used. To optimize the chemical compatibility or solubility of the peroxides, the organic character of these peroxides must be carefully chosen and peroxides which yield radicals with double bonds have higher grafting efficiency (Fink 2013).

The most important indicator for the activity of an initiator is its half-life ($t_{1/2}$), which is the time required to decompose half of the initial initiator content at a given temperature. For the first order decomposition, the half-life is given by Eq. 9.1:

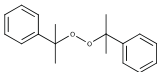
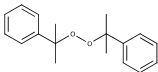
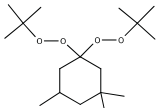
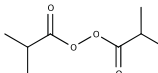
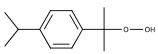
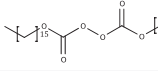
$$t_{1/2} = \ln \frac{2}{k_d} \quad (9.1)$$

where k_d is the constant of decomposition rate.

In general, when the residence time during REx is in the range of five times the half-life, the decomposition will be greater than 97%. However, if the half-life time is very short, the peroxide is decomposed mainly in the initial sections of the extruder, resulting in high concentrations of radicals in the polymer's backbone, which often results in an increase in crosslinking. Some examples of peroxide half-lives are shown in Table 9.2.

Based on the large difference between the types of peroxide, one can expect that their behavior and efficiency during grafting are also different, and as such, there are a large number of studies that have used different peroxide initiators, but few that directly compare their efficiency. The most studied polyester in light of peroxide

Table 9.2 Structures and half-life temperatures of some radical initiators

Compound	Structure	Initiator group	Half-life Temperature (°C)		
			10 h	1 h	1 min
DCP		Dialkyl peroxide	112	132	172
<i>tert</i> -butyl peroxybenzoate		Peroxyesters	103	122	160
1,1-di(<i>tert</i> -butylperoxy)-3,3,5-trimethylcyclohexane		Peroxyketal	85	105	148
Diisobutryl peroxide		Diacyl peroxides	23	39	73
Di-isopropylbenzene-mono hydroperoxide		Hydroperoxides	129	154	207
Dicetyl peroxydicarbonate		Peroxydicarbonates	48	65	100

efficiency is PLA. Several peroxides have been used to control Mw and it has been shown that dialkanoyl peroxide, dialkyl peroxydicarbonate, diaroyl peroxide, peroxy acid and peroxy ester, which have carbonyl groups in the molecular structure, prevented excessive chain scission, while peroxides such as dialkyl and diaralkyl peroxide did not (Coltelli et al. 2010). Similar studies showed that peroxides with a short half-life only induced partial crosslinking of PLA, since the decomposition was fast and PLA was not yet completely molten. However, if the half-life is close to the residence time, a uniform crosslinking occurs (Standau et al. 2019).


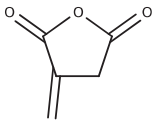
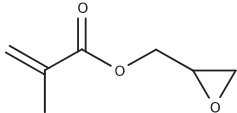
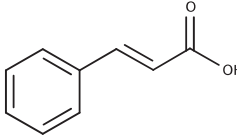
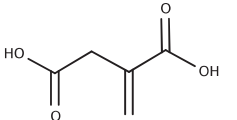
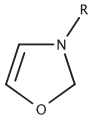
An alternative strategy to introduce free radicals for grafting are the so-called stable radicals, which are produced in two steps. A stable nitroxyl radical is grafted onto a polymer after which the grafted polymer of the first stage is heated in the presence of a monomer or oligomer at a temperature at which cleavage of the nitroxyl-polymer bond occurs and polymerization of the monomer is initiated in the polymer radical (Fink 2013). The benefit of this strategy is that the second step can be at a later stage, since the intermediate product can be stored for some time. Some examples of stable nitroxyl radicals can be 4-hydroxy-2,2,6,6-tetramethyl-piperidin-1-oxyl, 4-propoxy-2,2,6,6-tetramethyl-piperidin-1-oxyl, benzoic acid 2,2,6,6-tetramethyl-piperidin-1-oxyl-4-yl-ester and decanedioic acid bis(2,2,6,6-tetramethyl-piperidin-1-oxyl-4-yl) (Fink 2013).

9.4.2 Monomers

A wide variety of monomers have been grafted onto polyesters, the most important are listed in Table 9.3. Of these, MA is probably one of the most widely used reactive compatibilizers due to its good chemical reactivity, low toxicity and low homopolymerization potential. It is mainly chosen for its ability to react or interact with other polymers when the graft polymer is used as a compatibilizer in blends, especially polymers with functional groups such as $-\text{COOH}$, $-\text{NH}_2$ or $-\text{OH}$ (Maharana et al. 2015; Standau et al. 2019).

Itaconic anhydride (IAH) has its double bond located outside of the anhydride ring, which makes it more reactive than MA and could also be bioderived (da Silva and Galland, 2013; Petruš et al. 2016). Alternatively, maleate esters such as dibutyl maleate or diethyl maleate have lower toxicity and volatility compared to MA, although they are also less reactive (Fink 2013). MA and IAH typically also lead to significant chain scission, while grafting GMA has been shown to increase viscosity, inferring that less chain scission occurred (Kim et al. 2004).

Table 9.3 Functional groups commonly grafted onto polyesters

Type	Functional group	Chemical name	References
Anhydride		MA	Pascente et al. (2008) Raquez et al. (2008b) Signori et al. (2011) Haque et al. (2012) Maharana et al. (2015) Puteh et al. (2015) Petruš et al. 2016 Standau et al. (2019)
		IAH	
Epoxy		Glycidyl methacrylate (GMA)	Kim et al. (2004)
Carboxylic acid		Cinnamic acid	Signori et al. (2011)
		Itaconic acid	Krivoguz et al. (2003) Isiklan et al. (2010) da Silva and Galland (2013)
Oxazoline		2-oxazoline 3-oxazoline 4-oxazoline	John et al. (1998) Mani et al. (1999)

Itaconic acid presents an interesting opportunity for grafting. It has two ionizable groups, with different pKa values, which can form hydrogen bonds (Isiklan et al. 2010) allowing different compatibility strategies in polymer blends. On the other hand, oxazoline compounds can readily react with carboxylic acids, making them useful for chain extension and compatibilizers through amide-ester bonds (John et al. 1998).

9.4.3 *Mixing and Residence Time*

Grafting literature is mainly focused on reactions and processing conditions. However, it has also been shown that the mixture strongly influences the grafting process. The efficient mixing not only distributes the components to improve the overall grafting level, but high shear can also help the generation of free radicals. Mixing units, such as static or dynamic mixers instead of the regular extruder head, are a method to achieve this. Of these, a dynamic mixer is the most efficient (Fink 2013).

The screw configuration and the positioning of the mixing zones will have a significant impact on REx. This highlights that the residence time distribution (RTD) is not the only factor for determining the reactive progress. Screw design should thus be focused on a configuration with an optimal mix to maximize the degree of grafting. However, it must be remembered that mixing in an extruder is related to the degree of fill and the RTD. A good degree of fill can be achieved by selecting appropriate kneading blocks, such as a reverse-conveying kneading block with a narrow disc (Fang et al. 2008).

The rheology of the polymer, as well as the monomer and initiator solubilities also affect the mixture and can change the course of the reaction due to crosslinking and degradation (Fink 2013).

The most commonly used equipment for REx or grafting is co-rotating and intermingled twin-screw extruders. However, co-rotating, fully intermeshed, four parallel screw extruders, have been shown to have even better mixing. It has been suggested that these extruders have less dissipative heating, can prolong residence time and, due to the low-pressure and the release of volatiles are much more efficient (Calderon et al. 2019a).

The process is further complicated by some interactions between the mentioned variables, which may not be predictable when scaling up from batch processes. For example, during the production of PCL-*g*-MA, MA concentration is more important when an internal mixer is used, while for extrusion, the degree of grafting is more strongly influenced by the initiator concentration and reaction temperature (Morais et al. 2019).

The importance of mixing goes as far as the choice of the state of raw materials as well. By grafting PP with MA using extrusion, PP is fed as a powder or in granular form, where the latter is more successful due to a better initial mixing and less diffusional resistance.

The overall residence time is governed by throughput and can be adjusted by screw speed, screw design and extruder geometry. The peroxide lifetime/residence time ratio has been shown to affect the degree of crosslinking, where the initiators are broken down more rapidly, thus leading to a greater degree of crosslinking (Coltelli et al. 2010).

Higher screw speeds also promote better mixing, and therefore, the grafting is expected to increase. Nonetheless, this also leads to a reduction in residence time. In fact, for PCL grafting, where a significant variation in the degree of grafting was observed, grafting was shown to depend on the concentration of the initiator and screw speed (John et al. 1997b).

9.4.4 Polymer Structure

Grafting efficiency or the degree of grafting depends on the ease of hydrogen abstraction from the polymer chain by free radicals. For example, thermal decomposition of DCP forms cumyloxy radicals, which then abstract hydrogen from the polymer or undergo a dismutation (Lal et al. 1968). The higher abstraction rate (r_a)/hydrogen dissolution rate (r_d) ratio, the greater the ease of hydrogen extraction. The rate of hydrogen abstraction also depends on the type of hydrogen atom: non-activated, activated by a double bond or activated by an ether group. It was shown that the grafting was lower for polyolefins with high propene content due to the difference between chemical structures (Fink 2013).

The different polyesters presented above also vary significantly, depending on the length of the aliphatic section. For example, the grafting efficiency of poly(propylene carbonate) (PPC) is much higher than for PBS because PPC has tertiary carbons that are more reactive and less stable than the secondary carbons in the PBS structure (Calderon et al. 2019b). PLA and polyesters related with low aliphatic hydrocarbon content are relatively less reactive against radical graft modification, providing a relatively low degree of grafting (Dawidziuk et al. 2018).

9.4.5 Reagent Concentration

During reactive processing, the main aim is grafting the monomer onto the polymer chain. However, chain scission, crosslinking and homopolymerization of the monomer are competing reactions. Changing reagent concentrations alters the relative magnitude of each of these reactions since none of these reactions can be optimized individually. The exact optimal concentration is rather specific to each case, and is best illustrated with different grafting systems.

The effect of reagent concentration has been extensively studied and most studies have used an empirical approach to assess the effect of monomer and initiator concentration on the degree of grafting. The consensus is that the degree of grafting

depends largely on these two variables, but cannot be increased simply by increasing the concentration of either of them.

Increasing the initiator concentration generally leads to the formation of more free radicals formed through the decomposition of the initiator. A higher concentration of radicals results in a greater chain transfer to the polymer, and consequently, a higher degree of grafting. However, an increase in the initiator concentration can also reduce the M_w due to chain scission. Therefore, there is usually an optimal concentration that balances the grafting and chain scission (John et al. 1997a).

The degree of mixing or the processing method used (extrusion vs. batch mixing) also influences the degree of grafting and the reagent concentration cannot be considered in isolation (Fink 2013). Some authors have found that the effect of reagent concentration is different using a batch mixer instead of an extruder and that temperature is a dominant factor in the extruder. Grafting efficiency thus depends on the number of free radicals produced and their mobility (diffusion) and stability (Morais et al. 2019). Therefore, the optimization of the degree of grafting is first achieved by ensuring a high reaction temperature to induce the decomposition of free radicals, sufficient mixing to increase the probability of the monomer and radical species interacting and finally, by using an optimal amount of monomer and initiator to favor grafting instead of side reactions such as chain crosslinking and scission (Morais et al. 2019).

It has been shown that for grafting MA onto PCL, lower DCP concentrations result in a higher degree of grafting, independent of the monomer concentration, and an increase in the initiator concentration decreases the degree of grafting, which may be attributed to possible undesired reactions (Morais et al. 2019). Similarly, by grafting MA onto PPC and PBS, an increase in monomer concentration increased the degree of grafting, but it was accompanied by a significant reduction in M_w due to chain scission. It is also interesting to note that even at the same monomer and initiator concentration, the degree of grafting is very different for PPC and PBS (Calderon et al. 2019b).

Mani et al. (1999) grafted MA onto PLA, PBS and poly(butylene succinate-*co*-adipate) (PBSA). As expected, the degree of grafting increased with increasing initiator concentration up to a maximum of approx. 1 wt.%, after which a drastic drop was observed for PLA. In all cases studied, the intrinsic viscosity (i.e. M_w) decreased dramatically after that point as a result of chain scission. The increase in graft content was due to the increase in radical formation (initiator decomposition), and therefore, to a higher chain transfer to the polymer backbone. Although crosslinking is generally expected with an increase in initiator concentration, it was not observed for these systems. These authors suggested that the optimal grafting depends, therefore, on an optimal peroxide/monomer ratio, above which termination reactions become prevalent (Mani et al. 1999).

Grafting IAH onto PLA was extensively studied by Petruš et al. (2016) by varying monomer and initiator concentrations. These authors categorised the behavior into four classes of monomer to initiator concentration; low/low, low/high, high/low and high/high. An increase in the degree of grafting was observed with an increase in initiator concentration in the entire range (0.5–10 wt.% IAH) after the generation

of PLA macroradicals, which was favored at a high initiator concentration (Petruš et al. 2016).

At a low/low ratio, the formation of PLA macroradicals is favored because of limited IAH-free radical interactions. A relatively high degree of grafting was observed, as well as relatively few side reactions. However, at a low/high ratio, the desired reaction between PLA and free radicals predominates over IAH-free radical interactions due to a high concentration of reactive species and the viscosity of PLA reduces the extent of IAH interaction with free radicals.

As the initiator concentration increased, the concentration of PLA macroradicals increased, which led to chain crosslinking, scission and branching, as well as other termination reactions of the initiator. When the ratio becomes high/low, recombination of free radicals is unlikely and the main grafting reaction is favored. However, the conversion is low due to large amount of unreacted monomer.

When the ratio is high/high, the reaction between IAH and free radicals generates low reactivity IAH radicals which can be homopolymerized, due to lack of solubility of IAH in PLA. Although the degree of grafting is relatively high, the formation of other products is also prevalent (Petruš et al. 2016). These findings were similar to other investigations in which have shown that the yield of grafted polymer decreases with increasing monomer and initiator concentration (Kučera et al. 2017). A higher degree of grafting is accompanied by a higher extent of β -scission due to reactive tertiary carbon of IAH grafted onto the PLA backbone. Kučera et al. (2017) also found that the optimal reagent concentrations are a low monomer concentration (< 1 wt.%) and a high initiator concentration (> 0.5 wt.%).

Considering the effect of monomer concentration alone, the degree of grafting increased with increasing monomer concentration for PBS and PBSA, while it was relatively constant for PLA. At the same time, the intrinsic viscosity decreased with increasing monomer concentration because of increased chain scission (Mani et al. 1999). Similar behavior was observed for PCL and PBAT grafted with MA where an increase in MA concentration led to an initial increase in the degree of grafting. At low concentration, the free radicals formed from PCL combined directly with MA. As the concentration increased, termination reactions became more prevalent and the degree of grafting decreased. It was suggested using PBSA as an example that even in the presence of crosslinking and other degradative pathways, the degree of grafting generally increased with increasing monomer concentration, suggesting that MA inhibits crosslinking (John et al. 1997a; Signori et al. 2011).

9.4.6 Temperature and Pressure

In general, temperature is of the utmost importance in any chemical reaction. The degree of grafting depends on the amount, mobility and stability of the radicals formed during the reaction. However, too high processing temperatures cause degradation reactions, and the initiator decomposition may be too fast to be effective (Mani et al. 1999; Isiklan et al. 2010; Puteh et al. 2015).

For grafting PCL with MA, an increase in temperature leads to complete decomposition of the initiator, producing a higher number of free radicals, resulting in a higher degree of grafting. Higher temperatures also reduce viscosity and increase diffusion, both beneficial for grafting. However, at higher temperatures, radical recombination becomes more prominent, reducing the degree of grafting. Based on this, a maximum was observed in the degree of grafting as a function of temperature for PCL, which depends on the type of initiator used (John et al. 1997a; Morais et al. 2019). Similar observations were recorded for grafting natural rubber with IA where initially the degree of grafting increased as a result of the rapid decomposition of the initiator, but crosslinking was more prevalent as temperature increased, thus reducing the degree of grafting (Puteh et al. 2015).

9.4.7 *Inhibitors and Co-Monomers*

Other additives are often included in the grafting system to inhibit side reactions such as crosslinking or to promote the grafting efficiency of the monomer. Amides, sulfoxides and phosphites are effective in reducing crosslinking and chain scission, which is attributed to their electron donating properties. However, grafting can also be inhibited by adding phenolic stabilizers. The efficiency of stabilizers depends on their solubility in the polymer and the monomer, and will not only inhibit the side reactions, but also can reduce the grafting efficiency (Fink 2013; Petruš et al. 2018). Conjugated furan co-agents (e.g. butyl-3-(2-furyl) propenoate) are effective in increasing the degree of grafting of MA onto PP and have been shown to limit degradation (Signori et al. 2011). Similarly, cinnamic acid and ethyl cinnamate are effective for improving MA grafting by forming a weak adduct with MA, which increases the reactivity of MA (Signori et al. 2011).

The function of the co-agents is to react quickly with polymer macro-radicals, generating resonance-stabilized macro-radicals, thus preventing polymer chain scission. For example, butyl 3-(2-furyl) propenoate can be used for controlling M_w during grafting of MA onto PP. Functional nitroxides are also effective in controlling radical crosslinking through a reversible nitroxide-carbon radical coupling reaction, e.g. the addition of 2,2,6,6-tetramethylpiperidin-1-oxyl (TEMPO). It is effective due to the selectivity of TEMPO for radical termination with carbon-centered radicals instead of radical-initiated crosslinking. In another example, Petruš et al. (2018) found that 2,6-di-*tert*-butyl-4-methylphenol (BHT) was effective in preventing crosslinking and degradation in grafting IAH onto PLA. Similarly, Nerkar et al. (2014) and Standau et al. (2019) showed that multifunctional coagents, such as pentaerythritol triacrylate (PETA), triallyl isocyanurate (TAIC) and triallyl trimesate (TAM) reduce the PLA degradation and promote long chain branching.

Grafting with monomers such as MA and acrylic acid can be quite low and to overcome this, more than one monomer can be used to improve the overall grafting efficiency (White and Sasaki 2003). For example, styrene can be used as a comonomer to obtain high graft efficiency, with the additional benefit of less

degradation. The macroradicals formed onto the polymer backbone must react with the monomers before undergoing chain scission and if the primary monomer is not reactive enough towards the macroradicals, the benefit of the co-monomer is that it can react more quickly, thus preventing chain scission. However, the co-monomer must be easily copolymerized with the primary monomer to obtain the desired functionality of the graft-copolymer (Fink 2013).

9.5 Reaction Mechanisms

In this section, the mechanism *via* which free radical grafting occurs is discussed as an overview. The kinetics of these processes are examined in the subsequent section, which includes a detailed overview of potential side reactions.

9.5.1 Overall Mechanism

Free radical grafting occurs as a complex set of reactions occurring simultaneously, summarized as the following sequence (Fig. 9.3):

- Thermal decomposition of the initiator, generating primary radicals which can be further decomposed into secondary radicals.
- Formation of macroradicals through the hydrogen abstraction mainly from the tertiary carbon of the polyester backbone.
- Covalent bonding of the monomer onto the macroradicals.
- Termination of grafting by hydrogen donors.

Peroxides are commonly used as free-radical initiators. They decompose through homolytic scission, producing two free radicals, or primary radicals (RO^{\bullet}) and subsequently, hydrogen abstraction occurs from the polymer chain which allows the formation of macroradicals.

Primary radicals can also undergo β -scission to form secondary radicals. Secondary methyl radicals are more likely to participate in homopolymerization compared to bulky primary radicals. It is well known that the probability of abstraction depends on the polymer structure. Hydrogen abstraction typically occurs at the α -carbon with respect to the carbonyl group for saturated carboxylic acids and their derivatives because the radicals are stabilized due to their conjugation with the carbonyl group (John et al. 1997a; Mani et al. 1999). It has also been pointed out that the polymer structure could influence the grafting (Mani et al. 1999). For example, the degree of grafting in PPC was twice that of PBS using MA as a monomer. Calderon et al. (2019b) thought that the difference in grafting was due to the fact that the PBS only has secondary carbons, which are more stable than the tertiary carbons found in the chemical structure of PPC.

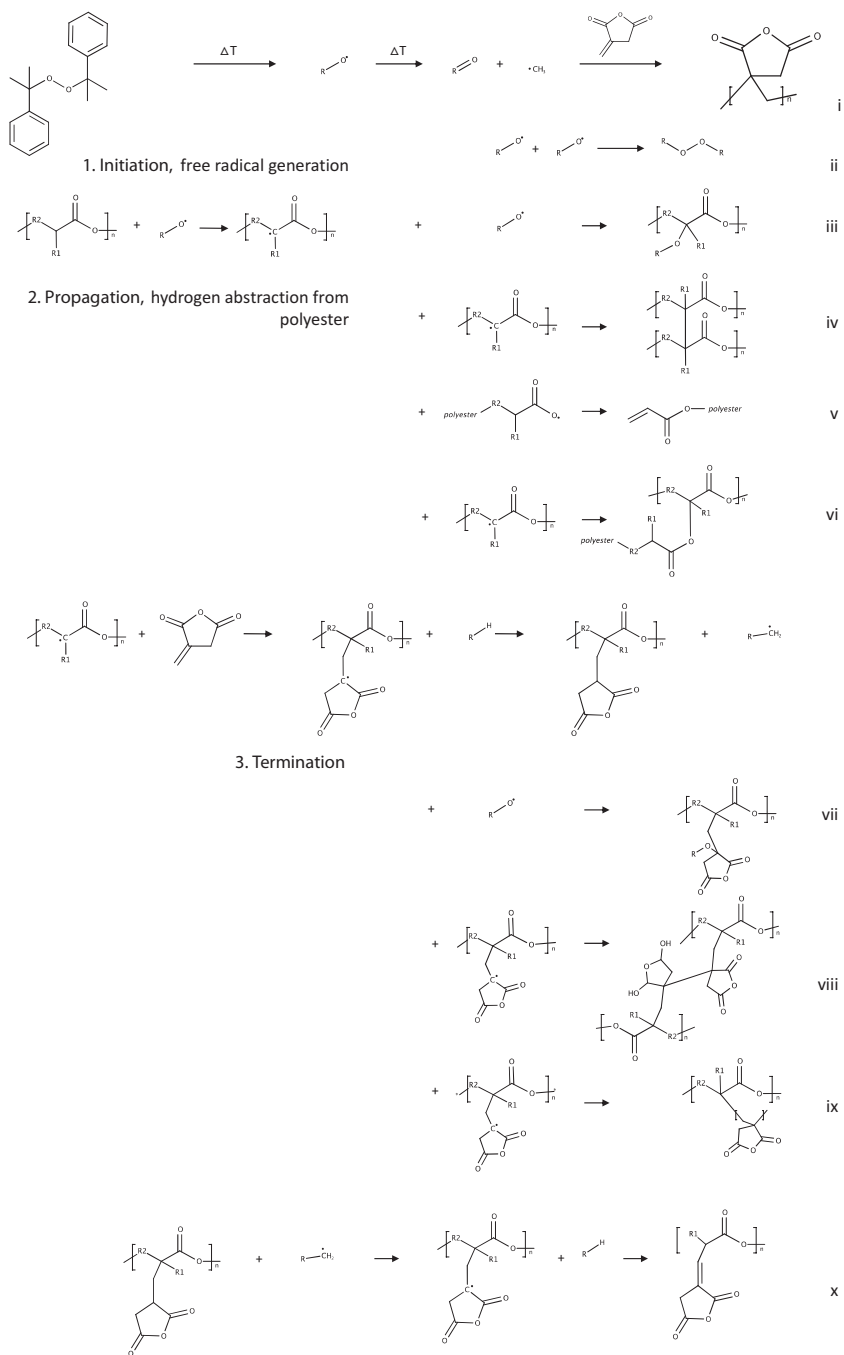


Fig. 9.3 Overall scheme of general reaction for grafting a monomer (IAH used as an example) onto a polyester. The main reactions are (1). Initiation, (2). Propagation and (3). Termination. Including side reactions, i to x

Propagation is the next step for generating a graft copolymer by a free radical mechanism which depends on the concentration of polymer radicals. This reaction continues until the initiator or the radicals have been consumed by the termination reactions. For the case of MA, the free radicals can abstract more hydrogens or combine with other free radicals (Kashani Rahimi et al. 2017) or alternatively the free radical can perform β -scission of the chain to produce a succinic anhydride end group. This typically occurs after the macro-radical has undergone a β -scission onto a radical chain end, as well as a vinylidene chain end (Mani et al. 1999).

Several authors have also suggested that MA could be grafted onto polyesters at the chain-end, based on the abstraction of the α -carbon hydrogen followed by β -scission and the formation of a vinylidene and macroradical chain end. The macroradical chain ends can then react with MA (Petruš et al. 2016; Kashani Rahimi et al. 2017; Morais et al. 2019).

During termination, when no more radicals are generated, the grafting slows down and eventually stops. To obtain a high degree of grafting, it is essential that the macro-radicals react with the monomers before undergoing side reactions. Grafting is accompanied by several possible side reactions, the extent of which depends on the reaction conditions (e.g. initiator and monomer concentration, radical reactivity, reaction temperature):

- Formation of secondary methyl radicals, which lead to the photopolymerization of monomers.
- Primary radicals can recombine, deactivating the free radical.
- Extinction of the active center by radical addition, or crosslinking, β -scission and branching.
- Addition of radicals onto grafted-chain macroradicals, which leads to the crosslinking of grafted chains.
- Hydrogen abstraction from the grafted polyester, which leads to β -scission.
- Non-radical side reactions, such as end-group reactions and polyester hydrolysis.

Several authors have proposed possible reaction mechanisms for PBAT (Kashani Rahimi et al. 2017; Muthuraj et al. 2017), PBS (Calderon et al. 2019b; Phua et al. 2012; Signori et al. 2011), PCL (John et al. 1997a; Mani et al. 1999; Kim et al. 2004; Morais et al. 2019), PLA (Ku Marsilla and Verbeek 2015b; Petruš et al. 2016) and PPC (Calderon et al. 2019b), all of which conform to the generalized mechanisms presented here. The only differences discussed in literature is the extent to which side reactions are taken into account. In general, homopolymerization of the monomer is not taken into account if grafting is performed about the ceiling temperature, however, it has recently been shown that this may have been an incorrect assumption (Petruš et al. 2016). In addition, the extent to which crosslinking occurs varies, depending on the system under consideration. For PLA, the first step, the formation of free alkoxy radicals, is the determining step for the degree of crosslinking. In the presence of radicals, PLA undergoes branching, crosslinking and chain scission, and reaction conditions are crucial for optimizing grafting (Standau et al. 2019). For example, primary *t*-butoxy radicals exhibit a high propensity for hydrogen abstraction, favorable for grafting. However, secondary methyl radicals tend to

participate in homopolymerization, as shown for grafting IAH onto PLA. The high reaction temperature favors scission of primary radicals into secondary radicals, which makes melt grafting less efficient than solution techniques, if homopolymerization is to be avoided (Kučera et al. 2017).

The monomer used can also influence the extent of side reactions, as evidenced by the differences detected with grafting glycidylmethacrylate (GMA) and MA onto PCL. Less chain scission occurred when GMA was grafted onto PCL compared to MA, however, the exact reason for this difference was not explained (Kim et al. 2004). Alternatively, when the reactivity of the monomer is low, co-monomers can be used to increase the degree of grafting, as explained above (Signori et al. 2011).

9.5.2 Kinetics

The kinetics of polymer grafting has been widely covered by White and Sasaki (2003) who have examined the kinetics: for the polymer grafting for natural rubber and polystyrene, and for REx of polyolefins and graft polymerization. More information on the kinetics of free radical modification for polyolefins in extruders can be found in the paper from Hamielec et al. (1991) and some other documents available for the kinetics of free radical grafting of PLA and other polyesters were recommended by Petruš et al. (2018).

First, the initiator must decompose to form the free radical which then attacks the respective polymer or monomer. For a compound to be an initiator it must have at least one bond with a low dissociation energy (100–200 kJ/mol) (Dossi et al. 2010). To produce a radical, the low dissociation energy bond (a single bond) is divided through homolysis (Dossi et al. 2010), so that each part produced retains one of the electrons in that bond. Thermal dissociation is the most common form, but redox initiation and photochemical initiation can also occur.

Redox or photochemical initiation are usually used in cases where the polymerization or grafting should be carried out at low temperature. Redox initiation is achieved by combining an initiator with a salt (e.g. ferrous) to produce the required radical. This can only work if the radical production rate is sufficiently fast to overcome the factors discussed above (e.g. the half-life). The photochemical option is also difficult, since it is activated very easily (Dossi et al. 2010).

Peroxide-based and azo-containing compounds typically undergo thermal decomposition according to Eq. 9.2. The velocity constant (k_d) is typically in the order of 10^{-4} – 10^{-6} s $^{-1}$ (Dossi et al. 2010) and can be described by an Arrhenius equation for temperature (Zhou and Zhu 1998).



The start of the grafting reaction occurs when the radical produced attacks the monomer (e.g. MA) or polymer itself. Each pathway has an associated reaction rate. For a radical attack on the monomer. This is described as follows:



where M represents the monomer.

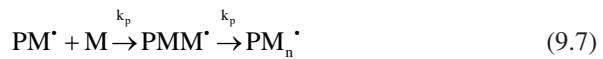
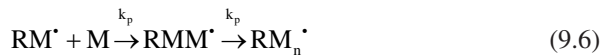
If the radical attacks the polymer, the analogous equation is applied:



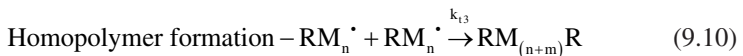
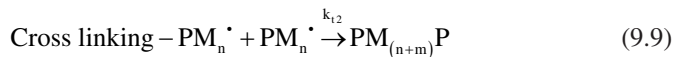
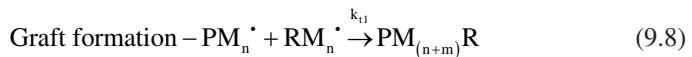
where RH is the radical attached to the hydrogen it extracts from the polymer itself. Consequently, the polymer now becomes the reactive species and in turn reacts with the monomer.



The result of any of these reactions is a highly reactive radical located on the monomer regardless of whether it is already bound to the polymer. Due to this free radical, propagation can occur causing an increase in Mw described below.



Finally, the reaction must end through one of the following three mechanisms. Graft formation is the desirable result (Eq. 9.8), where the monomer and polymer are joined, crosslinking (Eq. 9.9), where two reactive polymer chains are linked, or by the formation of homopolymers (Eq. 9.10), where two reactive monomers are joined.



Below is a comparison of the grafting reactions for a conventional polyolefin grafted with MA and PLA grafting with IAH (Petruš et al. 2016). Both reactions begin with the decomposition of the initiator into a free radical, the abstraction of a hydrogen from the polymer and the addition of the respective MA or IAH monomer.

Table 9.4 Kinetics of graft polymerization without homopolymerization

Steps	PP-g-MA
Radical formation	$I_2 \xrightarrow{k_d} 2R^*$
Hydrogen abstraction from polymer	$R^* + P \xrightarrow{k_{12}} P^* + RH$
Monomer addition	$P^* + M \xrightarrow{k_{13}} PM^*$
Monomer extension	$PM^* + M \xrightarrow{k_p} PMM^*$
Links to another polymer chain	$PM_n^* + PM_n^* \xrightarrow{k_t} PM_{(n+m)}P$
In the case of no MA impurities, where there is no homopolymerization due to steric hinderance	$-\frac{d[M]}{dt} = \frac{k_g \cdot \sqrt{2 \cdot k_d}}{1 + f} \sqrt{\frac{2 \cdot k_d}{k_t}} [I]^{1/2} [M]$
	$f = \frac{[PM^*]}{[P^*]}$

Source: White and Sasaki (2003)

Table 9.5 Kinetics of graft polymerization with homopolymerization

Monomer of radical attacks	$R^* + M \xrightarrow{k_p} RM^*$
Reactive monomer reacts with another monomer (homopolymerization)	$RM_n^* + M \xrightarrow{k_p} RM_{n+1}$
Termination occurs by reaction with another long chain of monomers	$RM_n^* + R^*M_m^* \xrightarrow{k_p} RM_{m+n}R^*$
Termination occurs by reaction with another polymer	$RM_n^* + PM_m^* \xrightarrow{k_p} RM_{m+n}P$
	$-\frac{d[M]}{dt} = k_g [M][P^*] + k_p [M]([PM_n^*] + [RM_m^*])$
	$-\frac{d[M]}{dt} = k_p \cdot \sqrt{\frac{2 \cdot k_d}{k_t}} [I]^{1/2} [M]$

Source: White and Sasaki (2003)

Both eventually end up with crosslinking *via* different mechanisms, but there is also the possibility of homopolymerization, which affects the reaction kinetics. Table 9.4 presents the case without homopolymerization. Table 9.5 shows the case with homopolymerization.

Homopolymerization occurs when the monomers are grafted repeatedly to form a long chain that can occur with or without the polymer as a substrate. Whether or not this reaction continues depends on the molecule that is grafted onto the polymer. For example, Cha and White (2001a) determined that MA was not

homopolymerized when it is partially grafted onto polyolefins due to steric hindrance by a 1–2-disubstitution of double bonds. In this particular study, a low concentration of peroxide and MA was used and processed at 230 °C well above the ceiling temperature of 150 °C (Cha and White 2001a). Methyl methacrylate (MMA) behaved similarly with a single unit grafted onto the polymer due to steric hindrance (Cha and White 2003).

In line with this, Cha and White (2001b) analyzed grafting styrene onto polyolefins. These authors pointed out that there was competition between grafting and homopolymerization. This complicates the termination reactions and affects the kinetics of the system.

The competition between grafting *vs.* homopolymerisation of styrene, as determined Fourier transform infrared (FTIR) analysis showed that at low 2,5-dimethyl-2,5-bis-(*t*-butylperoxy) hexane (DBHA) contents both reaction conversions increased linearly with the increase in initial styrene content. However, by increasing the DBHA content at 4% addition of styrene, the grafting only improved with more DBHA (Cha and White 2001b), thus indicating that grafting can be promoted under the correct conditions.

The grafting kinetics of polyesters are very similar. The same kinetic equations were presented by Ku Marsilla and Verbeek (2015a) for PLA-*g*-IAH using DCP. By reordering the overall kinetic equation for grafting without homopolymerization, the effective velocity constant for the grafting of PLA-*g*-IAH was calculated for this case, using the slope of the initiation reaction rate *vs.* monomer concentration, dM/dt . From this, it was shown that the effective velocity constant is mainly affected by the initiator concentration (Table 9.6) and is relatively independent of temperature (Ku Marsilla and Verbeek 2015b).

$$\frac{k_g}{1 + f\sqrt{k_t}} = \frac{\frac{d[M]}{dt} \left[\frac{1}{M} \right]}{\sqrt{2 \cdot k_d [I]^2}} \quad (9.11)$$

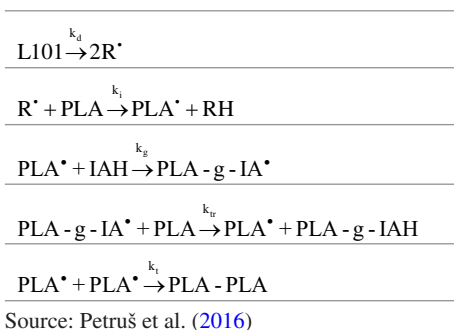
PLA has a particularly complex reaction route (Table 9.7). If instead of the monomer extending the PLA-*g*-IA, it removes a hydrogen from the PLA polymer, this becomes the reactive species and two PLA molecules can interact directly and cross link without the IA molecule involved.

The kinetics of PLA grafting are much more complex, and the main grafting reaction is described as a function of the initial concentration of the monomer and PLA macroradicals (Table 9.8) (Petruš et al. 2016). The overall reaction conversion is represented by α , and K is the initial reaction rate. The remaining parameters were determined experimentally by Petruš et al. (2016).

Whether or not IA undergoes homopolymerization during reaction with PLA is somewhat debatable. Most work excludes homopolymerisation as processing occurs well above the ceiling temperature, which is very low, 90 °C. Most authors do not consider homopolymerisation to occur if processing above the ceiling temperature. However, a recent study suggests that homopolymerisation of IAH can

Table 9.6 Kinetic parameters determined by Ku Marsilla and Verbeek (2015a)

Effective velocity constant (1/mol s) ^{1/2}	Initiator concentration (wt.%)	180 °C	200 °C
$\frac{k_g}{(1+f)\sqrt{k_t}}$	0.5	0.024	0.025
	1	0.027	0.03

Table 9.7 Reactions for PLA-g-IAH**Table 9.8** Kinetic equations for PLA-g-IAH

$$\begin{aligned} -\frac{d[\text{IAH}]}{dt} &= k_g \cdot [\text{PLA}^{\bullet}] \cdot [\text{IAH}] \\ k_i \cdot [\text{R}^{\bullet}] &= 2 \cdot f \cdot k_d \cdot \frac{[\text{L101}]}{[\text{PLA}]} \\ 2 \cdot f \cdot k_d \cdot [\text{L101}] &= k_t \cdot [\text{PLA}^{\bullet}]^2 \\ \frac{d\alpha}{dt} &= K \cdot (1-\alpha) \cdot [\text{L101}]^{1/2} \\ K &= \sqrt{\frac{2 \cdot f \cdot k_d \cdot k_g^2}{k_t}} \end{aligned}$$

Source: Petruš et al. (2016)

occur at processing temperatures as high as 190 °C when initiated with L101 (Kučera et al. 2017).

9.5.3 Side Reactions

Crosslinking, thermal degradation, hydrolysis and other side reactions decrease the overall grafting achieved.

9.5.3.1 Peroxide Induced Crosslinking

Peroxides are also capable of inducing crosslinking in PE (Zhou and Zhu 1998), PLA and PP, which is often exploited during extrusion through low addition levels of peroxide (Takamura et al. 2008). This process consists of three steps beginning with the decomposition of the initiator to produce primary radicals. These then extract a radical from an available carbon on the polymer to produce a polymer radical. The polymer radicals can then recombine and crosslink the polymer itself without undergoing grafting according to the reaction below (Takamura et al. 2008):

Primary radical generation



Hydrogen abstraction



Bimolecular recombination of polymer radicals



Takamura et al. (2008) examined the effect of the type of peroxide (initiator), and these were classified according to their thermal decomposition rates. These authors showed that peroxides (lauroyl peroxide - LPO and BPO) are rapidly decomposed, which leads to higher Mw fractions and more gelling, indicating that faster decomposition rates lead to partial crosslinking. In comparison, moderate (tri-*n*-butyltin hydride - TBTH and *tert*-butylperoxy 2-ethylhexyl carbonate - TBEC) or slow initiators (DCP), lead to a uniform crosslinking capacity in molten PLLA, and the average Mw and degree of crosslinking were correlated with the ability of the peroxide to abstract a hydrogen from the polymer.

The reaction kinetics for crosslinking of PE using peroxide has been well established and discussed by Zhou and Zhu (1998). This study highlights that the concentration, the reaction temperature and the type of peroxide, all affect the crosslinking *via* the mechanism described. Most importantly, the termination of the polymer radicals is a diffusion-controlled process and that, consequently, not all radicals react. Some radicals remained detectable after several months (Zhou and Zhu 1998).

9.5.3.2 Chain Scission

Carlson et al. (1999) determined that during the grafting process of PLA with MA, an increase in the amounts of the initiator (L101 - peroxide), resulted in a higher melt flow index (MFI) (83.4 g/10 min at 0.50 wt.% L101 vs. 27.8 g/10 min at 0 wt.%) at the same addition level of MA (2 wt.%). This suggests that chain scission

of PLA occurred as the viscosity decreased. This was similar to the behavior observed with PP. Chromatography also showed that when peroxide and MA are added, Mw decreased, suggesting an increase in chain scission corresponding to a decrease in intrinsic viscosity. These effects were worse at higher processing temperatures, suggesting that the degree of chain scission can be controlled between the initiator addition levels and the processing temperature.

Proposed mechanisms from this study include back biting and thermohydrolysis (Carlson et al. 1999). This is consistent with a previous study done by Carlson et al. (1998). Thermohydrolysis is a simple reaction in which free water at high temperature can cause the chain to split in two at the ester group (O-C=O), which leads to a molecule with a free hydroxyl group and a carboxylic acid (Fig. 9.4).

Backbiting occurs when a polymer which still contains a free radical rearranges and the radical attacks the group of esters, which leads to the same hydroxyl-containing molecule as before, but a cyclic molecule is produced instead of the carboxylic acid-containing molecule. Hydrolytic and thermal degradation along with backbiting can also occur in polymers that do not contain esters.

9.5.3.3 β -Scission

A reduction in viscosity has also been observed during grafting of PCL with MA when initiated by DCP. This is similar to the behavior of polyolefins, since it is believed that the peroxide initiates scission of the polymer backbone, thus creating smaller chains. Some control over the degree of scission can be achieved by controlling temperature and monomer concentration.

An increase in the MA content in this case favors grafting and with a higher concentration of MA, the occurrence of β -scission decreases as the macro radicals react immediately. Morais et al. (2019) demonstrated that β -scission was promoted

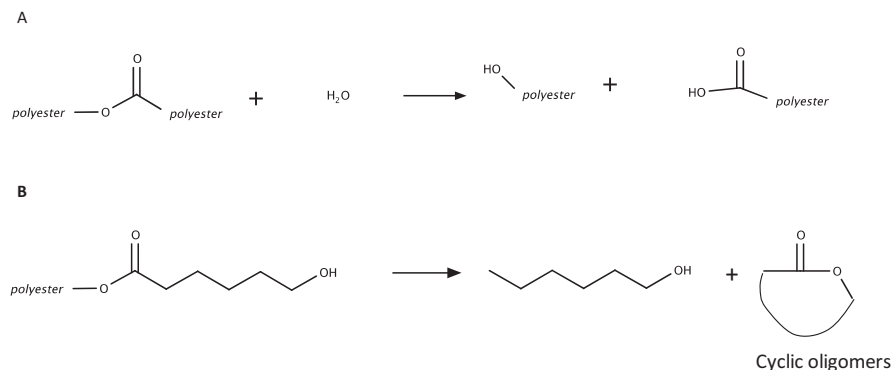


Fig. 9.4 Reaction mechanisms of chain scission by thermohydrolysis (A) and back-biting (B). Reproduced with permission from Carlson et al. (1999)

by high temperatures which initiated the decomposition of DCP. Signori et al. (2011) also suggested that β -scission can occur for PLA-g-MA.

All these degradation mechanisms can play a role during the processing of grafted polyesters. Al-Itry et al. (2012) discussed the exchange of between these mechanisms well, but noted that the velocity of a mechanism such as hydrolysis depends a lot on the water availability, the morphology of the polymer and the temperature. These authors also indicated that hydrolysis takes place between 150 and 215 °C which can directly compete with thermal degradation, which generally takes place above 180 °C, which can randomly break the polymer chain, thus leading to lower Mw chains. β -scission can also occur at this temperature. They also noted that for PLA cyclic oligomers are formed through backbiting (trans-esterification mechanism), while for PBAT, benzene rings are produced (Al-Itry et al. 2012). A reduction in Mw and melt strength for malleated PBAT has also been observed (Nabar et al. 2005).

9.5.4 Material Properties of Grafted Polyesters

This section outlines the changes in thermal behavior, rheology and mechanical properties which arise due to grafting. It mainly focuses on polyesters, however, some examples based on polyolefins are included for comparison.

9.5.4.1 Thermal Behavior

The addition of another component through grafting can affect the degree of crystallinity, the crystallization rate, the glass transition temperature (T_g) and melting temperature (T_m). It is common that grafting decreases the T_g and T_m values compared to pure polyester. This has been observed for PBS (Teramoto et al. 2005), PLA (Hassouna et al. 2011) and PLLA (Hwang et al. 2012) systems, which have been grafted with MA. Sometimes, these changes are minor, as with PLA grafted with MA in the presence of Lupersol, which caused a reduction in both T_g and T_m of only 0.5 °C (Hassouna et al. 2011). However, grafting also affects chain arrangement and increased the melting enthalpy by 3 J/g. Interestingly, for a combination of PLA + 10% MAG-PLA, the T_g and T_m were 0.5 °C higher than pure PLA alone, although the melting enthalpy coincided with pure PLA (Hassouna et al. 2011).

A similar decrease in T_g for grafted PLLA was also observed by Hwang et al. (2012) when grafted with MA using DCP. The addition of MA caused a decrease in T_g from 54.9 °C to 49.9 °C when 30 phr was added. A corresponding decrease in crystallinity also occurred from 13.0% to 10.2%. This was attributed to chain branching of MA onto PLLA, which causes a decrease in the regularity of the polymer and hinders the crystalline growth of PLLA. Thermal stability was also affected with a decrease in Mw for PLLA-g-MA samples due to the addition of MA (small Mw). Despite the differences in the thermal behavior of the PLLA-g-MA samples,

there was only a small variation in the mechanical properties of compression molded films from this material (Hwang et al. 2012).

Differential scanning calorimetry (DSC) analysis of PBS modified with IAH or MA in the presence of 1,4-butanediol and SA showed a very different thermal behavior to pure PBS (Teramoto et al. 2005). The most notable change was the decrease in melting enthalpy by increasing the itaconate or maleate content. The incorporation of these lower Mw units decreased the thermal stability of the material, reducing the degradation temperature from 389 °C to 377 °C and 373 °C for 15 mol % IAH and MA, respectively. T_g and T_m values were also reduced with MA, having a greater affect than IAH.

The effect of grafting on crystallinity and crystallization behavior has been examined in depth by You et al. (2013) by producing long-chain branched PLA *via* radical grafting. This was produced by grafting PLA with PETA using DCP. Through radical grafting the fraction of comb-like chains, as well as the number of arms was increased. A decrease in the crystallization temperature was observed as the branching level increased and the crystallization rate constant increased with PETA-*g*-PLA due to the presence of chain clusters which helped nucleation. This increased the crystallinity upon cooling from 0.94% (PLA) to 13.0% for a material produced from 0.3% DCP, 3% PETA and 0.2% antioxidant.

9.5.4.2 Rheology

Until recently, grafting of compounds such as IAH and MA onto polymers was focused on the addition of these groups to PE or PP. PP is naturally linear, has a low melt strength and has no strain hardening properties, making it unsuitable for applications such as blow molding and foaming where extensional forces occur.

A high melt strength polypropylene (HMSPP) can be obtained by free radical grafting in a two-step process. Initially, MA is grafted onto isotactic PP in a melt state to achieve PP-*g*-MA, before reacting with an epoxy to increase the branch length (Tang et al. 2008). The HMSPP produced *via* this method has a low MFI and sags less when stretched. The addition of epoxy chains also increased the degree of crystallinity and crystallization temperature. Similar results were observed when grafting is used to crosslink PE. The MFI of the material was also reduced, and the mechanical properties were affected with improved impact strength and creep resistance, while a reduction in ϵ_b values as reported from Tamboli et al. (2004) by Ku Marsilla and Verbeek (2015b).

In comparison, the grafting of MA onto PLA has been shown to affect the MFI of the material depending upon the temperature at which it is grafted. Carlson et al. (1999) evaluated the effect of the initiator Lupersol 101 at concentrations of 0–0.5 wt.%. Minor differences in the degree of grafting were detected between T_m of 180 °C (approx. 0.65% grafting) and 200 °C (0.672%), with 0.5% Lupersol, but a significant change in MFI occurred from approx. 85 to 135 (g/10 min). A corresponding change in intrinsic viscosity and Mw of the material also occurred and it is thought that this could have arisen through β -scission, back biting and/or

thermohydrolysis. This same study also highlighted the increase in melt viscosity, when only peroxide was used, or the reduction in melt viscosity in the presence of MA and a peroxide, was different from what occurs with polyolefins. For PE, the addition of peroxide alone or in combination with MA causes branching and gelation and for PP chain scission arises. Carlson et al. (1999) thought that the decrease of M_w in this case occurred due to competition between branching and grafting of MA.

It is important to understand the M_w changes due to these mechanisms. Kim et al. (2004) studied PCL systems grafted with MA and GMA. The increase in the polydispersity index (PDI) indicated that chain scission did not occur during grafting with GMA, instead chain extension/crosslinking occurred. In comparison, the grafting of MA onto PCL resulted in a decrease in M_w as the MAH content increased. Without BPO to initiate the grafting reaction, a decrease in M_w occurred; and there was also chain scission, which was promoted by higher processing temperatures (Kim et al. 2004).

9.5.4.3 Mechanical Properties

Free radical grafting with different monomers is widely used to improve the compatibility of the blends, e.g. PP/low density poly(ethylene) (LDPE) blends (1.3–2.7 °C) (Krivoguz et al. 2006), as well as some polyester blends. The grafted PLA can be used to make the PLA compatible with starch. For PLA-*g*-MA initiated by 2,5-bis(*tert*-butylperoxy)-2,5 dimethylhexane, the σ_m values increased from 61.6 MPa \pm 3.8 for pure PLA to 63.4 MPa \pm 1.6 for PLA-*g*-MA and the ϵ_b values remained constant: 5.2% \pm 0.5% (Zhang and Sun 2004). Once starch was added to the blend, the best σ_m value was 53.9 \pm 2.1 MPa. However, this is an improvement in the blend which did not contain PLA-*g*-MA which was reportedly 30.0 MPa \pm 2.6.

In comparison, an optimal amount of MAH-*g*-PLA was observed by Zhang et al. (2017) to occur in PLA/wood fiber composites at 30%, where the σ_m values increased up to this point from 43.5 MPa to more than 47 MPa, and ϵ_b values from 3.35 to 3.95%. The increase in PLA-*g*-MAH further decreased these properties until 50% of PLA-*g*-MAH was comparable to the absence of PLA-*g*-MAH in σ_m value and only a small improvement in ϵ_b value (3.65%).

PLA grafting with MA has also been explored by Yu et al. (2013) as an option to improve the melt strength of PLA for foaming applications. However, consistent with the other studies reported here, according to other results reported there, the production of PLA-*g*-MA decreased the melt strength together with M_w . This was attributed to the fact that the low M_w components produced by decomposition of PLA by peroxide can act as plasticizers, thus decreasing the melt strength. For foaming applications, the grafted PLA leads to broken cells on the surface of the foam beads and an open cell structure connected in the center. Overall, this study concluded that PLA-*g*-MA, which was linear in structure, could not resist elongation forces during cell growth. The result is a foam structure similar to foams produced at high temperature (Yu et al. 2013).

According to Jin et al. (2000), when maleic groups are incorporated into PBS together with SA and 1,4-butanediol (BD), a decrease in the ϵ_b values occurred from 58.1 to 52.2% or from 24 to 7%, depending on the ratio of the components SA/BD/MA (50/45/5) and (50/40/10), respectively (Jin et al. 2000). The ϵ_b values decreased as a result of the introduction of MA units into PBS. However, the ϵ_b and σ_m values were greatly improved by the chain extension when BPO was added through a solution-based method. PBS grafted with MA without BPO remained highly biodegradable with 12% degradation in 25 days compared to <2%.

The flexural and tensile properties, and impact strength for PBS, PBS-g-MA, and PBS/PBS-g-MA blends were examined by Muthuraj et al. (2015) together with composite samples containing miscanthus (grass) produced using DCP as an initiator. Regardless of the performance of the composite material, the tensile properties of PBS-g-MA and a PBS/PBS-g-MA blend in a 95/5 wt.% ratio was comparable to pure PBS (approx. 40 MPa). However, the YM of the PBS-g-MA was marginally greater than that of pure PBS and the addition of 5% PBS-g-MA produced a comparable value of 0.08 GPa, indicating that only a small addition was required to achieve comparable results. All three samples were comparable in flexural strength in this study, but the notched impact strength of pure PBS-g-MA was significantly higher but also more variable (64 J/m) which was attributed to partial crosslinking, which was produced during grafting (Muthuraj et al. 2015). Similar results were observed by Phua et al. (2013) for PBS-g-MA.

John et al. (1997a) indicated that the tensile properties of PCL-g-MA change very little compared to pure PCL, which had a σ_m of 550 N and an ϵ_b of >850%. Once grafted, regardless of whether it was performed in batch or by extrusion, the σ_m values oscillated between 589.5 and 640 N and the ϵ_b between 882 and 1070%. The authors attributed this to the minor changes in Mw and intrinsic viscosity.

John et al. (1998) also grafted two grades of PCL (787 and 767) with oxaline groups which were then compression molded to make traction bars. These authors reported that for 787 samples the σ_m values were inversely proportional with a decrease in ϵ_b values due to grafting. However, in the case of PCL 767, a decrease in both mechanical properties were observed. The difference in the properties of these materials grafted with PCL was attributed to changes in intrinsic viscosity and Mw. No change was observed for PCL 787, but a slight increase in Mw was observed for PCL 767.

9.6 Conclusions

Polymer grafting is a practical way to improve the properties of conventional polymers and is an emerging field as a mechanism for improving biobased or biodegradable polyesters for application in polymer blends. This chapter discussed polyester grafting in light of conventional grafting methods and technologies, focusing on REX.

It can be concluded that grafting of polyesters is better be optimized empirically. The influencing aspects of monomer and initiator concentration must be balanced

with the appropriate temperature profile, mixing, processing conditions, the rheology of the polymer and the possibility of side reactions. All of which can change during processing.

This chapter also highlighted recent changes in the field, including whether or not homopolymerization should be considered during grafting above the ceiling temperature, which was previously not thought to occur.

In general, this chapter provided an overview of the important aspects to consider for anyone looking to functionalize a bio-polyester to improve compatibility with other materials, petrochemical or not, or to manipulate the mechanical properties of these materials for a particular application.

Acknowledgements Acknowledgments are not reported.

Conflicts of Interest The authors declare no conflict of interest.

References

- Adrar, S., Habi, A., Ajji, A., & Grohens, Y. (2017). Combined effect of epoxy functionalized graphene and organomontmorillonites on the morphology, rheological and thermal properties of poly (butylenes adipate-*co*-terephthalate) with or without a compatibilizer. *Applied Clay Science*, 146, 306–315. <https://doi.org/10.1016/j.clay.2017.06.009>.
- Al-Itty, R., Lamnawar, K., & Maazouz, A. (2012). Improvement of thermal stability, rheological and mechanical properties of PLA, PBAT and their blends by reactive extrusion with functionalized epoxy. *Polymer Degradation and Stability*, 97(10), 1898–1914. <https://doi.org/10.1016/j.polyimdegradstab.2012.06.028>.
- Calderon, B. A., McCaughey, M. S., Thompson, C. W., & Sobkowicz, M. J. (2019a). Blends of renewable poly(butylene succinate) and poly(propylene carbonate) compatibilized with maleic anhydride using quad screw reactive extrusion. *Industrial and Engineering Chemistry Research*, 58(1), 487–495. <https://doi.org/10.1021/acs.iecr.8b04757>.
- Calderon, B. A., Soule, J., & Sobkowicz, M. J. (2019b). Synthesis and characterization of compatibilizers for blends of polypropylene carbonate and polybutylene succinate via free-radical grafting of maleic anhydride. *Journal of Applied Polymer Science*, 136(21). <https://doi.org/10.1002/app.47553>.
- Carlson, D., Dubois, P., Nie, L., & Narayan, R. (1998). Free radical branching of polylactide by reactive extrusion. *Polymer Engineering & Science*, 38(2), 311–321. <https://doi.org/10.1002/pen.10192>.
- Carlson, D., Nie, L., Narayan, R., & Dubois, P. (1999). Maleation of polylactide (PLA) by reactive extrusion. *Journal of Applied Polymer Science*, 72(4), 477–485. [https://doi.org/10.1002/\(sici\)1097-4628\(19990425\)72:4<477::aid-app3>3.0.co;2-q](https://doi.org/10.1002/(sici)1097-4628(19990425)72:4<477::aid-app3>3.0.co;2-q).
- Cha, J., & White, J. L. (2001a). Maleic anhydride modification of polyolefin in an internal mixer and a twin-screw extruder: Experiment and kinetic model. *Polymer Engineering & Science*, 41(7), 1227–1237. <https://doi.org/10.1002/pen.10824>.
- Cha, J., & White, J. L. (2001b). Styrene grafting onto a polyolefin in an internal mixer and a twin-screw extruder: Experiment and kinetic model. *Polymer Engineering & Science*, 41(7), 1238–1250. <https://doi.org/10.1002/pen.10825>.
- Cha, J., & White, J. L. (2003). Methyl methacrylate modification of polyolefin in a batch mixer and a twin-screw extruder experiment and kinetic model. *Polymer Engineering & Science*, 43(12), 1830–1840. <https://doi.org/10.1002/pen.10155>.

- Chen, F., & Zhang, J. (2009). A new approach for morphology control of poly(butylene adipate-co-terephthalate) and soy protein blends. *Polymer*, *50*(15), 3770–3777. <https://doi.org/10.1016/j.polymer.2009.06.004>.
- Chen, F., & Zhang, J. (2010). In-situ poly(butylene adipate-co-terephthalate)/soy protein concentrate composites: Effects of compatibilization and composition on properties. *Polymer*, *51*(8), 1812–1819. <https://doi.org/10.1016/j.polymer.2010.02.035>.
- Chikh, A., Benhamida, A., Kaci, M., Pillin, I., & Bruzaud, S. (2016). Synergistic effect of compatibilizer and sepiolite on the morphology of poly(3-hydroxybutyrate-co-3-hydroxyvalerate)/poly(butylene succinate) blends. *Polymer Testing*, *53*, 19–28. <https://doi.org/10.1016/j.polymeresting.2016.05.008>.
- Coltelli, M.-B., Bronco, S., & Chinea, C. (2010). The effect of free radical reactions on structure and properties of poly(lactic acid) (PLA) based blends. *Polymer Degradation and Stability*, *95*(3), 332–341. <https://doi.org/10.1016/j.polymerdegradstab.2009.11.015>.
- da Silva, M. A., & Galland, G. B. (2013). Preparation and characterization of PE-g-alt. *Macromolecular Symposia*, *330*(1), 177–184. <https://doi.org/10.1002/masy.201300025>.
- Dawidziuk, K., Simmons, H., Kontopoulou, M., & Parent, J. S. (2018). Peroxide-initiated graft modification of thermoplastic biopolyesters: Introduction of long-chain branching. *Polymer*, *158*, 254–261. <https://doi.org/10.1016/j.polymer.2018.10.053>.
- Dossi, M., Storti, G., & Moscatelli, D. (2010). Initiation kinetics in free-radical polymerization: Prediction of thermodynamic and kinetic parameters based on ab initio calculations. *Macromolecular Theory and Simulations*, *19*(4), 170–178. <https://doi.org/10.1002/mats.200900056>.
- Fang, H., Ma, X., Feng, L., Wang, K., & Cao, B. (2008). Effects of screw configurations on the grafting of maleic anhydride grafted low-density polyethylene in reactive extrusion. *Journal of Applied Polymer Science*, *108*(6), 3652–3661. <https://doi.org/10.1002/app.27158>.
- Fink, J. K. (2013). Chapter 15 - reactive extrusion. In J. K. Fink (Ed.), *Reactive polymers fundamentals and applications (second edition)* (pp. 339–371). Oxford: William Andrew Publishing. <https://doi.org/10.1016/b978-1-4557-3149-7.00015-2>.
- Fourati, Y., Tarrés, Q., Mutjé, P., & Boufi, S. (2018). PBAT/thermoplastic starch blends: Effect of compatibilizers on the rheological, mechanical and morphological properties. *Carbohydrate Polymers*, *199*, 51–57. <https://doi.org/10.1016/j.carbpol.2018.07.008>.
- Gardella, L., Calabrese, M., & Monticelli, O. (2014). PLA maleation: An easy and effective method to modify the properties of PLA/PCL immiscible blends. *Colloid and Polymer Science*, *292*(9), 2391–2398. <https://doi.org/10.1007/s00396-014-3328-3>.
- Guaras, M. P., Alvarez, V. A., & Luduena, L. N. (2016). Biodegradable nanocomposites based on starch/polycaprolactone/compatibilizer ternary blends reinforced with natural and organo-modified montmorillonite. *Journal of Applied Polymer Science*, *133*(44). <https://doi.org/10.1002/app.44163>.
- Gutiérrez, T. J., & Alvarez, V. A. (2017a). Eco-friendly films prepared from plantain flour/PCL blends under reactive extrusion conditions using zirconium octanoate as a catalyst. *Carbohydrate Polymers*, *178*, 260–269. <https://doi.org/10.1016/j.carbpol.2017.09.026>.
- Gutiérrez, T. J., & Alvarez, V. A. (2017b). Data on physicochemical properties of active films derived from plantain flour/PCL blends developed under reactive extrusion conditions. *Data in Brief*, *15*, 445–448. <https://doi.org/10.1016/j.dib.2017.09.071>.
- Gutiérrez, T. J., & Alvarez, V. A. (2017c). Films made by blending poly(ϵ -caprolactone) with starch and flour from Sagu rhizome grown at the Venezuelan amazons. *Journal Polymers and the Environment*, *25*(3), 701–716. <https://doi.org/10.1007/s10924-016-0861-9>.
- Gutiérrez, T. J., Guarás, M. P., & Alvarez, V. A. (2017). Chapter 9. Reactive extrusion for the production of starch-based biopackaging. In M. A. Masuelli (Ed.), *Biopackaging* (pp. 287–315). Miami, EE.UU. ISBN: 978-1-4987-4968-8: CRC Press Taylor & Francis Group. <https://doi.org/10.1201/9781315152349-9>.
- Gutiérrez, T. J. (2018). Biological macromolecule composite films made from Sagu starch and flour/poly(ϵ -caprolactone) blends processed by blending/thermo molding. *Journal Polymers and the Environment*, *26*(9), 3902–3912. <https://doi.org/10.1007/s10924-018-1268-6>.

- Hamielc, A. E., Gloor, P. E., & Zhu, S. (1991). Kinetics of, free radical modification of polyolefins in extruders – Chain scission, crosslinking and grafting. *The Canadian Journal of Chemical Engineering*, 69(3), 611–618. <https://doi.org/10.1002/cjce.5450690302>.
- Haque, M. M.-U., Errico, M. E., Gentile, G., Avella, M., & Pracella, M. (2012). Functionalization and compatibilization of poly(ϵ -caprolactone) composites with cellulose microfibrils: Morphology, thermal and mechanical properties. *Macromolecular Materials and Engineering*, 297(10), 985–993. <https://doi.org/10.1002/mame.201100414>.
- Hassouna, F., Raquez, J.-M., Addiego, F., Dubois, P., Toniazzo, V., & Ruch, D. (2011). New approach on the development of plasticized polylactide (PLA): Grafting of poly (ethylene glycol)(PEG) via reactive extrusion. *European Polymer Journal*, 47(11), 2134–2144. <https://doi.org/10.1016/j.eurpolymj.2011.08.001>.
- Hayes, D. G., Anunciado, M. B., DeBruyn, J. M., Bandopadhyay, S., Schaeffer, S., English, M., Ghimire, S., Miles, C., Flury, M., Sintim, H. Y., & Sintim, H. Y. (2019). Biodegradable plastic mulch films for sustainable specialty crop production. In T. J. Gutiérrez (Ed.), *Polymers for Agri-food applications* (pp. 183–213). Cham: Springer. https://doi.org/10.1007/978-3-030-19416-1_11.
- Herniou-Julien, C., Mendieta, J. R., & Gutiérrez, T. J. (2019). Characterization of biodegradable/non-compostable films made from cellulose acetate/corn starch blends processed under reactive extrusion conditions. *Food Hydrocolloids*, 89, 67–79. <https://doi.org/10.1016/j.foodhyd.2018.10.024>.
- Hwang, S. W., Lee, S. B., Lee, C. K., Lee, J. Y., Shim, J. K., Selke, S. E., Soto-Valdez, H., Matuana, L., Rubino, M., & Auras, R. (2012). Grafting of maleic anhydride on poly (L-lactic acid). Effects on physical and mechanical properties. *Polymer Testing*, 31(2), 333–344. <https://doi.org/10.1016/j.polymertesting.2011.12.005>.
- Isiklan, N., Kursun, F., & Inal, M. (2010). Graft copolymerization of itaconic acid onto sodium alginate using benzoyl peroxide. *Carbohydrate Polymers*, 79(3), 665–672. <https://doi.org/10.1016/j.carbpol.2009.09.021>.
- Jin, H.-J., Kim, D.-S., Lee, B.-Y., Kim, M.-N., Lee, I.-M., Lee, H.-S., & Yoon, J.-S. (2000). Chain extension and biodegradation of poly(butylene succinate) with maleic acid units. *Journal of Polymer Science, Part B: Polymer Physics*, 38(17), 2240–2246. [https://doi.org/10.1002/1099-0488\(20000901\)38:17<2140::aid-polb40>3.0.co;2-n](https://doi.org/10.1002/1099-0488(20000901)38:17<2140::aid-polb40>3.0.co;2-n).
- John, J., Tang, J., & Bhattacharya, M. (1998). Grafting of oxazoline functional group to polycaprolactone. *Journal of Applied Polymer Science*, 67(11), 1947–1955. [https://doi.org/10.1002/\(sici\)1097-4628\(19980314\)67:11<1947::aid-app14>3.0.co;2-r](https://doi.org/10.1002/(sici)1097-4628(19980314)67:11<1947::aid-app14>3.0.co;2-r).
- John, J., Tang, J., Yang, Z., & Bhattacharya, M. (1997a). Synthesis and characterization of anhydride-functional polycaprolactone. *Journal of Polymer Science, Part A: Polymer Chemistry*, 35(6), 1139–1148. [https://doi.org/10.1002/\(sici\)1099-0518\(19970430\)35:6<1139::aid-pola17>3.0.co;2-7](https://doi.org/10.1002/(sici)1099-0518(19970430)35:6<1139::aid-pola17>3.0.co;2-7).
- John, J., Tang, J., Yang, Z., & Bhattacharya, M. (1997b). Synthesis and characterization of anhydride-functional polycaprolactone. *Journal of Polymer Science Part A: Polymer Chemistry*, 35(6), 1139–1148. [https://doi.org/10.1002/\(sici\)1099-0518\(19970430\)35:6<1139::aid-pola17>3.0.co;2-7](https://doi.org/10.1002/(sici)1099-0518(19970430)35:6<1139::aid-pola17>3.0.co;2-7).
- Kashani Rahimi, S., Aeinhevand, R., Kim, K., & Otaigbe, J. U. (2017). Structure and biocompatibility of bioabsorbable nanocomposites of aliphatic-aromatic copolyester and cellulose nanocrystals. *Biomacromolecules*, 18(7), 2179–2194. <https://doi.org/10.1021/acs.biomac.7b00578>.
- Kim, C.-H., Jung, K.-M., Kim, J.-S., & Park, J.-K. (2004). Modification of aliphatic polyesters and their reactive blends with starch. *Journal of Polymers and the Environment*, 12(3), 179–187. <https://doi.org/10.1023/b:jooe.0000038550.11407.ab>.
- Krivoguz, Y. M., Pesetskii, S. S., & Jurkowski, B. (2003). Grafting of itaconic acid onto LDPE by the reactive extrusion: Effect of neutralizing agents. *Journal of Applied Polymer Science*, 89(3), 828–836. <https://doi.org/10.1002/app.12299>.
- Krivoguz, Y. M., Pesetskii, S. S., Jurkowski, B., & Tomczyk, T. (2006). Structure and properties of polypropylene/low-density polyethylene blends grafted with itaconic acid in the course

- of reactive extrusion. *Journal of Applied Polymer Science*, 102(2), 1746–1754. <https://doi.org/10.1002/app.23998>.
- Ku Marsilla, K. I., & Verbeek, C. J. R. (2015a). Modification of poly(lactic acid) using itaconic anhydride by reactive extrusion. *European Polymer Journal*, 67(C), 213–223. <https://doi.org/10.1016/j.eurpolymj.2015.03.054>.
- Ku Marsilla, K. I., & Verbeek, C. J. R. (2015b). Modification of poly(lactic acid) using itaconic anhydride by reactive extrusion. *European Polymer Journal*, 67, 213–223. <https://doi.org/10.1016/j.eurpolymj.2015.03.054>.
- Kučera, F., Petruš, J., Matláková, J., & Jančář, J. (2017). Itaconic anhydride homopolymerization during radical grafting of poly(lactic acid) in melt. *Reactive and Functional Polymers*, 116, 49–56. <https://doi.org/10.1016/j.reactfunctpolym.2017.05.004>.
- Lal, J., McGrath, J. E., & Board, R. D. (1968). Effect of polymer structure on ease of hydrogen abstraction by cumyloxy radicals. *Journal of Polymer Science Part A-1: Polymer Chemistry*, 6(4), 821–828. <https://doi.org/10.1002/pol.1968.150060411>.
- Liu, H. Y., Chen, F. Q., Guo, R. B., Zhang, G., & Qu, J. (2015). Effect of compatibilizer on the properties of PBS/lignin composites prepared via a vane extruder. *Journal of Polymer Engineering*, 35(9), 829–837. <https://doi.org/10.1515/polyeng-2015-0015>.
- Liu, W., Liu, T., Liu, H., Xin, J., Zhang, J., Muhidinov, Z. K., & Liu, L. (2017). Properties of poly(butylene adipate-co-terephthalate) and sunflower head residue biocomposites. *Journal of Applied Polymer Science*, 134(13). <https://doi.org/10.1002/app.44644>.
- Ma, P., Cai, X., Zhang, Y., Wang, S., Dong, W., Chen, M., & Lemstra, P. J. (2014). In-situ compatibilization of poly(lactic acid) and poly(butylene adipate-co-terephthalate) blends by using dicumyl peroxide as a free-radical initiator. *Polymer Degradation and Stability*, 102, 145–151. <https://doi.org/10.1016/j.polymdegradstab.2014.01.025>.
- Maharana, T., Pattanaik, S., Routaray, A., Nath, N., & Sutar, A. K. (2015). Synthesis and characterization of poly(lactic acid) based graft copolymers. *Reactive and Functional Polymers*, 93, 47–67. <https://doi.org/10.1016/j.reactfunctpolym.2015.05.006>.
- Mani, R., Bhattacharya, M., & Tang, J. (1999). Functionalization of polyesters with maleic anhydride by reactive extrusion. *Journal of Polymer Science Part A: Polymer Chemistry*, 37(11), 1693–1702. [https://doi.org/10.1002/\(sici\)1099-0518\(19990601\)37:11<1693::aid-pola15>3.0.co;2-y](https://doi.org/10.1002/(sici)1099-0518(19990601)37:11<1693::aid-pola15>3.0.co;2-y).
- Merino, D., Mansilla, A. Y., Casalengué, C. A., & Alvarez, V. A. (2019). Performance of bio-based polymeric agricultural mulch films. In T. J. Gutiérrez (Ed.), *Polymers for Agri-food applications* (pp. 215–240). Cham: Springer. https://doi.org/10.1007/978-3-030-19416-1_12.
- Mohanty, S., & Nayak, S. K. (2010). Aromatic-aliphatic poly(butylene adipate-co-terephthalate) bionanocomposite: Influence of organic modification on structure and properties. *Polymer Composites*, 31(7), 1194–1204. <https://doi.org/10.1002/pc.20906>.
- Morais, D. D. S., Siqueira, D. D., Luna, C. B. B., Araujo, E. M., Barros Bezerra, E., & Wellen, R. M. R. (2019). Grafting maleic anhydride onto polycaprolactone: Influence of processing. *Materials Research Express*, 6(5), 055312–055315. <https://doi.org/10.1088/2053-1591/ab050d>.
- Muthuraj, R., Misra, M., & Mohanty, A. K. (2015). Injection molded sustainable biocomposites from poly(butylene succinate) bioplastic and perennial grass. *ACS Sustainable Chemistry and Engineering*, 3(11), 2767–2776. <https://doi.org/10.1021/acssuschemeng.5b00646>.
- Muthuraj, R., Misra, M., & Mohanty, A. K. (2017). Biodegradable biocomposites from poly(butylene adipate-co-terephthalate) and miscanthus: Preparation, compatibilization, and performance evaluation. *Journal of Applied Polymer Science*, 134(43), 45448. <https://doi.org/10.1002/app.45448>.
- Nabar, Y., Raquez, J. M., Dubois, P., & Narayan, R. (2005). Production of starch foams by twin-screw extrusion: Effect of maleated poly(butylene adipate-co-terephthalate) as a compatibilizer. *Biomacromolecules*, 6(2), 807–817. <https://doi.org/10.1021/bm0494242>.
- Nerkar, M., Ramsay, J. A., Ramsay, B. A., & Kontopoulou, M. (2014). Dramatic improvements in strain hardening and crystallization kinetics of PLA by simple reactive modification in the melt state. *Macromolecular Materials and Engineering*, 299(12), 1419–1424. <https://doi.org/10.1002/mame.201400078>.

- Nitz, H., Semke, H., Landers, R., & Mulhaupt, R. (2001). Reactive extrusion of polycaprolactone compounds containing wood flour and lignin. *Journal of Applied Polymer Science*, *81*(8), 1972–1984. <https://doi.org/10.1002/app.1628>.
- Nocita, D., Forte, G., Drakopoulos, S. X., Visco, A., Gianporcaro, A., & Ronca, S. (2017). Processing and characterization of bio-polyester reactive blends: From thermoplastic blends to cross-linked networks. *Polymer*, *132*, 252–263. <https://doi.org/10.1016/j.polymer.2017.10.069>.
- Pascente, C., Marquez, L., Balsamo, V., & Muller, A. J. (2008). Use of modified poly(ϵ -caprolactone) in the compatibilization of poly(ϵ -caprolactone)/maize starch blends. *Journal of Applied Polymer Science*, *109*(6), 4089–4098. <https://doi.org/10.1002/app.28255>.
- Persenaire, O., Quintana, R., Lemmouchi, Y., Sampson, J., Martin, S., Bonnaud, L., & Dubois, P. (2014). Reactive compatibilization of poly(L-lactide)/poly(butylene succinate) blends through polyester maleation: From materials to properties. *Polymer International*, *63*(9), 1724–1731. <https://doi.org/10.1002/pi.4700>.
- Petruš, J., Kučera, F., Chamradová, I., & Jančář, J. (2018). Real-time monitoring of radical grafting of poly(lactic acid) with itaconic anhydride in melt. *European Polymer Journal*, *103*, 378–389. <https://doi.org/10.1016/j.eurpolymj.2018.04.030>.
- Petruš, J., Kučera, F., & Petrůj, J. (2016). Post-polymerization modification of poly(lactic acid) via radical grafting with itaconic anhydride. *European Polymer Journal*, *77*, 16–30. <https://doi.org/10.1016/j.eurpolymj.2016.02.016>.
- Phua, Y. J., Chow, W. S., & Mohd Ishak, Z. A. (2013). Reactive processing of maleic anhydride-grafted poly(butylene succinate) and the compatibilizing effect on poly(butylene succinate) nanocomposites. *Express Polymer Letters*, *7*(4), 340–354. <https://doi.org/10.3144/expresspolymlett.2013.31>.
- Phua, Y. J., Lau, N. S., Sudesh, K., Chow, W. S., & Mohd Ishak, Z. A. (2012). Biodegradability studies of poly(butylene succinate)/organo-montmorillonite nanocomposites under controlled compost soil conditions: Effects of clay loading and compatibiliser. *Polymer Degradation and Stability*, *97*(8), 1345–1354. <https://doi.org/10.1016/j.polymerdegradstab.2012.05.024>.
- Picard, M. C., Rodriguez-Urbe, A., Thimmanagari, M., Misra, M., & Mohanty, A. K. (2019). Sustainable Biocomposites from poly(butylene succinate) and apple pomace: A study on compatibilization performance. <https://doi.org/10.1007/s12649-019-00591-3>.
- Puteh, M., Klinpituksa, P., & Kaesaman, A. (2015). Grafting of itaconic anhydride onto natural rubber as compatibilizer for rubber blend, experimental optimization of grafting extent. *Applied Mechanics and Materials*, *754-755*, 94–98. <https://doi.org/10.4028/www.scientific.net/amm.754-755.94>.
- Raquez, J.-M., Nabar, Y., Narayan, R., & Dubois, P. (2008a). In situ compatibilization of maleated thermoplastic starch/polyester melt-blends by reactive extrusion. *Polymer Engineering & Science*, *48*(9), 1747–1754. <https://doi.org/10.1002/pen.21136>.
- Raquez, J.-M., Narayan, R., & Dubois, P. (2008b). Recent advances in reactive extrusion processing of biodegradable polymer-based compositions. *Macromolecular Materials and Engineering*, *293*(6), 447–470. <https://doi.org/10.1002/mame.200700395>.
- Riva, R., Lenoir, S., Jérôme, R., & Lecomte, P. (2005). Functionalization of poly(ϵ -caprolactone) by pendant hydroxyl, carboxylic acid and epoxide groups by atom transfer radical addition. *Polymer*, *46*(19), 8511–8518. <https://doi.org/10.1016/j.polymer.2005.03.105>.
- Signori, F., Badalassi, M., Bronco, S., & Ciardelli, F. (2011). Radical functionalization of poly(butylene succinate-co-adipate): Effect of cinnamic co-agents on maleic anhydride grafting. *Polymer*, *52*(21), 4656–4663. <https://doi.org/10.1016/j.polymer.2011.08.045>.
- Smith, M. J., & Verbeek, C. J. R. (2018). Energy absorption mechanisms and impact strength modification in multiphase biopolymer systems. *Recent Patents on Materials Science*, *11*(1), 2–18. <https://doi.org/10.2174/1874464811666180911122032>.
- Standau, T., Zhao, C., Murillo Castellón, S., Bonten, C., & Altstädt, V. (2019). Chemical modification and foam processing of polylactide (PLA). *Polymers*, *11*(2), 306. <https://doi.org/10.3390/polym11020306>.

- Takamura, M., Nakamura, T., Takahashi, T., & Koyama, K. (2008). Effect of type of peroxide on cross-linking of poly (L-lactide). *Polymer Degradation and Stability*, 93(10), 1909–1916. <https://doi.org/10.1016/j.polymdegradstab.2008.07.001>.
- Tamboli, S., Mhaske, S., & Kale, D. (2004). Crosslinked polyethylene. *Indian Journal of Chemical Technology*, 11, 853–864. Available in: [http://nopr.niscair.res.in/bitstream/123456789/9558/1/ijct%2011\(6\)%20853-864.pdf](http://nopr.niscair.res.in/bitstream/123456789/9558/1/ijct%2011(6)%20853-864.pdf).
- Tang, H., Dai, W., & Chen, B. (2008). A new method for producing high melt strength polypropylene with reactive extrusion. *Polymer Engineering & Science*, 48(7), 1339–1344. <https://doi.org/10.1002/pen.21105>.
- Teramoto, N., Ozeki, M., Fujiwara, I., & Shibata, M. (2005). Crosslinking and biodegradation of poly(butylene succinate) prepolymers containing itaconic or maleic acid units in the main chain. *Journal of Applied Polymer Science*, 95(6), 1473–1480. <https://doi.org/10.1002/app.21393>.
- Thirumizir, M. Z. A., Hazahar, M. D., & Mohd Ishak, Z. A. (2017). *Mechanical and morphological properties of poly(Butylene Succinate)/Poly(Hydroxybutyrate-co-Hydroxyhexanoate) Polymer Blends: Effect of blend ratio and maleated compatibiliser*. Paper presented at the International Conference on Material Science and Engineering Technology, ICMSET 2016, October 14, 2016 - October 16, 2016, Phuket, Thailand.
- Wenfei, L., Zhanhai, Y., Guowei, J., Xiaoci, Z., Lixia, L., & Jinghua, Y. (2010). Preparation, characterization, and properties of pre-irradiated linear low-density polyethylene grafted itaconic anhydride by reactive extrusion. *Journal of Macromolecular Science - Physics*, 49(1), 75–85. <https://doi.org/10.1080/00222340903344044>.
- White, J. L., & Sasaki, A. (2003). Free radical graft polymerization. *Polymer-Plastics Technology and Engineering*, 42(5), 711–735. <https://doi.org/10.1081/ppt-120024992>.
- Wu, C.-S. (2003). Physical properties and biodegradability of maleated-polycaprolactone/starch composite. *Polymer Degradation and Stability*, 80(1), 127–134. [https://doi.org/10.1016/S0141-3910\(02\)00393-2](https://doi.org/10.1016/S0141-3910(02)00393-2).
- Wu, C.-S. (2012a). Characterization of cellulose acetate-reinforced aliphatic-aromatic copolyester composites. *Carbohydrate Polymers*, 87(2), 1249–1256. <https://doi.org/10.1016/j.carbpol.2011.09.009>.
- Wu, C.-S. (2012b). Utilization of peanut husks as a filler in aliphatic-aromatic polyesters: Preparation, characterization, and biodegradability. *Polymer Degradation and Stability*, 97(11), 2388–2395. <https://doi.org/10.1016/j.polymdegradstab.2012.07.027>.
- Wu, C.-S. (2015). Influence of modified polyester on the material properties of collagen-based biocomposites and in vitro evaluation of cytocompatibility. *Materials Science and Engineering: C*, 48, 310–319. <https://doi.org/10.1016/j.msec.2014.12.013>.
- Wu, C.-S., Hsu, Y.-C., Liao, H.-T., Yen, F.-S., Wang, C.-Y., & Hsu, C.-T. (2014). Characterization and biocompatibility of chestnut shell fiber-based composites with polyester. *Journal of Applied Polymer Science*, 131(17), 8906–8915. <https://doi.org/10.1002/app.40730>.
- Xijun, L., Xiaohua, G., & Baoqing, H. (2013). Preparation of POE graft copolymer and its application of toughening modification for PA6. *Polymer-Plastics Technology and Engineering*, 52(4), 344–351. <https://doi.org/10.1080/03602559.2012.748801>.
- Yin, Q., Chen, F., Zhang, H., & Liu, C. (2015). Fabrication and characterisation of thermoplastic starch/poly(butylene succinate) blends with maleated poly(butylene succinate) as compatibiliser. *Plastics, Rubber and Composites*, 44(9), 362–367. <https://doi.org/10.1179/1743289815Y.0000000031>.
- You, J., Lou, L., Yu, W., & Zhou, C. (2013). The preparation and crystallization of long chain branching polylactide made by melt radicals reaction. *Journal of Applied Polymer Science*, 129(4), 1959–1970. <https://doi.org/10.1002/app.38912>.
- Yu, L., Toikka, G., Dean, K., Bateman, S., Yuan, Q., Filippou, C., & Nguyen, T. (2013). Foaming behaviour and cell structure of poly(lactic acid) after various modifications. *Polymer International*, 62(5), 759–765. <https://doi.org/10.1002/pi.4359>.

- Zarrintaj, P., Jouyandeh, M., Ganjali, M. R., Hadavand, B. S., Mozafari, M., Sheiko, S. S., Vatankhah-Varnoosfaderani, M., Gutiérrez, T. J., & Saeb, M. R. (2019). Thermo-sensitive polymers in medicine: A review. *European Polymer Journal*, *117*, 402–423. <https://doi.org/10.1016/j.eurpolymj.2019.05.024>.
- Zhang, J. F., & Sun, X. (2004). Mechanical properties of poly(lactic acid)/starch composites compatibilized by maleic anhydride. *Biomacromolecules*, *5*(4), 1446–1451. <https://doi.org/10.1021/bm0400022>.
- Zhang, L., Lv, S., Sun, C., Wan, L., Tan, H., & Zhang, Y. (2017). Effect of MAH-g-PLA on the properties of wood fiber/polylactic acid composites. *Polymers*, *9*(11), 591. <https://doi.org/10.3390/polym9110591>.
- Zhou, W., & Zhu, S. (1998). ESR study of peroxide-induced cross-linking of high density polyethylene. *Macromolecules*, *31*(13), 4335–4341. <https://doi.org/10.1021/ma970973s>.
- Zhu, N., Ye, M., Shi, D., & Chen, M. (2017). Reactive compatibilization of biodegradable poly(butylene succinate)/Spirulina microalgae composites. *Macromolecular Research*, *25*(2), 165–171. <https://doi.org/10.1007/s13233-017-5025-9>.

Chapter 10

Grafting of Electroactive Polymers



Arun K. Nandi, Radhakanta Ghosh, and Dhruva P. Chatterjee

Abstract The grafting of copolymers has received significant attention due to the successful integration of their properties, both the backbone and graft chain polymers. The matter becomes even more interesting when the reactive/stimuli responsive polymeric chains are grafted onto backbone polymer, which offers unique physical properties such as crystallization or optoelectronic properties, etc. Such graft copolymer materials are very promising for the opening of new horizons of applications both in industry and academia. The grafting of reactive/responsive polymer chains onto commercially available polymers for greater manipulation of their properties is an attractive field of research. Grafting onto commercially available membrane-forming polymers such as poly(vinylidene fluoride) (PVDF) has aroused significant interest due to the possibilities of stimuli dependent membrane pore size modulation, supramolecular interactions have boosted its applications for affinity-based chromatography. Similarly, graft copolymers based on conjugated polymer backbones are also very much interesting, since interactions of the grafted chains with the external chemical or physical stimuli (such as pH, photoirradiation, salts, surfactants, temperature changes, etc.) significantly affect the conformation of the backbone chain, both in the solution state, gel state and solid state. This leads to changes in the optical response of the backbone polymers which are very useful in sensor applications, since the photo-responsivity of polymer systems is much stronger than small molecules due to signal amplification even under tiny perturbation. In most cases, grafting is done following an uncontrolled free radical-driven polymerization protocol, which associates threats to backbone degradation, the formation of high molecular weight graft chains, which affect the native properties of the backbone irreversibly. However, in order to keep the native properties of the backbone polymer intact, the grafting of polymeric chains must be performed in a controlled manner. In the

A. K. Nandi (✉) · R. Ghosh
Polymer Science Unit, School of Materials Sciences, Indian Association for the Cultivation
of Science, Jadavpur, Kolkata, India
e-mail: psuakn@iacs.res.in

D. P. Chatterjee
Department of Chemistry, Presidency University, Kolkata, India

present chapter, different strategies for the controlled grafting of neutral or ionic polymeric chains onto electroactive polymers and impact of the reactivity of the grafted chains onto the polymer property will be discussed.

Keywords Poly(thiophene) · Poly(vinylidene fluoride)

10.1 Introduction

In order to make polymeric materials useful, two types of processes are generally used: (i) physical mixing of two polymers or by formation of composites and (ii) by chemical modification, e.g. copolymer or graft copolymer formation. The greatest difficulty in the former method is the limited miscibility between the two polymers, however, it is sometimes found that the microphase separation improves some properties (Parameswaranpillai et al. 2014). The composites, especially nanocomposites, greatly improve the mechanical and physical properties for commodity applications, but none of the physical mixing processes can tune the molecular properties of polymers and this can be achieved by chemical modification of polymers. Among the different chemical processes (copolymerization), the grafting is superior because it does not affect the properties of the main chain, rather it imparts new properties to the polymer coming from the pendent chains. Polymers are mainly insulator due to the difficulty in generating charge and its flow. A new class of polymers called electroactive polymers (EAPs) are very useful for this purpose. EAPs are those kinds of polymers which can generate charges under special conditions and, sometimes, charges can flow along the chain under an external field. They have good optoelectronic properties which can be modulated by varying their structure by grafting and varying external conditions. Grafting is a process that attaches pendent oligomers/polymers keeping intact the properties of main chain and providing new properties from the grafted chains. They have aroused great interest due to their possible applications as smart materials in the areas of actuators, batteries, membranes, sensors and also in the biomedical field.

However, among all known EAPs, poly(vinylidene fluoride) (PVDF) is the center of scientific attraction because of its highest known piezo- and pyro-electric properties (Gallantree 1983, Lang and Muensit 2006). In addition, this semi-crystalline fluoropolymer has excellent membrane formation capacity, chemical and weather resistance, biocompatibility and durability (Kuilta et al. 2017a). There are five different crystalline forms of PVDF (α , β , γ , δ and ϵ) (Lovinger 1982). Among these, α -polymorph is mostly produced in melting crystallization, which have monoclinic unit cell with $TGT\bar{G}$ chain conformation (Lovinger 1982, Kim et al. 2009, Martins et al. 2012). β -polymorph has an orthorhombic unit cell with an all *trans* conformation and exhibits the most important piezo- and pyro-electric properties (Morra and Stein 1982). γ phase has an orthorhombic unit cell with a $T_3GT_3\bar{G}$ chain conformation (Doll and Lando 1970). The δ and ϵ polymorphs are polar and antipolar analogs of α and γ form, respectively (Lando et al. 1966, Weinhold et al.

1979). The grafting of this polymer with a different polymer is interesting since the crystallinity, electrical and mechanical properties, membrane forming ability, miscibility, structure, etc., can be tuned.

Poly(thiophene) (PT) is another interesting EAP, which has a conjugated double bond along the chain and can conduct electricity and also exhibits optoelectronic properties (McCullough and Lowe 1992, Maity et al. 2018). The main drawback of this polymer is that it is infusible and insoluble in both hydrophilic and hydrophobic solvents (Das et al. 2015, Jaymand et al. 2015). It is thus difficult to process and grafting of short or long polymer chain overcomes this difficulty since the pendent chains prevent the strong π -stacking interaction between the thiophene units of the PT chain (Das et al. 2015, Jaymand et al. 2015). The grafted PT chains showing chromic response is an interesting candidate for the manufacture of smart materials (Le'vesque et al. 2000). The optoelectronic properties of PT-graft copolymer can be tuned effectively by varying the biomolecules, ions, light, pH, temperature, etc. (Maity et al. 2018). The fascinating area of application of these graft copolymers is the development of sensors for biological analytes, energy devices, logic gate and molecular thermometers (Das et al. 2015, Jaymand et al. 2015, Das et al. 2017, Maity et al. 2018). They are better than the small molecular analogues due to their mechanical superiority and the cooperative amplified response of each segment through the conjugated chain, even for a very small perturbation (Das et al. 2015, Das et al. 2017). In the following sections, the different methods of synthesis, characterization, properties and application from graft copolymers of the above EAPs, made so far will be discussed.

10.2 Grafting of Poly(Vinylidene Fluoride) (PVDF)

In view of the significant piezo- and pyro-electric properties (Lovinger 1982), good biocompatibility (Bagchi et al. 2016), excellent membrane forming capability (Hester et al. 2002, Chen et al. 2003), graft modification of PVDF is very desirable in order to exhibit improved antistaticity, biocompatibility and surface properties.

10.2.1 Conventional Approach

It has been a general practice to employ free radical polymerization for graft modification of commercial polymers. Free radical centers are generated into polymer backbone after exposing them to ionizing radiation, free radical initiators (Hester et al. 2002) or the introduction of peroxide groups onto the original polymer backbone by ozone treatment (Boutevin et al. 1992, Fargere et al. 1994, Kang et al. 1997, Wang et al. 1998, Liu et al. 2001). The radical centers so produced initiate polymerization of several desired comonomers. However, such uncontrolled polymerizations, mainly generate a significant amount of homopolymer together with the desired graft copolymer. In addition, commercial polymers such as PVDF are

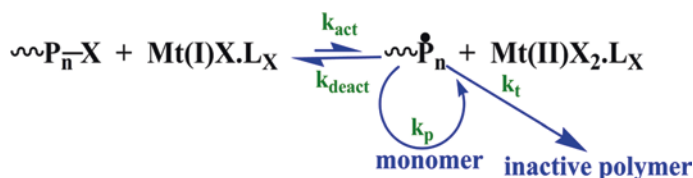
usually of high molecular weights (Mw), initial viscosity of the polymerization mixture remains high. Therefore, under uncontrolled polymerization conditions, there is a significant threat of gel formation or backbone degradation (Wang et al. 1999). An acceptable remedy for these problems is to use a controlled polymerization reaction during the synthesis of the grafted chains following the ‘grafting from’ strategy.

10.2.2 Grafting From Approach

In this respect, atom transfer radical polymerization (ATRP) technique is very acceptable due to its robust nature (with respect of the tolerance to various functional groups of monomers or solvents etc.), at relatively simple and profitable polymerization conditions. A schematic representation of the ATRP mechanism is given below (Scheme 10.1), where an alkyl halide R-X (or halogen-capped polymer chain P_n-X , X = Cl, Br) reversibly generates radical centers R^\bullet (or P_n^\bullet) by reacting with transition metal complex of lower oxidation state.

The radical centers produced react with vinyl monomers during chain propagation and are reversibly deactivated by the transition metal complex of higher oxidation state, which plays the role of ‘persistent radical’. Different transition metal complexes have been used as ATRP catalysts (Coessens et al. 2001; Matyjaszewski, & Xia 2001). However, the copper-based complexes have the most efficient performance. The main requisite in controlled radical polymerization is the initiation rate, which must be faster than propagation rate. However, due to very high bond strength of C-F bond and the relatively poor radical stabilization in the secondary carbon atom, this condition can never be achieved. Therefore, controlled polymerization initiated from the PVDF backbone is undoubtedly a challenge.

Hester et al. (2002) used for the first time ATRP of oxyethylene methacrylate (OEM) and *tert*-butyl methacrylate (*t*BMA) initiated from the PVDF backbone in homogeneous solution of *N*-methyl-2-pyrilidone (NMP) using CuCl/4,4'-dimethyl-2,2'-dipyridyl (DMDP) as catalysts. The initiation of the polymerization occurred from the secondary fluorine atoms present in the PVDF backbone. However, in view of the very high C-F bond strength (486 KJ/mole) and the appreciable stabilization of F-Cu^{II}L bond (Lanzalaco et al. 2017), neither the activation nor the deactivation occurred at a faster rate. This significantly affected the control over polymerization. The polymerization performance also recorded a significantly low yield, reaching ~42% *t*BMA conversion after 20 h and 20% OEM conversion after 19 h. The



Scheme 10.1 General scheme for atom transfer radical polymerization (ATRP)

¹H-NMR analysis indicated the presence of the poly(methacrylate) chains together with PVDF and the size exclusion chromatography (SEC) analysis exhibited a clean sweep of Mw distribution trace towards a lower elution volume compared to the PVDF macroinitiator. ¹H-NMR analysis is generally used to determine the graft chain Mw by using Eq. 10.1 (Expression for measuring Mw of graft copolymer).

$$\bar{M}_{n,\text{graft}} = \bar{M}_{n,\text{PVDF}} \left(1 + x \frac{M_o^{\text{comonomer}}}{M_o^{\text{PVDF}}} \right) \quad (10.1)$$

where x is the molar ratio of the comonomer units measured from nuclear magnetic resonance (NMR).

Hester et al. (2002) revealed through the use of dynamic scanning calorimetric (DSC) analysis that the melting temperature (T_m) and crystallinity were reduced after graft modification. However, the loss was more pronounced in the case of POEM graft chains, perhaps due to its greater flexibility and compatibility with the polar groups ($>CF_2$) of the PVDF backbone. Despite the lower degree of control over polymerization, the synthesized graft copolymers imparted the desired level of hydrophilicity to the PVDF backbone, which exhibited improved permeability towards aqueous analytes and protein antifouling properties when used in a 5% load with PVDF before membrane preparation by immersion precipitation technique.

The growth of hydrophilic chains on the surface of the PVDF membrane has been an acceptable strategy to impart hydrophilicity or antifouling property, retaining primarily the native properties of PVDF and the membrane framework. However, this is quite difficult to carry out the cleavage of C-F bond under heterogeneous conditions. With this in mind, Chen et al. (2006) reported a similar approach where surface-initiated atom transfer radical polymerization of poly(ethylene glycol) methyl ether methacrylate (PEGMA) or 2-dimethylaminoethyl methacrylate (DMAEMA) was carried out in water medium using CuCl/bipyridine (bpy) or CuBr/hexamethyltriethylenetetramine (HMTETA) complexes as catalysts. These authors performed a successful surface-initiated ATRP reaction from heterogeneous PVDF surface as a macroinitiator (Chen et al., 2006). Subsequently, the ‘living’ character of the surface grafted PPEGMA chains or poly(2-dimethylamino)ethyl methacrylate (PDMAEMA) has been established by a block copolymer with poly(styrene) (PS).

In view of the very high bond strength of C-F bond (486 kJ/mol compared to 339 kJ/mol for C-Cl bond) and the relatively poor stability of the secondary radical center in PVDF backbone compared to the tertiary/ α -ester group stabilized radical centers produced on monomer residues by C-Cl bond cleavage (during propagation). Thus, a slower initiation rate can be expected compared to the propagation rate. This should result in fairly poor control over the polymer chains and the ‘non-living’ character compared to any ATRP model system. It can also be expected that the control will be even lower during the surface initiated ATRP. Nevertheless, the work done by Chen et al. (2006) demonstrated a successful block copolymer formation with PS, which was established by ¹H-NMR analysis. Similarly, an appreciable antifouling property of the surface of hydrophilic polymer modified PVDF membrane with respect to the aqueous bovine serum albumin (BSA) solution was demonstrated.

Zhai et al. (2002) and Cen et al. (2004) reported a surface modification technique for modifying the surface of the PVDF membrane to impart antibacterial properties. Radiation-induced grafting of 4-vinylpyridine was carried out by Cen et al. (2004) on PVDF surface. Plasma pretreatment followed by exposure to air could create oxide or peroxide groups, and then graft copolymerization can be induced from them. The pyridine rings in the grafted chains were subsequently quaternized with hexyl bromide to generate *n*-hexylbromide groups onto the grafted poly(4-vinylpyridine) (P4VP) chains. A significant antibacterial property of the graft modified PVDF membrane was demonstrated by Cen et al. (2004) using *Escherichia coli* test compared to pristine PVDF membrane. The scanning electron microscopy (SEM) images showed numerous *E. coli* cells distributed on the upper fibers and interstitial spaces in contrast to the surface-modified membrane (PVDF-10) where no bacterial cells are found (Fig. 10.1a and b) (Cen et al. 2004).

In a fascinating approach, Singh et al. (2005) reported a methodology to convert commercially available PVDF microporous membranes into ion exchange membranes by grafting from primary anchoring poly(glycidyl methacrylate) (PGMA) monolayers. In order to avoid the ATRP initiation through a very strong C-F bond cleavage, PGMA layers were initially deposited on a plasma-pretreated microporous PVDF surface, where covalent anchoring with the PVDF surface was expected through reactive epoxy groups. Subsequently, the residual epoxide rings were opened with bromoacetic acid, and therefore, ATRP initiating sites were placed. The ATRP of 4-vinylpyridine was then carried out from these initiating sites using CuBr/Me₄Cyclam as catalysts in acetonitrile medium. The ion exchange capacities of the functionalized membrane were measured by generating titration curves of the pyridine groups on the membrane surface against 0.01 (M) HCl.

Pandey et al. (2003) also found that static ion exchange capacity was increased with the polymerization time during P4VP grafting, since a longer polymerization time had the introduction of a greater number of pyridine moieties onto the grafted chains. However, the ion exchange capacity observed was lower by the surface

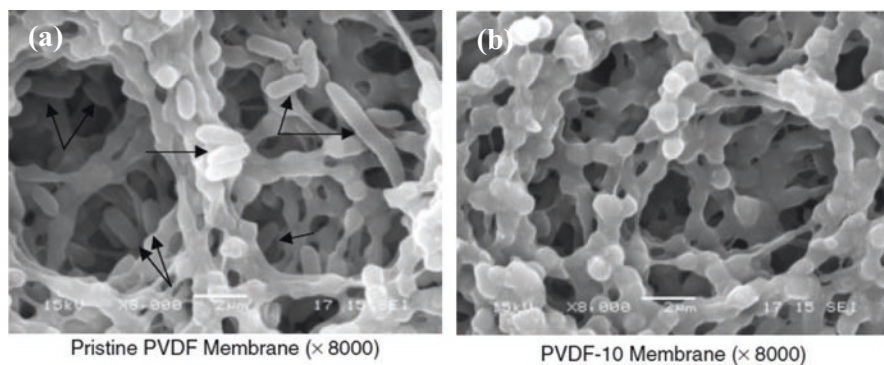


Fig. 10.1 SEM images of (a) Pristine PVDF and (b) modified PVDF-10 membrane. Reproduced with permission from Cen et al. (2004)

modified PVDF membrane compared to the commercially available ion exchange membranes (Table 10.1).

PDMAEMA is very interesting polymer due to its amphiphilic nature, thermo (lower critical solution temperature (LCST) at ~ 50 °C in neutral water) and pH responsive character. Most of the PDMAEMA's unique properties are due to their pendant tertiary amine groups ($-NMe_2$), which are very reactive. The easier availability of lone electron pair of the nitrogen atom can also induce supramolecular interactions with the positively charged carbon centers of PVDF ($>CF_2$) groups, and therefore, interesting bulk properties can be obtained. Apart from this, bulk modification of PVDF chains with PDMAEMA grafted chains was achieved, and therefore, the fabrication of membranes resulted in an improved affinity-based separation of the compounds from the analytes. In addition, given the hydrophilicity of the PDMAEMA chains, the membranes fabricated from bulk modified PVDF after the grafting solution phase of the PDMAEMA chains showed a better antifouling and antibacterial activity.

Xue et al. (2008) reported ATRP of DMAEMA initiated from the PVDF macro-initiator in *N,N*-dimethylformamide (DMF) medium using CuBr/pentamethyldiethylenetriamine (PMDETA) complex at 90 °C. The membrane fabrication was subsequently carried out using immersion precipitation technique. The analysis of the membrane surface composition was thoroughly performed by X-ray photoelectron spectra (XPS) analysis. The morphology of the membrane surface showed a significant dependence on external stimuli such as pH or temperature (Fig. 10.2). The PVDF-*g*-PDMAEMA synthesized by Xue et al. (2008) exhibited a significant antifouling property when studied in aqueous BSA solution. These materials also demonstrated a significant antibacterial property against *Staphylococcus aureus* compared to membranes fabricated from pristine PVDF (Fig. 10.3). In addition, the relatively low value of formation constant of CuBr/PMDETA complex resulted in a significant deactivation of the complex structure, particularly in reactive DMF solvent at elevated temperature as high as 90 °C. Therefore, a relatively poor degree of control over the graft chain polymer molecules is expected. Nevertheless, this work represents a significantly 'living' character of the grafted PDMAEMA chains, which is further established by the synthesis of the PDMAEMA-*b*-poly(naphthyl methacrylate) (PNM) block copolymer with fluorescent polymer PNM in the graft chains. Xue et al. (2008) also indicated that the initiation step during the synthesis of the block copolymer occurs from the fluoro-capped PDMAEMA graft chains and

Table 10.1 Ion-exchange capacities (mmol/g (meq/g)) for membranes prepared using different polymerization times. Reproduced with permission from Pandey et al. (2003)

Polymerization time (h)	Ion-exchange capacity ($\times 10^{-2}$ mmol/g ($\times 10^{-2}$ meq/g))
1	2.25
2	3.12
4	5.36
8	7.32

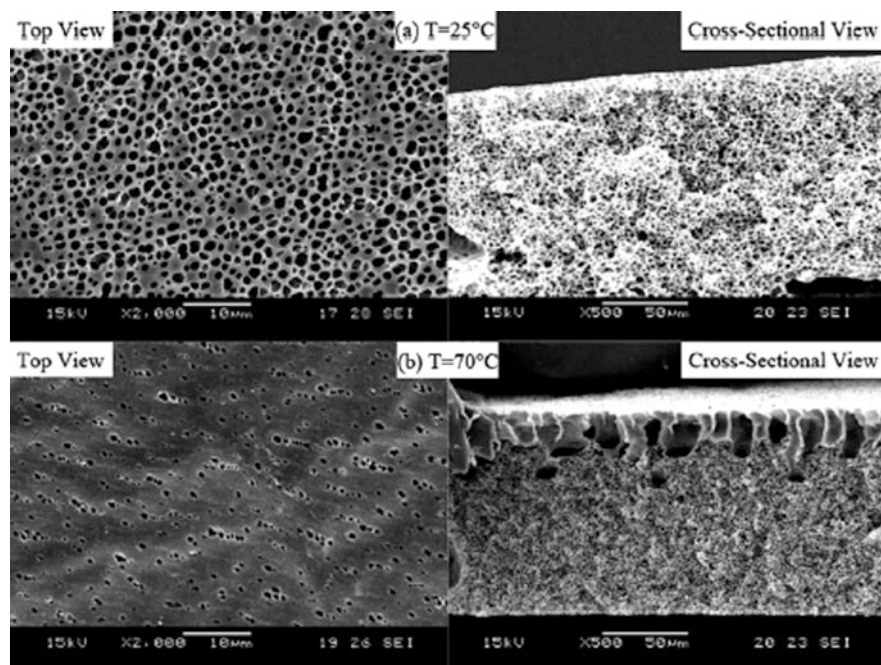


Fig. 10.2 SEM images of the surface (top) view and cross-sectional view of the PVDF-g-PDMAEMA copolymer membrane (from 2 h of ATRP fused at (a) 25 °C and (b) 70 °C in aqueous medium at pH 7. Reproduced with permission from Xue et al. (2008)

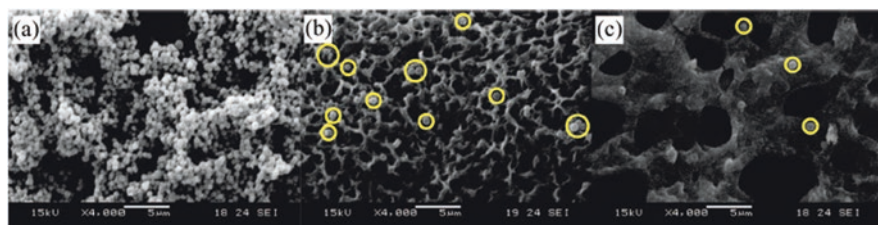


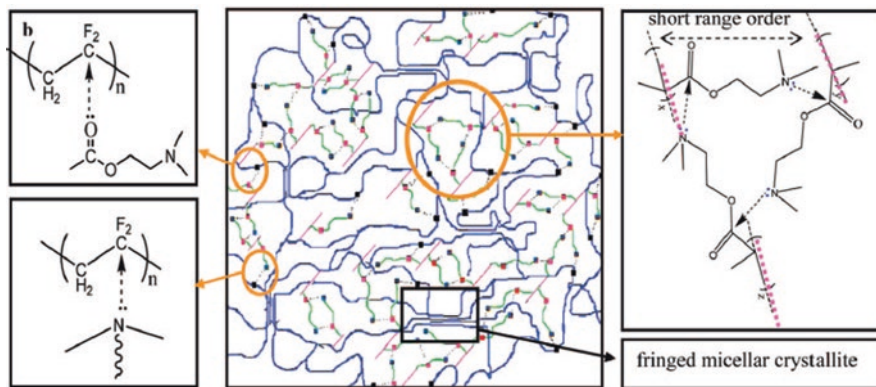
Fig. 10.3 SEM images of (a) the pristine PVDF membrane and the PVDF-g-PDMAEMA membranes from the copolymers with (b) 2 h and (c) 12 h of ATRP, after exposure to the *S. aureus* culture medium for 24 h. Reproduced with permission from Xue et al. (2008)

excludes any initiation from the residual backbone VDF moieties, as the temperature during the synthesis of the block copolymer with the same ATRP catalyst was maintained at 25 °C instead of 90 °C, and the fluorescence spectra of the PVDF-g-P(DMAEMA-*b*-NM) membrane casted from deionized water at 25 °C and pH 7 exhibited photoemission at ~364 nm when excited at 268 nm. Nevertheless, SEC analysis in support of the block copolymer synthesis was not given. Apart from providing hydrophilicity or antibacterial properties, the significantly reactive pendant tertiary amine ($-NMe_2$) groups of PDMAEMA graft chains can interact supra-molecularly with the ($>CF_2$) dipole of VDF units. This could result in a significant

development of the bulk properties of the PVDF-*g*-PDMAEMA graft copolymer. However, in order to achieve this, a significant amount of PDMAEMA chains is required to be grafted onto PVDF backbone.

Samanta et al. (2009) reported solution phase grafting of PDMAEMA chains onto PVDF macroinitiator in NMP medium at 80 °C using CuCl/DMDP catalyst. Unlike the CuBr/PMDETA catalyst used previously, CuCl/DMDP forms a much more stable catalytic complex having much greater efficiency to drive ATRP equilibrium. The polymerization kinetics was carefully monitored by gravimetric method, which exhibited about 39% monomer conversion for 24 h during grafting. The kinetic analysis showed a first order linear plot for the disappearance of monomers with a monomer conversion time of up to ~36%, and the evolution of Mw of the grafted chains with monomer conversion exhibited a linear relationship, as well as the SEC analysis confirmed the controlled nature of the polymerization through the clean sweep of the Mw distribution traces corresponding to the graft copolymers with increasing DMAEMA conversion, while the ¹H-NMR analysis proved to be quite useful for determining the exact Mw of the graft copolymers, graft length and graft density.

Very interesting, Samanta et al. (2009) also found that defect sites (H-H) of PVDF chains play a preferential role during the ATRP initiation. The ¹⁹F-NMR analysis of the graft copolymer with maximum DMAEMA conversion (39% monomer conversion in PD24) exhibited about 60% of the defective sites (H-H) responsible for the ATRP initiation, despite its abundance of only ~4.33% in the PVDF backbone, which of course is rich in (H-T) bonds (95.67%). The bulk modification of PVDF after grafting with hydrophilic PDMAEMA chains (as in PD24) was produced significantly, which is evident from the first-time report of PVDF-based graft copolymer being water soluble. The analysis of the thermal properties of the graft copolymer exhibited significant interactions between PDMAEMA graft chains and the PVDF backbone, resulting in a significant loss of crystallinity and a decrease in the T_m and degradation temperature of the graft copolymer. These effects were more pronounced by increasing graft conversion. Samanta et al. (2009) also suggested supramolecular interactions between the lone electron pairs on -NMe₂ group and the positively charged carbon atoms of >CF₂ groups, which results in the formation of 'fringed micelle' like crystallites for PVDF domains throughout the graft copolymer matrix (Scheme 10.2). The proposed supramolecular interactions are also supported from small angle X-ray scattering (SAXS), wide angle X-ray scattering (WAXS) and Fourier transform infrared (FTIR) analyses. The nanophases of the graft copolymer allow sufficient interaction between the components due to the increase in surface area. Samanta et al. (2009) also observed a dramatic increase in the toughness of the graft copolymer (~1970%) compared to PVDF, which was attributed to the unwinding of supramolecularly-organized rubbery PDMAEMA chains when stress is applied. In addition, the graft copolymer shows significant activity as an adhesive, which was able to withstand ~16 kg load when a pair of aluminum plates were fused using a thin film of PVDF-PDMAEMA (0.05 mm thickness and a square centimeter area). These authors indicated that this tremendous adhesive strength was caused by filler action of the nano dispersed PVDF



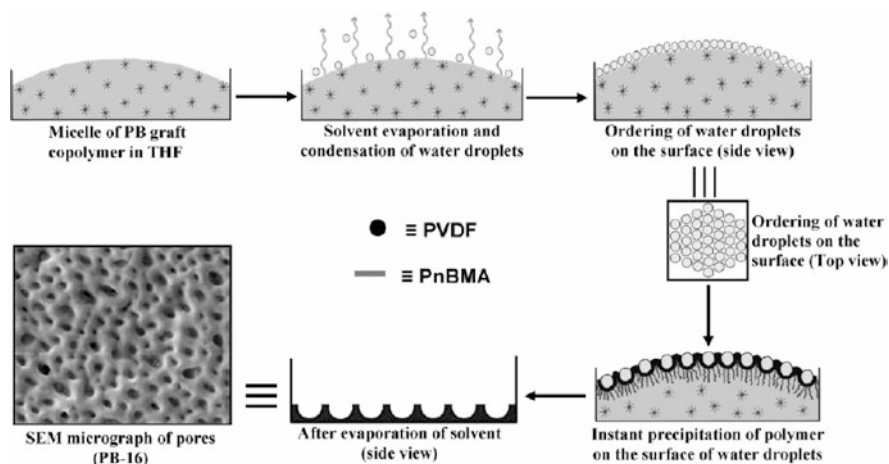
Scheme 10.2 Schematic model of PVDF-g-PDMAEMA graft chains with supramolecular interactions. Reproduced with permission from Samanta et al. (2009)

crystallites, and possibly in some degree of crosslinking by PDMAEMA chains during heating at 180 °C, before sealing the plates.

In another work, Samanta et al. (2010) carried out the ATRP grafting of poly(*n*-butyl methacrylate) (PnBMA) onto PVDF backbone under similar conditions to those considered for *tert*-butyl methacrylate (Hester et al., 2002). The polymerization kinetics exhibited first-order linear plot of almost 80% monomer conversion when the polymerization reaction was conducted in the presence of ~5% CuCl₂/DMDP complex with respect to CuCl/DMDP. The ¹⁹F-NMR analysis demonstrated defect sites (H-H) on the synthesized graft copolymer, which were the preferred site for ATRP initiation, while supramolecular interactions between the carbonyl ester group (>C=O) of the PnBMA chains and the (>CF₂) groups of PVDF were established by the FTIR analysis. The graft copolymer synthesized also shows appreciable mechanical properties, which were attributed to the supramolecular interactions between the ester carbonyl groups of grafted PnBMA chains and >CF₂ groups present on PVDF backbone. In addition, the graft copolymer showed appreciable solubility in low boiling organic solvent tetrahydrofuran (THF). Interestingly, honeycomb-like porous membranes were manufactured when film casting was done from the solution of the polymer in THF, following ‘breath figure’ mechanism (Scheme 10.3).

Samanta et al. (2010) also indicated that the graft copolymeric membrane casted from its THF solution exhibited a beautiful honeycomb-like morphology (Fig. 10.4) formed due to operation of the ‘breath figure’ mechanism. While the crystallinity of PVDF in the PVDF-*g*-PnBMA graft copolymer makes it a potential candidate to be used as a solid-state electrolyte in a Li⁺ ion battery. In fact, the graft copolymer film when doped with 5% Li⁺ ion (LiOTf), showed much an increased conductivity, as high as 1.04 × 10⁻⁵ S/cm compared to 2.0 × 10⁻¹⁰ S/cm dc conductivity of melt cooled Li⁺ ion doped PVDF film (Fig. 10.5) because of porosity of the film.

Another acceptable strategy for the synthesis of EAPs is graft copolymer based on PVDF keeping the reactive functional pendant groups, and subsequently modify



Scheme 10.3 A schematic model representing the pore formation of PB graft copolymers through 'breath figure' mechanism. Reproduced with permission from Samanta et al. (2010)

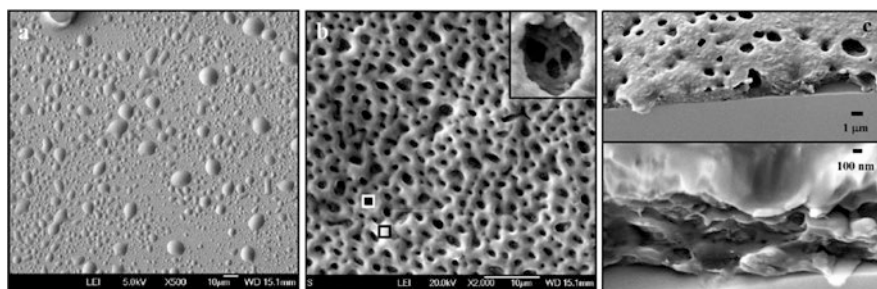
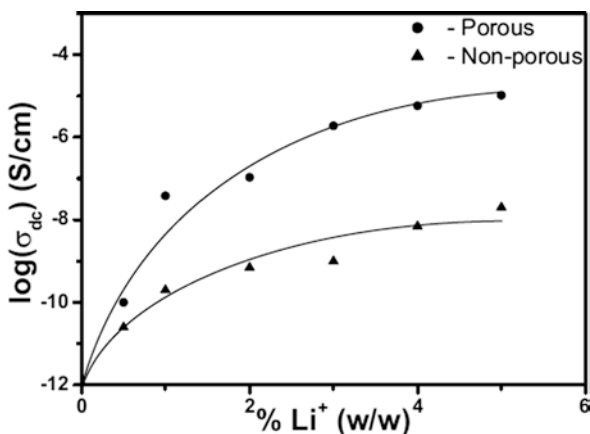


Fig. 10.4 Field emission scanning electron microscopy (FESEM) micrograph of (a) pure PnBMA, (b) PVDF-*g*-PnBMA films and (c) top: cross-section morphology of the PVDF-*g*-PnBMA film and bottom: high resolution micrograph of top. All films were cast from a THF solution in air at 30 °C. Reproduced with permission from Samanta et al. (2010)

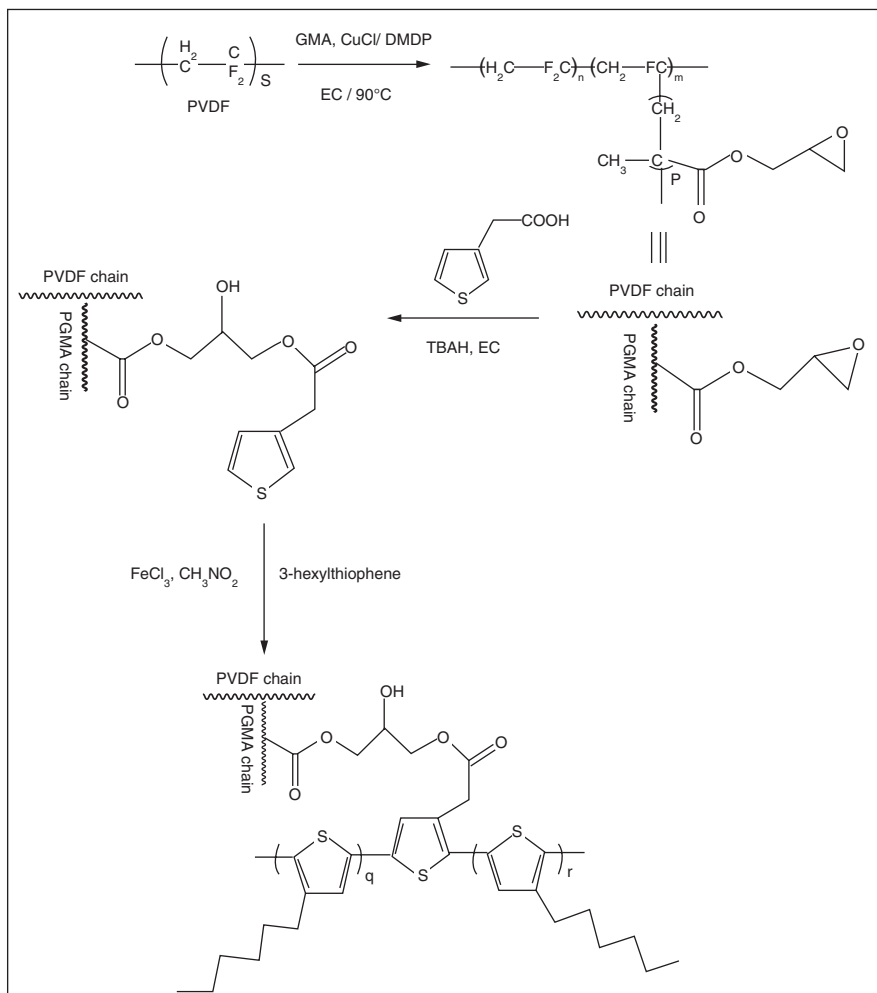
for the introduction of desired moieties before or after membrane fabrication. In this sense, Cai et al. (2011) reported on grafting of propargyl methacrylate (PMA) by thermal polymerization onto ozone pretreated PVDF backbone. This was followed by the manufacture of membranes by the phase inversion technique. Subsequently, the alkyne moieties present on the surface of the membrane were used for thiol-yne 'click' reaction with 3-mercapto-1-propanesulphonic acid sodium salt. Alternatively, alkyne-azide click reaction was performed to introduce β -cyclodextrin (β -CD) moieties to obtain mono(6-azido-6-deoxy)- β -cyclodextrin membrane surface. These moieties acted as hosts for the formation of inclusion complexes with diadamentyl-poly(ethylene oxide) (AD-PEO). Thus, polar PEO moieties were introduced on the membrane surface to impart significant antifouling properties. In fact, the PEO tethered membrane surface showed less than 25% γ -globulin adsorption compared to

Fig. 10.5 Plot of dc conductivity vs. Li^+ ion concentration of doped PVDF-*g*-PnBMA graft copolymer with porous and non-porous morphology. Reproduced with permission from Samanta et al. (2010)



the PVDF-*g*-PPMA precursor graft copolymer membrane. The high efficiency and the almost universal nature of the alkyne-azide click reaction allows additional extrapolation of the strategy developed for anchoring azide end capped polymeric chains of PEO monomethyl ether (azido-MPEO), poly[2-(*N,N*-dimethylamino) ethyl methacrylate](azido-PDMAEMA) and poly(*N*-isopropyl acrylamide) (azido-PNIPAM) on PVDF-*g*-PPMA membranes for the production of antifouling, pH and temperature responsive membranes.

Materials having a combination of orthogonal properties such as ferroelectricity and semi conductivity generate a significant interest in applications such as non-volatile data storage. Normally different inorganic materials are used for such applications. The ferroelectric properties of the β -phase of PVDF can be valuable in such applications if the semiconductor organic substances can be united with it. In this regard, poly(3-hexyl)thiophene (P3HT) has received significant attention as an organic semiconductor material, however, it is very difficult to covalently connect ferroelectric PVDF and semiconductor P3HT. With this in mind, Samanta et al. (2012a) designed a novel synthetic strategy for the preparation of covalently attached ferroelectric PVDF and semiconductor P3HT in a graft copolymer. In this work, the PGMA chains were first grown up *via* ATRP from the PVDF macroinitiator and then the 3-thiopheneacetic acid molecules were anchored after opening the epoxide rings. In the next step, the oxidative polymerization of 3-hexylthiophene was carried out with FeCl_3 in nitromethane medium in the presence of the above thiophene ring anchored PVDF graft copolymer (Scheme 10.4). The ATRP of glycidyl methacrylate (GMA) is quite difficult because of its tremendous susceptibility to acidic or basic impurities during the polymerization reaction which can lead to the epoxide ring opening and finally to irreversible gelation. The ATRP of GMA was conducted by Samanta et al. (2012a) in ethylene carbonate (EC) solvent with PVDF macroinitiator using CuCl/DMDP catalyst at 90°C . However, Mw evolution, polymerization kinetics and SEC analysis indicated a fairly controlled ATRP, which achieved a very poor monomer conversion of about 33% after 6 h. The epoxy rings of the PGMA graft chains were subsequently opened by heating with



Scheme 10.4 Synthesis of the PVDF-g-PGMA-g-P3HT copolymer using ATRP and oxidative polymerization techniques. Reproduced with permission from Samanta et al. (2012a)

thiophene 3-acetic acid and then oxidative polymerization of 3-hexylthiophene was carried out in the presence of the modified graft copolymer to synthesize PVDF-g-PGMA-g-P3HT (PGHT). The FTIR and crystallographic analysis indicated the presence of PVDF α -polymorph state in the PVDF-g-PGMA, which subsequently became β -phase in PGHT. The TEM micrograph of melt quenched PGMA samples exhibited a spherulitic structure of PVDF (Fig. 10.6), which disappears after the formation of PGHT showing the development of P3HT nanospheres. However, the analysis of dc conductivity shows an appreciably poor value of PGHT compared to P3HT, which was attributed to the largest energy barrier for hopping of the charge

carriers through the conductive P3HT nanospheres dispersed into the non-conducting PVDF-*g*-PGMA matrix.

On the other hand, Lanzalaco et al. (2017) reviewed the mechanism of PVDF backbone initiated ATRP, and evidenced that the slower initiation through the highly stable (C-F) bond breakage was the principal reason behind the poor control over the synthesized graft chains. These authors also suggested that the structure of the activator and deactivator catalyst complexes under the polymerization conditions was $[\text{Cu}^{\text{I}}(\text{DMDP})_2]^+[\text{CuCl}_2]^-$ and $[\text{Cu}^{\text{II}}(\text{DMDP})_2\text{Cl}_2]$, respectively. Therefore, after initiation through the PVDF macroinitiator, the expected structure of the deactivator complex should be $[\text{Cu}^{\text{II}}(\text{DMDP})_2\text{ClF}]\text{Cl}^-$. In this situation, Cl^- ions should provide a faster deactivation rate, although the relatively slow transfer of F^- (due to the greater Cu^{II}-F bond force) (Lanzalaco et al. 2017). Lanzalaco et al. (2017) also reported that the greater thermodynamic stability of C-F bond is decided on the propagating poly(methacrylate) graft chain ends. The last possibility must present a condition of slower chain reinitiation compared to the first, which results in poorly controlled polymerization. According to Lanzalaco et al. (2017) a greater monomer conversion in such polymerization can still be achieved due to the presence of a

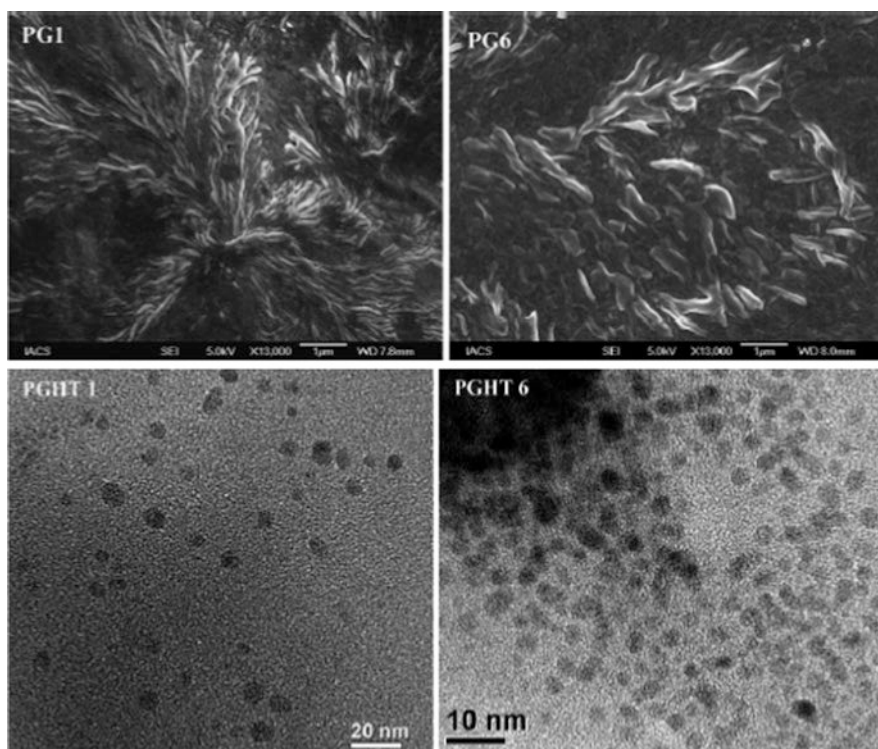


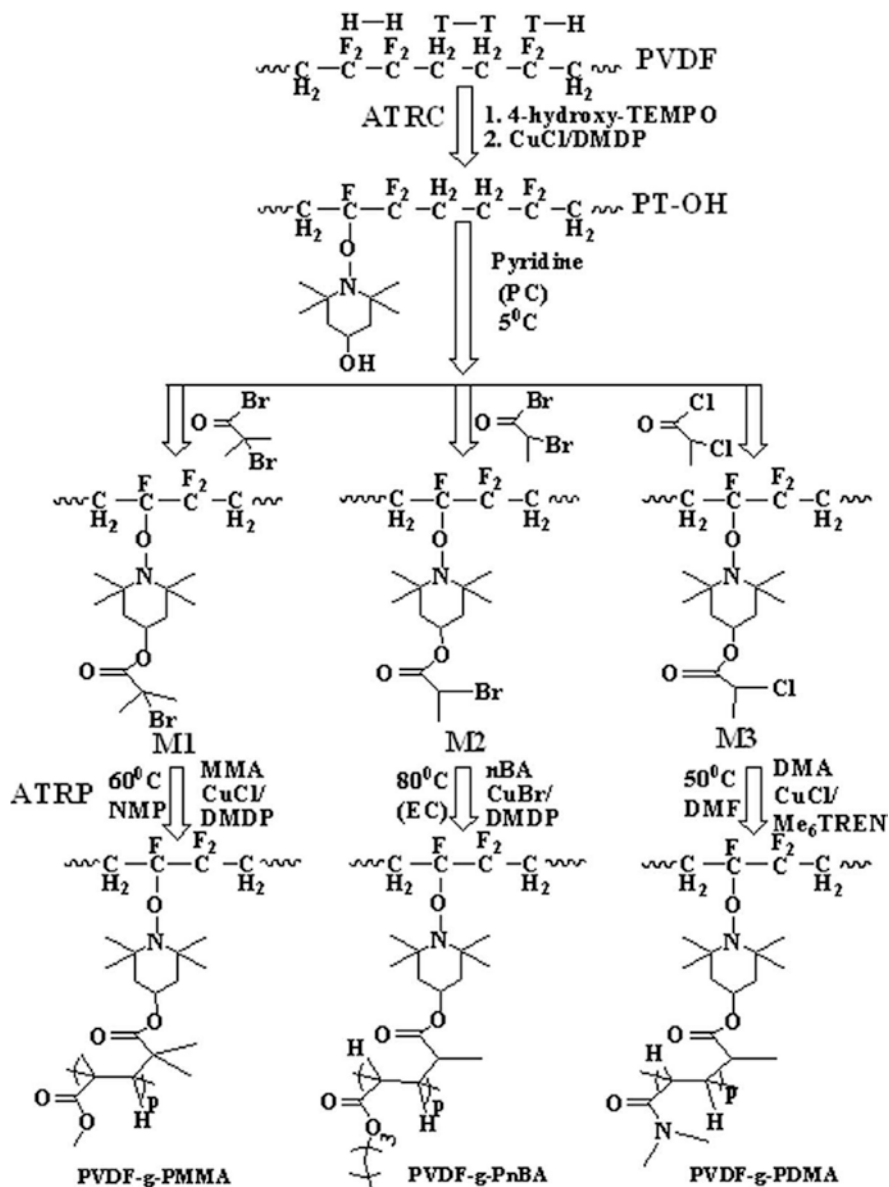
Fig. 10.6 TEM micrograph of PVDF-*g*-PGMA after 1 and 6 h of ATRP (PG1 and PG6). Corresponding samples after P3HT bonding (PGHT1 and PGHT6). Reproduced with permission from Samanta et al. (2012a)

large number of initiation sites distributed throughout the PVDF backbone. Therefore, a potential reason behind a relatively lower conversion, particularly in the case of monomers containing reactive pendant functional groups, should be catalyst deactivation. In line with this, the appreciably good nucleophilicity of the pendant $-NMe_2$ groups can replace the Cl atom from the primary valence sphere of the deactivator complex during polymerization of DMAEMA, resulting in the formation of deactivator complex such as $[Cu^{II}(DMDP)_2(DMAEMA)F]Cl$. This deactivator complex does not contain any Cl atom for providing deactivation, thus a very low deactivation rate can be expected for F^- ions. Under these conditions, the activator concentration decreases sharply due to non-establishment of the ATRP equilibrium, resulting in a poor monomer conversion until the end, even after an appreciable period of time (Lanzalaco et al. 2017).

In order to alleviate this problem and obtain a well-controlled polymerization from PVDF backbone, Kuila et al. (2014) introduced for the first time an approach for tethering model ATRP initiator onto the PVDF backbone, and therefore, to drive the polymerization. In this work, the first 4-hydroxyTEMPO moieties were anchored onto PVDF backbone using atom transfer radical coupling (ATRC) reaction based on $CuCl/DMDP$ (Kuila et al. 2014). This allowed the presence of hydroxyl groups distributed randomly onto PVDF backbone and then model ATRP initiators for various (meth)acrylate and acrylamide monomers were coupled to these sites by simple ester coupling reactions. All these strategies are presented in Scheme 10.5. The strategy applied presents a complete solution to the problem of slow initiation related with the cleavage of the C-F bond from PVDF backbone.

Many monomers have been successfully grafted from the PVDF backbone, which could not be done through direct ATRP. Table 10.2 shows many monomers having different reactivity. The highest polymerization rate of methyl methacrylate (MMA) using modified PVDF initiator compared to unmodified PVDF initiator is also given in Fig. 10.7a. As expected, Kuila et al. (2014) reported that during modified PVDF initiated polymerizations, the graft chain lengths were relatively longer compared to PVDF initiated graft chains. This was very evident by the relatively pronounced increase in the graft Mw with the conversion during the modified PVDF-initiated polymerization of MMA. Interestingly, the degrafted poly(methyl methacrylate) (PMMA) chains from the PVDF backbone of the modified PVDF-initiated graft copolymer, showed a linear increase in Mw with the conversion, thus maintaining an appreciably low Mw distribution (MWD or polydispersity index - $PDI = \text{weight-average apparent molecular weight } (M_w) / \text{number-average apparent molecular weight } (M_n)$), which shows an additional decrease as the conversion increases. In addition, the 'living' nature of the grafted PMMA chains when initiated from modified PVDF initiator is established by block copolymer synthesis with poly(methoxyethoxy)ethyl methacrylate (PMeO₂MA). According to Kuila et al. (2014) the superposition of SEC traces confirmed the ability to restart grafted PMMA chains of the grafted PMMA chains through clean sweep to reduce elution volume after block copolymer formation (Fig. 10.7b).

PVDF is highly hydrophobic in nature, initial attempts for attaching hydrophilic graft chains onto PVDF backbone have been aimed at imparting hydrophilicity to



Scheme 10.5 Synthetic scheme of different graft copolymers using the coupled ATRC and ATRP approach. Reproduced with permission from Kuila et al. (2014)

the membrane surface to improve antifouling properties and water permeation. A successful application of the strategy developed was demonstrated by Kuila et al. (2015) during the preparation of PVDF-*g*-PMe₂MA with almost 70% monomer conversion when the polymerization was conducted at 60 °C. The appreciable graft

Table 10.2 Reaction condition, conversion rate, Mw and PDI of different PVDF graft copolymers synthesized from PVDF and model initiators. Reproduced with permission from Kuila et al. (2014)

Entry	Macro initiator	monomer	Catalyst	Time (hrs)	Temp. (°C)	Conversion rate (%)	Mw (NMR) $\times 10^{-3}$	PDI
1	PVDF	MMA	A	32	60	62	180	1.5
2	M1	MMA	A	24	60	82	230	1.6
3	M1	<i>t</i> BMA	A	24	60	70	33 ^a	1.4
4	M1	DMAEMA	A	24	60	73	107	1.5
5	M1	MeO ₂ MA	A	24	60	70	421	2
6	M2	<i>n</i> BA	B	30	80	67	94	1.5
7	M2	<i>t</i> BA	B	30	80	32	87	1.4
8	M3	DMA	C	20	50	20	86	1.3

A = CuCl/DMDP or NMP, B = CuBr/DMDP or EC, C = CuCl/Me6TREN or DMF

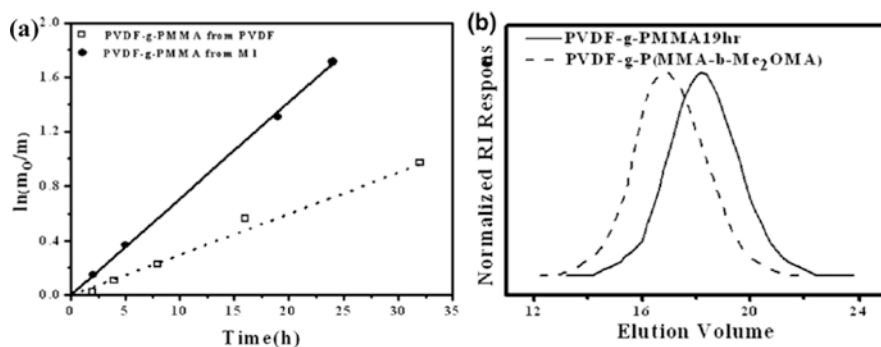


Fig. 10.7 (a) Disappearance of monomer with polymerization time and (b) SEC traces in THF of PVDF-*g*-PMMA and PVDF-*g*-P(MMA-*b*-MeO₂MA) block copolymer. Reproduced with permission from Kuila et al. (2014)

conversion during the synthesis of the hydrophilic PMeO₂MA chains made the water-soluble graft copolymer at low concentration. Kuila et al. (2015) also reported that the thermo-responsive character of the grafted PMeO₂MA chains in aqueous solution was reflected on the temperature-dependent aggregation/disaggregation behavior of the graft copolymer, and therefore, in its aqueous solubility (Fig. 10.8). The thermo-responsive character of the PMeO₂MA grafted chains was also performed by Kuila et al. (2015) for the demonstration of the antifouling character of the graft copolymer membranes casted by the ‘breath figure’ technique (Fig. 10.9). A digital image for the filtering configurations used for demonstrating the previous antifouling properties is shown in Fig. 10.10.

The development of the ATRP grafting from the PVDF surface in the last two decades has finally made the PVDF soluble in water or other protic solvents. Water soluble PVDF-*g*-PDMAEMA or PVDF-*g*-P(DMAEMA-*alt*-MeO₂MA) have been used for stabilization of gold nanoparticles (Au NPs) (Samanta et al. 2009) or silver NPs (Ag NPs) (Kuila et al. 2017b), respectively, in aqueous medium. A similar

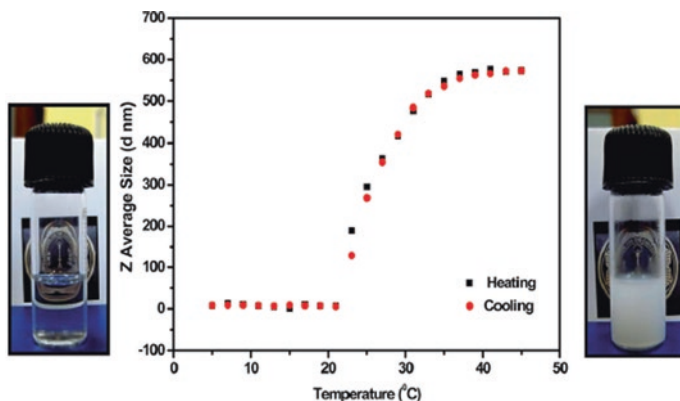


Fig. 10.8 Z average size vs. temperature plot of the PD-24 graft copolymer obtained from the study of dynamic light scattering (DLS) in aqueous solution (0.1% w/v). Reproduced from with permission Kuila et al. (2015)

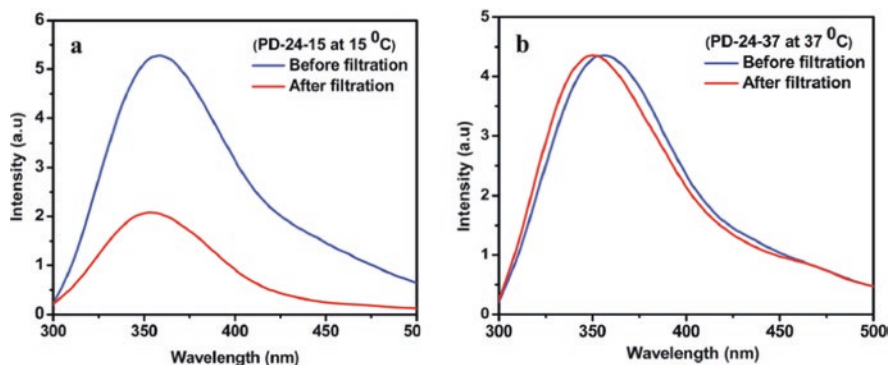


Fig. 10.9 Fluorescence spectra of aqueous solution of BSA before and after filtration through the graft copolymer film at (a) 15 °C and (b) 37 °C. Reproduced with permission from Kuila et al. (2015)

study was done by Kuila et al. (2016) by synthesizing PVDF-*g*-PMeO₂MA (PD) copolymer, demonstrating simultaneous presence of LCST and upper critical solution temperature (UCST) in water/methanol (40–60%) medium (Fig. 10.11).

Interestingly, He et al. (2014) with the objective of increasing the cytocompatibility of PVDF, studied the covalent bonding of the arginine-glycine-aspartic acid tripeptide (RGD) on the PVDF backbone, thus exploiting reactive epoxy groups of grafted PGMA chains onto PVDF. The synthesis of the material was carried out by coupled application of ATRP and alkyne-azide click chemistry, where the PGMA chains were directly grafted from the PVDF backbone by ATRP, subsequently, click coupling of the tripeptide was carried out after opening of the epoxide rings by azide ions (Scheme 10.6). The superior mechanical and physicochemical properties of these materials allow them to be applied to replace the defective function of a

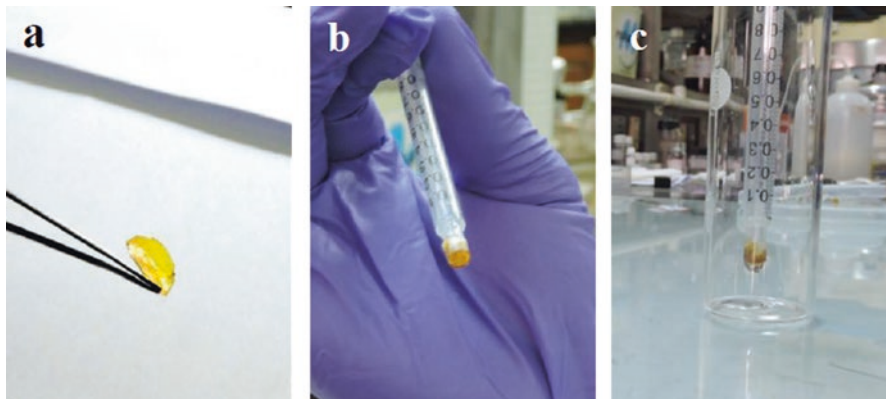


Fig. 10.10 (a-c) Digital images of filtering set up with PD-24

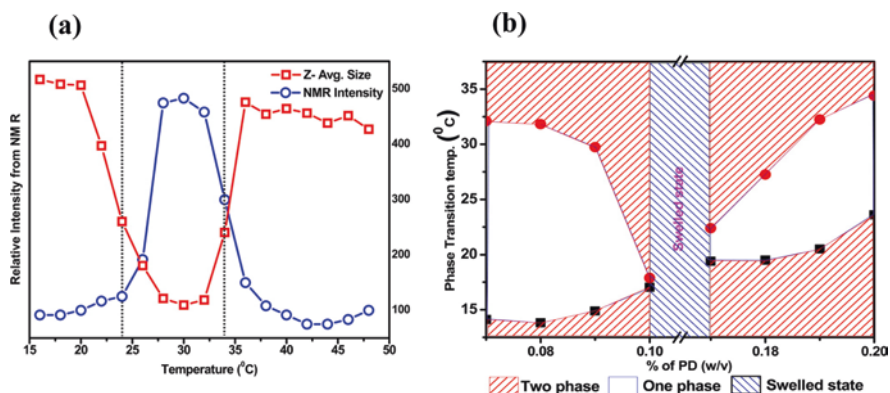
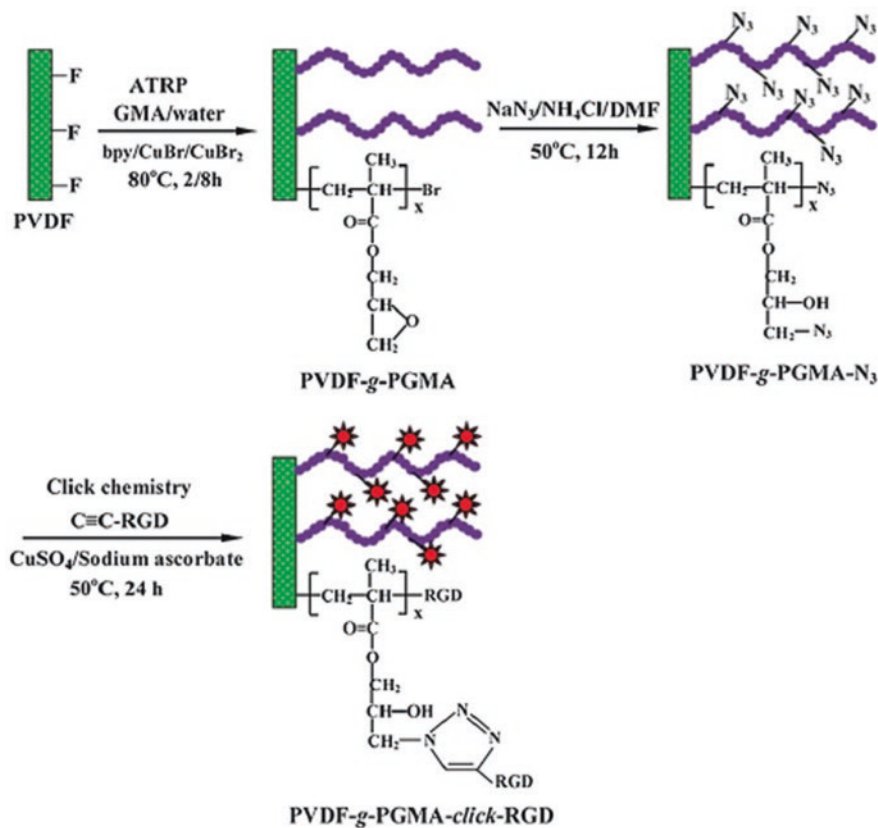


Fig. 10.11 (a) Comparison of the area of methylene peaks of grafted PMeO₂MA from ¹H NMR in MeOD-D₂O (1:1) and Z-average sizes of PD in methanol/water (1:1) at different temperature which show both UCST and LCST and (b) Quasi binary phase diagram of PD in methanol/water solution (1:1 v/v). Reproduced with permission from Kuila et al. (2016)

tissue or part of an organ. He et al. (2014) also found that the surfaces of the synthesized graft copolymeric materials improved cell attachment and proliferation of adipose derived stem cells (ASC) compared to the pristine PVDF or PVDF-*g*-PGMA film surfaces.

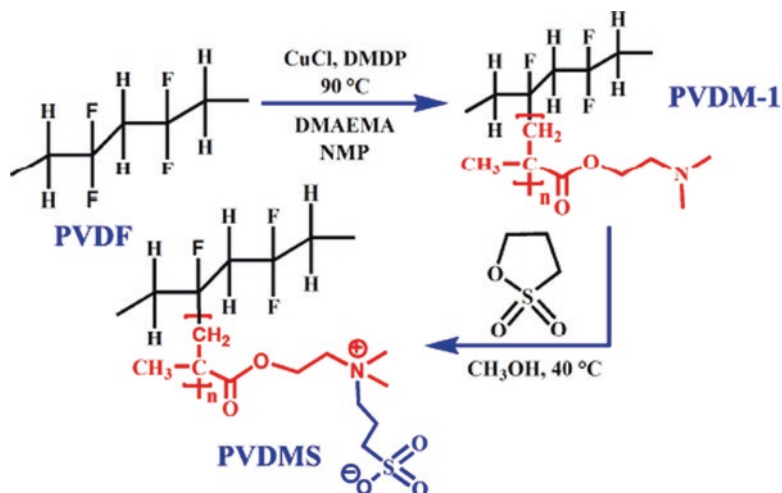
Given the technological importance and biocompatibility of PVDF, water-soluble PVDF-based polymeric materials are very desirable. In this respect, PVDF grafted with ampholytic graft chains with hydrophilicity or aqueous solubility is receiving considerable attention. With this in mind, Pakhira et al. (2019) synthesized a PVDF-based zwitterionic graft copolymer. The two-step strategy for synthesis is shown in Scheme 10.7, where at first, the PDMAEMA chains were grafted onto PVDF backbone by ATRP and then the pendant tertiary amine groups (-NMe₂) of the PDMAEMA chains were quaternized with 1,3-propane sultone. This was



Scheme 10.6 Schematic illustration of the surface-initiated ATRP process of GMA from the PVDF film to give the PVDF-g-PGMA film surface, subsequent addition of azide groups *via* ring opening reaction of the epoxy groups on the PGMA brushes with sodium azide to produce PVDF-g-PGMA- N_3 surface and the conjugation of the RGD peptide to the PGMA brushes *via* alkyne-azide click reaction. Reproduced with permission from He et al. (2014)

further fractionated by water to obtain the aqueous solution having much better optical clarity and emission properties with a quantum yield of 8%. This approach was very interesting since the molecule does not contain any conjugated fluorophoric moiety. The origin of such fluorescence emission with nonconjugated chromophores was attributed to the clustering of carbonyl groups.

Thus, great steps are made in the grafting of the technologically important PVDF using the ATRP technique with different polymeric chains to produce innumerable new functional materials. The works in this field has allowed the successful use of the ATRP in the controlled grafting of PVDF, where the C-F bond has a very high bond energy too difficult to activate (Kuila et al. 2014). In addition, after the initial attempt to carry out ATRP from the PVDF macroinitiator through C-F bond cleavage, the introduction of tethering model ATRP initiating sites onto PVDF backbone



Scheme 10.7 Synthesis of PVDF-based ampholytic graft copolymer. Reproduced with permission from Pakhira et al. (2019)

using ATRC to form a modified macroinitiator has thrown light for easier graft polymerization of different monomers with a substantial degree of polymerization. This could lead to producing interesting properties which can produce different functional materials, biomaterials, sensors, etc., in the near future.

10.3 Poly(Thiophene) (PT)

Up to three quarters of the twentieth century nobody would have believed that polymers could conduct electricity as metals. Polymers have been considered as insulators of electricity. About 40 years ago a new class of organic polymers was discovered whose have the remarkable ability to conduct electricity, classified as ‘electrically conducting polymers’ or ‘synthetic metals’ (Walton 1990). The discovery of poly(acetylene) by Hideki Shirakawa’s group opened a new window before us in the field of electroactive polymer due to its unique conjugated system (Shirakawa et al. 1977). The conjugated polymers (CPs) are organic macromolecules, characterized by a backbone chain of alternating double and single bonds, their overlapping π -orbitals create a system of delocalized π -electrons, which result in interesting and useful optical and electronic properties (Barford 2005). They also have a conductivity similar to metal with the following advantages: corrosion resistance, easy processing and recyclability, grater workability, lighter weight and low cost (Mac Diarmid 2001, Ignatyev et al. 2014).

After this advance, many new conjugated polymers such as poly(aniline) (PANI), poly(*p*-phenylene vinylene), poly(*p*-phenylene), poly(pyrrole), PT, etc. have been discovered, which have demonstrated an appreciably high value of electrical

conductance (sometimes even greater than metallic copper). Among all conducting polymers, PT is a well-known electroactive polymer showing tuneable fluorescence properties, Forster resonance energy transfer (FRET) and tunable electrical conductivity (Liu et al. 2002, Rasmussen et al. 2015, Westenhoff et al. 2005). The solubility in common organic solvents and in water is the greatest difficulty of pristine PT for its technological application (Das et al. 2015). Now, the processable materials in solution are always profitable and handier for technological applications. To overcome the processability problem, the attachment of flexible pendent groups onto the conjugated PT backbone is necessary (Das et al. 2015, Jaymand et al. 2015). Substituted PTs are semiconducting materials which have various technological applications particularly in the fields of field effect transistor (FETs), polymer light emitting diodes (PLEDs), solar cells and other optoelectronic devices due to its easy fabrication and tuneable optoelectronic properties (Andersson et al. 1999, Ong et al. 2004, Perepichka et al. 2005, Kim et al. 2006).

The attachment of different types of polar ionic pendent (anionic, cationic, zwitterionic) or the grafting of flexible polymers onto the PT backbone makes it stretchy enough to be solubilized in common organic solvents as well as in water (Das et al. 2015, Jaymand et al. 2015, Das et al. 2017). To achieve the water solubility of conventional PT, a widely used approach is to attach ionic ammonium, phosphate or sulfonate side groups onto hydrophobic π -conjugated backbones (Das et al. 2017). Ionic systems sometimes require adjusting the pH of the solution to avoid the aggregation of the polymers. In addition, the ion attached on the CP can migrate into the organic active layers of organic semiconductor devices and degrade their long-term stability. To overcome the drawbacks of ionic water-soluble CPs, another approach is to use some small non-ionic, highly polar, but neutral side groups to conjugate backbones, such as ethylene glycol and hydroxyl (Das et al. 2015). The grafting of polymer chains on PT backbone is more advantageous than the binding of small molecules due to the cooperative response of the graft polymers even in the presence of a small perturbation of the local environment (Das et al. 2015).

10.3.1 Grafting of PT

The idea of grafting flexible polymer chains onto the PT backbone is a fascinating way to produce processable PTs in solution. This approach is a useful tool to alter the solubility and mechanical properties of PT, and can also be used to introduce additional functional groups. The grafted chains can also introduce a controlled switching behavior in the main PT backbone, which leads to changes in the conformation, solubility, electrical and optical properties, which can be triggered by external stimuli, such as ion concentrations, pH changes, temperature or applied electrical potential (Maity et al. 2018). There are three approaches to grafting flexible polymer chains onto rigid backbone: (1) 'grafting from' when initiating sites located on the main polymer backbone initiate the polymerization of another monomer, (2) 'grafting to' when a growing polymer or a preformed polymer with reactive end

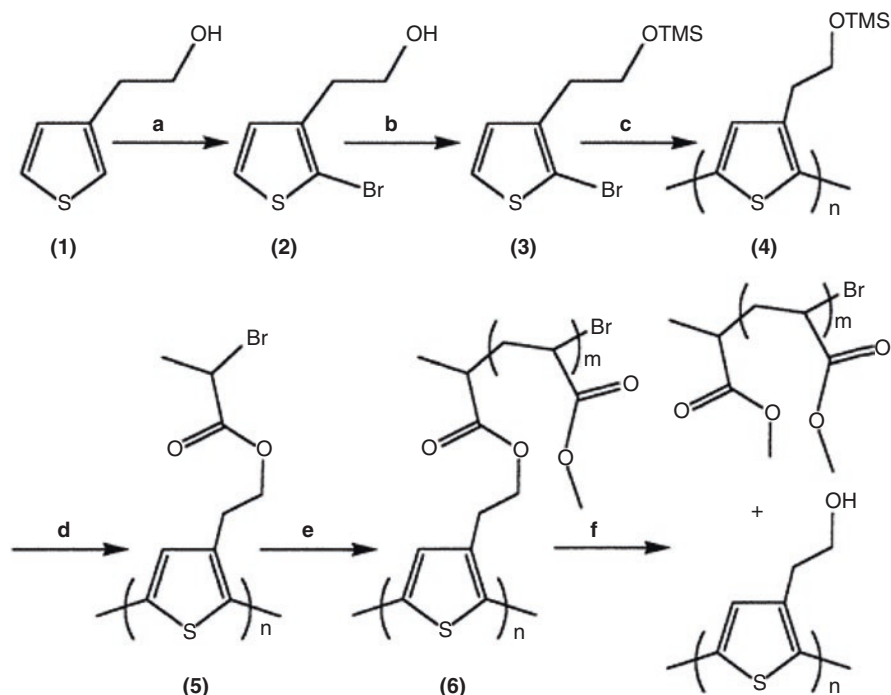
groups reacts with pendant functional groups located on another polymer and (3) ‘grafting through’, involves the synthesis of macromonomers, and then a low Mw monomer is radically copolymerized with the macromonomer.

10.3.1.1 ‘Grafting From’ Technique

Recently, grafting has emerged as a very common and important technique for polymer brush synthesis. The ‘grafting from’ method is the most widely reported and popular among the three methodologies due to the commercial availability of functionalized monomers, which can be readily linked from initiating sites. Here, an end-functionalized PT can be used as a macroinitiator for the chain polymerization of another monomer. The ‘grafting from’ technique includes the ATRP, reversible addition-fragmentation chain transfer (RAFT) and single-electron transfer living radical polymerization (SET-LRP) (Lee et al. 2010, Foster et al. 2017, Lligadas et al. 2017). Among these techniques, the ATRP is very robust, as it tolerates many functional groups such as allyl, amino, epoxy, hydroxy and vinyl groups present in the monomer or in the initiator (Lee et al. 2010).

Costanzo and Stokes (2002) presented for the first time an idea to incorporate highly dense poly(methyl acrylate) chains from PT macroinitiator using this technique. These authors first prepared a regioregular PT using the McCullough’s polymerization method (McCullough and Lowe 1992) of thiophene monomer containing a protected alcohol group, then the backbone was functionalized by incorporating 2-bromo-propionyl bromide (ATRP initiator) into the regioregular PT backbone. From these initiator sites, the methyl acrylate monomer was polymerized to produce well-defined polymer brushes (Scheme 10.8). Although the synthesized polymer was insoluble in water due to the hydrophobicity of poly(methyl acrylate) chains, the solubility and processability of the graft polymer in common organic solvents was increased. The graft segment also helped the backbone to obtain an extended conformation, thus avoiding π -stacking interactions of thiophene units. Thus, the non-radiative decay paths of PT excitations were decreased, which led to a 20-fold increase in fluorescence intensity relative to the PT macroinitiator with a quantum yield of 40% in solid state (Costanzo and Stokes 2002).

Balamurugan et al. (2005) adopted another technique in which the thiophene initiator, (3-[1-ethyl-2-(2-bromoisobutyrate)]thiophene, TI) was first prepared from thiophene-3-ethanol by coupling with the ATRP initiator moiety 2-bromoisobutyryl bromide in the presence of triethylamine. The PT macroinitiator was then synthesized by polymerization of the initiator containing thiophene monomer by oxidative polymerization using FeCl_3 as an oxidant. Finally, grafting of hydrophilic *N*-isopropylacrylamide (NIPAAm) monomer by ATRP from the initiator containing PT backbone was performed to obtain a highly water-soluble and thermally responsive poly(thiophene-*g*-NIPAAm) molecular brush (Scheme 10.8). These authors then demonstrated the temperature-induced structural transition of the graft polymer in water. At LCST, poly(*N*-isopropylacrylamide) (PNIPAAm) underwent a rapid and reversible conformational change from an extended hydrated coil to a



Scheme 10.8 Grafting of highly dense poly(methyl acrylate) chains from PT backbone. Conditions: **(a)** *N*-bromosuccinimide (NBS)/THF, **(b)** $\text{Me}_3\text{SiCl}/\text{NEt}_3/\text{THF}$; **(c)** dichloro(1,3-bis(diphenylphosphino)propane)nickel ($\text{Ni}(\text{dppp})\text{Cl}_2$), lithium diisopropylamide (LDA)/THF or ZnCl_2 , **(d)** THF/ NEt_3 /tetra-*n*-butylammonium fluoride (TBAF)/2-bromopropionyl bromide, **(e)** ATRP conditions and **(f)** $\text{H}_2\text{SO}_4/\text{THF}/\text{MeOH}$. Reproduced with permission from Costanzo and Stokes (2002)

collapsed hydrophobic globule, which led to a change in the effective conjugation length of the PT backbone with abrupt and reversible color and absorption intensity changes at 30–35 °C (Balamurugan et al. 2005). Following this typical protocol, many other researchers have successfully grafted several types of flexible monomer onto rigid PT backbone by ATRP. For example, Wang et al. (2008) grafted another hydrophilic monomer *N,N*-dimethyl aminoethyl methacrylate (DMAEMA) onto the PT backbone following the same protocol used by Balamurugan et al. (2005), and provided direct evidence of the molecular mechanism that drives the pH-induced conformational changes of PT, and optical properties. At low pH due to the repulsive interactions between the protonated PDMAEMA side chains, the PT backbone adopts a less folded and twisted conformation than at high pH. This caused a color change of the solution from yellow (deprotonated condition) to dark orange (protonated condition) with an increase in emission intensity. In this same line, Samanta et al. (2012b) developed a fully polymeric fluorescent molecular logic gate using the same graft polymer (PT-*g*-poly(dimethylaminoethyl methacrylate) (PT-*g*-PDMA, PD)) doped on methyl cellulose (MC) based hydrogel, in which

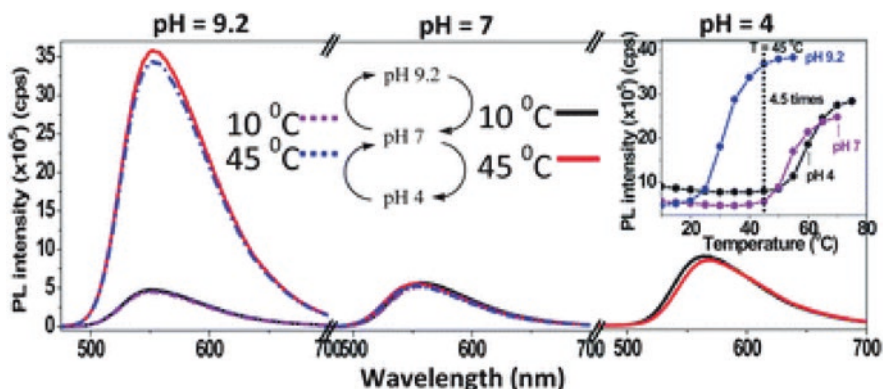


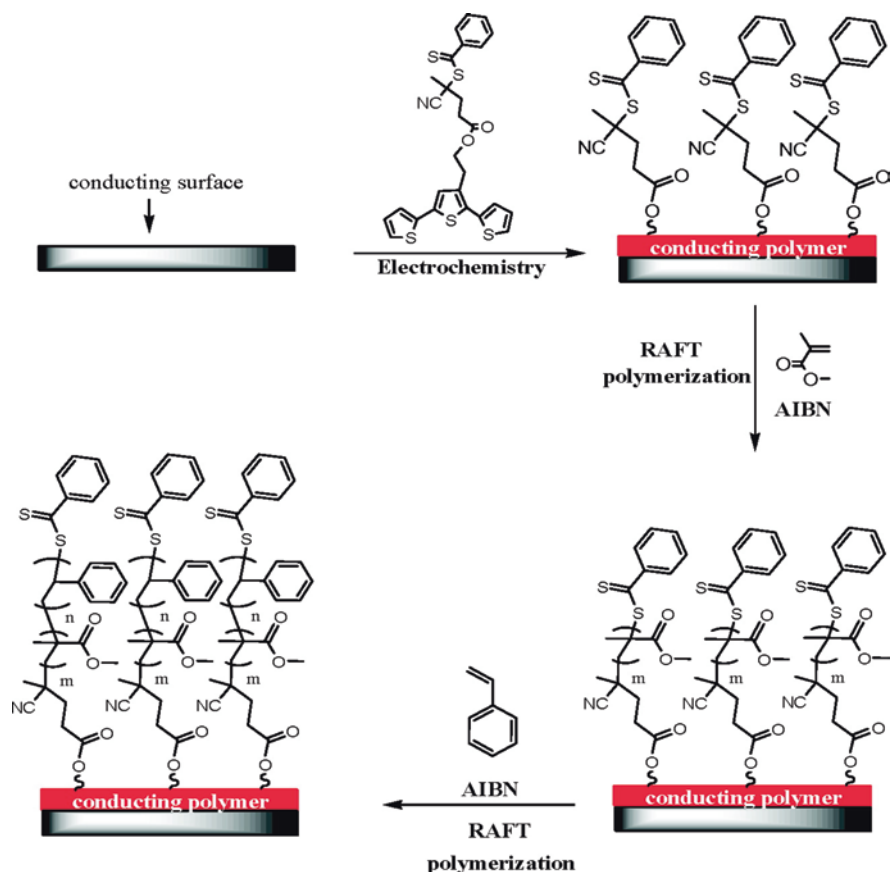
Fig. 10.12 Photoluminescence spectra of PD-doped MC hydrogel (5:1 wt. ratio) at 10 and 45 °C, at a pH cycle 9.2–7.0–4.0. Inset: pH-dependent PL intensity vs. temperature plot of PD-doped aqueous MC solution. Reproduced with permission from Samanta et al. (2012a, b)

showed LCST at 21 °C, which was gradually increased from 31 to 43 °C with increasing OEGMA concentration.

Das et al. (2013b) also grafted pH responsive PDMAEMA chains and temperature responsive PMeO₂MA onto PT backbone. This graft copolymer was used as a polymeric AND logic gate where pH and temperature were used as inputs and the fluorescence intensity was obtained as output. This graft copolymer was also used for the detection of nitroaromatics in solid/solution state, which is originated from the quenching of the PT excitons by the electron-poor nitro-substituted aromatic rings. This concept was further expanded by Das et al. (2014a) to obtain the maximum sensitivity of the logic operation under a lower pH by simple increasing the hydrophobicity of the grafted segments in which a *N,N*-dimethylamino ethyl methacrylate monomer was used.

Routh et al. (2012) successfully synthesized and stabilized Au NPs in water and tuned its morphological and electronic properties with ribonucleic acid (RNA) depending upon its assembled structure using the reducing capacity of PTDMA. The Au NPs embedded into PT-based polymer showed a dc-conductivity 6 times greater than that of the pure polymer due to the hopping process for charge carriers *via* Au NPs. This system also showed symmetric negative differential resistance (NDR) with a maximum NDR ratio of 64. This was possibly due to the fact that during the preparation of Au NPs, a large amount of charges were adsorbed on Au NPs, thus causing a hindrance to charge flow to reach a higher voltage when it releases the trapped charges completely, thereby giving almost zero current.

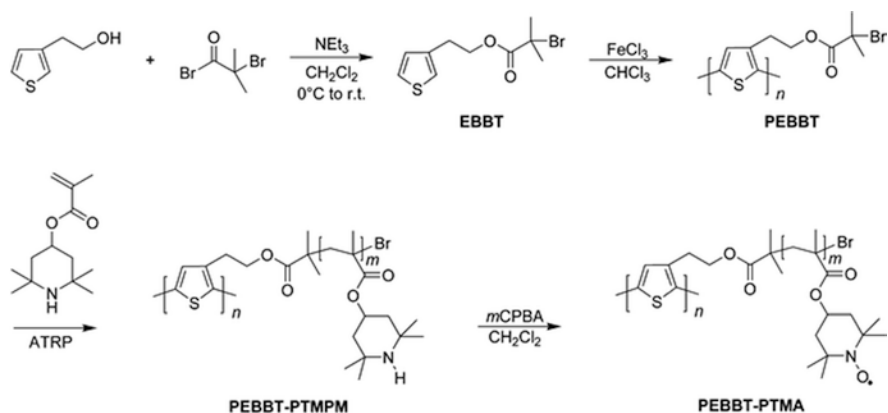
Lin et al. (2012) successfully grafted the PT backbones containing nitroxide radicals. These authors used a macroinitiator 2,5-poly(3-[1-ethyl-2-(2-bromoisobutyrate)]thiophene) (PEBBT) synthesized from 3-[1-ethyl-2-(2-bromoisobutyrate)]thiophene (EBBT) to be grafted onto poly(2,2,6,6-tetramethylpiperidin-4-yl methacrylate) (PTMPM) *via* ATRP, and then oxidized the PTMPM side chain with *m*-chloroperoxybenzoic acid (*m*CPBA) to



Scheme 10.10 General route for preparing homopolymer and block copolymers from electrochemically deposited terthiophene CTA. Reproduced with permission from Grande et al. (2011)

produce a high Mw PEBBT-*g*-poly(2,2,6,6-tetramethylpiperidin-1-oxyl-4-yl methacrylate) (PEBBT-*g*-PTMA) (Scheme 10.11). The electrochemical properties in the batteries of organic radicals showed that the polymer had a good cyclic and electrochemical stability, since it inhibited the dissolution into the electrolyte solvents. Thus, PEBBT-*g*-PTMA has potential as a cathode-active material in a rechargeable organic radical battery.

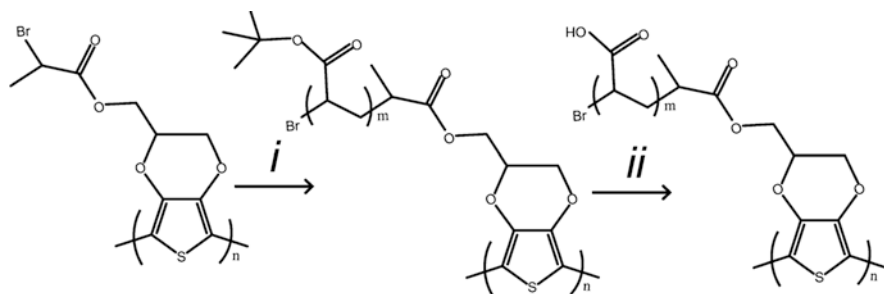
According to Fantin et al. (2016) direct grafting of methacrylic acid chains onto PT backbone is one of the biggest challenges for ATRP due to the intramolecular cyclization reaction, which leads to the loss of the carbon-halide chain-end functionality, thus resulting in the partial termination of the growing polymer chains. In this sense, Malmström et al. (2013) grafted poly(acrylic acid) (PAA) brushes from poly(3,4-ethylenedioxythiophene) (PEDOT). These authors first attached an ATRP initiator (2-bromopropionyl bromide) to the monomer 3,4-ethylenedioxythiophene (EDOT). The modified monomer (3,4-ethylenedioxythiophene)methyl



Scheme 10.11 Grafting of nitroxide radical-containing polymer onto PT backbone via ATRP. Reproduced with permission from Lin et al. (2012)

2-bromo-propanoate - BrEDOT) was then electropolymerized on large area gold-coated electrodes, and *tert*-butyl acrylate (*t*BA) brushes were grafted from the backbone by ATRP, followed by acid hydrolysis to give pH-responsive PAA brushes (Scheme 10.12).

Zhao et al. (2013) also forwarded a general approach of electropolymerization of EDOT to form an initiator group containing PEDOT. Neutral poly[oligo(ethylene glycol) methacrylate], POEGMA, poly(sulfobetaine methacrylate) (PSBMA) and zwitterionic poly([2-(methacryloyloxy)ethyl]dimethyl-(3-sulfopropyl)ammonium hydroxide) were grafted by SI-ATRP from the conducting polymer deposited on the surface. These grafted polymers prevented the binding of proteins and also showed the adhesion of the cells on the surface. In another work, Das et al. (2014b) also successfully grafted methacrylic acid chains onto a PT backbone by ATRP of *t*BMA followed by hydrolysis of *tert*-butyl groups using trifluoroacetic acid. The synthesized PT-*g*-PTMA polymer can be used as a template or a dopant for the synthesis of PANI nanostructures with motivational morphological and electronic properties. PTMA-doped PANI (PTPA) hybrids can be self-assembled in non-helical or single-handed helical nanorod with some morphology of small-sized spheroids depending on the amount of PANI ratio. The PTMA itself has a spheroidal morphology, while PTPA hybrids have a nanorod morphology. By increasing the aniline concentration with respect to PTMA, the nanorod becomes helical in nature, along with some spheroids. The PTPA hybrid has a maximum of 4.1×10^{-2} S/cm of dc-conductivity, while the PTMA has only a conductivity value of 5.6×10^{-7} S/cm. The PTPA hybrid exhibited reproducible photoconductivity by alternating between 'on' and 'off' switching of white light illumination with a semiconducting nature, and this photocurrent generation is a property of only PTPA hybrids, since no appreciable photocurrent is observed for the PT macroinitiator nor for the PMA-doped PANI. The core-shell type structure of PTMA with a conducting PANI coating was responsible for the good electrical conduction, because the doped-PANI produces an additional

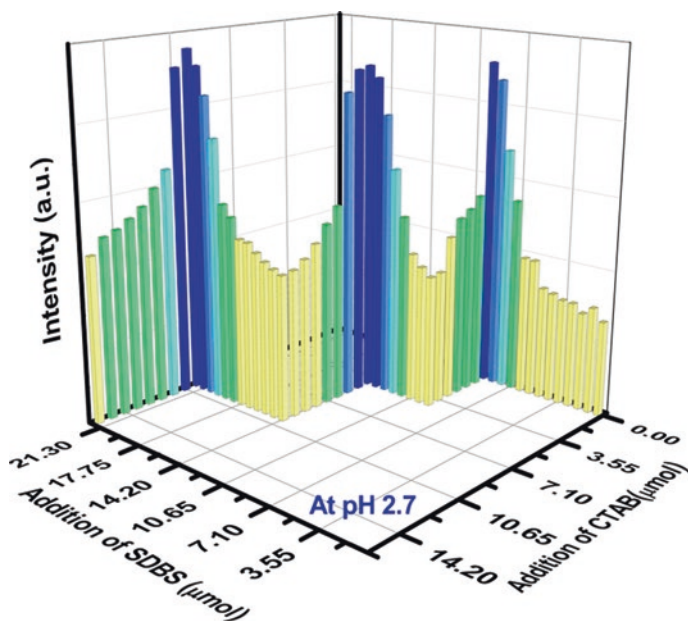


Scheme 10.12 Grafting of PAA brushes from the PBreDOT backbone. Conditions: (i) acetone/CuBr/PMDETA/*t*BA at 60 °C and (ii) 1% methanesulfonic acid in dichloromethane (DCM). Reproduced with permission from Malmström et al. (2013)

electrical conduction path. The molecular arrangement of PANI and PT in the PTPA samples can be attributed to the charges stored through resonance stabilization, thus producing a moderate capacitance value. The single semicircle in the Cole-Cole plot of real and imaginary parts of complex impedance can thus be obtained.

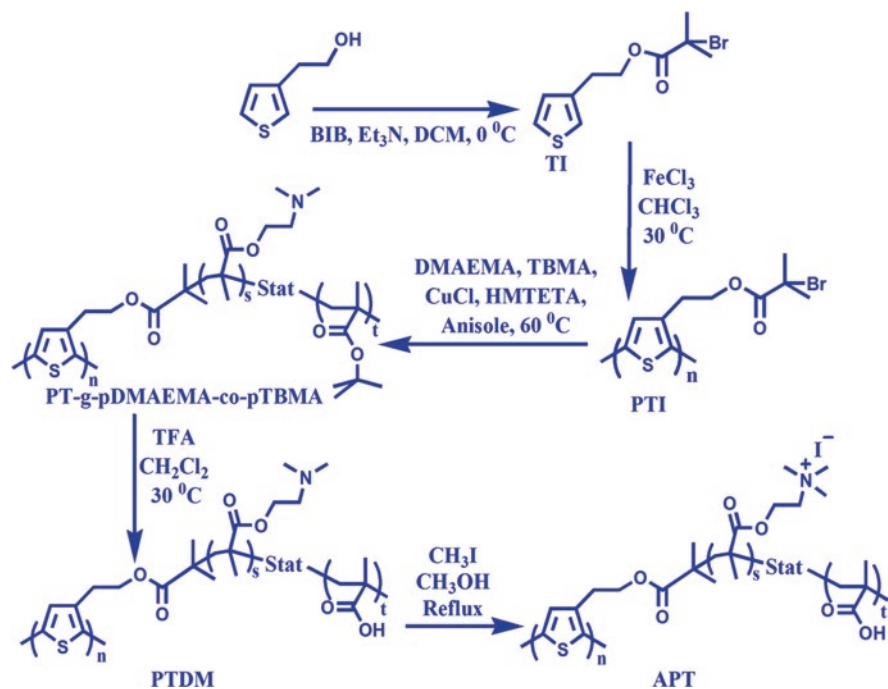
Ghosh et al. (2015) synthesized cationic PT-*g*-poly[(*N,N,N*-trimethylamino iodide)ethyl methacrylate] with iodide counter anion (CPT-I) from PTDMA, followed by quaternization of PDMAEMA segments using methyl iodide. The CPT-I has a lower fluorescence intensity than that of PTDMA due to the transfer of excitonic energy from the PT backbone to iodide ions. When the iodide anions were substituted by cyanide ions, the fluorescence intensity showed a huge rise depending on its concentration. Ghosh et al. (2016) also synthesized a PT-*g*-poly(ampholyte) (PTP) and studied the aggregation-disaggregation behavior with ionic surfactants with different charges at different pHs of the medium. For this purpose, the PTP was synthesized using *N,N*-dimethylaminoethyl methacrylate and *t*BMA monomers by grafting from the PT backbone, followed by hydrolysis. The PTP exhibited a reversible fluorescence on and off response in both acidic (Scheme 10.13) and basic medium with the sequential addition of ionic surfactants with different charge through self-assembly and de-assembly of the ionic aggregates, repeatedly.

An ampholytic PT (PT-*g*-poly[(*N,N,N*-trimethylamino iodide)ethyl methacrylate-*co*-methacrylic acid], APT) was also synthesized by Ghosh et al. (2017) synthesized in order to tune the optoelectronic properties of the PT chains depending on the position of Hofmeister iodide (I⁻) ion at different pH values. The APT was synthesized by copolymerization of *t*BMA and DMAEMA monomers from the PT backbone by ATRP technique (Scheme 10.14). The hydrolysis of the *t*BMA residues and the quaternization of the DMAEMA residues of the graft copolymer were then performed to produce the desired polymer. Under acidic conditions, the absorption and emission signals of the PT chromophore exhibited an appreciable blue shift in the presence of I⁻ only as a counter anion. The cooperative effect of non-dissociated -COOH and quaternary ammonium groups immobilized I⁻ near the apolar PT chain, causing the threading of grafted chains, and therefore, twisting of the backbone was attributed to the blue shift. The dethreading of PT backbone was produced as medium



Scheme 10.13 Reversible turn ‘on’ and ‘off’ plot of fluorescence intensity of PTP in aqueous solution with increasing amounts of sodium dodecylbenzenesulfonate (SDBS) then cetyltrimethylammonium bromide (CTAB) sequentially at pH 2.7. Reproduced with permission from Ghosh et al. (2016)

pH increased, due to the ionization of -COOH groups, thus releasing quencher iodide ions from the vicinity of the PT chains, resulting in a red shift in absorption and a sharp increase in fluorescence intensity. The dethreading was also found when APT interacts with RNA, which shows a significant increase of fluorescence for displacing iodide ions forming the nanofibrillar network morphology. Threading and dethreading also affected the capacitance (C), resistance (R2) and Warburg’s impedance (W) values of APT. The threading and dethreading of the grafted chains in APT also influenced the electrical properties of the system as follows from the impedance spectra (Nyquist plot, Fig. 10.13). APT at pH 2 and pH 4.5 showed a semicircle in the impedance spectra due to the presence of an equivalent circuit containing C and R2 in parallel with each other, while at pH 9 a semicircle and a linear hike corresponds to the presence of the W in the lower frequency region, whereas at a lower pH, the loss of planarity of the PT chain and the shield resisting the interchain hopping of charge carriers for the threaded nonconducting grafted chain caused a hindrance to the charge flow. APT has a maximum C value at pH 2, since the vesicle surface can easily store the charges at pH 4.5, due to the creation of partial negative charges, which leads to the charge annihilation, resulting in the lowest C value. At pH 9, APT showed an increase in C with W which arose for mass transfer because complete dethreading caused the I^- ions free to move into the nanofibrillar network. So, the influence of Hofmeister I^- ion was established for tuning



Scheme 10.14 Synthetic procedure for the preparation of amphoteric PT from 3-thiophene ethanol. Reproduced with permission from Ghosh et al. (2017)

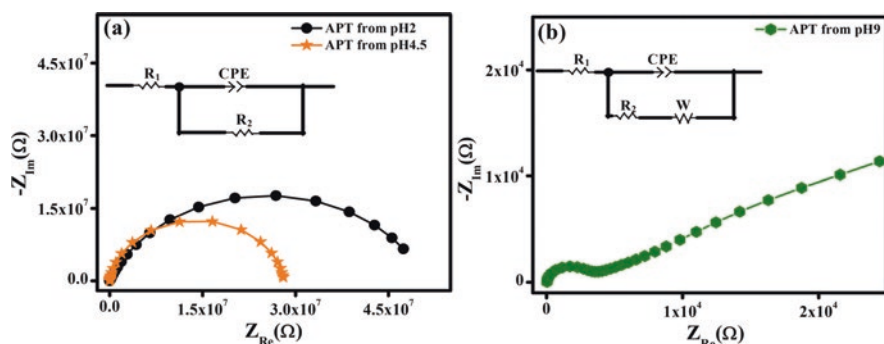


Fig. 10.13 Nyquist plots of APT under conditions of (a) pH 2 and pH 4.5 and (b) from pH 9 with their corresponding equivalent circuit. Reproduced with permission from Ghosh et al. (2017)

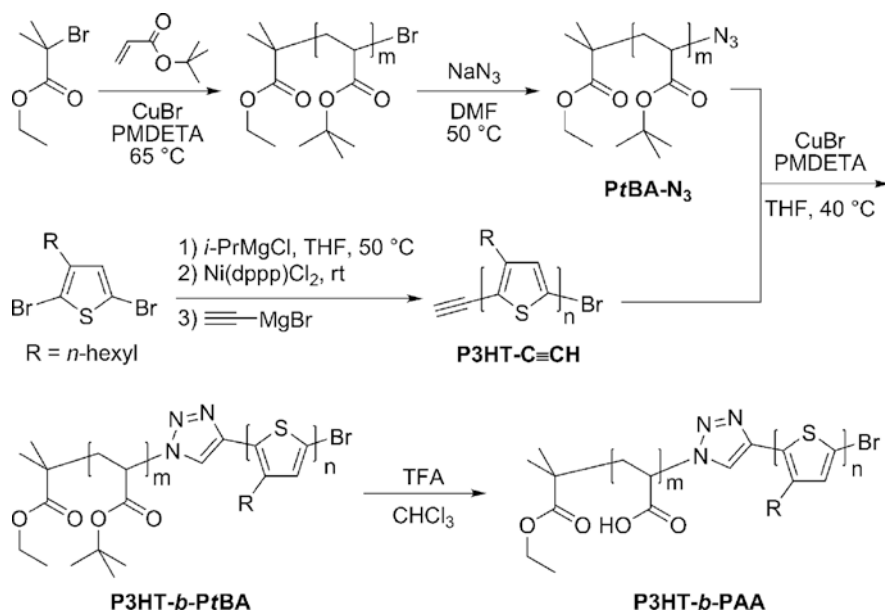
the optoelectronic properties of a novel PT-based polyampholyte by changing the pH or by conjugating with RNA (Ghosh et al. 2017).

Recently, Ghosh et al. (2018) anchored uracil moiety on PT backbone to modulate the electronic structure of a π -CP from the stimulus-sensitive side chains to

obtain the desired optoelectronic properties. For this purpose, PT-*g*-poly-[*N*-(6-methyluracilyl)-*N,N*-dimethylamino chloride)] ethyl methacrylate (PTDU) was synthesized by ATRP of the DMAEMA monomer from PT backbone followed by quaternization reaction with 6-chloromethyl uracil. The uracil moiety of the grafted chains when exposed to diffuse sunlight caused the absorption maximum of PTDU solution, showing a gradual blue shift of 87 nm and a gradual blue shift in emission maximum (46 nm) quenching its fluorescence (~7 times) with time. These effects occurred only in the absorption range of PT chromophore when exposed to direct exposure of light of different wavelengths, and the optimum wavelength was 420 nm. The uracil moieties after being exposed to visible light, these were moved towards the backbone to facilitate the photoinduced electron transfer (PET) between the PT and the uracil moieties, which was attributed to the variation of optoelectronic and phase transition properties. The transparent orange colored PTDU solution become cloudy with an increase in emission intensity when sodium halides were added and become reversibly transparent or cloudy when heated or cooled to a certain temperature. The screening of cationic centers of PTDU by varying halide anion concentration tuned the phase transition temperature. Thus, the light-induced variation of the backbone conformation was responsible for tuning the optoelectronic properties and regulates the thermal response capacity of the PTDU solution in the presence of halide ions (Ghosh et al. 2018).

10.3.1.2 ‘Grafting to’ Technique

In case of ‘grafting to’ technique at first, different polymer chains are synthesized separately and these pre-synthesized polymer chains are then linked onto the PT backbone. The Cu-catalyzed click chemistry and azide-alkyne cycloaddition are the simplest and most popular reaction procedures for the ‘grafting to’ process with high yield (Lutz et al. 2005). This method also avoids situations in which the ‘grafting from’ approach does not fit well. Although this method has not gained much popularity and has not been widely as ‘grafting from’ process due to the introduction of click chemistry and the steric hindrance has limited the chain growth of the polymer. Keeping this in view, Li et al. (2011) synthesized an amphiphilic rod-coil diblock copolymer (P3HT-*b*-PAA) using click reaction under the ‘grafting to’ approach between ethynyl-end regioregular P3HT with azide-end poly(*tert*-butyl acrylate) followed by acidolysis of P*t*BA (Scheme 10.15). Thus, Li et al. (2011) forwarded an idea to facilitate the synthesis and development of new block copolymers with high purity. In the same year, Wu et al. (2011) also reported on the synthesis of self-assembled P3HT-*b*-poly(*g*-benzyl-*L*-glutamate), which was the first report of PT/polypeptide-based diblock copolymer using Cu-catalyzed click chemistry. This copolymer could be self-assembled into hierarchical structures in solution and in solid state, and depending on the aggregation of the P3HT chains, the color of the THF solution of the polymer changes from orange to purple (the absorption peak shifts from 442 to 484 nm) by the slow addition of dimethyl formamide. Wei



Scheme 10.15 Synthesis of P3HT-*b*-PtBA and P3HT-*b*-PAA using grafting-to approach. Reproduced with permission from Li et al. (2011)

et al. (2015) reported the thiolated PEG binding to an alkene-functionalized poly(3,4-propylenedioxythiophene) (PProDOT) through thiol-ene click chemistry.

Recently, Mohamed et al. (2014) also reported water-soluble amphiphilic P3HT-*g*-PEO rod-coil conjugated random copolymers using the simple oxidative polymerization followed by simple click chemistry between azido-grafted random P3HT copolymers and ethynyl-end PEO (hydrophilic side chain). These authors stated that such P3HT polymers presenting PEO units on side chains are promising materials for a variety of bioengineering and biomedical applications (Mohamed et al. 2014). Kumari et al. (2015) also reported a new class of amphiphilic rod-coil conjugated block copolymer composed of regioregular P3HT and thermo-sensitive PNIPAAm by a Cu-catalyzed click reaction. The polymer exhibited LCST type thermo response capability and the luminescence and optical property of this block copolymer was different from its pure analogue and depended largely on the nature of the solvent or composition in a mixed solvent (Fig. 10.14) (Kumari et al. 2015).

10.3.1.3 ‘Grafting Through’ Technique

The macromonomer method or ‘grafting through’ method is one of the oldest and easiest ways to synthesize graft copolymers with very good control over graft chain length and PDI. Normally, a low Mw monomer can be radically copolymerized with an acrylate or methacrylate-functionalized macromonomer to avoid the

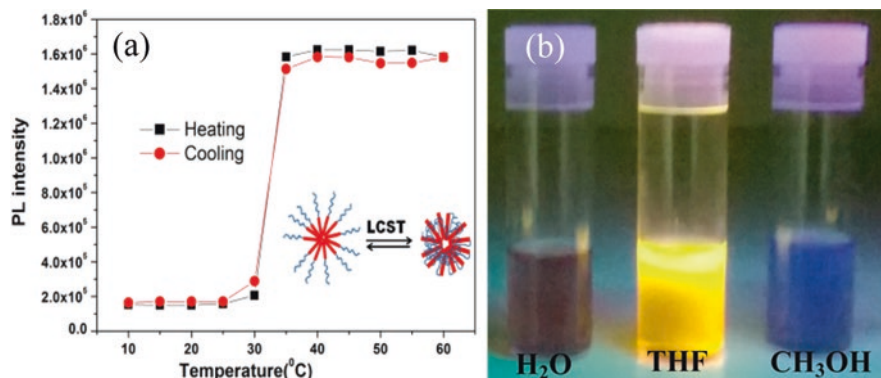
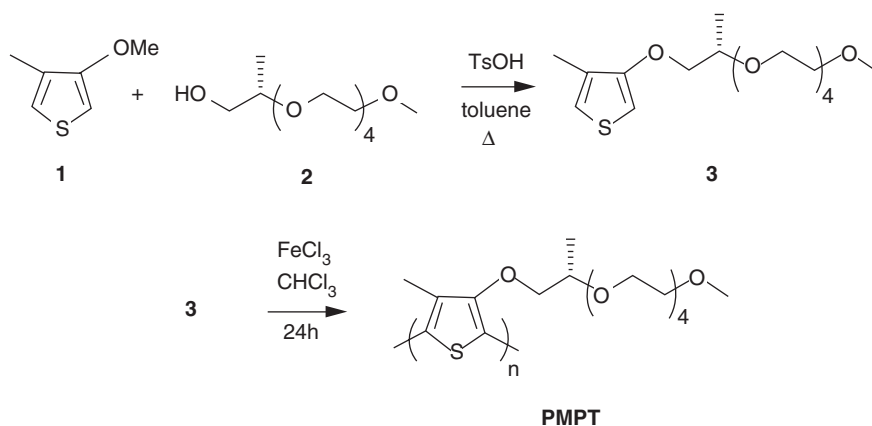


Fig. 10.14 (a) Variation in the PL intensity at different temperatures of the P3HT-*b*-PNIPAM solution in water and (b) emission color of P3HT-*b*-PNIPAM in various solvents under ultra-violet (UV) radiation. Reproduced with permission from Kumari et al. (2015)

steric effect of the macromonomers which can make polymerization difficult. In this sense, Levesque et al. (2000) reported a new regioregular PT derivative (poly(3-methylhexa(oxyethylene)oxy-4-methylthiophene) - PHEGMT) with side chains having exactly six oxyethylene units in each thiophene unit. The macromonomer (3-methylhexa(oxyethylene)oxy-4-methylthiophene) was first synthesized from 3-hexa(oxyethylene)oxy-4-methylthiophene. The PHEGMT was then obtained *via* chemical polymerization of the monomer with iron trichloride as an oxidizing agent. Due to the thermochromic and ionochromic behavior of this polymer, it was concluded that the hexa(oxyethylene) side chains induce a more planar conformation of the PT backbone than random length oxyethylene side chains with an average of seven oxyethylene units. Brustolin et al. (2002) also reported water-soluble regioregular PT (poly-{3-[(2*S*)-2-methyl-3,6,9,12,15-pentaoxahexadecyloxy]-4-methylthiophene} - PMPT), bearing enantiomerically pure oligo(ethylene oxide) side chains. The thiophene-based macromonomer (3-[(2*S*)-2-methyl-3,6,9,12,15-pentaoxahexadecyloxy]-4-methylthiophene) was first obtained by the transesterification of 3-methoxy-4-methylthiophene with (2*S*)-2-methyl-3,6,9,12,15-pentaoxahexadecanol using *p*-toluenesulfonic acid as a catalyst. The chemical polymerization of the macromonomer was performed to obtain the PMPT using iron trichloride as an oxidizing agent (Scheme 10.16).

Qi et al. (2006) synthesized thiophene copolymers and their derivatives with PEO side chains by chemical oxidation with FeCl_3 and electropolymerization. The starting monomers were 3-hexylthiophene and 2-(3-thienyl)ethanol with PEO grafted onto the side chains. Shao et al. (2013) also reported the synthesis of a water-soluble non-ionic PT derivative (poly(3-(2-(2-(2-methoxyethoxy)ethoxy)ethoxy)methylthiophene) - P3TEGT) with a hydrophilic tri-ethylene glycol side group on the backbone. The PT derivative was synthesized from 2-bromo-5-iodo-3-(2-(2-(2-methoxy-ethoxy)ethoxy)ethoxy)methylthiophen using Kumada catalyst-transfer polymerization. P3TEGT



Scheme 10.16 Synthesis of water soluble regioregular PMPT. Reproduced with permission from Brustolin et al. (2002)

films after thermal annealing exhibited a well-organized nano-fibrillar lamellar nanostructure which was originated from the strong π - π stacking of the backbones. p-type organic field-effect transistors (OFET) were fabricated from this water-soluble PT derivative, presenting the possibility of an environment friendly solvent for applications based on low-cost green solvent-processed devices.

Zhao et al. (2012) successfully synthesized a series of methyl- or benzyl-capped oligoethylene glycol-functionalized thiophene monomers, and also successfully polymerized the macromonomer by Grignard metathesis polymerization or reductive coupling polymerization following the ‘grafting through’ approach. The synthesized polymers showed high electroactivity and stability in aqueous solution and exhibited different colors depending on the doping state. In this same line, Bendrea et al. (2013) synthesized organic hybrid materials consisting of graft copolymers with a PT backbone and well-defined chains of PEG grafted onto the backbone by anodic polymerization of chemically synthesized pentathiophene macromonomers with methyl-capped PEG chains linked to the central thiophene. The synthesized polymer exhibited greater cell viability than steel and culture plate controls, thus suggesting that PEDOT films could be used as a promising tool for biomedical applications. Thus, the main bottleneck for PT application is its insolubility and rigidity in the backbone structure, which can be overcome by grafting a suitable polymer. These systems promise applications in manufacture of molecular logic gates, molecular thermometer, sensing of different toxic ions, sensors for biological molecules, surfactants, etc. The efficiency of these systems can be further tuned by changing the density of functional groups or by changing the graft density, graft Mw, co-grafting with different monomers, etc.

10.4 Summary and Outlook

In summary, this chapter presented the chronological development of graft copolymers of poly(thiophene) (PT) and poly(vinylidene fluoride) (PVDF), which are technologically very important as evidenced by their different uses. However, there is still much to be developed for its potential technological applications. A perspective for the future development of electroactive graft copolymers was given here, paying special attention to PVDF and PT.

Although PVDF has been grafted with a good number of acrylates, methacrylates and acrylamide-based monomers with several functional groups. There are still different monomer systems which have not been possible to graft from PVDF. Thus, different strategies of ATRP or RAFT polymerization can be designed to obtain new PVDF graft copolymers. However, the grafting of stimuli-responsive block copolymers onto PVDF has not yet been explored. This could help in the strategic design for producing smart polymers, both from its piezoelectric property and for making ion-selective, antibacterial and antifouling membranes. The introduction of thermo-sensitive and pH sensitive graft copolymers could also help to tune their electrical and piezoelectric properties under different conditions of ions, pH and temperature (Zarrintaj et al. 2019).

Another strategy for introducing desired complementary functionalities can be subsequent modification of PVDF graft copolymers, since the grafted chains have active functionalities. This strategy can be effective for producing materials combining orthogonal properties, e.g. PVDF piezoelectricity and semiconducting properties of organic or inorganic materials. For example, the conjugation of these copolymers with carbon nanotubes, CdS, CdSe and graphene quantum dots, as well as metal ions are very promising. This could help the manufacture of magneto-electric, multi-ferroic and data storage materials. PVDF graft copolymers can also act as compatibilizers, and reactive grafted groups could also help the manufacture of self-healing PVDF-based materials suitable for specific biological applications.

On the other hand, the increase in signal intensity for the cooperative response of the grafted PT chain segments makes it attractive for sensor application, developing sensors for toxic ions, surfactants, biological analytes, logic gates, etc. The efficiency can be further improved by introducing more responsive functionalities such as changing graft density and length, polymer grafts, etc. require new ATRP or RAFT polymerization reaction conditions. The modification of PT backbone by grafting with stimulus sensitive polymers also causes a significant change in the properties by changing external stimuli, e.g. biomolecules, ions, light, pH, surfactants, temperature, etc. The modification in PT-graft copolymer morphologies causes a change into the PT backbone conformations, which could change optical and electrical properties of PT. Thus, the grafting of liquid crystalline polymer onto PT backbone could allow to couple the optoelectronic properties of PT with the anisotropic properties of the liquid crystalline systems, thus opening new application possibilities, particularly in electronic displays with improved response.

The grafting of stimuli-responsive block copolymers onto PT backbone by 'grafting from' approach has not yet been well explored, which could help generate

new optoelectronic properties that can be tuned with the composition and length of the block, among others. The preparation of covalently/noncovalently-linked bioconjugates with stimuli-responsive PT-based graft copolymer using different biomolecules (e.g. nucleic acids, peptides, proteins, etc.) may be suitable for applications in biological assays in the understanding of detailed structure of biomolecules from the chromic properties of PT chains. Thus, the grafting of functional polymers onto electroactive polymers could help material engineers and scientists such as biotechnologists, device engineers and nanotechnologists, to manufacture different functional materials for applications in biomaterials, electronic appliances, energy devices, sensors, etc. Undoubtedly, it will stimulate collaborative research between this new field of polymer chemistry with the cutting edge of materials science and engineering for developing new technological devices.

Acknowledgments We gratefully acknowledge SERB, New Delhi (grant number EMR/2016/005302) and DST (grant number CS-189/2011) for financial support and CSIR, New Delhi (ES grant number 21(1055)/18/EMR-II) providing fellowship to Dr. R. Ghosh.

Conflicts of Interest The authors declare no conflict of interest.

References

- Andersson, M. R., Thomas, O., Mammo, W., Svensson, M., Theander, M., & Inganäs, O. (1999). Substituted polythiophenes designed for optoelectronic devices and conductors. *Journal of Materials Chemistry*, 9, 1933–1940. <https://doi.org/10.1039/a902859e>.
- Bagchi, B., Banerjee, S., Kool, A., Thakur, P., Bhandary, S., Hoque, N. A., & Das, S. (2016). Synthesis of eucalyptus/tea tree oil absorbed biphasic calcium phosphate–PVDF polymer nanocomposite films: A surface active antimicrobial system for biomedical application. *Physical Chemistry Chemical Physics*, 18(25), 16775–16785. <https://doi.org/10.1039/c6cp03493d>.
- Balamurugan, S. S., Bantchev, G. B., Yang, Y., & McCarley, R. L. (2005). Highly water-soluble thermally responsive poly(thiophene)-based brushes. *Angewandte Chemie, International Edition*, 44(31), 4872–4876. <https://doi.org/10.1002/anie.200500867>.
- Barford, W. (2005). *Electronic and optical properties of conjugated polymers*. New York: Oxford U. Press.
- Bendrea, A. D., Fabregat, G., Cianga, L., Estrany, F., del Valle, L. J., Cianga, I., & Alemán, C. (2013). Hybrid materials consisting of an all-conjugated polythiophene backbone and grafted hydrophilic poly(ethylene glycol) chains. *Polymer Chemistry*, 4(9), 2709–2723. <https://doi.org/10.1039/c3py00029j>.
- Boutevin, B., Robin, J. J., & Serdani, A. (1992). Synthesis and applications of graft copolymers from ozonized poly(vinylidene fluoride)—II. *European Polymer Journal*, 28(12), 1507–1511. [https://doi.org/10.1016/0014-3057\(92\)90143-p](https://doi.org/10.1016/0014-3057(92)90143-p).
- Brustolin, F., Goldoni, F., Meijer, E. W., & Sommerdijk, N. A. J. M. (2002). Highly ordered structures of amphiphilic polythiophenes in aqueous media. *Macromolecules*, 35(3), 1054–1059. <https://doi.org/10.1021/ma011334r>.
- Cai, T., Neoh, K. G., & Kang, E. T. (2011). Poly(vinylidene fluoride) graft copolymer membranes with “clickable” surfaces and their functionalization. *Macromolecules*, 44(11), 4258–4268. <https://doi.org/10.1021/ma2002728>.
- Cen, L., Neoh, K. G., Ying, L., & Kang, E. T. (2004). Surface modification of polymeric films and membranes to achieve antibacterial properties. *Surface and Interface Analysis*, 36(8), 716–719. <https://doi.org/10.1002/sia.1745>.

- Chen, Y., Ying, L., Yu, W., Kang, E. T., & Neoh, K. G. (2003). Poly(vinylidene fluoride) with grafted poly(ethylene glycol) side chains via the RAFT-mediated process and pore size control of the copolymer membranes. *Macromolecules*, 36(25), 9451–9457. <https://doi.org/10.1021/ma035194s>.
- Chen, Y., Liu, D., Deng, Q., He, X., & Wang, X. (2006). Atom transfer radical polymerization directly from poly(vinylidene fluoride): Surface and antifouling properties. *Journal of Polymer Science Part A-Polymer Chemistry*, 44(11), 3434–3443. <https://doi.org/10.1002/pola.21456>.
- Coessens, V., Pintauer, T., & Matyjaszewski, K. (2001). Functional polymers by atom transfer radical polymerization. *Progress in Polymer Science*, 26(3), 337–377. [https://doi.org/10.1016/s0079-6700\(01\)00003-x](https://doi.org/10.1016/s0079-6700(01)00003-x).
- Costanzo, P. J., & Stokes, K. K. (2002). Synthesis and characterization of poly(methyl acrylate) grafted from poly(thiophene) to form solid-state fluorescent materials. *Macromolecules*, 35(18), 6804–6810. <https://doi.org/10.1021/ma011638d>.
- Das, S., Samanta, S., Chatterjee, D. P., & Nandi, A. K. (2013a). Thermosensitive water-soluble poly(ethylene glycol)-based polythiophene graft copolymers. *Journal of Polymer Science Part A: Polymer Chemistry*, 51(6), 1417–1427. <https://doi.org/10.1002/pola.26514>.
- Das, S., Chatterjee, D. P., Samanta, S., & Nandi, A. K. (2013b). Thermo and pH responsive water soluble polythiophene graft copolymer showing logic operation and nitroaromatic sensing. *RSC Advances*, 3(38), 17540–17550. <https://doi.org/10.1039/c3ra42479k>.
- Das, S., Chatterjee, D. P., & Nandi, A. K. (2014a). Water-soluble dual responsive polythiophene-g-poly(methoxyethoxy ethyl methacrylate)-co-poly(*N,N*-diethylamino ethyl methacrylate) for different applications. *Polymer International*, 63(12), 2091–2097. <https://doi.org/10.1002/pi.4751>.
- Das, S., Chatterjee, D. P., & Nandi, A. K. (2014b). Supramolecular assembly of polythiophene-g-polymethacrylic acid-doped polyaniline with interesting morphological and opto-electronic properties. *Journal of Materials Chemistry A*, 2(30), 12031–12042. <https://doi.org/10.1039/c4ta01521e>.
- Das, S., Chatterjee, D. P., Ghosh, R., & Nandi, A. K. (2015). Water soluble polythiophenes: Preparation and applications. *RSC Advances*, 5(26), 20160–20177. <https://doi.org/10.1039/c4ra16496b>.
- Das, S., Routh, P., Chatterjee, D. P., Ghosh, R., & Nandi, A. K. (2017). Water-soluble ionic polythiophenes for biological and analytical applications. *Polymer International*, 66(5), 623–639. <https://doi.org/10.1002/pi.5295>.
- Doll, W. W., & Lando, J. B. (1970). Polymorphism of poly(vinylidene fluoride). III. The crystal structure of phase II. *Journal of Macromolecular Science, Part B: Physics*, 4(2), 309–329. <https://doi.org/10.1080/00222347008212505>.
- Fargere, T., Abdennadher, M., Delmas, M., & Boutevin, B. (1994). Synthesis of graft polymers from an ozonized ethylene vinyl acetate copolymer (EVA). I. Study of the radical polymerization of styrene initiated by an ozonized EVA. *Journal of Polymer Science, Part A: Polymer Chemistry*, 32(7), 1377–1384. <https://doi.org/10.1002/pola.1993.080311024>.
- Fantin, M., Isse, A. A., Venzo, A., Gennaro, A., & Matyjaszewski, K. (2016). Atom transfer radical polymerization of Methacrylic acid: A Won challenge. *Journal of the American Chemical Society*, 138(23), 7216–7219. <https://doi.org/10.1021/jacs.6b01935>.
- Foster, J. C., Radzinski, S. C., & Matson, J. B. (2017). Graft polymer synthesis by RAFT transfer-to. *Journal of Polymer Science Part A: Polymer Chemistry*, 55(18), 2865–2876. <https://doi.org/10.1002/pola.28621>.
- Gallantree, H. R. (1983). Review of transducer applications of polyvinylidene fluoride. *IEE Proceedings I - Solid-State and Electron Devices*, 130(5), 219–224. <https://doi.org/10.1049/ip-i-1.1983.0040>.
- Ghosh, R., Das, S., Chatterjee, D. P., & Nandi, A. K. (2015). Cationic polythiophene for specific detection of cyanide ions in water using fluorometric technique. *RSC Advances*, 5(112), 92564–92572. <https://doi.org/10.1039/c5ra17448a>.

- Ghosh, R., Das, S., Chatterjee, D. P., & Nandi, A. K. (2016). Surfactant-triggered fluorescence turn "on/off" behavior of a polythiophene-*graft*-polyampholyte. *Langmuir*, 32(33), 8413–8423. <https://doi.org/10.1021/acs.langmuir.6b01928>.
- Ghosh, R., Chatterjee, D. P., Das, S., Mukhopadhyay, T. K., Datta, A., & Nandi, A. K. (2017). Influence of Hofmeister Γ^- on tuning optoelectronic properties of ampholytic polythiophene by varying pH and conjugating with RNA. *Langmuir*, 33(44), 12739–12749. <https://doi.org/10.1021/acs.langmuir.7b03147>.
- Ghosh, R., Das, S., Bhattacharyya, K., Chatterjee, D. P., Biswas, A., & Nandi, A. K. (2018). Light-induced conformational change of uracil-anchored polythiophene-regulating thermo-responsiveness. *Langmuir*, 34(41), 12401–12411. <https://doi.org/10.1021/acs.langmuir.8b02679>.
- Grande, C. D., Tria, M. C., Jiang, G., Ponnappati, R., & Advincula, R. (2011). Surface-grafted polymers from electropolymerized polythiophene RAFT agent. *Macromolecules*, 44(4), 966–975. <https://doi.org/10.1021/ma102065u>.
- He, F., Luo, B., Yuan, S., Liang, B., Choong, C., & Pehkonen, S. O. (2014). PVDF film tethered with RGD-click-poly(glycidyl methacrylate) brushes by combination of direct surface-initiated ATRP and click chemistry for improved cytocompatibility. *RSC Advances*, 4(1), 105–117. <https://doi.org/10.1039/c3ra44789h>.
- Hester, J. F., Banerjee, P., Won, Y. Y., Akthakul, A., Acar, M. H., & Mayes, A. M. (2002). ATRP of amphiphilic graft copolymers based on PVDF and their use as membrane additives. *Macromolecules*, 35(20), 7652–7661. <https://doi.org/10.1021/ma0122270>.
- Ignatyev, I. A., Thielemans, W., & Beke, B. V. (2014). Recycling of polymers: A review. *Chem Sus Chem*, 7(6), 1579–1593. <https://doi.org/10.1002/cssc.201300898>.
- Jaymand, M., Hatamzadeh, M., & Omid, Y. (2015). Modification of polythiophene by the incorporation of processable polymeric chains: Recent progress in synthesis and applications. *Progress in Polymer Science*, 47, 26–69. <https://doi.org/10.1016/j.progpolymsci.2014.11.004>.
- Kang, E. T., Neoh, K. G., Tan, K. L., & Loh, F. C. (1997). Surface modified and functionalized polyaniline and polypyrrole films. *Synthetic Metals*, 84(1–3), 59–60. [https://doi.org/10.1016/s0379-6779\(97\)80664-9](https://doi.org/10.1016/s0379-6779(97)80664-9).
- Kim, G. H., Hong, S. M., & Seo, Y. (2009). Piezoelectric properties of poly(vinylidene fluoride) and carbon nanotube blends: β -phase development. *Physical Chemistry Chemical Physics*, 11(44), 10506–10512. <https://doi.org/10.1039/b912801h>.
- Kim, Y., Cook, S., Tuladhar, S. M., Choulis, S. A., Nelson, J., Durrant, J. R., Bradley, D. D. C., Giles, M., McCulloch, I., Sikha, C., & Ree, M. (2006). A strong regioregularity effect in self-organizing conjugated polymer films and high-efficiency polythiophene:Fullerene solar cells. *Nature Materials*, 5, 197–203. <https://doi.org/10.1038/nmat1574>.
- Kuila, A., Chatterjee, D. P., Layek, R. K., & Nandi, A. K. (2014). Coupled atom transfer radical coupling and atom transfer radical polymerization approach for controlled grafting from poly(vinylidene fluoride) backbone. *Journal of Polymer Science Part A-Polymer Chemistry*, 52(7), 995–1008. <https://doi.org/10.1002/pola.27081>.
- Kuila, A., Maity, N., Chatterjee, D. P., & Nandi, A. K. (2015). Temperature triggered antifouling properties of poly(vinylidene fluoride) graft copolymers with tunable hydrophilicity. *Journal of Materials Chemistry A*, 3(25), 13546–13555. <https://doi.org/10.1039/c5ta01306b>.
- Kuila, A., Maity, N., Chatterjee, D. P., & Nandi, A. K. (2016). Phase behavior of poly(vinylidene fluoride)-*graft*-poly(diethylene glycol methyl ether methacrylate) in alcohol-water system: Coexistence of LCST and UCST. *The Journal of Physical Chemistry. B*, 120(9), 2557–2568. <https://doi.org/10.1021/acs.jpcc.5b11736>.
- Kuila, A., Chatterjee, D. P., Maity, N., & Nandi, A. K. (2017a). Multi-functional poly(vinylidene fluoride) graft copolymers. *Journal of Polymer Science Part A-Polymer Chemistry*, 55(16), 2569–2584. <https://doi.org/10.1002/pola.28671>.
- Kuila, A., Maity, N., Chatterjee, D. P., & Nandi, A. K. (2017b). pH and temperature responsiveness in AgNPs stabilized by a new poly(vinylidene fluoride) random graft copolymer. *Journal of Polymer Science Part A-Polymer Chemistry*, 15(6), 960–970. <https://doi.org/10.1002/pola.28456>.

- Kumari, P., Bera, M. K., Malik, S., & Kuila, B. K. (2015). Amphiphilic and thermoresponsive conjugated block copolymer with its solvent dependent optical and photoluminescence properties: Toward sensing applications. *ACS Applied Materials & Interfaces*, 7(23), 12348–12354. <https://doi.org/10.1021/am507266e>.
- Lando, J. B., Olf, H. G., & Peterlin, A. (1966). Nuclear magnetic resonance and x-ray determination of the structure of poly(vinylidene fluoride). *Journal of Polymer Science Part A-Polymer Chemistry*, 4(4), 941–951. <https://doi.org/10.1002/pol.1966.150040420>.
- Lang, S. B., & Muensit, S. (2006). Review of some lesser-known applications of piezoelectric and pyroelectric polymers. *Applied Physics A*, 85(2), 125–134. <https://doi.org/10.1007/s00339-006-3688-8>.
- Lanzalaco, S., Fantin, M., Scialdone, O., Galia, A., Isse, A., Gennaro, A., & Matyjaszewski, K. (2017). Atom transfer radical polymerization with different halides (F, Cl, Br, and I): Is the process “living” in the presence of fluorinated initiators? *Macromolecules*, 50(1), 192–202. <https://doi.org/10.1021/acs.macromol.6b02286>.
- Lee, H., Pietrasik, J., Sheiko, S. S., & Matyjaszewski, K. (2010). Stimuli-responsive molecular brushes. *Progress in Polymer Science*, 35(1–2), 24–44. <https://doi.org/10.1016/j.progpolymsci.2009.11.002>.
- Le’vesque, I., Bazinet, P., & Roovers, J. (2000). Optical properties and dual electrical and ionic conductivity in poly(3-methylhexa(oxyethylene)oxy-4-methylthiophene). *Macromolecules*, 33(8), 2952–2957. <https://doi.org/10.1021/ma9917803>.
- Li, Z., Ono, R. J., Wu, Z. Q., & Bielawski, C. W. (2011). Synthesis and self-assembly of poly(3-hexylthiophene)-block-poly(acrylic acid). *Chemical Communications*, 47(1), 197–199. <https://doi.org/10.1039/c0cc02166k>.
- Lin, C. H., Chau, C. M., & Lee, J. T. (2012). Synthesis and characterization of polythiophene grafted with a nitroxide radical polymer via atom transfer radical polymerization. *Polymer Chemistry*, 3(6), 1467–1474. <https://doi.org/10.1039/c2py20048a>.
- Liu, J., Sheina, E., Kowalewski, T., & McCullough, R. D. (2002). Tuning the electrical conductivity and self-assembly of regioregular polythiophene by block copolymerization: Nanowire morphologies in new di- and triblock copolymers. *Angewandte Chemie, International Edition*, 41(2), 329–323. [https://doi.org/10.1002/1521-3773\(20020118\)41:2<329::aid-anie329>3.0.co;2-m](https://doi.org/10.1002/1521-3773(20020118)41:2<329::aid-anie329>3.0.co;2-m).
- Liu, Y., Lee, J. Y., Kang, E. T., Wang, P., & Tan, K. L. (2001). Synthesis, characterization and electrochemical transport properties of the poly(ethyleneglycol)-grafted poly(vinylidene fluoride) nanoporous membranes. *Reactive and Functional Polymers*, 47(3), 201–213. [https://doi.org/10.1016/S1381-5148\(01\)00030-X](https://doi.org/10.1016/S1381-5148(01)00030-X).
- Lligadas, G., Grama, S., & Percec, V. (2017). Recent developments in the synthesis of biomacromolecules and their conjugates by single electron transfer–living radical polymerization. *Biomacromolecules*, 18(4), 1039–1063. <https://doi.org/10.1021/acs.biomac.7b00197>.
- Lovinger, A. J. (1982). Poly(vinylidene fluoride). In D. C. Bassett (Ed.), *Developments in crystalline Polymers-I* (pp. 195–273). Dordrecht: Springer Netherlands. https://doi.org/10.1007/978-94-009-7343-5_5.
- Lutz, J. F., Borner, H. G., & Weichenhan, K. (2005). Combining atom transfer radical polymerization and click chemistry: A versatile method for the preparation of end-functional polymers. *Macromolecular Rapid Communications*, 26(7), 514–518. <https://doi.org/10.1002/marc.200500002>.
- Mac Diarmid, A. G. (2001). “Synthetic metals”: A novel role for organic polymers (nobel lecture). *Angewandte Chemie, International Edition*, 40(14), 2581–2590. [https://doi.org/10.1002/1521-3773\(20010716\)40:14<2581::aid-anie2581>3.0.co;2-2](https://doi.org/10.1002/1521-3773(20010716)40:14<2581::aid-anie2581>3.0.co;2-2).
- Maity, N., Ghosh, R., & Nandi, A. K. (2018). Optoelectronic properties of self-assembled nanostructures of polymer functionalized polythiophene and graphene. *Langmuir*, 34(26), 7585–7597. <https://doi.org/10.1021/acs.langmuir.7b04387>.
- Malmström, J., Nieuwoudt, M. K., Strover, L. T., Hackett, A., Laita, O., Brimble, M. A., Williams, D. E., & Sejdic, J. T. (2013). Grafting from poly(3,4-ethylenedioxythiophene): A simple route to versatile electrically addressable surfaces. *Macromolecules*, 46(12), 4955–4965. <https://doi.org/10.1021/ma400803j>.

- Martins, P., Costa, C. M., Benelmekki, M., Botelho, G., & Mendez, S. L. (2012). On the origin of the electroactive poly(vinylidene fluoride) β -phase nucleation by ferrite nanoparticles *via* surface electrostatic interactions. *Cryst. Eng. Comm*, 14(8), 2807–2811. <https://doi.org/10.1039/c2ce06654h>.
- Matyjaszewski, K., & Xia, J. (2001). Atom transfer radical polymerization. *Chemical Reviews*, 101(9), 2921–2990. <https://doi.org/10.1021/cr940534g>.
- McCullough, R. D., & Lowe, R. D. (1992). Enhanced electrical conductivity in regioselectively synthesized poly(3-alkylthiophenes). *Journal of the Chemical Society, Chemical Communications*, 1, 70–72. <https://doi.org/10.1039/c39920000070>.
- Mohamed, M. G., Cheng, C. C., Lin, Y. C., Huang, C. W., Lu, F. H., Changa, F. C., & Kuo, S. W. (2014). Synthesis and self-assembly of water-soluble polythiophene-graft-poly(ethylene oxide) copolymers. *RSC Advances*, 4(42), 21830–21839. <https://doi.org/10.1039/c4ra02433h>.
- Morra, B. S., & Stein, R. S. (1982). Morphological studies of poly(vinylidene fluoride) and its blends with poly(methyl methacrylate). *Journal of Polymer Science Polymer Physics Edition*, 20(12), 2261–2275. <https://doi.org/10.1002/pol.1982.180201208>.
- Ong, B. S., Wu, Y., Liu, P., & Gardner, S. (2004). High-performance semiconducting polythiophenes for organic thin-film transistors. *Journal of the American Chemical Society*, 126(11), 3378–3379. <https://doi.org/10.1021/ja039772w>.
- Pakhira, M., Ghosh, R., Rath, S. P., Chatterjee, D. P., & Nandi, A. K. (2019). Zwitterionic poly(vinylidene fluoride) graft copolymer with unexpected fluorescence property. *Langmuir*, 35(16), 5525–5533. <https://doi.org/10.1021/acs.langmuir.9b00039>.
- Pandey, A. K., Goswami, A., Sen, D., Mazumder, S., & Childs, R. F. (2003). Formation and characterization of highly cross-linked anion-exchange membranes. *Journal of Membrane Science*, 217(1–2), 117–130. [https://doi.org/10.1016/s0376-7388\(03\)00084-x](https://doi.org/10.1016/s0376-7388(03)00084-x).
- Parameswaranpillai, J., Thomas, S., & Grohens, Y. (2014). Polymer blends: State of the art, new challenges, and opportunities. In S. Thomas, Y. Grohens, & P. Jyotishkumarpp (Eds.), *Characterization of polymer blends* (pp. 1–6). Wiley. <https://doi.org/10.1002/9783527645602.ch01>.
- Perepichka, I. F., Perepichka, D. F., Meng, H., & Wudl, F. (2005). Light-emitting polythiophenes. *Advanced Materials*, 17(19), 2281–2305. <https://doi.org/10.1002/adma.200500461>.
- Qi, L., Sun, M., & Dong, S. (2006). Synthesis and characterization of novel polythiophenes containing poly(ethylene oxide) side chains. *Journal of Applied Polymer Science*, 102(2), 1803–1808. <https://doi.org/10.1002/app.23362>.
- Rasmussen, S. C., Evenson, S. J., & McCausland, C. B. (2015). Fluorescent thiophene-based materials and their outlook for emissive applications. *Chemical Communications*, 51(22), 4528–4543. <https://doi.org/10.1039/c4cc09206f>.
- Routh, P., Das, S., & Nandi, A. K. (2012). Polythiophene-*g*-poly(dimethylaminoethyl methacrylate) stabilized au nanoparticles and its morphology tuning by RNA with variation of electronic properties. *RSC Advances*, 2(30), 11295–11305. <https://doi.org/10.1039/c2ra21413j>.
- Samanta, S., Chatterjee, D. P., Manna, S., Mandal, A., Garai, A., & Nandi, A. K. (2009). Multifunctional hydrophilic poly(vinylidene fluoride) graft copolymer with supertoughness and supergluing properties. *Macromolecules*, 42(8), 3112–3120. <https://doi.org/10.1021/ma9003117>.
- Samanta, S., Chatterjee, D. P., Layek, R. K., & Nandi, A. K. (2010). Multifunctional porous poly(vinylidene fluoride)-*graft*-poly(butyl methacrylate) with good Li⁺ ion conductivity. *Macromolecular Chemistry and Physics*, 212(2), 134–149. <https://doi.org/10.1002/macp.201000472>.
- Samanta, S., Chatterjee, D. P., Layek, R. K., & Nandi, A. K. (2012a). Nano-structured poly(3-hexyl thiophene) grafted on poly(vinylidene fluoride) *via* poly(glycidyl methacrylate). *Journal of Materials Chemistry*, 22(21), 10542–10551. <https://doi.org/10.1039/c2jm30421j>.
- Samanta, S., Das, S., Layek, R. K., Chatterjee, D. P., & Nandi, A. K. (2012b). Polythiophene-*g*-poly(dimethylaminoethyl methacrylate) doped methyl cellulose hydrogel behaving like a polymeric AND logic gate. *Soft Matter*, 8(22), 6066–6072. <https://doi.org/10.1039/c2sm25145k>.

- Shao, M., He, Y., Hong, K., Rouleau, C. M., Geohagan, D. B., & Xiao, K. (2013). A water-soluble polythiophene for organic field-effect transistors. *Polymer Chemistry*, 4(20), 5270–5274. <https://doi.org/10.1039/c2py21020g>.
- Shirakawa, H., Louis, E. J., MacDiarmid, A. G., Chiang, C. K., & Heeger, A. J. (1977). Synthesis of electrically conducting organic polymers: Halogen derivatives of polyacetylene, (CH)_x. *J. Chem. Soc. Chemical Communications*, 16, 578–580. <https://doi.org/10.1039/c39770000578>.
- Singh, N., Husson, S. M., Zdyrko, B., & Luzinov, I. (2005). Surface modification of microporous PVDF membranes by ATRP. *Journal of Membrane Science*, 262(1–2), 81–90. <https://doi.org/10.1016/j.memsci.2005.03.053>.
- Walton, D. J. (1990). Electrically conducting polymers. *Materials & Design*, 11(3), 142–152. [https://doi.org/10.1016/0261-3069\(90\)90004-4](https://doi.org/10.1016/0261-3069(90)90004-4).
- Wang, M., Zou, S., Guerin, G., Shen, L., Deng, K., Jones, M., Walker, G. C., Scholes, G. D., & Winnik, M. A. (2008). A water-soluble pH-responsive molecular brush of poly(*N,N*-dimethylaminoethyl methacrylate) grafted polythiophene. *Macromolecules*, 41(19), 6993–7002. <https://doi.org/10.1021/ma800777m>.
- Wang, T., Kang, E. T., & Neoh, K. G. (1998). Surface modification of low-density polyethylene films by uv-induced graft copolymerization and its relevance to photolamination. *Langmuir*, 14(4), 921–927. <https://doi.org/10.1021/la971018z>.
- Wang, X. S., Luo, N., & Ying, S. K. (1999). Synthesis of EPDM-g-PMMA through atom transfer radical polymerization. *Polymer*, 40(16), 4515–4520. [https://doi.org/10.1016/S0032-3861\(98\)00693-4](https://doi.org/10.1016/S0032-3861(98)00693-4).
- Wei, B., Ouyang, L., Liu, J., & Martin, D. C. (2015). Post-polymerization functionalization of poly(3,4-propylenedioxythiophene) (PProDOT) via thiol-ene "click" chemistry. *Journal of Materials Chemistry B*, 3(25), 5028–5034. <https://doi.org/10.1039/c4tb02033b>.
- Weinhold, S., Litt, M. H., & Lando, J. B. (1979). Oriented phase III poly(vinylidene fluoride). *Journal of Polymer Science Polymer Physics Edition*, 17(9), 585–589. <https://doi.org/10.1002/pol.1979.130170907>.
- Westenhoff, S., Daniel, C., Friend, R. H., Silva, C., Sundström, V., & Yartsev, A. (2005). Exciton migration in a polythiophene: Probing the spatial and energy domain by line-dipole Förster-type energy transfer. *The Journal of Chemical Physics*, 122(9), 094903. <https://doi.org/10.1063/1.1855292>.
- Wu, Z. Q., Ono, R. J., Chen, Z., Li, Z., & Bielawski, C. W. (2011). Polythiophene–block–poly(γ -benzyl L-glutamate): Synthesis and study of a new rod–rod block copolymer. *Polymer Chemistry*, 2(2), 300–302. <https://doi.org/10.1039/c0py00299b>.
- Xue, J., Chen, L., Wang, H. L., Zhang, Z. B., Zhu, X. L., Kang, E. T., & Neoh, K. G. (2008). Stimuli-responsive multifunctional membranes of controllable morphology from poly(vinylidene fluoride)-graft-poly[2-(*N,N*-dimethylamino)ethyl methacrylate] prepared via atom transfer radical polymerization. *Langmuir*, 24(24), 14151–14158. <https://doi.org/10.1021/la801402u>.
- Zhai, G., Ying, L., Kang, E. T., & Neoh, K. G. (2002). Poly(vinylidene fluoride) with grafted 4-vinylpyridine polymer side chains for pH-sensitive microfiltration membranes. *Journal of Materials Chemistry*, 12, 3508–3515. <https://doi.org/10.1039/b206486c>.
- Zhao, H., Zhu, B., Sekine, J., Luo, S. C., & Yu, H. (2012). Oligoethylene-glycol-functionalized polyoxythiophenes for cell engineering: Syntheses, characterizations, and cell compatibilities. *ACS Applied Materials & Interfaces*, 4(2), 680–686. <https://doi.org/10.1021/am2012905>.
- Zhao, H., Zhu, B., Luo, S. C., Lin, H. A., Nakao, A., Yamashita, Y., & Yu, H. (2013). Controlled protein absorption and cell adhesion on polymer-brush-poly(3,4-ethylenedioxythiophene) films. *ACS Applied Materials & Interfaces*, 5(11), 4536–4543. <https://doi.org/10.1021/am400135c>.
- Zarintaj, P., Jouyandeh, M., Ganjali, M. R., Hadavand, B. S., Mozafari, M., Sheiko, S. S., Vatankhah-Varnoosfaderani, M., Gutiérrez, T. J., & Saeb, M. R. (2019). Thermo-sensitive polymers in medicine: A review. *European Polymer Journal*, 117, 402–423. <https://doi.org/10.1016/j.eurpolymj.2019.05.024>.

Chapter 11

Reinforced Polymers for Electroactive Devices



Anupama Gaur and Pralay Maiti

Abstract In this chapter, different electroactive polymers (EAPs) and reinforced polymer composites for device applications were discussed. Electroactive devices are widely used in all areas today. Electroactive devices show changes in shape and size when exposed to an electric field or give an electrical output signal when subjected to an external force. Their most common applications are in actuators and sensors. Previously, only ceramic materials were used to manufacture sensors and actuators. Ceramic materials can withstand a great force, but only a few can be deformed. In contrast, polymers can be greatly deformed at the same voltage, since the toughness and elongation at break of polymers are much higher than ceramics. Biocompatible polymers can also be used in the biomedical field. Some specific advantages of polymers are also discussed as electroactive material. These devices can be made of pure EAPs or filled polymers, especially with nanofiller geometry. Some nanofillers are piezo- or ferro-electric, and their inclusion into the polymers, in general, increases the electroactive properties of polymer composites. On the other hand, some nanofillers, such as nanoclay, can induce the electroactive phase in the polymer, even though the components are not intrinsically electroactive. A detailed discussion on the different nanofillers for making reinforced polymer composites for device applications was presented in this manuscript.

Keywords Electroactive polymers · Nanocomposites · Piezoelectricity

11.1 Introduction

In this era of technological development, polymers are replacing materials traditionally used, such as ceramics and metals in almost all fields. Due to the growing demand for polymeric materials, new processing techniques for the

A. Gaur · P. Maiti (✉)

School of Materials Science and Technology, Indian Institute of Technology (Banaras Hindu University), Varanasi, Uttar Pradesh, India

e-mail: pmaiti.mst@itbhu.ac.in

© The Editor(s) (if applicable) and The Author(s), under exclusive license to Springer Nature Switzerland AG 2020

T. J. Gutiérrez (ed.), *Reactive and Functional Polymers Volume Two*, https://doi.org/10.1007/978-3-030-45135-6_11

production of polymers are being developed with customized properties and cost-effective designs: lower weight and variable sizes (Gurunathan et al. 1999; Bar-Cohen 2004). Polymers have other advantages such as economical, flexible, fracture tolerant, light weight and easy to be processed and manufactured in different shapes and sizes (Bar-Cohen 2004). With the advancement of technology, various intelligent materials have also been developed, which can detect variations in the environment or the process against input, and act accordingly. Piezoelectric materials and shape memory alloys belong to this category (Zrínyi 2000). Intelligent polymers are also being studied under various stimuli, e.g. electric and magnetic field, light, pH, etc. (Bar-Cohen 2004; Bracone et al. 2016; Gutiérrez et al. 2016; Gutiérrez et al. 2017b; Gutiérrez 2018; Zarrintaj et al. 2019).

These polymers are generally known as active polymers. Active polymers can convert chemical or electrical energy into mechanical energy directly or vice versa. This property is used to manufacture miniature robot components (Courty et al. 2003). These active polymers have diverse properties and can detect changes in their environment, thus producing reversible or permanent responses according to the requirements. In the development of an intelligent structure, the toughness and resilience of the polymer is very important, since these properties in turn affect the properties of the fillers within the polymer matrix (so called 'reinforced polymers'). These reinforced polymers have improved properties and can exhibit better efficiency for designing electroactive devices.

11.1.1 Reinforced Polymers

Reinforced polymer is a class of composite materials in which the limitations of the polymer can be overcome by incorporating different types of fillers. These fillers can be fibers, nanoparticles (NPs), nanosheets, etc. depending on the requirement and the matrix polymer (Gutiérrez and Alvarez 2017). The final properties of the reinforced polymers depend mainly on the nature and properties of their components and on the type of interaction between the matrix and the filler (Gutiérrez et al. 2017a; Gutiérrez et al. 2018; Gutiérrez et al. 2019). The interaction or adhesion between the filler and the matrix also depends on the aspect ratio of the filler. The aspect ratio influences the electrical (Al-Saleh and Sundararaj 2010), mechanical (Zhang et al. 2007) and thermal (Meneghetti and Qutubuddin 2006) properties, as well as other properties of the composites. High-aspect ratio nanofiller-reinforced polymers such as carbon nanotubes, clay platelets and nanofibers have unique multifunctional properties. Fillers with nano-scale dimension and high aspect ratio improve the polymer properties even at low filler volume fractions. As a result, the low density of the matrix polymer, macroscopic homogeneity and opacity of the polymer can be maintained.

11.1.2 *Electroactive Devices*

Electroactive devices are those materials that provide chemical, mechanical or optical changes when an electric signal is given as input to them or vice versa, thus generating electric output if any chemical, mechanical or optical signal is applied to them. These are made of electroactive polymers (EAPs) or reinforced EAPs.

11.2 Development of EAP Materials

EAPs exhibit changes in shape and size under the influence of external electric field (Bar-Cohen and Zhang 2008; Carpi and Smela 2009). The basic activation mechanism of such polymers can be chemical, electrical, optical, pneumatic or magnetic stimuli, and outside of these, electrical excitation is most convenient and practical. EAPs have characteristics such as fracture tolerance, low weight, overall low cost and pliability to tailor properties to a particular application. There are different types of polymers within the category of EAPs, such as electrostrictive polymers (Zhang et al. 1998; Zhenyi et al. 1994), piezoelectric polymers (Furukawa and Seo 1990) and electrochemically actuated conducting polymers and gels (Smela et al. 1995; Elisabeth Smela and Gadegaard 1999; Fernandez Otero et al. 1999; Schreyer et al. 1999; Tamagawa et al. 1999), which are under investigation. The field of EAPs began in 1880, when Wilhelm Rontgen observed a change in the length of the rubber by several centimeters when the electric charge was sprayed onto the rubber (Keplinger et al. 2010). M.P. Sacerdote formulated a theory in 1899 about the strain response to an applied electric field following Roentgen's experiment. In 1925 the first piezoelectric polymer electret was discovered. In 1969, Kawai revealed the large piezoelectric effect of poly(vinylidene fluoride) (PVDF), which is considered as a breakthrough in this field. In 1977, the first electrically conducting polymer (polyacetylene) was discovered (Finkenstadt 2005) and by doping it with iodine vapor, its conductivity was to be close to that of metal. In the late 1980's numerous polymers were discovered which exhibit either conductivity or the piezoelectric effect. In 1990's, ionic polymer-metal composites were discovered, which showed superior electroactive properties than previous EAPs. High strain up to 380% and deformation at voltages as low as 1 or 2 volts were the main advantages of these ion polymer-metal composites. The first device commercially developed as an artificial muscle was produced by Eamex in Japan in 2002. In the last decade, a number of new materials have been developed which have shown great displacement under electrical stimulation. Due to this ability, these materials are widely used as actuators for their muscle-like work, damage tolerance, resilience and large strain producing ability: contracting, bending or stretching. The application of these materials is a multidisciplinary area which includes chemistry, computation, electromechanics, electronics and materials. EAP materials can be divided into two parts depending on the activation mechanism such as electronic and ionic.

Electronic EAPs In electronic EAPs, the actuation is due to electrostatic force between two electrodes, and therefore, squeezes the polymer, thus acting as capacitors which compress or expand the area due to the electric field arising from a very high strain. Electronic EAPs require a high actuation field ($>10 \text{ V}/\mu\text{m}$), but less electric power. The following are the different EAPs.

Ferroelectric polymers: These materials maintain a permanent electric polarization which is reversed or switched in the presence of an electric field. PVDF is a ferroelectric polymer and, due to its good piezoelectric (Gaur et al. 2018) and pyroelectric properties, it is also used in acoustic, electromechanical transducers, as well as in energy harvesting.

Electrostrictive polymers: In some graft polymers, backbone polymers and attached side chains crosslink and form crystal units to make polarized monomers, which generate dipole moments due to partial charges (Wang et al. 2004). The polymer unit rotates and causes strain because of these partial charges under an electric field.

Liquid crystalline polymers: Some groups are linked through mesogenic groups in these polymers. Due to temperature variations, these oriented elastomers exhibit high strain along the polymer chain direction, thus resulting in distinctive mechanical properties and applications in mechanical actuators.

Electronic EAP can be divided according to electric polarization and mechanical strain into electrostrictive and ferroelectric. Ferroelectric polymers have a linear relation between strain and polarization, while the strain is proportional to the square of polarization in electrostrictive polymers. PVDF is an example of a ferroelectric polymer, while its poly(vinylidene fluoride-*co*-trifluoro ethylene (P(VDF-*co*-TrFE)) copolymer is electrostrictive. Poly(urethane) is also an electrostrictive polymer used in energy harvesting (Kumar et al. 2017a).

Ionic EAPs In ionic EAPs, displacement of ions within the polymer causes actuation. These polymers require very low voltage but high electric power for actuation in these systems. High power is used to keep the actuator in the given position. Examples of these conducting polymers are ionic polymer-metal composites and responsive gels.

Electrorheological fluids: These fluids change the viscosity of solution when an electric field is applied, and the viscosity of the suspension increases with the application of a large electric field. Their applications are in engine mounts, acoustic dampers and shock absorbers (Glass et al. 1991).

Ionic polymer-metal composites: These exhibit very high deformations with low applied voltage and show low impedance due to electrostatic attraction between the cationic counter ions and the cathode for the applied electric field. These are mainly used in biomimetics as fibers and are composed of naturally occurring charged ionic polymers (Shahinpoor 1999). Commonly used ionic polymer metal composites are Nafion and Flemion (Park et al. 2008).

Stimuli-responsive gels: these materials change their volume due to variations in physical parameters such as chemical (concentration), electric field, light or

temperature, thus modifying their optical, mechanical or other properties, since the volume change is based on diffusion.

Ionic EAPs can also be divided into ionic polymer-metal composites (IPMC) and conductive polymer composites (Jean-Mistral et al. 2010). IPMCs work on ionic migration through a selective ionic membrane which allows the cations or anions pass through them. Nafion and Flemion are the examples of this category. Nafion is used in proton exchange membrane fuel cells (PEMFCs) in which there are selective migration of hydrogen ions. Conductive polymers in the presence of electrolytes undergo redox reactions and exhibit a change in volume, e.g. poly(aniline) and polypyrrole. Electrical energy harvesting from a conductive polymer composite through a mechano-chemo-electric process is an important way to maintain it in an electrolyte medium (Takashima et al. 1997). However, poly(dimethyl siloxane) (PDMS) and PVDF composites are widely used in energy harvesting as they have better electro mechanical coupling. Electronic EAPs require a high activation field ($> 10 \text{ V}/\mu\text{m}$) which is very close to the breakdown voltage level, while in ionic EAP activation can be achieved at low voltages (1–2 V) through of the transport of ions in electrolytes between the electrodes (Bar-Cohen et al. 2007). Of these EAPs, the piezoelectric polymers will be emphasized in detail. Different NPs and their effects to increase the properties and efficiency when embedded in polymers will also be discussed later.

11.3 Reinforced EAP Materials

The reinforced EAP material or EAP composites (EAPC) are those containing some filler material with the aim of improving their potential properties as EAP actuators, since they can change their shape and size in response to the applied electric field (Zhang et al. 2002; Bar-Cohen et al. 1998; Pei et al. 2000). This change can be controlled by the applied external field. Different fillers have been used to prepare these reinforced polymers and the nano dimension of filler help to improve the properties in a better way due to their greater surface area and improved interaction (Kumar et al. 2009). Studies indicate that improved mechanical properties of nano-composites depend on their aspect ratio and filler/matrix ratio (Sheng et al. 2004). The NP-induced properties are focused on improving electrical conduction, mechanical and barrier properties. Biron (2004) and Gloaguen and Lefebvre (2007) described a method for reinforcing polymer chains at the molecular level and generating two-phase material consisting of a matrix of basic polymers and nanofillers. The properties of composite materials can be easily altered by changing the content and dimension of the filler. Here, the three dimensions of nanofillers are discussed with their property improvement.

One-dimensional nanofiller: For this type of filler, two dimensions are confined and the nanotube and nanorod fall under this category. Dang et al. prepared a composite of PVDF and multiwalled carbon nanotubes (MWCNTs). MWCNTs were modified by chemical reaction and were then well dispersed in the polymer matrix.

The presence of carbon nanotubes (CNTs) increases the electroactive β -phase in the polymer and remarkably improved the dielectric properties over a wide range of temperature (Dang et al. 2007). Kim et al. (2009) added MWCNT to the PVDF matrix and prepared the composite using 0.2 wt.% of CNT. The piezoelectric β -phase increase in the drawn film and MWCNT helps in the conversion of α to β phase by acting as nuclei during crystallization. The result of the drawing and MWCNT increased the electroactive β -phase up to 96% together with the piezoelectric coefficient for the filler content of 0.2 wt.%. The β phase decreased as the filler content increased further, due to a higher conductivity of MWCNT, which caused depolarization (Kim et al. 2009). Lin et al. (2012) pre-treated MWCNTs through the oxidative unzipping process to use as filler to prepare nanocomposite with PVDF. This treatment achieved to solve the agglomeration problems of MWCNTs. The PVDF/CNT composite exhibited superior mechanical properties and an improved piezoelectric β -phase with only 0.3% filler. The piezoelectric coefficient obtained was as high as 38.4 pC/N. According to He et al. (2013) the nanocomposite also exhibited a 130% increase in storage modulus compared to pure PVDF.

Two-dimensional nanofiller: In this type of fillers a dimension is confined. Tiwari et al. (2013) prepared PVDF nanohybrids containing nanoclay through the solution route and found a dramatic change in structure. The polymer crystallized on the nanoclay surface which led to changes in structure and improvement of electrical and mechanical properties. After stretching at high temperature, the piezoelectric β -phase was increased by up to 90% for nanohybrid compared to 75% for pure PVDF, this due to the disposition of all trans (TTTT) on the surface of the clay platelets. The piezoelectric coefficient also increases in the nanohybrid more than pure PVDF (Tiwari et al. 2013). Rahman and Chung (2013) added reduced graphene oxide (RGO) into PVDF with the goal of improving piezoelectric and ferroelectric properties. The addition of 0.3 wt.% of RGO produced the complete conversion of the electroactive β -phase. The dielectric constant and the remnant polarization were increased by 320% and 200%, respectively. The high normalized strain of 16.66 pm/V was also found at this concentration (Rahman and Chung 2013). Rahman et al. (2013) showed that a lower concentration of GO in PVDF improved the piezoelectricity twice compared to pure PVDF. The energy harvesting capability of PVDF/RGO was better compared PVDF/GO and pure PVDF. This improvement in this property was explained through the specific interactions between PVDF and the functional groups present in partially RGO. The remnant polarization also increased by 53.2% in composite (Rahman et al. 2013). Gaur et al. (2016) prepared nanohybrid with 30B silicate clay through the solution route and reported better mechanical properties in the composites. After stretching of nanohybrid at elevated temperature, the electroactive β -phase increased by up to 75% compared to only 18% before stretching. The nanohybrid also showed improved remnant polarization and a piezoelectric coefficient (Gaur et al. 2016). The nanohybrid showed better piezoelectric properties than the pure PVDF due to epitaxial crystallization on the nanoclay layers (Gaur et al. 2017). The additional increase in piezoelectricity was obtained by uniaxial stretching at high temperature which improved

the piezoelectric β -phase, as well as the piezoelectric coefficient. Alluri et al. (2017a) prepared the PVDF composite containing 30% (v/v) of activated carbon through the sonication method. The nanocomposite was highly flexible and lightweight. The high electroactive β -phase was produced during sonication processing, which reduces the requirement for electric poling. The activated carbon acted as a stabilizer for the β -phase and also acted as an electrical conduction path between the PVDF dipoles. The stability test was performed for the nanogenerator measuring the output after 4 months and there was no deterioration in the response. Kumar et al. (2017b) prepared the RGO-containing PVDF nanocomposite for energy harvesting. The nanohybrids exhibited better mechanical and thermal properties.

Three dimensional nanofiller: When none of the dimensions of the fillers are confined, but in tens if it is a nanometer level, it is called as three-dimensional filler. Martins et al. produced magnetoelectric nanocomposites from P(VDF-co-TrFE) and CoFe_2O_3 NPs through solvent casting. The remnant polarization and the piezoelectric coefficient were increased to $16.3 \mu\text{C}/\text{cm}^2$ and $27 \text{ pC}/\text{N}$, respectively, at a concentration of 7 wt.% filler. At this very low filler concentration, the nanocomposite shows superior properties due to the increase in the electroactive phase, i.e. TTTT (all trans conformation β -phase) (Martins et al. 2011). In this same line, Gonçalves et al. (2013) used co-precipitation technique to produce magnetic iron oxide NPs of the order of 15 nm diameter and prepared their composites from PVDF through the solution route. PVDF was crystallized in the β -phase. This electroactive β -phase is proportional to the ferrite content, and crystallization is dominated by the electrostatic interactions between the polymer chains and the NPs. In addition, an increase in the β -phase content to $\sim 80\%$ was obtained using a 5% filler load in the composite. These composites exhibited better conductivity and magnetic properties (Gonçalves et al. 2013).

The mixture of two different types of nanofillers as reinforcing agents for the polymeric matrix have also been used. With this in mind, Geng et al. (2012) prepared a ternary composite made from PVDF containing organically modified montmorillonite (OMnt) and MWCNTs by melt mixing. The composite exhibited better damping, electrical, mechanical and piezoelectric properties. DC conductivity increased up to 8 order of magnitude for the composite loaded of MWCNT and 3 wt.% of OMnt. Similarly, at the percolation threshold, the PVDF/1.9 wt.% MWCNT/3 wt.% OMnt composite showed the best damping characteristics (Geng et al. 2012). Jeong et al. (2015) prepared a highly stretchable nanocomposite from lead magnesium niobite-lead titanate ($[(1-x)\{\text{Pb}(\text{Mg}_{1/3}\text{Nb}_{2/3})\text{O}_3\}-x\{\text{PbTiO}_3\}]$) - PMN-PT NPs and MWCNT in the silicon elastomer. The stretchable silver nanowire (Ag NW) electrode was deposited on top of the film, resulting in approx. 200% stretch capacity, and the stretchable Ag NWs give them a high degree of freedom with non-destructive stress relaxation without affecting the electrical properties (Jeong et al. 2015). Karan et al. (2016) prepared the aluminium oxide-RGO (AlO-RGO)-loaded PVDF nanocomposite. The AlO-RGO acted as an electroactive β -phase nucleator, thus improving the electrical properties and finding 90% stabilization of the β -phase with only 1 wt.% of the filler (Karan et al. 2016).

11.4 Fabrication and Performance of the Devices

There are several devices based on the above electroactive materials and different types of devices have been manufactured according on the type of application or the type of loads that are applied on them. Figure 11.1 shows different types of devices that are used for energy harvesting. The first type shown is generally used for impact types of loads (Fig. 11.1a), in which the reinforced material is coated with a conducting layer or the conducting layer is adhered on both sides of the electrodes. The assembly is then encapsulated in an insulating layer, such as PDMS. This type of device is used by several workers (Alluri et al. 2017a; Kumar et al. 2017b). Another type is shown in Fig. 11.1b, in which there is an active layer along with an inactive layer. The active layer is the reinforced polymer or EAP, and the structural layer is the insulating layer. This type of device is generally used for energy harvesting from different types of vibrations (Gaur et al. 2017; Zhou et al. 2016). A further type of device is shown in Fig. 11.1c, which is the laminated type, where different layers of electroactive materials are used, followed by another conducting layer deposited for electrode formation on both sides. This type of device is also used for compressive-type loads (Bhavanasi et al. 2016; Liao et al. 2014).

The performance of energy harvesting devices depends on the type of device used and the nature of the stress applied to the device. Keeping this in mind, Alluri et al. (2017a) prepared the activated carbon-loaded PVDF *via* sonication processing, the obtained nanogenerator showed an increase in dielectric constant and better electrical conductivity due to interfacial interactions and better dipole-dipole interactions. The unpoled PVDF and the composite nanogenerator produced an open-circuit voltage (OCV) and short-circuit current of 37.77 V, 299 nA and 37.87 V, 831 nA, respectively, at a 6.6 kPa pressure. No significant improvements were, however, observed when poling for the pure PVDF nanogenerator, but the composite generator exhibited an increase of $\sim 30\%$ in voltage and $\sim 96\%$ in current output. The output power density obtained was ~ 63.07 mW/m² (Fig. 11.2a) and can light up to 22 light emitting diodes (LEDs) (Alluri et al. 2017a). Kumar et al. (2017b) also prepared a device from RGO-loaded PVDF nanocomposites and obtained a maximum output at 1 wt.% filler content, thus showing a power density of 14 μ W/cm³, sufficient to drive self-powered devices. The prepared device had long-term stability for 2000 cycles under high stress (Kumar et al. 2017b). Alamusi et al. (2012)

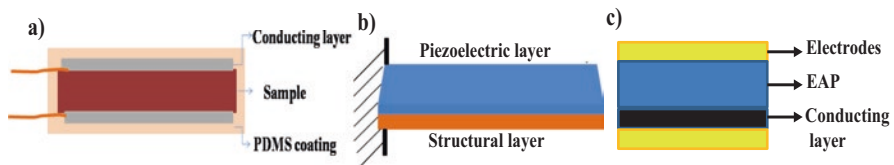


Fig. 11.1 Different types of devices used for energy harvesting: (a) composite device, (b) uni-morph or cantilever type device and (c) layered structure device

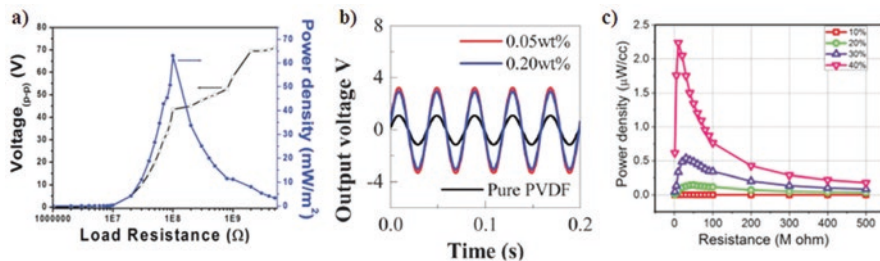


Fig. 11.2 Performance of different devices: (a) analysis of load resistance and calculations of powder density of the composite nanogenerator device after acceleration of 5 m/s^2 of load. Reproduced with permission from Alluri et al. (2017a), (b) output voltages of RGO/PVDF nanocomposite films (0.0 wt.%, 0.05 wt.% and 0.2 wt.%, at 30 Hz). Reproduced with permission from Alamusi et al. (2012), and (c) power density plots varying load resistances for different weight fractions of BZT-BCT NWs in the nanocomposite energy harvester. A maximum power density of $2.25 \mu\text{W}/\text{cm}^3$ was observed at an optimal resistance of $10 \text{ M}\Omega$ for 40 wt.% BZT-BCT NW/PDMS nanocomposite. Reproduced with permission from Zhou et al. (2016)

used graphene oxide (GO) varying the filler content from 0 to 0.2 wt.% in order to improve the piezoelectric properties of PVDF. The films were drawn and poled to induce the piezoelectric β -phase. The performance of the device was determined through the vibration test, and the maximum output was obtained at a vibration frequency of 30 Hz, where an output 293% higher than the pure PVDF was observed (3.28 V against 1.12 V in pure PVDF) (Fig. 11.2b) (Alamusi et al. 2012). Gaur et al. (2017) fabricated a unimorph of the stretched nanohybrid, and PVDF showed the generation of a peak-to-peak voltage of 2.5 V under an impulse load. For energy harvesting purpose, the samples were coated on both sides using Ag paste for electroding followed by different loading conditions. The maximum power output obtained was $25 \mu\text{W}/\text{cm}^3$, which was sufficient for miniaturized devices (Gaur et al. 2017). Zhou et al. (2016) prepared lead-free piezoelectric $0.5\text{Ba}(\text{Zr}_{0.2}\text{Ti}_{0.8})\text{O}_3-0.5(\text{Ba}_{0.7}\text{Ca}_{0.3})\text{TiO}_3$ (BZT-BCT) NWs. These NWs had a high piezoelectric coupling coefficient, and the energy harvesting performance of the NWs was measured by making polymer nanocomposites. The cantilever type energy harvester was fabricated, and the output performance was measured under different frequencies. The maximum voltage obtained was 6.25 V at the resonance frequency. The associated power was $2.25 \mu\text{W}/\text{cm}^3$ at $10 \text{ M}\Omega$ resistance (Fig. 11.2c) (Zhou et al. 2016). Bhavanasi et al. (2016) prepared the flexible bilayer P(VDF-co-TrFE) film loaded with GO for energy harvesting, which under the application of a 3.2 MPa compressive load produces a voltage output of 4 V and a power density of $4.41 \mu\text{W}/\text{cm}^2$.

Dhakras et al. (2012) prepared PVDF nanofibers loaded with the small amount of nickel chloride hexahydrate salt. The addition of hydrated salt helped to increase the piezoelectric β -phase from 0.64 to 0.92 fraction. The free vibration measurement showed the dynamic strain sensitivity, determined from voltage *per* unit strain, which varied between 0.119 and $0.548 \text{ mV}/\text{m}^3$ for PVDF and in composite in presence of hydrated salt, respectively. The charges were generated under the application of strain to the fibers which created the voltage differences and the peak was

observed in the positive direction, while the peak in the negative direction was during the release of the charges. These peaks corresponded to the compression and tension in the fibers, respectively. The performance increases increased with increasing β -phase fraction. Furthermore, by eliminating the beads in the fibers, the piezo response increased by 44% and the response increased by 157% due to the addition of a small amount of hydrated salt (0.5 wt.%) (Dhakras et al. 2012). Rahman et al. (2013) measured the output voltage for PVDF, PVDF/GO and PVDF/RGO. PVDF/RGO provided a maximum output voltage and the peak-to-peak voltages for pure PVDF, PVDF/GO and PVDF/RGO were 0.7, 0.9 and 1.3 V, respectively. The maximum voltages for PVDF, PVDF/GO and PVDF/RGO were 288, 312 and 436 mV, respectively, at the resonance frequency of 41 Hz. The output voltage with different load resistance was measured, and the maximum power of output reached a value of 704 K Ω which can generate a maximum power of 36 nW (Rahman et al. 2013). Soin et al. (2015) prepared spin coated PVDF films and quenched them to different quenching temperatures. These authors obtained a very high piezoelectric coefficient of 49.6 pm/V when the sample was quenched at -20°C without pore formation. The output voltage of the sample was determined by connecting the electrodes to the samples and a applying a maximum impact load of 100 N to obtain a 3 V OCV. This OCV was three times higher than the films quenched at 100°C , this mainly due to the variation in β -phase formation. Soin et al. (2015) also found that the corresponding piezoelectric coefficient was 49.6 pm/V. Tiwari et al. (2019) prepared nanoclay 30B-loaded PVDF composite nanofibers and were used for the energy harvesting application. The device prepared from these nanofibers produced an OCV of 70 V and a power of 68 $\mu\text{W}/\text{cm}^2$, as well as the device was stable even after repeated loading (Tiwari et al. 2019).

Gaur et al. (2016) fabricated unimorphs of pure poly(vinylidene fluoride-*co*-hexafluoro propylene) (P(VDF-*co*-HFP)) and its nanoclay 30B-loaded composite nanohybrid. This unimorph consisted of a structural and a piezoelectric layer and the thickness of each layer was taken such that the neutral axis of the unimorph was found in the structural layer. The electrodes were attached to both the sides of the unimorph, and the output voltage was measured under an impact load in order to determine the performance of the device. The voltage output of nanohybrid under the impact load was 1.2 V compared to 0.5 V for pure PVDF (Gaur et al. 2016). Karan et al. (2016) reported the manufacture of piezoelectric nanogenerator with high power density and energy conversion efficiency. The nanogenerator can convert different biomechanical and machine energy into electrical energy. The maximum OCV and short circuit current obtained in the finger imparting was ~ 36 V and ~ 0.8 μA , respectively, and with a power density of ~ 27.97 $\mu\text{W}/\text{cm}^3$. These authors achieved charge the capacitor (~ 6.1 V) in a short time-span (96.6 s) with a high energy conversion efficiency of $\sim 12.47\%$ (Karan et al. 2016).

Zhang et al. (2016) prepared barium titanate (BaTiO_3) NP/bacterial cellulose (BC) nanofiber-based piezoelectric paper having excellent output performance. The piezoelectric paper had an OCV of 14 V and a current density of 190 nA/cm 2 in the cyclic bending deformation from home-made bending stage (Zhang et al. 2016). Alam and Mandal (2016) prepared a piezoelectric nanogenerator based on native

cellulose microfiber and PDMS containing conducting fillers (MWCNTs). The prepared device had an OCV of ~ 30 V and a power density $\sim 9.0 \mu\text{W}/\text{cm}^2$ under repeated hand punching. These authors were also able to light up the LED and the liquid crystal display (LCD) screen from charged capacitor (Alam and Mandal 2016) (Fig. 11.3).

Some natural materials or biowastes have also been used as reinforcing materials to develop EAPs. Kumar et al. (2019) prepared a PVDF composite loaded with fish scales as biowaste and was used for energy harvesting, resulting in OCV and power density values of 70 V and $68 \mu\text{W}/\text{cm}^2$, respectively (Kumar et al. 2019). Maity et al. (2018) also used natural sugar as a reinforcing material in PVDF in order to manufacture EAPs to be used for energy harvesting. As a result, the maximum OCV and power density values obtained were 100 V and $33 \text{ mW}/\text{m}^2$, respectively, under human finger imparting (Maity et al. 2018). Tamang et al. (2015) used deoxyribonucleic acid (DNA) to induce the electroactive phase in PVDF, and the nanogenerator was fabricated for energy harvesting. These authors reported that the maximum OCV and power density values from finger tapping were 20 V and $115 \mu\text{W}/\text{cm}^2$, respectively (Tamang et al. 2015). Various other devices have been manufactured using different reinforced polymers. The following tables show different nanocomposites loaded with different types of fillers and their performances as devices (Tables 11.1, 11.2, 11.3).

11.5 Applications of Electroactive Devices

Electroactive devices are generally used as actuators and sensors, which can control the movement or measure certain physical parameters. Devices made of ionic polymer metal composites are used for this purpose, as they generate high strain at very low voltage (Palmre et al. 2015). The electric field applied on one side of the actuator forces the ions to other side and this causes the swelling on the other side, which in turn is reflected in the bending of the actuator. These actuators can also be used

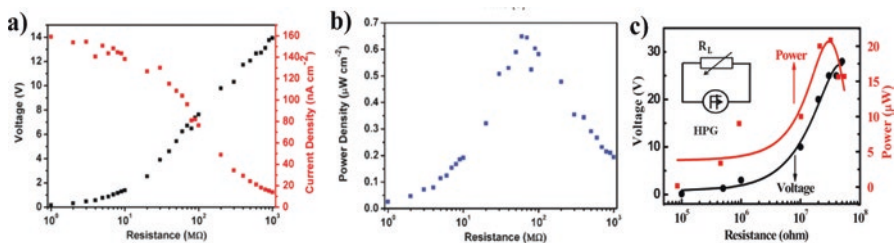


Fig. 11.3 The output voltage and (a) current density, (b) power density of the BaTiO_3/BC paper-based piezoelectric nanogenerator with different external load resistance. Reproduced with permission from Zhang et al. (2016), and (c) voltage and instantaneous power output as a function of the load resistance (the corresponding circuit diagram is shown in the box). Reproduced with permission from Alam and Mandal (2016)

Table 11.1 Performance of devices prepared from reinforced polymers using different inorganic and layered fillers

Materials and their composition	Method/processing	OCV, current, power and other parameters	References
PVDF/activated carbon	Poled at 8 KV/24 h at room temperature	~49.6 V, ~1.63 μ A and 63.07 mW/m ²	Alluri et al. (2017a)
PVDF/RGO (1 wt.%)	Solution method for composite preparation	Voltage peak-to-peak (V_{pp}) = 0.9 V, 150 nA and 14 μ W/cm ³	Kumar et al. (2017b)
NiCl ₂ salt-loaded PVDF nanofibers		0.119 mV/ μ e for PVDF nanofibers compared to 0.548 mV/ μ e for NiCl ₂ salt-loaded PVDF nanofibers	Dhakras et al. (2012)
PVDF/RGO (0–0.2 wt.%). Max. Output at 0.05 wt.%	Stretched 400–500% at 60 °C. Poled at 60 MV/m	3.28 V at 30 Hz	Alamusi et al. (2012)
Electrospun P(VDF-co-HFP)/Ag NP fibers	Electrospinning using a 6:4 <i>N,N</i> -dimethylformamide (DMF)/acetone ratio as solvent	3 V and 0.9 mA/cm ² at 2 Hz	Mandal et al. (2014)
PVDF/clay 30B at 4%	Stretching at high temperature	V_{pp} = 2.6 V, 100 nA and 25 mW/cm ³	Gaur et al. (2017)
P(VDF-co-HFP)/carbon black	Composite by solution route, then stretching and poling at 90 MV/m	3.68 V at 0.5 wt.% filler	Wu et al. (2014b)
PVDF/RGO	Max. for 0.05 wt.% RGO. 3.5 V poled at 900 kV/cm	4.5 W/m ³ in AC circuit and 2 W/m ³ in DC circuit	Wu et al. (2014a)
PVDF/ZnO NWs (0.1/1 w/w)	Uniaxial pressing and releasing at 50 mm/s	6.9 V, 0.96 μ A and 6.624 μ W	Saravanakumar et al. (2014)
Ce ³⁺ -doped electrospun PVDF/graphene composite nanofibers	Concentrations of PVDF, ammonium cerium sulfate dihydrate ((NH ₄) ₄ Ce(SO ₄) ₄ ·2H ₂ O) and graphene 12, 0.2, and 1 wt.%, respectively, with respect to the mixed solvent	Able to sense 2 Pa. Musical vibration. 11 V and 6.8 μ W maximum power at 6.6 kPa	Garain et al. (2016)
Cerium(III)- <i>N,N</i> -dimethylformamide-bisulfate (Ce(DMF)(HSO ₄) ₃) complex doped into PVDF	Electrode area: 1.5 × 2.5 cm	192 s for 4.7 μ F capacitor charging. 32 V for cerium complex-containing PVDF films at finger pressing	Garain et al. (2015)

(continued)

Table 11.1 (continued)

Materials and their composition	Method/processing	OCV, current, power and other parameters	References
PVDF/nanoclay nanofibers	DMF/acetone ratio (3:7) and 5 wt.% nanoclay content	0.83 V on finger pressing and 2.76 V in free vibration damping tests	Xin et al. (2016)
PVDF/graphene nanoplatelets	0.1 wt.% graphene content through electrospinning	7.9 V and 4.5 μ A at 0.2 MPa	Abolhasani et al. (2017)
P(VDF-co-TrFE)/Ag NPs and NWs (0.8 wt.%)	Al foil on polyethylene naphthalate nanocomposite and Al foil	67 mV at 1.2 wt.%	Chen et al. (2016)
FaPbBr ₃ NPs/PVDF (12 wt.%) formamidinium lead halide perovskite NPs	Drop cast, thermal annealing, poling 50 kV/cm for 1 h	3.3 μ F cap charge in 200 s up to 1.8 V, 30 V and 6.2 μ A/cm	Ding et al. (2017)

to move the wing spoiler of an airplane, which causing it to turn (Grau et al. 2016). The main benefits of the EAP-based devices are high strain or electromechanical bending on the low-voltage application (Jo et al. 2013) and their flexibility which allows them to mimic the motion of biological muscles and also in aqueous environment (Bar-Cohen 2006; Yeom and Oh 2009). These materials can also be used in underwater robotic applications, as well as aquatic propulsors (Palmre et al. 2015). These devices have potential in acoustic applications such as sound generation, noise and vibration control in loudspeakers (Zhao et al. 2016). Graphene-based electroactive devices have applications in broadband sensing and flexible energy harvesting (Rahman and Chung 2013). EAPs have a high dielectric constant, large deformations and energy conversion efficiency, as well as low elastic stiffness, noise and weight (Zhao et al. 2016). Different companies also offer customized EAPs (iRAP 2013). Parker Hannifin offers several advantages compared to traditional technology (Muir 2015), such as 10 times the battery life, 20% working strain for actuators, low power consumption and silent operation. Arkema Innovative Chemistry (2019) has developed fluorinated EAPs (terpolymers) having the large amount of energy storage capacity and showing larger changes in shape and size.

The flexible keypads have also been developed by the Algra Group (2019a) with the piezoelectric lacquer technique. Different forms and shapes have been made with piezoelectric lacquer technology (Algra Group 2019a). The most important advantage of this lacquering technique is its high sensitivity (approx. 1 V/N of applied force) and the wide operating temperature range compared to ferroelectrets. The Algra Group (2019b) also developed a piezoelectric button without batteries or cables. The energy to transmit the radio signals is generated by applying pressure to the button. This device is user-friendly, wear-free and click-free design (Algra Group 2019b). There are numerous applications of electroactive actuators such as

Table 11.2 Performance of devices prepared from reinforced polymers using ceramic fillers

Materials and their composition	Method/processing	OCV, current, power and other parameters	References
PDMS/BZT-BCT NW cantilever at 40 wt.%	Corona poling 15 kV 2 h	88 nW and 2.25 $\mu\text{W}/\text{cm}^3$ at 10 Ω	Zhou et al. (2016)
PVDF/ZnO NPs 50% suspension composite film acid etching acid etching-mesoporous film	Proof mass (65 g) on mesoporous structure (2 cm \times 1 cm \times \sim 28 μm)	0.16 mW/cm ³ at 60 Hz	Mao et al. (2014)
BaTiO ₃ NPs in 3D network of calcium alginate biopolymer	Single worm of 3.5 cm by hand force	70 mW/mw power by 2.5 cm device at 20 Hz and 11 N load	Alluri et al. (2017b)
KNbO ₃ /PDMS composite sandwiched by au/Cr-coated polymer substrates	0.38% strain and 15.2% strain rate	(+ve) 3.2 V, 67.5 nA and 9.3 nA/cm ²	Jung et al. (2012)
BaTiO ₃ nanotubes/PDMS	Poling 80 kV/cm for 12 h	5.5 V and 350 nA	Lin et al. (2012)
Processed wood fiber/ BaTiO ₃ piezoelectric paper	Corona poling	18 pC charge at 4 N	Mahadeva et al. (2014)
Electrospun BCZT NW/PDMS fibers	Poled at 4 kV/mm for 20 m. by electrospinning	V _{pp} = 2.2 + 1.2 V and I _{pp} = 180 nA	Fan et al. (2017)
PVDF/BaTiO ₃ NP nanofibers	Covered in PDMS max. at 16 wt.% BaTiO ₃	0.48 V at 6 mm deflection	Lee et al. (2016)
PDMS/BZT-BCT NPs	Indium tin oxide/ poly(ethylene terephthalate) film and Cu as electrodes	0.6 V and 7.6 nA	Kou et al. (2017b)
PDMS/BZT-BCT nanorods	Poling 3.5 kV/mm 20	0.8 V and 7 nA at finger pressing	Kou et al. (2017a)
P(VDF-co-TrFE)/0.78Bi _{0.5} Na _{0.5} TiO ₃ -0.22SrTiO ₃ (BNT-ST)	P(VDF-co-TrFE) and 60% BNT-ST filler using a DMF:Acetone (2:5:5) ratio	23.07 mV at wood door impact	Ji et al. (2017)
PDMS/KNbO ₃ NW (3 g PDMS+ 0.1-0.8 g KN)	Poling 5 kV/mm at room temperature for 1 h	10.5 V, 1.3 μA at 0.7 gm	Joung et al. (2014)

soft biomimetics for bioengineering applications such as active catheters and artificial muscles. According to Algra Group (2019b) a new implantable generator has been developed, which can convert heartbeat into energy. This device uses a nanoribbon piezoelectric element and can be placed in the heart to draw enough energy from its natural motion to power a pacemaker or other implantable devices. In this regard, a nano-dimension cochlear implant was developed and fully implanted with no external parts which works on piezoelectronic sensors and arbitrary waveform neutral stimulators. Currently, porous lead zirconate (PZT - Pb(Zr,Ti)O₃) is used in these devices, which are not biocompatible, but can be replaced by an alternative biocompatible EAP. Optimum energy waveform technology allows less power consumption, thus eliminating the need for parts that include a battery and power

Table 11.3 Performance of devices prepared from reinforced polymers using mixed fillers

Materials and their composition	Method/processing	OCV, current, power and other parameters	References
Silicon rubber/CNT/PMN-PT NPs.	Stretchable electrode coated	~4 V and ~500 nA at 50 kV/cm poling	Jeong et al. (2015)
PVDF/AIO-RGO (1% filler loading).	At 40 V at 46.8 KPa	~36 V and ~0.8 μ A. 40 V at 46.8 KPa. ~27.97 μ W/cm ³	Karan et al. (2016)
Fe-doped RGO/PVDF (2 wt.% loading).	Energy density of \approx 0.84 J/cm ³ at 537 kV/cm	5.1 V and 0.254 μ A. Finger pressing	Karan et al. (2015)
BaTiO ₃ NPs and BC, on a paper.	Paper was pressed and coated with PDMS then Ti/au. 13 V at 200 kV/cm poling	14 V, 190 nA/cm ² and 0.64 μ W/cm ² at 60 M Ω	Zhang et al. (2016)
K _{0.485} Na _{0.485} Li _{0.03} NbO ₃ -loaded PDMS.	NPs aligned with application of an AC field	V _{pp} = 16 at 5 N sinusoidal force	Deutz et al. (2017)
Cellulose microfiber/PDMS/MWCNT.		~30 V, ~500 nA and ~ 9.0 μ W/cm ³ at hand punch	Alam and Mandal (2016)
Zinc stannate (ZnSnO ₃)/PDMS/MWCNT.	Finger impact	40 V, ~0.4 μ A and ~ 10.8 μ W/cm ³	Alam et al. (2015)

supply. The stimulator component of the device uses a non-rectangular waveform which reduces power consumption by 15–35%. In addition to low power consumption, the implant can be configured to be used by adjusting the power input and can be charged wirelessly, thus eliminating the need of an external battery or power supply (Yip et al. 2015).

Some literatures have also shown the use of EAPs for real life applications. With this in mind, Jeong et al. (2015) prepared the silicon rubber composite loaded with CNT and PMN-PT NPs, which were highly elastic. As a result, the device can be used on the commercial LCD screen by repeating the stretching and releasing of the device, also this device can be used for smart clothing. These authors also stitched a stocking on the high and when the knee bends it produced 0.7 V and 50 nA, and can also illuminate the commercial LCD screen (Jeong et al. 2015). Alam et al. (2015) reported the lightening of different colored LEDs by charging the capacitor using the device made from PDMS loaded with MWCNTs and ZnSnO₃. Karan et al. (2016) also demonstrated that the piezoelectric nanogenerator can power various portable devices such as calculator and clock, mobile LCD screen, tweeter speaker and many LEDs. Many other papers have also demonstrated the LEDs lightening using manufactured EAPCs for stress applications (Alluri et al. 2017a; Alam and Mandal 2016; Kumar et al. 2019). In summary, electroactive devices can function as an energy source and also can act as an active sensor for implantable devices and in the automobile industries. These are highly desirable for large-scale application of flexible and portable electronics, and convert low-frequency mechanical energy into electricity.

11.6 Conclusion

Electroactive polymers (EAPs) have a wide area of applications. The properties of these polymers can be improved by loading different nanofillers in an optimal amount. The reinforced polymers have gained greater height in the area of device applications due to their biocompatibility, easy processability, unique toughness characteristics and added electroactiveness. EAPs can be used in batteries, chemical sensors, memory devices, photodiodes, photovoltaics, smart windows and supercapacitors. Carbon nanotube-reinforced polymers have applications such as electro-magnetic actuators, electrostatic dissipation and supercapacitors. Polymers reinforced with metal oxide nanowires and copper, gold, nickel, palladium, platinum and silver nanoparticles have applications for biological, chemical and gas sensors. Semiconductor reinforcement in the polymers is useful for applications in optical displays, photoconductors, photovoltaics and superconductors. Similarly, polymers with different types of reinforcements have applications in wider areas which are very useful. Thus, EAPs have become an integrated part of human life, as seen in their wide range of applications, including biodevices.

Acknowledgements The authors acknowledge the institute for the financial support.

Conflicts of Interest The authors declare no conflict of interest.

References

- Abolhasani, M. M., Shirvanimoghaddam, K., & Naebe, M. (2017). PVDF/graphene composite nanofibers with enhanced piezoelectric performance for development of robust nanogenerators. *Composites Science and Technology*, *138*, 49–56. <https://doi.org/10.1016/j.compscitech.2016.11.017>.
- Al-Saleh, M. H., & Sundararaj, U. (2010). Processing-microstructure-property relationship in conductive polymer nanocomposites. *Polymer*, *51*(12), 2740–2747. <https://doi.org/10.1016/j.polymer.2010.03.022>.
- Algra Group. (2019a). Retrieved April 15, 2019, from <https://www.algragroup.ch/en/trade-products/>
- Algra Group. (2019b). Wireless input system - piezo button without batteries and cables. Available in: <https://www.algragroup.ch/en/technologies/wireless-input-system-dynaptic-wireless/>
- Alam, M. M., Ghosh, S. K., Sultana, A., & Mandal, D. (2015). Lead-free ZnSnO₃/MWCNTs-based self-poled flexible hybrid nanogenerator for piezoelectric power generation. *Nanotechnology*, *26*(16), 165403. <https://doi.org/10.1088/0957-4484/26/16/165403>.
- Alam, M. M., & Mandal, D. (2016). Native cellulose microfibril-based hybrid piezoelectric generator for mechanical energy harvesting utility. *ACS Applied Materials & Interfaces*, *8*(3), 1555–1558. <https://doi.org/10.1021/acsami.5b08168>.
- Alamusi, Xue, J., Wu, L., Hu, N., Qiu, J., Chang, C., Atobe, S., Fukunaga, H., Watanabe, T., Liu, Y., Ning, H., Li, J., Li, Y., & Zhao, Y. (2012). Evaluation of piezoelectric property of reduced graphene oxide (rGO)-poly(vinylidene fluoride) nanocomposites. *Nanoscale*, *4*(22), 7250–7255. <https://doi.org/10.1039/c2nr32185h>.

- Alluri, N. R., Chandrasekhar, A., Jeong, J. H., & Kim, S. J. (2017a). Enhanced electroactive β -phase of the sonication-process-derived PVDF-activated carbon composite film for efficient energy conversion and a battery-free acceleration sensor. *Journal of Materials Chemistry C*, 5(20), 4833–4844. <https://doi.org/10.1039/c7tc00568g>.
- Alluri, N. R., Selvarajan, S., Chandrasekhar, A., Saravanakumar, B., Lee, G. M., Jeong, J. H., & Kim, S.-J. (2017b). Worm structure piezoelectric energy harvester using ionotropic gelation of barium titanate-calcium alginate composite. *Energy*, 118, 1146–1155. <https://doi.org/10.1016/j.energy.2016.10.143>.
- Arkema Innovative Chemistry (2019) Arkema acquires the PIEZOTECH startup company and speeds up its development in the fluorinated materials of the future. Available in: <https://www.arkema.com/en/media/news/news-details/arkema-acquires-the-piezotech-startup-company-and-speeds-up-its-development-in-the-fluorinated-materials-of-the-future/>
- Bar-Cohen, Y., Xue, T., Shahinpoor, M., Simpson, J. O., & Smith, J. (1998). Electroactive polymer actuators as artificial muscles for space applications. 28th Annual Meeting of the Fine Particle Society, April 1–3, 1998, Dallas, TX. Available in: <https://trs.jpl.nasa.gov/bitstream/handle/2014/19118/98-0345.pdf?sequence=1>
- Bar-Cohen, Y. (Ed.) (2004). Electroactive polymer (EAP) actuators as artificial muscles : Reality, potential, and challenges. ISBN: 978-0-81945-297-9. Volume: PM136. Pp. 816. Available in: <https://spie.org/publications/book/547465?websyncid=57381309-186d-1220-52ae-ae0191454&sessionguid=cdc86b71-ae3a-421b-cbb9-352c7a369794&ss=1>
- Bar-Cohen, Y. (2006). Biomimetic actuators using electroactive polymers (EAP) as artificial muscles. Available in: <https://trs.jpl.nasa.gov/handle/2014/39426>
- Bar-Cohen, Y., Kim, K. J., Choi, H. R., & Madden, J. D. W. (2007). Electroactive polymer materials. *Smart Materials and Structures*, 16(2). <https://doi.org/10.1088/0964-1726/16/2/e01>.
- Bar-Cohen, Y., & Zhang, Q. (2008). Electroactive polymer actuators and sensors. *MRS Bulletin*, 33(03), 173–181. <https://doi.org/10.1557/mrs2008.42>.
- Bhavanasi, V., Kumar, V., Parida, K., Wang, J., & Lee, P. S. (2016). Enhanced piezoelectric energy harvesting performance of flexible PVDF-TrFE bilayer films with graphene oxide. *ACS Applied Materials & Interfaces*, 8(1), 521–529. <https://doi.org/10.1021/acsami.5b09502>.
- Biron, M. (Ed.). (2004). *Thermosets and composites: Technical information for plastics users* (1st ed., p. 536). Elsevier Science. <https://doi.org/10.1016/b978-1-85617-411-4.x5000-1>. isbn:978-1-85617-411-4.
- Bracone, M., Merino, D., González, J., Alvarez, V. A., & Gutiérrez, T. J. (2016). Chapter 6. Nanopackaging from natural fillers and biopolymers for the development of active and intelligent films. In S. Ikram & S. Ahmed (Eds.), *Natural polymers: Derivatives, blends and composites* (pp. 119–155). New York. EE.UU: Editorial Nova Science Publishers, Inc. isbn:978-1-63485-831-1.
- Carpi, F., & Smela, E. (2009). *Biomedical applications of electroactive polymer actuators* (p. 496). John Wiley & Sons, Ltd. <https://doi.org/10.1002/9780470744697>. isbn:978-0-470-77305-5.
- Chen, H.-J., Han, S., Liu, C., Luo, Z., Shieh, H.-P. D., Hsiao, R.-S., & Yang, B.-R. (2016). Investigation of PVDF-TrFE composite with nanofillers for sensitivity improvement. *Sensors and Actuators A: Physical*, 245, 135–139. <https://doi.org/10.1016/j.sna.2016.04.056>.
- Courty, S., Mine, J., Tajbakhsh, A. R., & Terentjev, E. M. (2003). Nematic elastomers with aligned carbon nanotubes: New electromechanical actuators. *Europhysics Letters (EPL)*, 64(5), 654–660. <https://doi.org/10.1209/epl/i2003-00277-9>.
- Dang, Z. M., Wang, L., Yin, Y., Zhang, Q., & Lei, Q. Q. (2007). Giant dielectric permittivities in functionalized carbon-nanotube/electroactive-polymer nanocomposites. *Advanced Materials*, 19(6), 852–857. <https://doi.org/10.1002/adma.200600703>.
- Deutz, D. B., Mascarenhas, N. T., Schelen, J. B. J., de Leeuw, D. M., van der Zwaag, S., & Groen, P. (2017). Flexible piezoelectric touch sensor by alignment of lead-free alkaline niobate microcubes in PDMS. *Advanced Functional Materials*, 27(24), 1700728. <https://doi.org/10.1002/adfm.201700728>.

- Dhakras, D., Borkar, V., Ogale, S., & Jog, J. (2012). Enhanced piezoresponse of electrospun PVDF mats with a touch of nickel chloride hexahydrate salt. *Nanoscale*, 4(3), 752–756. <https://doi.org/10.1039/c2nr11841f>.
- Ding, R., Zhang, X., Chen, G., Wang, H., Kishor, R., Xiao, J., Gao, F., Zeng, K., Chen, X., Sun, X. W., & Zheng, Y. (2017). High-performance piezoelectric nanogenerators composed of formamidinium lead halide perovskite nanoparticles and poly(vinylidene fluoride). *Nano Energy*, 37, 126–135. <https://doi.org/10.1016/j.nanoen.2017.05.010>.
- Innovative Research and Products Inc. (iRAP) (2013) Electro-active polymer actuators and sensors - types, applications, new developments, industry structure and global markets. Available in: http://www.innoresearch.net/report_summary.aspx?id=83&pg=129&rcd=et-116&pd=3/1/2013
- Fan, H. H., Jin, C. C., Wang, Y., Hwang, H. L., & Zhang, Y. F. (2017). Structural of BCTZ nanowires and high performance BCTZ-based nanogenerator for biomechanical energy harvesting. *Ceramics International*, 43(8), 5875–5880. <https://doi.org/10.1016/j.ceramint.2017.01.057>.
- Finkenstadt, V. L. (2005). Natural polysaccharides as electroactive polymers. *Applied Microbiology and Biotechnology*, 67(6), 735–745. <https://doi.org/10.1007/s00253-005-1931-4>.
- Furukawa, T., & Seo, N. (1990). Electrostriction as the origin of piezoelectricity in ferroelectric polymers. *Japanese Journal of Applied Physics*, 29(4), 675–680. <https://doi.org/10.1143/jjap.29.675>.
- Garain, S., Jana, S., Sinha, T. K., & Mandal, D. (2016). Design of in situ poled Ce³⁺-doped electrospun PVDF/graphene composite nanofibers for fabrication of nanopressure sensor and ultrasensitive acoustic nanogenerator. *ACS Applied Materials & Interfaces*, 8(7), 4532–4540. <https://doi.org/10.1021/acsami.5b11356>.
- Garain, S., Sinha, T. K., Adhikary, P., Henkel, K., Sen, S., Ram, S., Sinha, C., Schmeißer, D., & Mandal, D. (2015). Self-poled transparent and flexible UV light-emitting cerium complex-PVDF composite: A high-performance nanogenerator. *ACS Applied Materials & Interfaces*, 7(2), 1298–1307. <https://doi.org/10.1021/am507522r>.
- Gaur, A., Kumar, C., Shukla, R., & Maiti, P. (2017). Induced piezoelectricity in poly(vinylidene fluoride) hybrid as efficient energy harvester. *ChemistrySelect*, 2(27), 8278–8287. <https://doi.org/10.1002/slct.201701780>.
- Gaur, A., Kumar, C., Tiwari, S., & Maiti, P. (2018). Efficient energy harvesting using processed poly(vinylidene fluoride) nanogenerator. *ACS Applied Energy Materials*, 1(7), 3019–3024. <https://doi.org/10.1021/acsaeam.8b00483>.
- Gaur, A., Shukla, R., Kumar, B., Pal, A., Chatterji, S., Ranjan, R., & Maiti, P. (2016). Processing and nanoclay induced piezoelectricity in poly(vinylidene fluoride-co-hexafluoro propylene) nanohybrid for device application. *Polymer*, 97, 362–369. <https://doi.org/10.1016/j.polymer.2016.05.049>.
- Geng, C., Wang, J., Zhang, Q., & Fu, Q. (2012). New piezoelectric damping composites of poly(vinylidene fluoride) blended with clay and multi-walled carbon nanotubes. *Polymer International*, 61(6), 934–938. <https://doi.org/10.1002/pi.4161>.
- Glass, J. E., Schultz, D. N., & Zukoski, C. F. (1991). Polymers as rheology modifiers: An overview. Available in: <https://ubir.buffalo.edu/xmlui/handle/10477/41535>
- Gloaguen, J.-M., & Lefebvre, J.-M. (2007). Nanocomposites polymères/silicates en feuillets. *Ref : TIP580WEB - "Matériaux Fonctionnels."* Available in: <https://www.techniques-ingenieur.fr/base-documentaire/materiaux-th11/materiaux-a-proprietes-mecaniques-42535210/nanocomposites-polymeres-silicates-en-feuillets-n2615/>
- Gonçalves, R., Martins, P. M., Caparrós, C., Martins, P., Benelmekki, M., Botelho, G., Lanceros-Mendez, S., Lasheras, A., Gutiérrez, J., & Barandiarán, J. M. (2013). Nucleation of the electroactive β -phase, dielectric and magnetic response of poly(vinylidene fluoride) composites with Fe₂O₃ nanoparticles. *Journal of Non-Crystalline Solids*, 361, 93–99. <https://doi.org/10.1016/j.jnoncrsol.2012.11.003>.
- Grau, G., Frazier, E. J., & Subramanian, V. (2016). Printed unmanned aerial vehicles using paper-based electroactive polymer actuators and organic ion gel transistors. *Microsystems & Nanoengineering*, 2(1), 16032. <https://doi.org/10.1038/micronano.2016.32>.

- Gurunathan, K., Murugan, A. V., Marimuthu, R., Mulik, U., & Amalnerkar, D. (1999). Electrochemically synthesised conducting polymeric materials for applications towards technology in electronics, optoelectronics and energy storage devices. *Materials Chemistry and Physics*, 61(3), 173–191. [https://doi.org/10.1016/s0254-0584\(99\)00081-4](https://doi.org/10.1016/s0254-0584(99)00081-4).
- Gutiérrez, T. J. (2018). Active and intelligent films made from starchy sources/blackberry pulp. *Journal Polymers and the Environment*, 26(6), 2374–2391. <https://doi.org/10.1007/s10924-017-1134-y>.
- Gutiérrez, T. J., & Alvarez, V. A. (2017). Cellulosic materials as natural fillers in starch-containing matrix-based films: A review. *Polymer Bulletin*, 74(6), 2401–2430. <https://doi.org/10.1007/s00289-016-1814-0>.
- Gutiérrez, T. J., González Seligra, P., Medina Jaramillo, C., Famá, L., & Goyanes, S. (2017a). Chapter 14. Effect of filler properties on the antioxidant response of thermoplastic starch composites. In V. K. Thakur, M. K. Thakur, & M. R. Kessler (Eds.), *Handbook of composites from renewable materials* (pp. 337–370). EE.UU: WILEY-Scrivener Publisher. <https://doi.org/10.1002/9781119441632.ch14>. isbn:978-1-119-22362-7.
- Gutiérrez, T. J., Ollier, R., & Alvarez, V. A. (2018). Chapter 5. Surface properties of thermoplastic starch materials reinforced with natural fillers. In V. K. Thakur & M. K. Thakur (Eds.), *Functional biopolymers* (pp. 131–158). EE.UU: Editorial Springer International Publishing. https://doi.org/10.1007/978-3-319-66417-0_5. isbn:978-3-319-66416-3. eISBN: 978-3-319-66417-0.
- Gutiérrez, T. J., Ponce, A. G., & Alvarez, V. A. (2017b). Nano-clays from natural and modified montmorillonite with and without added blueberry extract for active and intelligent food nanopackaging materials. *Materials Chemistry and Physics*, 194, 283–292. <https://doi.org/10.1016/j.matchemphys.2017.03.052>.
- Gutiérrez, T. J., Suniaga, J., Monsalve, A., & García, N. L. (2016). Influence of beet flour on the relationship surface-properties of edible and intelligent films made from native and modified plantain flour. *Food Hydrocolloids*, 54, 234–244. <https://doi.org/10.1016/j.foodhyd.2015.10.012>.
- Gutiérrez, T. J., Toro-Márquez, L. A., Merino, D., & Mendieta, J. R. (2019). Hydrogen-bonding interactions and compostability of bionanocomposite films prepared from corn starch and nano-fillers with and without added Jamaica flower extract. *Food Hydrocolloids*, 89, 283–293. <https://doi.org/10.1016/j.foodhyd.2018.10.058>.
- He, L., Xia, G., Sun, J., Zhao, Q., Song, R., & Ma, Z. (2013). Unzipped multiwalled carbon nanotubes-incorporated poly(vinylidene fluoride) nanocomposites with enhanced interface and piezoelectric β phase. *Journal of Colloid and Interface Science*, 393, 97–103. <https://doi.org/10.1016/j.jcis.2012.10.060>.
- Jean-Mistral, C., Basrou, S., & Chaillout, J.-J. (2010). Comparison of electroactive polymers for energy scavenging applications. *Smart Materials and Structures*, 19(8), 085012. <https://doi.org/10.1088/0964-1726/19/8/085012>.
- Jeong, C. K., Lee, J., Han, S., Ryu, J., Hwang, G. T., Park, D. Y., Park, J. H., Lee, S. S., Byun, M., Ko, S. H., & Lee, K. J. (2015). A hyper-stretchable elastic-composite energy harvester. *Advanced Materials*, 27(18), 2866–2875. <https://doi.org/10.1002/adma.201500367>.
- Ji, S. H., Cho, J. H., Paik, J.-H., Yun, J., & Yun, J. S. (2017). Poling effects on the performance of a lead-free piezoelectric nanofiber in a structural health monitoring sensor. *Sensors and Actuators A: Physical*, 263, 633–638. <https://doi.org/10.1016/j.sna.2017.07.016>.
- Jo, C., Pugal, D., Oh, I.-K., Kim, K. J., & Asaka, K. (2013). Recent advances in ionic polymer-metal composite actuators and their modeling and applications. *Progress in Polymer Science*, 38(7), 1037–1066. <https://doi.org/10.1016/j.progpolymsci.2013.04.003>.
- Joung, M.-R., Xu, H., Seo, I.-T., Kim, D.-H., Hur, J., Nahm, S., Kang, C.-Y., Yoon, S.-J., & Park, H.-M. (2014). Piezoelectric nanogenerators synthesized using KNbO_3 nanowires with various crystal structures. *Journal of Materials Chemistry A*, 2(43), 18547–18553. <https://doi.org/10.1039/c4ta03551h>.
- Jung, J. H., Chen, C.-Y., Yun, B. K., Lee, N., Zhou, Y., Jo, W., Chou, L.-J., & Wang, Z. L. (2012). Lead-free KNbO_3 ferroelectric nanorod based flexible nanogenerators and capacitors. *Nanotechnology*, 23(37), 375401. <https://doi.org/10.1088/0957-4484/23/37/375401>.

- Karan, S. K., Bera, R., Paria, S., Das, A. K., Maiti, S., Maitra, A., & Khatua, B. B. (2016). An approach to design highly durable piezoelectric nanogenerator based on self-poled PVDF/AIO-rGO flexible nanocomposite with high power density and energy conversion efficiency. *Advanced Energy Materials*, 6(20), 1–12. <https://doi.org/10.1002/aenm.201601016>.
- Karan, S. K., Mandal, D., & Khatua, B. B. (2015). Self-powered flexible Fe-doped RGO/PVDF nanocomposite: An excellent material for a piezoelectric energy harvester. *Nanoscale*, 7(24), 10655–10666. <https://doi.org/10.1039/c5nr02067k>.
- Keplinger, C., Kaltenbrunner, M., Arnold, N., & Bauer, S. (2010). Rontgen's electrode-free elastomer actuators without electromechanical pull-in instability. *Proceedings of the National Academy of Sciences of the United States of America*, 107(10), 4505–4510. <https://doi.org/10.1073/pnas.0913461107>.
- Kim, G. H., Hong, S. M., & Seo, Y. (2009). Piezoelectric properties of poly(vinylidene fluoride) and carbon nanotube blends: β -phase development. *Physical Chemistry Chemical Physics*, 11(44), 10506–10512. <https://doi.org/10.1039/b912801h>.
- Kou, Y., Chai, X., Yu, R., Liu, Y., & Wang, Z. (2017a). Bio-compatible BCTZ-based piezoelectric nanogenerator as energy harvester and waterdrop counter. *Ceramics International*, 43(9), 6666–6670. <https://doi.org/10.1016/j.ceramint.2017.02.028>.
- Kou, Y., Kou, Z., Zhao, D., Wang, Z., Gao, G., & Chai, X. (2017b). Fabrication of lead-free Ba ($Zr_{0.2}Ti_{0.8}$)O₃–(Ba_{0.7}Ca_{0.3})TiO₃ nanoparticles and the application in flexible piezoelectric nanogenerator. *Ceramics International*, 43(6), 4803–4806. <https://doi.org/10.1016/j.ceramint.2016.11.221>.
- Kumar, A., Ali, S. F., & Arockiarajan, A. (2017a). Energy harvesting from crystalline and conductive polymer composites. In D. Ponnamma, K. Sadasivuni, J. J. Cabibihan, & M. A. Al-Maadeed (Eds.), *Smart polymer nanocomposites* (Springer series on polymer and composite materials). Cham: Springer. https://doi.org/10.1007/978-3-319-50424-7_2.
- Kumar, A. P., Depan, D., Singh Tomer, N., & Singh, R. P. (2009). Nanoscale particles for polymer degradation and stabilization—Trends and future perspectives. *Progress in Polymer Science*, 34(6), 479–515. <https://doi.org/10.1016/j.progpolymsci.2009.01.002>.
- Kumar, C., Gaur, A., Rai, S. K., & Maiti, P. (2017b). Piezo devices using poly(vinylidene fluoride)/reduced graphene oxide hybrid for energy harvesting. *Nano-Structures & Nano-Objects*, 12, 174–181. <https://doi.org/10.1016/j.nanoso.2017.10.006>.
- Kumar, C., Gaur, A., Tiwari, S., Biswas, A., Rai, S. K., & Maiti, P. (2019). Bio-waste polymer hybrid as induced piezoelectric material with high energy harvesting efficiency. *Composites Communications*, 11, 56–61. <https://doi.org/10.1016/j.coco.2018.11.004>.
- Lee, C., Wood, D., Edmondson, D., Yao, D., Erickson, A. E., Tsao, C. T., Revia, R. A., Kim, H., & Zhang, M. (2016). Electrospun uniaxially-aligned composite nanofibers as highly-efficient piezoelectric material. *Ceramics International*, 42(2), 2734–2740. <https://doi.org/10.1016/j.ceramint.2015.10.170>.
- Liao, Q., Zhang, Z., Zhang, X., Mohr, M., Zhang, Y., & Fecht, H.-J. (2014). Flexible piezoelectric nanogenerators based on a fiber/ZnO nanowires/paper hybrid structure for energy harvesting. *Nano Research*, 7(6), 917–928. <https://doi.org/10.1007/s12274-014-0453-8>.
- Lin, Z.-H., Yang, Y., Wu, J. M., Liu, Y., Zhang, F., & Wang, Z. L. (2012). BaTiO₃ nanotubes-based flexible and transparent nanogenerators. *The Journal of Physical Chemistry Letters*, 3(23), 3599–3604. <https://doi.org/10.1021/jz301805f>.
- Mahadeva, S. K., Walus, K., & Stoeber, B. (2014). Piezoelectric paper fabricated via nanostructured barium titanate functionalization of wood cellulose fibers. *ACS Applied Materials & Interfaces*, 6(10), 7547–7553. <https://doi.org/10.1021/am5008968>.
- Maity, K., Garain, S., Henkel, K., Schmeißer, D., & Mandal, D. (2018). Natural sugar-assisted, chemically reinforced, highly durable piezoorganic nanogenerator with superior power density for self-powered wearable electronics. *ACS Applied Materials & Interfaces*, 10(50), 44018–44032. <https://doi.org/10.1021/acsami.8b15320>.
- Mandal, D., Henkel, K., & Schmeißer, D. (2014). Improved performance of a polymer nanogenerator based on silver nanoparticles doped electrospun P(VDF-HFP) nanofibers. *Physical Chemistry Chemical Physics*, 16(22), 10403–10407. <https://doi.org/10.1039/c3cp55238a>.

- Mao, Y., Zhao, P., McConohy, G., Yang, H., Tong, Y., & Wang, X. (2014). Sponge-like piezoelectric polymer films for scalable and integratable nanogenerators and self-powered electronic systems. *Advanced Energy Materials*, 4(7), 1–7. <https://doi.org/10.1002/aenm.201301624>.
- Martins, P., Lasheras, A., Gutierrez, J., Barandiaran, J. M., Orue, I., & Lanceros-Mendez, S. (2011). Optimizing piezoelectric and magnetoelectric responses on CoFe_2O_4 /P(VDF-TrFE) nanocomposites. *Journal of Physics D: Applied Physics*, 44(49), 495303. <https://doi.org/10.1088/0022-3727/44/49/495303>.
- Meneghetti, P., & Qutubuddin, S. (2006). Synthesis, thermal properties and applications of polymer-clay nanocomposites. *Thermochimica Acta*, 442(1–2), 74–77. <https://doi.org/10.1016/j.tca.2006.01.017>.
- Muir, A. (2015). *Electroactive Polymer (EAP) Technology*. Retrieved from <https://promo.parker.com/parkerimages/promosite/artificialmuscle/unitedstates/aboutelectroactivepolymer/pdf/eap-bulletin.pdf>.
- Fernandez Otero, T., Cantero, I., & Villanueva, S. (1999). EAP as multifunctional and biomimetic materials. In Y. Bar-Cohen (Ed.), *Smart structures and materials 1999: Electroactive polymer actuators and devices* (Vol. 3669, pp. 26–35). International Society for Optics and Photonics. <https://doi.org/10.1117/12.349699>.
- Palmre, V., Pugal, D., Kim, K. J., Leang, K. K., Asaka, K., & Aabloo, A. (2015). Nanothorn electrodes for ionic polymer-metal composite artificial muscles. *Scientific Reports*, 4(1), 6176. <https://doi.org/10.1038/srep06176>.
- Park, I.-S., Jung, K., Kim, D., Kim, S.-M., & Kim, K. J. (2008). Physical principles of ionic polymer-metal composites as electroactive actuators and sensors. *MRS Bulletin*, 33(3), 190–195. <https://doi.org/10.1557/mrs2008.44>.
- Pei, Q., Joseph, J., Kornbluh, R., & Pelrine, R. (2000). High-speed electrically actuated elastomers with strain greater than 100%. *Science*, 287(5454), 836–839. <https://doi.org/10.1126/science.287.5454.836>.
- Rahman, M. A., & Chung, G. S. (2013). Synthesis of PVDF-graphene nanocomposites and their properties. *Journal of Alloys and Compounds*, 581, 724–730. <https://doi.org/10.1016/j.jallcom.2013.07.118>.
- Rahman, M. A., Lee, B. C., Phan, D. T., & Chung, G. S. (2013). Fabrication and characterization of highly efficient flexible energy harvesters using PVDF-graphene nanocomposites. *Smart Materials and Structures*, 22(8). <https://doi.org/10.1088/0964-1726/22/8/085017>.
- Saravanakumar, B., Soyoon, S., & Kim, S.-J. (2014). Self-powered pH sensor based on a flexible organic-inorganic hybrid composite nanogenerator. *ACS Applied Materials & Interfaces*, 6(16), 13716–13723. <https://doi.org/10.1021/am5031648>.
- Schreyer, H. B., Shahinpoor, M., & Kim, K. J. (1999). Electrical activation of PAN-Pt artificial muscles. In Y. Bar-Cohen (Ed.), *Smart structures and materials 1999: Electroactive polymer actuators and devices* (Vol. 3669, pp. 192–199). International Society for Optics and Photonics. <https://doi.org/10.1117/12.349676>.
- Shahinpoor, M. (1999). Ionic polymer-metal composites (IPMC) as biomimetic sensors and actuators. In *Field responsive polymers*. Retrieved from <https://ci.nii.ac.jp/naid/10008212704/>.
- Sheng, N., Boyce, M. C., Parks, D. M., Rutledge, G. C., Abes, J. I., & Cohen, R. E. (2004). Multiscale micromechanical modeling of polymer/clay nanocomposites and the effective clay particle. *Polymer*, 45(2), 487–506. <https://doi.org/10.1016/j.polymer.2003.10.100>.
- Smela, E., Inganäs, O., & Lundström, I. (1995). Controlled folding of micrometer-size structures. *Science*, 268(5218), 1735–1738. <https://doi.org/10.1126/science.268.5218.1735>.
- Smela, E., & Gadegaard, N. (1999). Surprising volume change in PPy(DBS): An atomic force microscopy study. *Advanced Materials*, 11(11), 953–957. [https://doi.org/10.1002/\(sici\)1521-4095\(199908\)11:11<953::aid-adma953>3.0.co;2-h](https://doi.org/10.1002/(sici)1521-4095(199908)11:11<953::aid-adma953>3.0.co;2-h).
- Soin, N., Boyer, D., Prashanthi, K., Sharma, S., Narasimulu, A. A., Luo, J., Shah, T. H., Siores, E., & Thundat, T. (2015). Exclusive self-aligned β -phase PVDF films with abnormal piezoelectric coefficient prepared via phase inversion. *Chemical Communications*, 51(39), 8257–8260. <https://doi.org/10.1039/c5cc01688f>.

- Takashima, W., Uesugi, T., Fukui, M., Kaneko, M., & Kaneto, K. (1997). Mechanochemoelectrical effect of polyaniline film. *Synthetic Metals*, 85(1–3), 1395–1396. [https://doi.org/10.1016/s0379-6779\(97\)80289-5](https://doi.org/10.1016/s0379-6779(97)80289-5).
- Tamagawa, H., Popovic, S., & Taya, M. (1999). Phase transition behavior of an amphoteric polymer gel. In Y. Bar-Cohen (Ed.), *Smart structures and materials 1999: Electroactive polymer actuators and devices* (Vol. 3669, pp. 254–264). International society for optics and photonics. <https://doi.org/10.1117/12.349684>.
- Tamang, A., Ghosh, S. K., Garain, S., Alam, M. M., Haeberle, J., Henkel, K., Schmeisser, D., & Mandal, D. (2015). DNA-assisted β -phase nucleation and alignment of molecular dipoles in PVDF film: A realization of self-poled bioinspired flexible polymer nanogenerator for portable electronic devices. *ACS Applied Materials & Interfaces*, 7(30), 16143–16147. <https://doi.org/10.1021/acsami.5b04161>.
- Tiwari, S., Gaur, A., Kumar, C., & Maiti, P. (2019). Enhanced piezoelectric response in nanoclay induced electrospun PVDF nanofibers for energy harvesting. *Energy*, 171, 485–492. <https://doi.org/10.1016/j.energy.2019.01.043>.
- Tiwari, V. K., Prasad, A. K., Singh, V., Jana, K. K., Misra, M., Prasad, C. D., & Maiti, P. (2013). Nanoparticle and process induced super toughened piezoelectric hybrid materials: The effect of stretching on filled system. *Macromolecules*, 46(14), 5595–5603. <https://doi.org/10.1021/ma400603h>.
- Wang, Y., Sun, C., Zhou, E., & Su, J. (2004). Deformation mechanisms of electrostrictive graft elastomer. *Smart Materials and Structures*, 13(6), 1407–1413. <https://doi.org/10.1088/0964-1726/13/6/011>.
- Wu, L., Alamusu, Xue, J., Itoi, T., Hu, N., Li, Y., Yan, C., Qiu, J., Ning, H., Yuan, W., & Gu, B. (2014a). Improved energy harvesting capability of poly(vinylidene fluoride) films modified by reduced graphene oxide. *Journal of Intelligent Material Systems and Structures*, 25(14), 1813–1824. <https://doi.org/10.1177/1045389X14529609>.
- Wu, L., Yuan, W., Hu, N., Wang, Z., Chen, C., Qiu, J., Ying, J., & Li, Y. (2014b). Improved piezoelectricity of PVDF-HFP/carbon black composite films. *Journal of Physics D: Applied Physics*, 47(13), 135302. <https://doi.org/10.1088/0022-3727/47/13/135302>.
- Xin, Y., Qi, X., Tian, H., Guo, C., Li, X., Lin, J., & Wang, C. (2016). Full-fiber piezoelectric sensor by straight PVDF/nanoclay nanofibers. *Materials Letters*, 164, 136–139. <https://doi.org/10.1016/j.matlet.2015.09.117>.
- Yeom, S.-W., & Oh, I.-K. (2009). A biomimetic jellyfish robot based on ionic polymer metal composite actuators. *Smart Materials and Structures*, 18(8), 085002. <https://doi.org/10.1088/0964-1726/18/8/085002>.
- Yip, M., Jin, R., Nakajima, H. H., Stankovic, K. M., & Chandrakasan, A. P. (2015). A fully-implantable cochlear implant SoC with piezoelectric middle-ear sensor and arbitrary waveform neural stimulation. *IEEE Journal of Solid-State Circuits*, 50(1), 214–229. <https://doi.org/10.1109/jssc.2014.2355822>.
- Zarrintaj, P., Jouyandeh, M., Ganjali, M. R., Hadavand, B. S., Mozafari, M., Sheiko, S. S., Vatankehah-Varnoosfaderani, M., Gutiérrez, T. J., & Saeb, M. R. (2019). Thermo-sensitive polymers in medicine: A review. *European Polymer Journal*, 117, 402–423. <https://doi.org/10.1016/j.eurpolymj.2019.05.024>.
- Zhang, G., Liao, Q., Zhang, Z., Liang, Q., Zhao, Y., Zheng, X., & Zhang, Y. (2016). Novel piezoelectric paper-based flexible nanogenerators composed of BaTiO₃ nanoparticles and bacterial cellulose. *Advanced Science*, 3(2), 1500257. <https://doi.org/10.1002/advs.201500257>.
- Zhang, Q. M., Bharti, V., & Zhao, X. (1998). Giant electrostriction and relaxor ferroelectric behavior in electron-irradiated poly(vinylidene fluoride-trifluoroethylene) copolymer. *Science*, 280(5372), 2101–2104. <https://doi.org/10.1126/science.280.5372.2101>.
- Zhang, Q. M., Li, H., Poh, M., Xia, F., Cheng, Z.-Y., Xu, H., & Huang, C. (2002). An all-organic composite actuator material with a high dielectric constant. *Nature*, 419(6904), 284–287. <https://doi.org/10.1038/nature01021>.

- Zhang, R., Ni, Q.-Q., Natsuki, T., & Iwamoto, M. (2007). Mechanical properties of composites filled with SMA particles and short fibers. *Composite Structures*, 79(1), 90–96. <https://doi.org/10.1016/j.compstruct.2005.11.032>.
- Zhao, Z., Shuai, C., Gao, Y., Rustighi, E., & Xuan, Y. (2016). An application review of dielectric electroactive polymer actuators in acoustics and vibration control. *Journal of Physics: Conference Series*, 744(1), 012162. <https://doi.org/10.1088/1742-6596/744/1/012162>.
- Zhenyi, M., Scheinbeim, J. I., Lee, J. W., & Newman, B. A. (1994). High field electrostrictive response of polymers. *Journal of Polymer Science Part B: Polymer Physics*, 32(16), 2721–2731. <https://doi.org/10.1002/polb.1994.090321618>.
- Zhou, Z., Bowland, C. C., Malakooti, M. H., Tang, H., & Sodano, H. A. (2016). Lead-free $0.5\text{Ba}(\text{Zr}_{0.2}\text{Ti}_{0.8})\text{O}_3-0.5(\text{Ba}_{0.7}\text{Ca}_{0.3})\text{TiO}_3$ nanowires for energy harvesting. *Nanoscale*, 8(9), 5098–5105. <https://doi.org/10.1039/c5nr09029f>.
- Zrínyi, M. (2000). Intelligent polymer gels controlled by magnetic fields. *Colloid & Polymer Science*, 278(2), 98–103. <https://doi.org/10.1007/s003960050017>.

Index

A

Abrasion resistance, 126
Acetonitrile medium, 288
Acrylamide monomers, 224, 225
Acrylic acid monomers, 217, 222, 223
Acrylonitrile monomers, 223
Acrylonitrile-butadiene-styrene (ABS), 6
Additives, 225, 226
Adipose derived stem cells (ASC), 301
Agroindustrial inputs, 229
Aliphatic thermoplastic polyester (ATP), 26, 27
Alkyl acrylate, 105
 α -cyclodextrin (α -CD), 96
Alumina/aluminum oxide (Al_2O_3), 140, 149–151
AM-*g*-gellan gum copolymer, 225
Amides sulfoxides, 260
3-Aminopropyltrimethoxysilane 97% (APTMS), 150, 157
Ammonium persulfate (APS), 201, 203, 222, 227
Anti-biological crosslinked polymers, 100
Antidiabetic drug, 225
Applications of functional hydrogels
 biomedical
 biocompatibility, 187, 188
 biodegradability, 188, 189
 safety controls, 188, 189
 wound dressing, 187
 fire resistance glazing, 189–191
 healthcare, 186
 personal care/hygiene, 191
Artificial muscles, 101

Assimilation, 75
Atom transfer radical coupling (ATRC) reaction, 297
Atom transfer radical polymerization (ATRP), 286
Azide ions, 300
2,2-Azobis(isobutyronitrile) (AIBN), 34, 95

B

Backbone, 204, 208, 209, 212, 216, 217, 223–228, 230
Benzoyl peroxide (BPO), 31, 253
Biocompatibility, 98, 187, 188
Biodegradability, 188, 189
 application, 74
 assimilation, 75
 bacterial culture, 78
 biobased, 74
 biodegradation, 75
 biomass, 74
 blends, 76
 chemical degradation, 76
 control compositing condition, 76
 crosslinking agent, 78
 depolymerization, 75
 disadvantages, 74
 environmental conditions, 74
 genus *Citrobacter*, 78
 mineralization, 75
 Modic compatibilizer, 78
 PBS/PLA blends, 79
 PBS/PLA/BPO blends, 79
 PLA hydrolysis, 76, 77

- Biodegradability (*cont.*)
- PLA/PHBV, 76
 - polyesters, 78
 - properties, 74
 - pyrosequencing analysis, 78
 - steps, 75
 - thermophilic microorganism, 76
- Biodegradable blends crosslinking
- agents, 64
 - DCP, 64, 65
 - factors, 64
 - homopolymer system, 64
 - inter-chain, 64
 - melt blending technique, 64
 - partial crosslinking systems, 65
 - peroxides, 63, 65
 - PHB/PDLLA, 64
- Biodegradable polyesters, 26, 246
- blend compatibilizers, 250
 - factors
 - backbiting depolymerization/hydrolysis, 252
 - comonomers, 252, 260, 261
 - graft copolymerization, 252
 - inhibitors, 260, 261
 - initiators, 253, 254
 - macroradicals, 252
 - melt processing, 253
 - mixing and residence time, 256, 257
 - monomers, 255, 256
 - polymer structure, 257
 - pressure, 259, 260
 - processing and mixing parameters, 252
 - radical initiator/monomer, 252
 - reagent concentration, 257–259
 - temperature, 259, 260
 - kinetics
 - graft polymerization, 264
 - homopolymerization, 266
 - mechanisms, 265
 - parameters, 268
 - peroxide-based and azo-containing compounds, 264
 - PLA-*g*-IAH, 268
 - polyolefins, 264
 - radical attacks, 265
 - radical production, 264
 - redox/photochemical initiation, 264
 - low-cost petrochemical polymers, 249
 - material properties
 - mechanical properties, 273, 274
 - rheology, 272, 273
 - thermal behavior, 271, 272
 - mechanism
 - α -carbon hydrogen, 263
 - free radical grafting, 261
 - grafting, 263
 - homolytic scission, 261
 - homopolymerization, 263
 - hydrogen abstraction, 261
 - macro-radical, 263
 - peroxides, 261
 - polymer radicals, 263
 - reaction mechanisms, 263
 - secondary methyl radicals, 261

- PBAT, 250
 - PBS, 251
 - PCL, 251
 - PHAs, 252
 - PLA, 251
 - polyolefin materials, 249
 - side reactions
 - chain scission, 269, 270
 - crosslinking, 269
 - β -scission, 270, 271
- Biodegradable polymers
- ATP, 26
 - blend compatibilization (*see* Polymer blends compatibilization)
 - blending, 27
 - classification, 26
 - compatibilizer, 27
 - crosslinking (*see* Free radical crosslinking)
 - disadvantages, 26
 - maleated (*see* Maleated compatibilizer)
 - performance evaluation
 - biodegradability, 74–78
 - water absorption, 68–71
 - weathering, 71–74
 - petrochemical plastics wastes
 - accumulation, 25
 - research, 80
- Biodeterioration, 75
- Biological crosslinked polymers, 94
- Biomedical applications, 317
- biocompatibility, 187
 - biodegradability, 188, 189
 - safety controls, 188, 189
 - wound dressing, 187
- Biopolymers, 91
- Blend, 246, 248–251, 255, 256, 273, 274
- Block copolymers, 201
- Bovine serum albumin (BSA), 287
- Brominated copolymer isobutylene isoprene and chlorosulphonated polyethylene (BIIR/CSM), 122
- Bulk polymerization, 97

C

- Cancer research, 102
- Carbohydrate polymers, 200
- Catalyst, 209
- Cellulose, 140–142, 150, 152, 153
- Ceric ammonium nitrate (CAN), 205, 206
- Ceric ion-based graft copolymerization, 202, 203
- Cetyltrimethylammonium bromide (CTAB), 312
- Characterization techniques, functional hydrogels
 - microscopic analysis, 181
 - rheological analysis, 182–184
 - spectroscopic analysis, 180, 181
 - thermal analysis, 184
- Charge transfer complex (CTC), 44
- Chemical grafting
 - CAN, 205, 206
 - ceric ion initiation, 202, 203
 - FAS/H₂O₂ initiation, 202
 - free-radicals, 201, 207–209
 - living polymerization, 209
 - anionic, 211
 - cationic, 211
 - covalent, 212
 - free-radical, 212
 - persulfates, 203, 204
- Chemically crosslinked polymers, 93, 94
- Chemical modification, bio and mineral fillers
 - cellulose, 150, 152, 153
 - composite materials, 144
 - lignin, 154, 156
 - mechanical properties, 156, 157
 - SiO₂, 145, 146 (*see also* SiO₂ fillers)
 - surface functionalization, 144
- Chromatography, 270
- Cinnamoyloxy ethyl methacrylate (CEMA), 105, 106
- Compatibility process, 18
- Compatibilization
 - block copolymers, 10
 - block/graft copolymers, 16
 - challenges, 14
 - compatibilizers, 8, 9
 - copolymer A-*b*-B, 9
 - functional polymers, 9
 - maleation process, 17
 - mechanism, 17
 - morphology control, 11
 - nanomixtures, 16
 - polymer composites, 11
 - random copolymers, 8
 - spectroscopic techniques, 18
 - structural characterization, 11, 13
 - urethanes, 11
- Compatibilizers, 8, 248, 249, 251, 255, 256
 - biodegradable plastics, 27
 - block-copolymer, 62
 - block/graft copolymers, 27
 - crosslinking reaction, 54, 80
 - environmental degradation, 81
 - interfacial reaction, 58
 - MA, 73, 80
 - maleated (*see* Maleated compatibilizer)
 - melt blending, 57
 - NBR, 66
 - PHB-*co*-HHx-*g*-MA, 60
 - polymer chains, 66
 - synergistic effect, 81
 - types, 49
 - UHMWPE, 67
- Composite materials, 137
- Condensation polymerization, 97
- Conjugated polymers (CPs), 303
- Contact lenses, 102, 103, 176, 177
- Controlled drug release, 229
- Conventional curing system, 121
- Conventional polymerization techniques
 - bulk, 97
 - condensation, 97
 - free radical, 95–96
 - UV radiation, 97
- Conventional polymers, 27
- Copolymers, 96, 201
- Coupling, 1
- Covalently crosslinked hydrogels, 170, 171
- Critical gel, 166, 167
- Critical micelle concentration (CMC), 9
- Cross-linkable bio and inorganic fillers
 - application, 136
 - chemical modification (*see* Chemical modification, bio and mineral fillers)
 - functionalized surface fillers, 136
 - mechanical characteristics, 136
 - PMC (*see* Polymer matrix composites (PMC))
 - processing techniques, 136
- Cross-linked-compatibilized, biodegradable blends
 - advantage, 66
 - HDPE-*g*-MA, 67
 - inter- and intra-components, 66
 - NBR, 66
 - peroxides and multifunctional chemicals, 66
 - PVC/LDPE, 66
 - UHMEPE/HA, 67

- Cross-linked polymers
 alteration, 98
 forms
 biological, 94
 chemical, 93, 94
 physical, 93
 gel applications
 anti-biological, 100
 artificial muscles, 101
 cancer research, 102
 contact lenses, 102
 drug delivery, 103
 gene delivery, 104
 hydrophilic networks, 108
 ocular implants, 102
 oil sorbers, 105–107
 plastic replacement, 107
 soil erosion prevention, 107
 wound dressing, 107
 hydrophilic, 92
 natural, 93
 parameter, 93
 properties
 biocompatibility, 98
 DC, 99
 mechanical, 99
 swelling characteristics, 99, 100
 synthesis methods (*see* Conventional polymerization techniques)
 synthetic, 93
- Crosslinking
 chemical, 168
 chemical reactions, 118
 chitosan-based hydrogel, 169
 electron beam processing, 118
 entanglement, hydrogels, 171, 172
 functionalization techniques, 169
 hydrogels, 169–171
 mechanical properties, 118
 physical, 168
 polymer chemistry, 118
 radiation source, 118
 vulcanization (*see* Vulcanization)
- Cross-linking density
 abrasion resistance, 126
 BIIR/CSM, 126
 chemical methods, 123
 fillers, 126
 glass transition temperature, 131
 higher hardness values, 126
 mechanical properties
 BIIR/CSM, 125
 vulcanized rubber, 124
 Rheological method, 126–128
 solvent swelling method, 129, 130
 stress (σ)-strain (ϵ) method, 128, 129
 tear resistance, 127
 vulcanizing network, 123
- Crosslinking process
 conversion, 92
 covalent bonding, 92, 93
 definition, 92
 elastic and fragile, 92
 implementation, 92
 reversible/irreversible, 93
 types, 92, 93
- Crosslinking reaction mechanism, 51–53
 Cs-*g*-poly(ϵ -caprolactone) (PCL), 217
 CuBr/Me₆Cyclam, 288
 Curing, 119, 138
- D**
- β -D-anhydroglucopyranose units (AGU), 141
 Degree of crosslinking (DC), 99
 Degree of grafting (DG), 30, 31
 Depolymerization, 75
 Devolatilization, 58
 Diacyl peroxides, 253
 Differential scanning calorimetry (DSC), 184, 272
 2-Dimethylaminoethyl methacrylate (DMAEMA), 287
 2,5-Dimethyl-2,5-bis-(*t*-butylperoxy) hexane (DBHA), 267
 Dimethyl sulfoxide (DMSO), 208
 Di-*t*-butyl peroxide (DTBP), 253
 Dodecyl acrylate-*co*-ODA-*co*-vinyl acetate terpolymers (DOVs), 105
 Drug delivery, 103
 Dual-reactive compatibilization, 17
 Ductile biodegradable polymers, 43
 Dynamic light scattering (DLS), 300
 Dynamic mechanical analysis (DMA), 42
 Dynamic mechanical thermal analysis (DMTA), 62
 Dynamic scanning calorimetric (DSC), 287
- E**
- Efficient vulcanization curing system (EV), 121
 Electroactive polymer composites (EAPC), 329
 Electroactive polymers (EAPs)
 activation mechanism, 327

- applications, 335, 337–339
 - biomedical field, 284
 - category, 327
 - chemical processes, 284
 - conductivity/piezoelectric effect, 327
 - devices
 - ceramic fillers, 338
 - electroactive phase, 335
 - electrodes, 332, 334
 - energy harvesting, 332
 - graphene oxide, 333
 - inactive layer, 332
 - inorganic and layered fillers, 336–337
 - insulating layer, 332
 - mixed fillers, 339
 - nanocomposites, 335
 - nanogenerator, 334
 - nanowires, 333
 - natural materials/bio-wastes, 335
 - OCV, 334
 - output voltage, 335
 - performance, 333
 - β -phase fraction, 334
 - piezoelectric coefficient, 334
 - power density, 335
 - structural layer, 334
 - types, 332
 - electrostrictive, 328
 - external electric field, 327
 - ferroelectric, 328
 - field of, 327
 - former method, 284
 - ionic polymer-metal composite, 327, 328
 - liquid crystalline, 328
 - materials, 327
 - nanocomposites, 284
 - optoelectronic properties, 284
 - PT, 285
 - semi-crystalline fluoropolymer, 284
 - types of processes, 284
 - Electrorheological fluids, 328
 - Electrostrictive polymers, 328
 - Entanglement in hydrogels, 171, 172
 - Environmental remediation, 229, 230
 - Enzymatic methods, 217
 - 2-Ethylhexyl acrylate (EHA), 105
 - Ethylene carbonate (EC), 294
 - 3,4-Ethylenedioxythiophene (EDOT), 309, 310
 - Ethylene glycol diacrylate (EGDA), 105
 - Ethylene glycol dimethacrylate (EGDMA), 105
 - Ethylene-vinyl acetate (EVA), 149
 - Ethyl hydroxyl ethyl cellulose (EHEC), 93
 - 2-Ethylhexyl acrylate (EHA), 105
 - EVA-g-starch copolymers, 60
- F**
- Fatty acids, 153
 - Fenton's reagent ($\text{Fe}^{2+}/\text{H}_2\text{O}_2$), 202
 - Ferroelectric polymers, 328
 - Field emission scanning electron microscopy (FESEM), 293
 - Fillers, 126, 127, 132, 136
 - Fire resistance glazing applications, 189–191
 - Fire resistance mechanism, 190, 191
 - Flexural and tensile properties, 274
 - Forward recoil spectrometry (FRES), 11
 - Fourier transform infrared (FTIR), 11, 150, 267, 291
 - Free radical crosslinking
 - agents, 49
 - peroxides, 50, 53–57
 - reaction mechanism, 51–53
 - thermoplastic vulcanizates, 48
 - Free radical grafting, 30, 45
 - diazonium salts, 208
 - DMSO, 208
 - graft copolymers, 207, 209, 210
 - grafting efficiency, 209
 - homopolymerization, 209
 - oxidation, 208
 - vinyl and acrylic monomers, 217, 221
 - Free radical polymerization
 - acrylate-based molecules, 95
 - copolymers, 96
 - homopolymers, 95
 - IPNs, 96
 - semi-IPN, 96
 - swelling network, 95
 - synthetic methods, 95
 - usage, 95
 - Free radicals, 201, 207, 208, 214–217, 223, 226
 - Functional hydrogels
 - applications (*see* Applications of functional hydrogels)
 - characteristics (*see also* Characterization techniques, functional hydrogels)
 - mechanical properties, 176, 177
 - optical properties, 176, 177
 - stimulus response, 177–179
 - swelling, 175, 176
 - compositions, 178
 - crosslinking (*see* Crosslinking)

- Functional hydrogels (*cont.*)
 hydration enthalpy
 ionizable species, 173
 selection of anions, 174
 selection of cations, 174
 hydrogel starting materials, 172
 initiator, 172, 173
 salts, 173
 structure, 166–168
 synthesis, 174, 175
 water vs. ionizable species, 173
- Functionalization, 58
- Functional polymer surfaces, 1
- G**
- Gamma-irradiated graft polymerization, 216
- Gamma radiation-initiated graft copolymerization, 224
- Gene delivery, 104
- Gibbs free energy, 7
- Glycidyl methacrylate (GMA), 9, 294
- Graft copolymerization, 200, 202
- Grafting, 1, 17
 acrylamide monomers, 224, 225
 acrylic acid monomers, 217, 222, 223
 acrylonitrile monomers, 223
 additives, 225, 226
 agroindustrial inputs, 229
 backbone nature, 226
 chemical methods (*see* Chemical grafting)
 controlled drug release, 229
 conventional polymer backbone, 199
 environmental remediation, 229, 230
 enzymatic methods, 217
 graft copolymerization, 200
 initiator role, 227
 monomer, 227, 228
 physical methods (*see* Physical methods, grafting)
 polysaccharides, 200, 201
 temperature, 228
- Grafting functional groups
 biobased polymers, 246
 biodegradable polyesters, 246
 biodegradable polymers, 246
 convenient method, 246
 functional polymers, 246
 mechanical properties, 246
 polymer industry, 245
 sustainable polymer materials, 246
- Grafting reaction
 copolymer, 30
 DG and MA, 31, 32
 free radical grafting, 30
 maleated PHB, 31
 monomer concentration, 31, 33
 PBS, 31, 33
 peroxide radical initiator, 29
 polymer dissolution, 30
 processing parameter, 31
 reactive components, 31
 REx, 31
 solid-state, 30
- Grafting yield, 42
- H**
- Healthcare, 186
- High-energy ionizing radiation, 94
- High melt strength polypropylene (HMSPP), 272
- Homopolymers, 39, 95, 266
- Hyaluronan (HA), 67
- Hyaluronic acid (HA)-based crosslinked polymers, 102
- Hydrogel materials, 169
- Hydrogel networks, 171
- Hydrogen ions, 329
- Hydrolytic and thermal degradation, 270
- Hydrophilic polymers, 94
- Hydrophobic polymers, 93, 99, 102
- Hydroxyl/hydroperoxide index, 73
- I**
- Immiscible mixtures
 compatibilization, 9
 dispersed-phase domain size, 16
 free energy, 7
 heterogeneous nature, 6
 interfacial adhesion, 6
 NPs, 17
- Immiscible polymers, 7, 14
- Incipient gel, 166
- Infrared spectrophotometer, 180
- Initiator, 172, 173, 227
- Inorganic fillers, 139
- In-situ crosslinking, 93
- In-situ hydrogels, 93
- In-situ reactive compatibilization
 compatibility and adhesion, 58
 devolatilization, 58
 EVA-g-starch copolymers, 59, 60
 homopolymers, 58
 in-situ grafting, 59
 MA-induced chemical interaction, 60
 REx technological, 58, 59
 screw configuration, 58
- Interpenetrating polymer systems (IPNs), 96

- Intumescence fire retardation, 190
Ionically crosslinked hydrogels, 170
Ionic polymer-metal composites (IPMC)
 biomimetics, 328
 electrorheological fluids, 328
 stimuli-responsive gels, 328
Iron trichloride, 316
Irradiation-induced grafting, 215, 216
Itaconic anhydride (IAH), 255
- J**
Janus NPs (J NPs), 17
- K**
Kumada catalyst-transfer polymerization, 316
- L**
Lathe cutting technique, 102, 103
Lauryl acrylate (LA), 105
Lauryl methacrylate (LMA), 105
Leibler's theory, 8
Lewis acid, 211
Light emitting diode (LEDs), 332
Lignin, 142, 143, 154, 156
Lignin polycarboxylic acid (LPCA), 154, 156
Linear low-density poly(ethylene)
 (LLDPE), 216
Liquid crystalline polymers, 328
Living anionic polymerization, 211
Living cationic polymerization, 211
Living covalent polymerization, 212
Living free-radical polymerization, 212
Living polymerization, 209
Low density poly(ethylene) (LDPE), 273
Lower critical solution temperature (LCST),
 179, 289
- M**
MA-based compatibilizer, 27
Macromolecules, 98
Macromonomer method, 315
Macroradicals, 40, 73
MA-grafted PP (MAPP), 36
Maleated biodegradable polymers
 PBS, 41–43
 PCL, 46–48
 PHB, 43–44
 PLA, 44–46
Maleated compatibilizer
 additive, 28
 blends, 28
 interfacial adhesion, 28
 interfacial energy, 80
 MA reactive monomer, 28, 29
 organic peroxide initiator, 33–35
 physical-mechanical behavior, 28
 polymer industry, 80
 purification, 35, 36
 reaction (*see* Grafting reaction)
 reaction mechanism
 FTIR spectroscopy, 41
 functionalization, 36
 haemolytic scission, 36
 homolytic scission, 39
 MA grafting onto polyester, 39, 40
 MA grafting onto PP, 36, 39
 macroradicals, 40
 thermodynamic contributions, 28
Maleated PBS
 compatibilizer, 41
 DMA, 42
 grafting yield, 42
 ¹H-NMR analysis, 42
 melt grafting technique, 42
 molecular chain, 42
 PBAT/PBS blends, 42
 polyolefins, 41
 starch content, 41
 TPS/PBS, 42
Maleated PCL
 compatibilization techniques, 47
 ductile biodegradable polyester, 46
 FTIR analysis, 47
 grafting reaction, 47, 48
 homolytic scission, 48
 homopolymerization, 48
 solid state ¹³C-NMR analysis, 47
 solution grafting technique, 47
 starch, 48, 49
Maleated PHB
 conventional polymers, 43
 copolyesters, 43
 copolymerization, 43
 ductile biodegradable polymers, 43
 graft copolymerization, 43
 grafting reaction, 44
 homopolymerization, 43
Maleated PLA (PLA-g-MA)
 blends, 44
 free radical grafting, 45
 grafting, 44, 47
 macroradicals, 46
 melt grafting technique, 44
 St *co*-monomer, 45, 46
 St/MA/DCP ratio, 46
Maleic anhydride (MA), 9, 246

- MA reactive monomer, 28, 29
 Mechano-chemo-electric process, 329
 Melt flow index (MFI), 269
 Metformin hydrochloride (MTF), 225
 Methyl cellulose (MC), 306
 Methylene diphenyl diisocyanate (MDI), 11
 Methyl methacrylate (MMA), 267, 297
 Microscopic analysis methods, 181
 Microstructure, 168
 Microwave (MW) energy-induced initiation, 216–220
 Mineralization, 75
 Miscible mixtures
 entropic contribution, 7
 free energy, 7
 homogeneous nature, 6
 morphologies, 6
 Modic compatibilizer, 78
 Molecular weight (M_w), 8, 166
 Monomer, 176, 227, 228
 Mooney-Rivlin equation, 129
 Morphology control
 common pairs, 14
 interface, 14
 PA polymers, 12
 uncompatibilized mixing system, 11
 Mosaic grafting, 201
 Multifunctional crosslinkers, 94
 Multiwalled carbon nanotubes (MWCNTs), 329–331
 Multi-wave technique, 183
 MW radiation-irradiated free radical polymerization, 225
- N**
 Nafion, 329
 Nanocellulose (NC), 141
 Nanocomposites, 329–333, 335
 Nanohybrid, 330
 Nanoparticles (NPs), 9, 102
 Natural and synthetic polymers, 1
 Negative differential resistance (NDR), 308
 Nitrogen atom, 289
N-methyl-2-pyrilidone (NMP), 286
N,N-dimethyl aminoethyl methacrylate (DMAEMA), 306
N,N-dimethylformamide (DMF), 289
N,N'-methylene bis-acrylamide (MBA), 206, 216, 222
N,N',N''-tris(methacryloyl)melanine (MM), 106
N,N',N''-trisacryloyl melanine (AM), 106
- Non-modified fillers, 138
 Non-reactive compatibilization
 block copolymers, 62
 conventional polymers, 62
 diblock-copolymer, 62
 factors, 62
 PBS and PBT, 62, 63
 toughening approach, 62
 transesterification, 62
 Nuclear magnetic resonance (NMR), 11, 41, 131, 287
- O**
 Octadecyl acrylate (ODA), 105
 Octenestyrene-divinylbenzene (OS-DVB), 106
 Oil sorbers
 acrylates, 105
 alkyl acrylate, 105
 AM and MM, 106
 CEMA, 106
 crosslinked polymethyl sebacates, 106
 DC and hydrophobicity, 105
 DOVs, 106
 ODA, 105
 polyisobutylene, 105
 styrene monomer, 105
 synthetic variables, 105
 transesterification, 106
 Open circuit voltage (OCV), 334
 Optical properties, 176, 177
 Organically modified montmorillonite (OMnt), 331
 Organic field-effect transistors (OFET), 317
 Organic peroxide radical initiator
 BPO, 34
 crosslinking reaction, 35
 degradation, 34
 dehydrogenation, 33
 DG of MA, 34
 effects, 34
 reactive melt-blending technique, 34
 termination/combination reaction, 35
 Organosilanes, 145
 Oxyethylene methacrylate (OEM), 286
- P**
 PAAm polymer, 107
 Partial crosslinking systems, 65
 Pentaerythritol triacrylate (PETA), 260
 Permanganate ion, 208
 Peroxide efficiency, 253–254

- Peroxide radical crosslinking, 50
- Peroxides, 253, 261
- Peroxides concentration
 - chain branching, 54
 - DCP, 54–56
 - effects, 56
 - gel fraction, 54
 - grafting period, 53
 - LDPE, 54
 - partial crosslinking, 54
 - PHB/PDLLA, 56, 57
 - PLLA and PHBV, 53
- Peroxyl radicals, 174
- Personal care/hygiene application, 191
- Persulphate/ascorbic acid, 203, 204
- Phosphites, 260
- Photochemical grafting, 214
- Photopolymerization, 215
- Physically crosslinked polymers, 93
- Physical methods, grafting
 - irradiation-induced grafting, 215, 216
 - macromolecules, 214
 - MW energy-induced initiation, 216–220
 - photochemical, 214
 - photopolymerization, 215
 - plasma radiation-induced grafting, 215
 - reactive free radical, 214
- Piezoelectricity, 330
- Plasma radiation-induced grafting, 215
- Plasma treatment, 215
- Poly(acrylamide) (PAAm), 92, 94, 107
- Poly(acrylic acid) (PAA), 175
- Poly(amide 11)/poly(L-lactic acid) (PA11/PLLA), 17
- Poly(aniline), 329
- Poly(butylene adipate-*co*-terephthalate) (PBAT), 246, 250
- Poly(butylene succinate) (PBS), 251
- Poly(butylene succinate-*co*-adipate) (PBSA), 33
- Poly(caprolactone) (PCL), 251
- Poly(carbonate) (PC), 6
- Poly(carboxyethyl acrylate) (PCEA), 179
- Poly(*ε*-caprolactone) (PCL), 26, 246
- Poly(2-dimethylamino)ethyl methacrylate (PDMAEMA), 287
- Poly(dimethyl siloxane) (PDMS), 329, 332
- Polydispersity index (PDI), 273
- Poly(ethylene) (PE), 246
- Poly(ethylene glycol) (PEG), 92, 94, 96
- Poly(ethylene glycol) methyl ether methacrylate (PEGMA), 287
- Poly(glycidyl methacrylate) (PGMA), 288
- Poly(3-hexyl)thiophene (P3HT), 294
- Poly(hydroxyalkanoate)s (PHA), 252
- Poly(3-hydroxybutyrate-*co*-3-hydroxyhexanoate) (PHBHH), 252
- Poly(2-hydroxyethyl methacrylate) (PHEMA), 102
- Poly(lactic acid) (PLA), 246, 251
- Poly(L-lactic acid) (PLLA), 251
- Polymer blends compatibilization
 - cost-effective approach, 57
 - non-reactive, 62–63
 - procedure, 57
 - reactive (*see* Reactive compatibilization)
- Polymer grafting, 152
- Polymer matrix composites (PMC)
 - Al₂O₃ filler, 140
 - automotive/aerospace industry, 137
 - cellulose filler, 140–142
 - composite materials, 137
 - drawbacks, 138
 - epoxy, 138
 - lignin, 142, 143
 - nano/micro filler particles, 137
 - non-modified fillers, 138
 - properties, 137
 - reinforcement, 143, 144
 - role, 137
 - SiO₂ filler, 139, 140
 - thermoplastic/thermosetting polymers, 138
 - UPR, 138
 - waste materials, 138
- Polymeric hydrogels, 189
- Polymerization, 212
 - crosslinkers and initiators, 93
 - degradable/non-degradable, 97
 - hydrophilic molecules, 94
 - post-crosslinking process, 93
 - toxic chemicals, 98
 - types, 97
- Polymer mixtures
 - ABS/PC, 6
 - classification, 6
 - compatibilization (*see* Compatibilization)
 - definition, 6
 - miscibility, 6
 - thermodynamics, 7
- Polymers
 - biopolymers, 91
 - inter- and intramolecular interactions, 91
 - macromolecules, 91
 - synthetic, 91
- Poly(methyl methacrylate) (PMMA), 205, 212, 297

- Poly(naphthyl methacrylate) (PNM), 289
 Poly(*n*-butyl methacrylate) (PnBMA), 292
 Poly(propylene) (PP), 246
 Poly(propylene carbonate) (PPC), 257
 Polypyrrole, 329
 Polysaccharides, 200, 201, 229
 Poly(styrene-acrylonitrile)/poly(methyl methacrylate) (PSAN/PMMA), 6
 Poly(styrene-*co*-GMA-*co*-MA) ternary copolymers (SGM), 17
 Poly(styrene)/poly(phenylene oxide) (PS/PPO), 6
 Polysulfidic cross-links, 121, 122
 Poly(thiophene) (PT), 285
 - acidic conditions, 311
 - acidolysis, 314
 - azide-alkyne cycloaddition, 314
 - bioengineering and biomedical applications, 315
 - copolymer composition, 307
 - Cu-catalyzed click chemistry, 314
 - EDOT, 309, 310
 - electroactive polymer, 304
 - electrochemical properties, 309
 - emission intensity, 314
 - graft copolymer, 308
 - grafting through technique, 315–317
 - homopolymer and block copolymers, 309
 - hydrolysis, 311
 - ionic systems, 304
 - ionic water-soluble CPs, 304
 - light-induced variation, 314
 - macroinitiator, 305
 - metals, 303
 - methacrylic acid, 309
 - morphological and electronic properties, 308
 - nano-fibrillar network, 312
 - nitroxide radicals, 308, 310
 - Nyquist plots, 313
 - optical and electronic properties, 303
 - optoelectronic properties, 314
 - organic polymers, 303
 - photoluminescence spectra, 308
 - PL intensity, 316
 - PTPA, 310
 - technological applications, 304
 - temperature-induced structural transition, 305
 - 3-thiophene ethanol, 313
 - thiophene monomer, 305
 - trifluoroacetic acid, 310
 - uracil moiety, 314
 - water, 304
 Poly(vinyl alcohol) (PVA), 94
 Poly(vinyl chloride) (PVC), 92
 Poly(vinylidene fluoride) (PVDF), 284, 328
 - breath figure mechanism, 293
 - alkyne moieties, 293
 - ampholytic graft chains, 301
 - ampholytic graft copolymer, 303
 - ATRP, 286, 299, 302
 - azide ions, 300
 - carbonyl groups, 302
 - C-F bond, 287, 296
 - conventional approach, 285, 286
 - CuBr/PMDETA catalyst, 291
 - cytocompatibility, 300
 - ester carbonyl groups, 292
 - ferroelectric properties, 294
 - FESEM, 293
 - filtering configurations, 299
 - fluorescence spectra, 300
 - ¹⁹F-NMR analysis, 291, 292
 - FTIR and crystallographic analysis, 295
 - GMA, 294
 - graft copolymers, 298
 - heterogeneous conditions, 287
 - ¹H-NMR analysis, 287
 - hydrophilic chains, 287
 - hydrophobic, 297
 - immersion precipitation technique, 287
 - ion-exchange capacities, 289
 - kinetic analysis, 291
 - mechanism, 296
 - methylene peaks, 301
 - orthogonal properties, 294
 - plasma pretreatment, 288
 - polymerization kinetics, 291, 292
 - PVDF-*g*-PDMAEMA graft chains, 292
 - PVDF-*g*-PGMA-*g*-P3HT copolymer, 295
 - radiation-induced grafting, 288
 - SEM images, 290
 - solid-state electrolyte, 292
 - superior mechanical and physicochemical properties, 300
 - surface modification technique, 288
 - technological and biocompatibility, 301
 - thermal properties, 291
 - thermo-responsive character, 299
 - transition metal complexes, 286
 Poly(4-vinylpyridine) (P4VP), 288
 Potassium persulfate (KPS), 203, 204, 225, 227
 Processing techniques, 139
 Propargyl methacrylate (PMA), 293

- Proton exchange membrane fuel cells (PEMFCs), 329
- Psyllium mucilage, 223
- PT-*g*-poly(ampholyte) (PTP), 311
- PTMA-doped PANI (PTPA), 310
- p*-toluenesulfonic acid, 316
- R**
- Radiation grafting method, 215
- Raman spectroscopy, 180
- Random copolymer, 201
- Reactive and functional polymers, 1
- Reactive compatibilization, 17
- functionalization, 58
 - in-situ, 58–60
 - peroxide-induced crosslinking, 80
 - REx, 58, 60–62
- Reactive extrusion (REx), 31, 246
- benefits, 248
 - block copolymer, 249
 - carboxylic acids, 247
 - challenges, 248
 - chemical reactions, 247
 - compatibility, 248
 - free-radical grafting functional groups, 247
 - functional groups, 247
 - functional polyesters, 247
 - grafting, 247, 248
 - peroxide, 247
 - polyesters, 248
 - polymer's characteristics, 247
 - practical and profitable methods, 248
 - small molecules, 248
 - solution polymerization, 248
 - synthetic and natural polymer blends, 248
 - thermodynamic miscibility, 249
- Redox initiator, 202
- Reduced graphene oxide (RGO), 330
- Reinforced polymers
- fillers, 326
 - matrix, 326, 329
 - nanocomposites, 329
 - nanofillers, 329
 - high-aspect ratio, 326
 - one dimensional, 329, 330
 - three dimensional, 331
 - two dimensional, 330, 331 - nanoparticles, 329
- Reinforcement, 143–145, 150
- Residence time distribution (RTD), 256
- Rheological analysis
- crossover point, 184
 - gel point, hydrogels, 183, 184
 - multi-wave technique, 183
 - sinewaves, 183, 185
 - strain-time relationship, 182, 183
 - viscoelastic polymers, 182
- Rheological method, 126–128
- Rheology, 272, 273
- Ribonucleic acid (RNA), 308
- Ring opening polymerization (ROP), 174
- S**
- Saturated acids, 153
- Scanning electron microscopy (SEM), 13, 181, 288
- β -Scission, 270, 271
- Semi-efficient vulcanization curing system, 121
- Semi-inter penetrating network (Semi-IPN), 96
- Silanes, 145
- Silica NPs, 128, 130
- SiO₂ fillers, 145
- advantages, 144
 - Al₂O₃ fillers, 149–151
 - composite coatings, 147
 - cross-linking, 147, 148
 - grafting, 145
 - organosilanes, 145
 - PMC, 139, 140
 - process parameters, 146
 - reinforced composites, 148, 149
 - reinforcements, 145
 - silanes, 144, 146
 - surface functionalization, 145
 - surface modification, 147
 - TMVS, 146
- Size exclusion chromatography (SEC)
- analysis, 287
- Small-angle neutron scattering (SANS), 131
- Small angle X-ray scattering (SAXS), 291
- Sodium dodecylbenzenesulfonate (SDBS), 312
- Soft contact lenses, 187
- Solar radiation, 71
- Solid-state grafting, 30
- Solvent swelling method, 129, 130
- Spectroscopic analysis methods, 180, 181
- Stable radicals, 254
- Staphylococcus aureus*, 289
- Starch graft copolymer, 224
- Stearyl acrylate (SA), 105
- Stimuli-responsive gels, 328

- Stimulus response
 hydrogels, 177
 LCST, 179
 temperature-induced phase change, 178
 temperature *vs* light transmittance,
 178, 179
- Stress relaxation, 172
- Stress (σ)-strain (ϵ) method, 128, 129
- Styrene-GMA, 12
- Succinic acid (SA), 251
- Sulfate-free radical (SO₄⁻), 203
- Sulfur curing, 92
- Sulphur crosslinks, 121
- Sulphur curing systems, 120
- Sulphur-sulphur bonds, 121
- Sulphur vulcanization, 119
- Surface modification, 217
- Surface-initiated RAFT (SI-RAFT)
 polymerization, 307
- Swelling
 affinity, 103
 characteristics, 175, 176
 covalent/crosslinking, 99
 crosslinked polymer, 97
 DC, 99, 105
 interpenetrating networks, 95, 96
 networks, 100
 polymer bonds, 99
 property, 103, 105
- Synthetic polymers, 91
- T**
- Tear resistance, 127
- Temperature, 228
- Tert*-butyl methacrylate (*t*BMA), 286
- Tetrahydrofuran (THF), 47, 292
- 2,2,6,6-Tetramethylpiperidin-1-oxyl
 (TEMPO), 260
- Thermal analysis techniques, 184
- Thermal behavior, 271, 272
- Thermogravimetric analysis (TGA), 184
- Thermohydrolysis, 270
- Thermoplastic starch (TPS)/PLA blends, 35
- Thermoplastic vulcanizates, 49, 50
- Thermosetting polymers, 138
- Thiophene 3-acetic acid, 295
- Tissue engineering, 187
- Transesterification, 62, 106
- Transition alumina, 140
- Transmission electron microscopy (TEM), 16
- Triallyl isocyanurate (TAIC), 260
- Triallyl trimesate (TAM), 260
- Two-step REx compatibilization
 blend ratios, 60
 MA content, 61
 morphology, 61
 PCL, 61
 PHB-*co*-HHx, 60
 PLLA-*g*-MA, 61
 synergistic effect, 60
 twin-screw extruder, 60
- U**
- Ultra-high Mw polyethylene (UHMEPE), 67
- Ultraviolet (UV) radiation, 97
- Unsaturated fatty acids, 153
- Unsaturated polyester resin (UPR), 138
- Urethanes, 11
- UV irradiation technique, 216
- UV-visible spectroscopy, 180
- V**
- van Deur Waals forces, 91
- Vulcanization, 92, 94
 BIIR/CSM, 122
 chemical bonds, sulphur vulcanized
 rubber, 121
 chemical probes, 121
 conventional curing system, 121
 cross-linked C-C monosulfidic bonds,
 122
 cross-linking density (*see* Cross-linking
 density)
 curing, 119
 EV, 121
 microwave energy/ultrasound, 119
 monosulfide, 123
 polysulfide cross-links, 121–123
 rheological curves, 119
 rubber macromolecules and chemical
 structure, 120
 rubber processing methods, 119
 rubber technologies, 118
 semi-efficient vulcanization curing
 system, 121
 sulphur crosslinks, 121
 sulphur curing systems, 120
 sulphur-sulphur bonds, 121
 temperature, 120, 121
 types of cross-links, 120
 vulcanized rubber, 118
 vulcanizing agents, 119, 120
 vulcanizing chemical agents, 119
 vulcanizing network, 118, 120
- Vulcanizing chemical agents, 119

W

Waste materials, 138

Water absorption

- alteration, biodegradable polymer blends, 68
- crystallinity of biodegradable blends, 69
- degree of crystallinity, 68
- hydrolysis, 69
- PDLA/PVA, 69
- physical properties, 70
- PLA, 68
- polymer blends morphology, 68
- starch-based blends, 70
- starch content, 69, 70
- TPS/PBS, 70

Weathering test

- blend composition, 73
- elements, 71
- mechanical properties, 71
- PEC/PVA blend, 73

photodegradation, 71, 72

PLLA/PBS, 73

polymer blends, 71, 73

PP/PBT blends, 72, 73

pure components, 73

solar radiation, 71

Wide angle X-ray scattering (WAXS), 291

Winter-Chambon criteria, 184

Wound dressing, 107

X

XG-g-AA copolymer, 226

X-ray diffraction (XRD) spectroscopy, 181

X-ray photoelectron spectra (XPS)

analysis, 289

Y

Young's module (YM), 251